UNIVERSIDADE DO ALGARVE

INTERACTION OF VANADIUM COMPOUNDS WITH DNA

Nataliya Butenko

Dissertação para obtenção do Grau de Doutor em Química

Trabalho efetuado sob a orientação de:
Prof. Doutora Isabel Maria Palma Antunes Cavaco

2013

Interaction of Vanadium Compounds with DNA

Declaração de autoria de trabalho

Declaro ser a autora deste trabalho, que é original e inédito. Autores e trabalhos consultados estão devidamente citados no texto e constam da listagem de referências incluída:

Dedication

I dedicate my work to Isabel Cavaco and Lidiia Svirenko

"Whatever you are, or whatever has happened, just be glad. Be glad because you are here. You are here in a beautiful world; and all that is beautiful may be found in this world... Just be glad, and you always will be glad. You will always have better reason to be glad. You will have more and more things to make you glad. For great is the power of sunshine, especially human sunshine. It can change anything, transform anything, remake anything, and cause anything to be become as beautiful as itself. Just be glad and your fate will change; a new life will begin and a new future will dawn for you". ***Cristian D. Larson***

Acknowledgements

I would like to express my profound gratitude to my advisor Prof. Dr. Isabel Cavaco for her excellent supervision, knowledge, all practical teachings, especially in agarose gel electrophoresis, immense help, continuous encouragement and support during my PhD work.

I wish to acknowledge several people who contributed to this work directly and indirectly:

- Professor João Costa Pessoa for giving me the opportunity to work in Centro de Química Estrutural, for welcoming and accepting me into his group, for keen interest and valuable suggestions;
- Professor José Paulo Pinheiro for teachings in voltammetry, constant support and willingness to help;
- Professor Vera Ribeiro for sharing her knowledge on plasmid DNA preparation and the opportunity to work in her laboratory;
- Professor Susana Etcheverry and her PhD student Ignacio León for collaboration, for kind and positive attitude in work;
- Doctor Isabel Tomaz for practical teachings and help in conducting Circular Dichroism and UV-Vis experiments as well as in synthesizing vanadium complexes, for her sincere interest and impressive dedication to work;
- Doctor Isabel Correia for practical teachings in NMR, for her boundless support, encouragement and friendship along these years;
- A big group in Centro de Química Estrutural, namely, Sérgio Marques, Sofia Gama, Gisela Gonçalves, Pedro Adão and many others for a very enjoyable work environment and the help to easily find my way around the laboratory;
- Professor Igor Khmelinskii and Professor Jorge Martins for allowing to use spectrofluorometry equipment;
- Miguel Manuel for practical teaching in Fluorescence;
- José Paulo da Silva for mass spectrometry experiments and corresponding discussions;

- Doctor Rosário Lopes, Doctor Hélio Martins and Engineer Catarina Pires for the constant help in organizing my working process and friendly work environment;
- My lab mates, Ana Luísa Ribeiro, Ana Catarina, Jorge Correia, Ana Guerreiro, Ana Margarida Eufigénia, and Rute Félix, for creating an excellent atmosphere in the laboratory and constant help;
- A great team from International mobility office (namely, Mercês Covas, Paula Simões, Marleni Azevedo, Celia Oliveira, Sofia Nunes) and Igor Khmelinskii for taking care of organizational and paper work, and amicable relationships;
- My family, especially my mother, for being always there for me;
- All my friends for unconditional acceptance and boundless support, for being the sourse of continuous joy and laughter.

With deep respect and gratitude, in memory of Professor Lidiia Svirenko (1939-2011) who was my teacher and supervisor at the National Academy of Municipal Economy, Kharkiv (Ukraine). She was the first to introduce me to research and helped to carry out my first investigation. Special thanks to my teacher Yuri Vergeles. If it were not for him, I would probably not have learnt about the Erasmus Mundus program and the great opportunity to study in Portugal. I am also very grateful to my teacher Oleksandr Spirin who keeps my spirit high, encourages my personal development, and is always helpful in many aspects.

This work was financially supported by the **Erasmus Mundus External Cooperation Window Lot 6** and **Fundação para a Ciência e Tecnologia (SFRH/BD/69444/2010).** Thanks to their granting, my work was successfully completed.

I would like to acknowledge Portuguese people for their hospitality and cordiality, willingness to help and create a delightful environment for foreigners.

THANK YOU.

Abstract

The DNA cleavage activity of several vanadium complexes (VC) was studied. The focus was on vanadium acetylacetonate, $V^{IV}O(acac)_2$, **1**, and several β-diketonate oxidovanadium(IV/V) derivatives: $V^{IV}O(hd)_2$ (**2**, hd = 3,5-heptanedione), $V^{IV}O(Cl\text{-}acac)_2$, (**3**, Cl-acac = 3-chloro-2,4-pentanedione), $V^{IV}O(Et\text{-}acac)_2$ (**4**, Et-acac = 3-ethyl- 2,4-pentanedione) and $V^{IV}O(Me\text{-}acac)_2$ (**5**, Me-acac = 3-methyl-2,4-pentanedione), $V^{V}{}_2O_4(acac)_2$ (**6**), $V^{V}O_2(acac)(phen)$ (**7**, phen = 1,10-phenanthroline) and $V^{V}O(OH)(OMe)(acac)$ (**8**). The nuclease activity of 28 additional vanadium, copper and nickel complexes was also analysed and compared.

The experimental techniques involved digestion of plasmid DNA (pDNA) followed by agarose gel electrophoreses to evaluate nuclease efficiency. pDNA was prepared and purified to assure the absence of interference from EDTA (ethylenediaminetetraacetic acid) and Tris present in commercial pDNA. The stability of complexes in aqueous solutions was studied by UV/vis spectroscopy and electroanalytical techniques, cyclic (CV) and square wave voltammetry (SWV). The nature of DNA cleavage mechanisms was assayed using fluorescent probes and ^{1}H and ^{51}V NMR spectroscopy.

$V^{IV}O(acac)_2$ was found to be efficient in cleaving pDNA. The extent of this pDNA cleavage is dependent on buffer media. In organic buffers (Tris, HEPES MOPS) no significant changes are observed, whereas in phosphate medium the nuclease activity is remarkable. The activity of the different complexes follows the order **3**>**1**≥**2**>>**4**~**5**. The V(V) derivatives, **6**-**8**, do not show any significant activity, except in the presence of an oxidant activating agent. CV results show that **1**-**3** have a quasi-reversible electrochemical behaviour, while of **4** and **5** have an irreversible one, similar to **6**.

The DNA cleavage by these complexes takes place through an oxidative mechanism. Complex **1** also cleaves DNA hydrolytically, however the reaction is too slow to compete with the radical mechanism.

In conclusion, phosphate buffer potentiates the DNA cleavage by $V^{IV}O(acac)_2$ derivatives through a species which presents a quasi-reversible redox behaviour and facilitates the formation of ROS, probably a mixed V(IV)-V(V)-acac-phosphate complex.

Keywords: Inorganic nucleases, DNA cleavage, Vanadyl acetylacetonate, Oxidovanadium (IV/V) complexes, Phosphate, ROS, Agarose Gel Electrophoresis.

Resumo

Este trabalho estuda a interação de complexos de vanádio com ADN, em particular a atividade nuclease do acetilacetonato de oxovánadio(IV), $V^{IV}O(acac)_2$, **1**, e alguns dos seus derivados: $VO(hd)_2$ (**2**, hd = 3,5-heptanodiona), $VO(Cl\text{-}acac)_2$, (**3**, Cl-acac = 3-cloro-2,4-pentanodiona), $VO(Et\text{-}acac)_2$ (**4**, Et-acac = 3-etil-2,4-pentanodiona) e $VO(Me\text{-}acac)_2$ (**5**, Me-acac = 3-metil-2,4-pentanodiona), $V_2O_4(acac)_2$ (**6**), $VO_2(acac)(phen)$ (**7**, phen = 1,10-fenantrolina) and VO(OH)(OMe)(acac) (**8**). O objetivo inicial foi identificar a(s) espécie(s) metálicas presentes em solução responsáveis pela degradação do ADN.
A atividade nuclease de seis compostos de vanádio e três compostos de cobre contendo aminoácidos e 1,10-fenantrolina e/ou 2,2'-bipiridina como co-ligandos, **10**-**36**, foi também analisada.

A eficiência da clivagem do ADN pelos complexos metálicos em soluções tamponizadas a pH 7 foi determinada por electroforese em gel de agarose. Comparou-se o efeito de diferentes tampões de pH sobre a atividade. A estabilidade dos complexos em solução aquosa foi estudada por espectroscopia de absorção molecular no UV-Vis e por técnicas electroanalíticas (voltametria cíclica e voltametria de onda quadrada). A natureza radicalar ou hidrolítica dos mecanismos de clivagem foi averiguada recorrendo a compostos modelo e usando técnicas de fluorescência molecular e de ressonância magnética nuclear.

O $VO(acac)_2$ mostrou ser extremamente eficiente na clivagem de ADN (pADN), em particular em soluções tamponizadas com fosfato. Não requer agentes ativadores, ar ou fotoirradiação para degradar o pADN. A clivagem de uma cadeia simples ("nicking") observa-se na presença de concentrações de metal na ordem dos 1,2 µM (correspondendo a ri = 0,08, onde ri é a razão da concentração de metal para a concentração do ADN, em pares de bases). A extensão da clivagem aumenta à medida que a concentração de **1** aumenta, e para concentrações de metal da ordem dos 10 µM (ri = 0,7) observa-se a clivagem da dupla cadeia. Quando ri = 1,7 observa-se a degradação completa da forma superenrolada (Sc) do pADN.

Todos os complexos estudados apresentam atividade nuclease, dependente da concentração. O complexo **2** é uma nuclease um pouco menos eficiente do que **1**, atingindo a degradação completa da forma Sc para ri = 3,3. O complexo **3** é muito pouco solúvel em solução aquosa, mas ainda assim demonstra uma atividade nuclease razoável, sugerindo ser mais eficiente do que os anteriores. Os complexos **4** e **5** têm atividades semelhantes e muito inferiores a **1**, não chegado a linearizar o pADN excepto para ri > 6,7. Os complexos **4** e **5** promovem a clivagem simples de uma cadeia a ri = 1,7.

O $VOSO_4$ é frequentemente considerado um controlo negativo em ensaios de atividade nuclease de compostos de vanádio. Neste estudo verificou-se que o $VOSO_4$ (**9**) tem um comportamento pouco reprodutível, nalguns ensaios apresenta uma atividade nuclease dependente da concentração tão forte como **1**, enquanto noutros não apresenta qualquer atividade. É possível que esta falta de reprodutibilidade seja devida nalguns casos precipitação do oxovanádio como hidróxido. A precipitação resulta em pouca ou nenhuma atividade observada. Caso as condições da precipitação e a sua extensão sejam irreprodutíveis, a atividade observada resulta também irreprodutível.

A estabilidade em solução aquosa dos complexos **1**–**5** e **9** foi avaliada por espectroscopia de absorção molecular no UV/Vis. Verificou-se que **1** e **2** são razoavelmente estáveis nas primeiras 24 h em tampão fosfato, havendo apenas pequenas alterações no espectro ao fim de 2-4 h. Os complexos **4** e **5** têm um comportamento totalmente diferente, observando-se uma hidrólise significativa em menos de 1 h. O mesmo sucede com o complexo **9**. O complexo **3** não é suficientemente solúvel em água, mas é muito estável em DMSO.

A diferente atividade dos complexos relaciona-se com a sua estabilidade em solução aquosa, seguindo a ordem **1**≥**2**>>**4**~**5**. As nucleases fracas (**4** e **5**) são complexos instáveis que são rapidamente oxidados e hidrolisados a complexos de V(V) durante a primeira hora após dissolução numa solução tamponizada a pH 7. Esta observação é confirmada pelos resultados de voltametria cíclica: **1**-**3** apresentam um comportamento semelhante entre si, e muito diferente de **4** e **5**. O comportamento electroquímico dos primeiros é quase-reversível, enquanto o dos segundos é claramente irreversível com um voltamograma semelhante ao do derivado de oxovanádio(V) (**6**).

Estudos de atividade nuclease dos complexos na presença de excesso de ligando mostram que deve ser outra espécie que não $V^{IV}OL_2$ a responsável pela atividade. A adição de excesso de ligando favorece a formação desta espécie em solução, relativamente ao metal livre e ao complexo $V^{IV}OL^{+}$. Ao adicionar excesso de acac a **1**, observa-se uma diminuição progressiva da atividade à medida que a razão ligando/metal aumenta de 80 para 160.

O efeito da presença de agentes redutores e de agentes oxidantes foi testada juntando oxona ou ácido mercaptopropiónico (MPA) à mistura reacional. Observou-se que a oxona favorece a eficiência da clivagem por **1**. Por outro lado, o MPA reduz a atividade nuclease destes compostos, mas não totalmente. Estes efeitos são observados tanto quando a digestão é feita ao ar como em atmosfera de azoto.

A presença de H_2O_2 favorece fortemente a clivagem. O aumento da concentração de H_2O_2 tem um efeito muito menos significativo na degração do pADN do que o aumento da concentração de complexo.

A atividade nuclease dos derivados de oxidovanádio(V), **6**-**8**, faz-se notar apenas na presença de oxona e em tampão fosfato. É improvável que o monovanadato (V_1), o produto mais comum da hidrólise e oxidação do vanádio(IV) em solução aquosa, seja a espécie responsável pela atividade nuclease de **1**. Por si só, o V_1 não exerce efeitos no pADN. Embora na presença de oxona possa causar clivagem da cadeia simples, é muito menos eficiente do que **1**.

A natureza e a concentração do tampão de pH são determinantes para a atividade nuclease. Demonstra-se que a extensão da clivagem do pADN causada por **1** depende grandemente do meio tampão, sendo maior em tampão fosfato do que em tampões orgânicos como HEPES, Tris e MOPS. A reação é sempre inibida na presença de MOPS, mesmo quando existe excesso de fosfato em solução, mas progride até à linearização do pADN na ausência daquele. O efeito do tampão foi estudado por electroforese em gel de agarose, espectroscopia de UV-Vis, voltametria cíclica e voltametria de onda quadrada e RMN de ^{1}H e ^{51}V.

Os resultados apontam para que as espécies responsáveis pela degradação observada no ADN em tampão fosfato sejam provavelmente espécies mistas contendo V(IV) e V(V), e os ligandos acac e fosfato, apresentando um comportamento redox quase reversível. Os

resultados de voltametria de onda quadrada indicam a formação de pelo menos três espécies diferentes, possivelmente: $VO(acac)_2(H_2PO_4)^-$, $VO(acac)(H_2PO_4)_2^-$ e $VO(H_2PO_4)_2$.

A clivagem do ADN ocorre através de um mecanismo radicalar. A formação de radicais OH foi observada em ensaios de hidroxilação do ácido tereftálico (TPA), um método muito sensível para a sua detecção. Observa-se um aumento notável na intensidade de fluorescência, devida à formação de ácido hidroxitereftálico, ao misturar TPA com soluções aquosas de **1**. Na presença de H_2O_2 a intensidade de fluorescência torna-se muito mais alta do que na sua ausência, confirmando a libertação de •OH. No entanto é possível que o radical superóxido ou radicais ligados ao complexo metálico sejam de fato as ROS que causam a clivagem oxidativa observada na ausência de agentes oxidantes.

Estudos por RMN de ^{1}H e ^{51}V, com modelos da ligação fosfodiéster mostram que o $VO(acac)_2$ é capaz de clivar e promover a clivagem hidrolítica do ADN, e que as espécies responsáveis são provavelmente tetravanadatos. No entanto, esta hidrólise é demasiado lenta (>24 h a 50 ºC) para competir com a reação radicalar que ocorre no tempo de incubação típico de 1 h a 37ºC.

A atividade nuclease de outros complexos de oxidovanádio(IV) e alguns complexos de cobre foi também avaliada e discutida.

Os complexos $VO(acac\text{-}Naf)_2$ (**10**, acac-Naf = acetonaftalina), $VO(tmh)_2$ (**11**, tmh = 2,2,6,6-tetrametil-3,5-heptanodiona), $VO(pbd)_2$ (**12**, pbd = 1-Fenil-1,3-butadiona)), $VO(acac\text{-}NH_2)_2$ (**13**, acac-NH_2 = acetoacetamida), $VO(acac\text{-}NMe_2)_2$ (**14**, N,N-dimetilacetoacetamida) são outros derivados de **1** que foram estudados neste trabalho. Com a excepção de **10**, que não induz qualquer clivaegem do ADN, **11**-**14** promovem a clivagem simples da dupla cadeia.

$Cu(acac)_2$ (**15)** e $Ni(acac)_2$ (**16**) foram testados como complexos com uma estrutura quadrangular plana, com coordenação semelhante a **1**. Ao contrário de **16**, que não apresenta qualquer atividade nuclease, **15** induz “nicking”, mas aparentemente não dependente da concentração de complexo. A adição de agentes ativadores aumenta significativamente a atividade nuclease de **15**, especialmente na presença de MPA, situação em que se observa a destruição completa do pADN. Este efeito do MP sugere um

mecanismo radicalar desencadeado pela redução do Cu(II) a Cu(I) pelo MPA. O complexo **16** também não apresenta efeitos sobre o ADN na presença de MPA.

Outro grupo de complexos estudados contém ácido picolínico na sua estrutura: $VO(MPA)_2$ (**17**, MPA = ácido 6-metil-2-picolínico), $VO(dmpp)_2$ (**18**, dmpp = 1-(3,4-dimetil-fenil)-piperazina) e $VO(PA)_2$ (**19**, PA = ácido picolínico). O complexo **19** é o mais ativo, seguido de **17** e **18**. Tanto as bandas Nck como Lin aparecem para concentações de 25, 50 e 100 µM (ri 1.67, 3,3 e 6,7, respetivamente).

VO(oda) (**20**), VO(oda)phen (**21**) e VO(oda)bipy (**23**), onde "oda" é o ligando oxodiacetato e phen denota fenantrolina, são outros exemplos de nucleases eficientes. $VO(phen)_2$ (**22**) foi estudado como termo de comparação. Os quatro complexos interagem prontamente com o pADN, causando clivagem simples e dupla.

$VO(morin)_2$ (**24**), $VO(chrysin)_2$ (**25**), VO(clor) (**26**), e $VO(silibinin)_2$ (**27**), complexos que demonstaram efeitos antitumurais, não promovem qualquer clivagem significativa, mesmo quando ativados com oxona ou MPA.

Palavras-Chave: nucleases, Clivagem do ADN, acetilacetonato de vanádio, complexos de oxidovanadio(IV), fosfato, ROS, electroforese em gel de agarose.

Abbreviations

acac	acetylacetone
AGE	agarose gel electrophoresis
ADME	adsorption, distribution, metabolism and excretion
ATP	adenosine 5´-triphosphate
BEOV	bis(ethylmaltolato)oxidovanadium(IV)
bipy	2,2'-bipyridine
chrysin	5,7-dihydroxyflavone
Clor	chlorogenic acid
Cl-acac	3-chloro-2,4-pentanedione
CD	Circular dichroism
CV	cyclic voltammetry
Cvs	cyclic voltammograms
EDTA	ethylenediaminetetraacetic acid
Et-acac	3-ethyl-2,4-penthanedione
Gly	glycine
GSH	glutathione
HAS	human serum albumin
hd	3,5-hepthanedione
HEPES	4-(2-hydroxyethyl)-1-piperazineethanesulfonic acid
HTPA	2-hydroxyl-terephtalate
IR	insulin receptor
Lin	linear form of plasmid DNA
L-Phe	L-phenylalanine
Me-acac	3-methyl-2,4-penthanedione
MOPS	3-(N-morpholino)propanesulfonic acid
Naf	naphthalene
MES	2-(N-morpholino)ethanesulfonic acid
MPA	mercaptopropionic acid
NMR	nuclear magnetic resonance
Nck	open circular form of plasmid DNA

oda	oxodiacetate
oxone	active oxygen (potassium peroxomonosulfate compound, min 4.5%)
PBS	phosphate buffered saline
pDNA	plasmid DNA
phen	1,10-phenanthroline
PO_4	phosphate buffer
PTP(s)	protein tyrosine phosphatase(s)
ROS	reactive oxygen species
RT	room temperature
Sal	salicylic acid
Sc	supercoiled form of plasmid DNA
SDS	sodium dodecyl sulfate
SWV	square wave voltammetry
SWvs	square wave voltammograms
Tf	transferrin
TPA	terephthalic acid
Tris	2-amino-2-hydroxymethyl-propane-1,3-diol
Trizma base	tris(hydroxymethyl)aminomethane
UV-vis	UV-visible
V_1	monovanadate
V_2	divanadate
V_4	tetravanadate
V_5	pentavanadate
V_{10}	decavanadate
VC	vanadium complex(es)

Contents

List of Tables

Chapter I:

Chapter II:

Chapter III:

Chapter IV:

Chapter V:

List of Figures

Chapter I:

Chapter II:

Chapter III:

Chapter IV:

Chapter V:

Chapter VI:

List of Publications

Present work has originated the following publications:

PAPERS IN INTERNATIONAL SCIENTIFIC PERIODICALS WITH REFEREES:

1) "The effect of phosphate on the nuclease activity of vanadium compounds", **N. Butenko**, J.P. Pinheiro, A.I. Tomaz, I. Correia, V. Ribeiro, J. Costa Pessoa, I. Cavaco. Manuscript under preparation;

2) "Vanadium and copper Schiff base complexes: evaluation of the interaction with HSA and DNA and its cytoxicity", S. Roy, S. Borovic, I. Correia, A.I. Tomaz, **N. Butenko**, I. Cavaco, R.F.M. Almeida, S. Mehtab, M.H.V. Garcia, F. Marques, V. Moreno, J. Costa Pessoa. Manuscript under preparation;

3) "Vanadium and cancer treatment: antitumoral mechanisms of three oxidovanadium(IV) complexes on a human osteosarcoma cell line", I. León, **N. Butenko**, A. Di Virgilio, C. Muglia, E. Baran, I. Cavaco, S. Etcheverry. Accepted for publication in Journal of Inorganic Biochemistry, DOI 10.1016/j/jinorgbio.2013.10.009;

4) "Application of $V^{IV}O(acac)_2$ type complexes in the desulfurization of fuels with ionic liquids", A. Mota, **N. Butenko**, J.P. Hallett, I. Correia. *Catalysis Today* **2012**, 196, 119-125;

5) "Plasmid DNA cleavage and cytotoxicity of VO(oda)phen complex on normal and tumour lines in culture", I.E. León, **N. Butenko**, E. Baran, I. Cavaco, S.B. Etcheverry. *Biocell* **2011**, 35 (Suppl – CB-P46): S70;

6) "Antioxidant, DNA cleavage, and cellular effects of silibinin and a new oxidovanadium(IV)/silibinin complex", L.G. Naso, E.G. Ferrer, **N. Butenko**, I. Cavaco, L. Lezama, T. Rojo, S.B. Etcheverry, P.A.M. Williams. *J. Biol. Inorg. Chem*. **2011**, 16, 653–668;

7) "Cyto- and genotoxicity of a vanadyl(IV) complex with oxodiacetate in human colon adenocarcinoma (Caco-2) cells. Potential use in cancer therapy", A.L. Di Virgilio, J. Rivadeneira, C.I. Muglia, M.A. Reigosa, **N. Butenko**, I. Cavaco, S.B. Etcheverry. *BioMetals* **2011**, 24, 1153–1168;

8) "DNA Cleavage Activity of $V^{IV}O(acac)_2$ and Derivatives", **N. Butenko**, A.I. Tomaz, O. Nouri, E. Escribano, V. Moreno, S. Gama, V. Ribeiro, J.P. Telo, J. Costa Pessoa, I. Cavaco. *J. Inorg. Biochem*. **2009**, 103, 622-632.

PAPERS IN CONFERENCE PROCEEDINGS:

1) "Nuclease Activity Of $V^{IV}O(acac)_2$ derivatives", I. Cavaco, **N. Butenko**, A.I. Tomaz, J.P. Pinheiro, V. Ribeiro, J. Costa Pessoa, Book of abstracts, *FIGIPAS10th* **2009** (PO 33);

2) "Cytotoxicity and oxidative stress induced by a complex of Cu (II)-valsartan in osteoblast cell lines", A.L Di Virgilio, P.A.M. Williams, M.A. Reigosa, **N. Butenko**, I. Cavaco, S.B. Etcheverry. *Biocell* 34 (Suppl.) **2010** (CB-P11);

3) "Studies on the Mechanism of Action of an Efficient Vanadium Inorganic Nuclease, $V^{IV}O(acac)_2$" I. Cavaco, **N. Butenko**, A.I. Tomaz, V. Ribeiro, J. Costa Pessoa. *J. Biol. Inorg. Chem*. **2009**, 14 (Suppl 1): S183.

List of Communications

Present work was presented on the following scientific meetings:

ORAL COMMUNICATIONS:

1) "Nuclease Activity Of $V^{IV}O(acac)_2$ and its derivatives", **N. Butenko**, A. I. Tomaz, J.P. Pinheiro, J. Costa Pessoa, I. Cavaco, *Workshop on Metal Containing Drugs*, Meeting of the Inorganic Chemistry Committee of the Szeged Branch of HAS, 30-31st August **2011**, Szeged, Hungary (Speaker: I. Cavaco);

2) "DNA Cleavage activity of $V^{IV}O(acac)_2$ and derivatives", **N. Butenko**, A.I. Tomaz, O. Nouri, E. Escribano, V. Moreno, S. Gama, V. Ribeiro, J.P. Telo, J. Costa Pessoa, I. Cavaco, *6th International Symposium on the Chemistry and Biochemistry of Vanadium*, 17-19th July **2008**, Lisbon, Portugal (Speaker: I. Cavaco).

POSTER COMMUNICATIONS:

1) **N. Butenko**, J.P. Pinheiro, A.I. Tomaz, I. Correia, V. Ribeiro, J. Costa Pessoa, I. Cavaco "The Effect of Phosphate on the Nuclease activity of Vanadium Compounds", *11th European Biological Inorganic Chemistry Conference (EUROBIC11)* 12-16th of September **2012**, Granada, Spain (Poster presentation: N. Butenko);

2) **N. Butenko**, I. Correia, J. Costa Pessoa, I. Cavaco "Studies of hydrolytic DNA cleavage activity of $V^{IV}O(acac)_2$", *International Symposium on Metal Complexes 2012 (ISMEC2012*), also the XXIII Italian-Spanish Congress on Thermodynamics of Metal Complexes, 18-22nd of June **2012**, Lisbon, Portugal (Poster presentation: N. Butenko);

3) I. E. León, **N. Butenko**, E.J. Baran, I. Cavaco, S.B. Etcheverry "Cytotoxicity and plasmid DNA cleavage of three vanadyl(IV) complexes containing the oxodiacetate ligand on a human osteosarcoma cell line in culture", *International Symposium on Metal Complexes 2012 (ISMEC2012)*, also the XXIII Italian-Spanish Congress on Thermodynamics of Metal Complexes, 18-22nd of June **2012**, Lisbon, Portugal (Poster presentation: N. Butenko);

4) J. Costa Pessoa, S. Roy, S. Borovic, S. Mehtab, I. Cavaco, **N. Butenko**, R. F.M. Almeida, A.I. Tomaz, M.H.V. Garcia, F. Marques, V. Moreno, I. Correia "Vanadium and copper Schiff base complexes: evaluation of the interaction with HSA and DNA and its cytoxicity", *International Symposium on Metal Complexes 2012 (ISMEC2012)*, also the XXIII Italian-Spanish Congress on Thermodynamics of Metal Complexes, 18-22nd of June **2012**, Lisbon, Portugal (Poster presentation: I. Correia);

5) I. E. León, **N. Butenko**, E. Baran, I. Cavaco, S. B. Etcheverry "Plasmid DNA cleavage and cytotoxicity of VO(oda)phen complex on normal and tumour lines in culture", *47th Annual Meeting Argentine Society for Biochemistry and Molecular Biology*, 30th of October–2nd November **2011**, San Luis, República Argentina (Poster presentation: I.E. León);

6) **N. Butenko**, A. I. Tomaz, J.P. Pinheiro, J. Costa Pessoa, I. Cavaco "DNA cleavage activity of $VO^{IV}(acac)_2$ and derivatives", *4th European Conference on Chemistry for Life Science*, 31st August-3rd September **2011**, Budapest, Hungary (Poster presentation: N. Butenko);

7) S. Nigam, **N. Butenko**, I. Cavaco "Uncertainty in measuring the efficiency of inorganic nucleases", 4th European Conference on Chemistry for Life Science, 31st of August-3rd of September **2011**, Budapest, Hungary (Poster presentation: I. Cavaco);

8) P.A.M. Williams, M.A. Reigosa, **N. Butenko**, I. Cavaco, S.B. Etcheverry "Cytotoxicity and oxidative stress induced by a complex of Cu (II)-valsartan in osteoblast cell lines", *SAIB – 46th Annual Meeting Argentine Society for Biochemistry and Molecular Biology*, 30th of November-3rd of December, **2010**; Puerto Madryn, Chubut, Argentina (Poster presentation: Di Virgilio A.L.);

9) **N. Butenko**, A. I. Tomaz, J. P. Pinheiro, J. Costa Pessoa, I. Cavaco "Searching for the culprit species in $V^{IV}O(acac)_2$ nuclease activity", *7th International Symposium on the Chemistry and Biochemistry of Vanadium*, 6-9th October **2010**, Toyama, Japan (Poster presentation: I. Cavaco);

10) **N. Butenko**, A. I. Tomaz, J. P. Pinheiro, J. Costa Pessoa, I. Cavaco "Voltammetric studies of micromolar aqueous solutions of $V^{IV}O(acac)_2$ and derivatives, in relation to their nuclease activity", *7th International Symposium on the Chemistry and Biochemistry of Vanadium*, 6-9th October **2010**, Toyama, Japan (Poster presentation: N. Butenko);

11) I. Correia, A. Mota, I. Cavaco, **N. Butenko**, J. Hallett "Solvatocromic behaviour of $V^{IV}O(acac)_2$ and derivatives in ionic liquids", *7th International Symposium on the Chemistry and Biochemistry of Vanadium*, 6-9th October **2010**, Toyama, Japan (Poster presentation: I. Correia);

12) **N. Butenko**, A. I. Tomaz, V. Ribeiro, J. P. Pinheiro, I. Cavaco, J. Costa Pessoa "DNA cleavage by oxidovanadium(IV) complexes of acac derivatives", *4th SPB Clinical Biochemistry Workshop*, 29th of January **2010**, University of Algarve, Faro, Portugal (Poster Presentation: N. Butenko);

13) **N. Butenko**, A. I. Tomaz, V. Ribeiro, J. P. Pinheiro, I. Cavaco, J. Costa Pessoa " $V^{IV}O(acac)_2$ derivatives as efficient Inorganic Nucleases", *10th International Symposium on Applied Bioinorganic Chemistry (ISABC10)*, 25-28th September, **2009** Debrecen, Hungary (Poster Presentation: J. Costa Pessoa);

14) **N. Butenko**, A. I. Tomaz, V. Ribeiro, J. P. Pinheiro, J. Costa Pessoa, I. Cavaco "Studies on the Mechanism of Action of an Efficient Vanadium Inorganic Nuclease, $V^{IV}O(acac)_2$", *International Conference on Biological Inorganic Chemistry* (*ICBIC 14)*, 25-30th July, **2009** Nagoya, Japan (Poster Presentation: I. Cavaco);

15) **N. Butenko**, I. Cavaco, A. I. Tomaz, J. P. Pinheiro, V. Ribeiro, J. Costa Pessoa "Nuclease Activity Of $V^{IV}O(acac)_2$ derivatives", *10th Meeting In Inorganic Chemistry (FIGIPAS)*, 1-4th July **2009** Palermo, Sicily (Poster Presentation: N. Butenko).

Chapter I

Introduction

I. Introduction

I.1 Objectives

Current interest in biochemistry of vanadium-containing compounds (VC) falls into four fields: (1) study of its natural occurrence in biological system; (2) insulin-enhancing properties in the treatment of diabetes *mellitus* [1-4]; (3) potent artificial enzymes in gene manipulation procedures; (4) antitumor effect in cancer therapy [5,6].

When considering the therapeutic applications of VC many questions arise, namely whether and how VC can enter cells. Considering they do, an important question must be addressed: will they interact with DNA and, if so, how harmful (or beneficial, in case of anticancer drugs) will this interaction be? The effects over DNA may be dramatic (resulting in cytotoxicity) or subtle, and may not be detected within the timeframe of traditional clinical trials. A thorough understanding of these possible effects is essential to assure the safety of metallodrugs.

The central aim of this work is to evaluate the nuclease activity of vanadium compounds, and to establish which is/are the active species in the DNA cleavage.

Our particular focus are oxidovanadium(IV) complexes containing acetylacetonate ligands, primarily $V^{IV}O(acac)_2$, which have been considered as good candidates for the anti-diabetic drugs. Many diverse studies have been conducted with this family of compounds, however, little is known about its structure and chemistry in an aqueous solution at biologically relevant concentrations capable of cleaving DNA.

The main objective of this work is to understand how VC can cleave DNA, and which are the most active species involved. With this in mind, the work is divided into: (a) the synthesis and characterization of VC, (b) aqueous solution speciation via electrochemical and stability studies, (c) understanding of the role of buffer media and (d) determination of the mechanism of DNA cleavage action.

Along this work the following compounds were studied:

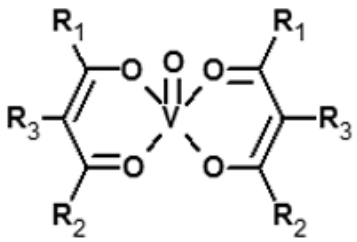

1 - $VO(acac)_2$: $R_1 = R_2 = CH_3$; $R_3 = H$
2 - $VO(hd)_2$: $R_1 = R_2 = C_2H_5$; $R_3 = H$
3 - $VO(Cl\text{-}acac)_2$: $R_1 = R_2 = CH_3$; $R_3 = Cl$
4 - $VO(Et\text{-}acac)_2$: $R_1 = R_2 = CH_3$; $R_3 = C_2H_5$
5 - $VO(Me\text{-}acac)_2$: $R_1 = R_2 = R_3 = CH_3$
13 - $VO(acac\text{-}NH_2)_2$: $R_1 = CH_3$; $R_2 = NH_2$; $R_3 = H$
14 - $VO(acac\text{-}NMe_2)_2$: $R_1 = CH_3$; $R_2 = N(CH_3)_2$; $R_3 = H$

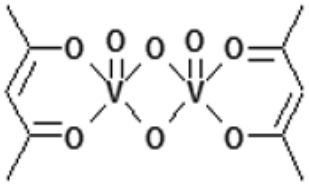

$V_2O_4(acac)_2$ (**6**)

$VO_2(acac)(phen)$ (**7**)

$VO(OH)(OMe)(acac)$ **(8)**

$VOSO_4$ (**9**)

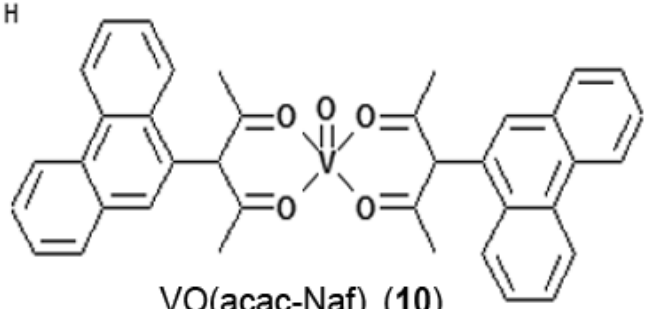

$VO(acac\text{-}Naf)_2$ (**10**)

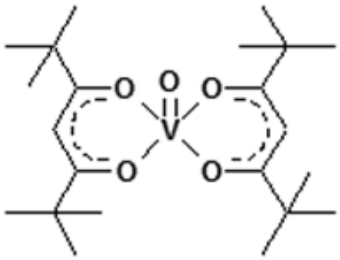

$VO(tmh)_2$ (**11**)

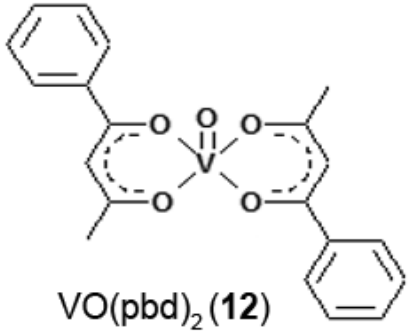

$VO(pbd)_2$ (**12**)

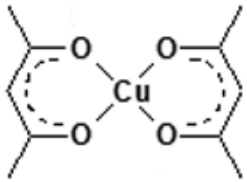

$Cu(acac)_2$ (**15**)

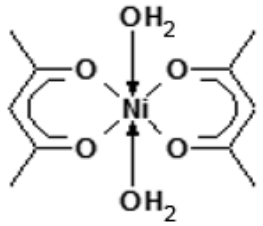

$Ni(acac)_2$ (**16**)

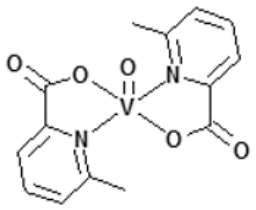

VO(MPA)$_2$ (**17**)

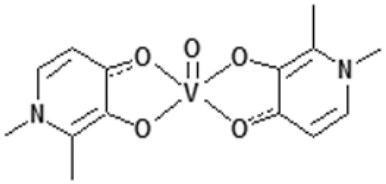

VO(dmpp)$_2$ (**18**)

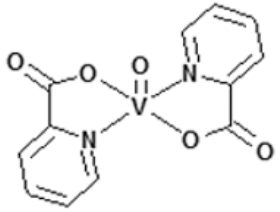

VO(PA)$_2$ (**19**)

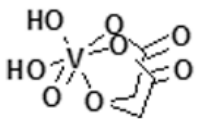

VO(oda) (**20**)

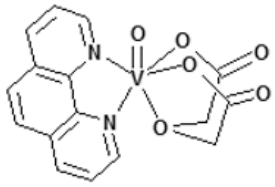

VO(oda)phen (**21**)

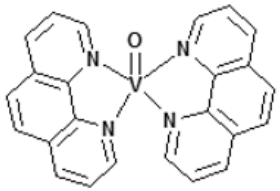

VO(phen)$_2$ (**22**)

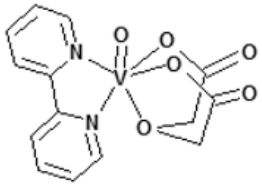

VO(oda)(bipy) **(23)**

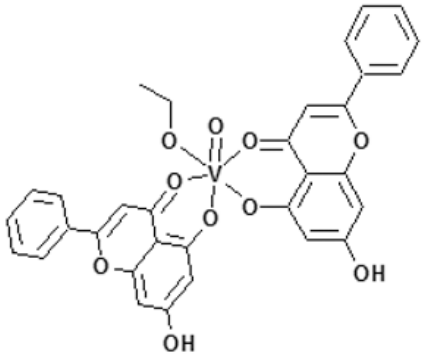

VO(chrysin)$_2$ (**24**)

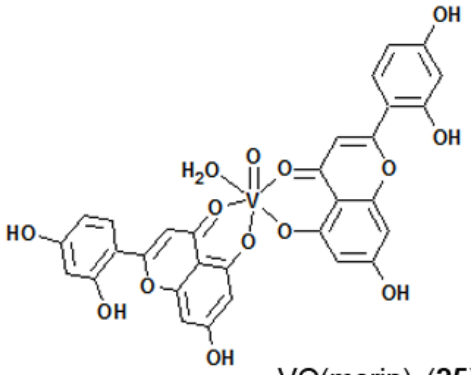

VO(morin)$_2$ (**25**)

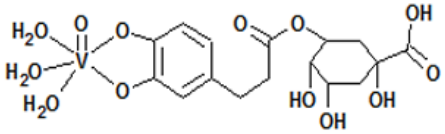

VO(Clor) (**26**)

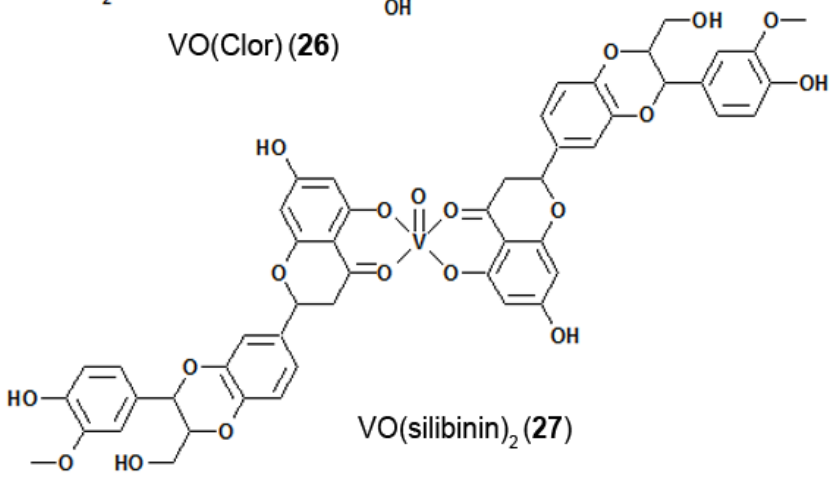

VO(silibinin)$_2$ (**27**)

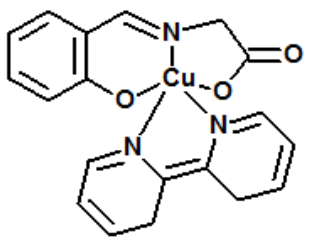

Cu(Sal-Gly)(bipy) (**28**)

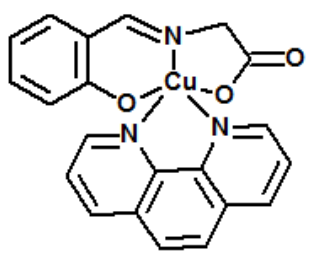

Cu(Sal-Gly)(phen) (**29**)

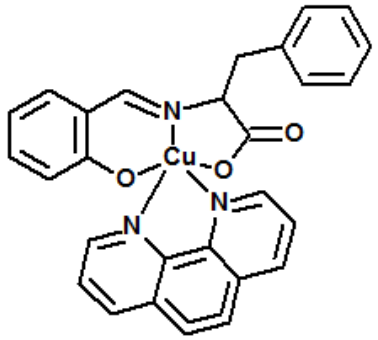

Cu(Sal-L-Phe)(phen) (**30**)

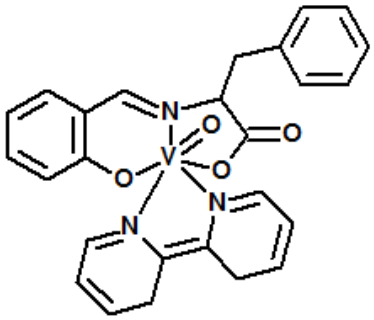

VO(Sal-L-Phe)(bipy) (**31**)

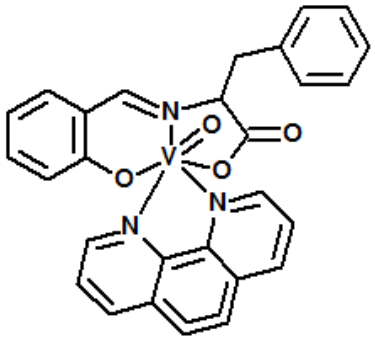

VO(Sal-L-Phe)(phen) (32)

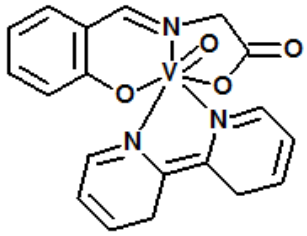

VO(Sal-Gly)(bipy)$_2$ (**33**)

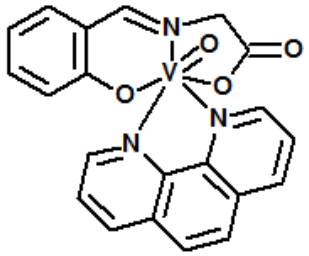

VO(Sal-Gly)(phen) (**34**)

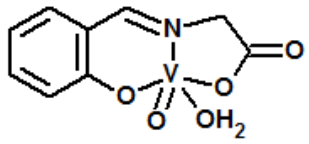

VO(Sal-Gly)(H_2O) (**35**)

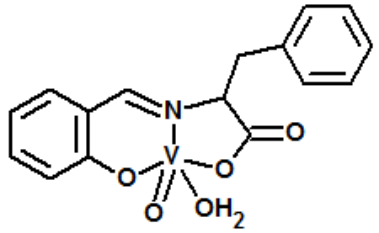

VO(Sal-L-Phe)(H_2O) (**36**)

I.2 General concerns on vanadium chemistry

I.2.1 Chemical and physical properties

Vanadium is a transition metal, member of the first transition series of group 5 (VB), d-block of the periodic table. The atomic number and mass are 23 and 50.9415, respectively, and symbol is V. The ground state electron configuration is [Ar] $3d_3$ $4s_2$, and the main oxidation states are +2, +3, +4 and +5. Oxovandium(V) is diamagnetic d_0, metal can be present in tetrahedral (VO_4), pentahedral (VO_5) and octahedral (VO_6) coordination environment and tends to form polyoxoanions [7]. Oxidovanadium(IV) (d_1, paramagnetic) is also stable and mostly present in square pyramidal or pseudo-octahedral coordination as an isolated cation. Other oxidation states such as oxidovanadium(III) (d_2, paramagnetic) and oxidovanadium(II) (d_3) are less stable and only present under reducing conditions [8,9].

I.2.2 History, isolation and application

Discovered in Mexican lead ore in 1801 by Spanish-Mexican mineralogist A. M. del Rio, vanadium was initially named panchromium, meaning "all colours". The element was re-named later to erythronium (*erytho-* means "red") as most of its alkaline salts became red upon heating (forming V_2O_5) or treating with acids (decavanadates, namely $[H_4V_4O_{28}]^{4-}$). Del Rio's claim of the new element was rejected in 1805 by French chemist H.V. Collet-Descotils, who erroneously concluded that "the new element" was nothing but impure chromium. The element was re-discovered nearly 30 years later (1830) by Swedish chemist N. G. Sefström, who named it vanadium in honour of the goddess of beauty and fertility, Vanadis (old Norse name for Freya in Scandinavian mythology) [9]. Until 1869, when English chemist H.E. Roscoe obtained for the first time pure (metallic) vanadium by reduction of VCl_2 with hydrogen, it was used in the form of V_2O_5. The first major synthesis of pure vanadium (99.9%) was carried out in 1927 by the Westinghouse Lamp Co by heating a mixture of oxidovanadium(III), Ca and $CaCl_2$ at 760 ºC.

Most of the pure vanadium metal produced these days is obtained by reduction of V_2O_5 with calcium in a pressure vessel using iodide process (thermolysis of VI_3, van Arkel-de Boer process) [9]. The metal is relatively inert toward oxygen, nitrogen, and hydrogen at room temperature. However, when heated in air at different temperatures, it oxidizes to a brownish black trioxide, a blue black tetraoxide, or a reddish orange pentoxide. It reacts with chlorine at fairly low temperatures (180 ºC) forming vanadium tetrachloride; with carbon and nitrogen at high temperatures forming respectively VC and VN. The most common commercially available vanadium compounds are V_2O_5, $VOSO_4$, $NaVO_3$, Na_3VO_4, NH_4VO_3.

Industrially, almost 80% of the annual world production of vanadium (~38 000 tons) is used in ferrovanadium alloy (reduction of the crude vanadium and iron oxides with coal, ~1:1) for fabrication of particularly strong and durable steels as it makes steel shock-, rust- and vibration-resistant. For this reason vanadium is considered a strategic metal, since a part of the steel production goes into the weapon manufactory. Vanadium alloys are used in aerospace industry also, e.g. titanium–aluminium–vanadium alloys for aero-engine gas turbines and undercarriages of planes. Vanadium finds use in nuclear applications because of its low fission neutron cross section; as well as in ceramics, electronics, dyes for textiles and leather [7], vanadium redox batteries [10].

Certain vanadium compounds have a specific use in industry. Vanadium sulphate and vanadium tetrachloride, for example, are used as mordants in the dyeing industry. Vanadium silicates are used as catalysts. Vanadium dioxide and vanadium trioxide are employed in metallurgy. However, the most significant compounds in terms of industrial health hazards are vanadium pentoxide and ammonium metavanadate [11].

I.2.3 Occurrence

Vanadium is a trace element, the most abundant in marine environment (after molybdenum), where it exists as monomeric vanadate, vanadate oxoanion, and most commonly, in the form of ion pairs $Na^+H_2VO_4^-$ at the average concentration of ca. 0.03 µM. Its amount in the fresh waters is significantly higher than in the ocean [12]. The

cosmic abundance (0.0001%) is similar to that of zinc and copper. In the earth's crust, it is the 18th most abundant element (0.0019% w/w) [13], similar to zinc and nickel (~0.008%). Vanadium is found in about 152 minerals, among which the important sources are vanadinite, carnotite, roscoelite and patronite. In most minerals vanadium is present at II, IV and V oxidation states in the form of oxide and seldom in as metal cation. Shales are especially rich in vanadium, contain 0.012% w/w [9]. Vanadium is also present in phosphate rock, certain iron ores, some crude oils in the form of organic complexes, e.g. V–porphyrin complexes [14]. The major sources of vanadium are titaniferrous magnetite ores from mines in Australia, China, Russia and South Africa (98% world's production) [7,15].

I.2.4 Aqueous oxidovanadium chemistry

Water is a constituent essential for the processes of life, participates in all essential reaction in biological system, act as a solvent, reaction medium and reactant. When studying physiological action of transition metals, solution chemistry recognition is of high importance. Understanding the behaviour of metal compound in aqueous environment allows predicting possible redox reactions and forming species in order to assure a successful implementation *in vivo.*

The aqueous oxidovanadium chemistry is very complex. With a variety of oxidation states, +2 (V^{II}), +3 (V^{III}), +4 (V^{IV}) and +5 (V^{V}), the metal can undergo hydrolytic, acid-base, condensation and redox reactions. These reactions are highly affected by the pH of a solution (Figure I.1), and the presence of potential ligands, which upon coordination with vanadium, can form stable complexes with different coordination geometries [12].

Depending on the oxidation state, vanadium acidic solutions have different colouring: V^{2+} (violet), V^{3+} (green), $V^{IV}O^{2+}$ (blue) and $V^{V}O_4^{2-}$ (yellow). Except the last one, all ions exist in the form of cations. Vanadium(II) compounds are reducing agents, whereas those of vanadium(V) are oxidizing. Vanadium(IV) compounds often exist as oxidovanadium derivatives which contain the VO^{2+} center. Biological relevance is found

for all four oxidation states, i.e., II/III/IV (nitrogenases), III/IV (ascidians), IV (amavadin), IV/V (bacterial respiration), V (haloperoxidases) [9,13].

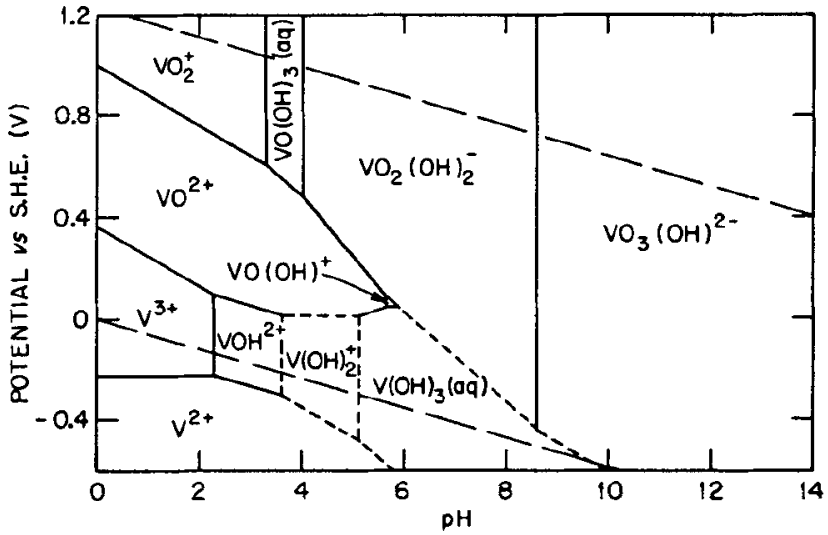

Figure I.1. The Pourbaix diagram of vanadium, expressing the vanadium speciation as a function of pH and potential at 25°ºC and an ionic strength of 1 M [16].

Due to the rapid oxidation of vanadium(II) and (III) in aqua media, unless prevented by complexation with sufficiently reducing ligands, the studies of aqueous vanadium chemistry are mainly focused on vanadium(IV) and (V). Much is known about the redox properties and reactions of both vanadium(IV) and (V) in organic solvents, however, little knowledge is obtained in aqueous system [12,17]. The chemistry of these two oxidation states, in the forms of oxidovanadium(IV) and (V) ($V^{IV}OSO_4$, vanadate(V), peroxidovanadates(V)), is particularly relevant since these compounds are typically employed in classical treatment of diabetic animals and seldom in humans [13,18]. However, biological studies with vanadium are complicated by the aqueous chemistry of vanadium(IV) and (V), and the facility with which these oxidation states convert in aqua media.

In the physiological pH range, vanadate(V) is readily dissolved in water and is more stable as free vanadate, (~90% $[H_2VO_4]^-$ + 10% $[HVO_4]^{2-}$ hereinafter referred to as V_i,

monomeric vanadate ion). V_i readily undergoes condensation reactions with many nucleophilic ligands, including other vanadium derivatives. In solution containing millimolar and higher vanadate concentrations, at pH 3 to 6 the major condensed species is $V_{10}O_{28}^{6-}$/ $HV_{10}O_{28}^{5-}$ (V_{10} decavanadate), which forms yellow-orange solutions. At pH 6 to 10, the major oligomers include a dimer $H_2V_2O_7^{2-}$/$HV_2O_7^{3-}$ (V_2, divanadate), cyclic tetramer $V_4O_{10}^{4-}$ (V_4, tetravanadate) and cyclic pentamer $V_5O_{12}^{5-}$ (V_5, pentavanadate) which are colourless. At neutral pH all vanadium(V) species present in water are anionic, below pH 3 and above pH 10 respectively, the cationic and anionic monomers are the major species. The cationic VO^{3+} and VO_2^+ exist only when stabilised by ligands which prevent precipitation of hydroxides. Due to a hydrolytic resistance of V_{10}, usually heating is necessary to convert it to colourless oligomeric species. Oxidovanadium(IV) is rapidly oxidized by molecular oxygen [19] or precipitated in the form of insoluble hydroxides In the latter case, the concentration of VO^{2+} is between micromolar and nanomolar range regardless of the amount of oxidovanadium(IV) compound dissolved in solution [9,12,13].

In *vivo,* under aerobic conditions, V^V is stable whereas, in anoxic environments (e.g., in cytoplasm), reducing agents such as ascorbate, glutathione and NADH readily reduce $V^VO_2^+$ to $V^{IV}O^{2+}$. In the form of V_i, V^V is less likely to be reduced. The reduction of $V^{IV}O^{2+}$ to V^{3+} does not occur under common conditions. These redox reactions are well described by Rehder [9] and are based on the redox potentials of these inorganic vanadium species at pH 7 (
Table I.1).

Solution chemistry of vanadium compounds has been explored by electronic and vibrational spectroscopies. Diamagnetic oxidovanadium(V) is often studied by nuclear magnetic resonance (NMR) spectroscopy whereas, oxidovanadium(IV) is examined by electron absorption (UV-Vis) and electron paramagnetic resonance (EPR) spectroscopy, and less commonly, electron spin echo envelope modulation (ESEEM) and hyperfine sublevel correlation (HYSCORE) spectroscopies [12].

The speciation in the aqueous vanadophosphate [20] and peroxovanadate system [21], vanadate-ligand and peroxovanadate-ligand system [22], $H^+/H_2VO_4^-/H_2O_2$/citrate [23] and $H^+/H_2VO_4^-/H_2O_2$/phosphate system [24,25] has been thoroughly studied by Petterssons' group, employing a combination of proton potentiometry and ^{51}V NMR spectroscopy. T. Kiss [26-28] and D. Crans [19,29-31] studies vanadium(IV/V) speciation of complexes with variety of ligands mostly by H^+ potentiometry, UV-Vis and EPR spectroscopy. J. Costa Pessoa and T. Kiss explored the speciation of vanadium in human serum [32,33]. Many other studies have been conducted regarding the redox reactions of vanadium complexes in aqueous media [34-36] using and aforementioned techniques.

Table I.1. Redox potentials for inorganic vanadium species.E (V) vs. normal hydrogen electron (NHE) [9].

Species	E^0	$E^{pH=7}$
VO^{2+}/V^{3+} (V^{IV}/V^{III})	+0.359	-0.462
$[H_2VO_4]^-/VO^{2+}$ (V^V/V^{IV})	+1.31	-0.34
NAD^+/NADH		-0.315
Pyruvate/Lactate		-0.185
1/2(GS)2GSH		-0.10
Dehydroascorbate/ascorbate		+0.06
VO_2^+/VO^{2+}(V^V/V^{IV})	+1.016	+0.19
O_2/H_2O_2	+0.695	+0.295
$^1O_2/H_2O$	+1.23	+0.815

Many aspects of aqueous vanadium chemistry remain unclear, as a consequence, the lack of proper interpretation of the results in *vivo* studies. Rapid conversion between the vanadium(IV) and (V) oxidation states makes it difficult to even specify the oxidation state of the active vanadium species.

I.3 Vanadium in biology

Table I.2 lists most important dates in the history of vanadium's biological chemistry [16,37-41].

Table I.2. Milestones in the history of development of vanadium biology and chemistry.

1830	Discovery of vanadium (N. Sefström).
1899	First report of vanadium salts as probes of metallotherapeutics (B. Lyonnet and co-workers).
1911	First report of high levels of vanadium in tunicates (Ascidiacea *Phallusia mamillata*) (M. Henze).
1933-36	Discovery of the role of vanadium in nitrogen fixation (H. Bortels).
1972	Isolation of amavadin from the fly agaric (E. Bayer).
1977	Discovery of the role of vanadate as an efficient inhibitor of Na^+, K^+-ATPases (L. J. Cantley).
1980-	Development of vanadium compounds for the treatment of diabetes mellitus.
1983	Isolation of the first vanadium enzyme, vanadate-dependent bromoperoxidase, in the marine alga *Ascophyllum nodosum* (H. Vilter). Discovery of the affinity of vanadium for transport proteins (Chasteen and co-workers).
1986	Isolation of a vanadium nitrogenase from *Azotobacter ninelandii* (Sussex Nitrogen Fixation Group).
1993	Discovery of high levels of vanadium in fan worms *Pseudopotamilla occelata* (T. Ishii and co-workers).
1997-	Discovery and development of vanadium-binding proteins (vanabins) in *Ascidia sydneiensis samea* (Michibata and co-workers).
1998	First report on isolation of vanadium-containing (molybdenum-free nitrate reductase) enzyme from *Pseudomonas isachenkovii* and *Thioalkalivibrio nitratireducens* (Antipov and co-workers).
2003	Phase I of clinical trials of a designed vanadium-based pharmaceutical agent (bis(ethylmaltolato)oxidovanadium(IV), BEOV) (C. Orvig and K. Thompson).
2010	Discovery of the ability of vanadium nitrogenase from Azotobacter vinelandii to catalyze the reduction of CO (W. Ribbe and co-workers).

I.3.1 Vanadium in biological systems

Vanadium's essentiality was determined in the 1970s through studies in rats [83]. The beneficial and essential role in humans is still uncertain and yet to be discovered. To animals and humans vanadium is mostly supplied via food and drinking water and is chiefly accumulated in bones, kidneys and liver. The concentration level in blood and tissue, respectively, is ca. 0.2 and 6 µM, respectively. Vanadium can enter the food chain via soil and water, where it is transferred to plants (beans, beets, barley, and wheat etc.) accumulated in roots and seeds. Most food has naturally occurring low concentrations of vanadium (average ca. 30 µg/kg) [13]. Common sources of vanadium in food are dill seeds, black pepper, garlic, parsley, cereals, seafood, meat, fish, mushrooms, olives, grains, vegetable oils, and fats [42]. Since vanadium is the second most abundant element in marine environment, seafood is richer in vanadium than meat from land animals.

I.3.2 Absorption

Vanadium's absorption rate is still unclear. When administered orally, the absorption in the gastrointestinal tract is minimal (i.e., ~2% in humans and 40% in some animals). As vanadium is poorly absorbed, ingested vanadium compounds mainly in the form of VO^{2+} hydroxides are eliminated with faeces. When applied intravenously, vanadium is rapidly distributed in body via blood circulation. The accumulation begins in kidneys, liver and spleen, excreted with urine probably in the form of V^{IV} bound to iron-containing complexes such as albumin, transferrin or ferritin [33,43]. Bones and muscles retain with vanadium the longest. A biological half-life of vanadium is 20-100 h [44].

I.3.3 Vanadium in living organisms and life processes

Vanadium has been proven to be a necessary part of the diet of rats and chickens, but only in very small amounts. Deficiencies of vanadium causes reduced growth and impair reproduction. Vanadyl sulfate and sodium metavanadate have been used in dietary supplements for athletes and body builders [31,45].

Vanadium is certainly essential for some living organisms, which either accumulate (ascidians, fly agaric and fan worms) or employ vanadium in life processes (bacterial respiration, vanadium-dependent haloperoxidases, nitrogenases and nitrate reductases).

Ascidians[1]*,* known as marine tunicates or sea squirts, contain high levels of vanadium. They accumulate vanadium from sea water, where it is present at the average concentration of 0.03 μM, but may vary increasing up to 10^7.

In 1911, Henze discovered extraordinary levels of vanadium in the blood cells (coelomic cell, named vanadocytes) of *Phallusia mamillata*. Since then much interest has been developed towards the redox mechanism and possible physiological roles of vanadium in tunicates. It is worth mentioning, that in the early findings there was an assumption on the respiratory importance of vanadium and vanadium compound(s) present in vanadocytes of ascidians in terms of oxygen transport. These compound(s) were called 'haemovanadin', however such function was refuted because no parallelism to iron-based haemoglobins and the copper-based haemocyanins exist [9].

Vanadate is assumed to enter the organism of these marine creatures via phosphate and sulphate channels. It is then reduced, presumably by tunichromes[2] (blood pigments) to VO^{2+} and V^{3+} [46]. Depending on the species of tunicates, vanadium(III) is accumulated in the form of aqua-sulfato complexes ($V(H_2O)_4(OH)(HSO_4)^+$) in tunic, mantle, branchial, serum and mainly in vanadocytes at concentrations up to 0.3 M (350 mM V(III), 500 mM SO_4^{2-} at pH 1.9). The lower the pH is, the more vanadium appears to be accumulated [9]. Michibata's group has extensively studied ascidians [47,48]. One of their most significant contributions is development of vanadium-binding protein, vanabins. They suggested that the accumulated metal ions may be a source of oxidizing energy for redox reactions in vanadocytes or in other tissues. Recent studies

[1] Ascidians are marine animals, knows as filter feeders. They are sessile animals (remain firmly attached to substratum such as rocks and shells) that found all over the world, usually in shallow water with salinity over 2.5%. Tunicates are phylogenically classified into the phylum Chordata between Invertebrata and Vertebrata, while the adult individuals do not contain a vertebral column, the juvenile larvae show features in common with vertebrates [9,48]. These animals feature a tunic. The main constituents of this tough outer mantle are a mucopolysaccharide–protein substance, contain blood cells and tunicin fibres which contain cellulose.

[2] Tunichromes are small tri- or dipeptides**,** referred to a class of DOPA (3,4-dihydroxyphenylalanine) and hydroxyl-Dopa-containing peptides. The theory about tunichromes being associated with vanadocytes, was turned down [9].

of vanadium-rich species have shown that vanadium accumulation in ascidians is associated with enhanced capacity of metabolize glucose-6-phosphate via pentose phosphate pathway [49].

Amanita muscaria[3]*,* A. *regalis* and A. *velatipes* are three species of the genus *Amanita* (poisonous mushrooms), that were found to accumulate amavadin, a vanadium-containing anion. This anion is an octa-coordinated V^{IV} non-oxo complex, which bonded with two tetradentate ligands derived from N-hydroxyimino-2,2'-dipropionic acid. This complex was discovered in 1931 but isolated and identified only in 1972 by Kneifel and Bayer. Although, muscarin, the poisonous part of this mushroom, is not in any known relationship with amavadin, the latter may serve as a toxin for protection of the mushroom [50]. The concentration of vanadium in *A. muscaria* was found to be approximately 400 times higher than that in plants. The element is not evenly distributed since the bulb accumulates the most, up to 1000 mg/kg dry weight, and the lamellae up to 400 mg/kg, whereas spores contained only 1-2% of the lamellar vanadium. Interestingly, the amount of vanadium in these mushrooms is independent of the vanadium content in soil [9].

The biological function of amavadin is still unknown. Its reversible one-electron redox properties have been related to the possible role in biology as a one-electron redox mediator. Studies have shown that amavadin can catalyze thiol oxidation in the absence of H_2O_2 [51] and in the presence of hydrogen peroxide, it can perform halogenation, hydroxylation, and oxygenation of alkyl and aromatic substrates [52]. Fraústo Silva et al. have found that amavadin electro-catalyze the oxidation of some thiols to the corresponding disulfides [53] and that amavadin could convert methane into acetic acid in the presence of peroxodisulfate salt and trifluoroacetic acid [54]. Hubregtse et al. suggested that amavadin may acts as peroxidase via the reaction with H_2O_2 for the regeneration of damaged tissues [55].

[3] *A. muscaria* is commonly known as fly agaric or toadstool

Fan worms[4] are the second marine organisms which in 1993 were reported to contain high levels of vanadium [37]. Vanadium content is 320-1350 µg/g dry weight of the whole body. About 90% of the overall vanadium is found in the branchial crown as ($V(H_2O)_5(HSO_4)^{2-}$). This speciation is similar to that of vanadocytes in ascidians [9].

To date, the role of vanadium in ascidians, fan worms and amanita remains unclear.

Vanadate-dependent haloperoxidases (VHPO) form a group of enzymes that have been isolated from seaweeds, fungi and lichen. These enzymes catalyse the oxidation of a halide (X^-) by hydrogen peroxide to corresponding hypohalous acid (HOX) according to the following scheme [31]:

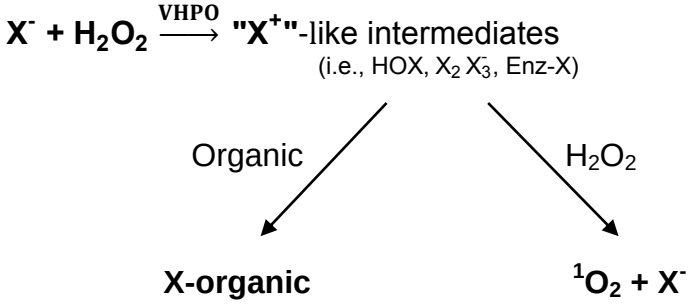

VHPOs is the first specific vanadate-dependent enzyme. In 1983, Vilter isolated the first representative of the large family of VHPO, vanadium bromoperoxidase (VBrPO) from brown alga *Ascophyllum nodosum* (knobbed wrack), where it is widely distributed. VHPOs are also found in red (such as *Corallina pilulifera* and *Cor. officinalis*), and green alga (*Halimeda* sp.), the fungi (*Curvularia inaequalis* and *Botrytis cinerea)* and in the terrestrial lichen *Xanthoria parietina* [9]. With the discovery VHPOs, there are now three distinguished classes of peroxidases: non-metallo haloperoxidases, Fe-Haeme haloperoxidases and vanadate-dependent haloperoxidases.

[4] *Pseudopotamilla occelata* is a class Polychetes (bristle worms), belong to phylum Annelida

In all of the VHPOs the active centre is hydrogen vanadate ($H_2VO_4^-$) which does not change its redox state during catalysis. The metal most probably functions as Lewis acid coordinating and activating the substrates in such a way that catalysis occurs.

VHPOs are divided into two related groups which are alga bromo/iodo peroxidases and fungal chloroperoxidases. The enzymes are termed iodo-, bromo- or chloroperoxidases. Iodoperoxidases (VIPO) can oxidise only iodide, bromoperoxidases (VBrPO) iodide and bromide, while chloroperoxidases (VClPO) are able to oxidise all three halides VHPOs are very chemo- and thermostable enzymes, remains active at high temperatures (~70 ºC). Unlike haeme haloperoxidades, VHPOs are resistant to excess of H_2O_2, organic solvents and hypohalous acid. These properties facilitate their isolation and characterization. Depending on the source, about 100 mg of fully active enzyme can be recovered from 10 kg of finely chopped and freeze-dried algal material [9].

The physiological role of VBrPO is assumed to be in the biosynthesis of the halogenated marine natural products. These products range from relatively simple volatile halomethanes (e.g., $CHBr_3$, CH_2Br_2, $CHBr_2Cl$) to more complex compounds, such as halogenated indoles and terpenes. Halomethanes contribute to the ozone degradation and thus, to the global ozone balance. The production of $CHBr_3$ by marine algae is ca. 10^4 tons per year [56].

Vanadium nitrogenase (VNase) is vanadium-containing bacterial enzyme that promote nitrogen fixation. VNases are found in free-living nitrogen-fixing bacteria of the genus *Azotobacter* (*chroococcum*, *vinelandii* and *amylobacter*). Biogenic reductive nitrogen fixation occurs when atmospheric nitrogen (N_2) is converted to ammonia (NH_3) by nitrogenases, making nitrogen available for assimilation by plants. The nitrogenases are responsible for cycling about 10^8 tons of nitrogen per year from the atmosphere to the soil [57].

For many years molybdenum was considered essential for N_2 fixation and the majority of nitrogenases that have been widely studied contain a molybdenum nitrogenase (MoNase) system. In 1930, Bortels in his research of an alternative substitute for Mo,

determined that vanadium compounds almost match molybdenum, showing the positive effect on N_2 fixation by *Azotobacter* [9]. In 1986, Robson and coworkers (Sussex Nitrogen Fixation Group) [58] purified a vanadium-containing nitrogenase from *A. vinelandii*[5]. Since then, VNases are mostly isolated from *A. vinelandii* and *A. chroococcum*.

VNases are considered to be less efficient than MoNase because the reduction equivalents used for N_2 reduction are 50%, whereas for Mo they are 75%. Generally, VNases are less stable, which creates a problematic crystallization (the structural information from X-ray diffraction data is not available to date), also it produces some hydrazine, whereas no such is observed with MoNases [59]. VNases are expressed in case of MoNases deficiency and low temperatures.[6]

The main constituents of MoNase/VNase are two metalloproteins, Fe-protein and MoFe-protein/VFe-protein, encoded by structural genes (i.e., *nif*- and *vnf*-encoded for Mo and V, respectively). Both nitrogenases utilize a catalytic mechanism that involves ATP-dependent electron transfer from a reductant (i.e., *nif*H- or *vnf*H-encoded Fe-protein) to the catalytic component (i.e., *nif*DK-encoded MoFe-protein or *vnf*DGK-encoded VFe-protein) followed by the reduction of N_2 at the cofactor site (i.e., FeMoco or FeVco) of the catalytic component. Although, VFe-protein and MoFe-protein are biochemically similar, the expression of VNases does not simply occur by substituting Mo with V in MoFe-protein. It is because they possess different substructures, $\alpha_2\beta_2$ in MoFe-protein and $\alpha_2\beta_2\delta_2$ in VFe-protein. The α subunits in VNases contain the so-called ***M*** cluster (termed FeVco for iron–vanadium– cofactor), with the composition of seven iron ions, nine bridging sulfide ions ($VFe_7[\mu_6\text{-}C]S_9$) [60] and the active centre - vanadium, which is bound to a histidine and the vicinal hydroxide and carboxylate of homocitrate [13]. This ***M*** cluster is responsible for the reductive protonation of N_2 to NH_4 (1).

$$N_2 + 12e^- + 14H^+ + 40\ (\text{or } 24)\ MgATP \rightarrow 2NH_3^+ + 3H_2 + 40\ (\text{or } 24)\ MgADP + 40\ (\text{or } 24)P_i \quad (1)$$

[5] *Azotobacter vinelandii*, member of the family *Azotobacteriaceae,* contains three genetically distinct nitrogenase system, i.e., a Mo-containing nitrogenase, a V-containing nitrogenase and an Fe-only nitrogenase, encoded by nitrogen fixation genes. These genes have shown to play roles in the biosynthesis of the Mo- and the V-protein.
[6] Low temperatures create more effective system for the reductive protonation of nitrogen to the ammonium ion.

Recently, Ribbe and co-workers [61] discovered that in a total atmosphere of CO, with no nitrogen present, VNases are able to reduce CO (2) with the production of (C_2H_4), (C_2H_6) and (C_3H_8). The fact that the reduction of both N_2 and CO are industrially important processes makes VNases commercially applicable in the future.

$$2CO+4H^{+}+4e^{-}\rightarrow C_2H_4+ 2H_2O\ [+H_2] \quad (2)$$

In the end of the 1990s, Antipov et al. [39] reported the isolation of molybdenum-free nitrate reductase from two bacteria, *Pseudomonas isachenkovii*, which contains vanadium, and *Thioalkalivibrio nitratireducens* which is consistent of vanadium and iron (ratio 1:3). The nitrate reductase activity was found to depend on vanadium content in *P. isachenkovii*. The enzyme purified form *T. nitratireducens* in addition to nitrate reduction, reduces nitrite, bromate and selenate. The existence of vanadium-dependent nitrate reductase is yet to be confirmed.

Another biological function of vanadate is to be a primary substrate for electron delivery in bacteria such as *Pseudomonas vanadium-reductans*, *P. isachenkovii* and *Shewanella oneidensis*. Unlike higher animals and plants, which use oxygen for the respiration, bacteria and archaea employs high-valent ions such as Fe^{3+}, Mg^{3+} and oxometal ions such as arsenate(V), selenate(VI), molybdate(VI) and vanadate(V). Most metals in aqueous, non-acidic, oxygenated environments such as soil and sea, exist in the form of insoluble oxides and hydroxides and thus cannot be utilized by microorganisms. Since iron is the most essential in respiration of microbes, they scavenge Fe^{3+} by releasing high-affinity iron compounds (siderophores, i.e., “iron carriers”). Siderophores form chelators with Fe^{3+} in iron-containing minerals, which results into formation of soluble iron complexes. The solubility thus makes the metal more bioavailable for further uptakes. Siderophores that chelate vanadium (“vanadium carriers”) were named **vanadophores**. More information on vanadium-siderophore complexes can be found in [9,31].

I.3.4 Biochemical action

The biochemical role of vanadium has been reviewed many times [31,44,45,62,63]. Vanadium is likely to be essential considering its various biological functions. Starting from 1977, the discovery of the inhibition effect on Na,K adenosine triphosphatases (ATPase), vanadium was generally accepted as a bio-metal. The interest in vanadium metallobiochemistry is mostly due to structural and chemical similarities of vanadate and phosphate, especially in the tetrahedral trianionic forms (VO_4^{3-} and PO_4^{3-}). One difference is that at neutral pH, the V_1 exists primarily as a monoanion ($[H_2VO_4]^-$), whereas phosphate is present in its dianion form ($[HPO_4]^{2-}$). Another one is that unlike H_3VO_4 which undergoes redox chemistry under physiological conditions, H_3PO_4 is highly stable.

Being an active competitor of the phosphate, vanadate (four-coordinated) seems to be involved in variety of regulations of phosphate-dependent processes. Vanadate mimics cellular metabolites because its esters and anhydrites were established as functional analogues of those of phosphate. The examples of vanadium-cofactor analogous of adenine monophosphate (AMP) [64] and nicotinamide adenine dinucleotide phosphate (NADP) such as AMV, ADPV, and NADV [65,66] have been reported. NADV is considered to be more potent than NADP since it forms the cyclic derivative for which the active enzyme has greater affinity. Both oxidovanadium(V) anion and oxidovanadium(IV) cation inhibit phosphorylases such as alkaline, acid and protein phosphatases, ribonuclease [67,68] and ATPases.

One of the prominent functions of vanadium compounds is the insulin-mimetic effect on cells, diabetic animals, and humans. Administration of pharmacological doses of vanadium to experimentally diabetic animals mimics the effect of insulin and growth factor. As a results, glucose tolerance increases, other diabetes symptoms decline; DNA synthesis, osteoblast proliferation and collagen formation are induced in bones, and along with the rise of vanadium in bone, osteogenesis and bone repair are promoted [9].

I.3.5 Toxicity and hazard

While no nutritional requirement of vanadium has been established in humans, exposures to high level concentrations of any form of the metal are known to be toxic. Toxicity can occur via oral administration, intravenous application and inhalation. A dose of an immediate danger of vanadium for an average human is 10 mg/kg orally, 7 mg intravenously and 35 mg/m^3 of inhaled substance. The oral intake is less hazardous due to poor absorption of vanadium in the gastrointestinal tract. The main side effects are green tongue coloration, weakness, gastrointestinal problems, failure to gain weight.

Vanadium compounds are encountered relatively rarely by most people. The amount of vanadium found in food is out of the hazardous range. In the laboratory, unless known otherwise, all vanadium compounds should be regarded as highly toxic. Vanadium metal powder is a fire hazard. In some industrial smoke pollution vanadium compounds may cause lung cancer. Industrial regulations exist to keep exposure to V_2O_5 dust under control. No studies were located regarding the carcinogenicity in humans after inhalation exposure to vanadium [9,16].

I.4 Medicinal interest

Metal coordination compounds as therapeutics for different medical applications are currently one of the most demanding subjects in the biochemical research. More and more metal complexes are recognized as effective drugs in diseases such as cancer, diabetes, HIV, and malaria. Diabetes *mellitus* (DM)[7] and cancer are among the most spread diseases. Metallotherapeutic interest in vanadium rose as early as 1899, when Lyonnet and his colleagues first tried sodium metavanadate as a drug in oral uptakes, observing the lowering of glucose level in urine of two out of three diabetic individuals. However, these studies were left undeveloped due to parallel exploration of constituents of pancreas with eventual discovery of insulin (1921-1922). Rapid and successful implementation of insulin in the treatment of diabetes eclipsed the research of vanadium compounds for the same purpose. This discovery was assigned as miraculous, since people with severe diabetes and only days left to live were saved. With daily insulin injections into the subcutaneous tissue (in case of Type 1 diabetes) they could live an almost normal life. However, the daily injections are painful both physically and mentally. To eliminate such undesirable defects, creation and development of new therapeutic compounds to replace insulin injections (insulin is a peptide hormone, oral application is impossible) and synthetic therapeutics are being explored to improve the lives of diabetic patients. The extensive studies of different metals, especially those which are essential for humans, such as iron, copper, zinc, selenium, and their relationship with numerous diseases, resulted in the development of numerous metallopharmaceuticals such as the platinum-containing anticancer drug, cis-platin, and the gold-containing rheumatoid arthritis drug, auranofin. That time vanadium was mostly explored for its biological effects and functions. After the discovery of high levels of vanadium in tunicates in 1911 and its participation in nitrogen fixation (1936), vanadium was recognized as a metal with ubiquitous nature. This led to a massive research for the significance of vanadium in biological systems and raised question marks around its

[7] There are two principal forms of DM: Type I and II DM. **Type I**, also called insulin-dependent DM (IDDM), results from the pancreas failure to produce insulin (e.g., inherited or virus-induced auto-immune reaction or damage of the pancreas); most frequently developed in children and adolescents and treated only by daily insulin injections (~10% of diabetics). **Type II** occurs due to the body's inability to properly respond to insulin still produced in the pancreas. The reason is in the occurring resistance of special receptors, which insulin needs to attack in order to lower the glucose. This type of DM most frequently occurs in elderly adults and treated by several types of synthetic therapeutic substances together with a controlled diet and physical exercise (~90% of diabetes cases).

pharmacological effects. First, it was studied as a potential cholesterol-lowering agent, gradually moving to abundant exploration of physiological, metabolic and enzymatic effects, stimulatory and inhibitory. The research continued with the studies of anti-diabetic and anti-cancer agents. Special attention and constant emphasis was paid to the solution chemistry in aqua media, precisely, the physiological interconversion of vanadium compounds between cationic (V^{IV}) and anionic (V^{V}) species.

This section will provide a brief introduction into the role of vanadium in medicine, namely the main findings for treatment of DM and cancer. Special acknowledge is given to the following research groups which contributed into the research of vanadium anti-diabetic, -cancer and –parasitic effect the most: Cantley; Chasteen; McNeill, Thompson and Orvig; Sakurai; Pessoa, Tomaz and Correia; Rehder, Crans, Willsky and Godzala; Kiss, Jakusch and Buglyó; Garribba and Micera; Brichard and Reul; Etcheverry, Williams and Baran; Gambino. These reviews can be consulted for further reading [13,16,31,45,63,69-77,116]. A series of articles about anti-cancer activity of variety metal compounds can be consulted in special issue [78].

I.4.1 Vanadium in diabetes treatment

The interest in the insulin-enhancing[8] effect of vanadium received its development only in the 1980s, i.e., two decades after the observation of Lyonnet, and has thoroughly been explored since. The most important studies are reflected in Table I.3.

[8] Initially, the effect was called both insulin-enhancing and –mimetic since vanadium compounds were believed to be able to mimic the effect of insulin. However, after some studies it became clear that vanadium will never be able to substitute insulin but rather works in synergistic way by augmenting the efficiency of insulin. Since then the term 'insulin-enhancing' was thoroughly used.

Table I.3. Development of vanadium and vanadium compounds as anti-diabetic agents, presented chronologically.

Year	Research	Ref.	Brief description
1897–98	Tests of aqueous solutions of sodium vanadate on humans in the L'Hôtel-Dieu hospital in Lyon	9	The first report on vanadium's possible benefits in the treatment of 44 subjects with various health problems, including anemia, tuberculosis, rheumatism, arnyotrophia, hysteria, neurasthenia and diabetes (three individuals).
1960s	Vanadium as potential cholesterol-lowering pharmaceutical agent	79	Despite of modest inhibitory effect on serum cholesterol, no negative side effects were observed even at high doses of "di-ammonium vanado-tartrate".
	Synthesis and characterization of numerous V^{IV} and V^{V} complexes, particularly $VO(acac)_2$	80	Spectral characterization of vanadium(IV) and (V) complexes became possible and the characteristic eight-line vanadyl EPR spectrum was described. The coordination chemistry of oxidovanadium(IV) was first summarized in 1965.
	Extensive studies on essentiality of vanadium		This launched an elaborate study of vanadium's metabolism, effect on growth, possible deficiency effect and served as a preamble to the studies of vanadium from a medicinal point of view.
1979-1980	First in *vitro* studies of the insulin-mimetic action of vanadate	81,82	V^{V} was found to be responsible for glucose oxidation via reduction to V^{IV} which in turn inhibits cellular phosphatase.
mid-1980s	Recognition of vanadium compounds as important metallo-pharmaceuticals		The potent pharmacological effects and physiological interconversion between cationic (V^{IV}) and anionic (V^{V}) species attracted a great interest which significantly advanced research in this field.
1980-1985	First reports on vanadium's insulin-like action in vivo	83	Pioneer experiments of Heyliger, McNeill and Meyerovitch's groups. Studies on animal models of diabetes, namely, alloxan[9]-diabetic and streptozotocin (STZ)[10]-diabetic rats. In these assays vanadate was dissolved in the drinking water of animals, where it is present at millimolar concentrations as a mixture of $\boldsymbol{H_2VO_4^-}$, $\boldsymbol{H_2V_2O_7^{2-}}$ and $\boldsymbol{V_4O_{12}^{4-}}$.Concentrations of vanadium in *vivo* tissue were found to be in the nanomolar to micromolar range.

Continued on the next page

[9] Alloxan is a toxic glucose analogue, which selectively destroys insulin-producing cells in the pancreas (that is beta cells) when administered to rodents and many other animal species. This causes an insulin-dependent diabetes mellitus (called "Alloxan Diabetes") in these animals, with characteristics similar to type I diabetes in humans

[10] Streptozotocin is an antibiotic that is produced by *Streptomyces achromogenes*; intravenously applied, it destroys the insulin-producing β-cells in the pancreas and thus induces type I diabetes. STZ rats are thus animal models of human type I diabetes.

Table 1.3. – *Continued*

1987	Peroxovanadate as potential anti diabetic drug	84,85	First noted in the form of a synergistic effect when incubating adipocytes (fat cells) with a combination of vanadate and hydrogen peroxide. Among the effects noted was the stimulation of the insulin receptor[11] tyrosine kinase/inhibition of phosphotyrosine phosphatase. Despite a particularly high efficacy, its in *vivo* applicability is questionable. Oral application peroxovanadates will hardly survive the passage through the gastrointestinal tract (GIT); in case of intact absorption, will readily be decomposed by catalase to form vanadate.
1988-1995	Numerous tests of V^{IV} salts as p Potent candidates for anti-diabetes	86-89	Vanadium salts, at doses ranging from 0.1–0.7 mM/kg/d, in a variety of animal models of diabetes, normalized blood glucose and lipid levels, altered thyroid hormone deficiency, improved insulin sensitivity, and prevented or reversed secondary complications, such as cardiomyopathy, cataract development, impaired antioxidant status and excessive food/ fluid intake.
1989	Insulin-like activity of $V^{IV}OSO_4$ in STZ rats	18,90, 91	$VOSO_4$ is advantageous over vanadate because it is sufficiently less toxic. Its drawback is a low rate of absorption in the gut, estimated to be 1% or less.
early 1990s	Development and testing of VC with organic ligands for anti-diabetic purposes		Due to potential toxicity of vanadate and the low absorption rate for the less toxic $VOSO_4$ these inorganic compounds were considered to be excluded from potential use as anti-diabetic drugs. As an alternative, vanadium coordination compounds containing organic ligands began to be tested. This allowed developing vanadium anti-diabetic drugs with desired properties which in turn would help to increase their bioavailability.
1990	$V^{IV}O(Cys\text{-}Me)_2$ as promising anti-diabetic agent	92	The efficacy of this complex was found to be equivalent to $VOSO_4$.
1992	$V^{IV}O(malto)_2$ as a glucose lowering agent	93-96	*Bis*(maltolato)oxidovanadium(IV), BMOV, was found to be more effective than $VOSO_4$ as a glucose lowering agent. BMOV was better tolerated than inorganic vanadium salts, and resulted in reliable glucose-lowering in all animal models of diabetes in which it was tested. Also, overall bioavailability of vanadium from BEOV was three times higher than from $VOSO_4$.

Continued on the next page

[11] Insulin receptors are receptors with high-affinity cell surface (trans-membrane) that are activated when the insulin is secreted. They belong to the large class of tyrosine kinase proteins. By targeting insulin receptors, insulin decreases glucose levels.

Table 1.3. – *Continued*

1995-2009	Insulin-mimetic V^{IV}-picolinate complexes	75, 97-102	After $V^{IV}O$(pic)2 exhibited *in vitro* insulin-mimetic activity in isolated rat adipocytes and in *vivo* hypoglycemic ability in STZ-rats, many analogues were prepared to mainly study relationship between the structure and anti-diabetic activities. Oxidovanadium(IV) complexes with picolinato ligands were found to be stable against oxidation in the blood and forming the ternary system (oxidovanadium(IV)–L_A–L_B–Tf, where L_A = picolinate or picolinate-containing ligand; L_B = low molecular mass serum constituents; Tf = transferrin). Only systems that contain phosphates or citrate along with picolinato ligand were proven to survive to a certain extent in the blood.
1995	Tests of vanadate and $V^{IV}OSO_4$ on humans for insulin-enhancing purposes	103, 104	The second report involving human subjects. The treatment of five type I and five type II diabetics with sodium (or ammonium) vanadate and $VOSO_4$ at the Joslin Diabetes Center in Boston, MA and at the Diabetes Research Center, Albert Einstein College of Medicine, NY. In all cases only a modest improvement in insulin sensitivity and glycemic control was observed at the dose of ~1 mM V/d and duration of 6 weeks
1995-present	Studies of the interaction of insulin-mimetic vanadium compounds with the high (ATP, GHS, HAS, Tf) and low (lactate, oxalate, phosphate, citrate) molecular mass serum components	26, 105-113	Vanadium(III,IV,V) undergoes parallel ligand exchange and redox reactions with bioligands when given orally. Serum constituents were considered to be potential transporters of $V^{IV}O^{2+}$ in blood. This field was widely researched and many interesting results were obtained. The main finding is that little of the vanadium remains bound to the original carrier because citrate and transferrin displace most of the carrier molecules; phosphate is able to partially replace of one the functionalities. V^{IV} ions were found to bind specifically into two iron biding sites of transferrin and to a histidine of the N-terminal end of albumin
1996, 1999, 2000, 2005	$VO(acac)_2$ and derivatives as efficient insulin-enhancing complexes	18, 114-117	$VO(acac)_2$ and $VO(Et\text{-}acac)_2$ were found to have long-term in *vivo* insulin mimetic effects in STZ-diabetic Wistar rats. The effectiveness of these compounds in reducing the final glucose levels in STZ-diabetic rats after 12 weeks was compared to the one of $VOSO_4$ and $VO(malto)_2$ and was found to be as follows: $VO(acac)_2$ > $VO(Et\text{-}acac)_2$ > $VO(malto)_2$ > VO^{2+}. Complex speciation in the aqueous speciation liquid was related to its effectiveness in plasma glucose lowering. The concentration of the 1:1 hydrolysis product (one ligand is substituted with molecules of water) is in the order $VO(acac)_2$ > $VO(Et\text{-}acac)_2$ > $VO(malto)_2$ > VO^{2+}, which is the same order as observed for the in *in vivo* effectiveness, suggesting an active role of this species. Another derivative of $VO(acac)_2$, $VO(Me\text{-}acac)_2$, had also attracted interest since it as $VO(malto)_2$ formed similar species when dissolved in water.

Continued on the next page

Table 1.3. – *Continued*

1997	VC with tetradentate salen-type ligands as insulin-enhancing agent	118, 119	The ability of $V^{IV}O$(salen) to reverse the hyperglycemic condition of alloxan-induced diabetic rats to near normal. However, the rats tended to become hypoglycemic, and withdrawal of treatment brought an immediate return to hyperglycemia.
1999, 2003	$VO(opt)_2$ and $VO(opd)_2$	72, 120, 121	$VO(opt)_2$ (opt=1-oxy-2-pyridinethiolato) and $VO(opd)_2$ (opd=1-oxy-2-pyridonato) are particularly stable complexes that have been shown to lower free fatty acid (FFA)[12] levels. When orally administered, $VO(opd)_2$ was more effective at lower doses than $VO(opt)_2$
2000	Phase I clinical trial using V^{IV}(Et-maltolato)$_2$ coordination complex	39	Safety, tolerability, pharmacokinetics and bioavailability of escalating doses of a vanadium complex, were possible with *bis*(ethylmaltolato)oxidovanadium(IV), BEOV in treatment of DM. A range of doses from 10 to 90 mg, given orally to 40 non-diabetic volunteers, resulted in no adverse effects; all biochemical parameters remained within normal limits. The trials were carried out by Medeval Ltd in Manchester, UK. Comparison studies revealed that vanadium from $VOSO_4$ was absorbed more slowly than vanadium delivered from BEOV.
2000-2002	Development of V^{III} and V^{V} complexes with organic ligands as potential anti-diabetic agents	115, 11,29, 122, 123	Most of the active complexes that have been tested over the years contain tetravalent vanadium. However, some of V^{V} complexes such as $V^{V}O_2$(dipic) and V5dipic-NH_2 exhibited insulin-enhancing activity. Also, some trivalent vanadium complexes were found to be as active as pentavalent, e.g., V(maltolate)$_3$.
2008	Phase II clinical trial with BEOV	77	The trials were carried out by Akesis Pharmaceuticals, Inc. (La Jolla, CA). Successful completion of phase II of human clinical trials made BEOV the benchmark anti-diabetic drug candidate; since then the results of vanadium compound newly tested for anti-diabetic activity are always compared with those of BEOV. First reported by C. Orvig.
2005-2010	Tests of V^{IV}-allixinate, pyridinone, kojicate compounds and derivatives; V^{III}, V^{IV} and V^{V}-malto-, allomalto-, and isomaltolate as potential drug candidates	124-126	After a successful phase I and II clinical trials with BEOV, these complexes were tested assuming their potential anti-diabetic activity due to the structural similarities with BEOV. All complexes were found to be active, however none was better than BEVO.

[12] FFA (indicator of habitual dietary fat intake in middle-aged adults) increase in patients with uncontrolled type 2 diabetes mellitus and are an indicator of insulin resistance.

Diabetes is a chronic illness, one of the main epidemic challenges of the future. The World Health Organization estimated the amount of people worldwide affected by diabetes to be around 150 million, forecasting the increment in number of affected people (Type II diabetes). DM is a chronic disease, caused by a deficiency or insufficient supply of the pancreatic hormone insulin, or resistance of cellular insulin receptors to insulin. The lack of insulin results into a failure of glucose balance and lipid metabolism, which in turn leads to accumulations of glucose in the blood and urine in the first case, and disequilibrium of the acid-base balance of the blood by the byproducts of alternative fatty acid metabolism in the second case. Typical complications associated with DM are kidney failure, heart diseases, damage of the peripheral blood vessels retinopathy and neuropathy.

Vanadium ions alone and coordinated with variety organic ligands have been demonstrated to exert numerous insulin-enhancing and anti-diabetic effects in *vitro* (cells cultures) and in *vivo* (diabetic animals and sporadically humans) systems. Although the mechanism by which metal ion works as insulin-mimetics has yet to be established, there is some generally accepted basic understanding of the mode of action of vanadium as an insulin-enhancing agent.

I.4.1.1 Mechanism of insulin-enhancing and/or anti-diabetic activity

Potential mechanisms of anti-diabetic activity of vanadium that have been found and investigated to date are stimulation of glucose uptake, glycogen and lipid synthesis in muscle, adipose and hepatic tissues, inhibition of gluconeogenesis, and the activation of the gluconeogenic enzymes (phosphoenol pyruvate carboxykinase and glucose-6-phosphatase in the liver and kidney as well as lipolysis in adipocytes). Physiological effects of vanadium are expected to result from the structural resemblance between phosphate and vanadium, as well as from the fact that vanadium can form cationic and anionic compounds.

Since insulin has only one action site (i.e., insulin receptor), while oxidovanadium(IV) ion has been found to have multiple action sites in the adipocytes, the mechanism of

action was called an ‘‘ensemble mechanism’’ (Figure I.2). Oxidovanadium(IV) and its complexes act on at least four sites in this ‘‘ensemble mechanism’’. They are the tyrosine kinase of the insulin receptors, signal transduction glucose transporter and protein kinase B, and phosphodiesterase [75,127].

A detailed description of the mode of mechanism can be found in [13,63,75,128].

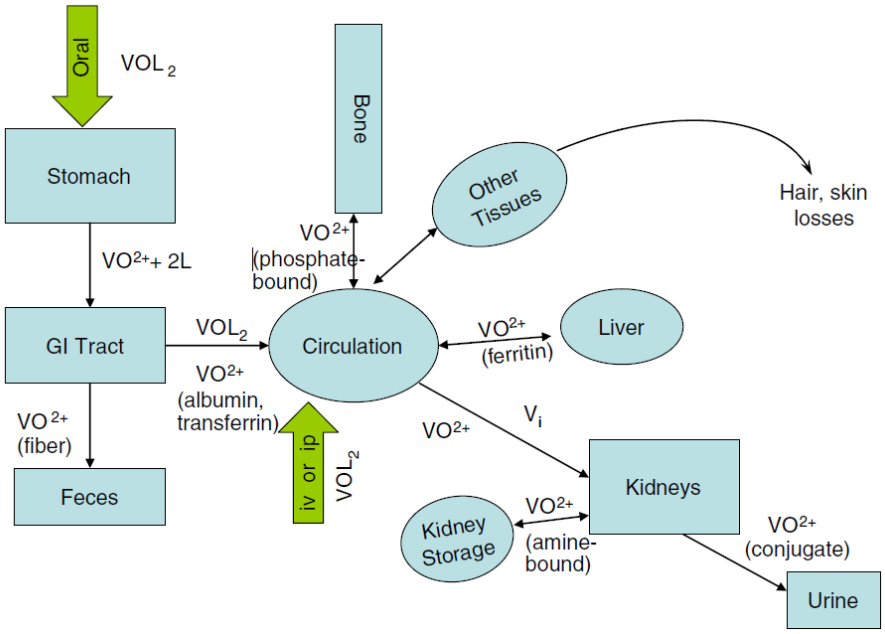

Figure I.2. Schematic model of absorption, distribution, metabolism and excretion of vanadium compounds of the general form VOL_2 [63]. I.p. - intraperitoneal and i.v. – intravenous.

Absorption, distribution, metabolism and excretion of vanadium complexes

Drug delivery to cells and then through the cell membrane can be a problem. Bioavailability of vanadium administered orally differs from when the metal is internalized intravenously of via inhalation. The distribution of vanadium in a biological system is related to aqueous chemistry of V^{IV} and V^{V} at different pH. When vanadium complex of $V^{IV}OL_n$ (Figure I.2) composition enters a cell, there are four possible “transformations” the drug can undergo [9,13,63]:

1. Upon complex decomposition of VO^{2+} cation is freed and oxidized to H_2VO_4 which in turn due to structural and chemical similarities with phosphate can use phosphate channels to penetrate the membrane;
2. The complex bind to iron-containing complexes, i.e., transferrin, albumin which partly ($VO_{2+}(L)_nTf/Alb$) or completely ($VO_{2+}Tf/Alb$) substitute the functionalities. The latter species is stable and since it contains transferrin, it is assumed to be recognized by cellular transferrin receptor and internalized via endocytosis.[13]
3. The complex is sufficiently stable to remain intact, and sufficiently lipophilic to be able to slowly cross the cellular membrane via diffusion (passive diffusion was observed in cells in *in vitro* studies).

Unequal exposure time to vanadium and different administered doses in human individuals and animals, mainly rats, are the reasons that the effect of vanadium observed in humans is not as dramatic as in animals

Many coordination complexes of vanadium, mainly oxidovanadium(IV), have been demonstrated as potent insulin-like compounds (Table I.3) and several of them have proven to be specially effective. Great efforts have been made to prepare vanadium(IV) and (V) complexes of high activity and low toxicity that are readily absorbed. Figure I.3 presents some complexes with potential anti-diabetic properties.

[13] Endocytosis is a process of the taking in of matter by a living cell via invagination of its membrane to form a vacuole.

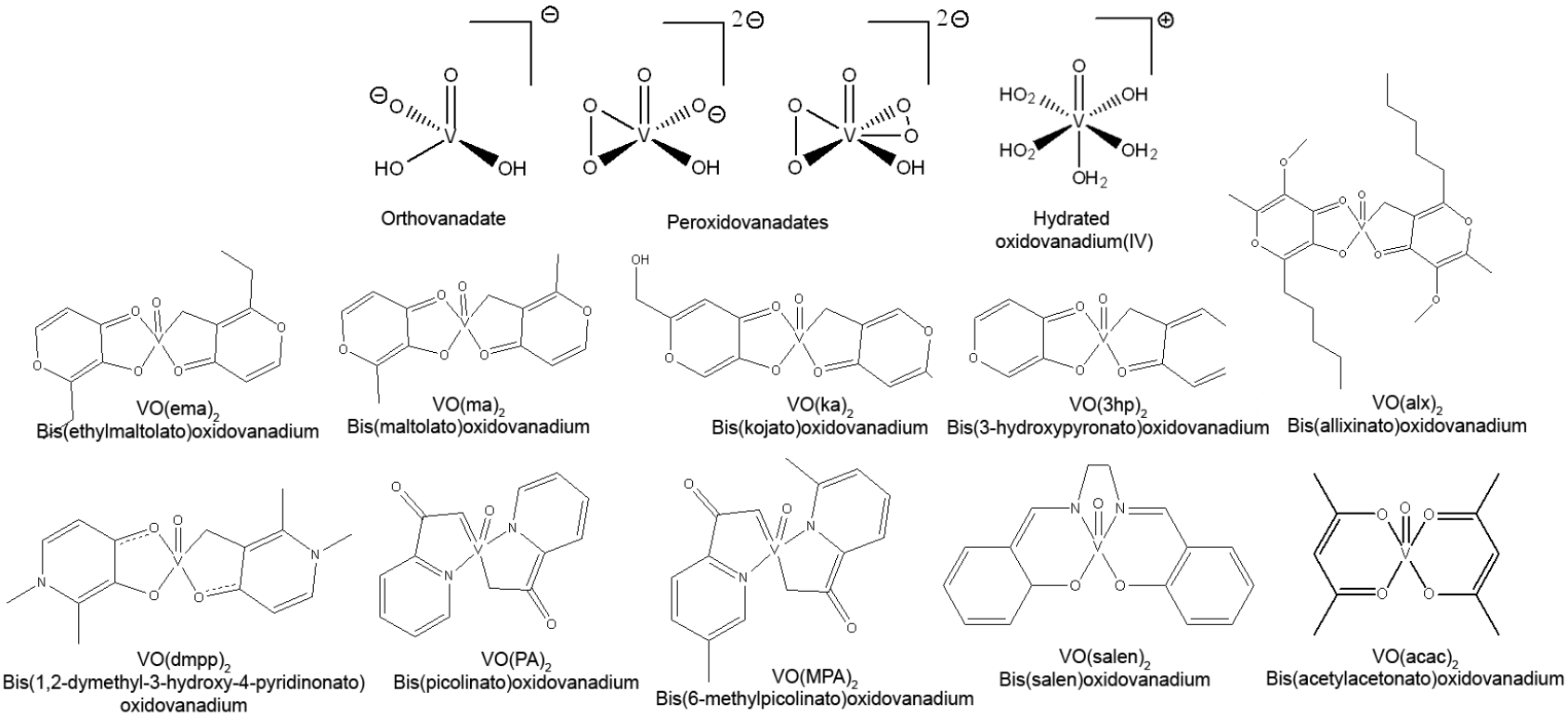

Figure I.3. Examples of potential anti-diabetic complexes. $VO(ema)_2$, $VO(ma)_2$, $VO(ka)_2$, $VO(3hp)_2$ and $VO(alx)_2$ are BEOV derivatives.

BEOV to date remains to be the most promising candidate in this field, none of vanadium complexes with insulin-mimetic properties so far has surpassed BEOV for glucose- and lipid-lowering in an oral administration; however, variety of conditions in different studies such as rodent species, levels of glycemia, residues of insulinemia etc., make unable a proper comparison of effect of all tested compounds. Since it became clear that ligands serve as "delivery system" of oxidovanadium(IV) to the target cells, the choice of functionalities became an important task. One of the important requirements is a high dissociation degree, since the compounds that do not dissociate readily have been found to show no insulin-mimetic effect *in vivo* [74,129]. Complexes BMOV, BEOV, $VO(pic)_2$, $VO(6MPA)_2$, $VO(acac)_2$, and $VO(Et\text{-}acac)_2$ seemed to comply with such requirement [130]. However, the use of a non-toxic ligands such as maltol or ethyl maltol, which are approved in many countries as food additives [131], was given preference to the use of ligands with a known problematic toxicity profile, e.g., acetylacetonate [132] or picolinic acid [133].

I.4.1.2 Vanadium in cancer treatment

According to Domingo [134], metals could be divided into four groups: (1) metals with greatest toxicity that are widespread in the environment (arsenic, cadmium, lead, mercury, and uranium), (2) essential trace metals (chromium, cobalt, manganese, selenium, and zinc), (3) metals with biological importance (nickel and vanadium), and (4) metals of pharmacological interest (aluminium, gallium, and lithium). Interestingly, some metals being carcinogenic are able to treat cancer and vice versa - some metals that are essential micronutrients, can cause cancer directly or indirectly [78]. Both their carcinogenicity and aptitude to cure cancer can be explained by their ability to generate reaction oxygen species (ROS).[14] Vanadium and arsenic are considered to be such cases [135-138]. By causing oxidative stress ROS damage macromolecules such as nucleic acids, proteins and lipids. As a result, chromosomal instability, variety of

[14] Reactive oxygen species OS are oxygen species, by-product of various metabolic processes of molecular oxygen. ROS include superoxide anion radical (O^{2-}), singlet oxygen ($^1O_2$), hydrogen peroxide (H_2O_2), the highly reactive hydroxyl radical (•OH) and so-called crypto-radicals. The deleterious effects of oxygen are assumed to result from its metabolic reduction to these highly reactive and cytotoxic species which have been implicated in the etiology of a wide array of human diseases, including cancer.

mutations, loss of organelle functions, damage of cell membrane [139], all of which are a straight road to cancer.

The term ‘cancer’ refers to more than 100 forms of this disease and each of these forms has unique features. However, the basic process that develops tumours is similar. Almost every tissue in the body can spawn malignancies and some can yield several types [140]. The development of cancer is mainly triggered by two gene classes, proto-oncogenes and p53 tumour suppressor genes. In normal conditions, they maintain the life cycle of a cell by participating in cell’s division and proliferation. Proto-oncogenes act as stimulators of growth, whereas tumour suppressor genes are inhibiting it. The importance of their tandem lies in the regulation of the cell life cycle, namely proliferation. Upon mutation, which is most likely to be induced via oxidative stress, the loss of regulation in both genes occurs. The mutations induce changes in the protein structure of proto-oncogenes thus turning them into carcinogenic oncogenes. This modification provokes uncontrolled excessive cell multiplication. Tumour suppressor genes, in contrast, contribute to cancer when they are inactivated by mutations. The resulting loss of functional suppressor proteins deprives the cell of crucial brakes that prevent inappropriate growth. Since cells that actively dividing are in a greater risk for acquiring such mutations, tumours generally originate from rapidly proliferating tissues, which means that proto-oncogenes are more likely to ‘host’ a tumour than tumour suppressor genes.

Cancer tumour development occurs in stages. When normal cells undergo genetic mutations, the cell proliferation begins to increase. As a consequence of excessive expression, hyperplasia[15] (over reproduction) takes place. At this stage these changes are not reflected on the appearance of cells. With time, typically of a year scale, some of these altered cells undergo secondary mutation. The behaviour of the cells now is different because in addition to high-speed division (uncontrolled mitosis[16]), ‘new-born’ mutated cells possess abnormal shape and orientation. At this phase dysplasia (abnormality of development) occurs. For the cancer to develop to clinical disease, the

[15] Hyperplasia is the enlargement of an organ or tissue caused by excessive proliferation; considered as an initial stage in the development of cancer.
[16] Mitosis is a type of cell division that results in two daughter cells each having the same number and kind of chromosomes as the parent nucleus, typical of ordinary tissue growth.

cells need to suffer another mutation and consequently many others. The affected cells become even more abnormal in growth and appearance. This is an early form of cancer, and in case of the absence of invasion of tumour cells into the surrounding tissue, it is called *in situ* carcinoma. Numerous attempts have been made to define the actual number of mutations that are responsible for cancer. When it became apparent that most tumours harbour many mutations, the number was estimated to be from ten to tens of thousands [141]. Nevertheless, many of these mutations do not contribute to the development of the tumour. In the case when series of mutations actually promote the tumour invasion, the mass is considered to have become malignant. Cancer begins to penetrate surfaces and barriers of body going through body structures and tissues (local invasiveness) and spread to other sites within the body (metastasize) by permeating or entering into the lymphatic vessels (regional metastasis)[17] and/or the blood vessels (distant metastasis).

Death from cancer worldwide is projected to continue rising, with an estimated 13.1 million deaths in 2030 [142]. The development of targeted anticancer therapeutics is a hot topic in medicinal research. Despite of a great advancement of knowledge towards discovery of a cancer cure, the progress in this field has been relatively slow.

When it comes to designing a drug, many challenges rise instantaneously. The most common hurdles in the drug discovery process (*in vitro* ADME tests) are stability of a chosen compound in physiological conditions, toxicity issues, mode of administration to a body, drug delivery to tumours, minimal exposure of normal tissue to the drug etc. However, one of the main challenges in the design of anti-cancer or any other type of drugs is an acute identification of a disease target. In the case of cancer DNA has always been considered a common molecular target [143]. Only recently a clinical relevance of the insulin-like growth factor has been demonstrated and identified as another target [141].

Platinum compounds are known for their wide application in cancer chemotherapy, in fact they are to date the only ones used in the treatment of patients diagnosed with cancer [144]. These pharmaceuticals act by binding to DNA. Cisplatin (square planar

[17] Metastasis is the development of secondary malignant growths at a distance from a primary site of cancer.

Pt(II) complex (cis-dichlorodiamine platinum(II)) occupies the top position in the platinum drug pyramid [145]. Cisplatin was approved in 1978 as the first line therapy and clinically used ever since. The main drawbacks of this compound such as high toxicity, large volume intravenous infusions, lack of oral bioavailability and inherited or acquired resistance of some population of cancer cells, prompted a necessity to start searching for alternative drugs. The research led to development of second (carboplatin, 1986) and third (satraplatin, has not received an approval, phase III clinical trials in 2007) generation of anti-cancer pharmaceuticals. Carboplatin though showing similar to cisplatin clinical activity, has lesser effect on cytotoxicity of cancer cells. However, higher stability, which allows more time for the drug to reach the target molecule in its original form, makes carboplatin advantageous and more desirable for the therapy. Satraplatin received a great interest since it is the first orally active platinum-based chemotherapeutic drug. In tumour models it was found to behave similarly to cis- and carboplatin, and showed the activity against some acquired *cis*platin-resistant tumour cell lines [143,146].

The success of cisplatin and carboplatin stimulated an intense search of other metal-based cancer drugs with favourable toxicity. A wide range of metals such as ruthenium, palladium, gallium, iridium, rhodium, tin, vanadium, titanium, copper and gold are being studied as possible candidates in cancer treatment [147,148]. Ruthenium[18] complexes [149-153] being in the lead are now a proven effective alternative to Pt-based complexes, followed by gallium, rhodium, titanium and vanadium compounds [43,154].
Vanadium, known for possessing insulin mimetic and osteogenic effects [155], has been also found to have anti-tumour activity [5]. Moreover, vanadium compounds exhibit cytotoxic, mainly due to the generation of oxidative stress that can trigger apoptosis of cancer cells, and genotoxic effects [156,157]. Versatility of redox vanadium chemistry, i.e., many oxidation states and rapid interconversion between V^{IV} and V^{V}, allows vanadium to participate in biological redox chemistry and undergo ligand exchange reactions. The ability of vanadium compounds to interact and coordinate with biological

[18] From all tested compounds, KP1019 ([IndH]*trans*-[$RuCl_4(Ind)_2$)] (Ind = indazole)) and NAMI-A ([ImH][*trans*-$RuCl_4$(DMSO-S)Im] (Im = imidazole)) are in the lead as they have both completed Phase I clinical trials. For more information see a detailed review by I. Tomaz and J. Costa Pessoa [43]. Another promising ruthenium anti-cancer agent is ONCO4417 has been reported by Antonarakis and Emadi in [152].

molecules has awoken a great interest in scientists on their way to ‘overturn the platinum paradigm’ [143]. The first report on cytostatic effects of vanadate appeared in 1965 [29]. The anti-tumour potential of organovanadium compounds, namely vanadocene Cp_2VCl_2, was demonstrated on Ehrlich ascites tumour in 1986 [158].

Discovery of diverse biological effects of vanadium compounds (i.e., insulin-like action and reduction of hyperlipidemia and hypertension) established the potential therapeutic applications of these compounds. According to Evangelou [5], who wrote the first comprehensive review on vanadium in treatment of cancer, in last few decades, vanadium compounds have been considered as a new class of metal-based antitumor agents and are assumed to act through generation of ROS. Interestingly, Liu et al. [159] in their most recent studies of vanadium in the PC-3 human prostate cancer cell line, detected and speculated the capability of vanadium to control diabetes and cancer simultaneously. They interpreted and related this dual potential of vanadium as a result of vanadium-induced ROS generation.

Vanadium complexes that have been reported to have anti-cancer potential, namely, to supress the proliferation of cancer cells, are presented in Figure I.4. Bis(η5-cyclopentadienyl)vanadium(IV) (vanadocene, Cp_2VCl_2), derivatives are described in [160], bis(4,7-dimethyl-1,10-phenanthroline) sulfatooxidovanadium(IV) (metvan) and related compound [5,161-166]. Others compounds reported are vanadate [159]; oxidovanadium(IV) silibinin, $VO(silibinin)_2$ [167]; oxidovanadium(IV) oxodiacetate, VO(oda) [156]; V-cysteine complex [168], and vanadium(V) complexes with salicylaldehyde semicarbozone derivatives [169]. $VO(acac)_2$ was found to block permanently the cell cycle in a human hepatoma cell line [170]. This compound was also tested as an MRI probe in studies for early detection of cancer [171]. Although the majority of tests of vanadium compounds as anti-cancer agents are typically performed *in vitro*, the number of studies *in vivo* impetuously increases [6,13,143,164,168,172-175,180]. No tests in humans have been reported to date.

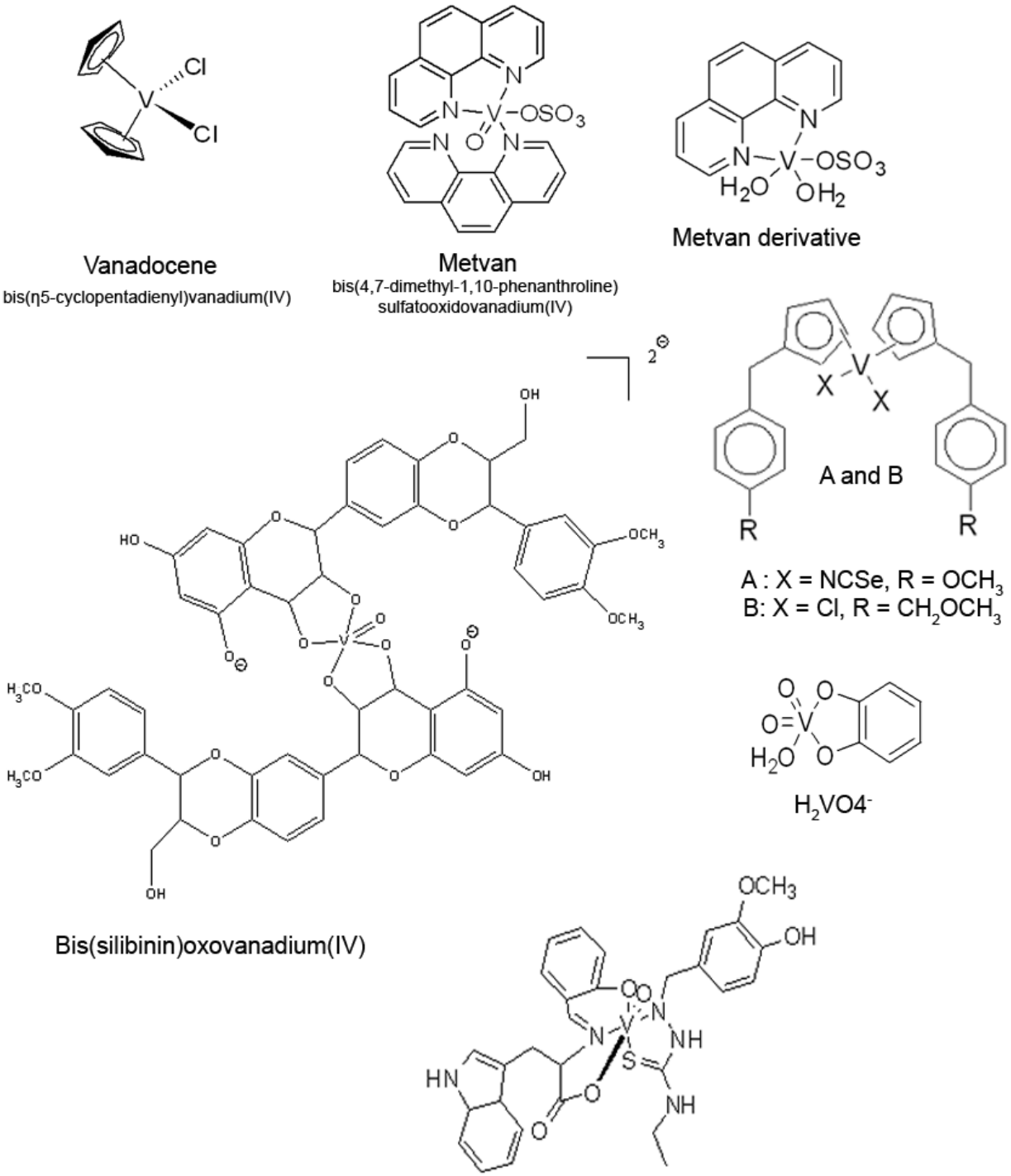

Figure I.4. Examples of vanadium compounds with anti-tumour effect.

Mechanisms of action of potent vanadium anti-cancer agents

Cancer conditions vary significantly from case to case. In order to design a proper drug, accurate identification of a disease target is required. Most of the chemotherapeutic drugs are DNA-targeted thus DNA molecule is often chosen in studies with putative anti-cancer compounds. This was the reason for many scientists to study DNA cleavage activity of various metal-based compounds (section “Inorganic nucleases”).

Evangelou in his review [5], highlighted the main capabilities of any designed drug that are crucial for achievement of an effective treatment. These properties are antiproliferation effect (reduction of cellular growth rate), cytostatic and/or cytotoxic effects - inhibition of cell growth and division, necrotic (uncontrolled) or apoptotic (programmed) cell death -, antimetastatic effect (reduction and/or inhibition of the cancer cells invasion and the metastatic potential), antiresistant effect (a drug should possess potency to sensitize drug-resistant cancer cells). Vanadium compounds seem to fulfil aforementioned criteria. They can act individually or in tandem with another metal-based drug, e.g. *cis*platin. Vanadium chelated by EDTA was found to reduce the resistance of human ovarian cancer to *cis*platin allowing this drug to fully exert its cytotoxic effect [176].

The main pathways for vanadium compounds to exert antiproliferative and cytotoxic effects on normal and malignant cell lines appear to be mainly via cell cycle arrest and interactions with DNA. Cell cycle arrest is expected to mediate through the inhibition of PTPs, however, it may also be exerted via activation of mitogen activated protein kinases (MAPKs superfamily) signalling pathway [5,177]. Metvan was found to induce cell apoptosis by inhibiting mitochondrial transmembrane potential, the generation of reactive oxygen species and depletion of glutathione [178]. $VO(acac)_2$ was able to block the cell cycle permanently at the G1 phase on HepG2 cells in human hepatoma cell line [170]. Vanadyl sulfate, cysteine and V(III)-cysteine were found to exert antitumor effects on leiomyosarcoma bearing Wistar rats [175]. Also, $VOSO_4$ promoted DNA damage in in human lymphocytes and HeLa cells [179]. Treatment with orthovanadate resulted in an inhibition of MDAY-D2 lymphosarcoma cells in mice assumed to act through generation of ROS [180]. Antitumor activity of vanadocene complexes, namely vanadocene dishloride, was found to take place via interaction with DNA’s nucleotide

phosphate groups. As a result, labile vanadocene-DNA complexes form causing alterations in nucleic acid metabolism [181]. The mechanism of Cp_2VCl_2 interaction with DNA differs from that of *cis*platin which forms covalent DNA adducts that are potentially mutagenic [5]. VO(oda) is another compound that exerts cytotoxicity via interaction with DNA. It was tested in human colon adenocarcinoma (Caco-2) cells and suggested to augment oxidative stress and thus DNA damage of the malignant cells [156].
Given the increasing number of reports on vanadium anti-cancer activity in the last two decades, vanadium compounds have a possibility to become a new class of nonplatinum metal antitumor agents. However, more intensive basic and applied research is required.

In addition to anti-diabetic and anti-cancer properties, vanadium complexes have shown activity against parasitical diseases. Rehder in his recent publication reviewed [13] potential vanadium compounds in the treatment of epidemic tropical diseases, which to date remain to be a serious problem taking away thousands human lives yearly. While, in the past few decades, there has been observable progress with respect to insulin-enhancing and chemopreventive role of vanadium, little is explored about its effect on other diseases.
Nowadays this gap is slowly becoming filled since many vanadium complexes are being investigated and tested as anti-parasitic [182-188], spermicidal [189,190], anti-viral [191], anti-HIV [192-195], and anti-tuberculosis agents [196-198].

I.5 Vanadium(IV) acetylacetonate

Oxobis(2,4-pentanedionato-*O,O´*)vanadium(IV) ($VO(acac)_2$,) is a well-known compound among vanadium studies [199,200]. Since the discovery of the $VO(acac)_2$ insulin-mimetic activity in cell cultures [114], the interest to study its behaviour greatly increased. The efficiency of $VO(acac)_2$ was found to be superior to that of $VOSO_4$ which was intensively investigated for insulin-enhancing potential. $VO(acac)_2$ received the attention as a promising anti-diabetic agent in the beginning of this millennium after the report of Reul et al. [18]. In this publication $VO(acac)_2$ and $VO(Et\text{-}acac)_2$ were shown to be more effective in glucose lowering in insulin-deficient diabetic rats than $VO(malto)_2$, which was already well known for its insulin-mimetic properties, and by the time being had entered phase I clinical trials in humans. This finding allowed investigators to assume that $VO(acac)_2$ and its H-acac derivatives may be superior to $VO(malto)_2$ as insulin-mimetic agents. This hypothesis has perceptibly triggered new studies on the way to understanding the biologically relevant aqueous chemistry of $VO(acac)_2$.

The first preparation of $VO(acac)_2$ was recorded over a century ago, in 1876 [201]. In 1914 Morgan et al. [199] reported synthesis and characterization of $VO(acac)_2$ and four decades later, in 1961, its crystal structure was published [200]. Since then, the physical properties of the compound have been extensively studied [202,203,204]. The IR spectrum of $VO(acac)_2$ in the spectral range between 1600-400 cm^{-1} was first investigated by Nakamoto et al. in 1961 [205] and complete IR and Raman data of the complex in the 4000-200 cm^{-1} range, were reported by Vlčková et al. [206]. The characteristic $\upsilon(V=O)$ stretch is observed at ca. 1000 cm^{-1} (often 998 cm^{-1}) [207,208,209].

$VO(acac)_2$ has been used as an oxidizing agent in organic synthesis [210,211,212,213], precursor for the synthesis of VC [214,215,216,217,218] and catalyst for selective epoxidation of allylic alcohols in combination with terbuthyl hydroperoxide [11,219, 220]. The biological significance of vanadium compounds in a wide variety of biological systems has augmented also the studies of $VO(acac)_2$ regarding its electrochemical behaviour and solution chemistry [115,119,116,209,221-223]. $VO(acac)_2$ acts as nonspecific phosphotyrosine phosphatases inhibitor such as PTP1B, exhibits weight

and fat-reducing effect by enhancing signal traducer and activator of transcription 3 phosphorylation induced by centrally administered leptin to normal rats [224]. In conjunction with insulin-enhancing activity [117,225], anti-cancer potential of $VO(acac)_2$ came into focus. The complex was found to inhibit the cell growth in a human hepatoma cell line in a dose- and time-dependent manner [170]. As an important part in understanding insulin-mimetic behaviour, Costa Pessoa et al. [119]. studied the stability and nuclease activity of $VO(acac)_2$ and several oxidovanadium(IV) salen and salan complexes, as well as $V^{IV}O(phen)_2(SO_4)$. A variety of $VO(acac)_2$-type complexes were explored on the way of searching new water soluble $VO(acac)_2$-derived complexes for biological activity [209,226-229]. Among these derivatives are $VO(hd)_2$, $VO(acac\text{-}NH_2)_2$ and $VO(acac\text{-}NMe_2)_2$ [230,231], $VO(Et\text{-}acac)_2$ and $VO(Me\text{-}acac)_2$ [116,221]. These complexes were synthesized and characterized, and examined as inorganic nucleases together with $VO(acac)_2$. $VO(Et\text{-}acac)_2$ and $VO(Me\text{-}acac)_2$ were also studied as potential insulin-mimetic compounds. Another study involving these compounds and $VO(Cl\text{-}acac)_2$ is desulfurization of fuels with their ionic liquids [232]. Additionally, $VO(Et\text{-}acac)_2$ and $VO(Me\text{-}acac)_2$ were tested in inhibition of alkaline phosphatase along with $VO(acac)_2$, $VO(CF_3acac)$, and $VO(Benzac)_2$ [233].

The coordination number and geometry of vanadium is ligand dependent [234]. In the solid state and in some non- or weakly-coordinating organic solvents (such as benzene, CH_3Cl and even in acetonitrile), $VO(acac)_2$ is a pentacoordinate complex [201]. However, when placed into aqua media or other polar solvents (such as methanol, DMF and pyridine), it becomes six-coordinated [235]. This mononuclear complex is coordinated by four oxygen atoms lying in a distorted square pyramidal coordination (Figure I.5). The vanadium atom lies above the basal equatorial plane (0.55 Å). The V=O bond length measured from the crystal structure is 1.5922 Å [116]. Upon dissolution in organic solvents, the vanadium coordinates a donor ligand (L) in the vacant site, generating products expressed as $[VO(acac)_2L]$ [236,237]. In aqueous media $VO(acac)_2$ was determined by EPR and visible spectroscopy to form three species (Figure I.6) which are *trans*-$VO(acac)_2 \cdot H_2O$ (A), *cis*-$VO(acac)_2 \cdot H_2O$ (B) adducts, a hydrolysis product assigned as 1:1 vanadium atom with one $acac^-$ group (C), and another vanadium(IV) species which is NMR and EPR-silent. In freshly prepared

solutions A (85%) and B (5%) species are predominant, whereas the species C is not observed; the remaining 10% are assigned to vanadium(IV)-acac complexes with strongly antiferromagnetically coupled spins (such as the dimeric VO(acac) complexes). Solution of $VO(acac)_2$ recorded after several days, showed significantly higher concentrations of C; species A remained relatively intact [116,209]. After 24 days at room temperature, the same solution contained about 25% A and 65% C. The species C can be observed in the reaction with polydentate ligands, where one $acac^-$ group is substituted, and the second $acac^-$ group remains resistant [238-241].

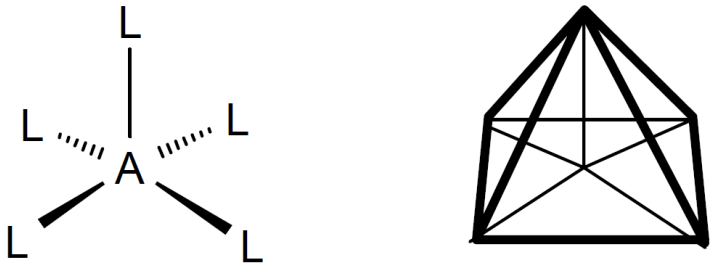

Figure I.5. Square pyramidal geometry of pentacoordinate $VO(acac)_2$.

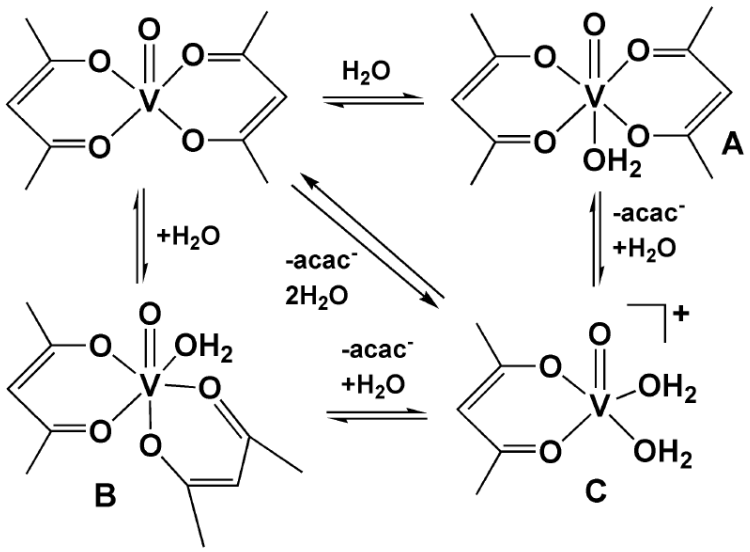

Figure I.6. Structure and possible isomers of oxobis(2,4-pentanedionato)vanadium(IV). The *trans* (species A) and *cis* (species B) isomers have the H_2O molecule coordinated respectively *trans and cis* to V=O; and the 1:1 hydrolysis product (species C) may contain two or three coordinated water molecules and have an overall charge of +1 or neutral. Species A is identified to be the major species upon dissolution of $VO(acac)_2$.

The electronic spectra of acetylacetonate are dominated by the $n \rightarrow \pi^*$ and $\pi \rightarrow \pi^*$ transitions of the carboxylic groups. The spectra of $VO(acac)_2$ have been intensively investigated and it has been shown that they are markedly solvent dependent [242,243]. $VO(acac)_2$ spectra, located in the range 380-800 nm, show three bands indicating three "d-d" transitions. They were assigned to the $b_2 \rightarrow e^*$, $b_2 \rightarrow b_1$, $b_2 \rightarrow a_1^*$ transitions [207-209], following the energy level scheme derived originally by Ballhausen and Gray [244] from a molecular orbital study for a square pyramidal structure of C_{4v} symmetry (Figure I.7).

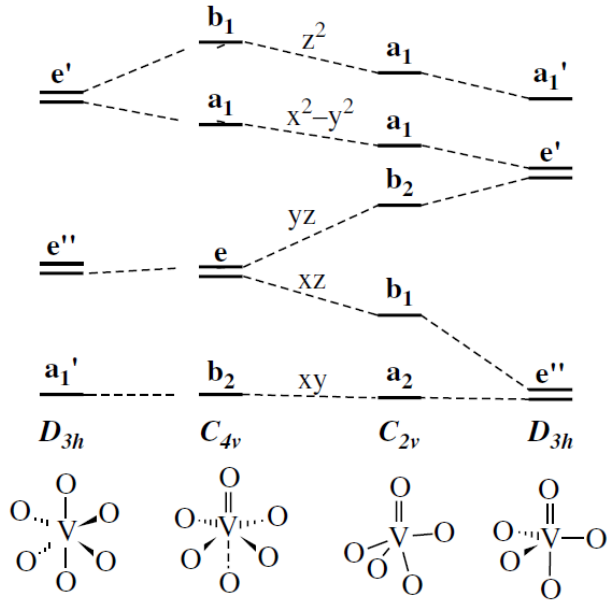

Figure I.7. Orbital correlation diagram for the transformation of a square pyramid to a trigonal bipyramid ($C_{4\upsilon} \rightarrow C_{2\upsilon} \rightarrow D_{3h}$) and an octahedron to a trigonal prism ($D_{3h} \leftarrow C_{4v}$) under idealised local symmetries [9].

I.6 Inorganic nucleases

Nucleases are any enzymes that cleave nucleic acids. Natural nucleases, which belong to the class of enzymes called hydrolases, are usually specific in action, ribonucleases and deoxyribonucleases acting respectively only upon ribonucleic (RNA) and deoxyribonucleic acids (DNA). Some enzymes having a general action (such as phosphoesterases, which hydrolyse phosphoric acid esters) can be called nucleases because nucleic acids are susceptible to their action. Nucleases are found in both mammals and plants [245].

Nucleases that cut only those DNA molecules in which they recognize particular subunits are called restriction enzymes. Some of them cleave the target DNA molecule at random sites (Type I), but others split the molecule only at the recognition site (Type II) or at a fixed distance from the recognition site (Type III). Type II and III restriction enzymes are powerful tools in the elucidation of the sequence of bases in DNA

molecules. They play a fundamental role in the field of recombinant DNA technology, or genetic engineering.

Inorganic nucleases are inorganic compounds which have demonstrated enzyme-activity towards DNA. They are becoming increasingly important. They may function as artificial restriction enzymes offering the possibility for a) designing systems with sequence specificities different from those of natural endonucleases, for which inorganic nucleases showing site specificity are particularly interesting [246,247]; b) targeting DNA sequences to block gene expression at the molecular level in chemotherapy[19] [147]; c) studying nucleic acid conformations. A different and equally important motivation to study these compounds comes from predicting a possible undesirable DNA damage following the use of metal compounds as new options for therapeutic use on other diseases. According to Mancin et al. review [248], the development of these synthetic agents is advantageous as they may be even more efficient DNA cleavers than natural enzymes.

Since DNA is sensitive to oxidative cleavage, which is known to be promoted by ROS via oxidative stress, many researchers have focused on metallonucleases capable of cleaving DNA oxidatively. In spite of their high efficiency and versatility, the products of cleavage by these complexes are not readily amenable to further enzymatic manipulations, and thus have limited use. Hydrolytic cleaving agents, on the contrary, do not possess these drawbacks. Their ability to efficiently cleave nucleic acids in a non-degradative manner with different levels of selectivity, made them preferable to oxidative agents. The hydrolytic cleavage is targeted at the phosphate ester bonds linking the nucleosides. Finding metallohydrolases capable of mimicking the function of natural endonucleases is a primary goal in this area of research.

Transition metal complexes of Fe, Cu, V, Ni and Mn, among others such as Pt, Ru, Rh, Cr, Co, Y and Os, have been reported to mediate DNA oxidation in the presence of oxidants or reductants or without any assistant agents [246,249,250]. These complexes attack the sugar or base moieties of DNA and the mechanism of action often involves

[19] Mainly, as potential substitutes for cisplatin in cancer chemotherapy, which is the case of Gallium, Ruthenium, Rhodium, Titanium, Tin and Vanadium compounds.

generation of reactive oxygen or metal-oxo species (ROS/MROS). Many excellent reviews on artificial metallonucleases can be further consulted [194,246,248,249,251-261], some of which have been recently published [262-264].

I.6.1 Vanadium nucleases

Among several transition metals that have shown nuclease activity, some examples are of VC. Some of them are known for their insulin-mimetic properties, and have been studied as possible therapeutic agents for diabetes *mellitus* since the very discovery of this disease [75].

The first case of nuclease activity by VC was reported in 1985 [265] for bleomycin vanadyl(IV) in the presence of hydrogen peroxide. This complex system was found to be more effective in attacking G-A (5´→3´) sequences than the bleomycin-iron complex system. In 1992, Sakurai et al. [266] tested DNA cleavage by hydroxyl radicals generated in a vanadyl ion-hydrogen peroxide system and have found $V^{IV}O^{2+}$ in the form of $VOSO_4$. Another publication [267] reports about $[VO(phen)(H_2O)_2]_2^{+}$, a new antitumor VC, which showed a strong cleavage towards supercoiled plasmid Col E1 DNA. A year later [268], $VOSO_4$ was shown to damage DNA which was explained by Fenton-like generation of hydroxyl radicals. The interest in V nucleases has since increased. In the beginning of this millennium many oxidovanadium(V) and peroxidovanadium(V) complexes were investigated as chemical nucleases and were found to cleave DNA on photoexposure to UV-A light [269-274]. In 2000, several cationic V(III) dimeric complexes with phenanthroline and similar ligands were shown to promote nuclease activity. In the same publication, Heater et al. [275] reported a strong nuclease activity for the V(IV) complex with phenanthroline. Another publication about $VOSO_4$ appeared in 2001 by Stemmler and Burrows [276]; they studied guanine and deoxyribose damage in DNA oxidation by vanadyl and vanadate. In 2004, complexes of V(IV) with hydroxysalen ligands showed nuclease activity in the presence of an activating agent, either a reducing (MPA) or an oxidizing one (oxone) [277]. The authors did not establish the actual active vanadium species. Later, several cases were reported on photocleavage activity by V(V) complexes with ligands containing polyaromatic

groups (either derivatives of phenanthroline or naphthalene) which can dock to DNA. The photocleavage activity of phenanthroline peroxovanadate complexes was extensively studied by Sam et al. [270] and Chen et al. [274] who observed photocleavage activity with site selectivity by a V(V) complex with the Schiff base of 2-hydroxy-1-naphthaldehyde and L-phenylalanine. Kwong et al. [271] examined another example of sequence-specific photocleavage by a V(V) peroxo complex. Since the time $VO(acac)_2$ has been proposed as a particularly efficient insulino-mimetic/insulin-enhancing compound [115], much interest has been focused in its *in vivo* biological behaviour. Costa Pessoa et al. [119], when comparing the nuclease activity of several different types of V(IV)Cs with salen-, salan-, and pyran-type ligands for possible therapeutic application, also studied $VO(acac)_2$ and $VO(phen)_2$. They found these two compounds to be very active towards DNA.

Most of the DNA-vanadium cleaving agents developed over the past few years promote photo-induced DNA cleavage, whereas their “chemical nuclease activity” is relatively poor even in the presence of activating agents. Chakravarty’s group [278-282] greatly contributed in the study of photocleavage activity of oxidovanadium(IV) complexes. They explored VC with different phenanthroline derivatives and often observed an efficient DNA photocleavage activity. In 2009, Leelavathy et al. [283] studies of DNA cleavage properties of macrocyclic binuclear $V^{IV}O$ complexes showed a significant promotion of oxidative DNA cleavage under physiological conditions in the presence of H_2O_2. Continuing DNA photocleavage activity studies, Du et al. [284] tested two mixed-ligand (thiosemicarbazones and bipyril) oxidovanadium(IV) complexes. Two novel oxidovanadium(IV) complexes of phenanthroline bases investigated by Prasad et al. [285] induce a single-strand DNA cleavage under oxidizing conditions (H_2O_2). Another example of oxidative DNA cleavage is found in research by Raman et al. [286]; they assumed that the hydroxyl radicals are likely to be the reactive species responsible for the cleavage of plasmid DNA by the synthesized complexes containing a pyrazolone derivative Schiff base. Recently, Patel et al. [287] synthesized several oxidovanadium(IV) complexes with ciprofloxacin and uninegative bidentate ligands such as 1-(2-hydroxyphenyl)ethanone, salicylaldehyde, 2-hydroxy-1-naphthaldehyde, 2-hydroxy-5-methyl-propiophenone, 5-bromosalicylaldehyde, 3,5-dibromosalicylaldehyde

and investigated their DNA cleavage without any activating agents. Cationic μ-oxo V(III) dimers of the type $[V_2OL_4Cl_2]^{2+}$ (L = 1,10-phenanthroline, 3,4,7,8-tetramethyl-1,10-phenanthroline, 4,7-diphenyl-1,10-phenanthroline, or 2,2´-bipyridine) have been shown to bind strongly to DNA and lead to its degradation, assuming the involvement of oxidative base loss [275]. Islam et al. [288] have reported the DNA cleavage and the *in vitro* insulin-mimetic activity of four *bis*(maltolato)vanadium(III)-polypyridyl complexes. Two of these complexes (dpq and dppz ligands) have been found to promote DNA cleavage, requiring no external additives such as H_2O_2. They concluded that neither hydroxyl nor superoxide radicals are involved. The research group of Parac-Vogt [289,290,291] has been thoroughly investigating the hydrolytic cleavage of RNA and DNA by polyoxovanadates by NMR spectroscopy using DNA-model substrates, 4-nitrophenyl phosphate and bis-4-nitrophenyl phosphate. Their two most recent works are devoted the hydrolysis of serine-containing peptides by vanadates [292] and the mechanism of p-nitrophenyl acetate (pNPA) hydrolysis by vanadate ions [293].

Evidently, VCs have been widely explored for their possible nuclease activity. In many reported cases the possible DNA damage is evaluated prior to conducting studies on insulin-mimetic effect and considering any compound for the treatment of diabetes. Typically, nuclease activity studies are performed at micromolar metal ion concentrations, at which the metal ion speciation is unknown. This can explain why to date it is not yet clear which vanadium species are actually active towards DNA breakage.

I.6.2 Other nucleases

Many coordination complexes with metal centres were prepared to serve as nuclease mimics. Interest in the development of chemical nucleases is constantly increasing. A majority of the metal compounds reported to cleave DNA oxidatively, however a considerable progress has been made in the design and study of metal complexes that promote phosphodiester hydrolysis.

Literature survey revealed numerous publications on a variety of transition metal complexes with enzyme-like action as well as some articles on some lanthanide

complexes tested as nucleic acid cleavage agents. In many cases metal ions, chosen to synthesize a compound that will be further tested as a possible nuclease, are divalent. Divalent (Cu, Fe, Mn, Zn, Co, Ni, Cd, Cr, Ru and Pt) and some tetravalent metal ions, such as V and Cr, are important catalytic centres in a designed metallonuclease [294-296]. Among such a diversity of metals, copper and iron compounds seem to have taken a leading role; they possess the highest number of studies conducted on the way to finding efficient artificial nuclease.

After it has been reported that lanthanide and transition metal ion complexes can promote the hydrolysis of DNA [297], a new wave of research on the development of artificial metallonucleases, namely synthetic DNA hydrolytic agents containing metal ions, grew intensively. It is well known that DNA is particularly resistant to spontaneous hydrolysis. Estimated half-life time at 25 ºC and pH 7 is between hundreds of thousands to hundreds of millions of years [298]. Although many natural enzymes have metal ions, such as Ca(II), Mg(II) and Zn(II), Fe(III) and Fe(II) as their active centres, their synthetic analogues, apart from Fe(III), which is a promising candidate, are far from being competitive with them. In fact, as shown in the literature, these metal ions are not as popular as the others (e.g., Fe(III) and Cu(II)), when it comes to choosing a catalyst for designing a nuclease. Synthetic catalysts for DNA hydrolysis with good activity have been obtained by using Ce(IV), Cu(II), and Fe(III) complexes, but Zn(II)-based agents are generally less efficient [299-301].

According to the review of Hegg and Burstyn [247] in order to promote hydrolysis of phosphate esters in DNA molecule, a metal ion should possess the following features: a) lability to substitution (ability to exchange ligands very rapidly); b) strong Lewis acids (ability to polarize carbonyl bonds); c) high charge density (ability to bind to the hard oxygen anions of the negatively changed phosphodiester backbone). The combination of these characteristics makes a metal a potent candidate for the role of nuclease.

In accordance with the aforesaid key criteria for effective hydrolytic activity, the most effective hydrolytic metal ions have been shown to be lanthanide ions (Ln(III), Eu(III), Dy(III), Ce(IV)), as well as Zn(II), Ca(II), Cu(II) and, to some extent, Fe(III) [253]. However, literature suggests that metal ions, other than lanthanides, are sporadically

effective in DNA hydrolytic cleavage. Indeed, trivalent lanthanides were demonstrated to accelerate the hydrolysis of DNA and a number of papers were published on hydrolysis of phenyl phosphate esters and DNA by La(III), Er(III), Tm(III), Yb(III) and Lu(III) ions [302-309].

Among transition metals that showed a great merit in cleaving DNA, mainly in a oxidative manner, are copper, iron, platinum, ruthenium, zinc, cobalt, manganese and a few others. A brief overview of artificial nucleases that most often appear in the literature is presented below.

I.6.2.1 Copper nucleases

Copper complexes have attracted attention due to their redox properties. Countless experiments have been carried out testing different copper compounds as enzyme mimics. Several well-known and thoroughly studied cleavage agents are $[Cu(phen)_2]^+$ (phen = 1,10-phenanthroline)[20] [310-323], Cu-BLM (BLM = bleomycin) [324,325], metalloporphyrin [326-328], cuprous ion with flavonoids [329] etc. Copper complexes are typically used in the development of oxidative-cleaving agents [246,325,330-346]; however many examples of Cu(II) complexes promoting hydrolytic mechanism of DNA cleavage are also reported [347-357].

I.6.2.2 Platinum nucleases

Since platinum compounds were the first metal based complexes used as antitumor agents in cancer therapy, they were soon studied as inorganic nucleases. Cisplatin as the most effective anti-tumour compound and a representative of all potential platinum anti-cancer drugs is known to act via interaction with DNA. However, the acting mechanism is not cleaving but rather unwinding. Cisplatin binds to DNA molecules via chloride ligand exchange [358]. The planar aromatic cation intercalates between adjacent base pairs which leads to unwinding and distortion of the strands [359,360,361]. After cisplatin is administered, one of the chloride ligands is slowly substituted by water (an aqua ligand), in a process termed aquation. The aqua ligand in

[20] The 1,10-phenanthroline-copper complex was the first synthetic coordination complex demonstrated to have an efficient nucleolytic activity

the resulting $[PtCl(H_2O)(NH_3)_2]^+$ is itself easily displaced, allowing the platinum atom to bind to bases. Of the bases on DNA, guanine is preferred [362].

I.6.2.3 Ruthenium nucleases

Ruthenium compounds are becoming popular in anti-cancer research, and have gained a special attention as inorganic nucleases. The targets of ruthenium based potential anti-cancer complexes continue to be debatable [43]. As in the case of platinum compounds, the majority of ruthenium complexes promote intercalative binding to DNA instead of cleaving it [147,154,363-366]. NAMI-A and KP1019, two important anti-cancer agents, showed irrevocable coordination with DNA. To date their final targets and the mechanism of action are still unclear [367], nevertheless, some tests showed that their antitumor activities have stronger effect on plasma proteins and glutathione than on DNA [153]. Ruthenium(III) and (II) complexes with phenanthroline, phenanthroline-dione, dipyridophenazine [368], diimine, bypiridine, dipyridoquinoxaline, nitrofurylsemicarbazone ligands [369] were found to bind to DNA in a non-covalent manner prior to the photo- [154] or oxidative cleavage [370]. Ruthenium(II) polypyridyl complex was found to hydrolytically cleave DNA in a enzyme-like mode [371]. Organomettalic Ru(II)-arene compounds, developed by the groups of Sadler [148,372] and Dyson [373], were found to directly coordinate to the DNA bases.

I.6.2.4 Iron nucleases

Since the natural antitumor antibiotic iron-bleomycins (Fe-BLMs) [374-376] were found to efficiently promote double-strand DNA cleavage, many studies of iron-containing complexes have been carried out. Considering that Fe-BLMs, effective chemical nucleases, act only in the present of external additives, many attempts have been made to develop iron-containing cleaving agents with different functional groups in order to augment the cleaving effect. Among many tested complexes, there are examples of $[Fe(EDTA)]_2$ [377], methidiumpropyl-EDTA-iron [378], (μ-oxo)diiron(III) complexes [379-381], and ferrocenes [382]. Compounds reported to date mainly promote oxidative breakage [383,384], however, studies of hydrolytic cleavage can also be found [385,386].

Other metals such as zinc [337,346,355,387-391], manganese [392-394], nickel [337,340,344,355,394-396], cobalt [337,342,344,346,397], chromium [394,398-400,], molybdenum [401,402], rhodium(III) [43,403], yttrium(III) [404] gadolinium(III) [405] with varying ligands are also reported, though explored to a lesser extent, since their compounds are not as effective as those aforesaid.

It is also important mentioning salen metal complexes, which have been designed as nucleic acid reagents to induce specific damage in DNA or RNA. Mn [406], Ni [407], V [119,277], Cu [408,409], Co [410], Ru [411], Fe [412] salen-containing complexes [413] were demonstrated as effective DNA cleavers.

Impressive progress towards obtaining efficient metallonucleases has been achieved since their first report. However, the successful practical implications are still complicated by a number of things, among which are absence of selectivity and satisfying cleavage efficiency specified by double strand scission. The design of a really effective model of metallonuclease is one of the most demanding tasks in biochemical research field.

I.6.3 Methodologies for studying inorganic nucleases

Mechanistic studies of DNA molecule as a substrate are complicated by the extraordinary resistance of the phosphodiester bond. Supercoiled plasmid DNA, being a more accessible substrate, is typically used for such studies.

The most common method in efficient evaluations of cleavage reaction of metallonucleases is digestion of plasmid DNA in controlled conditions followed by gel electrophoresis analysis of the three products of degradation of the pDNA which are Sc, Nck and Lin forms. Some of the major methodologies frequently used in the field of metallonucleases are listed in Figure I.8. In practical applications it is common to combine two or more techniques to get more valuable information.

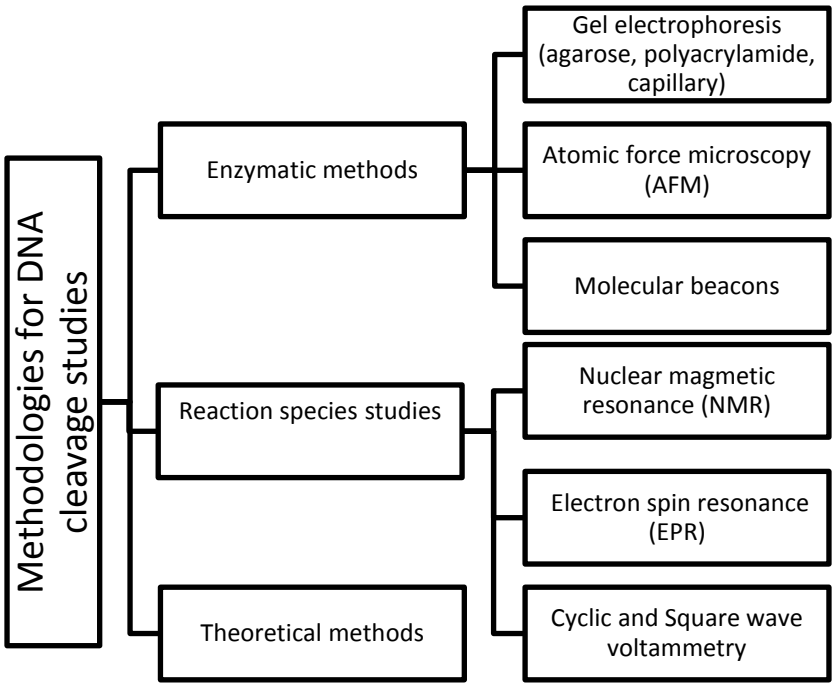

Figure I.8. Methodologies used to study DNA cleavage activity of inorganic nucleases (adapted from 246).

I.7 DNA and DNA Cleavage

I.7.1 Briefly about DNA

The nucleus of every cell contains a DNA molecule, a carrier of genetic instructions, used in the development and functioning of all known living organisms and many viruses. The molecule consists of two strands that wrap around each other to resemble a twisted ladder (double-stranded helix), whose sides, made of sugar and phosphate molecules, are connected by "rings" of nitrogen-containing chemicals called bases. Each strand is a linear arrangement of repeating similar units called nucleotides, which are composed of one sugar (deoxyribose), one phosphate (related to phosphoric acid), and a nitrogenous base, presented by purine bases (adenine and guanine) and pyrimidine (thymine and cytosine) (Figure I.9). Adenine (A) always pairs with thymine (T) via two hydrogen bonds. Guanine (G) is connected to cytosine (C) via three hydrogen bonds. These four nitrogenous bases of DNA are arranged along the sugar-

phosphate backbone in a particular order (the DNA sequence), encoding all genetic instructions for an organism. The two DNA strands are held together by weak bonds between the bases. Each time a cell replicates, DNA molecule undergoes unwinding and the breakage of the bonds between the base pairs.

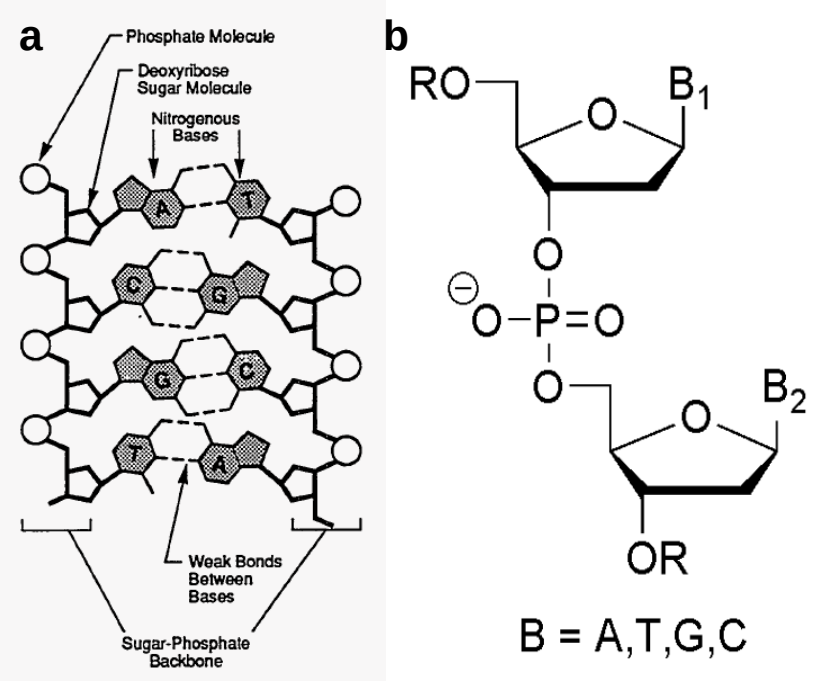

Figure I.9. Schematic structure (a) and chemical composition of DNA (b).

DNA molecules are classified into genomic linear (encountered in majority living organisms) and plasmid DNA (found mainly in bacteria). DNA molecule in bacteria cells is commonly found in the form of cyclic supercoiled double strand. One single strand scission unravels the supercoiled DNA (form I) to a relaxed open circular one (nicked, form II), while a second scission on the complementary strand, generates a linear DNA form (form III). These three DNA forms can be easily separated and quantified by gel electrophoresis (Figure I.10) allowing a simple and rapid analysis [246].

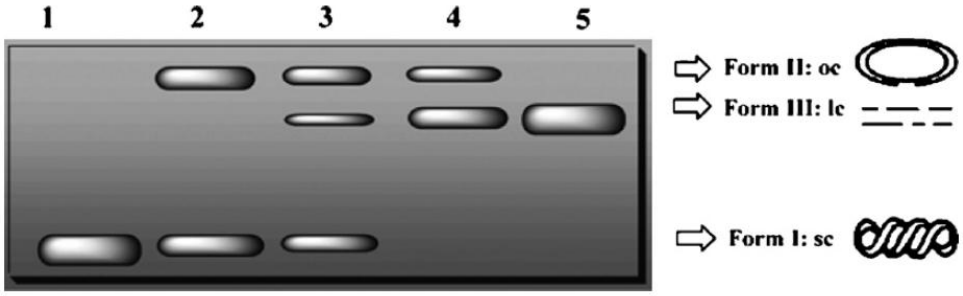

Figure I.10. Cleavage of the plasmid DNA, three form of the DNA molecule.

Due to local deviations in the sugars or the bases, DNA can isomerize into different forms. The most important forms are A-DNA, B-DNA (both right handed helices) and Z-DNA (left handed helix) (Figure I.11) [414].

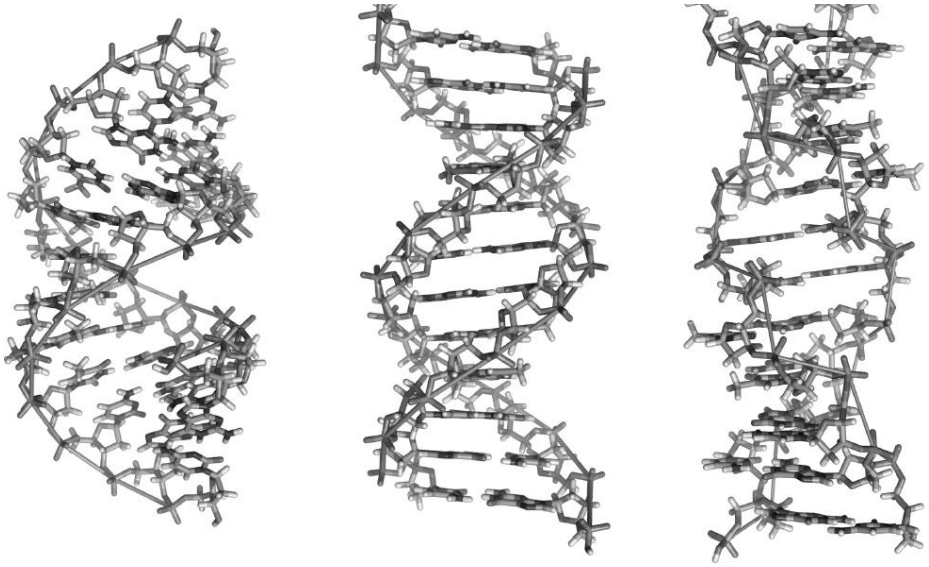

Figure I.11. Three different forms of DNA; A-DNA (left), B-DNA (center) and Z-DNA (right).

I.7.2 DNA cleavage

In all living systems from bacteria to humans, DNA cleavage is a crucial process operated by natural enzymes called hydrolases [415]. Since they are ubiquitous in a living organism, they function in all situations where partial or complete digestion of nucleic acid is required. This is the case of not only degradation and senescence but also replication and recombination[21]. Nucleases that break the phosphodiester bond within a polynucleotide chain are named endonucleases, and those that cut at the end of the chain bear the name of exonucleases. This type of cleavage, where the phosphodiester bond undergoes scission, is recognized as the DNA hydrolysis and is encoded in the program of every living cell. The other two types are oxidative and photocleavage. In both cases reactive oxygen species (ROS) are responsible for DNA damage. Similar reduced oxygen species that are generated as reactive intermediates make photochemical and oxidative DNA cleavage almost undistinguishable. However, ROS can originate from completely different sources. Development of artificial nucleases has shown that most of them cleave DNA molecule mainly via an oxidative mechanism [416].

I.7.2.1 Hydrolytic cleavage

The phosphodiester bonds in biopolymers are cleaved in a base-specific manner by the type II restriction endonucleases, which are considered to be the best studied of the nucleases to date as to both their in vivo role and their use as tools in the techniques of molecular biology. However, the role of their metal centres, particularly Zn^{II}, Mg^{II} and Fe^{II}, in natural hydrolases is yet to be elucidated. This is one of the reasons why synthetic metallohydrolases are important to study [247]. The interest in designing synthetic systems capable of reproducing the effective activity of natural hydrolases is stimulated by the possibility of providing useful alternatives to the restriction enzymes currently used as laboratory tools in biotechnology and molecular biology.

[21] To date, evidence for the involvement of nucleases in the replication and recombination processes in eukaryotes is chiefly circumstantial.

Phosphate esters bonds in DNA molecule are remarkably resistant towards hydrolysis[22] [417], nevertheless, natural nucleases are able to cleave them very efficiently with impressive rate acceleration [264]. A nucleophilic attack at the DNA phosphate backbone is the generally accepted mechanism of the DNA hydrolysis reaction, resulting into formation of a five coordinate intermediate (Figure I.12), which can be stabilized by the catalyst. Subsequent cleavage of either the 3'-PO, typical in enzymatic systems, or the 5'-PO results in a strand scission.

The presence of the metal ions, acting as Lewis acids, always favours the breakage of the phosphodiester bonds by 1) activating water or hydroxide as nucleophile; 2) activating phosphate group towards nucleophilic attack; and 3) increasing the leaving group ability of the departing alcohol (Figure I.12) [247,298,418-420].

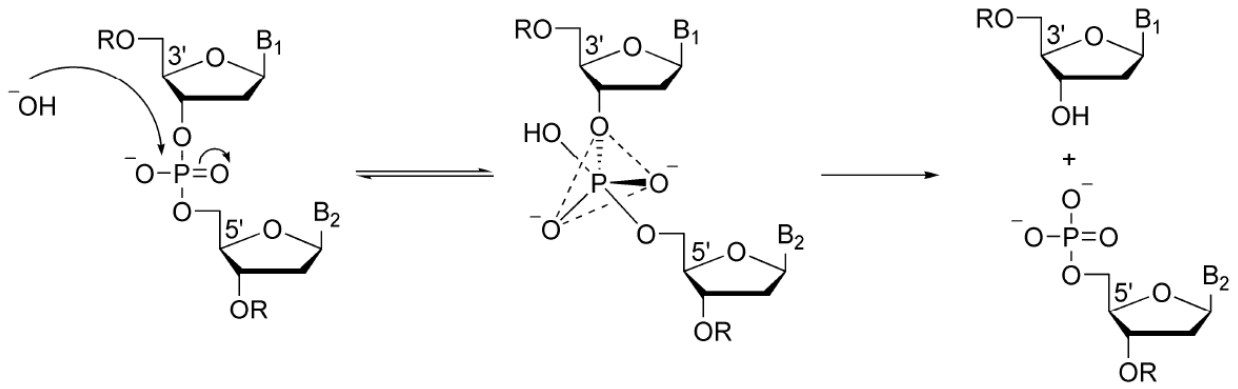

Figure I.12. Reaction mechanism of the DNA hydrolysis by natural enzymes [416]. The scission is shown via activation of water or hydroxide as nucleophile (left), activation the phosphate group to facilitate nucleophilic attack (centre) or increment of the leaving group ability of the departing alcohol (right).

[22] The half-life for hydrolysis of phosphodiester bond in DNA at physiological conditions (pH 7 and 25 ºC) has been estimated to be 130 000 years [247]. This peculiarity makes it difficult to perform any mechanistic tests using DNA as a substrate.

Many natural enzymes such as phosphatases[23], nucleases or topoisomerases that are capable of catalysing the hydrolysis reaction of a phosphate bond, act via a similar mechanism.

I.7.2.2 Oxidative cleavage

Since DNA cleavage under physiological conditions is practically inert toward P–O hydrolytic cleavage, spontaneous DNA degradation occurs mainly through different pathways, involving C–O cleavage, nucleobase ring opening or radical attack which means an oxidative type of cleavage. Numerous amount of reviews have been published on this topic [139,421-433].

Oxidative DNA damage is involved in diverse biological phenomena and consists of several kinds of lesions, mainly, strand breaks, base modifications, and DNA-protein crosslinking. However, little is known about the existence of a chemical relationship among them or the ratio by which these different types of lesions are produced.

The oxidation of DNA and its components takes place in the presence of reactive oxygen, nitrogen, or chlorine species (ROS/RNS/RCS) such as hydrogen peroxide (H_2O_2), hypochlorous acid (HOCl), hydroxyl radical ($^{\bullet}OH$), superoxide ($^{\bullet}O_2^-$) , singlet oxygen ($^1O_2$), nitryl chloride (NO_2Cl), peroxynitrite ($ONOO^-$), nitrous acid (HNO_2) [423]. They are generated in vivo by various exogenous and endogenous mechanisms such as aerobic metabolism, mitochondria, peroxisomes, cytochromes P450, xanthine oxidase, the neutrophil respiratory burst, other phagocytes, and hypoxia reperfusion injury, xenobiotics, ionizing radiation, UV irradiation, ultrasonication etc. [429]. ROS normally exist in all aerobic cells in balance with biochemical antioxidants. Oxidative stress occurs when this critical equilibrium is disrupted because of excess ROS, antioxidants depletion, or both. This leads to a damage of nucleic acids (variety of DNA lesions including chemical modification of both purine and pyrimidine bases), proteins and lipids [427].

[23] The role of phosphatases is to remove a phosphate group from its substrate by hydrolysing phosphoric acid monoesters into a phosphate ion and a molecule with a free hydroxyl group. Nucleases, including restriction enzymes, protect a cell against virus infection by cleavage of the foreign DNA or by degrading cellular DNA during apoptosis (programmed cell suicide) of the affected cell. Topoisomerases resolve topological problems of DNA in replication, transcription and other cellular transactions by cleaving one or both strands of the DNA

Numerous types of ROS can be formed by all body tissues [427]. Oxygen itself is, thermodynamically, a potent oxidizing agent [423]. The most common oxygen centered free radicals are as $^{\bullet}OH$, $^{\bullet}O_2^-$, H_2O_2 and $^1O_2$ [430,432]. An attack of these different species on DNA can be distinguished by the pattern of damage that is caused to the other DNA bases. For instance, $^{\bullet}OH$ produces a multiplicity of products from all four DNA bases, whereas singlet oxygen is selective for guanine, the most oxidisable base in DNA [434,435], in fact, 8-hydroxyguanine is the most widely used ‘‘marker’’ for oxidative DNA damage [436].

The **hydroxyl radical** is a highly reactive species that can cause non-enzymatic scission of DNA. Hydroxyl radical is short-lived, but the most damaging radical within the body. It is thought to be generated within cells and tissues where it can attack proteins, lipids, and DNA, thus initiating secondary radical reactions that can produce irreparable cellular damage. This type of free radical can be formed from $^{\bullet}O_2^-$ and H_2O_2 via the Harber-Weiss reaction [437]. The reaction is very slow and is catalysed by iron. The first step of the catalytic cycle involves reduction of ferric ion to ferrous:

$$Fe^{3+} + {}^{\bullet}O_2^- \rightarrow Fe^{2+} + O_2$$

The second step is the Fenton reaction:

$$Fe^{2+} + H_2O_2 \rightarrow Fe^{3+} + OH^- + {}^{\bullet}OH$$

$$^{\bullet}O_2^- + H_2O_2 \rightarrow {}^{\bullet}OH + OH^- + O_2$$

The interaction of iron with H_2O_2 produces $^{\bullet}OH$ as first observed by Fenton and described in 1894 [438]. These reactions are significant as the substrates are found within the body and could easily interact [462].

Superoxide anions are formed when molecular oxygen (O_2) acquires an additional electron, leaving the molecule with only one unpaired electron. Within the mitochondria $^{\bullet}O_2^-$ is being formed continuously. The rate of formation depends on the amount of oxygen flowing through the mitochondria at any given time and the presence of

exogenous components (redox cycling compounds) [439,440]. While superoxide radical can be directly toxic [441], in the presence of lipids it has a limited reactivity, raising a question about its true toxicity. Thus, its action is frequently considered to result from a secondary production of the more reactive $^{\bullet}OH$ species by the iron-catalyzed Haber-Weiss reaction. As that production may be limited *in vivo*, it was proposed that nitric oxide reacting with $^{\bullet}O_2^-$ generates secondary cytotoxic species (peroxinitrite anion). Superoxide is often cited as the species responsible for the toxicity of oxygen [442].

The **hydrogen peroxide** is produced in vivo by many reactions, mainly by enzymatic ones. Corresponding enzymes are located in microsomes, peroxysomes and mitochondria. In plant and animal cells, superoxide dismutase is able to produce H_2O_2 by dismutation of $^{\bullet}O_2^-$, thus contributing to the lowering of oxidative reactions [421]. The natural combination of dismutase and catalase shows a true cellular antioxidant activity by contributing the removal of H_2O_2 which is also able to diffuse easily through cellular membranes. Interestingly, H_2O_2 is unique in that it can be converted to the highly damaging hydroxyl radical or be catalysed and excreted harmlessly as water. H_2O_2 is converted to water during the conversion of glutathione to oxidized glutathione by glutathione peroxidase. If H_2O_2 is not converted into water $^1O_2$ is formed.

The **singlet oxygen** is not a true radical but can be formed during radical reactions and also cause further reactions acting as a catalyst for free radical formation. It is reported to be an important ROS especially in reactions related to UV exposition [443,444,445].

Another type of radical that has been often mentioned in the past few decades is **"crypto-OH"** radical, so-called "non-free" radical [384,446]. Though the oxygen species formed by "crypto-OH" radicals are assumed to mimic those of $^{\bullet}OH$-radicals, their reactions differ since "crypto-OH radical" is expected to form under oxygen limited conditions. This type of radicals was found to resist the inhibition by traditional $^{\bullet}OH$ radical scavengers [446,447]. Interestingly, many studies on generation of free radicals carried out in phosphate buffer, which is a medium widely used in physiological reaction systems, obtained results that indicate the formation of "crypto-OH radical" rather than of common $^{\bullet}OH$ radical [448-452].

As in the hydrolysis of DNA, the contribution of metal ions is very significant for the oxidative cleavage. Due to the ability to participate in one-electron transfer reactions redox-active metal ions favour the generation of ROS. These metals are most of transition metals. Some of them are found at the active sites of most oxidases and oxygenases, again due to their ability to accept and donate single electrons [453].

Fe(II)\(III) and Cu(I)\(II) are the most common transition metal ions that suggested to mediate oxidative damage of DNA via activating ROS and RNS [454-459]. These deleterious species are believed to be generated from the less damaging reactive oxygen species - superoxide radical anion and hydrogen peroxide - in a Fenton reaction catalyzed by iron(II) or cuprous ions (Fenton-like reaction). Interestingly, generation of ROS and RNS is suggested to be the unifying factor in determining the toxicity and carcinogenicity of metals such as Fe, Cu, Cr, V, Cd, Hg and Ni. The first four metals, i.e., Fe, Cu, Cr and V, undergo redox-cycling reactions, while Cd, Hg and Ni, as well as Pb, deplete glutathione and protein-bound sulfhydryl groups [431,453]. Mixtures of two or five metal ions, Fe^{II}, Cd^{II}, Ni^{II}, Cr^{III}, Cu^{II}, results into formation of 8-hydroxy-deoxyguanosine and strand breaks in DNA by Fenton-type reactions [460].
Common mechanisms involving the Fenton reaction, generation of the superoxide radical and the hydroxyl radical appear to be also involved for chromium, vanadium and cobalt and are primarily associated with mitochondria, microsomes and peroxisomes. However, for the Fenton reaction to occur *in vivo* enough of 'catalytic' metal should be present. As reported by Halliwell and Gutteridge [432,461], despite of high content of iron in body fluids, particularly blood, there is no 'free' iron is available *in vivo* that would be capable of promoting Fenton chemistry as efficiently as *in vitro*, unless iron ions remain unabsorbed after some extra supplementation or in the special case of iron overload. [383]. Therefore, iron, being a powerful promoter of free-radicals reaction in vitro [462], may not be as powerful in *in vivo* environment, where it and especially other catalytic metal ions seem to be available only to a very limited extent [463]. This means that the importance of the Fenton reaction has been proven under *in vitro* conditions, but not under *in vivo* conditions. On the other hand, if both H_2O_2 and copper or iron catalysts are available *in vivo*, then $^{\bullet}OH$ will be formed in biologically-significant

amounts. The question “Does the Fenton reaction actually produce $^{\bullet}$OH radicals?” had been raised repeatedly in the past few decades [432,447,464]. Despite of increasing amount of evidences ‘against’ the relevance of Fenton reaction, many scientists reported and discussed iron-dependent free-radical reactions insisting on their existence *in vivo* and considering ROS important mediators of oxidative damage [429,430,432,451,462, 465,466].

One of the most studied DNA oxidative mechanisms is by natural compound bleomycin which is used in the clinical treatment of certain cancers [457]. Its activity is thought to rely on its capability to oxidize both strands of the DNA molecule at once - direct double strand cleavage. Since bleomycin is such an effective DNA-cleaving agent which can damage the DNA of the affected cells triggering apoptosis, many research groups have made (synthetic) models of bleomycin, to study various aspects of the DNA cleavage process. Fe^{II} bleomycin system is well studied (Figure I.13) [374,467].

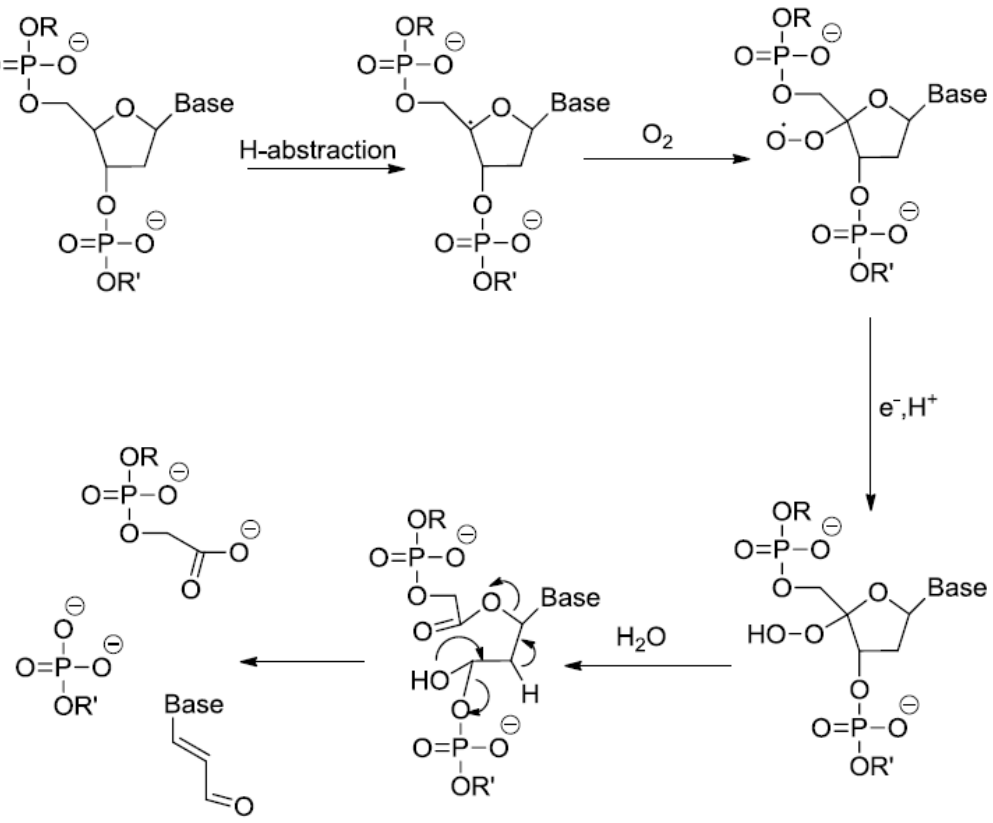

Figure I.13. Proposed mechanism of oxidative cleavage by bleomycin.

I.7.2.3 Photocleavage

Photocleavage possesses oxidative mechanism of DNA cleavage by photochemical means via 1) generation of ROS by organic compounds or metal complexes [250] and 2) direct UV-induced DNA damage, which involves a direct UV-promoted dimerization reaction between two pyrimidine residues (thymine and cytosine) to form mutagenic and cytotoxic DNA lesions [468]. It is important to emphasize that most DNA-cleaving agents are not directly responsible for the observed DNA damage but rather create labile sites for the further cleavage or more likely – generate highly reactive intermediates which affect sugars [467] or nucleobase intermediates [249]. When designing systems with photoexcitable or redox active metal centres that bind/cleave specific sites of the DNA strand, both direct (oxidation of deoxyribose residues by hydrogen abstraction or electron transfer from nucleobases to the metal ion) and

indirect mechanisms (generation of reactive species such as the hydroxyl radical or singlet oxygen mediated by the metal centre) for DNA cleavage can be included.

Photochemical DNA damage can be divided into two types (Figure I.14): a one electron process (type I) and a pathway involving singlet oxygen (type II). Both processes start with the photosensization of the DNA cleavage agent and result in the oxidation of guanine base.

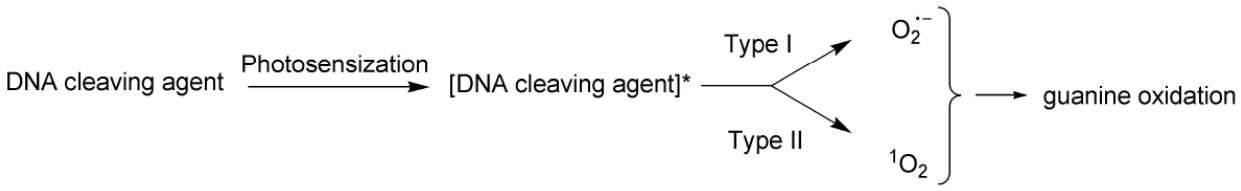

Figure I.14. Type I and II photochemical cleavage of DNA.

Chapter II

Experimental Techniques

II. Experimental techniques

In this study agarose electrophoresis was chosen as the main technique to explore DNA cleavage properties of vanadium compounds. Circular dichroism was used to study DNA-vanadium interactions. These were the only techniques where plasmid DNA was used. Other techniques such as cyclic and square wave voltammetry, UV/Vis, fluorescence and NMR spectroscopy were employed to examine vanadium solution chemistry, i.e., redox reactions, compound stability, possible vanadium species and free radicals formation under organic and inorganic buffers.

In this chapter the principles of each technique is briefly described.

II.1 Electrophoresis. Agarose gel electrophoresis (AGE)

Electrophoresis is the easiest, most popular and important molecular biological technique for both analysis and purification of nucleic acids [469]. It is the technique by which mixtures of charged macromolecules, including proteins, nucleic acids, and carbohydrates, are rapidly resolved in an electric field. When a mixture of different nucleic acids is allowed to move through a gel matrix, they can be separated on the basis of their shape and size. There are three methods of nucleic acid electrophoresis: agarose gel electrophoresis (AGE), polyacrylamide agarose gel electrophoresis (PAGE) and capillary electrophoresis (CE). Each type is suited to a particular task. The function of both agarose and polyacrylamide matrices is to provide different sized holes in the molecular sieve. Therefore, the main difference between these two techniques is the size of pores in the gel matrix, which automatically means that the DNA fragments being separated are of different size. AGE is useful for the separation of DNA fragments ranging from 50 base pair to several millions of bases, while PAGE permits conformational analysis of proteins from 5 to 2000 kDa and correspondingly sized DNA fragments. Typically, AGE is performed in a horizontal tank, whereas PAGE is run vertically. Finally, CE is an increasingly important technique, performing electrophoretic separation of biopolymers in narrow buffer-filled capillaries. CE is particularly important for protein separation because the charge of proteins at a particular pH depends on the

distribution of charged amino acid side-chains, therefore they can be separated electrophoretically in liquids. CE can also be carried out in gels as well as in liquids, but it is a difficult task to make gels in very fine capillaries. CE is a useful technique for determination of diffusion coefficients of small DNA molecules, detection of DNA-buffer interactions, and analysis of the sequence dependence of counterion binding in free solution (without sieving liquid polymers) [470].

II.1.1 Theoretical considerations

Electrophoresis is a movement of electrically charged particles or molecules in a conductive liquid medium, usually aqueous, under the influence of an electric field (Figure II.1).

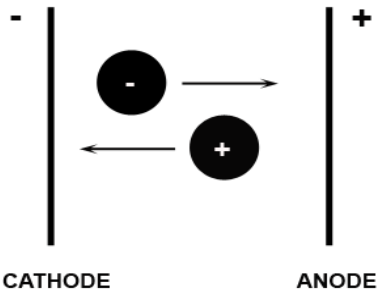

Figure II.1. Principles of separation.

When an electric field is applied to the negatively charged nucleic acid, the molecule is able to migrate through the gel matrix submerged in a conductive medium. In water, poorly conductive medium, only the few positive and negative ions that are present will move to the electrodes of opposite sign. However, in a highly conductive aqueous medium, an electrical circuit is completed. As current flows, the aqueous part of the medium is subjected to electrolysis: the generation of hydrogen gas (H_2) and alkali (OH^-) at the negative electrode (cathode), and oxygen gas (O_2) and acid (H_3O^+) at the positive electrode (anode). This phenomenon is called electrolysis of water:

$$2e^- - 2H_2O \rightarrow H_2 + 2OH^- \quad \text{(eq. II.1)}$$

At the positive electrode, electrons can be removed from water to produce oxygen gas and acid:

$$H_2O - 2e^- \rightarrow \frac{1}{2}O_2 + 2H^+ \quad \text{(eq. II.2)}$$

A molecule under an electric field is affected by the force (F) which is dependent on the net charge of the molecule (q) and the strength of the field (E/d, V·cm^{-1}) into which it is placed:

$$F_e = \frac{E}{d} \cdot q \quad \text{(eq. II.3)}$$

where
E = potential difference between the electrodes (V)
d = distance between them (cm)

Upon the movement of molecules, a frictional force is initiated that diminishes the migration of particles toward an electrode. This force is dependent on the size and shape (radius, r) of the molecule and the viscosity of the medium (η, Pa·s = kg/(s·m)), through which it passes with a certain velocity (υ, cm·s^{-1}). Therefore:

$$F_d = 6\pi r \eta \upsilon \quad \text{(eq. II.4)}$$

By combining eq. II.3 and II.4, we obtain:

$$\frac{E}{d} \cdot q = 6\pi r \eta \upsilon \quad \text{(eq. II.5)}$$

Now, when an electrical field is established, and the electrical force equals frictional force ($F_e = F_d$), the particles move with a terminal velocity that can be expressed as:

$$\upsilon = \frac{Eq}{d6\pi r\eta} \quad \text{(eq. II.6)}$$

Therefore, the velocity at which the molecule moves is proportional to the field strength and net charge and inversely proportional to the size of the molecule and the solution viscosity (stiffness of the gel). The proportionality constant is called the absolute electrophoretic mobility, μ, $cm^2V^{-1}s^{-1}$:

$$\mu = \frac{\upsilon}{E} = \frac{q}{d6\pi r\eta} \quad \text{(eq. II.7)}$$

Two fundamental parameters are important for understanding the mechanism of electrophoresis. The first one is described by Ohm's law: the voltage (E, volts) is directly proportional to the electrical current (I, amperes) and resistance (R, ohms):

$$E = I \cdot R \quad \text{(eq. II.8)}$$

The second parameter is the power (P, watts), which measures the amount of heat produced. It is directly proportional to *E* and *I* and can be expressed as:

$$P = E \cdot I \quad \text{(eq. II.9)}$$

Substitution of *E* with the product $I \cdot R$ from eq. II.8 gives the following:

$$P = I^2R \quad \text{(eq. II.10)}$$

Agarose and polyacrylamide gel matrices must be as electrically neutral as possible. Otherwise a phenomenon known as electroendosmosis (EEO) takes place. It is the mass movement of water toward the cathode, against the movement of the macromolecules, which is usually towards the anode. The mass flow of water towards

the cathode is caused by fixed negative charges in the agarose gel (sulphate and carboxyl groups on the agarose).

Agarose is a polysaccharide extracted from red algae and used for a variety of life science applications, especially in gel electrophoresis. The apparatus for conducting AGE is relatively simple: an electrophoresis chamber and power supply; gel casting trays; sample combs, around which molten agarose forms sample wells in the gel. After an agarose gel solidifies, it is placed inside the chamber filled with electrophoresis buffer, usually TBE (Tris-Borate-EDTA) or TAE (Tris-Acetate-EDTA), and covered with a transparent lid. Before samples are electrophoresed, a loading buffer should be added. This buffer consists of glycerol (30%) and bromophenol blue with xylene cyanol (0.25% each). Glycerol is important for two reasons: 1) it increases the density of a sample to prevent the dissolution in the running buffer and thus ensure its sinking into the gel pocket; 2) due to its viscosity the DNA-complex cleavage reaction is believed to be diminished or ceased. Bromophenol blue and xylene cyanol serve as tracking dyes that allow visual monitoring of migrating samples.

Another important component in AGE is ethidium bromide (EtBr). It is a fluorescent dye that intercalates between bases of nucleic acids and allows very convenient detection of DNA fragments in gels. It can be incorporated into agarose gels, or added to samples of DNA before loading to enable visualization of the fragments within the gel. As might be expected, binding of EtBr to DNA alters its mass and rigidity, and therefore its mobility. Supercoiled DNA has a lower ability to bind EtBr, therefore it is important to multiply a value obtained from form I DNA by a correction factor [393].

The separation of the molecules is achieved by the movement of negatively charged nucleic acid molecules through an agarose matrix in the formed electric field. The movement depends on the length and conformation of the molecule. The main benefit of AGE is that it can be a preparative technique as DNA can also be recovered without any harm to it at the end of the process. Agarose gel is not supposed to interact with DNA samples [471].

DNA strand breaks are quantified by measuring the transformation of the supercoiled form into nicked circular and linear forms. After the DNA is cleaved, its integrity is impaired and nucleic acid is present in the gel as fragments. The double-stranded plasmid DNA exists in a compact supercoiled conformation (Sc, I form). Upon formation of strand breaks, the supercoiled form of DNA is disrupted into the nicked circular form (Nck, single strand cleavage, II form) and the linear form (Lin, double strand cleavage, III form). If one strand is cleaved, the supercoiled form will relax to produce a nicked circular form. If both strands are cleaved, a linear form will be produced. Due to differences in shape and size, these three forms migrate with different velocities: Sc>Lin>Nck [329,460]. Three are different modes of migration: Ogston sieving, reptation, rigid rods.

Ogston sieving

When nucleic acid fragments are present in the gel as tumbling globules, Ogston sieving occurs. The probability of the passage through the matrix depends on the radius of gyration[24], meaning that molecules can pass if they possess a radius of gyration less than that of the matrix pores. On the contrary, when the radius of gyration is significantly bigger than the cross-sectional area of a pore, DNA fragments are expected not to pass, and thus to not separated.

Reptation

It is established that the electric field can deform nucleic acids, which are initially present as globules. The reptation mode is a good example since the DNA fragments start as molecules with globule-shaped conformation and switch upon electrical supply to linear-shaped molecules (coiled or helical) that enter the gel ‘end-on’, migrating in a reptile-like movement. A larger fragment will therefore migrate with lower mobility than a shorter one.

[24] The radius of gyration is the average radius of the area swept by a molecule as it undergoes random thermal tumbling.

Rigid rods

To separate larger molecules more quickly, it is necessary to increase the strength of the electric field. However, this increase influences the coiled or helical shape of DNA fragments since the high voltage stretches the molecules towards the positive electrode. The stretched molecules thus adopt a rigid, rode-like shape. On one hand, this phenomenon progresses the migration through the gel matrix. On the other hand, however, the separation of the molecules will be significantly impaired since the rigid rod structure of the nucleic acids allows them to proceed through the passage at size-dependent rates.

II.2 UV-vis spectroscopy

Spectrophotometry is a branch of spectroscopy that measures the radiant energy transmitted or reflected by a body as a function of wavelength. Ultraviolet and visible[25] (UV/Vis) spectroscopy is a routine technique in analytical chemistry for analysis of clinical samples, environmentally significant pollutants, industrial and forensic samples, and the quantitative determination of different analytes, such as transition metal ions and highly conjugated organic compounds (e.g., DNA, RNA, proteins). It is particularly useful in detecting and quantifying colourless substances in solution; the detection limit is 10^{-5}-10^{-6} mol·L^{-1}. Spectroscopic analysis is commonly carried out in solutions but solids and gases may also be studied [472,473].

Solutions of transition metal ions can be coloured (i.e., absorb visible light) because d electrons within the metal atoms can be excited from one electronic state to another. Therefore, absorption measures transitions from the ground to the excited state:

$$M(\text{ground state}) + h\upsilon \rightarrow M^{*}(\text{excited state})$$

[25] Ranges of electromagnetic spectrum: ultraviolet (UV, 200-380 nm), visible (Vis, 380-780 nm) and infrared (IR, 780-$3x10^5$ nm)

The colour of metal ion solutions is strongly affected by the presence of other species, such as certain anions or ligands. This, in turn, changes the wavelength of maximum absorption.

Molecules containing π-electrons or non-bonding electrons (n-electrons) can absorb the energy in the form of ultraviolet or visible light to excite these electrons to higher anti-bonding molecular orbitals. When light of certain intensity (I_0), at certain wavelength (λ) passes a solution of certain concentration placed into a cuvette, a part of this light will be absorbed (Figure II.2) [474].

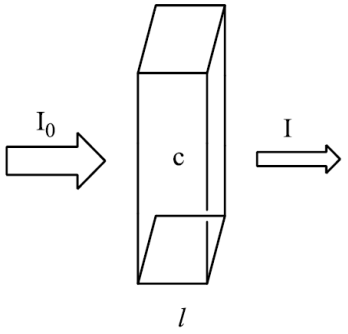

Figure II.2. Schematic representation of a beam of light (I_0) passing through an absorbing medium, in a quartz cuvette, and being absorbed (I). The intensity of light is represented by the thickness of the arrows.

The absorption or reflectance in the visible range directly affects the perceived colour of the chemicals involved. In this region of the electromagnetic spectrum, molecules undergo electronic transitions.

II.2.1 Theoretical considerations

According to the Lambert-Beer's law, the absorbance of a solution is directly proportional to the concentration of the absorbing species in the solution and the path length:

$$A = \varepsilon C l \qquad \text{(eq. II.11)}$$

where

A = absorbance

ε = extinction coefficient ($M^{-1}cm^{-1}$)

C = concentration of the analyte (M)

l = optical path length of the cuvette through which the light passes and is absorbed by the analyte (cm)

Absorbance is also expressed as:

$$A = -logI/I_0 \qquad \text{(eq. II.12)}$$

Many different types of spectrophotometers have been designed, nonetheless all have a similar assembling (Figure II.3), i.e., a light source (often Tungsten filament (300-2500 nm), a deuterium arc lamp, which is continuous over the ultraviolet region (190-400 nm), Xenon arc lamp, which is continuous from 160-2000 nm; or more recent - light emitting diodes for the visible wavelengths), a monochromator for wavelength dispersion, a sample holder, a transparent sample container (typically quartz cuvette), a light detector (typically, a photomultiplier tube, a photodiode, a photodiode array or a charge-coupled device), and a readout device for measuring output from the detector.

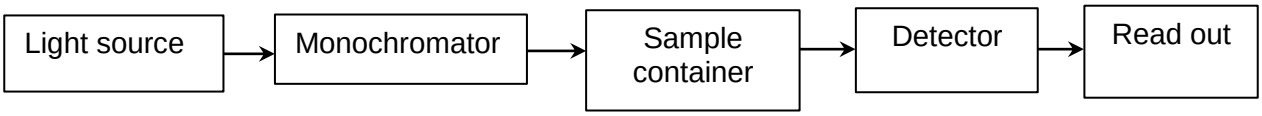

Figure II.3. The components of typical absorption elements in a spectrophotometer.

II.2.2 UV–vis spectroscopy of VC

Unlike vanadium(V), which is a diamagnetic d^0 metal, V(IV) is paramagnetic d^1 and can be conveniently studied using UV-Vis spectroscopy. A square pyramidal V(IV) complex, normally containing the VO^{2+} centre, in ideal conditions[26] [244], possesses $C_{4υ}$ symmetry (d_{xy} ground state, Figure I.7) and therefore, represents an axial system (Figure II.4). The electron can be excited into the doubly degenerate *e* level (d_{xz}, d_{yz}), the a_1 [$d(x^2-y^2)$] or the *b1* [$d(z^2)$] level, consequently giving rise to three bands.

Under realistic conditions, distortion occurs, which reduces the $C_{4υ}$ symmetry to $C_{2υ}$, (rhombic system). The degeneracy of the *e* level is lifted (Figure I.7) and four transitions can be observed. Despite the changes caused by distortion, the d-d transition model remains. A $3d^1$ metal ion electronic configuration of vanadium(IV) complexes normally give rise to three bands (Table II.1). Band I is the lowest energy band that often appear as one broad band but consequently splits in two, IA and IB. Band III is mainly covered by the intense charge-transfer (CT) bands or appears just as a shoulder on the low-energy side of the CT band. This is especially the case if a considerable π interaction between vanadium and its ligand system [9].

[26] Model of molecular orbital treatment proposed by Ballhausen and Gray for the $[VO(H_2O)_5]^{2+}$ [244].

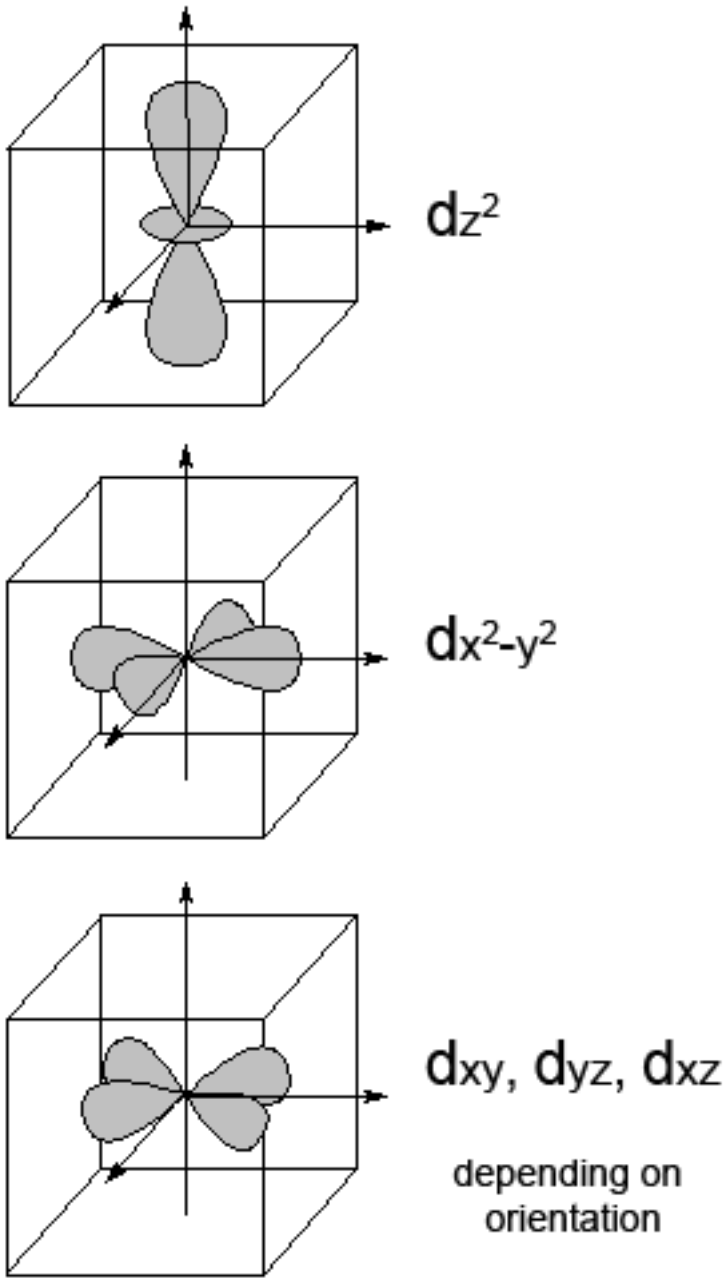

Figure II.4. The orientation of d orbitals towards the faces and edges of a cube.

Table II.1. Typical ranges of vanadium bands in UV-Vis spectroscopy.

Bands	IA	IB	II	III
C_{4v}	$b_2 \rightarrow e$ $d(xy) \rightarrow d(xz, yz)$		$b_2 \rightarrow a_1$ $d(xy) \rightarrow d(x^2 - y^2)$	$b_2 \rightarrow b_1$ $d(xy) \rightarrow d(z^2)$
C_{2v}	$a_2 \rightarrow b_1$ $d(xy) \rightarrow d(xz)$	$a_2 \rightarrow b_2$ $d(xy) \rightarrow d(yz)$	$a_2 \rightarrow a_1$ $d(xy) \rightarrow d(x^2 - y^2)$	$a_2 \rightarrow a_1$ $d(xy) \rightarrow d(z^2)$
λ, nm	900-620		690-530	480-330

II.3 Circular Dichroism

Circular dichroism (CD) occurs in a UV–Vis spectrum if there is a chiral (the one that cannot be superposed on its mirror image) element, commonly a centre of chirality, in the compound. In substances with optical activity (chiral) the left and right circularly polarized beams are traveling at different speeds and are absorbed to a different extent [9,414].

Light is an electromagnetic radiation which has an electrical and a magnetic component. These components are perpendicular to each other and to the direction of propagation of the light wave (Figure II.5). CD deals with circularly polarized light in which the electric field vectors trace out helices. Electrons of a chiral molecule, since it has no reflection plane, move in a helical manner. Hence, the interaction between a chiral molecule and left- and right-handed photons is different. Therefore, CD is the difference in absorption, *A*, of the left and right circularly polarized light of a chiral molecule (eq. II.13). “Dichroism” is used to denote direction-dependent light absorption.

$$CD = A_l - A_r \qquad \text{(eq. II.13)}$$

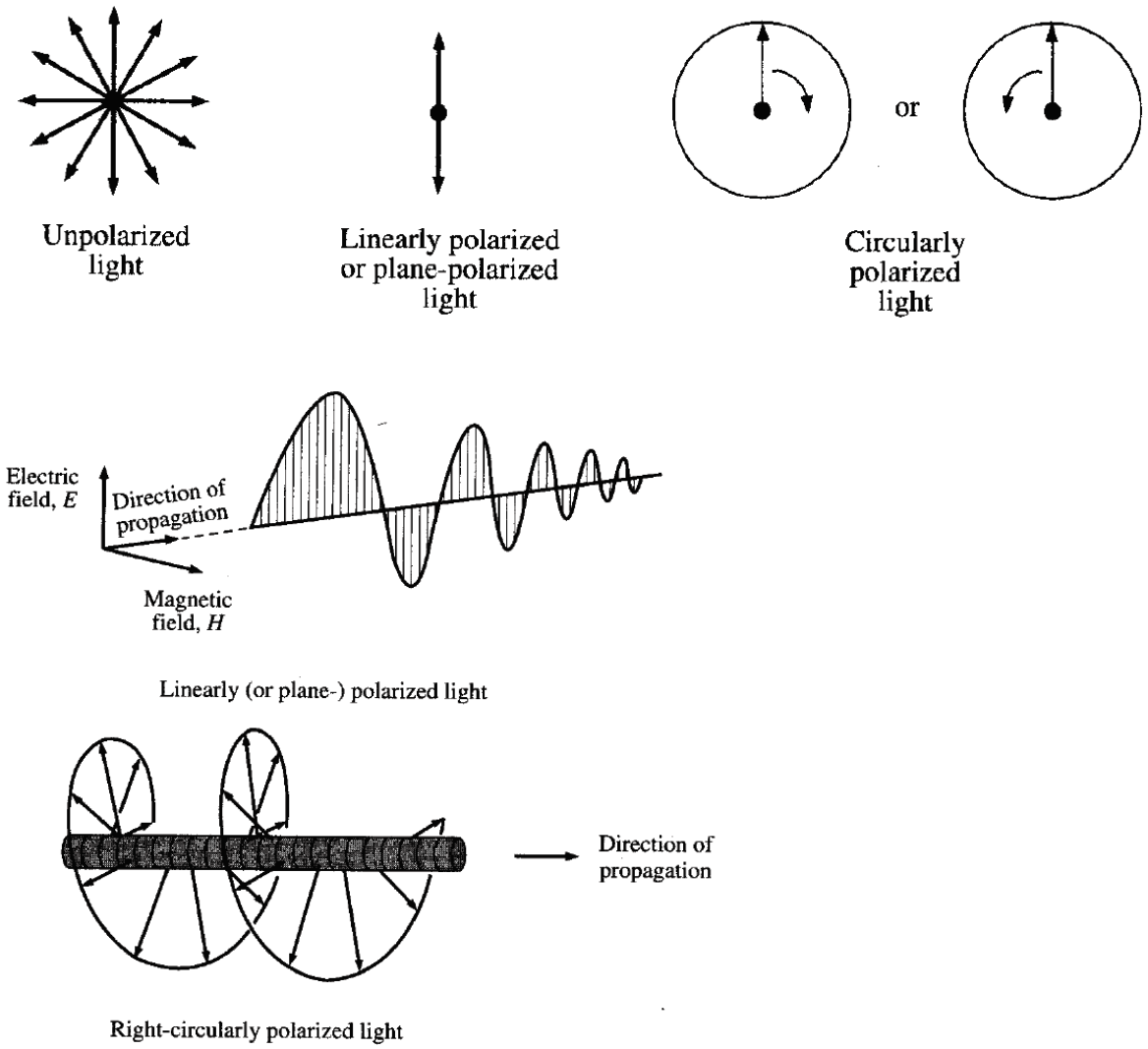

Figure II.5. Types of light polarization: linear (electric vector direction constant, magnitude varies) and circular (electric vector direction varies, magnitude constant) [414].

The difference between the molar absorption coefficients for left and right circularly polarised light, $\Delta\varepsilon = \varepsilon_L - \varepsilon_R$, is called circular dichroism. $\Delta\varepsilon$ can be calculated from the ellipticity[27] which emerges from different absorptions of the left and right hand polarized

[27] Ellipticity refers to the elliptically polarized light which is the polarization of electromagnetic radiation such that the tip of the electric field vector describes an ellipse composed of unequal contributions of right and left circular polarized light. Most CD spectropolarimeters, although they measure the changes of intensity (the true differential absorption of light), produce a CD spectrum in units of ellipticity, θ. Nowadays this unit is regarded as obsolete.

components [414]. Any chiral molecule exhibits both positive and negative CD signals. The CD version of the Lambert-Beer's law (eq. II.11):

$$A = (\Delta\varepsilon)Cl \qquad \text{(eq. II.14)}$$

CD is a very popular technique to study biological systems, much more than non-biological systems. Due to the large size of biomolecules, detailed structural analysis of their CD data is hardly possible. However, changes in the conformation of the macromolecule and its interaction with small molecules, especially achiral ones that do not solely induce CD, are successfully probed. Many advantages of CD as an instrument for high quality analysis of biomolecules have been reported [475]. Using CD, it is simple to identify the type of DNA geometry in the tested sample, i.e., A, B or Z-form (Figure I.11). Since CD spectra is easy to measure, it is often the simplest technique to use to probe DNA conformational changes as a function of a wide range of variables such as pH, ionic strength, temperature etc., and to obtain information on the effect of added ligands and solvent concentration.

Interestingly, without chirality the biochemical processes in our bodies would not function. As nucleotide molecules form the structure of DNA, they develop a twist that forms the double helix structure of DNA. It is the chirality or handedness of consisting components that gives DNA the spiral shaped helical structure. The chiral part of the DNA molecule is composed of ribose sugar units, without which the phosphate and the bases are achiral. The moment they are bonded together, the entire molecule becomes chiral and their transitions are able to produce CD spectra. Thus, the chirality of DNA molecules originates from the ribose sugar, helical structure and supercoiled (double-stranded DNA) conformation. Single-stranded DNAs are structurally less well defined than duplex DNAs and their CD signal is smaller. Measuring CD spectrum means probing the asymmetry of the system. The purine bases show a negative CD signal, whereas the pyrimidine bases have a positive one.

CD instruments, known as dichrometer or spectropolarimeter are used to obtain CD spectra (Figure II.6). The apparatus typically consists of a xenon lamp (170-1000 nm), a source of light which, when passing through the monochromator, becomes left and right

circularly polarized light, a monochromator, polariser, photoelastic modulator, emission and transition detectors. Since the CD of molecules is generally weak, a polarizer is implemented to ensure the induction of circularly polarized light. A photoelastic modulator produces alternatively left and right circularly polarized light with a switching frequency of 50 kHz, a frequency most commonly employed. This frequency becomes significant when an intensity fluctuation (different absorption of left and right circularly polarized light) appears after the light of a constant intensity passes through a sample and exhibits CD [476,477].

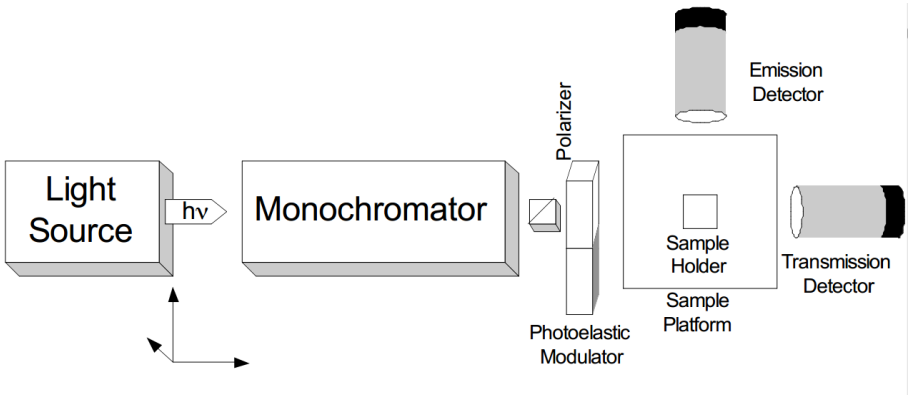

Figure II.6. Schematic representation of CD spectropolarimeter [475].

II.4 Voltammetry

In contrast to many chemical measurements, which involve homogeneous bulk solutions, electrochemical processes take place at the electrode-solution interface. The main types of electroanalytical methods include potentiometric and potentiostatic measurements. Both types require at least two electrodes (conductors) that are immersed into a sample solution (electrolyte). These components constitute an electrochemical cell. The electrode surface is thus a junction between an ionic conductor and an electronic conductor. One conductor responds to the target analyte and is thus termed the *working* electrode. The other one, the *reference* electrode, is of

constant potential, i.e., independent of the properties of the solution. Electrochemical cells are of two types, electrolytic (when they consume electricity from an external source) and galvanic (when they are used to produce electrical energy).

Voltammetry as one of the controlled-potential (potentiostatic) techniques, concerns the study of charge transfer processes at the electrode-solution interface, and is based one dynamic (non-zero-current) situations. The electrode potential here is being used to derive an electron transfer reaction and the resultant current is measured. The role of the potential is analogous to that of the wavelength in optical measurements. This parameter “forces” the chemical species to gain or lose an electron (reduction or oxidation, respectively). The resulting current reflects the rate at which electrons move across the electrode-solution interface. All potentiostatic techniques can measure any chemical species that is electroactive. i.e., that can be reduced or oxidized. Controlled-potential techniques offer a wide range of advantages, from portable low-cost instrumentation with variety of electrodes to extremely low detection limits with very small (5-20 µL) sample volumes.

II.4.1 Theoretical considerations

The objective of controlled-potential electroanalytical experiments is to obtain a current response that is related to the concentration of the target analyte. This can be accomplished by monitoring the transfer of electron(s) during the redox process of the analyte:

$$O + ne^- \rightleftharpoons R \qquad \text{(eq. II.15)}$$

where O and R are the oxidized and reduced forms, respectively, of the redox couple. This reaction will occur in a potential region that makes the electron transfer thermodynamically or kinetically stable. For systems controlled by the laws of thermodynamics, the potential of the electrode can be used to establish the concentration of the electroactive species at the surface [$C_O(0,t)$ and $C_R(0,t)$] according to the Nernst equation:

$$E = E^{\circ} + \frac{2.3R}{nF} \log \frac{C_O(0,t)}{C_R(0,t)} \qquad \text{(eq. II.16)}$$

where E^o is the standard potential for the redox reaction, R is the universal gas constant (8.314 $JK^{-1}mol^{-1}$), T is the Kelvin temperature, n is the number of electrons transferred in the reaction, and F is the Faraday constant [96487 C (coulombs)]. On the negative side of E^o, the oxidized form thus tends to be reduced, and the forward reaction (reduction) is more favourable. The current resulting from a change in oxidation state of the electroactive species is termed the faradaic current because it obeys Faraday's law, i.e., the reaction of 1 moL of substance involves a change of n x 96487 C. The resulting current-potential plot, known as the voltammogram, is a display of current signal (ordinate) versus the excitation potential (abscissa). The exact shape and magnitude of the voltammetric response is governed by the process involved in the electrode reaction. The total current is the summation of the faradaic currents for the sample and the blank solution as well as the nonfaradaic charging background current [478-480].

II.4.2 Cyclic voltammetry

Cyclic voltammetry (CV) is one of the most versatile electroanalytical techniques for the study of electroactive species. It allows rapid observation of redox behaviour over a wide potential range. CV involves the cycling of the potential of an electrode, which is immersed in an unstirred solution, and measuring the resulting current. The controlling potential applied across these two electrodes is an excitation signal. For CV, the excitation signal is a linear potential scan with a triangular waveform (Figure II.7). A cyclic voltammogram is obtained by measuring the current at the working electrode (often DME – dropping mercury electrode) during the potential scan. The voltammogram is a display of current versus potential (Figure II.8). In CV, a potentiostat applies a potential to the electrochemical cell and a current to a voltage converter which measures the resulting current. The current is displayed on a recorder as a function of the applied potential.

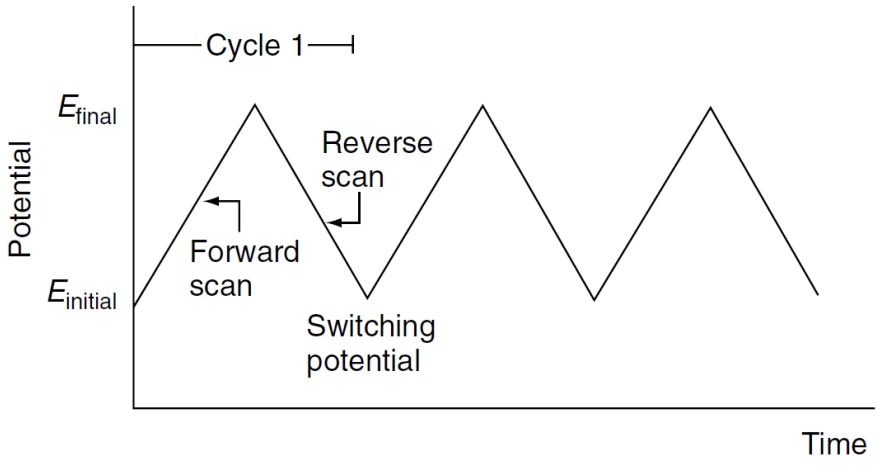

Figure II.7. Potential time excitation signal in a cyclic voltammetric experiment [478].

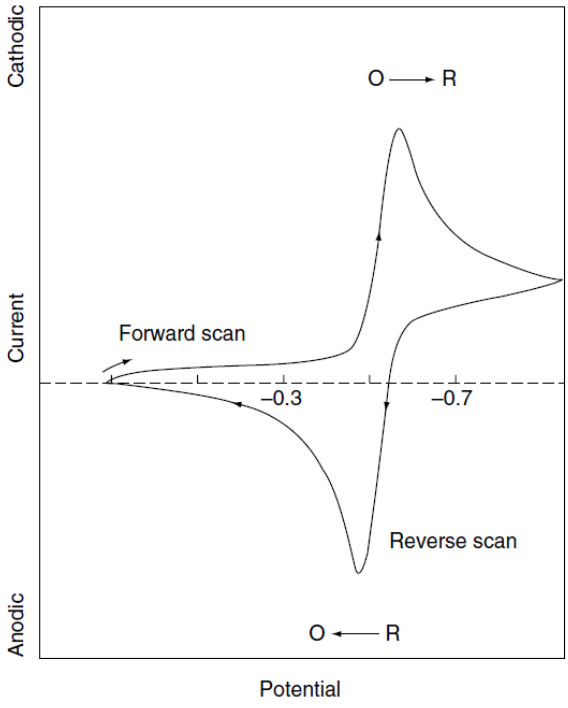

Figure II.8. Typical cyclic voltammogram for a reversible $O+ne^- \rightleftharpoons R$ redox process [478].

The utility of CV is highly dependent on the analyte being studied. The analyte has to be redox active within the experimental potential window. It is also highly desirable for the analyte to display a reversible wave. A reversible wave is obtained when an analyte is

reduced or oxidized on a forward scan and is then re-oxidized or re-reduced in a predictable way on the return scan as shown in Figure II.8. Even reversible couples contain polarization overpotential and thus display a hysteresis between absolute potential and the reduction (cathodic peak, E_{pc}) and oxidation peaks (anodic peak, E_{pa}). This overpotential emerges from a combination of analyte diffusion rates and the intrinsic activation barrier of transferring electrons from an electrode to analyte. Reversible couples will display a ratio of the peak currents passed at reduction (i_{pc}) and oxidation (i_{pa}) that is near unity (1 = i_{pa}/i_{pc}). Accordingly, when i_{pa}/i_{pc} is less than or greater than 1, voltammograms are quasi-reversible or non-reversible [481].

The method uses a working electrode in conjugation with an auxiliary electrode and reference electrode as a three-electrode system (Figure II.9). The working electrode is the one on which the reaction of interest occurs. The auxiliary electrode, often referred to as counter electrode, is the one in which an electrical current is expected to flow. Finally, the reference electrode is an electrode that has a stable and well-known electrode potential. Electrolyte is usually added to the test solution to ensure sufficient conductivity. The combination of the solvent, electrolyte and specific working electrode material determines the range of the potential. Electrodes are static and stay in unstirred solutions during CV. This "still" solution method results in cyclic voltammetry's characteristic diffusion controlled peaks. This method also allows a portion of the analyte to remain after reduction or oxidation where it may display further redox activity. Stirring the solution between CV scans is important for supplying the electrode surface with fresh analyte for each new experiment. The solubility of an analyte can change drastically with its overall charge. Since cyclic voltammetry usually alters the charge of the analyte, it is common for reduced or oxidized analyte to precipitate out onto the electrode. This layering of analyte can insulate the electrode surface, display its own redox activity in subsequent scans, or at the very least alter the electrode surface. For this and other reasons it is often necessary to clean electrodes between scans. DME[28],

[28] DME is a working electrode made of mercury. Like other electrodes this electrode is often used in electrochemical experiments. A flow of mercury passes through an insulating capillary producing a droplet which grows from the end of the capillary in reproducible way. Each droplet grows until it reaches a diameter of about a millimeter and then is releases into the analyte. As the electrode is used mercury collects in the bottom of the cell. Each released drop is immediately followed by the formation of another drop. The drops are generally produced at a rate of about 0.2 Hz. In addition, the drops growth causes capacitive current and faradaic current.

however, does not need to be cleaned or polished due to the self-renewing mercury droplets which have a smooth and uncontaminated surface free from any adsorbed analyte or impurity.

Common working electrodes can consists of inert metals such as gold, silver or platinum, or inert carbon such as glassy carbon or pyrolytic carbon, DME and film electrodes. A regular working electrode has a radius within an order of magnitude of 1 mm. Having a controlled surface area with a defined shape is important for interpreting CV results. To run CV experiments at high scan rates a regular working electrode is insufficient. High scan rates create peaks with large currents and increased resistances which result in distortions. Ultramicroelectrodes can be used to minimize the current and resistance.

The counter electrode, also known as the auxiliary or second electrode, can be of any material that conducts easily and does not react with the bulk solution. Reactions occurring at the counter electrode surface are unimportant as long as it continues to conduct current well. To maintain the observed current, the counter electrode will often oxidize or reduce the solvent or bulk electrolyte.

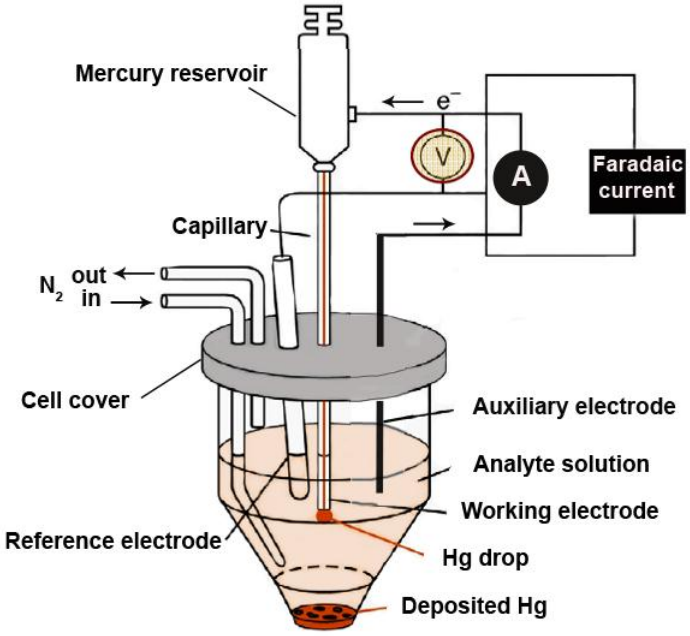

Figure II.9. Schematic diagram of an electrochemical cell with a three-electrode setup.

II.4.3 Square wave voltammetry

Like cyclic voltammetry, square wave voltammetry (SWV) is a derivative of linear sweep chronoamperometry technique, often referred as linear sweep voltammetry. However, more specifically, SWV is considered to be an improvement of staircase voltammetry. In SWV experiments the same three-electrode setup is employed. The current at the working electrode is measured while a waveform composed of a symmetric square wave is superimposed on the potential staircase sweep (Figure II.10). Oxidation or reduction of species is registered as a peak or trough in the current signal at the potential at which the species begins to be oxidized or reduced. In staircase voltammetry the potential sweep represents a series of stair steps. The current is measured at the end of each potential change, right before the next, so that the contribution to the current signal from the capacitive charging current is minimized. The differential current is then plotted as a function of potential, and the reduction or oxidation of species is measured as a peak or trough (Figure II.11) [478,482].

Since the SWV waveform diminishes the capacitance current, the detection limits of this technique are at concentrations as low as 10 nM [483]. Broader dynamic range and higher speed are an advantage of SWV over CV. Frequencies of 1-100 cycles per second permit the use of extremely fast potential scan rates due to which the entire voltammogram is recorded on a single mercury droplet.

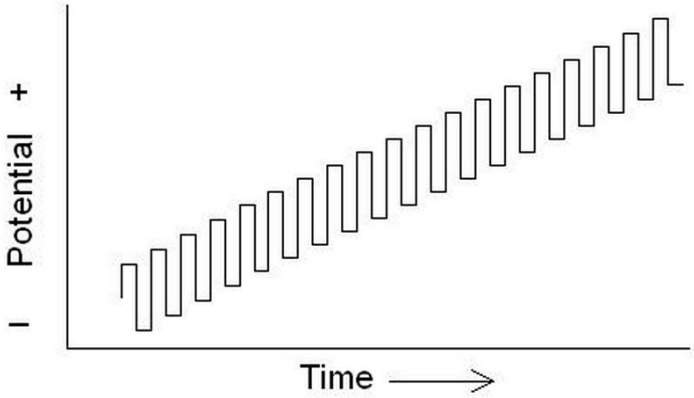

Figure II.10. Square-wave waveform potential sweep [480].

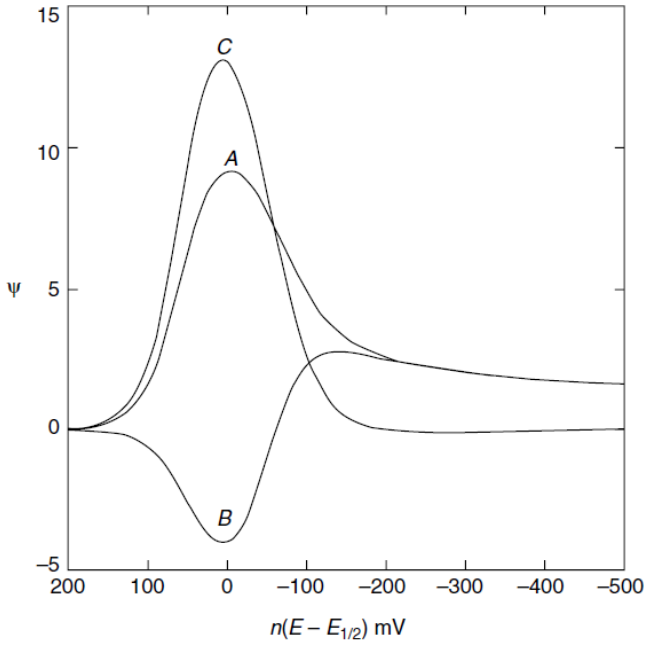

Figure II.11. Square-wave voltammograms for reversible electron transfer: Forward (A), reverse (B) and net (C) are three SWV currents.

II.5 Fluorescence spectroscopy

In this work we used fluorimetry, a highly sensitive technique for studying ROS, to analyse reaction mixtures of $VO(acac)_2$ with terephthalic acid (TPA) under phosphate and MOPS buffers. Hydroxylated aromatic compounds are often used to detect OH radicals. The use of terephthalate has been extensively reported for the detection of hydroxyl radicals *in vitro* [484-488] and *in vivo* studies [489,490,491]. Unlike other dosimeters, e.g. salicylate and benzoate [455,492-494], used to detect •OH, the hydroxylation of terephthalic acid (TPA) yields only one product, i.e., 2-hydroxyl-terephtalate (HTPA), which has a strong fluorescent emission around 435 nm when excited at 323 nm. Moreover, the efficiency of HTPA is at least three times higher than that of salicylate and benzoate [484]. The reaction is very sensitive and the detection limit of HTPA is as low as 0.5 nM [433].

In contrast to absorption, which measures transitions from the ground state to the excited state, fluorescence deals with transitions from the excited state to the ground state. The significant advantages of fluorescence over absorption spectroscopy are 1) the ability to separate compounds on the basis of either their excitation or emission spectra, as opposed to a single spectra in UV-Vis; 2) low signal to noise, since emitted light is read at right angles to the exciting light; 3) high-sensitivity detection, i.e., fluorescence sensitivity is approximately a thousand times greater than in absorption spectrophotometric methods; 4) micromolar levels of concentration can be used. A major disadvantage of fluorescence is the sensitivity of fluorescence intensity to fluctuations in pH and temperature [473].

Fluorescence occurs when a molecule absorbs photons in the UV/Vis light spectrum (200-900 nm) and shifts to a high-energy electronic state, known as excitation, and then emits photons as it returns to the ground-state orbital. The lifetime of the fluorescence, which is the average time between its excitation and its return to the ground-state, less

than 10^{-9} sec, is affected by temperature, pressure, quenchers[29], and the different type of matrices used.

Fluorimetry characterizes the relationship between absorbed and emitted photons at specific wavelengths. Emitted energy is less than the exciting energy; correspondingly, the emission wavelength is always longer than the excitation wavelength. This difference is due to the loss of energy through heat or vibration. Fluorescent compounds or fluorophores, commonly aromatic molecules, can be identified and quantified on the basis of their excitation and emission properties [495]. Spectral data are generally presented as emission spectra. A fluorescence emission spectrum is a plot of the fluorescence intensity versus wavelength.

Once a molecule has absorbed energy in the form of electromagnetic radiation, there are a number of routes by which it can return to the ground state (the statistically most common energy state for room temperature chemical species). A Jabłoński diagram shows a few of these processes. (Figure II.12). The singlet ground, first, second and *n* electronic states are respectively depicted by S_0, S_1, S_2 and S_n. When the light is absorbed, several processes occur: 1) a fluorophore is usually excited to some higher vibrational level of S_2 to possibly S_n (photon absorption, A); 2) molecules in condensed phases rapidly relax to the lowest vibrational level of S_1. This process is termed internal conversion (IC, represented by zigzag arrow), typical lifetime is 10^{-12} s or less; 3) return to the ground state which results into fluorescence emission (F) and occurring on the way from the lowest-energy vibrational state of S_1 (thermally equilibrated excited state) to the ground state of S_0. Typically, the emission spectrum is a mirror image of the absorption spectrum of the $S_0 \rightarrow S_1$ transition. This implies that the spacing of the vibrational energy levels of the excited states is similar to that of the ground state.

From the S_1 level molecules can undergo a spin conversion to the second triplet state, T_2 via intersystem crossing (ISC). When the $S_1 \rightarrow T_2$ conversion occurs, molecules

[29] Quenching is a decrease in the fluorescence intensity. Quenching can occur by a variety of processes. Fluorescent compounds can form nonfluorescent complexes with quenchers. This type of quenching occurs in the ground state and is considered to be a static one. Another type of quenching occurs via molecular collisions when the excited-state fluorophore is deactivated upon contact with some other molecules in solution or air. Among a variety of molecule-quenchers are examples of oxygen, halogens, amines, acrylamide etc. Molecular oxygen is a good example.If a fluorophore in the excited state collides with O_2, the former returns to the ground state without emission of a photon, i.e. fluorescence does not occur.

undergo $T_2 \rightarrow T_1$ IC, followed by emission from T_1. This loss of energy, when the spin state of the initial and final energy levels is different (e.g. $T_1 \rightarrow S_0$), is called phosphorescence. Since fluorescence is statistically much more likely to occur than phosphorescence for most molecules, the lifetimes of fluorescent states are very short (10^{-5} to 10^{-8} seconds) and phosphorescence somewhat longer (from 10^{-4} seconds to minutes or even hours) [473].

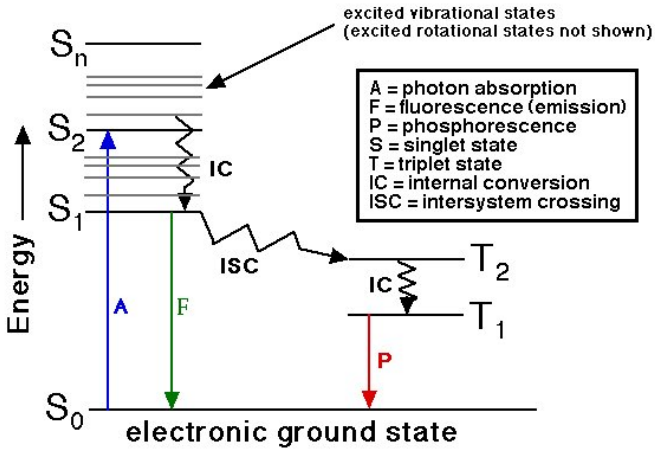

Figure II.12. One form of Jabłoński diagram illustrating the absorption and the emission processes. The singlet ground state, first, and second electronic states are depicted by S_0, S_1, and S_2, respectively.

The three basic elements of any fluorescence-detecting instrument are a source of light, sample holder and detector. The spectrofluorometer (Figure II.13) consists of a light source, usually mercury or xenon, two monochromators for operating with the emission and excitation wavelength, a sample chamber equipped with working and reference cells, photomultiplier tubes as detector and appropriate electronic devices for quantifying the fluorescence [495].

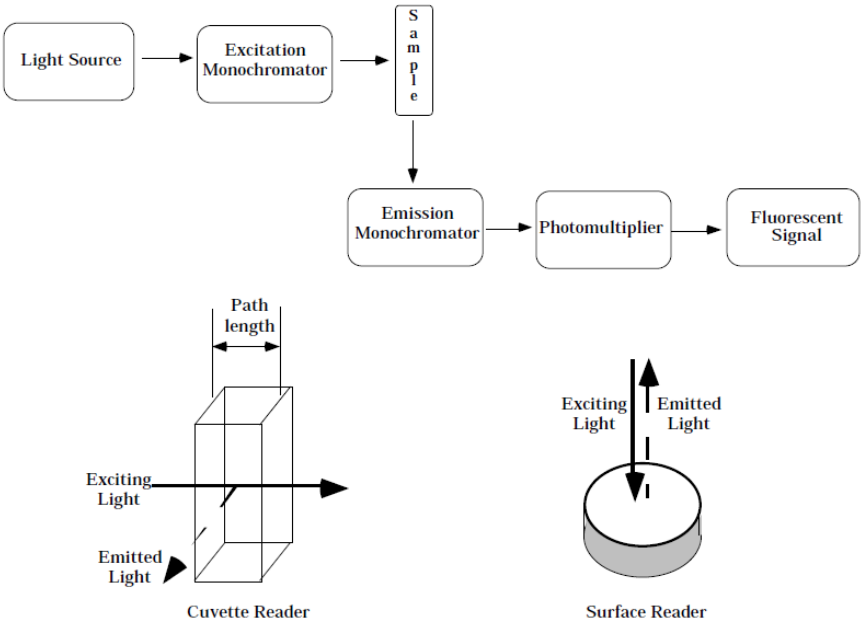

Figure II.13. Schematic illustration of a spectrofluorometer.

II.6 Nuclear magnetic resonance spectroscopy (NMR)

In any form of spectroscopy, depending on the case, an electromagnetic field excites the molecules, atoms, electrons, or nuclei from the lower energy level to the upper one followed by the reversing transition (i.e., from excited to ground state). The intensity of the spectroscopic transition is determined by the difference in population of the two levels. In nuclear magnetic resonance (NMR) spectroscopy, where the upward transitions outnumber the downward ones by only one in 10^4 - 10^6, it is as if one detects only one nucleus in every 10^4 - 10^6. Unlike fluorescence spectroscopy, which allows working with micromolar level of concentration, NMR spectroscopy is effective within millimolar and molar range.

All chemical elements possess a nucleus with a mass and charge. Most nuclei have at least one naturally occurring magnetic isotope with an intrinsic angular momentum known as spin. Since spinning charge creates a magnetic field, there is a magnetic moment, μ, associated with the angular momentum. These magnetic properties of certain nuclei are exploited using NMR spectroscopy most often to seek structural

information of the molecule [473,474]. When a magnetic nucleus is placed in a magnetic field, it adopts one of a small number of allowed orientations of different energy. For example, the proton has two permitted alignments with respect to the direction of the applied field. The nuclei can be aligned either with the field direction, or opposed to it (Figure II.14). The two orientations are not equivalent, and separated by an energy ΔE, which depends on the size of the nuclear magnetic moment and the strength of the magnetic field [472]. This energy is required to change the more stable alignment to the less stable one. By applying electromagnetic radiation of frequency, υ, which causes the nuclei transition (commonly called as 'spin flip') from the lower energy level to the upper one, ΔE can be measured. The relation between ΔE and υ is called the Planck relation [496]:

$$\Delta E = h\upsilon \qquad \text{(eq. II.17)}$$

where *h* is the Planck constant which is the quantum of action in quantum mechanics.

Thus, NMR spectroscopy pursuits the measurement of ΔE, the energy required to change the alignment of magnetic nuclei in the applied magnetic field.

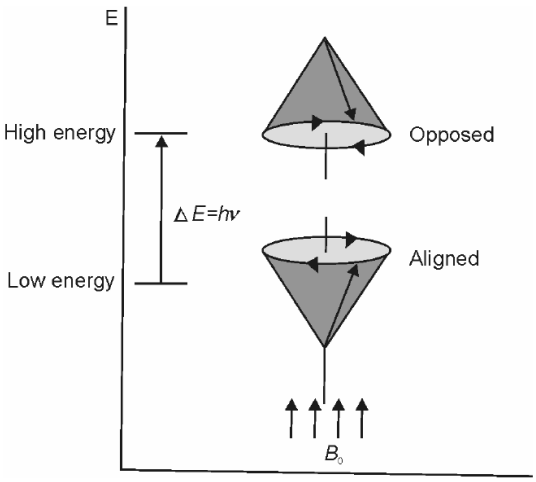

Figure II.14. Schematic illustration of possible alignment of magnetic nucleus in an applied magnetic field.

II.6.1 Theoretical considerations

When a sample is placed in an external magnetic field, the nuclear spin states come into existence; NMR active nuclei such as ^{1}H or ^{13}C absorb electromagnetic radiation at a frequency characteristic of the isotope. The NMR phenomenon is based on the nuclei that exhibit this phenomenon, their magnetic properties that make it possible, and the meaning of resonance [497,498].

Nuclei important for NMR are the ones with a fundamental property, i.e. spin. Nuclei are either spinning or nonspinning. The angular momentum of the spinning nucleus is defined in terms of spin angular momentum quantum number, *I* (spin quantum number). In the case of a nonspinning[30] nucleus, *I* = 0, whereas for the spinning one *I* = 1/2. The magnitude of spin angular momentum |I| of the spinning nucleus is quantized in units of $\hbar(=\boldsymbol{h/2\pi})$ and is related to the spin angular momentum quantum number:

$$I = \sqrt{I(I+1)}\hbar \qquad \text{(eq. II.18)}$$

where ħ is the reduced Planck constant which is the quantum of angular momentum in quantum mechanics.

The magnetic moment, μ, of a spinning nucleus is proportional to its spin angular momentum, I:

$$\mu = \frac{g_N e}{2m} I \qquad \text{(eq. II.19)}$$

where, g_N is called the nuclear g-factor which is characteristic of the particular nucleus, *e* is the charge of a proton and *m* is the mass of the proton. Altogether, $\frac{g_N e}{2m} = \gamma$, which is known as the gyromagnetic ratio.

The magnetic moment vector is in the same direction as the angular momentum vector. By substituting the value of the magnitude of spin angular momentum in eq. I.15 from

[30] Nuclei with even number of protons and neutrons have I = 0 (e.g., ^{4}He, ^{12}C and ^{16}O) and are spherical nonspinning nuclei. Nuclei with odd number of protons and neutrons have integral value of I (e.g. 1, 2) are nonspherical and thus nonspinning. Nuclei having odd value for the sum of protons and neutrons have half integral value of I (e.g., ^{1}H and ^{15}N have I =1/2 and ^{17}O has I =5/2). Spherical nonspinning nuclei have a magnetic moment, μ = 0, whereas for spherical spinning nuclei μ ≠ 0.

eq. I.16 the relationship between the magnitude of magnetic moment and spin angular momentum quantum number is expressed:

$$|\mu| = \frac{g_N e}{2m_p}\sqrt{I(I+1)}\hbar = g_N \mu_N \sqrt{I(I+1)} \qquad \text{(eq. II.20)}$$

where $\mu_N = e\frac{\hbar}{2m_p}$ is called the nuclear Bohr magneton.

Frequency (υ) and magnetic field (B) are principal in the mechanism of resonance. Resonance is the condition under which a 'spin-flip' occurs: the nuclei in the lower spin state absorb the radiation and are excited to a higher energy state [474,496]. The NMR frequency of the nucleus radiation required for a transition from the lower to the upper level is determined by its gyromagnetic ratio *γ*, and the strength *B* of the magnetic field a nucleus experiences:

$$\upsilon = \frac{\gamma}{2\pi}B \qquad \text{(eq. II.21)}$$

For the magnetic fields used in the NMR instruments, this frequency falls in the radiofrequency region of the spectrum. In other words, a suitable radiofrequency radiation can cause the transition from the lower to the upper spin state.

The resonance frequency slightly depends on the chemical environment of the nucleus in the molecule, an effect known as a chemical shift. It distinguishes, for example, the three types of hydrogen atom in ethanol[31] and, moreover, gives separately detectable signals for the hundreds of protons in a protein.

Experimentally, there are two different ways to achieve resonance: 1) varying the frequency at a fixed magnetic field strength (frequency sweep method), and 2) varying the magnetic field strength while keeping the frequency constant [496]. In both setups the different protons (nuclei) are brought into resonance one by one by continuously varying either the field or the frequency (continuous wave spectrometry). This method, being popular to about the end of 1960s, is used nowadays in some lower resolution

[31] Liquid ethanol, CH_3CH_2OH,has three different kinds of H atom which exhibit different resonance frequencies and thus give rise to three separate peaks distinguished by their integrated areas reflecting the number of protons of each type: OH, CH_2, CH_3 with corresponding ratio 1 : 2 : 3.

instruments. Most modern instruments use pulse Fourier Transform technique (Figure II.15). An FT-NMR spectrometer consists of a superconducting magnet, control console, detector and amplifier, radiofrequency detector, and a coil of wire that serves as an antenna for transmitting and receiving the radiofrequency radiation.

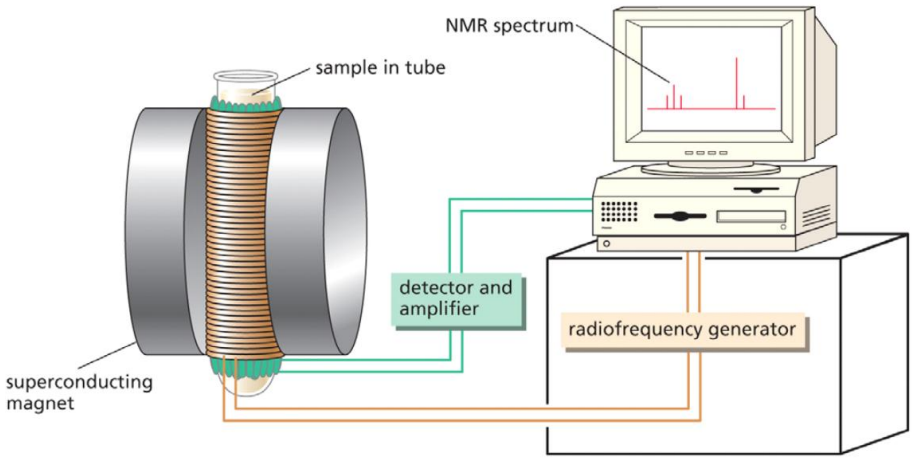

Figure II.15. Schematic illustration of an NMR spectrometer.

II.6.2 ^{51}V NMR

The aqueous speciation in some vanadium-organic ligand systems of biochemical interest can be determined by ^{51}V NMR spectroscopy. In order to be accessible to ^{51}V NMR, a vanadium compound has to be diamagnetic. This is the case for $V^{V}(d^0)$, low-spin V^{III} (d^2), low spin V^{I} (d^4), V^{-I} (d^6) and V^{-III} (d^8). In addition, dinuclear V^{IV} (d^1) centres with strong anti-ferromagnetic coupling are detectable by NMR [9].

The popularity of ^{1}H as an NMR nucleus can be explained by its large gyromagnetic ratio and high natural abundance which are favourable for maximizing ΔE. Nucleus ^{51}V is considered to be unique among the transition metal nuclei with excellent NMR properties. High natural abundance and big gyromagnetic ratio, as in the case of the proton nucleus, explain its great receptivity[32].

[32] Receptivity of ^{51}V magnetic nucleus relatively to ^{1}H is 0.38.

Nucleus ^{50}V exhibits less favourable NMR-relevant properties and therefore is not commonly employed in analytical NMR spectroscopy. NMR is a powerful tool in characterising peroxidovanadium complexes, especially ^{17}O NMR [9].

To define ^{51}V NMR chemical shifts, typically, $VOCl_3$ is used as reference. The chemical shift of $VOCl_3$ is set to zero. Due to its fast hydrolysis in moist air, the use of others, more easily manageable standards is considered. An aqueous solution of 1 M sodium metavanadate at pH 12 is sometimes employed, which contains the anions VO_4^{3-} (δ = -535.7 ppm) and $V_2O_7^{4-}$ (δ = -535.7 ppm).

As reviewed in I.2.4, V_i, the monomeric vanadate ion, in solution at millimolar and higher concentrations, under different pH, is susceptible to form oligomeric species such as V_2, V_4, V_5 and V_{10}. This is well demonstrated by the distribution diagram presented in Figure II.16.

The ^{51}V NMR chemical shifts are presented as a function of pH [9]. Pettersson's group carried out this investigation [21]. Due to the decavanadate structure which contains three structurally different vanadium atoms (two central (Va), four corner (Vb) and four capping (Vc)), three resonances with the integral ratio 1:2:2 were obtained. Except for the cyclic tetramer, c-V_4, and pentamer, V_5, the shifts depend on pH, the nuclearity and protonation state. The tetrahedral vanadates all resonate in the range −534 to −586 ppm. Concentration of ionic medium also plays a significant role, for example, at physiological pH, the tetramer is the dominant species in the medium with the highest concentration (160 mM), and the monomer dominates in the medium with lowest concentration (0.3 mM).

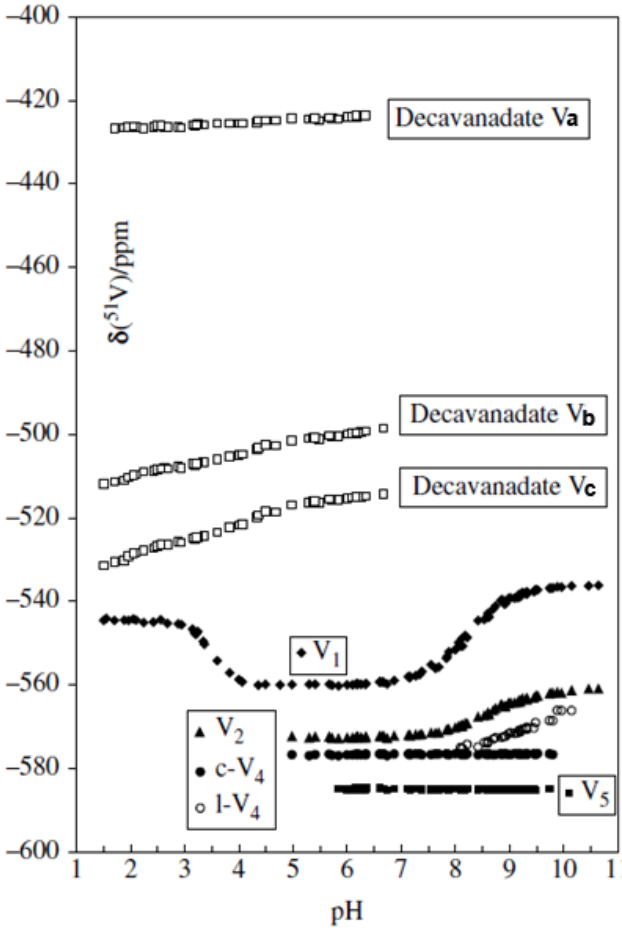

Figure II.16. ^{51}V chemical shifts as a function of pH for the H^+ - $H_2VO_4^-$ system in the range 0.3 < V < 160 mM: decavanadate (for the three vanadium sites, Va, Vb and Vc), monovanadate [V_1 = $H_xVO_4^{(3-x)-}$ and, below pH ≈ 2, VO_2^+], divanadate [V_2= $H_xV_2O_7^{(4-x)-}$], cyclic tetravanadate (c-V_4 = $V_4O_{12}^{4-}$), linear tetravanadate (*l*-V_4 = $V_4O_{13}^{6-}$) and pentavanadate ($V_5O_{15}^{5-}$) [21].

Chapter III

Experimental Part

III. Experimental Part

All studies were performed with Millipore (MilliQ®) water-purification system of conductivity <0.054 μS/cm. All chemicals used were of analytical grade.

III.1 Synthesis

***Chemicals*.** Vanadium acetylacetonate ($VO(acac)_2$, 98%, Aldrich), vanadium sulphate trihydrate ($VOSO_4 \cdot 3H_2O$, 97%, Aldrich), 2,4-pentanedione (Hacac, 99.5%, Merck), 3,5-heptanedione (Hd, 98+%, Sigma-Aldrich), 3-chloro-2,4-pentanedione (Cl-acac, 97%, Aldrich), 3-ethyl-2,4-pentanedione (Et-acac, 98%, Aldrich), 3-methyl-2,4-pentanedione (Me-acac, 85%, Aldrich), sodium metavanadate (Riedel-de Haën), sodium acetate trihydrate (99.5-100.5%, MERCK), 1,10-phenanthroline (99.5%, Riedel-de Haën) were used.

Characterization. Elemental (C, H, N) analysis was performed by Laboratório de Análises at Instituto Superior Técnico, Lisbon. Fourier transform infrared spectroscopy (FTIR) spectra in the range of 4000-400 cm^{-1} were recorded on a Jasco FT/IR-4100 spectrometer in KBr pellets.

Procedure. $VO(acac)_2$ **1**, $VOSO_4$ **9**, $Cu(acac)_2$ **15**, and $Ni(acac)_2$ **16**, are commercially available, were used without further purification. Oxidovanadium(IV) complexes **2-5** were obtained by reaction of vanadyl sulphate trihydrate with a slight excess of ligands [116,230].

$VOSO_4 \cdot 3H_2O$ (1.78 g, 8.21 mM) dissolved in water (25 mL) was placed into a water bath at 70 ºC. A 10-mL aqueous solution of sodium bicarbonate (2.30 g, 16.9 mM) was added dropwise under constant stirring (pH 4.8). This resulted in a colour change from light blue to dark blue-green. To this mixture 3,5-heptanedione (2.21 g, 17.2 mM) was added dropwise causing an immediate precipitation of green solid. The mixture was stirred at 70 ºC for 35 min and filtered upon cooling to room temperature. The green solid was washed with two 5 mL portions of water and dried under vacuum.

Oxidovanadium(V) complexes **6**-**8** were synthesized by three different published procedures [226-229].

μ-Dioxo-bis[oxo-(acetylacetonato)vanadium(V)], $V_2O_4(acac)_2$. [226,228]. To a 50-mL aqueous solution of sodium monovanadate tetrahydrate (4.8 g, 40 mM) was added 2,4-pentanedione (4 g, 40 mM). After stirring for 20 min at 50 ºC, the mixture was cooled down to room temperature and HCl was added dropwise to lower pH from 8 to 1.5. The solution immediately turned from yellow to orange and gradually, with pH decrease, became red-brown. To obtain a crystalline product, the mixture was stored at 4 ºC for 20 h, washed with water and acetone, and dried under vacuum.

Dioxo(2,4-pentanedionato(1,10-phenanthroline)vanadium(V), **$VO_2(acac)(phen)$** [227]. To a solution of **1** (0.45 g, 1.69 mM) in dichloromethane (18 mL) a solution of 1,10-phenanthroline monohydrate (2.5 mM) in the same solvent (18 mL) was added. The mixture was purged with air for 5 h. Precipitation of red-brown crystals occurred after ca. 3 h. To compensate the solution evaporation during the aeration time, dichloromethane (8 mL) was added. The crystals were filtered off, washed with diethyl ether, and dried under vacuum. Since the solid still contained dichloromethane, recrystallization from 1:1 methanol-acetylacetone mixture (v/v) was performed.

Hydroxomethoxooxo(pentane-2,4-dionato)vanadium(V), VO(OH)(OMe)(acac) [229]. A solution of $V_2O_4(acac)_2$ (0.36 g, 18.6 mM) in methanol (50 mL) was purged with nitrogen for 3 h until the volume was reduced by 50%. Obtained red-brown crystals were washed with cold methanol (3 mL) and dried under vacuum.

Complexes **10**-**14**, **22**; **17**-**19**; **20**, **21**, **23**-**27** and **28**-**36** were provided by Isabel Cavaco; Gisela Gonçalves; Susana Etcheverry and Somnath Roy, respectively.

Elemental analysis and IR spectral data.

Complex **2**: dark green solid; 74.7% yield; elemental analysis (%): calculated for $[VO(C_7H_{11}O_2)_2]$ (found): C = 52.34 (51.52); H = 6.90 (7.16). IR (KBr, cm^{-1}): 1552, 1534, 1411, 1371, 1311, 1248, 1186, 1170, 1076, 1000 (V=O), 991, 954, 861, 810, 779. Complex **3**: light green; 91.6% yield; elemental analysis (%): calculated for $[VO(C_5H_6O_2Cl)_2]$ (found): C = 35.96 (36.01); H = 3.62 (3.48). IR (KBr, cm^{-1}): 1576, 1464, 1424, 1374, 1352, 1298, 1049 (V=O) [233], 1024, 1015, 905, 703, 638, 617, 509, 469, 451. Complex **4**: green; 54% yield; elemental analysis (%): calculated for $[VO(C_7H_{11}O_2)_2]$ (found): C = 52.34 (52.19); H = 6.90 (7.12). IR (KBr, cm^{-1}): 1559, 1467, 1454, 1376, 1331, 1296, 1259, 1173, 1066, 1000 (V=O), 958, 916, 790, 780, 722, 686, 618, 490, 463, 441. Complex **5**: green; 70% yield; elemental analysis (%): calculated for $[VO(C_6H_9O_2)_2]$ (found): C = 49.16 (49.05); H = 6.19 (6.93). IR (KBr, cm^{-1}): 1563, 1481, 1429, 1337, 1300, 1178, 998 (V=O), 982, 899, 732, 660, 619, 491, 468. Complex **6**: dark brown; 61% yield; elemental analysis (%): calculated for $[V_2O_4(C_5H_7O_2)_2]$ (found): C = 31.03 (30.45); H = 3.65 (3.85). IR (KBr, cm^{-1}): 1580, 1534, 1413, 1384, 1348, 1294, 1283, 1033, 991 (V=O), 983, 949, 934, 818, 790, 775, 672, 604. Complex **7**: light brown; 72% yield; elemental analysis (%): calculated for $[VO_2(C_{17}H_{15}N_2O_2)]$ (found): C = 56.37 (48.65); H = 4.17 (3.69); N = 7.73 (6.40). IR (KBr, cm^{-1}): 1612, 1515, 1425, 1385, 1263, 1227, 1189, 1139, 1027, 945, 932, 915 (V=O), 889, 868, 852, 777, 736, 728, 703, 669. Complex **8**: light green; 64% yield; elemental analysis (%): calculated for $[VO(C_6H_{11}O_4)]$ (found): C = 33.66 (26.76); H = 5.18 (4.43). IR (KBr, cm^{-1}): 1590, 1530, 1384, 1360, 1285, 1045, 1011, 978 (V=O), 968, 757.

III.2 Nuclease activity studies

III.2.1 DNA preparation

The plasmid DNA (pDNA), used in AGE experiments, was pA1, which consists of a full-length cDNA from Cytochrome P450 CYP3A1 inserted in the pBS plasmid vector (pBluescript[33], Stratagene, UK) [499]. The pDNA was amplified in *Escherichia coli,* Mach1, and purified using Nucleobond® AX Anion Exchange Columns[34] for quick purification of nucleic acids from MACHEREY-NAGEL.

All manipulations with pDNA were always performed in MilliQ® autoclaved water.

Chemicals. Tryptone enzymatic (Fluka), yeast extract (Fluka),, $MgCl_2$, $MgSO_4$, glucose, ampicillin sodium salt (Sigma-Aldrich), sodium chloride (99.5÷100.5%, Carlo Erba), isopropanol (Panreac, 99.8%), 70% ethanol (Panreac, 99,9%), filter Whatman polyethersulfone membrane (Puradisc™ 25 AS) were used.

Instrumentation. BECKMAN Avanti™ Coulter™ Centrifuge J-251 with rotors J-14 and J-20, Eppendorf centrifuge 5418 and 5804, incubator, shaking incubator, pH meter from HANNA Instruments pH 211 with 7.0 and 4.0 pH standard solutions, autoclave machine (20 min, 121 ºC, liquid cycle), vortex were employed.

Solution preparation. Luria-Bertani (LB) medium was prepared by dissolving under constant stirring tryptone enzymatic (10 g), yeast extract (5 g) and sodium chloride (5 g) in 1 L of water and after sterilized together with 30 mL open centrifuge tubes, 1000 mL Erlenmeyer flasks and 250 mL tapped centrifuge tubes (BECKMAN).

[33] The type of plasmid, especially the size and the origin of replication (ori) has a crucial influence on DNA yield. In general, the larger the plasmid or the cloned insert is, the lower is the expected DNA yield due to a lower copy number. Plasmids based on, for example pBR322 or pACYC, cosmids or BACs are maintained at copy numbers < 20 down to even only 1, whereas vectors based on for example pUC, pBluescript or pGEM can be present in several hundred copies per cell [469].

[34] Nucleobond® is a patented silica-based anion-exchange resin, developed by MACHEREY-NAGEL. It is developed for routine separation of different classes of nucleic acids like oligonucleotides, RNA, and plasmids. NucleoBond® Xtra Silica Resin consists of hydrophilic, macroporous silica beads functionalized with MAE (methyl-amino-ethanol). The dense coating of this functional group provides a high overall positive charge density under acidic pH conditions that permits the negatively charged phosphate backbone of pDNA to bind with high specificity

Ampicillin stock (50 mg/mL) solution was prepared by Ana Luisa Ribeiro and Jorge Correia (2.5 g in 50 mL of H_2O, filter sterilized, divided into 1 mL aliquots per 1.5 mL eppendorfs, stored at -20 ºC).

LB agar solution was prepared by adding 15 g of agar to 1 L of LB, autoclaved. When this mixture had cooled down to 50 ºC, ampicillin was added to a final concentration of 50 µg/mL. Under continuous flame, 30-35 mL of the medium was poured into 85 mm petri dishes and set aside until the agar hardened.

Super optimal broth[35] with catabolite repression (SOC) was prepared by adding tryptone (2 g), yeast extract (0.5 g), NaCl (1 mL of 1 M) and KCl (0.25 mL of 1 M) to 97 mL distilled water, stirred to dissolve, autoclaved and cooled to room temperature. Then, 1 mL of 2 M Mg^{2+} stock (1 M $MgCl_2 \cdot 6H_2O$, 1 M $MgSO_4 \cdot 7H_2O$) and 1 mL of 2 M glucose stock[36] were added, each to a final concentration of 20 mM. Finally, the complete medium was filtered through a 0.2 µm filter unit.

Procedure. The preparation of pDNA involved four following steps:

1. Amplification of the pDNA
2. Growth of the bacterial culture
3. Harvest of the bacteria
4. Bacteria lysis and the pDNA purification

III.2.1.1 Amplification of the pDNA

The transformation of the competent bacteria started by thawing Mach1 cells on ice (5 min), carefully pipetting them up and down. Cells for each transformation were aliquoted (50 µL) into a 15 mL conical screw cap tubes (falcon) that had been pre-chilled on ice. To each tube was added 1 µL (50 ng) of pA1 pDNA, inverting the tubes carefully and incubating on ice for 30 min. The tubes were then submerged into 42 ºC water bath (heat shock) for 30 sec and places on ice for 2 min. Meanwhile, the SOC medium was pre-warmed at 37 ºC and added to each tube (240 µL), inverting carefully.

[35] Super optimal broth (SOB) is a nutrient-rich bacterial growth medium used for microbiological culture, generally of *Escherichia coli*. SOC is the SOB with added glucose.
[36] Mg^{2+} and glucose stock were filter-sterilized 25 mm filter with pores of 0.2 mm.

The tubes were positioned horizontally inside of the shaking incubator and left for 1 h at 37 ºC and 180 rpm (rotations per minute). Each transformation (300 µM) was plated onto petri dishes with agar-LB using an L-shaped glass spreader. The plates were left to dry and then incubated inverted overnight at 37 ºC. Cells with no plasmid were the transformation controls.

The next morning single colony was picked from agar plate with a disposable inoculating loop and transferred into a falcon tube containing 4 mL of SOC with 4 µL of ampicillin (50 mg/mL). The mixture was incubated overnight (~ 8 h) at 37 ºC and ~ 300 rpm. Into 1.5 mL sterile eppendorfs with 70% glycerol (500 µL) was added 500 µL of grown culture. The mixtures were gently pipetted up and down and immediately placed into a freezer at -78 ºC. Before starting a maxipreparation[37], typically, minipreparation was performed.

All manipulations were performed under open flame.

III.2.1.2 Growth of the bacteria culture

Bacterial cultures were typically grown from a bacteria-glycerol stock stored at -78 ºC and sometimes directly from single colony picked from an agar plate. LB broth, recommended for standard high-copy plasmids, [469,500] was always chosen as starter medium. After sterilization, the broth was cooled down to room temperature and 1 mL of ampicillin (50 mg/mL in H_2O) was added to ensure plasmid propagation.[38]

The next step was then to divide the medium in four and pour into 1000 mL Erlenmeyer flasks[39], approximately 200 mL in each. A tube with Mach1 cells was taken out from the freezer, placed on ice and left thawing for 5-10 min. Using inoculating loops, the bacteria were introduced with LB in each Erlenmeyer, which was immediately tapped

[37] Maxipreparation he starting *E. coli* culture volume is 100-200 mL of LB broth and the expected DNA yield is 500-850 µg, whereas in minipreparation DNA yield is 20-30 µg depending from the cell strain.
[38] Cell cultures should be grown under antibiotic selection. Besides a high probability of contamination in the absence of antibiotics, cells tend to lose a plasmid during cell division.
[39] Using a vessel with a volume of five times greater the volume of the medium is essential for bacteria growth since it ensures a better saturation with oxygen.

with aluminium foil. Four flasks were placed into a shaking incubator and kept overnight (10-16 h) at 37ºC and 220 rpm. Growth was observed by the increasing of the turbidity.

All manipulations with bacteria were also performed under continuous flame.

III.2.1.3 Harvest of the bacteria

The bacterial culture was tested for sufficient growth by measuring the optical density (OD_{600}) after ~ 12 h of incubation: under open flame a sample of the culture was taken from one of the flasks, diluted 1:10[40] with fresh LB. Absorbance was measured at 600 nm with two cuvettes, one contained LB (control) and the other one grown culture (working sample). Typically, flasks with the culture were kept incubating for more 2-4 h to ensure higher cell masses. However, the incubation longer than 16 h and can lead to cells overgrowing which could result into a partial degradation of pDNA or its contamination with chromosomal DNA [500].

The appropriate culture volume, important for obtaining high-copy plasmids, was selected according to the OD_{600} value (Table III.1).

Table III.1. Recommended culture volume for high-copy plasmids (adapted from 500).

NucleoBond Xtra	**Rec. ODV[41]**	**OD_{600}=2**	**OD_{600}=4**	**OD_{600}=6**	**OD_{600}=8**	**OD_{600}=10**
Maxi prep (mL)	1200	600	300	200	150	120

III.2.1.4 Plasmid DNA purification

In the Nucleobond® Xtra plasmid purification system the bacterial cells are lysed by a set of buffers based on the NAOH/SDS lysis method of Birnboim and Doly [501]. The Nucleobond® Xtra Maxi kit contains [500]:

[40] It is recommended to dilute the culture sample for a correct OD determination, especially if OD_{600} exceeds 0.5.
[41] OD volume (ODV) = OD_{600} x Vol [mL]

- RNase A[42]
- Resuspension buffer (RES)
- Lysis buffer (LYS, sodium hydroxide/SDS)
- Neutralization buffer (NEU, potassium acetate)
- Equilibration buffer (EQU)
- Washing buffer (WASH)
- Elution buffer (ELU)
- Nucleobond® Xtra Maxi Columns
- Nucleobond® Xtra Maxi Columns Filters

The OD_{600} of *E. coli* cell mass was typically 2-4, and according to the Table III.1, it corresponds to the culture volume 600-300 mL, respectively. For higher yields, the volume of the cell culture was usually increased.[43] The necessary volumes for the RES, LYS and NEU buffers were calculated based to the culture volume and OD_{600}:

Vol. [mL] = Culture Volume [mL] x OD600 / 50

For example, for 427 mL of the bacterial culture (OD_{600} = 2.81), 24 mL of each buffers were used.

After the incubation, the culture was transferred from Erlenmeyer flasks to a 250 mL tapped tubes and centrifuged for 15 min at 5524 x G and 4 ºC (rotor ID: JA-14; speed (rpm/rce): 6000). Using RES buffer (24 mL), the cell pellet was re-suspended by a slow pipetting up and down followed by addition of buffer LYS[44] (24 mL). The mixture was carefully inverted five times in order not to shear and release contaminating chromosomal DNA from cellular debris into the suspension. It was then left incubating for 5 min at room temperature. The next step was the equilibration of a Nucleobond® Xtra Column Filter inserted in a Nucleobond® Xtra Column with buffer EQU (25 mL). In the meantime, buffer NEU (24 mL) was added to the lysate, homogenized by careful inverting the tubes, after centrifuged for 10 min at 3836 x G and 4°ºC (rotor ID: JA-14;

[42] RNase A was dissolved in buffer RES, when the kit was used for the first time,
[43] Using too much cell material leads to inefficient cell lysis and precipitation, might reduce the plasmid yield and purity. Therefore, lysis buffer volumes was always increased by factor 3-5 when applying larger culture volumes.
[44] LYS buffer was always checked for precipitated SDS prior to use. In case white precipitate was visible, the buffer was warmed for several minutes at 30-40 °C until dissolved completely, cooled down to room temperature before use.

speed (rpm/rce): 5000). The cleared lysate was loaded onto the column and left filtering by gravity flow. Buffer EQU (15 mL) was applied to the rim of the filter washing out the remaining lysate. The filter was then discarded and the buffer WASH (25 mL) was applied to the column. To elute the pDNA, the buffer ELU (15 mL) was added. The eluate was collected in a 30 mL centrifuge tubes. To precipitate the eluted pDNA, isopropanol (10.5 mL) was added; the mixture was vortexed for 2 min and centrifuged for 30 min at 15000 x G and 4 ºC (rotor ID: JA-20; speed (rpm/rce): 27216). The supernatant was discarded.

After addition of ethanol (5 mL, 70%), the pellet was centrifuged for 5 min at 15000 x G and 24 ºC (rotor ID: JA-20; speed (rpm/rce): 27216). The supernatant was carefully removed by pipetting out small quantities. The pellet was left to dry at room temperature for 10 min, transferred into a sterile eppendorf with 300 µL of sterile water, and pipetted carefully up and down to homogenize.

The samples of the nucleic acids (aliquots of the cleared lysate, column flow-through, wash flow-through and eluate) collected during DNA purification were precipitated by adding isopropanol (0.7 volumes), centrifuged for 30 min at 15000 x G and 4 ºC. The pellet was washed with 70% ethanol, centrifuged for 10 min at 15000 x G and 25 ºC, dried at room temperature (10 min) and dissolved in 100 µL of sterile water. Finally, the samples (20 µL) were analysed by AGE.

Determination of plasmid yield.

The plasmid yield was determined by UV spectrophotometry at 260 nm. DNA stock solution was diluted[45] 1:1000 prior to the measurements. The concentration of pA1 pDNA was calculated from the obtained value considering that one absorbance 1 (1 cm path length) is equivalent to 50 µg DNA/mL.

[45] The absolute measured absorbance should lie between 0.1 and 0.7 in order to be in the linear part of Lambert-Beer's law. Therefore, dilution of DNA sample before UV spectrophotometric measurements is important for the accurate determination of the plasmid yield.

Plasmid quality and integrity were checked by running a 20 µL sample (18 µL of water and 2 µL of diluted to 100 µg/mL pDNA) on a 1% agarose gel in 0.5x TBE. Calculations of the pDNA recovery after the precipitation by isopropanol were based on the yield of the eluted and precipitated DNA.

III.3 Agarose gel electrophoresis

Chemicals. Trizma® base (≥99.9%, Sigma-Aldrich), phosphate buffered saline (PBS, Sigma-Aldrich)[46], agarose powder (Type I, low EEO, Sigma-Aldrich), 3-(N-morpholino)propanesulfonic acid (MOPS, 99.5%, Fluka), di-potassium hydrogen phosphate (99%, Panreac), hydrogen peroxide (30%, Panreac), 4-(2-hydroxyethyl)-1-piperazineethanesulfonic acid (HEPES, ≥99.5%, Sigma), mercaptopropionic acid (MPA, >99%, Acros), potassium peroxomonosulfate compound (oxone, active oxygen, min 4.5%, Acros), acetylacetone (99.5%, Merck), titriPUR® NaOH solution (Merck), suprapur® nitric acid (65%, Merck), ammonium-metavanadate (>99.% Riedel-de Haën), boric acid (99.5%, Riedel-de Haën), EDTA (99.5%, AnalaR BDH), ethidium bromide powder (EtBr, Sigma), dimethyl sulfoxide (DMSO, ≥99.7%, Fisher Scientific) were used.

Instrumentation. AGE was performed using an electrophoresis chamber and power supply (CONSORT E143). AlphaImager from Alpha Innotech was used to visualize and photograph the bands of gels under UV light.

Densitometry. To analyse a gel image after electrophoresis, Lane Densitometry (1-D Multi) in AlphaEaseFC™ software (Alpha Innotech) was used. This tool is designed for measuring and quantitating the intensity of bands in each lane of the gel image. This quantitative estimation can be achieved in two ways, using Auto Lane or Auto Grid function. The latter was always used as it allows defining band parameters manually, while the Auto Lane is completely automated feature.

[46] PBS is a pH 7.4 phosphate buffered medium with controlled ionic strength: 10 mM phosphate buffer, 2.7 mM KCl, 137 mM NaCl=.

After bands were visualized under UV light and photographed by AlphaImager, a gel image was opened in AlphaEaseFC™ software. The enhancement tools were used to modify the image display, e.g., zoom, rotate-flip, annotate. These features allow adapting the image only on the monitor[47] and do not change the original quantitative data.

To measure the areas of each band, the enhancement function was switched to analysis tools, specifically, to 1D-Multi tab (set of densitometry tools,) to display the Auto Grid template on the image. After specifying the correct number of lanes (typically 14-16) and the scan width[48], which is the area for measuring the pixel density (defined by green lines), the borders of the template (red lines) should be adjusted in such a way that they frame the lanes to be scanned and the adjacent lines lie between each of the lanes. When these parameters are set and the 'AUTOGRID' button is clicked, the areas of each band are automatically measured. The next important step was checking peaks of each lane. Although, 1D-Multi by default identifies the peaks of each band and integrates the area - band intensity – correspondingly, often, manual addition/deletions of existing peaks or the readjustment of their boundaries is necessary (Figure III.1). The data table is automatically updated to reflect the resultant changes.

[47] To preserve the applied adjustments on the screen, the image was saved as a different file (typically TIF format) and could be later opened and viewed/changed with this AlphaEaseFC; however, the modifications, such as annotated information, were never displayed when opening the image with Photoviewer, Adobe Photoshop or any other software, able reading TIF files. In such cases, "Print" option was used for printing either on paper or as a PDF file. This permitted to check and share the results of any experiment when the software was unavailable.

[48] A proper specification of the scan width is important. A scan width is too narrow may not include enough information and can result in a noisy graph with many undesired peaks, while a wide scan can incorporate background pixels that will reduce the pixel average and dilute the actual data.

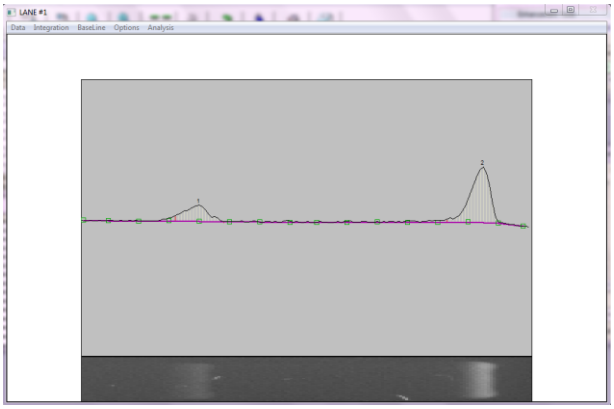

Figure III.1. Example of the lane densitometry. Nck (left) and Sc (right) bands of one reaction mixture represented by a lane. Areas of each band are adjusted manually if necessary.

After peaks of each lane were detected, the quantitative data were output and saved as a text file. From this point the data were managed using Microsoft Excel.

The values of peak areas for the Sc form were corrected by the factor of 1.47 to account for its lower staining capacity by ethidium bromide [393] and used to calculate the percentage (%) of each form (Sc, Nck and Lin).

The variability of results was estimated from the analysis replicate digestions using $VO(acac)_2$ as a reference standard metallonuclease. Standard deviation for repeatability (s_r, measures the random variability within each experiment) for the peak area within the same gel was estimated as 8, 6 and 8% for the Sc, Nck and Lin forms, respectively [502]. The s_r of the whole experimental procedure, including the preparation of solutions and incubation was 10, 6 and 3%, for the Sc, Nck and Lin forms, respectively. These values were estimated from analysis of variance (single factor ANOVA) of duplicates from 11 different runs. s_r for the peak area was estimated from duplicates of plasmid DNA (not incubated). s_r for a whole procedure was estimated from duplicates of samples incubated with metal complex. All experiments were done in duplicate, and the gel of best quality was presented as example.

Solutions preparation. Stock solutions of VC were typically prepared by weighing the appropriate amount of the compounds (ca. 6 mg) and dissolving in 100 mL of water to

obtain a 200 μM solution. The natural uncertainty coming from this procedure is ca. 10% due to the small weighted mass.

When testing the DNA cleavage activity of monovanadates (V_1), NH_4VO_3 was used. Most important point in the preparation of the monovanadate solution is to maintain a high pH to prevent the formation of decavanadate [503,504]. To prepare V_1 solution, MilliQ® water was buffered with NaOH (0.1 M) to adjust the pH to 10. This water was used to dissolve NH_4VO_3 to make a 50 mM solution. Water bath (~70 ºC) was used to heat up the solution for 10 min. Ready solution was transferred and stored in a plastic bottle.

A 100-mM stock solution of phosphate, HEPES or MOPS buffer was prepared in water. The pH was adjusted between 7.0 and 7.4 by adding dropwise nitric acid or sodium hydroxide. PBS was prepared by dissolving one tablet in 20 mL of water to obtain a 100 mM solution; pH (typically 7.39) was verified by a pH meter.

A 10x stock of TBE (89 mM Tris-borate and 1 mM EDTA, pH 8.0), chosen as electrophoresis buffer, was prepared in water at and stored at 4ºC. Typically the buffer was freshly diluted to the working concentration of 0.5x prior to a gel preparation.

Stock solution of EtBr (50 mg/mL) was prepared by dissolving the powder in water and was stored at RT in a plastic tube wrapped up in aluminium foil. Loading buffer was prepared in water by Professor Isabel Cavaco. Autoclaved MilliQ® water was always used in preparation of reaction mixtures with pDNA.

Agarose gel preparation. Agarose gels were typically of 1.0% in 0.5x TBE containing ca 3 μg/mL of EtBr. A gel was prepared by adding 150 mL of 0.5x TBE to 1.5 g of agarose powder in Erlenmeyer (~5 mm thick gel). The mixture was heated in a microwave oven at medium power until no agarose grains were visible. While the gel-TBE solution was warming up, a gel casting plate, which is composed of UV-transparent plastic, was sealed with tape to close the open edges in order to compose a mold, and set on the even horizontal surface. A comb with typically 14-16 teeth was chosen to

form sample slots in the gel. The comb was positioned 0.5-1 mm above the plate so that a complete well is formed when the agarose is added to the mold.

Upon cooling the mixture to approximately 60 ºC, 10 µL of EtBr was added, swirling the Erlenmeyer vigorously to ensure a thorough distribution of DNA dye. Warm agarose solution was poured into the mold and left for 1 h at RT to cool and solidify. The gel was checked for air bubbles that are likely to form under or between the teeth of the comb or anywhere on the surface. In the molten gel these bubbles were easily removed by poking them with a pipette tip.

After the gel hardened, the comb and tape were carefully removed, and the mold with the gel was submerged into 0.5x TBE (~ 1 mm depth) in the electrophoresis chamber.

Procedure. DNA cleavage activity was evaluated by monitoring the conversion of Sc plasmid DNA to Nck and Lin DNA. Each reaction mixture was prepared by adding (in this order) 6 µL of water, 2 µL of 100 mM buffer solution, 2 µL (100 µg/mL) of supercoiled pA1 DNA and 10 µL of the aqueous solution of VC. Phosphate (K_2HPO_4/HNO_3) and MOPS/NaOH buffers were used in most experiments[49], unless indicated otherwise. Working concentrations of VC were usually 3, 6, 12, 25, 50 and 100 µM.

Typical plasmid, purified from E. *coli* cells, after being cleaved, shows three bands (DNA forms) in agarose gel. They are closed circular supercoiled (I, supercoiled, Sc, the fastest one), linear (III, Lin, the middle band) and open circular (II, relaxed, nicked, Nck, the slowest one). Samples of the DNA control, which always contained only pA1, are normally represented by two bands – Sc and Nck, while those of the Lin control, which were obtained by digesting pA1 plasmid DNA with *Hind*III[50], show Nck and Lin forms (Figure III.2). In most experiments a mixture of 10 mM phosphate buffer and 50 µM of $VO(acac)_2$ digested with pA1 was used as a reference of the linearized DNA form. The

[49] Initially, HEPES buffer, or sometimes TRIS, was chosen for AGE experiments. When we started to work with cyclic and square wave voltammetry, José Paulo Pinheiro, having tested a variety of different buffers from the electrochemical point of view, suggested MOPS buffer as non-interactive one, and thus HEPES was substituted with MOPS in electrochemical tests as well as in all AGE experiments.

[50] *Hind*III is a restriction enzyme (type II site-specific), isolated from *Haemophilus influenzae,* that cleaves DNA via hydrolysis. This endonuclease was used as a reference in our AGE experiments.

endonuclease, *Hind*III, was only employed on the initial stage of our investigation to mark the band position of double strand cleavage.

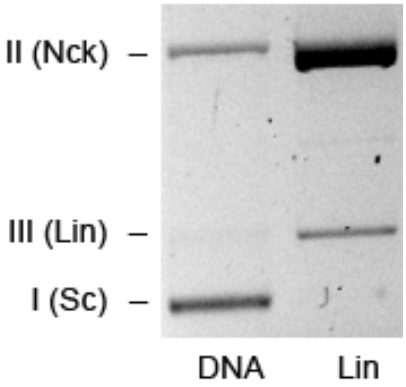

Figure III.2. Agarose gel image of the lanes "DNA" – pA1 (plasmid DNA control) and "Lin" – pA1digested with *Hind*III. Bands Sc, Nck and Lin correspond to **I** (supercoiled), **II** (nicked) and **III** (linear) forms of DNA.

When the reaction involved addition of activating agents, radical scavengers [462] or hydrogen peroxide, the initial volume of water was reduced to 4 µL, and 2 µL of the agent/scavenger/H_2O_2 aqueous solution (NaBz, NaN_3 and DMSO[51]) were added prior to metal complex. MPA and oxone were chosen as reducing and oxidizing agents, respectively. The final concentrations of the activating agents and radical scavengers were 200 µM and 40 mM, respectively. Their control samples were prepared in the absence of metal complex. Stock solutions of ~ 1 mM hydrogen peroxide were freshly prepared from 30% H_2O_2, their concentration was measured spectrophotometrically ($\varepsilon_{230\ nm}$ = 74 M^{-1} cm^{-1}) [505] and diluted as needed immediately before addition to the reaction mixture.

The samples were incubated at 37 ºC for 1 h, wrapped in aluminum foil. The reactions were quenched by the addition of 5 µL of loading dye and the samples were loaded onto 1% agarose gel in a horizontal electrophoresis tank containing 0.5x TBE buffer,

[51] NaBz, and DMSO are known hydroxyl radical scavengers, while NaN_3 is also recognized as a strong quencher of the singlet oxygen reactivity [462].

which served as electrolyte, and subjected to electrophoresis. Controls of supercoiled and linearized plasmid were included in both extremes of a 14 or 16-well gel plate.

Experiments under inert atmosphere were carried out using Schlenk techniques and a vacuum and nitrogen line. Solvents for the preparation of VC solutions were degassed prior to the dissolution of the complex under nitrogen. Eppendorfs containing the DNA and buffer solutions were arranged inside a Schlenk flask. They were submitted to vacuum and N_2-atmosphere consecutively three times before the careful addition of the complex solution using a micropipette and under a continuous flux of nitrogen gas. The Schlenk was closed, submitted to vacuum and then nitrogen and left under nitrogen to incubate for 1 h at 37 ºC.

Experiments under UV light were conducted preparing the reaction mixtures as described, and incubating them in open Eppendorfs under a 8-W blacklight blue 370 nm lamp for 1 h at RT. Experiments in the dark were carried out preparing all solutions in a dark room with red light, and incubating the reaction mixtures for 1 h at 37 ºC wrapped in aluminum foil.

III.4 Circular Dichroism

Circular dichroism (CD) spectra were recorded at t = (26 ± 1) ºC on a Jasco J-720 spectropolarimeter with a 180-800 nm photomultiplier using 1 cm path-length cylindrical quartz cells.

Stock solutions of **1** (250 µM) in 100% PBS were freshly prepared prior to each measurement. Four independent solutions of **1** with pDNA (ri[52] 0, 0.3, 0.75 and 1.5) were prepared and kept in a water bath during 25 h at 37 ºC stirring sideways (60 rpm). After the incubation aliquots of these solutions were collected in a 1.5 mL eppendorfs and stored at -20 ºC for analyses by AGE. Spectra were recorded in the 200–400 nm range at the time zero (no incubation), 6, 18 and 25 h.

[52] 'ri' is the ratio of the metal concentration to DNA concentration, measured as base pairs per liter.

III.5 Solution studies

Chemicals. HEPES (≥99.5%, Sigma), MOPS, (99.5%, Fluka), K_2HPO_4 (99%, Panreac), DMSO (≥99.7%, Fisher Scientific), titriPUR® NaOH solution (Merck), suprapur® nitric acid (65%, Merck) were used. In all cases, MilliQ® water (resistivity > 18MΩ.cm) was used, unless otherwise mentioned.

Instrumentation. UV-vis spectra were recorded at room temperature on a Hitachi U-2000 double beam spectrometer with 1 or 4 cm path-length quartz cell in the 350-950 nm range. Voltammetric studies were carried out using an Eco Chemie Autolab Potentiostat/Galvanostat 12 in conjunction with a Metrohm 663VA stand. A three electrode stand with a mercury drop working electrode, a saturated calomel reference electrode (SCE) or an Ag/AgCl, and a Pt wire auxiliary electrode.

III.5.1 UV-vis spectroscopy

Visible absorption spectroscopy was employed to analyse the stability of the complexes **1**-**5** and **9** in 10 mM PBS and HEPES media at physiological pH. Buffer solutions were prepared in deionized water and used as VC solvents. Absorption UV-vis spectra were obtained for millimolar solutions for **2**, **4**, **5** and **9** in 100% PBS (pH 7.4) were 1.2 mM concentration; **1** and **3** were of 2 mM in 1 and 100% DMSO, respectively.

The majority of these complexes are poorly soluble in water, therefore their dissolution was complete by sonication (5-10 min). Complex 3 showed a scarce dissolution in aqueous medium even with prolonged up to 1 h sonication.

Spectra were recorded immediately after solution preparation.

III.5.2 Electroanalytical methods

The electrochemical behaviour of **1**-**6** and **9** was studied by cyclic and square wave voltammetry (CV and SWV) in phosphate and MOPS buffers (10, 30 and 100 mM).

Cyclic and square wave voltammograms (Cvs and SWvs) were measured at 50 mV/s scan rate and 25 Hz, respectively. High-purity N_2 gas was used to purge solutions prior to each scan for at least 15 min. During all measurement a continuous flow of nitrogen passed through an electrochemical cell to ensure a maximum possible removal of dissolved oxygen. Typically, measurements started by filling an electrochemical cell with a buffer solution (25 mL), purging with nitrogen and measuring the first scan (blank voltammogram), followed by addition and scanning of VC solutions.

Stock solutions of the complexes were always prepared in deionized water immediately before use. Complex concentrations were similar to those used in digestion with pDNA, i.e., 2, 5, 10, 20 and 50 µM.

In experiments varying the concentration of phosphate buffer from 1 to 20 mM, the measurement started by running a scan of 1 mM buffer (blank), followed by addition of **1** to a final concentration of 50 µM. The experiment continued with subsequent additions of the appropriate volumes of concentrated buffer (100 mM) to 25 mL of solution, thus increasing the buffer concentration to 2, 3, 4, 6, 10, 15 and 20 mM. The solution volume in the end of the experiment was 30 mL, corresponding to a dilution of VC by maximum of 20%.

Similar procedures were followed in the experiments increasing the concentration of phosphate buffer in the presence of MOPS, and vice-versa. Peak potentials and currents were determined from the voltammograms using General Purpose Electrochemical Chemistry software (GPES, version 4.9, Eco Chemie B.V. Utrecht, the Netherlands).

III.6 Mechanistic studies

Chemicals. Terephthalate (disodium salt, 98%, Sigma-Aldrich), 4-nitrophenyl phosphate disodium salt hexahydrate (NPP, Sigma), bis-*p*-nitrophenyl phosphate sodium salt (BNPP, Sigma), hydrogen peroxide (30% Panreac), deuterium water (D_2O, 99.9% D, Euriso Top), 4,4-dimethyl-4-silapentano-1-sulfonic acid (DSS) were used.

Instrumentation. Fluorescence spectra were recorded on a FluoroMax®-3 spectrofluorometer in a 3 cm quartz rectangular spectrofluorometer cuvette (Sigma-Aldrich). NMR measurements were performed using a Bruker Avance 400 spectrometer in glass NMR tubes (NORELL® ST500-7).

III.6.1 Fluorescence spectroscopy

Spectrofluorometry was chosen to monitor the formation of ROS in aqueous solutions of VC (**1**, **4** and **9**) through the hydroxylation reaction of terephthalic acid (TPA) with a single fluorescent product, HTPA.

Excitation spectra of HTPA were scanned in the 250-400 nm range at emission of 435 nm, whereas the emission spectra were monitored at excitation of 323 nm in the range of 350-500 nm. The slit width was 1 nm (excitation and emission) and the scan rate was set on 1 nm/s.

The stock solutions of TPA, prepared in phosphate or MOPS buffer (solution A), and **1** in water (solution B) were 400 and 125 µM, respectively. Typically, 10 mL of solution A was mixed with 8 mL of solution B and 2 mL of water or H_2O_2 to a final volume of 20 mL. Blanks were prepared with 200 µM solution A in phosphate or MOPS buffer (pH 7.4). The final buffer concentration varied from 5 to 20 mM. All solutions were kept at room temperature between the measurements. TPA is poorly soluble in water and the dissolution was complete using water bath (~ 80 ºC) instead of sonication since the ultrasound in liquids is known to produce free radicals [487].

III.6.2 NMR studies

Hydrolysis of two widely used DNA model substrates, nitrophenyl phosphate (NPP) and bis-4-nitrophenyl phosphate (BNPP) (4 mM), by **1** (sat, C≤3 mM) was followed by ^{1}H and ^{51}V NMR spectroscopy.

The acquisition parameters were 33 KHz spectral width, 25 μs pulse width, 0.5 s acquisition time, and 10 Hz line broadening. Solutions were buffered with either MOPS or PBS (40 mM) prepared in H_2O or D_2O (pH 7.2-7.4). Dissolved DSS and a capillary containing a saturated solution of metavanadate were used as ^{1}H and ^{51}V references, respectively. The reaction mixtures were places in an oil bath, kept at 50 °C and followed during 10 days. The ^{51}V NMR chemical shift data of aqueous solutions of **6**-**8** were obtained in 10 mM phosphate and HEPES buffers. The NMR signals were assigned according to the literature [506].

Chapter IV

DNA Cleavage Activity

IV. DNA cleavage activity

IV.1 Results

This chapter presents the results obtained from AGE technique when studying the interaction of plasmid DNA with vanadium compounds (VC) containing acetylacetonate ligand. Some results on the interaction of VC with pDNA obtained by Circular Dichroism are also demonstrated.

During this work a total of 238 agarose gels were prepared, 115 of which were selected for this thesis and can be found in Annex A. Each electrophoresis experiment was aimed to show the extent of the DNA cleavage activity of **1**-**9** mainly. Complexes **10-36** were tested for comparison purposes and the results are also presented.

We examined different effects on the nuclease activity of VC. Table IV.1 lists the complexes with the studied effects. Nuclease activity was measured by the extent of the degradation of the supercoiled form of plasmid DNA (Sc) into the nicked form (Nck) and the linear form (Lin) after incubation with a metal complex.

Table IV.1. Studies of the nuclease activity of vanadium and copper complexes: effect of 1 – complex concentration; 2 – incubation time; 3 – excess ligand; 4 – buffer media; 5 – light; 6 – H_2O_2; 7 – atmosphere (air vs. nitrogen); 8 –activating agents; 9 – radical scavengers; 10 – observation of phantom bands. Gel images are presented in Annex 1 numbered as A1, A2, A3…An[53].

Complex	Studied effect									
	1	**2**	**3**	**4**	**5**	**6**	**7**	**8**	**9**	**10**
$VO(acac)_2$ (1)	A1-A20, A37-A39, A53, A92-A94, A110, A111, A113	A21-A25	A27-A29	A1-A3, A7, A10, A30-A37, A94	A38, A39	A40		A47, A49, A50, A58		A110, A111, A113
$VO(hd)_2$ (2)	A7, A11, A13, A19, A20	A26		A7						
$VO(Cl\text{-}acac)_2$ (3)	A11, A14, A19, A20									
$VO(Et\text{-}acac)_2$ (4)	A11, A15, A19, A20			A34, A35						
$VO(Me\text{-}acac)_2$ (5)	A11, A16, A19, A20									
$V_2O_4(acac)_2$ (6)	A46			A34, A35				A33, A47		
$VO_2(acac)(phen)$ (7)	A46							A47		
VO(OH)(OMe)(acac) (8)	A46							A47		
$VOSO_4$ (9)	A4, A8-A10, A13, A18, A19, A20, A41-A45, A53, A62-A64, A92-A94			A10, A31, A34, A35, A43-A45			A41, A42	A66, A98, A99		
$VO(acac\text{-}Naf)_2$ (10)	A6, A19, A20									
$VO(tmh)_2$ (11)	A11, A17, A19, A20									

[53] The table demonstrates the numbers of the figures to the complex and studied effect correspondingly. These figures are collected in the Annex A. in Complex **1**, besides the experiments where it was purposefully tested, is present in every gel at 50 μM concentration digested with pA1 plasmid DNA under phosphate buffer, i.e., control ofr the linearized DNA form.

$VO(pbd)_2$ (12)	A11, A18, A19, A20									
$VO(acac\text{-}NH_2)_2$ (13)	A19, A20		A27-A29	A34, A35						
$VO(acac\text{-}NMe_2)_2$ (14)	A19, A20		A27-A29							
$Cu(acac)_2$ (15)	A51, A53, A54, A58			A51, A54				A54, A56, A58		
$Ni(acac)_2$ (16)	A52, A53, A55, A58			A52, A55, A57				A55, A57, A58		
$VO(MPA)_2$ (17)	A59-A61, A111-A112									A110-A112
$VO(dmpp)_2$ (18)	A59-A61									
$VO(PA)_2$ (19)	A62-A64									
VO(oda) (20)	A65-A67, A88, A89, A110			A65, A67, A68, A88, A89				A66, A67, A90, A91	A32, A68	A110
VO(oda)phen (21)	A69-A75, A88, A89			A69, A70, A88, A89		A76-A79		A71-A75, A90, A91	A76-A79	
$VO(phen)_2$ (22)	A71-A75, A110-A112									A110-A112
VO(oda)bipy (23)	A80, A81, A88, A89			A80-A83, A88, A89		A84-A87		A82, A83, A90, A91	A84-A87	
$VO(chrysin)_2$ (24)	A92-A94									
$VO(morin)_2$ (25)	A92-A96			A97				A97		
VO(clor) (26)	A95, A96, A113									A113
$VO(silibinin)_2$ (27)	A98, A99							A98, A99		
Cu(Sal-Gly)(bipy) (28)	A100, A101, A107							A103,		

								A105, A109		
Cu(Sal-Gly)(phen) (**29**)	A100, A101, A102, A107, A108							A103, A105, A109		
Cu(Sal-L-Phe)(phen) (**30**)	A100, A101, A102, A107, A108							A103, A105, A109		
VO(Sal-L-Phe)(bipy) (**31**)	A100, A101, A107							A103, A105		
VO(Sal-L-Phe)(phen) (**32**)	A100, A101, A107							A103, A105		
VO(Sal-Gly)(bipy) (**33**)	A100, A101, A107							A104, A106		
VO(Sal-Gly)(phen) (**34**)	A100, A101, A107							A104, A106		
VO(Sal-Gly)(H_2O) (**35**)	A100, A101, A107							A104, A106		
VO(Sal-L-Phe)(H_2O) (**36**)	A100, A101, A107							A104, A106		
NH_4VO_3	A48-A50			A48				A49, A50		

Normally, the **effect of complex concentration** is the first step in determining the nuclease activity of a metal complex. This effect was studied for all complexes listed in Table IV.1 typically at 3, 6, 12, 25, 50 and 100 µM, which corresponds to metal:bp ratio (ri) of 0.2, 0.4, 0.8, 1.67, 3.3 and 6.7.

Except for the complexes **7**, **8**, **10**, **15**, **16**, **24**-**36** and NH_4VO_3 (Figure A46, A6, A51, A52, A92, A95 and A48, respectively) nuclease activity of the studied complexes is concentration dependent, especially under phosphate buffer.

Complex **1** is a very active nuclease promoting a strong cleavage, the extent of which is directly dependent on the buffer media and complex concentration (Figure A1-A3).

Figure A11 shows the results of the effect of complex concentration on the nuclease activity of **1**-**5**, **9**, **11** and **12** at 50 and 100 µM (ri 3.3 and 6.7) under phosphate. All complexes are active towards pDNA at these concentration levels. To determine whether each of these complexes breaks the DNA strands at lower concentrations, the corresponding tests were carried out for 3-100 µM (ri 0.2-6.7) and the images of these gels are summarized in Annex in Figures A7, A8, A10, A13-A18.

VC with ligands composed of oxodiacetate (Figure A65-A91) or picolinic acid (Figure A59-A64) were also found to promote a concentration-dependent cleavage.

A particularly strong concentration effect was observed on the nuclease activity of VO(oda)phen, which was found to promote a linearization of the DNA strands even under MOPS (Figure A89).

Effect of buffer media was tested using inorganic (phosphate) and organic (HEPES or MOPS) buffers. DNA cleavage was found to be usually stronger under phosphate buffer. Exception is the complexes containing oxodiacetate ligand (Figure A91). Complex **1** can be an excellent example to demonstrate this difference (Figure A1-A3). Figure A20 shows the results of the nuclease activity of **1**-**5** and **9**-**14** under MOPS buffer. No significant change can be observed.

Not only was the nature of the buffer found to affect the extent of the DNA cleavage but also its concentration (Figure A34). When searching for the optimal buffer media concentration, at which the extent of DNA scission would be the highest, different concentrations were tested. According to the calculated percentage of each DNA form obtained after the cleavage, the most efficient cleavage among 1, 2, 3, 4, 6, 10, 15 and 20 mM concentration is observed at 6 mM (Figure A33).

To support the assumption that the activity under organic buffers might be affected due to their scavenging effect, the extent of DNA cleavage was tested in the presence of both buffers at the ratio 1:1 and 1:2 (Figure A36). The results show that the nuclease activity of **1** is stronger under phosphate buffer and the extent of the DNA cleavage decreased with addition of MOPS buffer.

The **effect of excess ligand** was studied by incubating solutions of **1**, **13** and **14** with an excess of corresponding ligands, i.e., acac, acac-NH_2 and acac-NMe_2 respectively, up to ~160. No increase of nuclease activity was observed. Instead, there is a clear decrease in the nuclease activity of **1** when acac is added. In the case of excess ligands added to solutions of **13** and **14**, the inhibition of the cleavage is considerably smaller (Figure A28).

Ligands of the active complexes were often assumed to be relevant to the extent of DNA cleavage. Thus, ligands were typically examined next to the corresponding complexes. From Figure A63, A73 and A83 it can be seen that none of the tested ligands *per se* induced the DNA breakage.

To check the **effect of light** on the nuclease activity of **1**, the samples were incubated for 1 h at 37 ºC under a 370-nm UV lamp (Figure A38). Although a distinct separation of Sc and Lin forms cannot be observed, it is clear that **1** promotes an efficient concentration dependent cleavage of both tested plasmids. When the incubation was

carried out in the dark (Figure A39), results demonstrate similar behaviour of **1** to that observed under natural light or incubated under UV light.

Often, for the DNA cleavage to occur additional stimulating agents are required. MPA and oxone were used as reducing and oxidizing activating agents, respectively. These agents simulate reducing conditions as may be found inside biological cells, and oxidizing conditions as may be found in blood or in contact with the air.

For most of the tested compounds, the **effect of activating agents** on their nuclease activity was found to be significant. Oxone seemed to always increase the extent of the cleavage or, when a complex was initially non-active, to induce it. (Figure A58 and A90). MPA, on the other hand, in some cases had no effect on the extent of the cleavage (Figure A49 and A97), and many times demonstrated an inhibition effect (Figure A47, lane 8; Figure A58, lane 14; Figure A67, lane 9). The results, where MPA increased the extent of the cleavage, were also common (Figure A47 lane 7; Figure A99 lane 8). In some cases the cleavage in the presence of MPA was much stronger than with oxone regardless of the buffer medium (Figure A90 and A91, lane 11).

Interesting results with MPA were obtained for the compounds containing copper as a metal centre: the activity in the presence of the reductant is so strong that the plasmid undergoes a complete destruction, once more independently of the buffer medium. As the consequence, no bands indicating these samples can be observed in a gel (Figure A54).

Usually, the effect of activating agents was always stronger for more active compounds towards DNA cleavage, especially under phosphate buffer.

Assuming that the cleavage is of oxidative nature and that ROS are probably involved in the cleavage process, studying the **effect of radical scavengers** was of a high importance. Commonly used scavengers of free radicals (DMSO and NaBz) and singlet

oxygen (NaN_3), were chosen for these tests. Normally, such experiments were conducted with the compounds that demonstrated an efficient nuclease activity. The involvement of the reaction oxygen species (ROS) was judged by the decrease in the DNA cleavage upon addition of the scavengers. Principally, the cleavage was inhibited in the presence of either of the agents (Figure A68 and A86). In some cases the extent of the inhibition was higher with NaN_3 than with DMSO or NaBz (Figure A76). The scavengers under MOPS buffer could have a different effect from that observed under phosphate for the same compound (Figure A78).

Experiments related to the **effect of atmosphere** carried out under inert atmosphere gave results similar to those performed under usual conditions, i.e., under air. Though a slight decrease in the extent of DNA cleavage is noticeable under N_2 (Figure A41 and A42), the scission remains significant.

Continuing to study the involvement of OH radicals in the reaction of **1** with pDNA, nuclease behaviour of **1** was examined in the presence of H_2O_2 at physiological concentrations. According to the obtained results, a significant **effect of hydrogen peroxide** on the activity of **1** towards DNA cleavage is observed upon addition of ca. 1 µM and seems to augment with the complex concentration (Figure A40). However, further increasing the concentration of H_2O_2 does not seem to alter the extent of scission.

The **effect of incubation time** on the nuclease activity of **1** was studied with the time intervals of 15 or 30 min. A difference in the extent of the cleavage between the sample incubated for 5 min and the one digested for 4 hours can be observed (Figure A23). A dependence of the intensity of the DNA cleavage on the time digestion does not seem to be dramatic.

Circular Dichroism studies

The circular dichroism spectrum of pDNA in PBS buffer shows a negative band with λ_{max} = 246 nm and a positive band at λ_{max} = 274 nm with zero at 257.5 nm (Figure IV.1, A). A slight change is observed between 0 and 6 h, more in the positive than negative band. After 25 h of incubation the intensity of both negative positive bands increases. The changes in the molar ellipticity of pDNA caused by **1** at 45, 112,5 and 225 μM (ri 0.3, 0.75 and 1.5) are shown in Figure IV.1 (B). At the highest ri, the intensity of the negative band increases and that of the positive band decreases, both by 6%. At the positive band no significant difference in the intensity change is observed between ri 0.3 and 0.75, whereas at the negative one it is increased by 13%. Some changes can be observed in the 220-230 nm range both in the absence and presence of **1**.

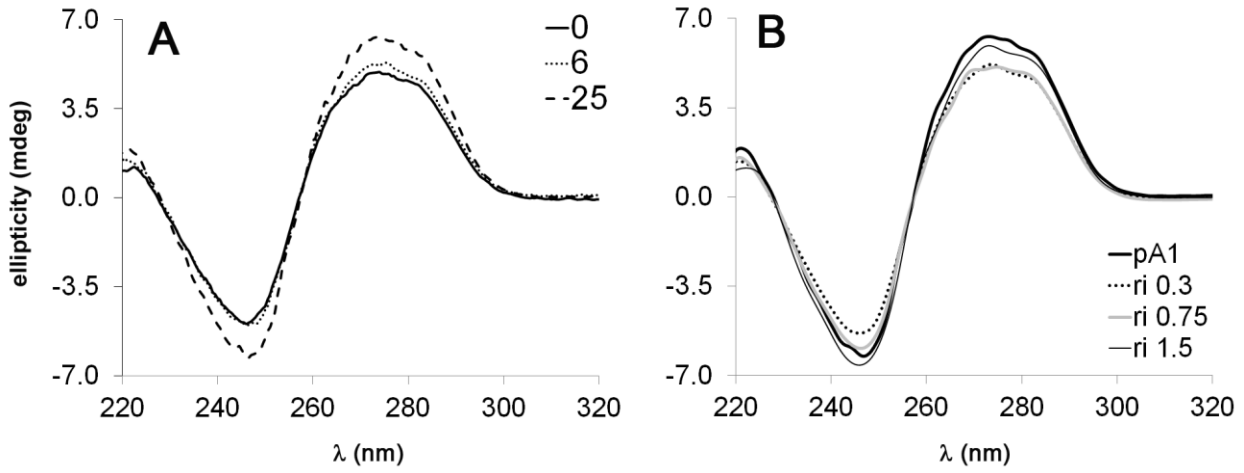

Figure IV.1. Circular dichroism spectra of pDNA in PBS at the time of reaction mixture preparation, after 6 and 25 h incubating at 37 °C (A, numbers in the legend present hours) and after addition of **1** (B) at different ratios of metal:bp, i.e., 0.3, 0.75 and 1.5; 'pA1' is pDNA with no complex in PBS.

AGE carried out after the CD measurements for the same samples shows significant degradation of pDNA (Figure IV.2; A (ri 0.3), B (ri 0.75) and C (ri 1.5), lanes 4, 5 and 6, respectively). The increase in the amount of nicked and linear DNA is associated with

the increase of metal:bp ratio: the Nck form A – 47%, B – 75% and C – 87%; the Lin form 3.9%, 4.8% and C 6.1% respectively, whereas the amounts of these two DNA forms for Lin control (pA1 DNA incubated 1 h at 37 ºC with **1**, ri 3.3; lane 2 and 7) are 74% (Nck) and 2.2% (Lin).

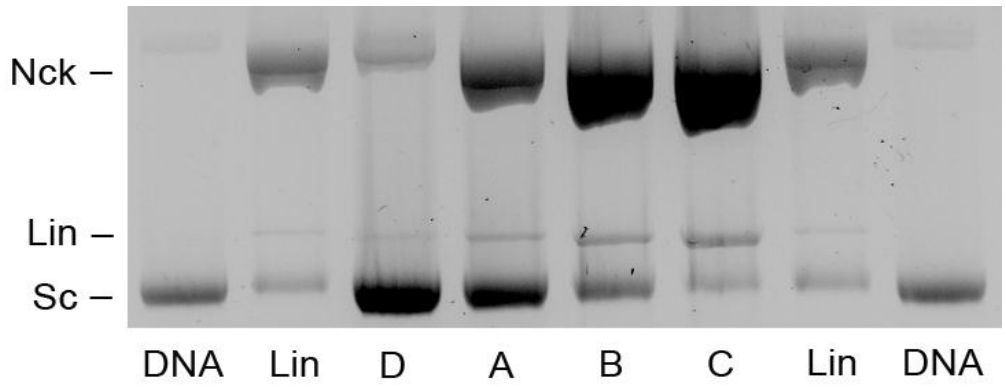

Figure IV.2. AGE of the reaction mixtures used at CD measurements (Figure IV.1, B): pDNA in PBS, no complex (D), ri 0.3 (A), ri 0.75 (B), ri 1.5 (C), "DNA" and "Lin" – controls for native and linearized plasmid, respectively. Incubation 25 h at 37 ºC.

IV.2 Discussion

IV.2.1 Effect of complex concentration

When trying to assess a possible toxic effect of vanadium, namely its effect on plasmid DNA (pDNA), which is assumed to occur upon metal penetration into the cells, the following questions were of interest:

1) Does vanadium interact with DNA? Does this interaction lead to a cleavage of DNA strands?

2) Which concentration of vanadium is sufficient for the cleavage to occur?

In pilot studies with other vanadium compounds [119] such as $V^{IV}O(phen)_2$, $V^{IV}O(phen)(SO4)$, $V^{IV}O(salan)$, $V^{IV}O(pyren)$, complex **1** showed the DNA cleavage in the absence of oxidizing (oxone) and reducing (MPA) agents exhibiting different behaviour in phosphate and organic (TRIS and HEPES) buffers. Both activating agents increased the extent of the cleavage much less in the presence of organic buffers. All the experiments on the nuclease activity of $VO(acac)_2$ carried out during the present study support these results obtained.

$VO(acac)_2$ and its derivatives promote the DNA cleavage with remarkably different efficiencies (Figure IV.3). Based on obtained AGE data, two types of nucleases, strong and weak, in oxidovanadium(IV) acac family can be distinguished. The least active compounds are also less stable ones towards hydrolysis.

When a complex is active towards DNA, increasing metal:bp ratio “ri” will augment the extent of the cleavage. In other words, complexes exhibiting the nuclease activity generally induce concentration dependent cleavage.

Comparison of the DNA degradation by **1** at different concentrations (Figure IV.4) demonstrates a strong concentration dependent cleavage. Single-strand cleavage occurs at the lowest tested concentration of 6 μM (ri 0.4) and gradually increases up to 100 μM (ri 6.7), as can be seen from the increase in the percentage of Nck at the cost of Sc. Above ri 6.7 a significant decrease in the relative intensity of the Nck band suggests further cleavage of this form to produce linear DNA. A tail-like smear observed below the Lin bands (Figure A113) is evidence of linear DNA undergoing destruction to form shorter strands, indistinguishable by AGE.

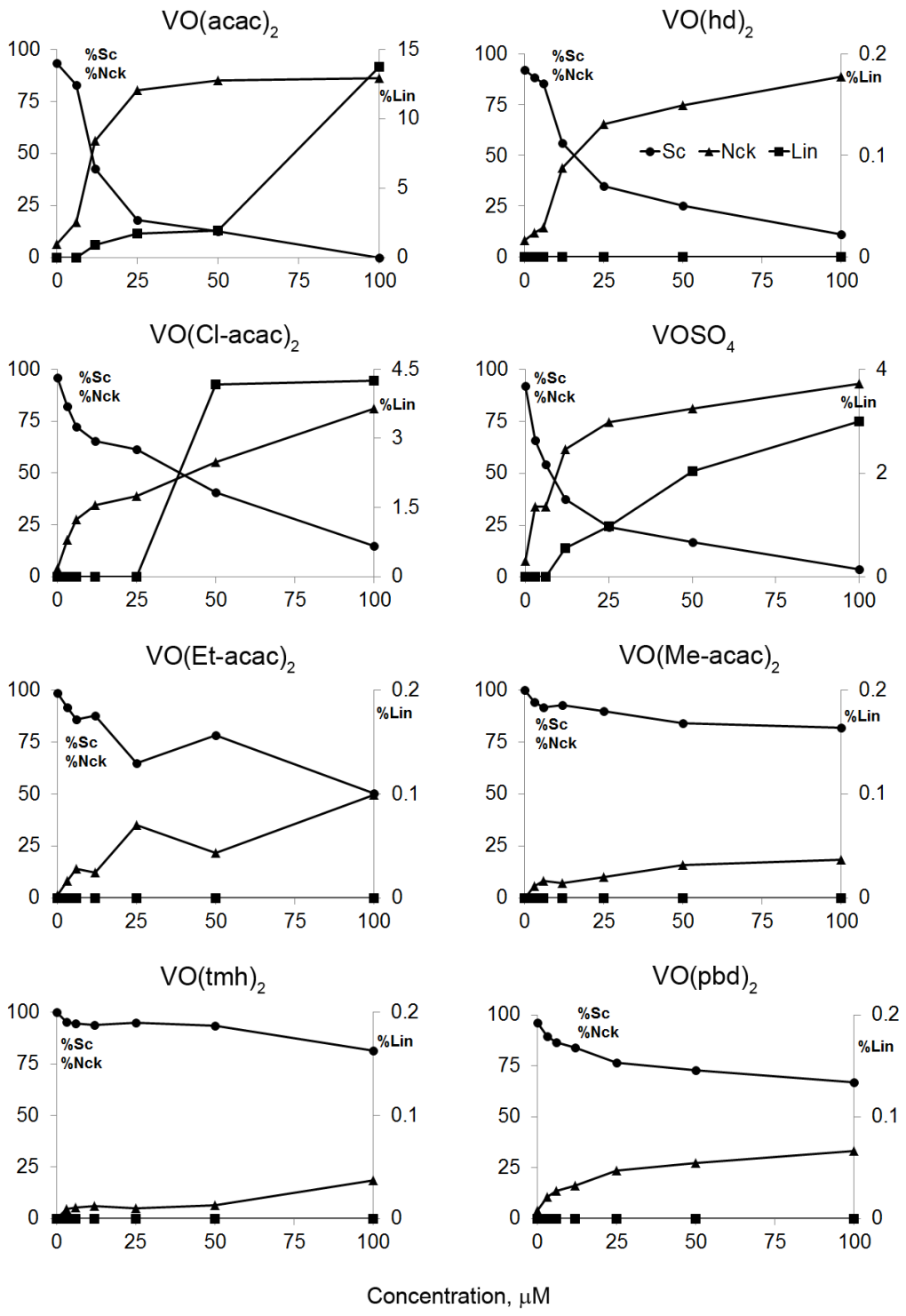

Figure IV.3. Cleavage of pA1 pDNA by **1**-**5**, **9**, **11** and **12** at 0 (DNA control), 3, 6, 12, 25, 50 and 100 μM (ri 0.2, 0.4, 0.8, 1.7, 3.3 and 6.7) under phosphate buffer. Percentage calculated from the areas of Sc, Nck and Lin bands *vs.* complex concentration. Data extracted from the gels in Figures A13-A18, A43 and A113.

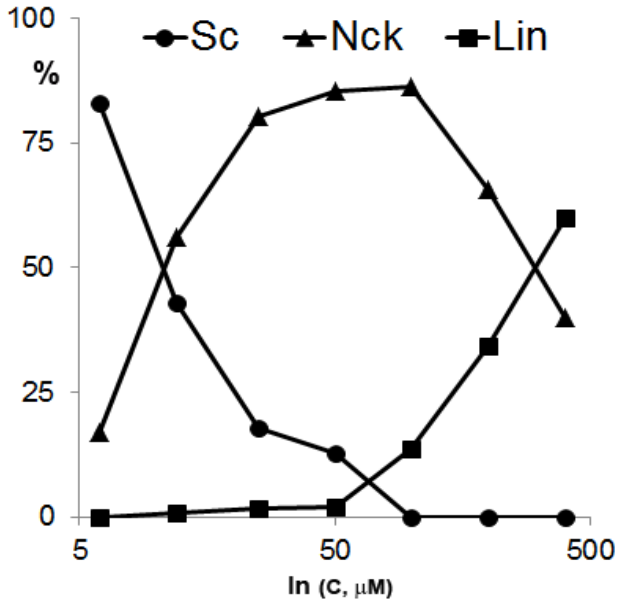

Figure IV.4. Percentage of the Sc, Nck and Lin DNA forms demonstrating the extent of the nuclease activity of **1** vs. complex concentration (6, 12, 25, 50, 100, 200 and 400 μM corresponding to ri 0.4, 0.8, 1.67, 3.3, 6.7, 13.3 and 26.67) under phosphate buffer. 'C' indicates concentration. Data extracted from the gel in Figure A113.

Complexes **2**-**5** were synthesized and their nuclease activity was compared with that of **1**. Figure IV.5 presents the results for **1**-**5** under phosphate buffer at 50 and 100 μM (ri 3.3 and 6.7). The presence of both single and double-strand cleavage suggests that all complexes are active towards DNA scission. Clearly, complex **1** is the most active; it is the only complex that induces a complete degradation of the Sc DNA at ri 6.7 with 8.6% of the Lin form. Even at ri 3.3 the double-strand cleavage of **1** is higher than that of any of complexes at the same or higher ri. The same is observed for single-strand cleavage, with the only exception observed in the presence of complex **3** which promotes stronger nicking at ri 6.7 (91%) than **1** at ri 3.3 (88%). Considering the fact that **3** is scarcely soluble in water, it is likely that its nuclease activity is even stronger than that of **1**. The absence of the linearization and a scarce change in the relative intensity of the Nck band, suggest that **4** and **5** as well as **11** and **12** are weak nucleases. The cleavage activity of all seven complexes tested at ri 3.3 and 6.7 seems to be concentration dependent. Based on these and other results obtained in the course

of this work, the order of activity of **1**-**5, 11** and **12** under phosphate buffer is assumed to be the following:

3 > **1** ≥ **2** >> **4** ≥ **5** > **12** > **11**

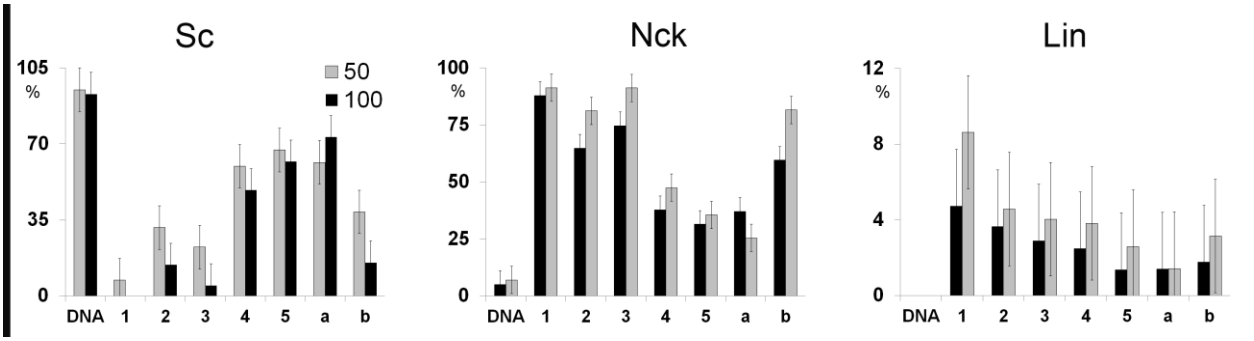

Figure IV.5. Comparison of the nuclease activity of **1**-**5**, **11** (a) and **12** (b) under PBS buffer at 50 and 100 µM (ri 3.3 and 6.7). "DNA" is the control for native DNA incubated in the absence of metal Solutions of 50 and 100 µM of **1**, **2**, **4**, **5** were prepared by dilution from 200 µM stock solutions. Due to the scarce solubility of **3**, **11** and **12** in water, 1:2 and 1:4 dilutions from a saturated solutions (<<200 µM) were used. Error bars represent S_r. Data extracted from the gel in Figure A11.

Not all oxidovanadium(IV) complexes with acac ligand show concentration dependent activity. Complex **10**, for instance, does not seem to promote any cleavage (Figure IV.6). This may be due to its poor solubility in water, which is however, not the case of the complexes **3**, **11** and **12**, despite their low solubility, they are active towards pDNA.

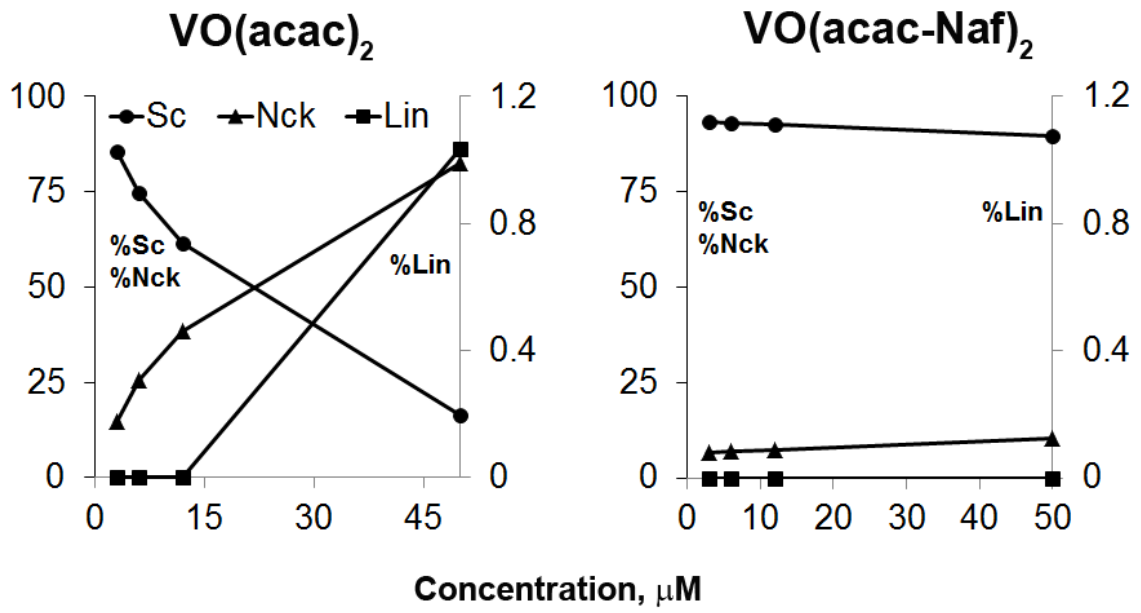

Figure IV.6. The extent of DNA cleavage promoted by **1** and **10** at 3, 6, 12 and 50 μM under phosphate buffer, presented as the percentage of the Nck, Lin and Sc forms *vs.* complex concentration. Data extracted from the gel in Figure A6.

A proper comparison of the efficiency of DNA cleavage by artificial metallonucleases measured by different research groups is normally impeded by the large variety of reaction conditions used. These can be incubation time, type of buffer media and plasmid DNA, concentration of ethidium bromide in a gel, solubility of complexes etc. No absolute method is yet established to allow comparison of the efficiency of different complexes examined as inorganic nucleases at different conditions.

According to Cowan [507], a Poisson distribution can be used to describe the cleavage process, and the efficiency of a complex can be defined as S/M, where S is the average number of strand scissions occurred in each plasmid per micromole of metal complex per hour at 37 ºC, and M is the metal concentration in micromole. S equals -ln(f_{Sc}) where f_{Sc} is the fraction of the Sc DNA form (%Sc) in the case only the Nck and Sc forms are obtained.

Figure IV.7 compares the efficiencies of tested complexes with **1** presented as ln (%Sc) *vs.* complex concentration. The ln (%Sc) was calculated from the percentage of the Sc

form measured from bands in AGE gel images. The results are displayed as a straight line where the slope relates the decrease of the intensity of the Sc band with the complex concentration. Supporting earlier conclusion, under phosphate buffer complex **1** comparing to the derivatives, is the most efficient DNA cleaving agent followed by **2** and **4**. Complex **3** is probably even a stronger nuclease than **1** and **2**, however its scarce solubility does not allow to accurately estimate the extent of its nuclease activity.

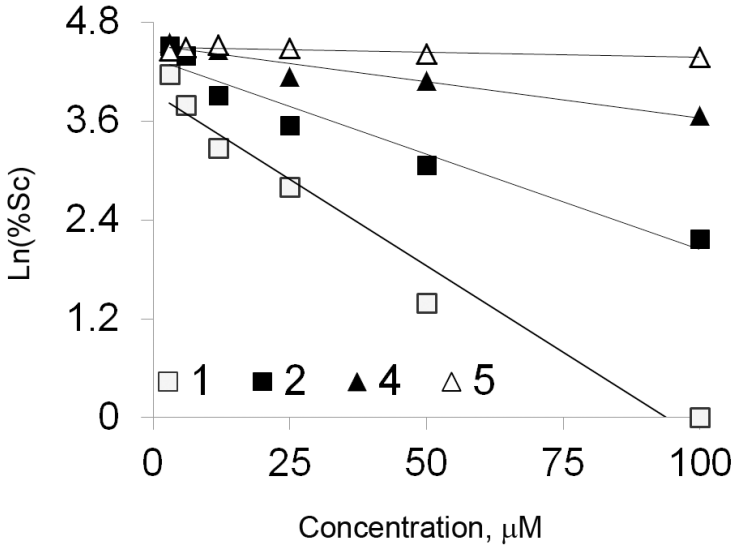

Figure IV.7. Comparison of the nuclease efficiencies of **1** and **2**, **4** and **5** at 3, 6, 12, 25, 50 and 100 μM (ri 0.2, 0.4, 0.8, 1.7, 3.3 and 6.7) under phosphate buffer. Complexes-derivatives **3**, **6**-**8** and **10**-**12** are not included for comparison since they do not dissolve completely in H_2O, thus the concentration might be somewhat different from the expected value.

Quantification of the nuclease activity in phosphate buffer can be observed in Table IV.2, ln (%Sc) *vs.* concentration. Table IV.3 presents the calculations of the absolute slope values of the lines for phosphate buffer and the potency order for this activity (intervals for 95% confidence).

Table IV.2. Values of ln (%Sc) corresponding to 0, 5, 10, 25, 50 and 100 μM complex concentration under phosphate buffer. Sampe with complex concentration '0' is the the one with plasmid DNA and no complex added.

Concentration, μM	**ln (%Sc)**			
	1	**2**	**4**	**5**
3	4.169	4.517	4.554	4.462
6	3.799	4.402	4.484	4.502
12	3.280	3.919	4.469	4.525
25	2.800	3.555	4.140	4.484
50	1.392	3.067	4.091	4.415
100	*	2.174	3.673	4.382

* Sc not detected due to complete degradation into Nck and Lin.

Table IV.3. Calculated slopes for –ln (%Sc) *vs.* complex concentration for **1**, **2**, **4** and **5** under phosphate buffer. Intervals for 95% confidence are presented.

Complex	**1**	**2**	**4**	**5**
$\boldsymbol{m} \pm \Delta\boldsymbol{m}$	-0.056±0.013	-0.023±0.007	-0.009±0.003	-0.001±0.001

$VO(acac)_2$ and derivatives **2**-**5** including complexes **11** and **12** exhibit different activities towards pDNA degradation. This fact suggests an important role of a ligand in the complex activity. This assumption was verified by testing the nuclease activity of **9** which, in aqueous solution, is the oxidovanadium(IV) aqua complex, VO^{2+}. The results reveal a strong DNA cleavage activity which, seems to be similar to **1** (Figure IV.8). Apparently, some other species are responsible for the efficient DNA degradation, different from those formed in aqueous solution of **1**. Nonetheless, **1** seems to be a stronger nuclease, particularly at 100 μM concentration.

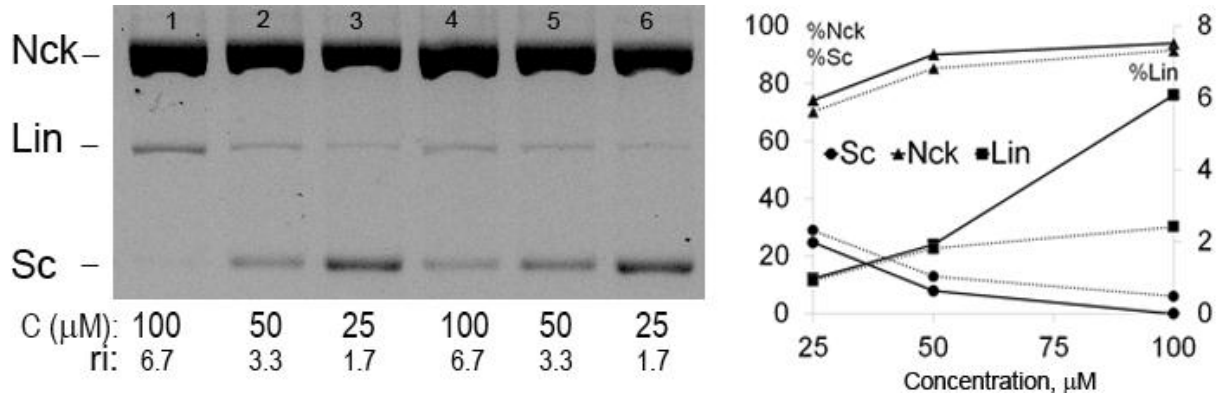

Figure IV.8. Comparison of the nuclease activity of **1** and **9** under phosphate buffer at three concentration levels. *Left:* Agarose gel image; samples 1-3 were digested with **1** and samples 4-6 with **9**. *Right:* Percentage of three DNA forms calculated from the areas obtained by densitometry; **1** represents a solid line, while **9** – a dotted one. Data extracted from the gel in Figure A10, lanes 8-13.

$VOSO_4$, though commonly reported as an inactive towards DNA degradation [277], in the present work shows concentration dependent activity. However, often irreproducible behaviour is observed. It can show an activity as high as **1** in some assays, or weaker activity in others. This lack of reproducibility may be explained by the hydrolysis and precipitation of vanadium hydroxides at neutral pH which occurs more readily for aquo complex than for vanadium complexes that are stabilized by bidentate ligands such as acac. The precipitation is a very irreproducible process and may affect the DNA degradation by itself. The kinetics of the precipitation will depend strongly on factors such as the room temperature and the process of mixing the solutions, which were not specifically controlled in these experiments. The absence of nuclease activity observed in some tests and reported in the literature may be due to extensive precipitation of the metal as a hydroxide. When this precipitation is slower or not so extensive, nuclease activity can be observed, with a similar behaviour to **1**, especially under phosphate buffer, since in the presence of organic buffers, HEPES or MOPS, **9** seems to exhibit more activity than **1**.

Similar to **9**, the extent of the DNA cleavage was obtained for oxidovanadium(IV) perchlorate under MOPS buffer (Figure IV.9), suggesting that the same species are responsible for nuclease activity of these complexes.

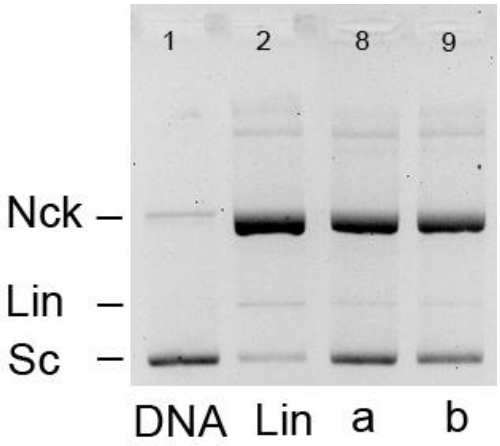

Figure IV.9. Comparison of the nuclease activity of **9** (a) and $V^{IV}O(ClO_4)_2$ (b) at 50 μM under MOPS buffer. Data extracted from the gels in Figure A32, lanes 8 and 9.

To determine whether the active species in pDNA degradation are products of the oxidation of **1**, three vanadate (V^V) complexes containing acac as a ligand, **6**-**8**, were synthesized and digested with pDNA. Comparing the relative intensities of the Nck and Sc bands of the DNA control sample (plasmid digested in the absence of metal) with those of the samples with complexes, a weak single-strand cleavage by **6** and **7** can be distinguished, especially at the highest tested concentration (Figure IV.10).

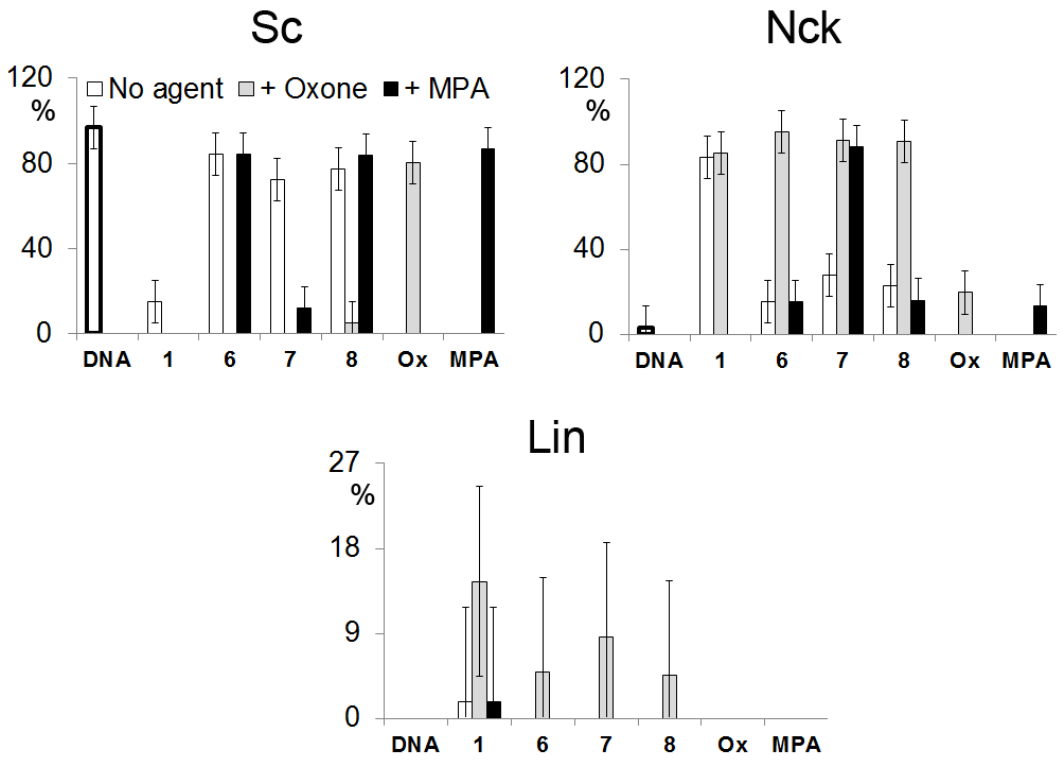

Figure IV.10. Comparison of the nuclease activity of **6**-**8** under phosphate buffer in the presence of activating agents. The complexes did not dissolve completely in water. Their concentration is 1:4 of the stock solution, which was prepared to be 200 μM. "DNA" and "Lin" are the controls of the Sc (native plasmid DNA) and Lin (50 μM of **1** digested with pA1 pDNA under 10 mM phosphate buffer) forms, respectively. Complex **1** with oxone was added for comparison. Error bars represent S_r. Data extracted from the gel in Figure A47.

The results of the nuclease of monovanadate, an expected product of oxidation of dilute aqueous solutions of V^{IV}-complexes (Figure IV.11), suggest that V_1 is apparently not the active species either. No DNA cleavage under phosphate buffer even at 200 μM (ri 13.3) and merely a moderate single-strand scission in the presence of MOPS are observed. A gradual decrease in the intensity of the Sc band under MOPS indicates a concentration dependent cleavage. Complex **1** is much more active especially under phosphate buffer.

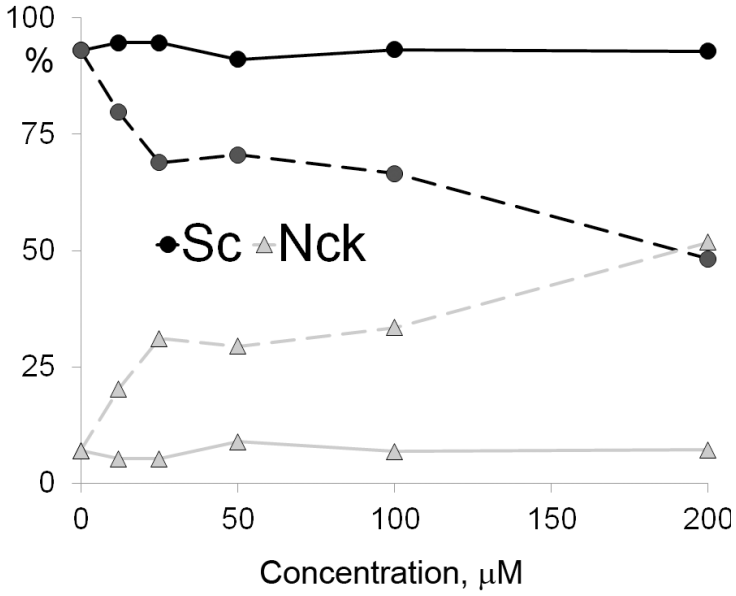

Figure IV.11. Extent of the DNA cleavage induced by V_1 under phosphate (solid line) and MOPS (dashed line) buffers presented as the percentage of the Sc and Nck forms *vs.* complex concentration. Data extracted from the gel in Figure A48.

The effect of complex concentration on the nuclease activity of other complexes, **10**-**36**, mainly oxidovanadium(IV) compounds with different ligands was studied in comparison with **1** (Figure IV.12–Figure IV.19). None of these complexes demonstrated higher activity than that of **1**. Exception is VO(oda)phen (**21**) which exhibits more efficient activity than **1** especially under MOPS buffer. In fact, it is the only complex out of total 36 examined in this work that seems to be a stronger nuclease than **1**.

Two other complexes with oxodiacetate ligand “oda”, VO(oda) (**20**) and VO(oda)bipy (**23**), are also efficient nucleases (Figure IV.12). The principal complex, **20**, has been reported as a possible candidate in evaluation related to the search of alternative therapeutics in cancer treatment, induces both nicking and linearization. Complexes **21** and **23**, synthesized as VO(oda) derivatives, readily interact with pDNA causing both single and double-strand cleavages. However, unlike with phenanthroline (phen), addition of bipyridine ligand (bipy) does not increase the reactivity of **20** much, the extent of the DNA cleavage seems to be similar. Figure IV.13 compares the nuclease activity of **21** and **23** under both buffers. Strong cleavage by **21**, including linearization,

is observed already at ri 0.3 under phosphate as well as under MOPS. Complete conversion of the Sc into Nck and Lin occurs only under phosphate at ri as low as 1.7. Complex **23** is much weaker nuclease, linearization takes place also at ri 0.3 but to considerably lower extent than observed with **21**. The difference in the activities is probably due to the binding affinity of phenanthroline which in the series of mononuclear mixed ligand copper(II) complexes is stronger than the one of bipyridine [508].

In the presence of MOPS a double-strand cleavage occurs only at the highest tested concentration, ri 6.7. The difference in the activities is more likely due to the presence of phenanthroline (phen). Known for its strong affinity to DNA, this ligand may bind to the DNA by intercalating the nucleobases, making it more susceptible to scission.

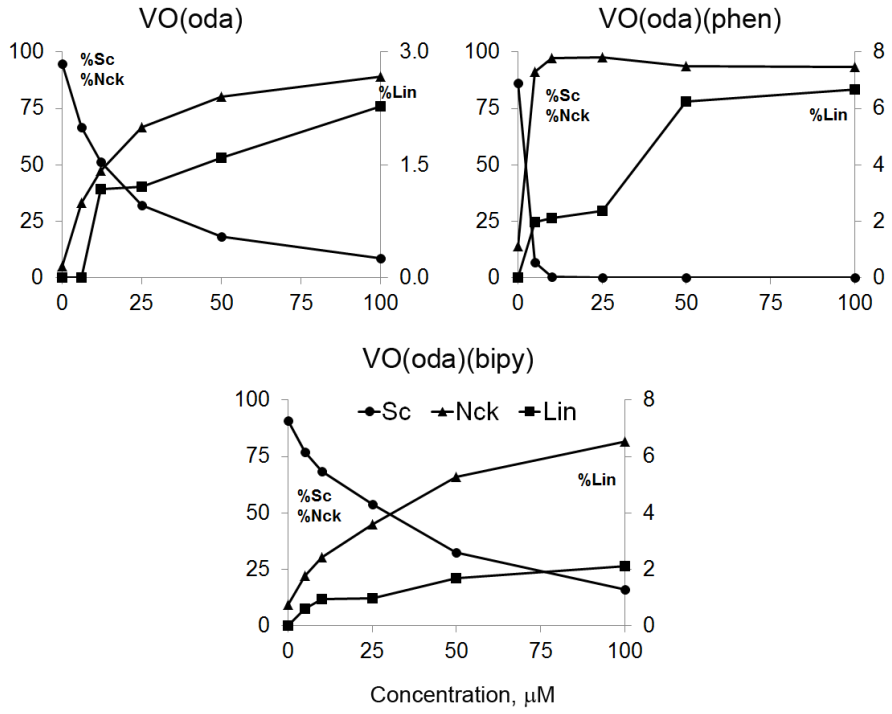

Figure IV.12. Cleavage of pA1 pDNA by **20**, **21** and **23** at 5, 10, 25, 50 and 100 μM (ri 0.3, 0.7, 1.7, 3.3 and 6.7) under phosphate buffer. Data extracted from the gels in Figures A65, A70 and A80, respectively.

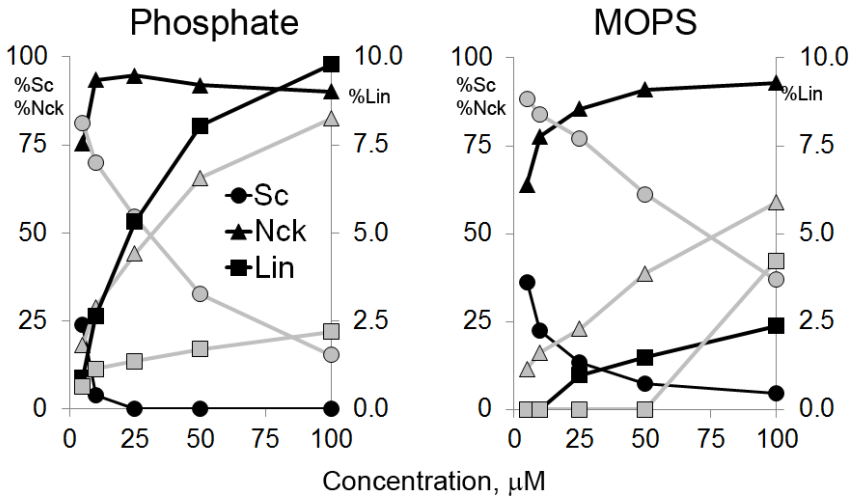

Figure IV.13. Comparison of the nuclease activity of **21** and **23** (black and grey lines, respectively) at 5, 10, 25, 50 and 100 μM (ri 0.3, 0.7, 1.7, 3.3 and 6.7) under phosphate and MOPS buffers. Data extracted from the gels in Figures A69 and A80.

Figure IV.14 compares the extent of the nuclease activity of **20**, **21** and **23** which is presented as the slope of the straight lines of ln (%Sc) *vs.* complex concentration. It is clear that the DNA cleavage ability of **23** is similar to that of **20**, while **21** has a much higher nuclease activity. Quantification of the nuclease activity in phosphate buffer and calculated slopes together with the intervals for 95% confidence can be observed in Table IV.4 and Table IV.5, respectively. For **21** under MOPS the values of ln (%Sc) *vs.* concentration diverge somewhat from linearity because, simultaneously to the cleavage of the Sc, cleavage of the Nck into Lin form also takes place.

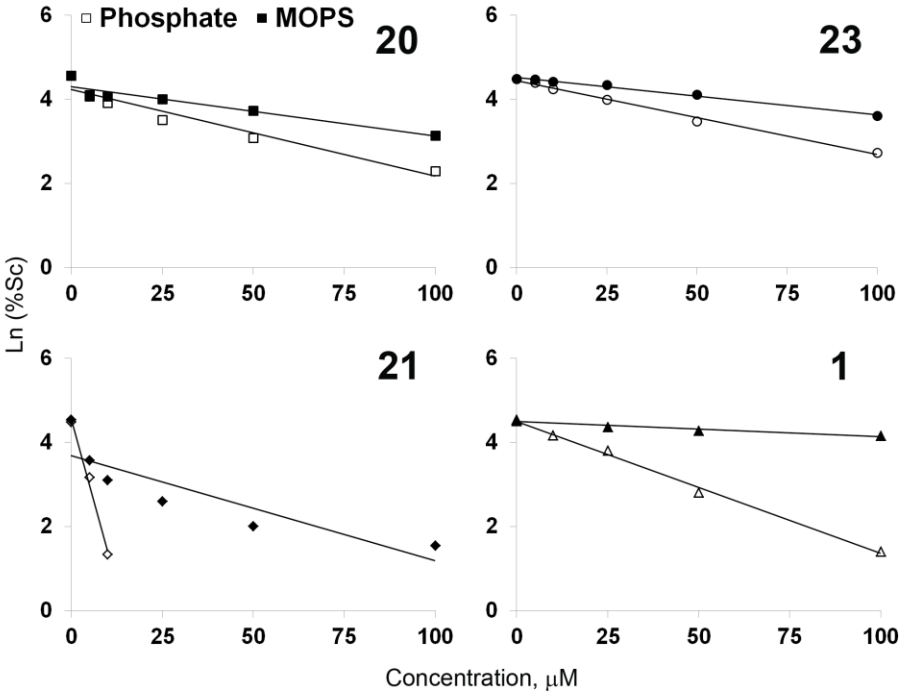

Figure IV.14. Comparison of the extent of pDNA cleavage by **20**, **21** and **23** and VO(oda)phen with the one of **1** under phosphate and MOPS buffers, ln (%Sc) *vs*. complex concentration.

Table IV.4. Values of ln (%Sc) corresponding to 0, 5, 10, 25, 50 and 100 μM complex concentration under phosphate buffer. Sampe with complex concentration '0' is the the one with plasmid DNA and no complex added.

Concentration, μM	**ln (%Sc)**			
	1	**20**	**21**	**23**
0	4.513	4.571	4.495	4.491
5	**	4.105	3.169	4.398
10	4.168	3.918	1.346	4.248
25	3.805	3.515	*	4.000
50	2.808	3.091	*	3.485
100	1.405	2.299	*	2.733

* Sc not detected due to complete degradation into Nck and Lin.

** Not tested

Table IV.5. Calculated slopes for ln (%Sc) *vs.* complex concentration for **20**, **21** and **23** and **1** under phosphate buffer. Intervals for 95% confidence are presented.

Complex	1	20	21	23
$m \pm \Delta m$	--0.031±0.004	-0.021±0.008	-0.3±0.4	0.018±0.002

Other oxidovanadium(IV) complexes that showed a concentration-dependent activity are presented in Figure IV.15. Except for VO(clor) (**26**), all three complexes promote single and double-strand DNA scissions at ri 1.7, 3.3 and 6.7. $VO(PA)_2$ (**19**) is the most active followed by $VO(MPA)_2$ (**17**), $VO(dmpp)_2$ (**18**). Complex **26** seems to be the least active despite similar increase in the percentage of the Nck form as with **18**. No linearization is observed even at ri 6.7. The cleavage activity of all four complexes is considerably lower than that of **1**.

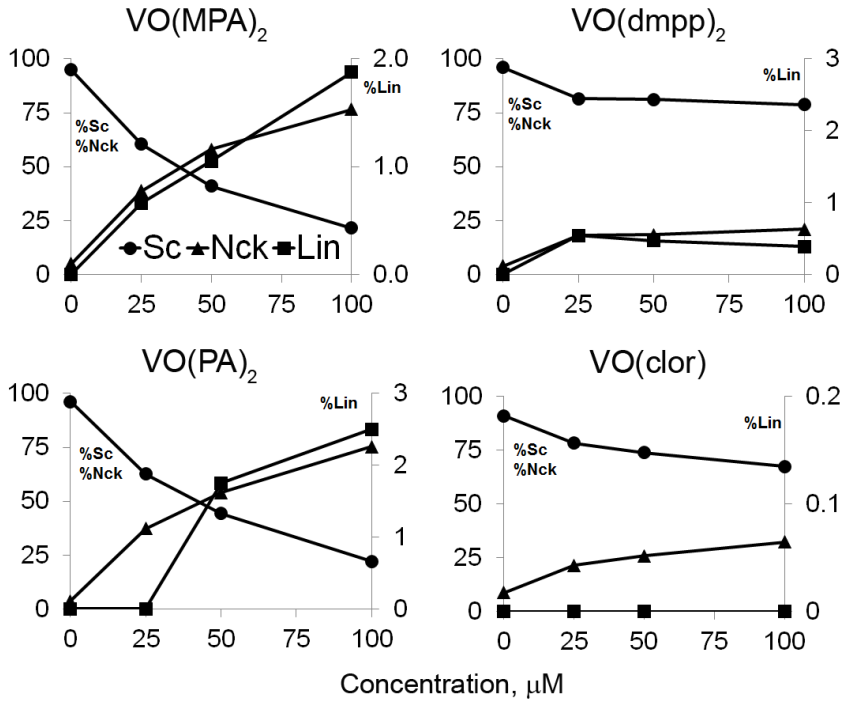

Figure IV.15. Relation of the nuclease activity of **17**-**19** and **26** under phosphate buffer with the metal:bp ratio presented as the percentage of each DNA form *vs*. complex concentration. The percentage was calculated from the areas measured by densitometry in the gels from Figures A60, A62 and A113.

Complex **17** and **19** exhibit similar DNA cleavage activity under both buffers (Figure IV.16) can be considered for the further studies as potential inorganic nucleases.

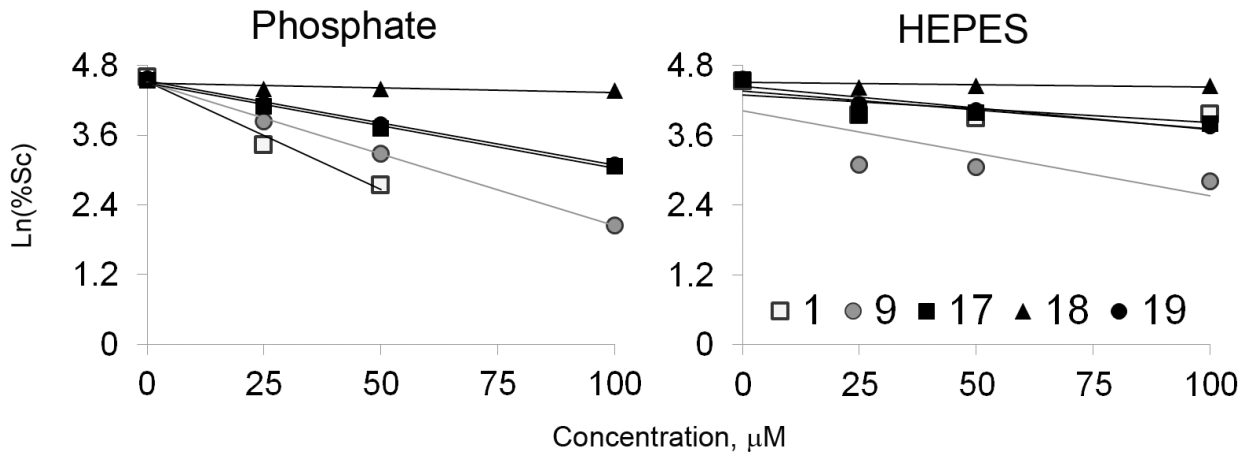

Figure IV.16. Efficiencies in DNA degradation promoted by **17**-**19** compared with those of **1** and **9** under at 25, 50 and 100 μM (ri 1.7, 3.3 and 6.7) phosphate and HEPES buffers. Data extracted from the gels in Figures A59, A60, A62 and A63.

Table IV.6 and Table IV.7 show respectively calculated values of ln (%Sc) and slopes for -ln (%Sc) together with the intervals for 95% confidence. According to these results, the potency order of activities under phosphate and HEPES buffers are **1**>**9**>**17**~**19**>**18** and **9**>**19**>**17**>**1**>**18**, correspondingly. Organic buffers, in this case HEPES, seem inhibit the nuclease activity of **1** considerably.

Table IV.6. Values of ln (%Sc) corresponding to 0, 5, 10, 25, 50 and 100 μM complex concentration under phosphate buffer. Sampe with complex concentration '0' is the the one with plasmid DNA and no complex added.

Buffer	Concentration, μM	ln (%Sc)				
		1	**9**	**17**	**18**	**19**
Phosphate	**0**	4.605	4.562	4.553	4.565	4.567
	25	3.436	3.835	4.102	4.400	4.138
	50	2.737	3.287	3.713	4.396	3.789
	100	*	2.053	3.073	4.365	3.097
HEPES	**0**	4.537	4.554	4.566	4.568	4.556
	25	3.956	3.097	3.954	4.419	4.140
	50	3.895	3.053	3.988	4.453	4.033
	100	3.959	2.813	3.800	4.454	3.754

* Sc not detected due to complete degradation into Nck and Lin.

Table IV.7. Calculated slopes for –ln (%Sc) *vs.* complex concentration for **1**-**9**, and **17**-**19** under phosphate buffer. Intervals for 95% confidence are presented.

$m \pm \Delta m$	**1**	**9**	**17**	**18**	**19**
Phosphate	-0.04±0.07	-0.024±0.003	-0.015±0.004	-0.0017±0.04	-0.015±0.002
HEPES	-0.005±0.02	-0.015±0.03	-0.006±0.01	-0.0008±0.004	-0.007±0.007

$VO(chrysin)_2$ (**24**) [156], $VO(morin)_2$, (**25**) [157] and $VO(silibinin)_2$ (**27**) [167], as the complexes that were studied for their antitumor effect by our collaboration group of Dr. Susana Etcheverry, in the DNA cleavage activity studies do not show any significant activity (Figure IV.17) even after addition of activating agents. Only **27** seems to exhibit a weak single-strand cleavage at tested ri 3.3.

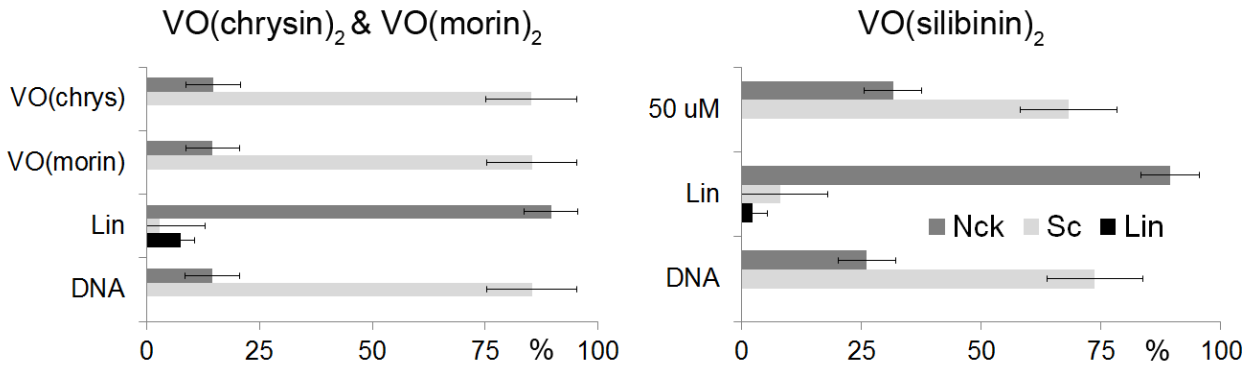

Figure IV.17. DNA cleavage activity of **24**, **25** and **27** under phosphate buffer related to the complex concentration. Error bars represent S_r. Data extracted from the gels in Figures A92 and A98.

$Cu(acac)_2$ (**15**) and $Ni(acac)_2$ (**16**), possessing similar structure to **1**, were tested to determine the role of the metal center in the DNA cleavage activity of acac-containing complexes. Unlike **16**, which does not show any nuclease activity, **15** induces nicking with no apparent concentration dependence (Figure IV.18). Addition of activating agents increases the nuclease activity of **15** significantly, especially in the presence of MPA – plasmid seems to undergo a complete destruction. Complex **16** still shows no effect on the pDNA.

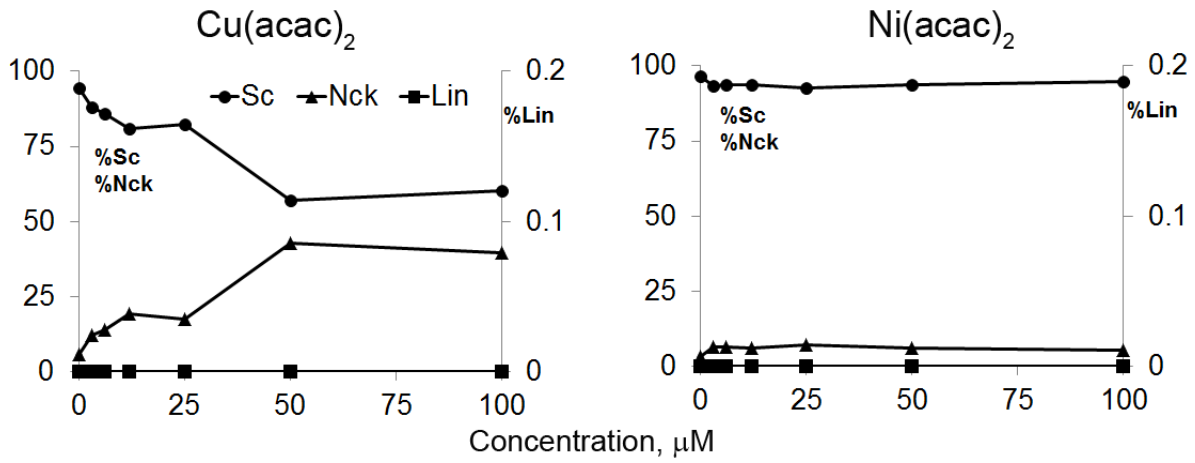

Figure IV.18. Cleavage of pA1 pDNA by **15** and **16** at 3, 6, 12, 25, 50 and 100 μM (ri 0.2, 0.4, 0.8, 1.7, 3.3 and 6.7) under phosphate buffer presented as percentage of the Sc, Nck and Lin forms *vs*. complex concentration. Data extracted from the gels in Figures A51 and A52.

The nuclease activity of six vanadium and three copper complexes containing amino acids and phen or bipy as co-ligands, **28**-**36**, is compared in Figure IV.19. These complexes are of biological importance and possess therapeutic properties (e.g., anti-cancer). Except for VO(Sal-L-Phe)(bipy) (**31**), which exhibits a low single-strand cleavage, none of these vanadium complexes induces the cleavage at the tested concentration of 50 μM (ri 3.3). Stronger cleavage of pA1 pDNA by copper complexes, namely Cu(Sal-Gly)(phen) (**29**) and Cu(Sal-L-Phe)(phen) (**30**), could be explained by the presence of phen ligand, which, as aforementioned, is a good DNA intercalator able to mediate the DNA breakage.

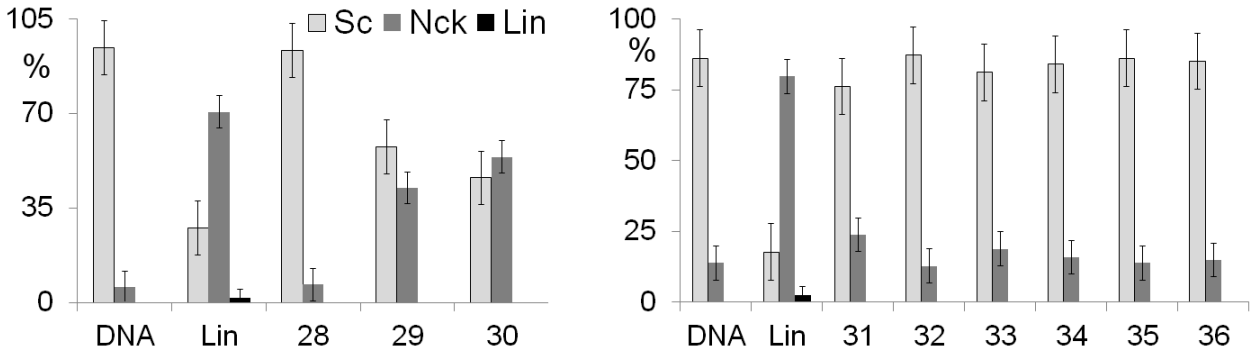

Figure IV.19. Cleavage of pA1 pDNA by **28**-**36** at 50 μM (ri 3.3) under phosphate buffer. All complexes were dissolved in 5% EtOH. Error bars represent S_r. Data extracted from the gels in Figures A101 and A110.

IV.2.2 Effect of buffer media

To understand the importance of buffer media in the studies of DNA cleavage activity of metal complexes, the following questions were of importance:

Do the concentration and nature of the pH buffer affect the nuclease activity of vanadium compounds? Is there any difference in the nuclease activity of **1** when it is dissolved in water and in buffer?

Organic, most often Good's buffers[54] [469,509-511] such as MOPS, MES, HEPES, are common pH buffer media in biochemistry laboratories and are typically reported in the studies of the nuclease activity of metal complexes. Considering the fact that these organic buffers are weak radical scavengers [462,512], it is not expedient to use only them for testing inorganic nucleases, assuming the DNA cleavage is commonly

[54] Good buffers (or Good's buffers) are twelve buffering agents selected and described by Norman E. Good and colleagues in 1966. He developed buffers based on several criteria that made them useful candidates for biochemical research: pKa values between 6-8, good solubility in water, cell membrane impremeability, minimal salt, temperature and ionic strength effects, well defined or nonexistent interactions with mineral cations, biochemical inertness, chemical stability, optical absorbanse (should not absorbe visible or ultraviolet light) purity, non-toxicity, ease of preparation and low cost. *Tris is **not** one of the Good's buffers*. It exhibits large shifts in dissociation with temperature changes. Tris buffer solution at pH 7 will drop to 5.95 at 37 ºC. Also its pH decreases approximately 0.1 pH unit per tenfold dilution.

promoted via oxidative mechanism; cases of DNA being cleaved hydrolytically are still rare given the stability of DNA towards hydrolysis (half-life is approximately 130 000 years at neutral pH and 25 ºC). Phosphate buffer is an ideal alternative for such studies. Unlike, MOPS, HEPES or TRIS, it does not possess radical scavenging properties, moreover it is an important biogenic ligand, one of the major constituents of human blood serum and interstitial fluids, where it is present at the approximate concentration of 1.1 mM [513]. The choice of phosphate buffer for pDNA digestion studies is not random: physiological conditions such as incubation temperature (37 ºC) and buffer pH (6.9-7.4) together with the medium itself that is biologically important, allows projecting *in vitro* results for *in vivo* application. Therefore, complexes were typically studied under two buffers – organic (HEPES, MOPS or TRIS) and inorganic (phosphate).

The results in Figure A31–Figure A37 show that the mixture of phosphate buffer with **1** equals a strong pDNA cleavage, whereas MOPS, HEPES or TRIS buffer do not favour this reaction (Figure A1–Figure A3). Figure III.20 compares the extent of the DNA cleavage by **1**-**5** and **9** at 50 μM under MOPS buffer. All complexes promote only single-strand cleavage and according to the calculated percentage the order of activity can be as follows: **1**>**2**>**4**~**9**>**3**~**5**.

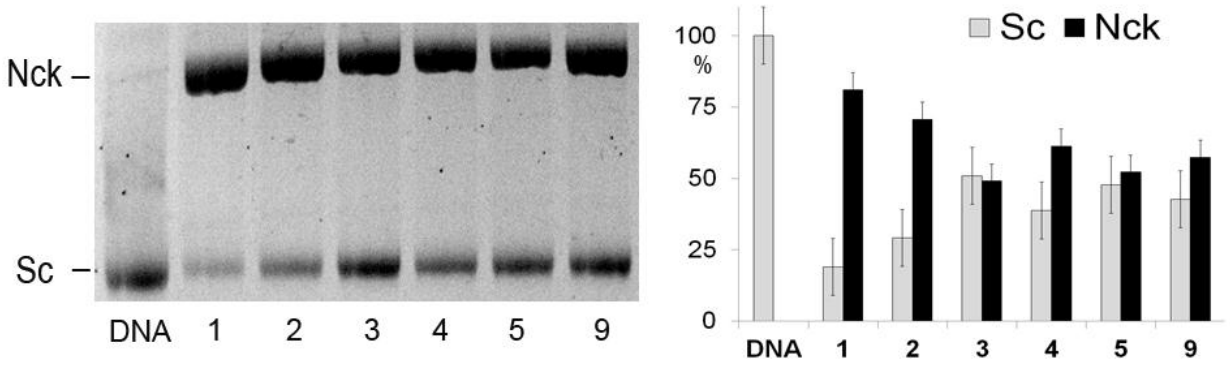

Figure IV.20. *Left*: Agarose gel of pA1 incubated with **1**-**5**, **9** under MOPS buffer (pH 7.0). "DNA" - native DNA digested in the absence of metal. Numbers 1-5 and 9 refer to corresponding complexes. Complex concentration for **1**, **2**, **4**, **5** was 50 µM (ri 3.3), prepared from stock solutions of 100 µM; **3** was diluted 1:2 from a saturated solution at room temperature. *Right*: Percentage calculated by densitometry. Error bars represent S_r.

Results of the nuclease activity of **1** expressed as a slope of the decrease of ln (%Sc) related with the increase of complex concentration (Figure IV.21), shows that the complex exhibits an insignificant activity in the presence of organic buffers, whereas under phosphate the difference is striking. Under TRIS the values of ln (%Sc) *vs.* concentration diverge somewhat from linearity most probably because the cleavage is not concentration dependent.

Complex **9** seems to behave similarly in all tested buffers (Figure IV.22) exhibiting stronger DNA cleavage activity under HEPES. Since **9** was found to precipitate under phosphate, this could explain the lower activity than under HEPES.

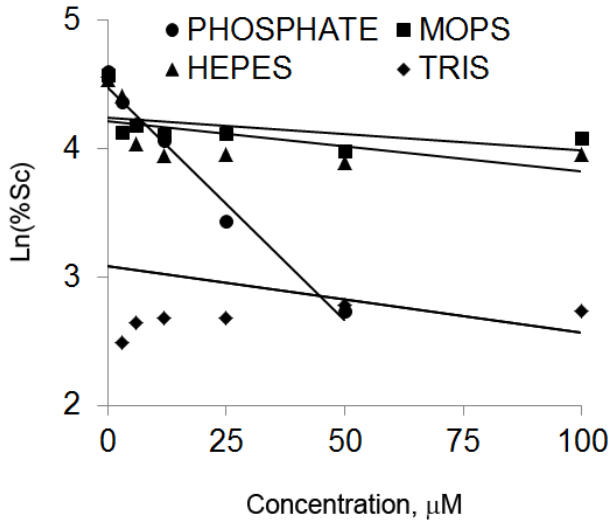

Figure IV.21. Comparison of the extent of pDNA cleavage by **1** under phosphate, MOPS, HEPES and TRIS buffers, expressed as ln (%Sc) *vs.* complex concentration. There is no Sc at 100 μM under phosphate buffer as pDNA was linearized completely.

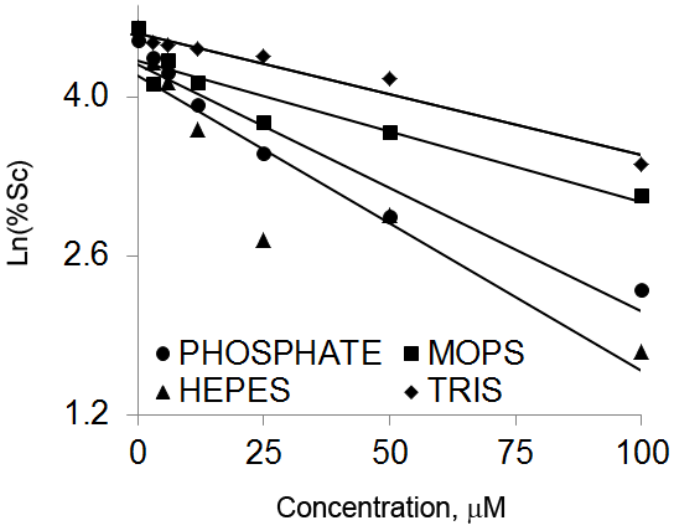

Figure IV.22. Comparison of the extent of pDNA cleavage by **9** under phosphate, MOPS, HEPES and TRIS buffers, expressed as ln (%Sc) *vs.* complex concentration. Data extracted from the gels in Figures A44 and A45.

Not only was the nature of the pH buffer but also its concentration found to affect the extent of the DNA cleavage activity of vanadium complexes. Comparison the DNA cleavage activity of **1**, **4**, **6**, **9** and VO(acac-NH_2)$_2$ at 12 μM (ri 0.8) and 25 μM (ri 1.7) under 10 and 100 mM phosphate buffer (Figure A35 and A36) showed that all complexes exhibit stronger DNA cleavage at lower buffer concentration.

Presuming that the DNA cleavage activity of the majority tested chemical nucleases follows oxidative pathways, the possibility that the formation of ROS in the aqueous solution of **1** is the culprit of its efficient behaviour towards DNA degradation was considered. This hypothesis together with that MOPS can act as a radical scavenger was clarified by examining the DNA cleavage by **1** under phosphate buffer with addition of MOPS (Figure IV.23). The nuclease activity of **1** is much higher in the absence of MOPS, linearization of pDNA 0.8% and 1.6% occurs at 5 and 10 mM of phosphate, respectively. On the contrary, the DNA degradation is always inhibited when MOPS is added and the extent of the inhibition is higher for higher concentrations of MOPS. Apparently, the generation of ROS by **1** is greatly increased in the presence of phosphate at millimolar concentrations and is always inhibited with MOPS due to its scavenging action.

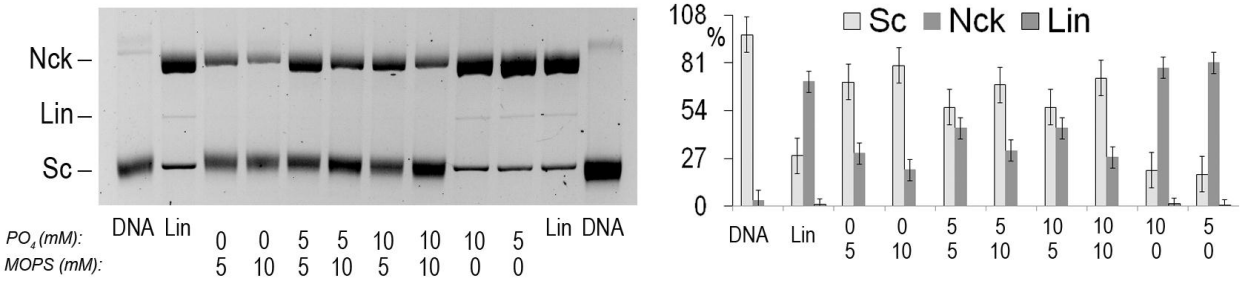

Figure IV.23. Effect of mixtures incubation with DNA buffered with mixtures of MOPS and phosphate buffer on the DNA cleavage activity of **1** (50 μM). *Left*: AGE image. "Lin" and "DNA" are the controls for linearized and native DNA. *Right*: Results obtained from densitometry measurements. Error bars represent S_r.

As phosphate buffer was found to play a significant role in the nuclease activity of **1**, the question how exactly arose immediately. According to Saran et al. [447] and Reinke et al [449] Fe(II) ions in solutions with neutral pH have a tendency to autoxidize to Fe(III) and most likely to precipitate in form of insoluble hydrates. When this solution is phosphate medium, the precipitation is prevented by formation of Fe(III)-phosphate complex. This could be true for V(IV) ions as well, but in the case of **1** it is less likely due to the presence of the ligands coordinated to the complex. However, the assumption that phosphate buffer increases the chances of **1** for autoxidation has been made. It is reasonable to assume that oxidovanadium(IV) complexes undergo a structural change in this medium: phosphate interacts with 1, for example by stabilizing the mono-chelated complex, $V^{IV}OL^{+}$. This assumption could explain the stability of **1** and **2** observed in UV-vis spectra, taking into account that the compounds were directly dissolved in buffer. Since phosphate is an abundant component in physiological buffer system, its possible complexation with metal complexes, particularly **1**, is crucial for the future in vivo studies.

Reported studies of the interaction of inorganic phosphate with $V^{IV}O^{2+}$ [34 ,514] show a formation of protonated 1:1 and 1:2 complexes in acidic pH range, it then precipitates at pH ~4.5, and re-dissolves at pH~8.5, forming mononuclear mixed hydroxo species in addition to various poorly characterized oligonuclear hydroxo-bridged complexes. To our knowledge, no speciation studies for $VO(acac)_2$ in phosphate media have been reported. This has been done for maltolate, a small bidentate ligand with a stability similar to $VO(acac)_2$ [28,515]. Above pH 6, when the ratio metal:maltonate:phosphate is 1:5:5, phosphate cannot compete with maltolate for binding to vanadium. In the modelled physiological condition (phosphate and metal concentrations of 1 mM and 10 µM, respectively), it was predicted that 8% of vanadium forms a binary complex with maltolate and phosphate. The stability constant of $VO(acac)_2$ is close to that of $VO(maltolato)_2$ (15.6 and 16.3), thus it is possible that a micromolar solution of $VO(acac)_2$ in a 10 mM phosphate buffer will also contain a fraction of the ternary complex $V^{IV}O(acac)$-(phosphate). This assumption can be supported by SWV results

which indicate a possible formation of at least three different species: $VO(acac)_2(H_2PO_4)^-$, $VO(acac)(H_2PO_4)_2^-$ and $VO(H_2PO4)_2$.

IV.2.3 Effect of excess ligand

Assuming that the active species towards DNA cleavage is the one that is stable upon formation in an aqueous solution, it is possible that the predominant species is the one containing vanadium and at least one functional group as acac coordinated to vanadium ensures its stability.

Considering the importance of ligands in a coordination complex, two following questions were of interest:

1) Do the ligands of the active complexes cause the pDNA degradation *per se*? In other words, can ligands be responsible for the nuclease activity of tested complexes?

2) Does the increasing of the complex stability by addition of excess ligand mean a higher DNA cleavage?

Excess ligand favours the stability of $V^{IV}OL_2$ which is predominant species in an aqueous solution of **1**. Speciation studies [116] show that when one equivalent of Hacac is added to the aqueous solution of $VO(acac)_2$, the 1:2 species, i.e., $V^{IV}OL_2$, can be stable for 7 days. Speciation studies [231] of $VO(acac\text{-}NH_2)_2$ and $VO(acac\text{-}NMe_2)_2$ metal-ligand system showed that at 1:80 metal ion to ligand ratio (L/M), 80% are in the $V^{IV}OL_2$ form. Our group tested the effect of excess ligand on the nuclease activity of $VO(acac\text{-}NH_2)_2$, $VO(acac\text{-}NMe_2)_2$ by incubating the solutions, where the complex at 50 µM (ri 3.3) under phosphate buffer was stabilized by addition of an excess of ligand up to ~300 fold. Following this example, similar experiments with L/M of 1.25, 2.5, 5, 40, 80 and 160 were carried out (Figure A27-A29). No increase in the DNA cleavage is observed up to L/M of 160. Instead, a noticeable decrease in the activity of all three complexes is detected upon ligand addition. The inhibition of the DNA cleavage that is

especially prominent at higher excess of ligands, suggests that stabilization of the 1:2 species is not a determinant factor in a high nuclease efficiency observed in the presence of **1**.

Taking into account that $VO(acac)_2$ was reported [238, 240] to react with polydentate ligands having one acac group substituted, with the second acac group remaining resistant to substitution, it is likely that upon addition of aqueous solution of **1** to a sample containing pDNA and phosphate buffer during 1h incubation at 37 ºC, phosphate substitutes one $acac^-$ group. As a result $VO(acac)(H_2PO_4)^-$ species is formed which is the one possible responsible for the cleavage we observe. Therefore, there are two possible explanations for the inhibition of DNA cleavage upon addition of excess ligands. First, stabilization of the complex prevents the species from forming especially taking into account the fact that ligands were added before the complex. Second, if the species is formed despite the increased amount of ligands and assuming that this species favours the formation of ROS, i.e., the mechanism of cleavage is radical, it is possible that such high concentration of ligand acts as a radical scavenger.

IV.2.4 Effect of time

Studies of the effect of incubation time allowed answering the following questions:

1) How does the nuclease activity of VC change with the incubation time?

2) What is the minimum incubation time necessary for the DNA cleavage to be observed?

The DNA cleavage in the presence of **1** was found to increase with longer incubation time. Though no significant change is observed between the results obtained after 15 and 135 min incubation, a noticeable increase in the percentage of the Nck form at 3 μM (ri 0.2) and gradual linearization at 25 μM (ri 1.67) (Figure IV.24) suggest that the longer the time of pDNA digestion with **1**, the higher the extent of strands breaks. Nonetheless, it is clear that 15 min of incubation is sufficient for an efficient DNA scission, especially at 25 μM. In the experiment, where the lowest amount of time tested

was 5 min at 25 μM of **1** (Figure IV.25), the presence of both single and double-strand cleavages indicates that the DNA cleavage reaction at 37 ºC is rapid. Most likely that with longer incubation time the DNA degradation will continue increasing until completely destroyed. This assumption is supported by the calculated percentage of DNA forms presented in Figure IV.25. Increased incubation time up to 4 h resulted into gradual complete and increasing linearization.

The fact that the Lin band can be observed at 3 μM in the first 15 min of incubation suggests a very strong ability of **1** to cleave DNA.

Taking into account that the DNA cleavage occurs as early as 5 min of being incubated and still continues to be induced after 4 h, chosen incubation time of 1h in a typical AGE experiment might be considered as optimal for studies of DNA cleavage by VC.

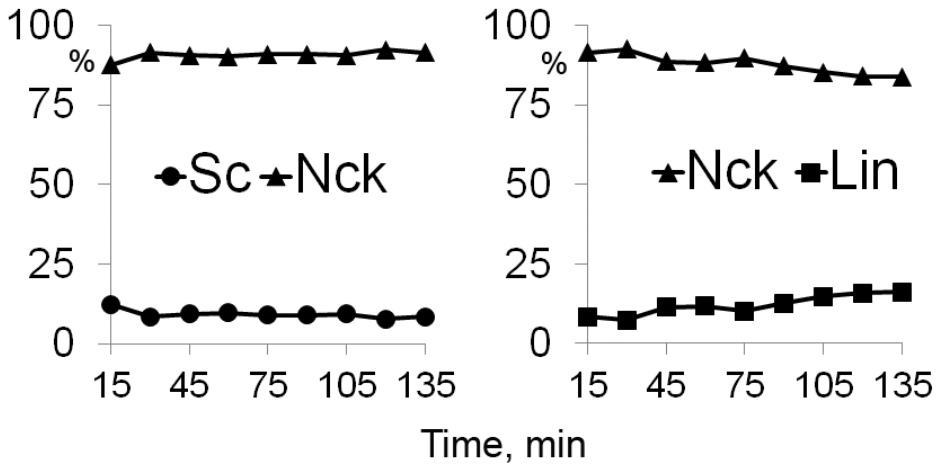

Figure IV.24. Relation of the nuclease activity of **1** and the time of its digestion with pDNA. Complex concentrations are 3 (left) and 25 mM (right) under phosphate buffer. Data extracted from the gels in Figures A21 and A22, respectively.

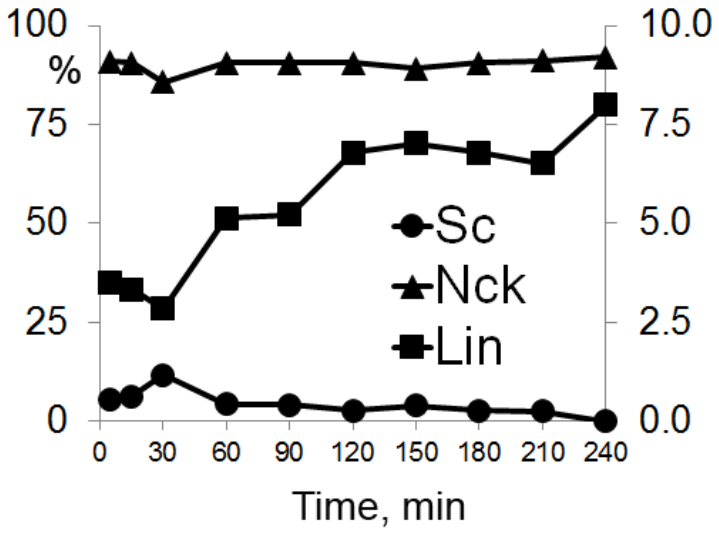

Figure IV.25. Effect of incubation time on the nuclease activity of **1** (25 μM, ri 1.67) under phosphate buffer expressed as the percentage of Sc, Nck and Lin DNA forms *vs.* time. Data extracted from the gel in Figure A23.

IV.2.5 Effect of light

Many chemical nucleases, including VC, have been found to break DNA photochemically [278-282].

Our group previously did some studies of the effect of light on the nuclease activity of **1**, determining that photocleavage is not an important process in the reaction with pDNA Results of the experiments where the incubation was carried in the dark (Figure A40), and those where the samples were incubated under a UV lamp at 370 nm (Figure A39), do not differ significantly from the experiments where incubation was carried out under natural light. Though the complete absence of light could not be guaranteed, it still seems like light does not affect the nuclease activity of **1**. The progress of the cleavage is evident with the increase of complex concentration (Figure IV.26).

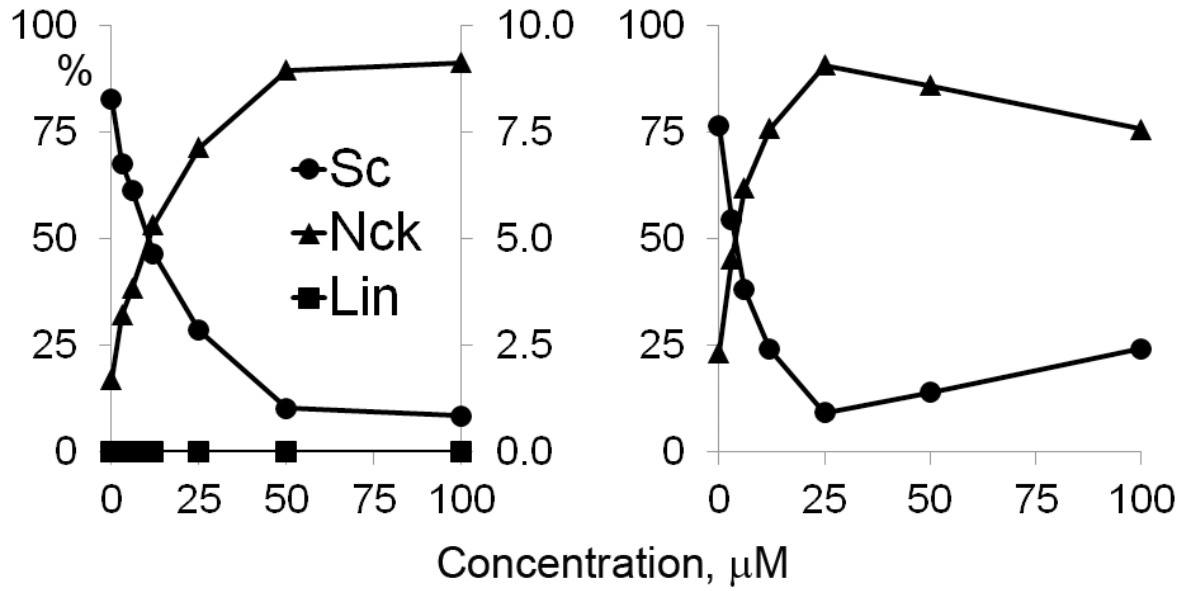

Figure IV.26. Nuclease activity of **1** at 3, 6, 12, 25, 50 and 100 μM (ri 0.2, 0.4, 0.8, 1.67, 3.3 and 6.7, respectively) under phosphate buffer. *Left*: samples were incubated wrapped in aluminium foil to ensure the protection from light. *Right*: samples were incubated under a 370 nm UV lamp. Data extracted from the gels in Figures A38 and A39.

IV.2.6 Effect of activating agents

Our group has previously tested the effect of the presence of an oxidizing and reducing agent on the nuclease activity of **1**. Oxone enhanced the complex nuclease efficiency, and it was observed that supercoiled DNA is totally broken into its Nck and linear forms. The activating effect of oxone was found to be similar both under air and inert atmosphere. In contrast, the reducing agent MPA inhibited the nuclease activity, although some degradation of the Sc form into the Nck form was still observed. This inhibiting effect also took place to the same extent under air and under inert atmosphere, but it appeared to be less dramatic under N_2 because activity is already low in the absence of any agent.

For most of the tested complexes in this work the addition of oxone or MPA ensured a significant change in the extent of the DNA cleavage. Such dramatic difference

indicates that the oxidation of V(IV) in the presence of oxone greatly affects the DNA breakage. Addition of oxone promotes oxidation of V(IV) to V(V) in the process involving the formation of ROS. Since oxidovanadium(V) complexes, **6**-**8**, exhibit rather moderate DNA cleavage activity, tit is unlikely that V(V)acac species that result from the oxidation of **1**, are the ones responsible for the strong nuclease activity. On the other hand, the role of ROS generated during the oxidation process may be crucial.

Addition of activating agents, especially oxone, to **6**-**8** increased the percentage of the DNA cleavage significantly. Linearization is observed for all three complexes with the higher extent for **7** followed by **6** and **8** (Figure IV.10). Hence, these oxidovanadium(V) derivatives of **1**, do not promote a significant nuclease activity unless a strong oxidant is present.

Monovanadate on its own has no effect on pDNA (Figure IV.27). The absence of the DNA cleavage in the presence of MPA, suggests that no reduction of V(V) took place. Upon addition of oxone a slight increase in activity is observed. This is unexpected, as V(V) is already in its highest oxidation state and cannot be further oxidized by oxone. Nevertheless, some explanation can be found from the reduction potentials of monovanadate and oxone. The equilibria for the redox pairs and the standard reduction potentials are:

$$HSO_5^- + 2H^+ + 2e^- \rightleftharpoons HSO_4^- + H_2O \qquad E^0 = 1.44V \qquad \text{(eq.IV.1)}$$

$$VO_2^+ + 2H^+ + e^- \rightleftharpoons VO^{2+} + H_2O \qquad E^0 = 1.00V \qquad \text{(eq.IV.2)}$$

When corrected for pH 7 buffered solutions, the conditional reduction potentials $E^{0'}$ become 1.03V and 0.17V. The Nernst equation can be used to estimate the reduction potential of a redox pair at 25ºC:

$$E_{ox/red} = E^{0'} - \frac{0.05916}{n} \log\left(\frac{[red]}{[ox]}\right) \qquad \text{(eq.IV.3)}$$

where, for a general redox equilibrium ox + $ne^- \rightleftharpoons$ red, $E_{ox/red}$ is the reduction potential of the redox pair ox/red, $E^{0'}$ is the conditional reduction potential for the pair at pH 7, n is the number of electrons exchanged and [red] and [ox] are the concentrations of the reduced and oxidized species. Applying to the present study,

$$E_{HSO_5^-/HSO_4^-} = E^{0'} - \frac{0.05916}{2} \log\left(\frac{[HSO_4^-]}{[HSO_5^-]}\right) \quad \text{(eq.IV.4)}$$

$$E_{VO_2^+/VO^{2+}} = E^{0'} - 0.05916 \log\left(\frac{[VO^{2+}]}{[VO_2^+]}\right) \quad \text{(eq.IV.5)}$$

Oxone is a triple salt $2KHSO_5 \cdot KHSO_4 \cdot K_2SO_4$ where HSO_5^- is the oxidant species undergoing the reduction to produce HSO_4^-, already present in solution at an initial concentration which is half that of HSO_5^-. The solution of monovanadate is not expected to contain any residues of V(IV), which would make its reduction potential practically infinite. It is thus reasonable to expect that vanadate will oxidize oxone (HSO_4^- to HSO_5^-) to a very small extent. As this process will involve ROS, it may justify the small nuclease activity observed when adding oxone to monovanadate.

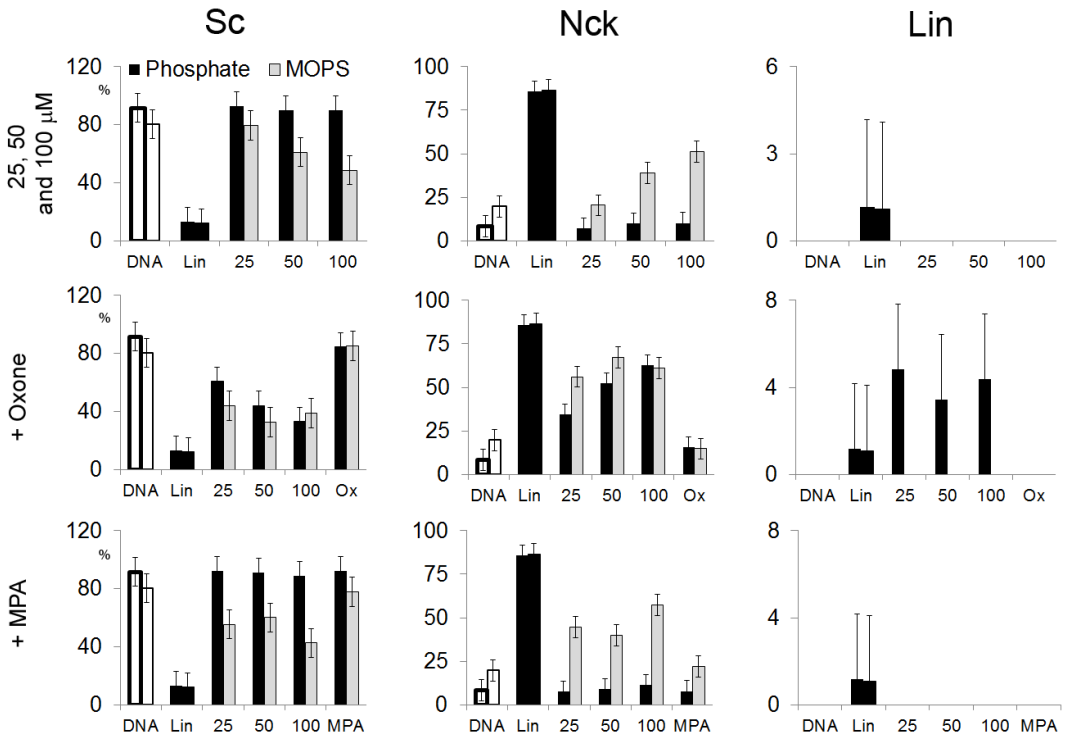

Figure IV.27. DNA cleavage activity of monovanadate at 25, 50 and 100 µM in the presence of activating agents under phosphate and MOPS buffers. Data extracted from the gels in Figure A49 and A50. The columns "DNA" compare two samples of DNA control from two gels. As reaction mixtures for the DNA controls typically do not contain any buffer medium, the columns are not filled with colours that were chosen to represent phosphate (black) and MOPS (grey). As reactions mixtures for the Lin controls are always prepared with phosphate buffer, both columns "Lin" are shown in black.

The effect of activating agents on the nuclease activity of **9** seems to be as significant as for **1**. There seems to be a difference in the effect of MPA under phosphate and MOPS buffers (Figure IV.28). Under MOPS buffer the situation is considerably different: in the presence of MPA the extent of the cleavage by **9** is much stronger than with oxone. The same behaviour is observed for **21**. The most efficient DNA cleavage seems to occur in the presence of MPA under MOPS buffer.

Regarding **20** and **23**, under both buffers the extent of the cleavage is affected by MPA or oxone but not dramatically (Figure IV.29). Activated by oxone and MPA, the nuclease behaviour of **21** is different from what was expected, i.e., being increased with oxone

and inhibited by MPA. A complete linearization takes place when the complex is not activated by the agents. Interestingly, under MOPS the amount of the Lin (9.6%) is considerably bigger than under phosphate (5.5%). Oxone seems to augment a double-strand cleavage under phosphate (11.3%) and inhibit under MOPS (4.8%). Addition of MPA to 50 μM of **21** increases the linearization under both buffers to 13.3% and 33.9% in phosphate and MOPS, respectively. Such a high percentage of the Lin form in the presence of MPA under MOPS, suggests extremely efficient nuclease ability. Moreover, the pDNA degradation seems to still be an on-going process. Clearly, the Lin form is increased at the cost of the Nck. A tail-like smear (Figure A91, lane 11) suggests that the Lin destruction into smaller fragments.

Complexes **20** and **23** also seem to cleave pDNA at higher extent under MOPS buffer. For **20**, the percentage of the Lin form in the absence of activating agents is 2 and 4.3% under phosphate and MOPS, respectively. With oxone it is 3 and 4.3%, and with MPA – 2.9 and 3.8%.

In the case of **23**, the percentage of linearization with no agents is 2.8 and 4.4% under phosphate and MOPS, respectively. Upon addition of oxone, it decreased to 2.7 and 3.9%; in the presence of MPA it is 3 and 3.6%.

Finding a plausible explanation for an efficient nuclease behaviour under MOPS and MPA, it is likely that both **9** and **21** cleave pDNA via mechanism other than radical. Another possibility is another type of ROS which are not scaveged by MOPS.

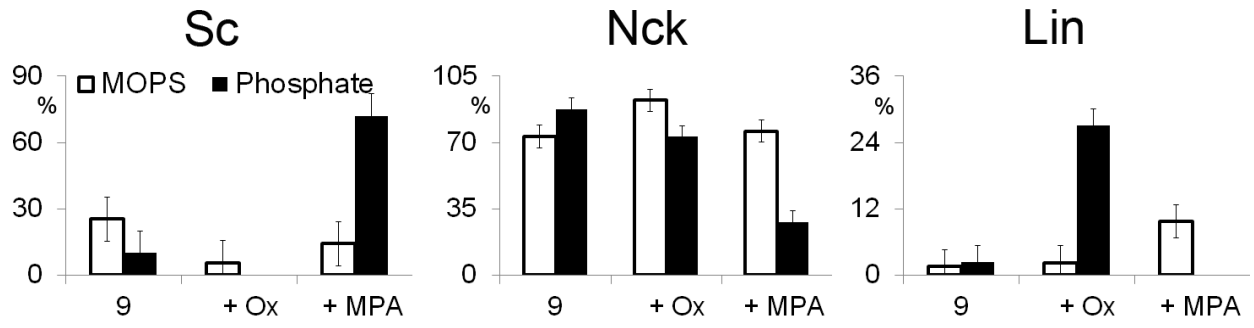

Figure IV.28. Percentage of the Sc, Nck and Lin forms of pDNA after incubating **9** with oxone and MPA under phosphate and MOPS buffers. Data extracted from the gels in Figure A98 (lanes 12-14) and A99 (lanes 7-9).

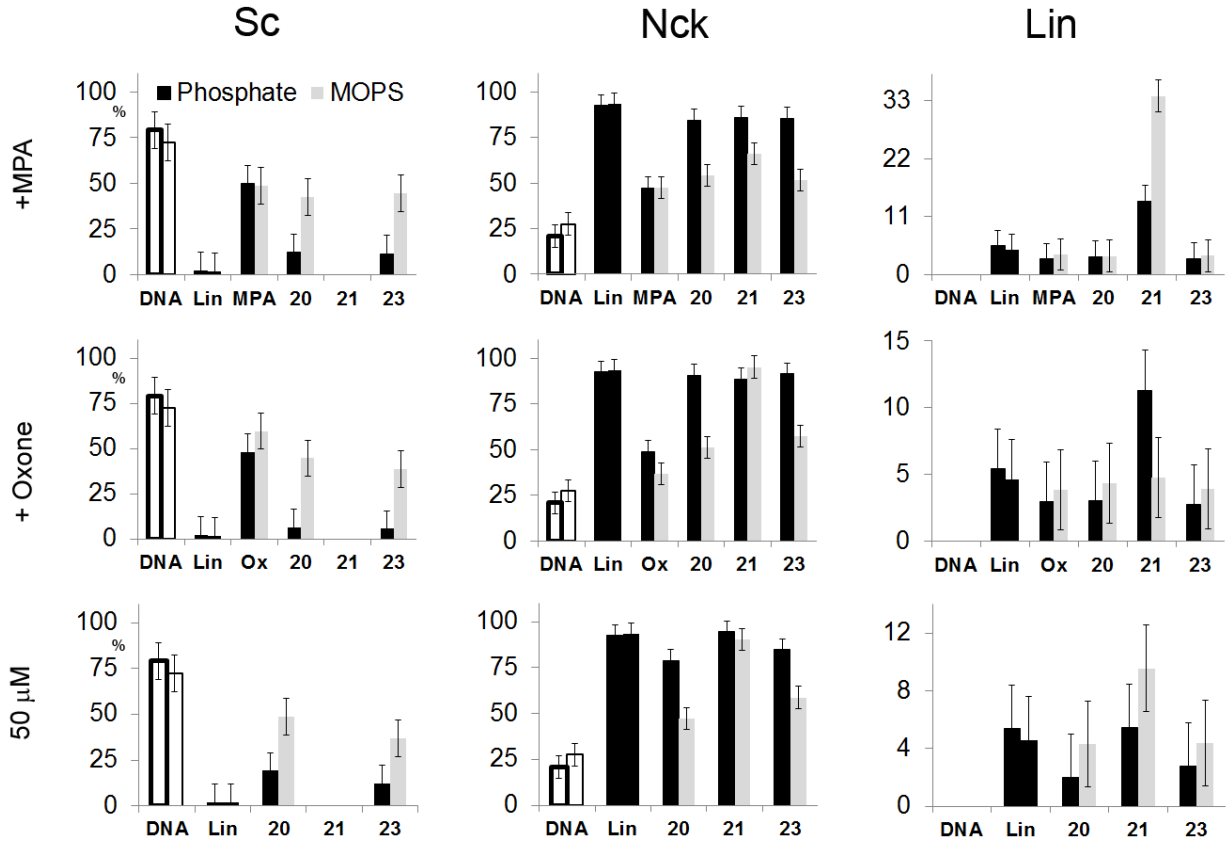

Figure IV.29. Effect of oxone and MPA on the nuclease activity of of **20**, **21** and **23** at 50 µM (ri 3.3) under phosphate and MOPS buffers. Data extracted from the gels in Figures A90 and A91. Error bars represent Sr.

The presence of activating agents is expected to intensify the extent of the DNA cleavage. It is assumed to be especially true for phen-containing compounds. Due to intercalation of phen, the DNA undergoes the strand breakage more readily. Addition of activating agents is supposed to augment the strength of the cleavage. The results of the effect of activating agents on DNA cleavage activity of phen-containing copper and vanadium complexes, Cu(Sal-Gly)(phen) (**29**), Cu(Sal-L-Phe)(phen) (**30**), VO(Sal-L-Phe)(phen) (**32**) and VO(Sal-Gly)(phen) (**34**), support this assumption. After a 5h-digestion, **32** and **34** in the presence of MPA (Figure A105 and A106) promote both single and double-strand cleavage, and induced a complete linearization of the Sc DNA with oxone (Figure A103 and A104).

Similarly, in the presence of oxone or MPA, **29** and **30** break the plasmid into very small fragments that are possibly eluted in a gel and cannot be detected after visualization by UV-light. This is the reason of the missing bands observed in gels (Figure IV.30). These results were obtained following a long digestion of 5 h. At was the usual incubation of 1 h, in the presence of oxone the complexes behaved similarly, i.e., the plasmid underwent destruction (Figure A109, lanes 8 and 11). Effect of MPA seems to be less dramatic. The bands are well defined but the tail-like smears (lanes 9 and 12) suggest that pDNA undergoes the extensive degradation.

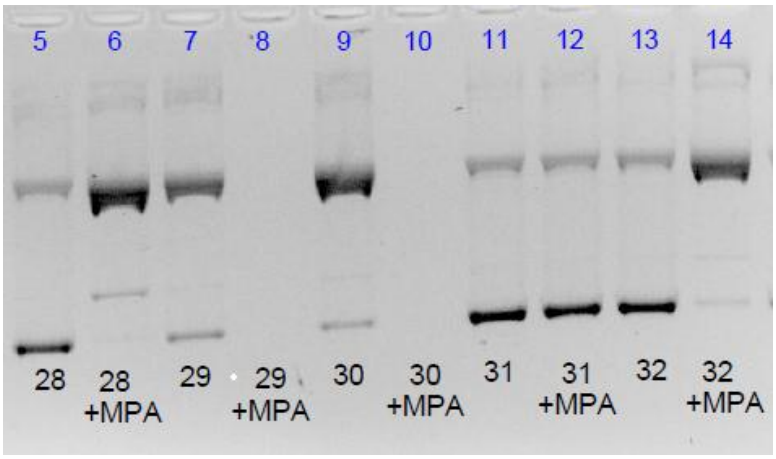

Figure IV.30. Effect of the reductant on the nuclease activity of **28**-**32** under PBS. Example of the complete breakage of pDNA by copper complexes with MPA. The snip of the gel image is from Figure A105.

These are not the only copper complexes that behave in such way towards DNA degradation. In fact, all copper complexes that were tested in this work by AGE, promoted the destruction of the plasmid in the presence of MPA. A good example is **15**. Regardless of the buffer medium, the complex seems to completely destroy the plasmid that no band can be observed under UV light Figure IV.31). Considering the fact that a typical concentration of MPA used in AGE experiment, i.e., 200 µM, might be too high, **15** and $CuCl_2$ at 50 µM were examined in the presence of 10, 25, 50, 100 and 200 µM Of MPA (Figure IV.32). A tail-like smear observed for both complexes at 25 µM (lanes 5 and 11) suggests that the destruction is taking place and already at 50 µM (lanes 6 and 12) the plasmid is completely degraded. A plausible reason for this high reactivity is that copper(II) is reduced by MPA to copper(I) in a mechanism involving reactive ROS which can cleave DNA [331, 516].

.

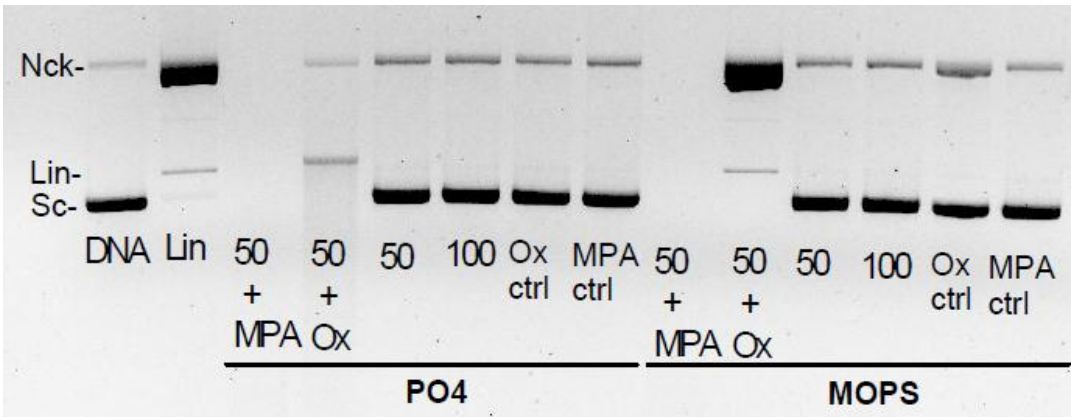

Figure IV.31. Extracted from Figure A54.

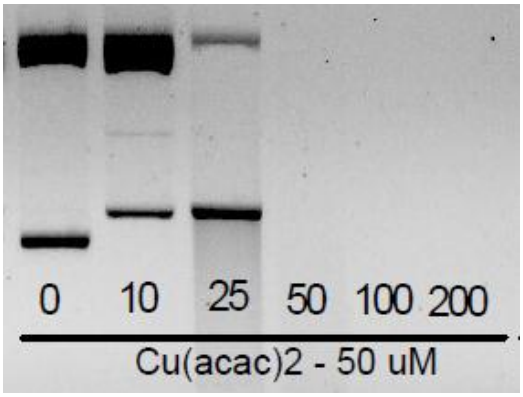

Figure IV.32. Extracted from Figure A56.

Examples of vanadium complexes which were not activated by oxone nor MPA under any tested pH buffer are $VO(morin)_2$ (**25**), VO(clor) (**26**) and $VO(silibinin)_2$ (**27**) (Figure A96-A98 and A99). This fact allows considering, as already aforementioned, possible important role of the ligands in the cleavage activity of VC. In the case of **25** and **26** he lack of the DNA cleavage can be explained by their solubility. Although they seem to visually dissolve in H_2O, DMSO is the solvent that is typically used in their solution preparation.

IV.2.7 Effect of radical scavengers and H_2O_2

The nuclease activity of many inorganic complexes has been attributed to oxidative pathways of the cleavage mainly via formation of OH radicals by Fenton-type reactions [246]. Literature survey on the reported potential vanadium nucleases points to the oxidative mechanism of DNA cleavage.

The use of known radical scavengers such as NaN_3, NaBz, DMSO in the AGE tests with active VC helped clarifying the nature of the mechanism of cleavage, which seems to be purely oxidative. Our group has previously shown that the pDNA cleavage of **1** is completely inhibited in the presence of all scavengers suggesting the involvement of activated oxygen species in the degradation process. Addition of sodium azide, a known scavenger of singlet oxygen, to the reaction mixture seems to significantly inhibit the DNA cleavage, suggesting the involvement of $^1O_2$ in the reaction of pDNA with **1**. The quenching of the reaction by two other scavengers (NaBz and DMSO) suggests a mechanism involving the formation of OH radicals, as intermediates. This assumption can be confirmed by the results obtained in the tests of VC with hydrogen peroxide, an important constituent of the reactions leading to hydroxyl radical formation. A dramatic increase in the DNA cleavage is observed (Figure IV.33). Increasing the concentration of H_2O_2 showed a much less significant effect on DNA degradation than increasing the complex concentration. This fact suggests that the oxidative mechanism is not very sensitive to the concentration of oxidant.

VC whether are being introduced intravenously, intramuscularly or orally are expected to interact with body's fluids. In living systems, H_2O_2 is formed by dismutation of superoxide anions, which are generated in several systems such as xanthine-oxidase, NADPH oxidase and NADH-dependent cytochrome P-450 systems and in neutrophils [517,518], and which can be generated by the oxidation of the metal centre in the presence of molecular oxygen [519]. Hence, addition of oxone or H_2O_2, most likely, will induce the oxidation of V(IV) with the production of ROS such as superoxide O_2^-, which may further react with V(V), yielding peroxidovanadium(IV). This product can be the cause of the DNA breakage. Liochev and Fridorovich in their numerous publications on

vanadate-stimulated oxidation of NAD(P)H [520-522], report the reaction of V(V) with by O_2^-, yielding a peroxidovanadium(IV), which is likely to be responsible for the univalent oxidation of NAD(P)H. VO^{2+} is the active form of vanadium that plus H_2O_2 can could oxidize NAD(P)H by a process dependent on hydroxyl radicals [523]. Thus, V(IV) can reduce H_2O_2 yielding •OH in Fenton-like reaction [524] via the same pathway as does Fe(II) and Cu(I).

The nuclease behaviour of **20**, **21** and **23** in the presence of scavengers is distinctively different under phosphate and MOPS buffers. As an example, Figure IV.34 compares the efficiency of **21** in the presence of the scavengers under both buffers. Clearly, scavenging effect under phosphate buffer is much stronger than under MOPS. This difference suggests that in the presence of phosphate buffer, ROS are the cause of the remarkable nuclease activity of **21**, as in the case of **1**.

Under MOPS buffer all three complexes of oda family (Figure IV.35) cleave pDNA more efficiently than **1**. Moreover, in the case of **21**, the extent of the pDNA cleavage induced under MOPS is as high as that with phosphate. Therefore, a mechanism by which **21** interacts with pDNA in MOPS is rather different from that of **1**. The same can be assumed under phosphate medium since the DNA degradation by **21** most likely is greatly dependent on the binding affinity of phenanthroline.

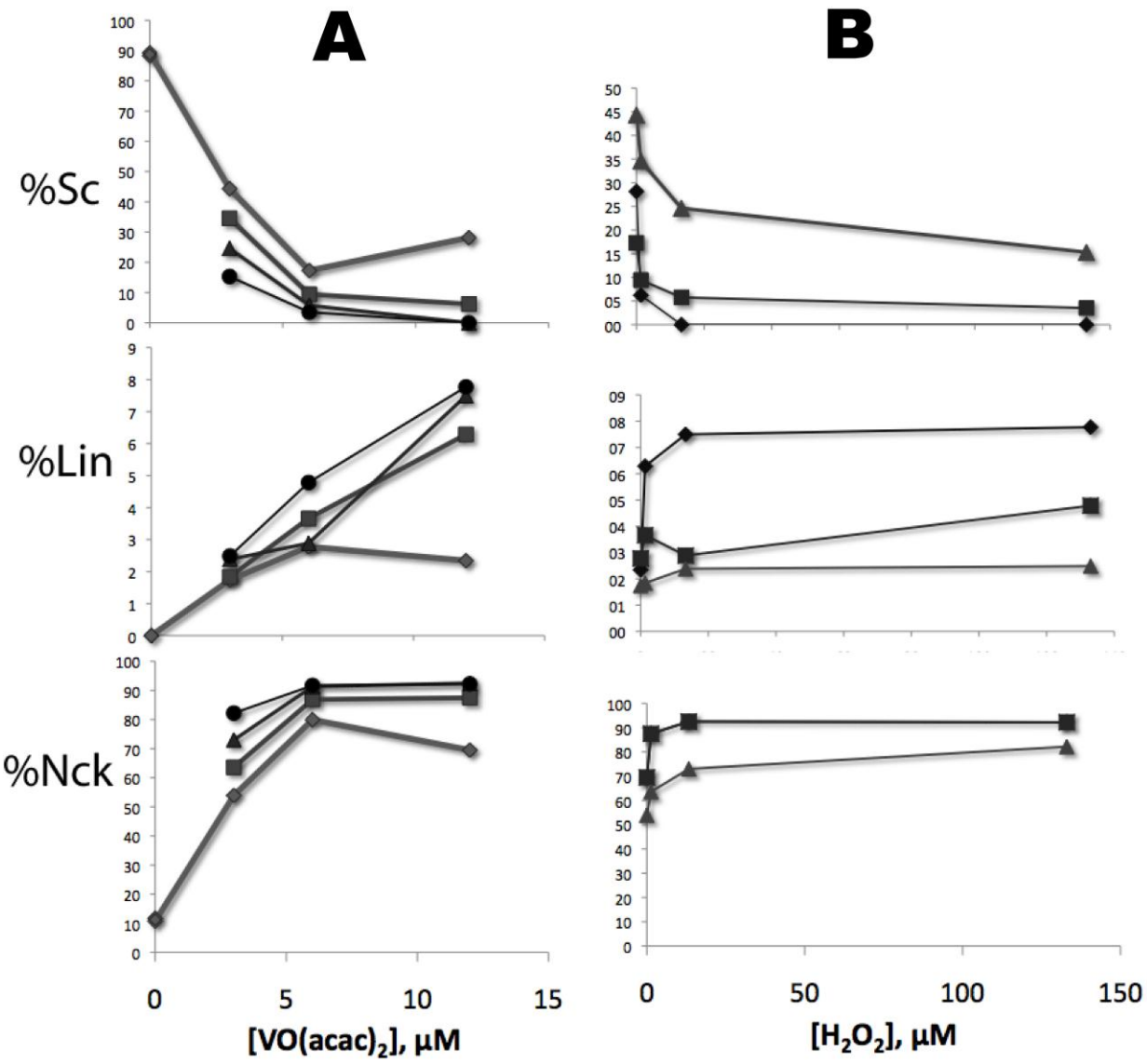

Figure IV.33. Effect of H_2O_2 on the nuclease activity of **1**. (A) Effect of complex concentration with constant peroxide content: (♦) no added H_2O_2 (■) 1 µM (▲) 10 µM (●) 100 µM H_2O_2. (B) Effect of H_2O_2 with constant complex concentration: (▲) 3 µM (■) 6 µM (♦) 12 µM $VO(acac)_2$.

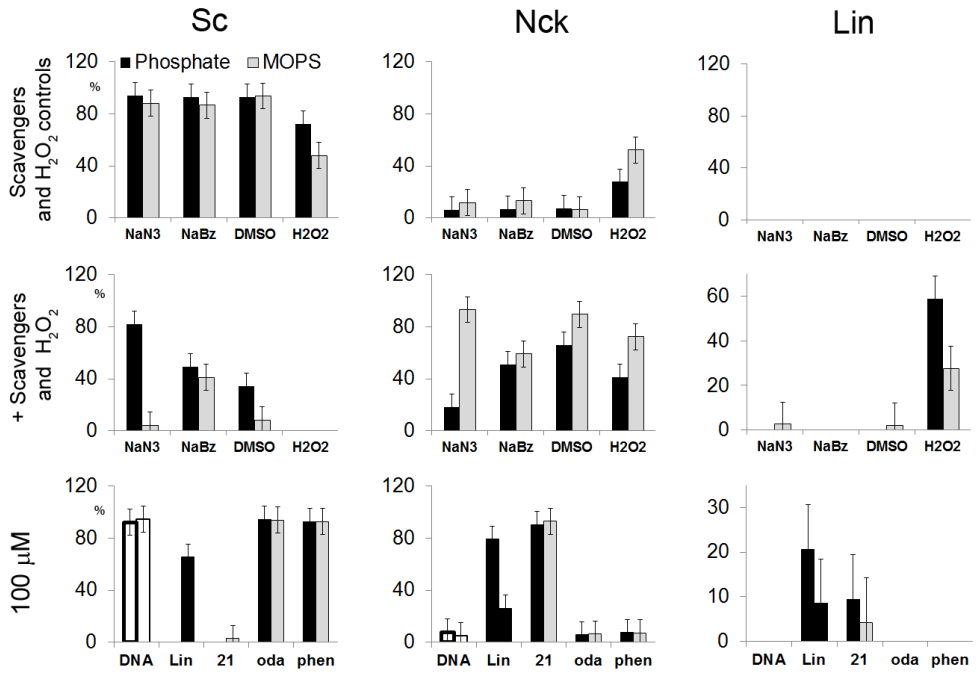

Figure IV.34. DNA cleavage activity of **21** at 100 µM (ri 6.7), under MOPS and phosphate buffers in the presence of scavengers. NaN_3, NaBz and DMSO are the controls of the scavengers. The data are extracted from Figures A77 and A79, respectively. Error bars represent S_r.

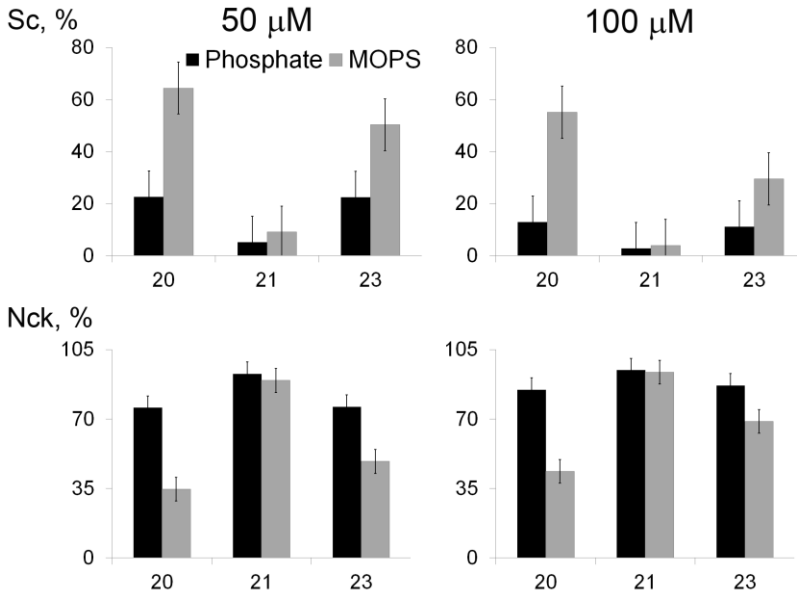

Figure IV.35. Percentage of the Sc and Nck forms obtained after pDNA cleavage by **20**, **21** and **23** at 50 and 100 µM under phosphate and MOPS buffers. Error bars represent S_r. Data extracted from Figure A90.

IV.2.8 Effect of atmosphere (air and nitrogen)

Atmospheric oxygen is an important constituent in many chemical and biochemical reactions. In the presence of metal cations such as V, Fe(II) Cu(I) it may cause the oxidation of the metal centre with the production of superoxide radicals [519].

The nuclease activity of **1** under inert atmosphere was studied previously in our group. The extent of the DNA cleavage decreased but only in a slight manner, a significant effect of **1** could still be noticed.

A slight inhibition of nuclease activity under N_2 is also observed for **9** under phosphate buffer. In the experiment with HEPES buffer the decrease is higher (Figure IV.36). These results, as in the case of **1**, indicate that air does not have a primary role in the nuclease activity of **9** which is possibly taking place through more than one mechanism in parallel, possibly radical, one at least involving atmospheric oxygen.

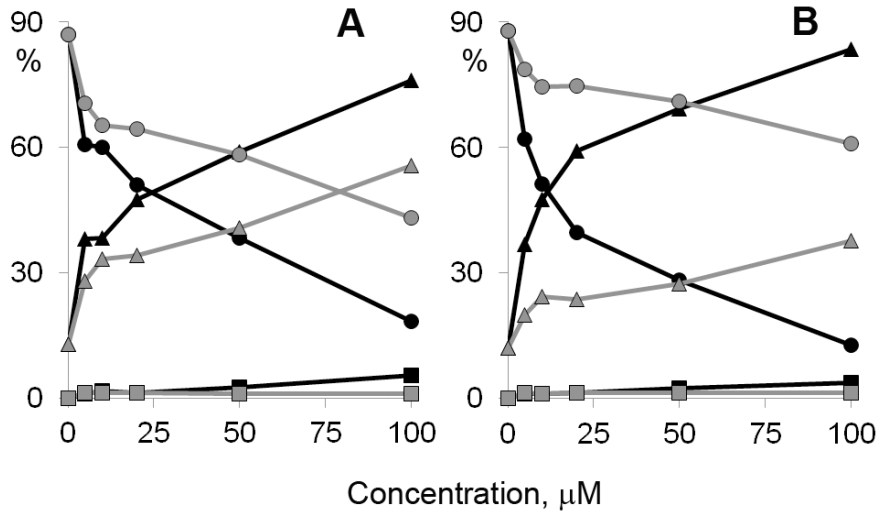

Figure IV.36. DNA degradation induced by **9** in phosphate (black lines) and HEPES buffers (grey lines), increasing the concentration of the complex. Samples were prepared and incubated under air (A) and nitrogen (B). The percentage of the DNA forms – Sc (●), Nck (▲) and Lin (■) was calculated by densitometry. Data extracted from Figure A42 and A43.

IV.2.9 'Phantom bands'

Interpretation of the results obtained by AGE consists of comparing the working samples (i.e., containing metal complexes, the nuclease activity of which is to be determined) with the controls for the supercoiled and linear DNA forms. As stated earlier, depending on the nuclease efficiency of a tested complex, two (Sc and Nck, single-strand cleavage) or three (Sc, Nck and Lin, double-strand cleavage) bands are expected to appear and be observed under UV-light on account of EtBr present in a gel. However, the data collected as the images of gels during AGE experiments revealed the present of some additional bands. They can be observed almost in every image, especially in the tests of compounds with a high nuclease activity. As the interest in the origin of these extra bands grew, we decided for the time being to call them '***phantom bands'***.

The intensity of 'phantom bands' seems to increase with the complex concentration. Gels A110- A113 contain the results of experiments specially dedicated to testing these bands, which we named as A1, A2, A3 and B1.

The 'phantom bands' are absent from the controls of native pDNA and from samples not containing metal (see for example samples containing ligand *oda* in gel A112), but always appear in samples containing vanadium. Samples incubated with copper complexes also present phantom bands in similar positions (see for example gels A102, A103, A109).

Figure IV.37 compares the percentage of the Sc, Nck and Lin DNA forms with that of 'phantom bands'. The intensity of B1 appears to correlate with the intensity of the linear form, while A2, and A3 follow the intensity of the Nck form. Band A1 is generally more irregular and harder to analyse than the other two. Lin and B1 are purposefully presented with the same symbol to better show an assumed relation between them.

The increase of the B1 band is apparently affected by the intensity of the double-strand cleavage. A3 seem to always be present in all samples with pDNA and a complex even if no cleavage takes place. In the controls of the Sc DNA form, no 'phantom bands' can

be observed signifying that these bands are the product of the nuclease activity of the tested complexes and not just some gel artefacts.

To our knowledge, no information on these extra bands is available in the literature. Typically, in scientific reports, a gel image is presented as a snip which is cut right above the Nck form and below the Sc or Lin forms; no additional records are usually provided. Such bands must represent a fraction of pDNA with a different electrophoretic mobility, which can occur due to a change in molecular mass, geometry or electrical charge. 'Phantom bands' can be a result of vanadium causing the distortion of the pDNA structure and changing its geometry. Another hypothesis is that vanadium ions bind to the phosphate backbone, changing the global charge of the pDNA. This binding would lower the overall negative charge of the phosphate backbone and thus lower the mobility of the DNA fragments. B1 would correspond to partially neutralized Lin form, while A1, A2 and A3 to partially neutralized Sc and Nck forms. ~

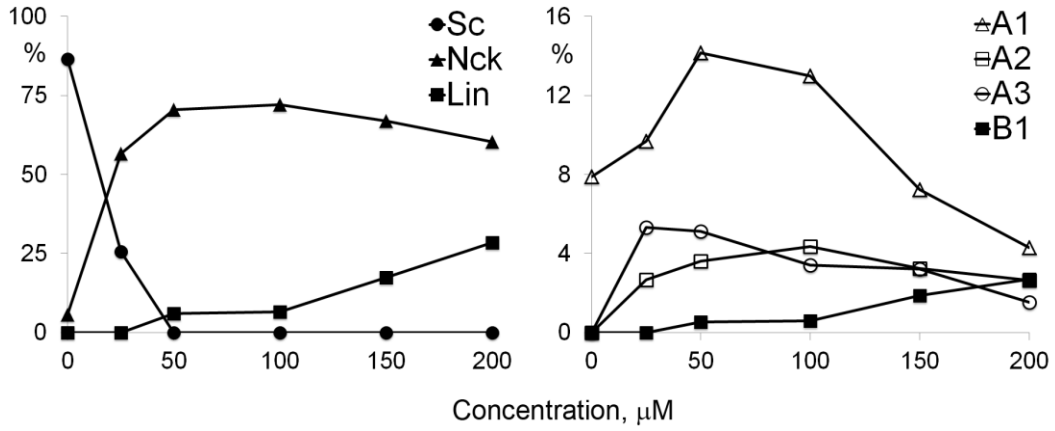

Figure IV.37. Change in the percentage of the Sc, Nck and Lin DNA forms (left) and A1, A2, A3, B1 (phantom bands; right) *vs.* concentration of **1**. Data extracted from Figure A110.

IV.2.10 Variability of gels

The results obtained in AGE can vary from gel to gel. The following are the most common problems that were encountered during AGE tests. In such cases an experiment was normally repeated:

1) gel of an inferior quality (e.g., a gel is contaminated or the agarose particles were not homogenised) (Figure IV.38);

2) poor resolution of the gel image (e.g., the bands are non- or only partially visible (Figure IV.39) or are not sharp (Figure IV.40)); .

3) poor separation of the bands (Figure IV.41), especially Lin and Sc (Figure IV.42, lanes 11 and 12);

3) possible contamination of all tested samples (Lin band is present in all lanes including references of Sc DNA (Figure IV.43);

4) significant difference in the percentage of the DNA forms in the bands of the controls of native and/or linearized DNA (typically, two controls of Sc and Lin forms of plasmid were included in both extremes of a 16/18-well gel plate) (Figure IV.44, lanes 1 and 14).

As a rule, especially in the beginning of this research, experiments were repeated whenever any of the above cases would take place. Later, two replicate gels were run on regular basis for purposes of the results reliability.

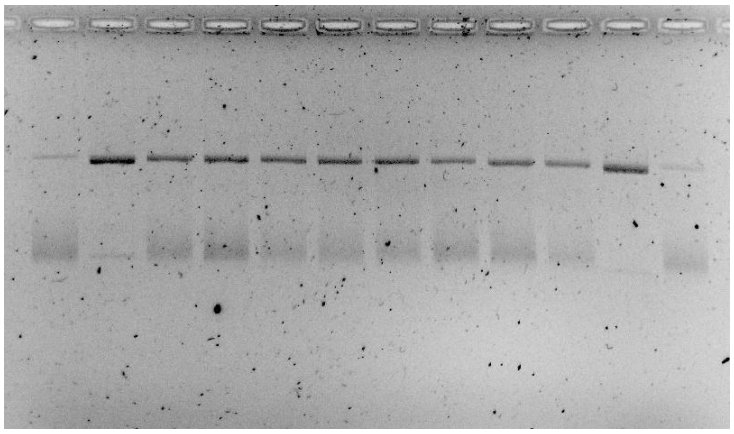

Figure IV.38. Example of a gel contaminated with some external material, small dots are probably undissolved particles of agarose.

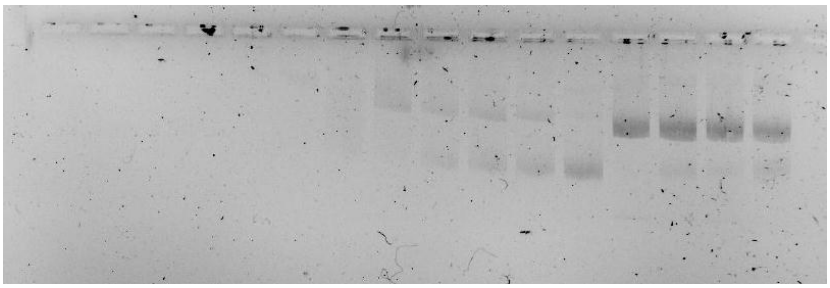

Figure IV.39. Example of the gel with a poor image resolution.

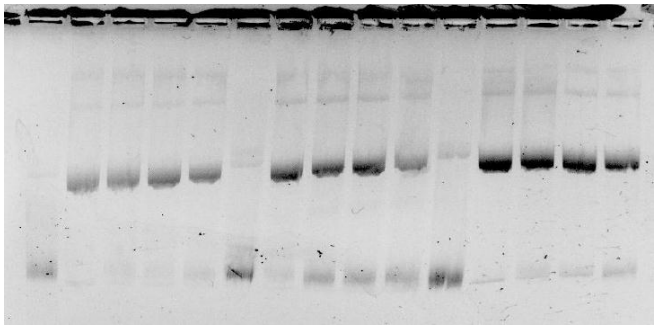

Figure IV.40. Example of the gel with distorted bands, low sharpness.

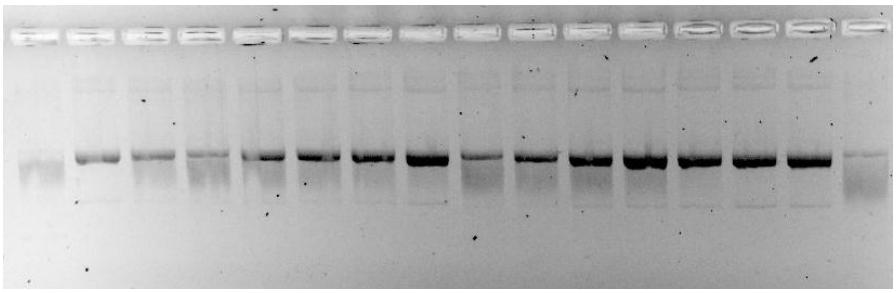

Figure IV.41. Example of the gel with a poor separation of the bands.

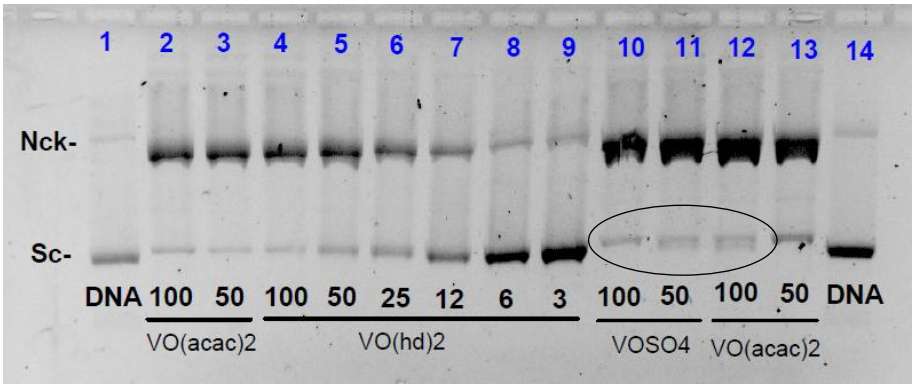

Figure IV.42. Example of the gel with a poor separation of the Lin and Sc bands.

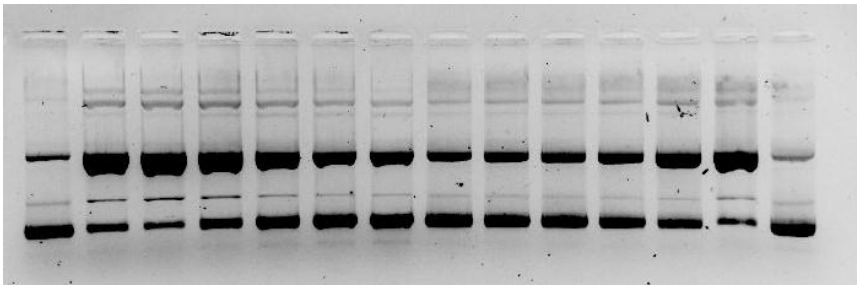

Figure IV.43. Example of the gel, where all the samples, including both references of the pDNA (first and last lanes), contain a Lin band.

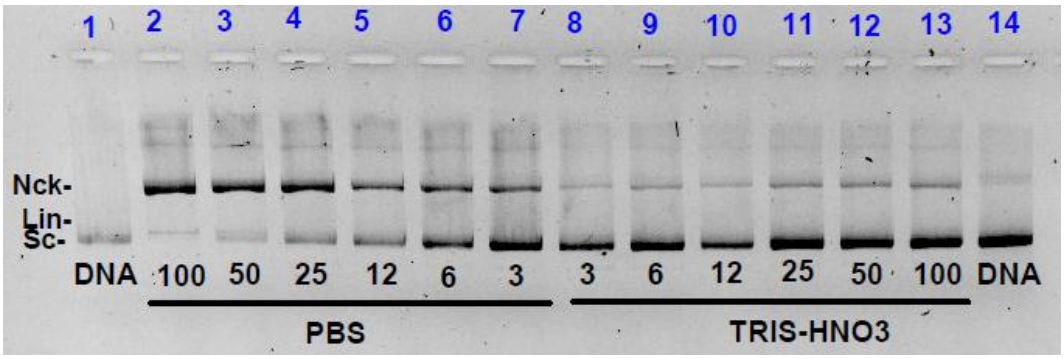

Figure IV.44. Example of the gel in which the percentage of the Sc form differs significantly in the samples-controls of native pDNA (lanes 1 and 14).

IV.2.11 Circular Dichroism studies

Obtained spectra suggest the CD signature of B-form DNA [322, 525]. A positive band (274 nm) is due to the base stacking, while a negative one (264 nm) appear at the cost of the DNA helicity. The CD spectra of native pA1 changes with time: the intensity of both bands increases by 27% in 25 h (Figure IV.1, A). This is a significant change, when compared with the intensity of the same bands in the presence of metal complex - maximum change is 20% (Figure IV.1, B). These changes in the 220–230 nm range could be due to some degradation of the DNA molecule without extensive change of either helix form or base-stacking.

The changes observed in the pA1 DNA bands are consistent with its degradation. A good correlation between the “asymmetry” and the % of linear form can be observed. (Figure IV.45). Comparison of the DNA control (native pDNA incubated 1 h at 37 ºC, lane 1 and 8) with pA1 used in the CD measurements (D, lane 3, 25 h incubation) shows a significant difference in the amount of DNA conformations 3.5% and 12% for Nck and 96% and 85% for Sc form, moreover there is a linearization of 3% in the latter. This could be due to a long incubation, during which plasmid DNA started to decompose.

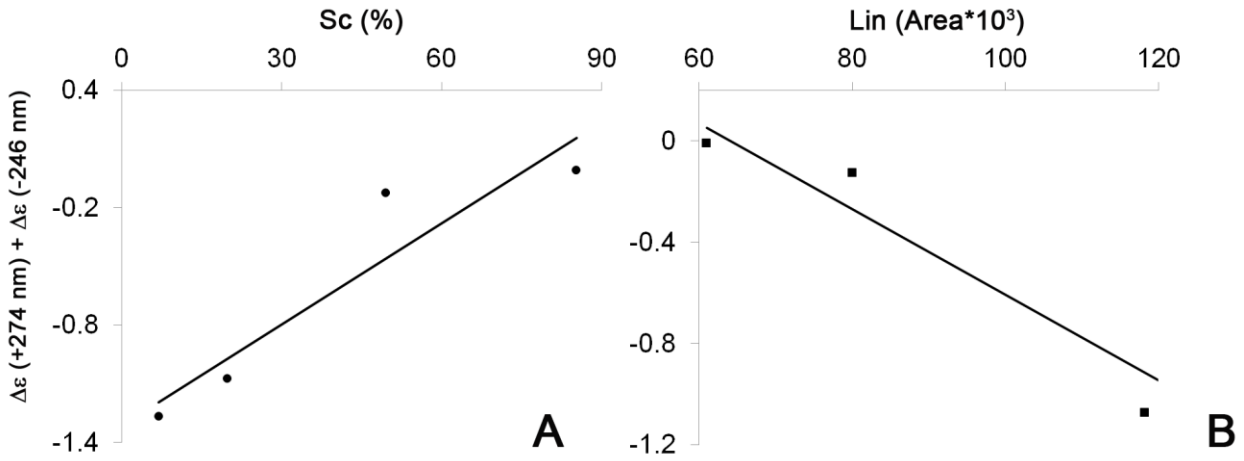

Figure IV.45. Correlation of the "asymmetry" (Δε (+) + Δε (-)) of the DNA bands with the degradation of pDNA presented as percentage of the Sc form (A) and as area of the Lin form (B). Data extracted from Figure IV.2.

Pure DNA bands are always approximately symmetric. Addition of **1** induces a decrease in the intensity of the positive band that is not followed by the negative band, thus increasing the "asymmetry" of the two bands. This effect increases with time and with DNA concentration. No correlation could be found between DNA degradation and the intensity of CD bands (Figure IV.46).

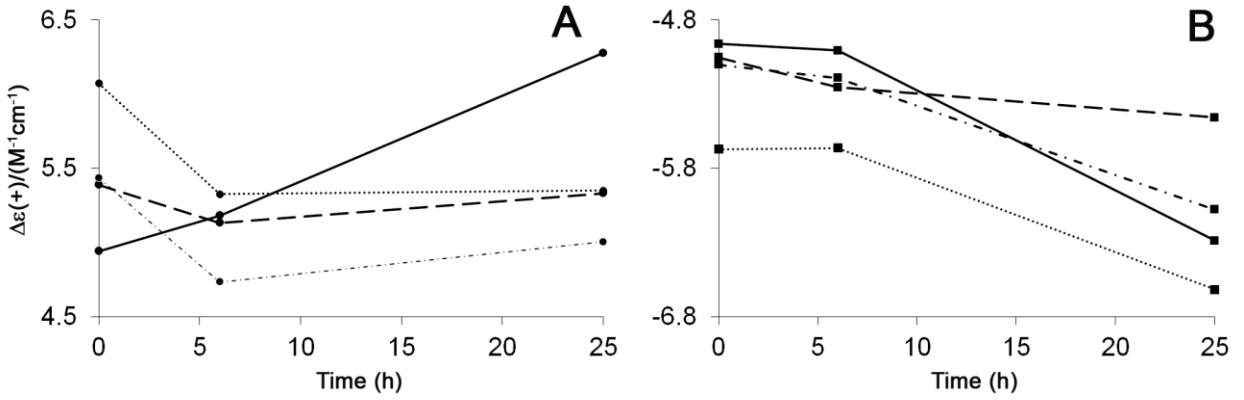

Figure IV.46. Effect of the incubation time on the CD intensity of 274 nm (positive band, A) and 246 nm (negative band, B), with increasing metal:bp ratio. Plasmid DNA at 274 nm(+)/246 nm(-) (solid line), ri 0.3 (dashed), ri 0.75 (dot-dashed), ri 1.5 (dotted).

Chapter V

Solution Studies

V. Solution Studies

V.1 Results

Solution characterization of **1**-**5** and **9** involved studies by UV/visible spectroscopy (complex stability), cyclic and square wave voltammetry (redox chemistry). In addition, ^{51}V NMR spectroscopy was used to check for oxidation products of V(IV) complexes.

V.1.1 Stability studies

The electronic absorption spectra of **1**-**5** and **9** were determined in PBS and HEPES buffers at pH 7.4 (Figure V.1 and Figure V.2). The spectrum of **3** was determined in 100% DMSO due to a scarce solubility of this complex. Solutions of **4** and **5** were sonicated for ca. 10 min to ensure a complete dissolution.

Obtained spectra were identified according to the model of molecular orbital treatment proposed by Ballhausen and Gray for the $[VO(H_2O)_5]^{2+}$ described in the Section I.5 (Figure I.7). The complexes show d-d transitions that within a typical range were assigned to the obtained bands are present in Table V.1.

Complex **1** is stable for at least 24 h; no significant changes could be detected during this time. A noticeable decrease and a shift in the position are observed after 2 h for the band III. In HEPES buffer the intensity of all bands decrease gradually with time, especially in the band IA.

Complex **2** exhibits stability for 2 h and after the intensity starts decreasing. A shift in the positions of the bands IA (from 840 to 845 nm) and II (from 585 to 590 nm) is observed. There is no difference in the spectra between 2 and 4 h. After 24 h there is still no change in the intensity of the band IA. The intensity of the band II, on the contrary,

continues to decrease and shifts to 580 nm. Under HEPES buffer the intensity decreases continuously; the most significant change is observed in the first 2 h. There is also a shift in the bands IA (from 830 to 825 nm) and II (from 565 to 570 nm).

The electronic absorption spectra of **3** changes insignificantly. Only a slight gradual decrease can be observed during 24 h. Measurements were performed in 100% DMSO since the aqueous solubility of this complex is assumed to be too low for UV-vis studies. Attempts to prepare the solution in 5, 10 or 50% of DMSO were unsuccessful as the addition of the buffer followed the dissolution in DMSO would cause the turbidity.

Complexes **4** and **5** upon dissolution in either of the buffers decompose gradually which is especially noticeable within the first 2 h. Under HEPES buffer no bands are observed even for the freshly prepared solutions (i.e., 0 h).

In the case of **9**, the biggest change is observed also in the first 2 h. Not only is there a shift in the band II (from 595 to 590 nm) but also a significant shift in the spectra due to which the band II at the time 0 h is not easily identified. Between 2 and 24 h, the decrease in the intensity of the bands is gradual. Under HEPES buffer no d-d transitions bands are observed, the positions of the spectrum shifts along time.

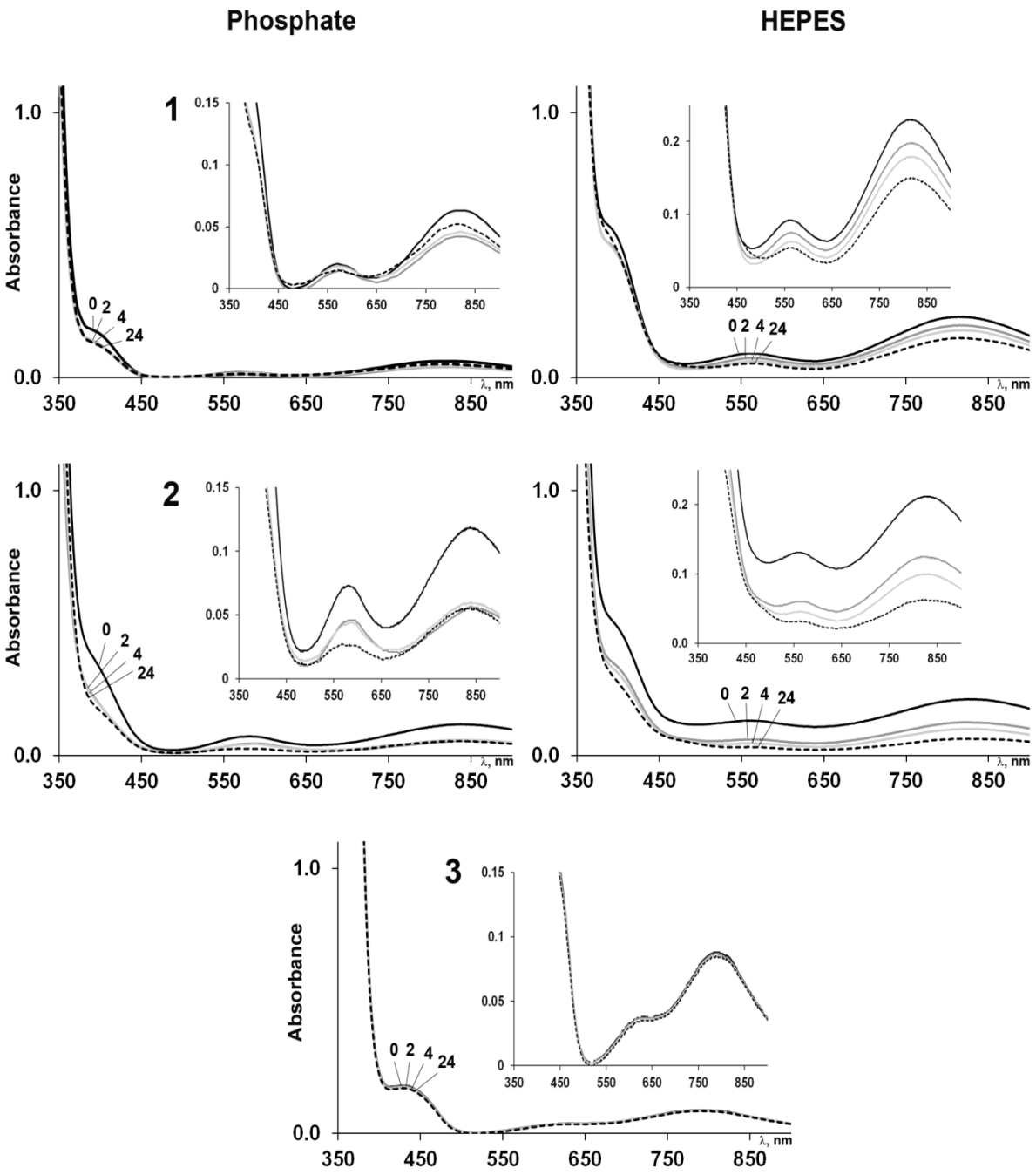

Figure V.1. Time evolution of the UV-vis absorbance spectra of aqueous solutions of **1** (2 mM in PBS/1% DMSO; 1.2 mM in HEPES), **2** (1.2 mM) and **3** (1.2 mM in 100% DMSO). Numbers indicate time (h) after dissolution: 0, (a spectrum taken immediately after solution preparation) 2, 4 and 24 h are presented as black, grey, light grey and black dashed lines, respectively.

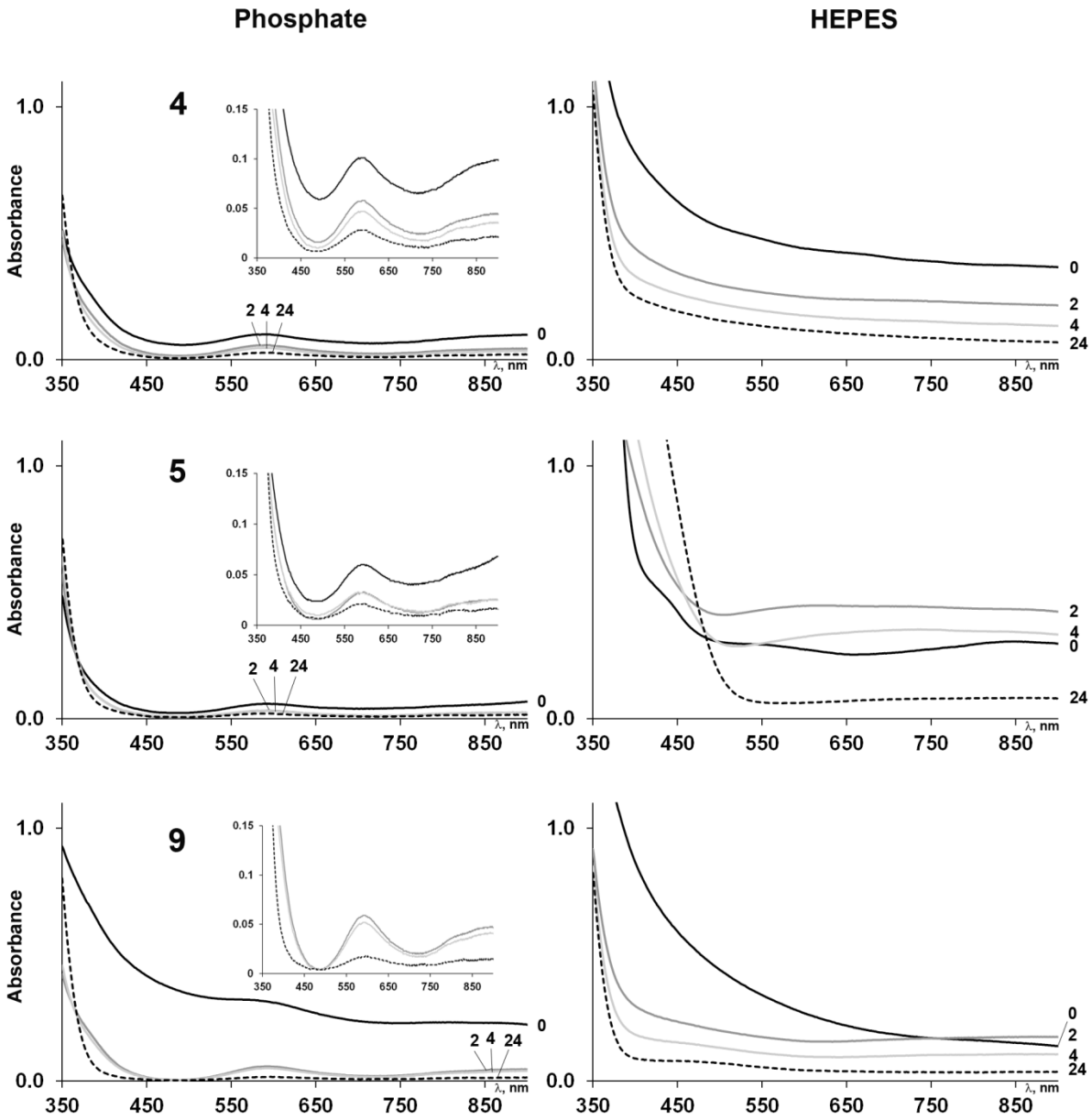

Figure V.2. Time evolution of the UV-vis absorbance spectra of aqueous solutions of **4**, **5** and **9** (1.2 mM) in phosphate and in HEPES buffer. Numbers indicate time (h) after dissolution.

Table V.1. Bands in the electronic absorption spectra of **1**-**5** and **9** identified according to the typical range.

Band	C4v	C2v	Typical range (nm)	PBS/ HEPES	PBS/ HEPES	DMSO	PBS/ HEPES	PBS/ HEPES	PBS/ HEPES
				1	**2**	**3**	**4**	**5**	**9**
IA	b2-e	a2-b1	900-620	820/820	840/830	795	865/-	895/-	895/-
IB		a2-b2		-/-	-/-	-/-	-/-	-/-	-/-
II	b2-a1	a2-a1	690-530	570/565	585/565	620	595/-	590/-	595/-
III	b2-b1	a2-a1	480-330	400/400	410/410	435	-/-	-/-	-/-

V.1.2 Redox chemistry

The electrochemical behaviour of **1**-**5** and **9** under phosphate and MOPS buffers are CV measurements were conducted using the potential scan rate of 50 mV/s. This choice was preceded by testing **1** at 20 μM in 100 mM phosphate buffer at different scan rates (i.e., 25, 50, 100, 150, 200, 250, 300, 350, 400, 450 and 500 mV/s). Though, the scan rate affects the shape of a voltammogram, the change is insignificant and behavioural pattern remains unaltered. Therefore in Figure V.3, we present only the voltammograms taken at 25, 50, 100, 250 and 500 mV/s.

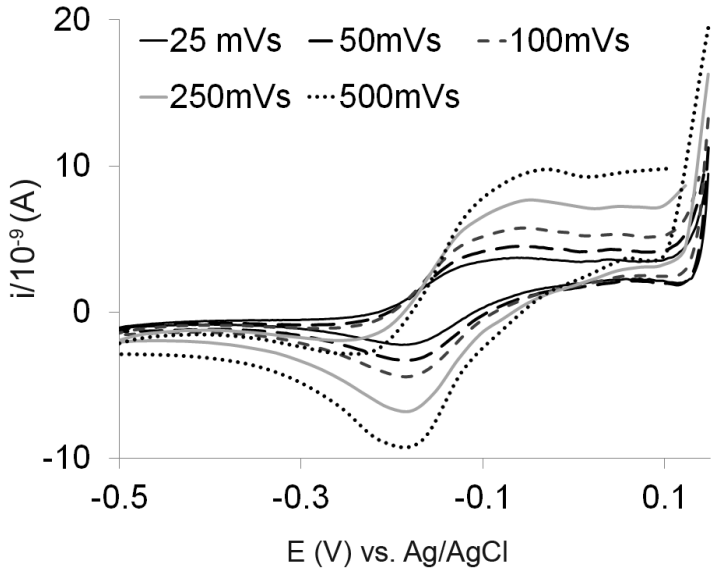

Figure V.3. Effect of the scan rate on the electrochemical response of **1** (20 μM) in 100 mM phosphate buffer.

The results of all experiments, CV and SWV, are summarized in Annex B. There, Figures B1-B4, B11 and B12 show the voltammograms of **1**, **2** and **9**, respectively, under phosphate and MOPS buffers (10, 30 and 100 mM). Results of the redox behaviour of **3**-**5**, **13** and **14** under 10 and 100 mM buffer media are presented in Figures B5-B10, B13-B16. Figures B17-B18 contain correspondingly cyclic and square wave voltammograms (Cvs and SWvs, respectively) of **6**, **19**, **11** and **12**.

The first measurements of the electrochemical behaviour of **1**-**5** and **9** were carried out under 100 mM phosphate and MOPS buffers. The voltammograms are demonstrated in Figure V.4 and Figure V.5. Under 100 mM phosphate buffer complexes **1**-**3** and **9** show quasi-reversible behaviour, whereas **4** and **5** behave irreversibly as well as all complexes under MOPS buffer. The cathodic and anodic potentials are given in Table V.2.

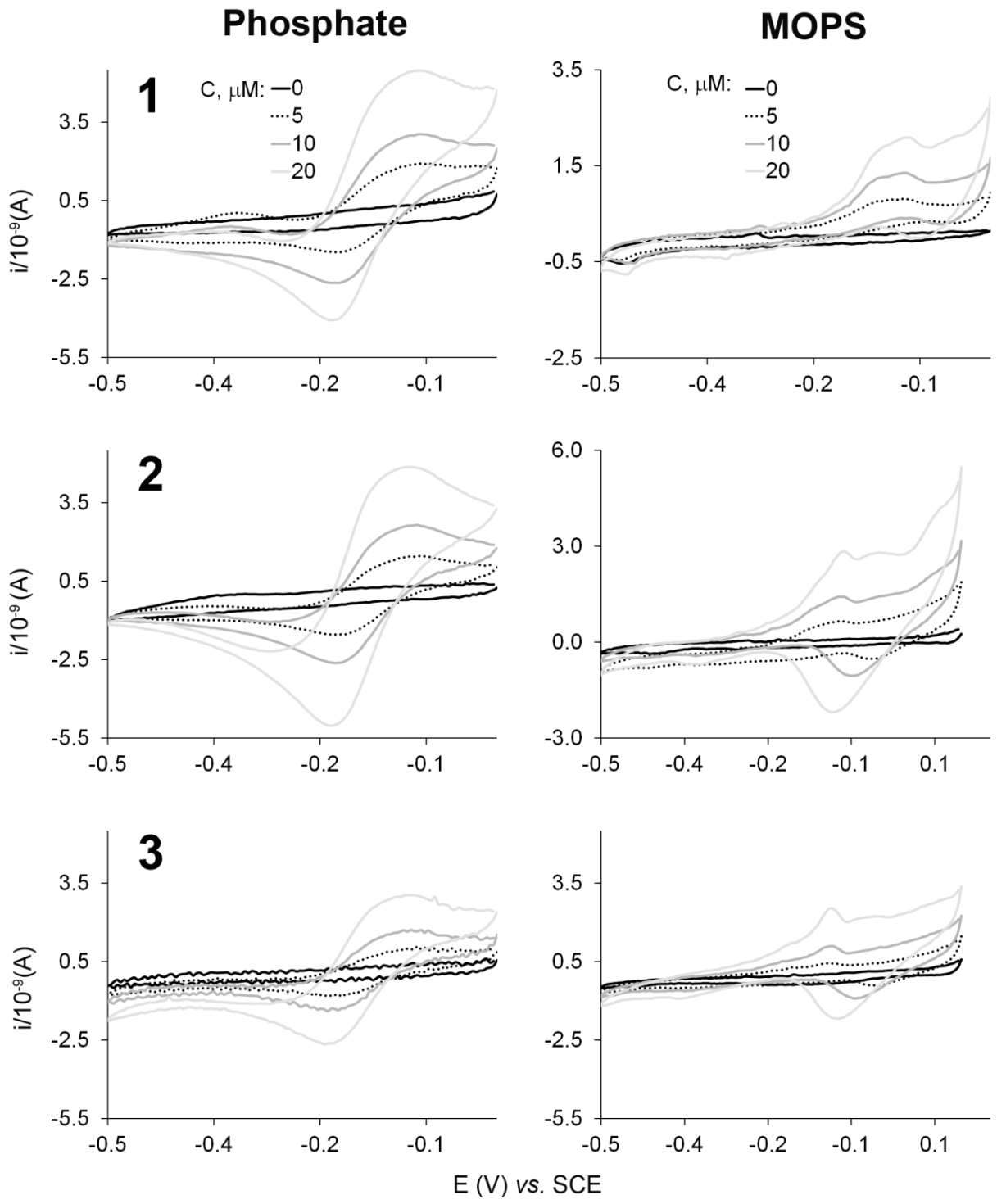

Figure V.4. Evolution of Cvs with increasing concentration of **1**, **2** (0, 5, 10 and 20 μM) and **3** in phosphate and MOPS buffers (100 mM). Due to a poor solubility, the exact concentrations of **3** are unknown but lower than the other complexes.

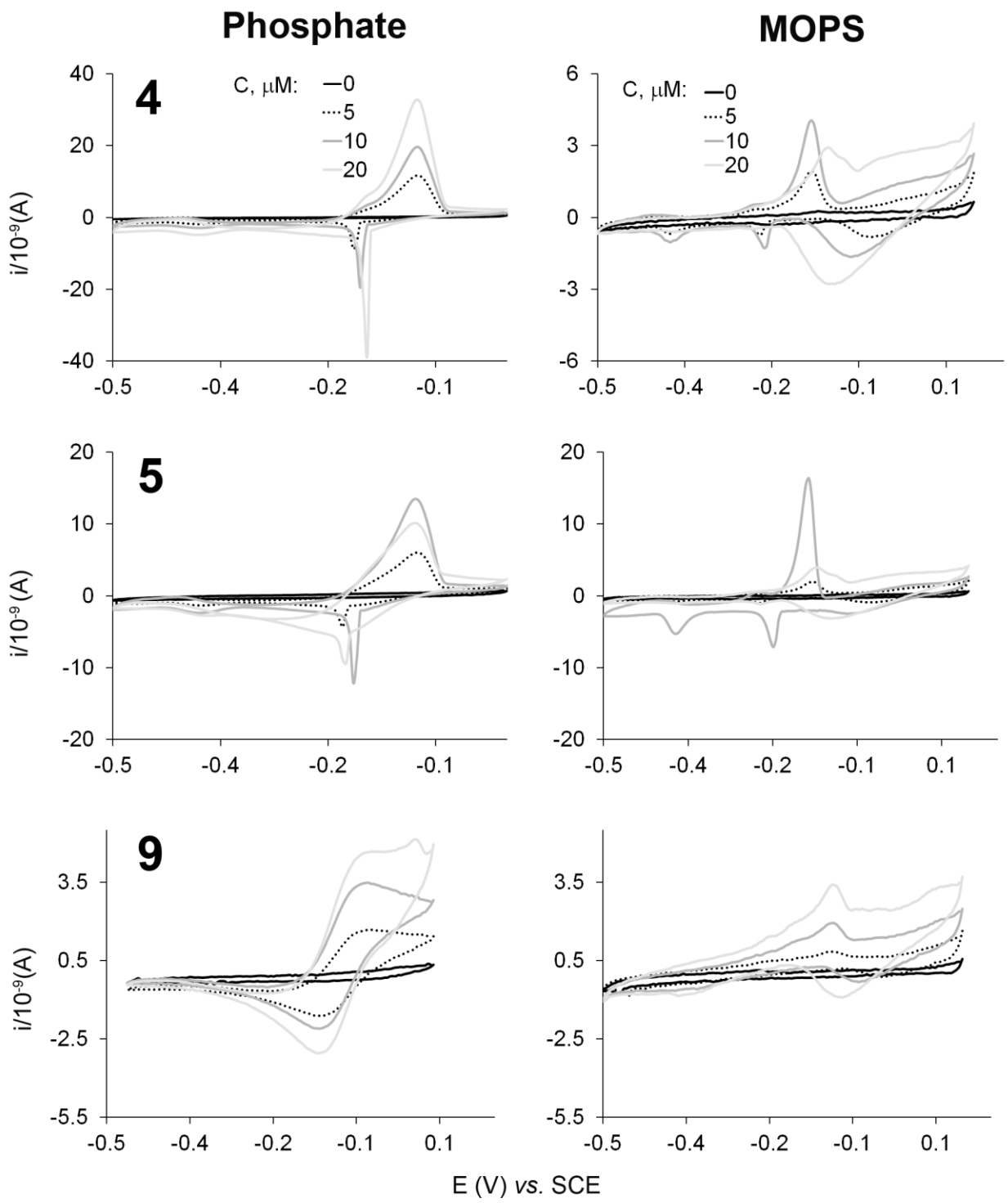

Figure V.5. Evolution of Cvs with increasing concentration of **4**, **5** and **9** aqueous solutions at 0, 5, 10 and 20 μM in phosphate and MOPS buffers (100 mM).

Table V.2. Summary of electrochemical data for **1**-**5** and **9** at 20 μM concentration in phosphate and MOPS buffers.

Complex	Phosphate		MOPS	
	Ep_c (V)	Ep_a (V)	Ep_c (V)	Ep_a (V)
1	-0.182	-0.060	-0.056	-0.069
2	-0.186	-0.072	-0.085	-0.065
3	-0.186	-0.072	-0.075	-0.087
4	-0.158	-0.078	-0.098	-0.103
5	-0.193	-0.096	-0.094	-0.127
9	-.0.156	-0.065	-0.069	-0.086

Changing concentration of phosphate buffer gave a different electrochemical response of **1** (Figure V.6). Progressive changes with increase of the buffer concentration from 1 to 20 mM are well defined in the SWvs (direct and reverse). Under 1 mM phosphate the two bands, A (0.19 V) and B (-0.29 V), can be observed in the reverse scan. Band A disappears at 2 mM of buffer, while band B increases progressively with increasing buffer concentration, reaching a maximum between ca. 4 and 6 mM.

CV results of these reaction mixtures are presented in the same Figure. In the reverse scan at least three species can be observed, i.e., -0.11 (I), -0.19 (II) and -0.05 V (III). In the direct scan there are two species (IV and V). Band IV increases with the concentration moving towards more positive potential, -0.22 V at 1 mM changes to -0.18 V at 20 mM. Band V appears at the lowest concentration, i.e., 1 mM at -0.28 V but is almost non-distinguishable even on the zoomed scale. Only at 20 mM it is easily noted at more positive potential (-0.23 V). At the lowest buffer concentration species II is predominant. Increasing buffer concentration gives a rise to bands I and III. Band II, on the contrary, decreases. Significant change in the intensity of the bands is observed between 2 and 4, 10 and 20 mM voltammograms. These tests were carried out in parallel with AGE experiments (Figure A32 and A33).

The same experiment was repeated controlling ionic strength with $KClO_4$ (Figure V.7). No changes can be observed in either of the scans. Results of the experiments with **2**-**5** are presented in Figure B19-B22.

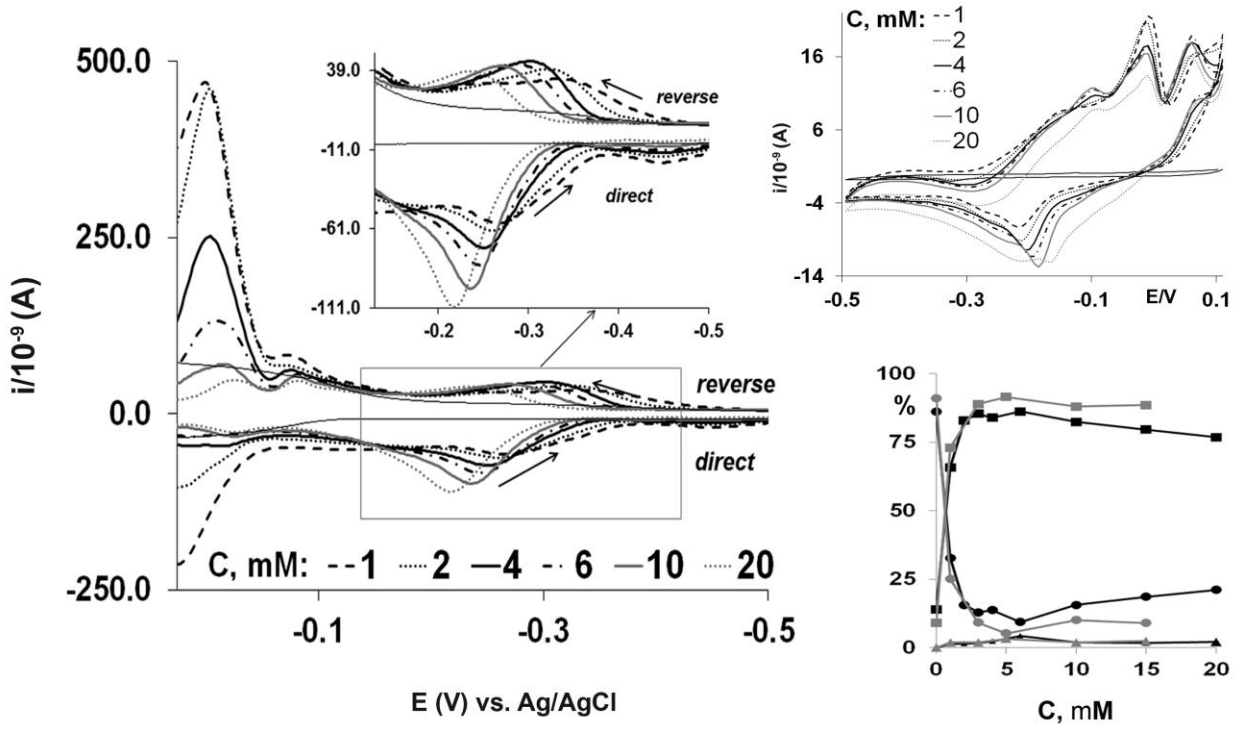

Figure V.6. Studies of the electrochemical response and the nuclease activity of **1** under increasing concentration of phosphate buffer: 1, 2, 3, 4, 6, 10, 15 and 20 mM. *Left*: Direct and revers SWvs. *Top right*: Cvs of the same solutions. *Bottom right*: Results of AGE represented as percentage of each DNA *vs.* buffer concentration extracted from Figure A34.

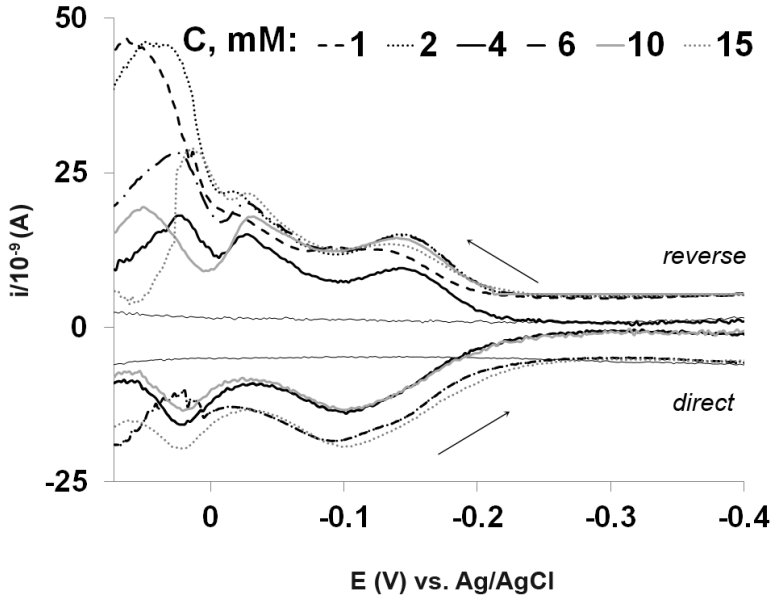

Figure V.7. Square wave voltammetry results of the electrochemical behaviour of **1** changing concentration of phosphate buffer (1, 2, 4, 6, 10, and 15 mM) with increased ionic strength controlled by $KClO_4$.

V.2 Discussion

When studying the biological activity of metal complexes it is important to understand whether the complex is stable in solution or if it decomposes with time into different species. Upon dissolution in water, vanadium complexes will be hydrated and competition of water molecules with the ligand for coordination to the metal may cause hydrolysis of the complex and, depending on the pH, oxidation to V(V). Buffer medium may compete for coordination positions and cause a degradation of the original complexes. Depending on the binding affinities of the ligands as well as their concentrations, a mixture of species may be formed in solution including the original complex, mixed species with the original ligand and water and/or buffer molecules, aquo complexes and vanadates.

V.2.1 Stability Studies

According to the obtained electronic spectra (Figure V.8 and Figure V.9), in aqueous PBS solution all complexes seem to be more stable than in HEPES. Complexes **1** and **2**, and most likely **3**, are the most stable.

Complex **1** is more stable than **2** in aqueous solution regardless of the pH buffer, but both complexes are significantly more stable than complexes **4** and **5**. When dissolved in HEPES buffer, complexes **4** and **5** do not present absorbance spectra in the visible region, suggesting that their hydrolysis is rapid and complete. Under phosphate buffer they present weak visible spectra with band II well defined at 595 nm, and band I apparently very weak and with maxima above 950 nm. These bands in the visible region disappear rapidly with time confirming a fast hydrolysis also in phosphate buffer. Complex **9** hydrolyses rapidly in both buffer solutions. Less active complexes, **4** and **5**, seems to hydrolyse/oxidize significantly in the first 2 h and continued to decompose up to 24 h.

Considering that all tests in the present work were typically performed in phosphate and HEPES/MOPS buffers at physiological pH, it is likely that the complex structure upon dissolution differs from what has been reported for the solid phase.The stability and solution structure of **1** has been previously subjected to extensive studies [4,115,116,222,223,231]. According to the studies of Crans [116], freshly dissolved $VO(acac)_2$ in aqueous solution is present as $VO(acac)_2 \cdot H_2O$ adduct, i.e., *trans* (species A, 85%) and *cis* (species B, 5%) isomers (Figure I.6), which remain intact for several days. After 24 days at ambient temperature the dominant species (65%) is the product of hydrolysis (1:1 complex) is species C in which one acac ligand is replaced with molecules of water; species A is reduced to 25%.

The spectrum of **1** in HEPES buffer presents clearly the bands characteristic of a V(IV) complex, 820 nm (band I), 565 nm (band II) which were attributed to species A [116], and 400 nm where band III appears as a shoulder of an intense charge transfer band. The same complex dissolved in phosphate buffer shows a very similar spectrum with the band II shifted to longer wavelengths by 5 nm, but the normalized spectra present

some clear differences (Figure V.8). The normalization of spectra to a certain wavelength, typically a wavelength of maximum absorbance, allows a better comparison of the relative intensities of bands. In this case, the intensities of bands I and III relative to band II are lower in phosphate buffer. Evolution with time in both buffers shows a slight decrease in the intensity of the absorbance spectra, but no change in the position of the bands, suggesting a slow oxidation of the V(IV) complex into V(V) along time with disappearance of the bands in the visible region.

When the spectra of evolution with time are normalized at band I for **1** and **2** (Figure V.9), the main change seems to be take place under HEPES buffer after 24 h at the change transfer band, i.e., band III. In PBS buffer, the changes can be observed in the band II which decreases similarly for **1** and **2**. Interestingly, the decomposition of both complexes does not progressing equally with time. In the case of **1**, there is an increase in the intensity of this band between 0 and 2 h. Then, the spectra taken after 2 and 4 h are on the same position, while the one after 24 h, demonstrates a significant decrease in the intensity which is lower the spectrum “0 h”. The pattern of the complex decomposition/speciation is similar for **2**. However, the rate of the increase/decrease is higher than for **1** and after the intensity of the band increased from after 2 h, the spectra after 4 h is no longer on the same position but decreases considerably. Probably, the rate of the species formation and their possible further decomposition differs for **1** and **2**.

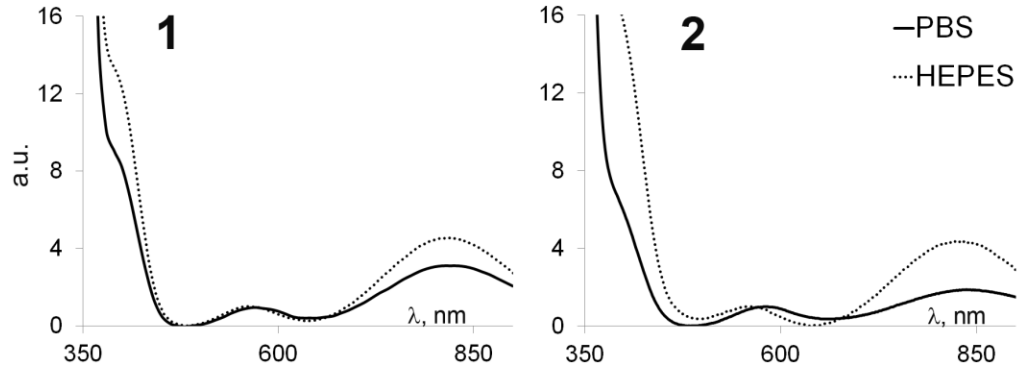

Figure V.8. Comparison of the absorption spectra of freshly dissolved **1** and **2** in phosphate and HEPES buffers. Spectra have been normalized to the relative maxima at band II (ca. 565 nm).

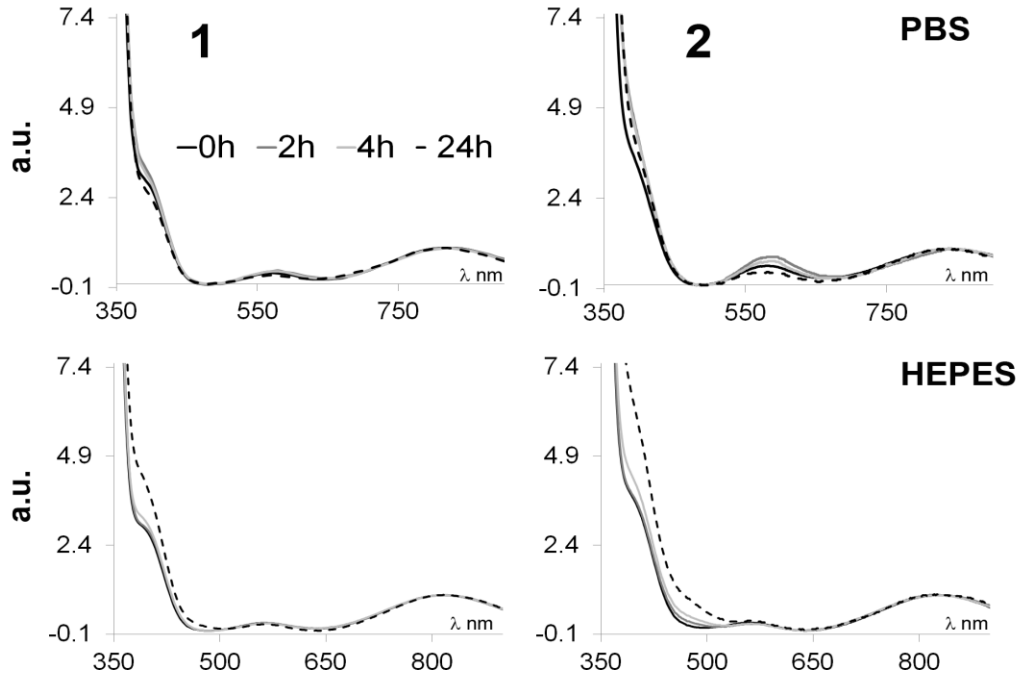

Figure V.9. Comparison of the electronic absorption spectra of **1** and **2** under PBS and HEPES buffers along time (0, 2, 4 and 24 h). The spectra are normalized to the relative maxima at band I (ca. 820 and 840 nm for **1** for **2**, correspondingly).

^{51}V NMR spectrum of **1** freshly dissolved in PBS shows the presence of V_1, V_2 and V_4 peaks (Figure V.10) suggesting a rapid oxidation and hydrolysis of the complex to some extent upon dissolution. No peaks of V^V are observed when **1** is prepared in water,

which is in agreement with the results presented by Crans [116] that the complex is stable in water. ^{51}V NMR spectrum of V^{V}(acac) derivatives, **6**-**8**, presented for comparison (Figure V.11), shows peaks only of V_1, V_2 and V_{10}. Since the complexes did not dissolve completely, the absence of the peaks assignable to the complexes suggests that the complexes dissolved only to the extent of their hydrolysis, and that any solubilized complex was found in concentrations below the detection limit of the technique.

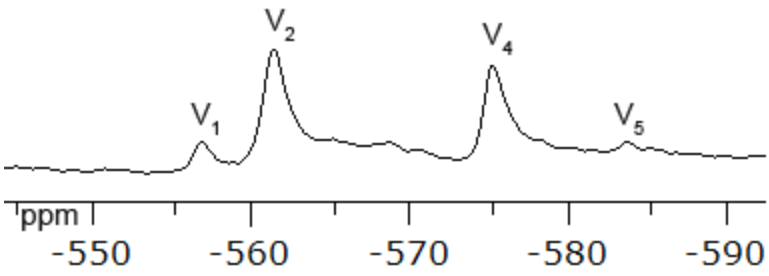

Figure V.10. ^{51}V NMR spectrum of **1** (2 mM) under 10 mM of PBS.

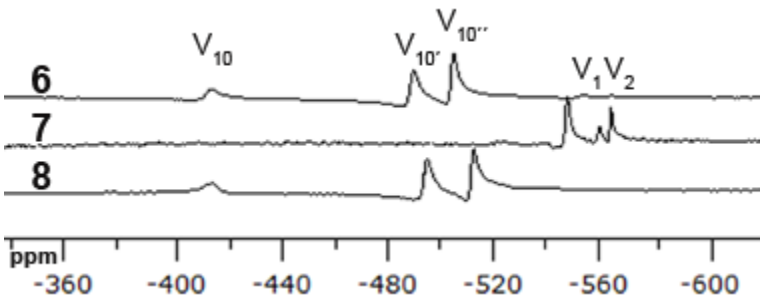

Figure V.11. ^{51}V NMR spectrum of saturated solutions of **6**-**8** in 10 mM PBS buffer.

In HEPES buffer the normalized spectrum of **2** is similar to **1**. The position and the relative intensities of the bands I and II are identical in both complexes (Figure V.12). Some differences appear between both complexes when dissolved in phosphate buffer:

bands I and II in **2** shift ca. 10 and 20 nm, respectively, to longer wavelengths. The relative intensities are also different, with bands I and III much weaker for **2** than for **1**.

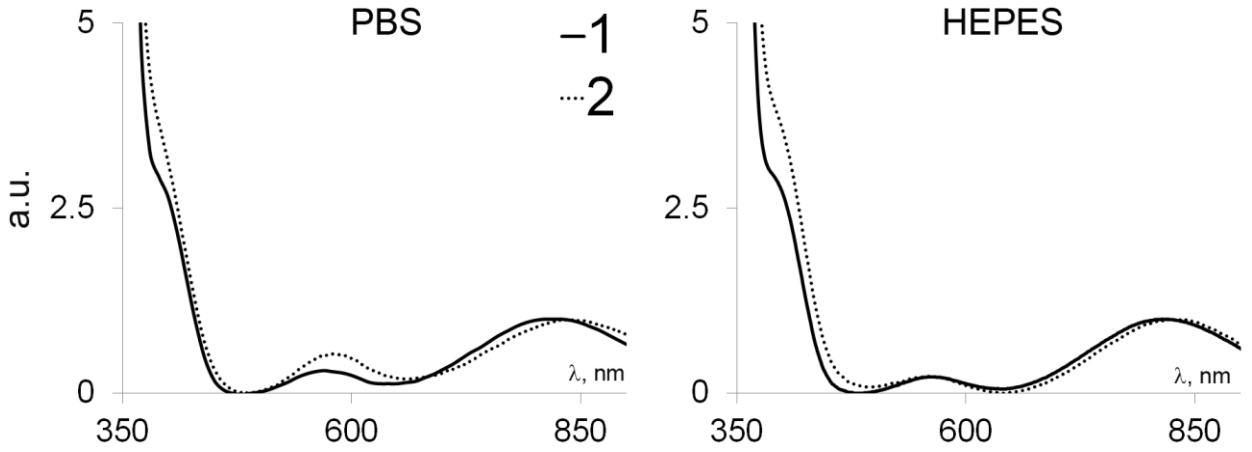

Figure V.12. Comparison the absorption spectra of **1** and **2** in phosphate (left) and HEPES (right) buffers. Spectra have been normalized to the relative maxima at band I (ca. 820 and 840 nm for **1** for **2**, respectively).

The solution structure of complexes **1** and **2** is therefore different when dissolved in phosphate buffer, but is similar when dissolved in HEPES buffer.

Figure V.13 compares the normalized spectra of all complexes under phosphate buffer. Complexes **4**, **5** and **9** show similar spectra which differs greatly from those of **1** and **2**.

It is likely that, like **9**, which dissolves as an aquacomplex of V(IV), complexes **5** and **9** are present in solution as oxidised V(V) and in the form of monomeric $V^{IV}O^{2+}$ which depending, on the pH, can be in the form of $[VO(H_2O)_5]^{2+}$ or $[VO(H_2O)_4(OH)]^{+}$ [115].

The fact that **1** and **2** are more stable complexes and have similar, much higher DNA cleavage efficiencies than **4**, **5** and **9** suggests that it is the neat complexes, and not the products of their decomposition, that have a relevant role in DNA degradation.

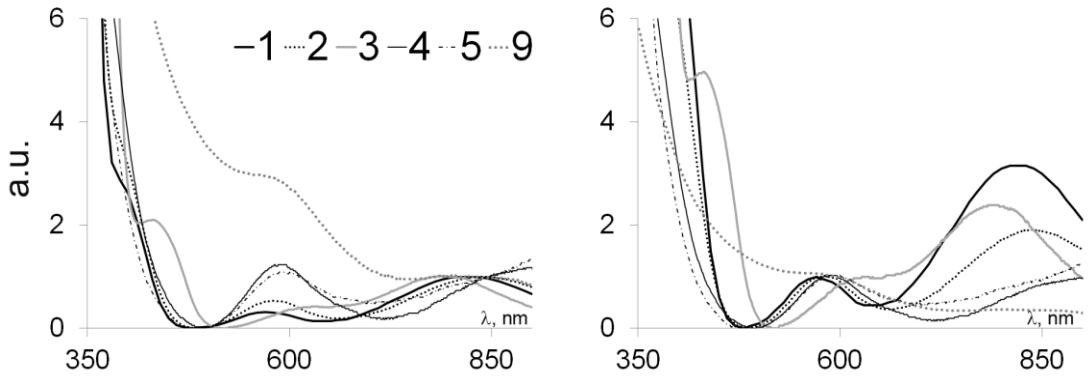

Figure V.13. Electronic spectra of **1**-**5** and **9** at the time of mixing in PBS, normalized to the relative maxima at band I ca. 830 nm (left) and II ca. 590 (right).

V.2.2 Redox chemistry

Due to the low extinction coefficients associated with the metal d-d electronic transitions, UV-vis spectroscopic studies of VC cannot be performed at complex concentrations below millimolar. The studies on the speciation of vanadium complexes in aqueous solutions that have been published to date are typically conducted at millimolar metal concentrations. Studies at micromolar concentrations can be performed using mass spectrometry, particularly ESI-MS. This technique, often in combination with other spectroscopic techniques like NMR, IR, UV-vis, and theoretical calculations, is reported to be a powerful tool for obtaining direct information of the structure and the chemistry of peroxo vanadates in solutions [526].

The biologically relevant interaction of metal complexes with DNA occurs at micromolar levels of concentration, thus the competition of the solvent and buffer molecules for the binding sites of the metal can change the metal speciation dramatically.

In contrast with UV-vis absorption spectroscopy, often employed for monitoring species in aqueous solutions, electroanalytical techniques such as cyclic (CV) and square wave voltammetry (SWV), allow studying the species formation at much lower detection limits. These two methods were chosen to study redox chemistry of complexes **1**-**5** and **9** in

aqueous solutions at concentration level of the metal as low as 2 μM using the dropping mercury electrode (DME). Though DME has the advantage of achieving much lower detection limits than other electrodes, the available potential window is shifted to more negative potentials (+0.4 to -1.3 V) which makes it accessible only for analysis of more positive potential range.

At complex concentrations of 5, 10 and 20 μM, and buffer concentration of 100 mM the cyclic voltammograms (Cvs) present a striking pattern that differentiates the group of complexes with stronger nuclease activity (**1**-**3**, Figure V.4) from the weak ones (**4** and **5**, Figure V.5). Under phosphate buffer the first group of complexes exhibits a quasi-reversible one electron response, with very similar Cvs. Even though complex **3** could not be dissolved completely, it exhibits a clear pattern, similar to **1** and **2**. The cathodic peaks appear at -0.182, -0.186 and -0.186 V (*vs.* SCE) for **1**, **2** and **3**, respectively, corresponding to V(V)/V(IV) reduction, and the anodic peaks at -0.060, -0.072 and -0.072 V. The distance between the two peaks for an ideal reversible redox couple at 25 ºC would be $\Delta E = 59$ mV/n, where *n* is the number of electrons exchanged. This distance is 122 mV for **1** and 114 mV for **2** and **3**. The peak intensities ratio is close to **1**, and the position of the peaks did not change when the scan ratio varied. This is consistent with a reversible electrochemical reaction involving dimerization with the exchange of one electron:

$$2\ V^{V}O(L)(P) + e^{-} \rightleftharpoons V^{V}OV^{IV}O(L)(P)^{-} \qquad \text{(eq.V.1)}$$

However, such behaviour is not observed under an organic buffer. Cvs of the same complexes under MOPS show an irreversible behaviour, and weaker signals suggesting the formation of a mixture of species which probably have sluggish electron exchange.

The Cv of **9** (Figure V.4) in the same conditions shows a pattern similar to **1**, however the cathodic peak is at a less negative potential, -0.156 V (*vs*. SCE) while the anodic peak maintains a position close to -0.065 V. This suggests that the redox pair formed

when dissolving **1**, **2** or **3** in phosphate buffer is different from the one obtained when dissolving **9**, and the difference lays in the stabilization of the reduced form (V^{IV}) by the presence of a bidentate acac ligand lowering the reduction potential of the species formed from **1** and **2** to more negative values. Phosphate, as a pH buffer ion, is a strong competitor for metal binding sites due to the extremely high ligand to metal ratio (>5000) and may displace the acac molecules in the physiological pH range [28, 515]. Most likely that in the case of **1**-**3** only one $acac^-$ group is being replaced, since the second functional group has been found to resist the substitution [238, 239]. It is probable that these complexes equilibrate with phosphate ions to form mixed stable species $V^{IV/V}O(Lx)(Py)$. Another possibility of phosphate binding to the complexes is via replacement of water molecule of *trans* or *cis* isomers [223].

Complexes **4** and **5** in phosphate present sharp cathodic peaks - characteristic of adsorption at the surface of the working electrode. Adsorption significantly affects the electrochemical response resulting in Cvs of irreversible shape [478]. In such cases the redox processes that take place on the surface of the dropping mercury electrode differ greatly from those which involve dissolved species in the bulk and, hence, cannot be compared. This suggests the formation of hydrophobic complexes.

Figure V.14 shows the change accompanying several consecutive scans of **4**. The intensities of the adsorption anodic peak increase with a shift of potential Ep_c from -0.085 to -0.075 V and of the desorption cathodic peak, also shifting from Ep_a ~ -0.175 to -0.146 V. This is consistent with the formation of an adsorbed film promoted by the oxidation, and its desorption on reduction. The cathodic peak is sharper than the anodic one, suggesting that it is a desorption process. Another, weaker, process can be seen at potentials close to -0.4 V. Direct scans start each cycle by lowering the potential down to -0.5 V and then increasing it back to +0.05 V. On each consecutive cycle, the concentration of adsorbed vanadium species in the mercury drop increases, resulting into higher intensity of the cathodic peak. A reverse scan starts at the negative potential -0.5 V and moves to +0.05 V before lowering back to -0.5 V. The first reverse scan in Figure V.14 shows an oxidation peak at -0.163 V, which disappears with consecutive

scans while a second anodic peak appears at -0.08 V, suggesting that a new species is formed by the oxidation of the adsorbed film.

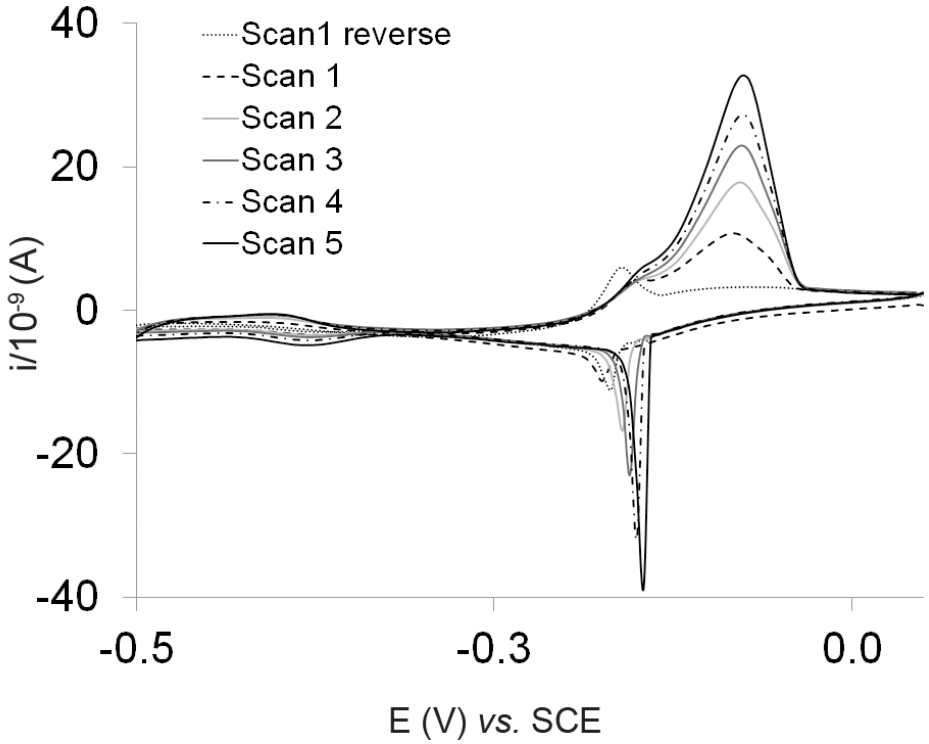

Figure V.14. Consecutive scans of **4** at 20 µM in 100 mM phosphate buffer. Five consecutive forward and one reverse scans**.** Only the first reverse scan is presented, the subsequent ones are similar to the direct scans.

The formation of the adsorbed film could be due to polyoxidovanadium species, polymerizing into less soluble, hydrophobic structures.

$$V^{IV}OL_2 \rightarrow (V^{IV}OL_2)_2(PO_4) \rightleftharpoons (V^{IV}OL_2)(V^{V}OL_2)(PO_4)\ \text{(ads when L=Et, Me)} \rightarrow V_2O_4(L)_2(PO_4)_{(ads).}$$

Figure V.15 compares the Cv of complex **4** with the one of a vanadium(V) dimer complex of acac, complex **6**. Both show a similar adsorption-desorption pattern.

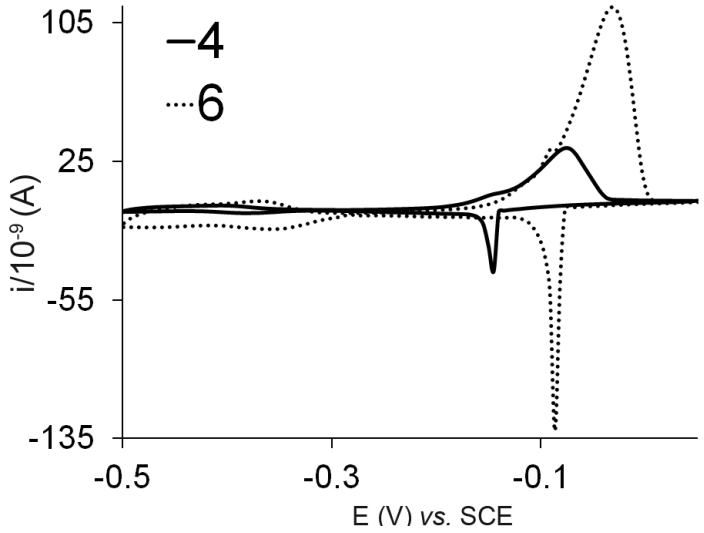

Figure V.15. Comparison of Cvs of **4** and **6** at 20 μM in 100 mM phosphate buffer.

Summarizing above written, under phosphate buffer all complexes show relatively simple quasi-reversible redox behaviour, involving species containing both the original ligand and phosphate, probably dimers or polymers bridged by phosphate. The voltammograms of complexes **4** and **5** indicate the formation of hydrophobic species upon oxidation, due to which different reactions are taking place at the electrode surface. This behaviour is similar to complex **6** and it is reasonable to assume that oxo-bridged vanadium(V) species will form near the surface of the electrode, under the high concentrations allowed by the adsorption. In the presence of MOPS buffer all complexes behave irreversibly and voltammograms show weak and multiple peaks reflecting the formation of multiple electrochemically active species. Cvs of **4** and **5** in MOPS are more complex (Figure V.5), showing the cathodic peak at ca. 0.0 - 0.1 V increasing with vanadium concentration, and two weaker ones at ~-0.2 and -0.4 V. At lower concentrations a sharp anodic peak at ~0.19 V suggests adsorption, but it disappears with increasing concentration.

To understand whether buffer concentration plays a role in the redox response of the complexes, measurements in 10 and 30 mM of phosphate and MOPS buffers were also performed (Figures B1-B16).As before, similar electrochemical behaviour was observed for complexes **1**-**3**, different from complexes **4**-**5**. The electrochemical behaviour of **1** is compared in 10, 30 and 100 mM phosphate and MOPS buffers (Figure V.16). Clearly, at lower concentrations of phosphate buffer the system becomes irreversible with more peaks and more complex species involved. This suggests that phosphate stabilizes the formed species or, more likely, that phosphate is an important part of the species. On the other hand, results obtained under 10 mM MOPS buffer show signals as weak as observed under 100 mM MOPS.

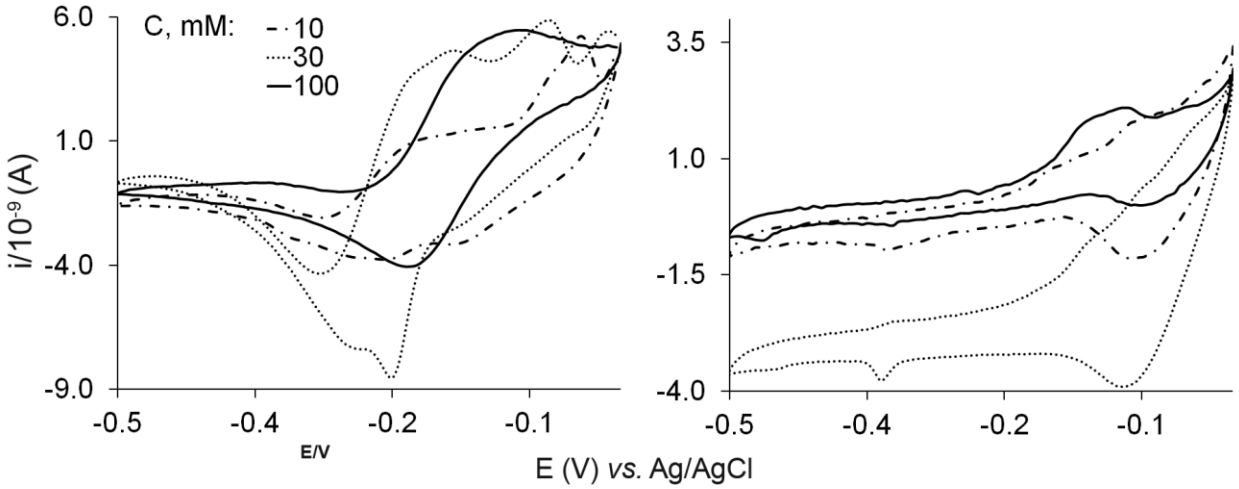

Figure V.16. Cvs of **1** at 20 µM in 10, 30 and 100 mM phosphate (left) and MOPS (right) buffers.

Since the AGE studies are typically carried out in the presence of 10 mM phosphate buffer, CV results obtained at this concentration were of high interest. Figure V.17 and Figure V.18 compare complex **1** as a representative of the strong nucleases, and **4** of the weak ones.

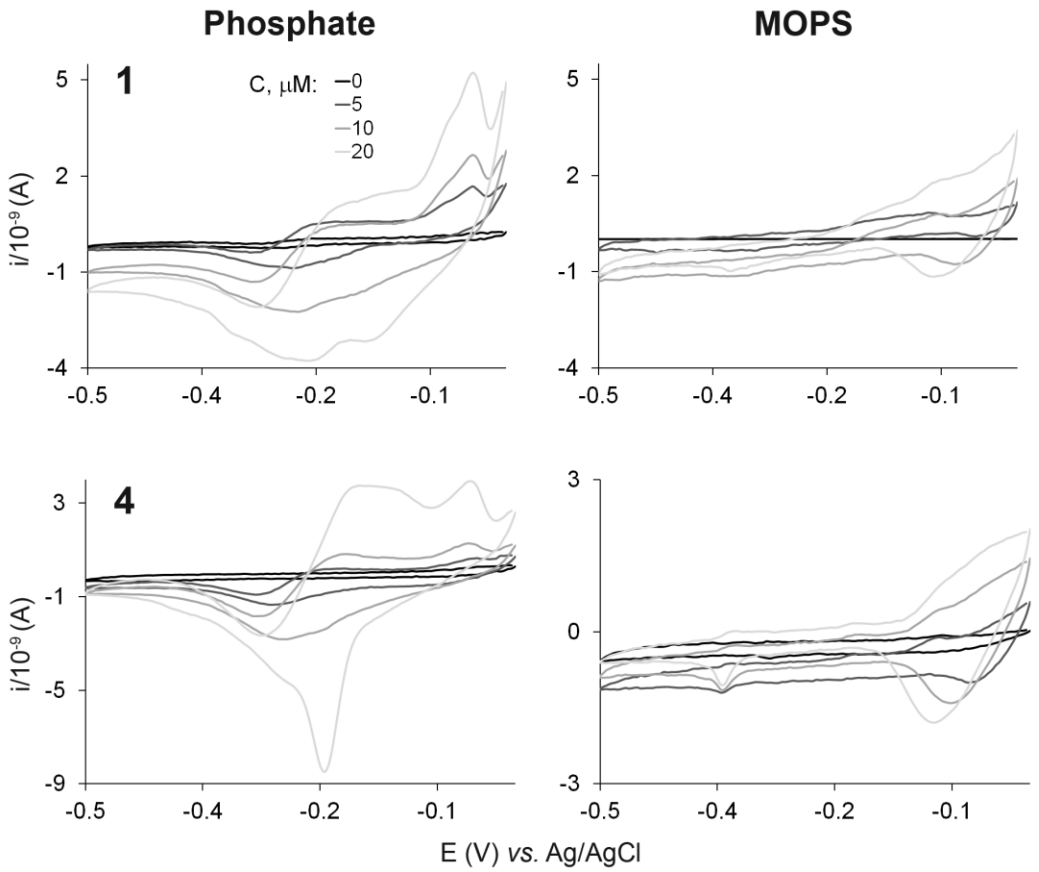

Figure V.17. Electrochemical behaviour of **1** and **4** at 0, 5, 10 and 20 μM in 10 mM phosphate (left) and MOPS (right) buffers.

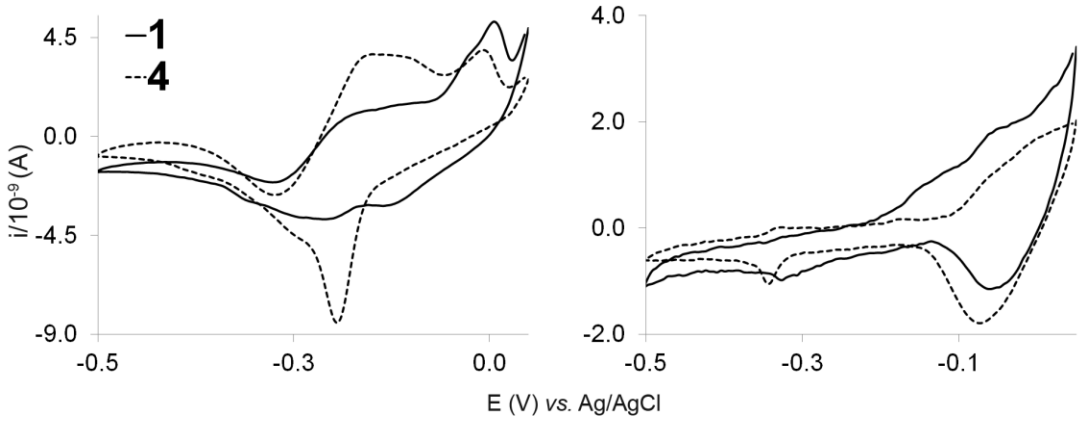

Figure V.18. Comparison of the Cvs of **1** and **4** at 20 μM in 10 mM phosphate (left) and MOPS (right) buffers.

SWV method was chosen for the studies of electrochemical behaviour due to a much broader dynamic range, higher speed and lower detection limits in comparison to CV. The concentration at which analytical determinations can be made using SWV can be as low as 10 μM [483] which allows studying aqueous solutions of VC at the micromolar concentrations, similar to those used in DNA assays.

In tests of the effect of buffer concentration SWV results (Figures B19-B22) seem to be easier to interpret than those obtained from CV. Two observed overlapped bands that centered at ca. -0.19 and -0.29 V probably correspond to two different species A and B, respectively that are formed in the reverse (oxidative) scan. The reason these bands are gradually shifted to more negative potentials with increasing buffer concentration is probably due to increasing ionic strength and was not observed in replicate experiments where ionic strength was controlled by the addition of excess potassium perchlorate (Figure V.7). Species causing bands A and B are expected to be mixed complexes of vanadium and phosphate, presumably $VO(acac)_2(H_2PO_4)^-$ (A) and $VO(acac)(H_2PO_4)$ (B), while oxidovanadium phosphate, $VO(H_2PO_4)_2$ (C), is expected to form only at very higher phosphate concentrations. The nuclease activity of **1** was found to depend on the concentration of phosphate, showing a maximum at ca. 6 mM phosphate buffer (Figure V.19) which is in agreement with the SWV results.

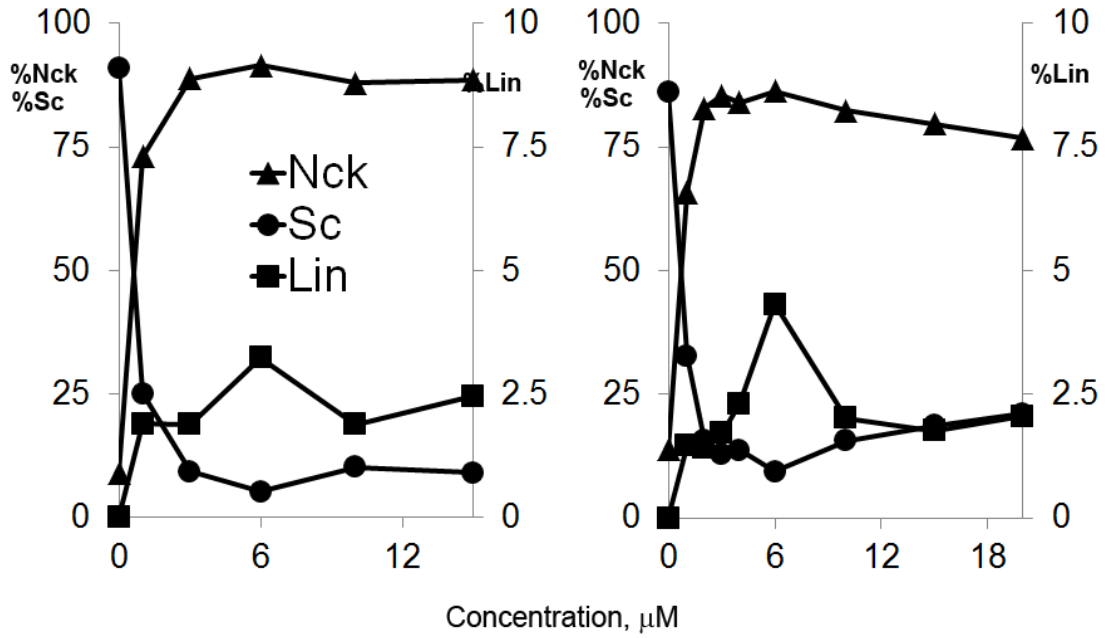

Figure V.19. Change in DNA degradation by **1** at 50 μM with increasing concentration of phosphate buffer (1, 3, 6, 10 and 15 mM). The right graphic is the replicate with three more concentrations, i.e., 2, 4 and 20 mM. Percentage of Sc, Nck and Lin forms is calculated from Figure A32 and A33.

Results obtained from the addition of phosphate buffer to a solution of **1** in MOPS (Figure V.20) showed the formation of a series of species similar to the ones observed in phosphate buffer. On the contrary, adding MOPS to a solution of **1** in phosphate did not cause a significant change in the voltammograms, except what was caused by dilution.

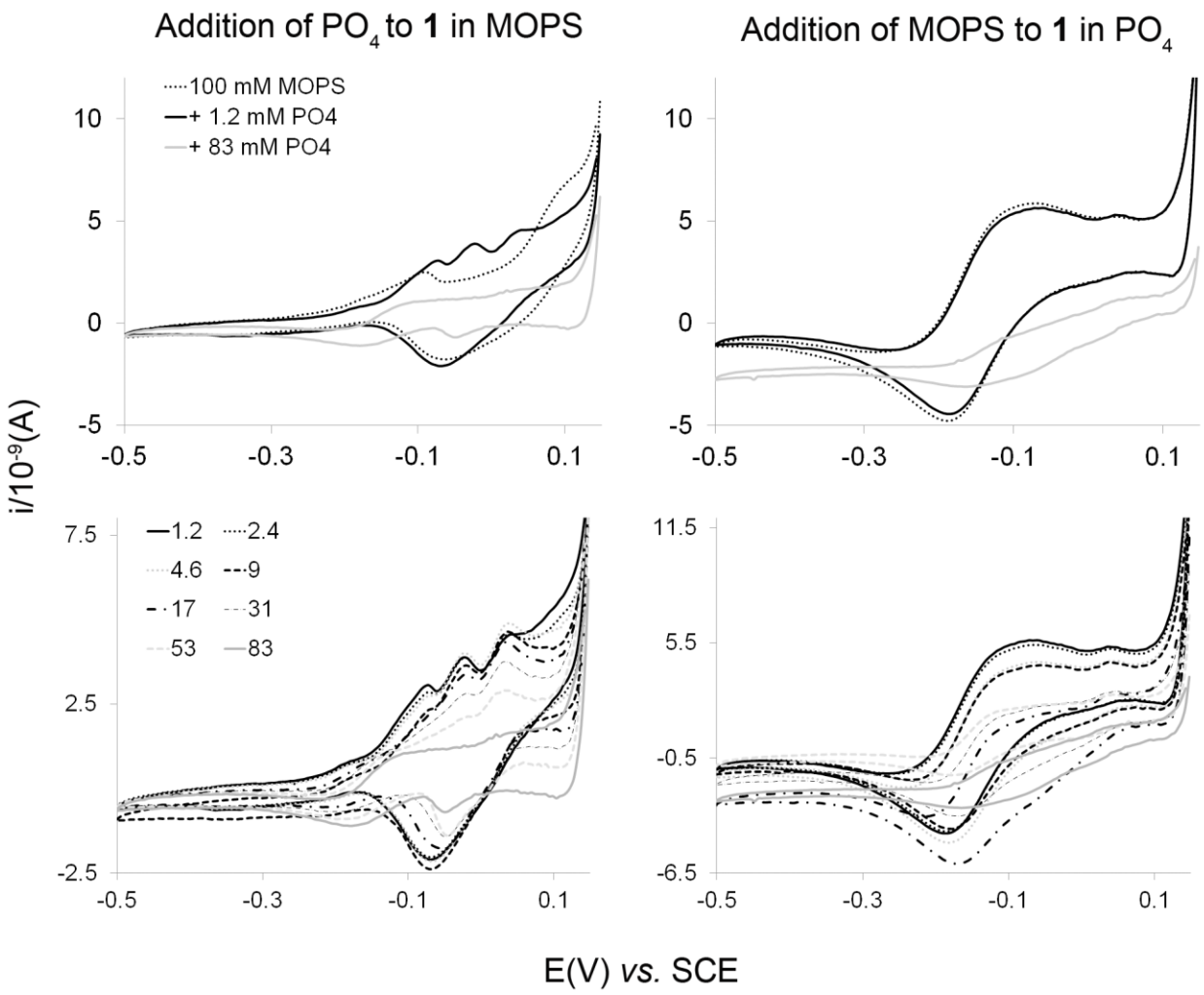

Figure V.20. Changes in redox behaviour of 1 at 20 µM in MOPS buffer (left) with addition of phosphate and in vice versa. Numbers indicate concentration (mM).

The electroanalytical results show that speciation of vanadium complexes in media buffered by phosphate is affected by small changes in the concentration of buffer. These changes in turn affect the nuclease activity of the VC. The nuclease activity of the studied complexes increases in the presence of phosphate, and is closely dependent on its concentration.

Chapter VI

Mechanistic Studies

VI. Mechanistic Studies

VI.1 Results

The evaluation of oxidative and hydrolytic mechanisms is presented. The formation of ROS in aqueous solutions of the VC was observed by fluorescence spectroscopy, and the hydrolysis of DNA phosphoester bond was studied by ^{1}H, ^{31}P and ^{51}V NMR.

VI.1.1 Oxidative cleavage

Generation of ROS that are presumed to be the cause of the cleavage induced by **1** was assessed through hydroxylation reaction of terephthalic acid (TPA) upon which a fluorescent 2-hydroxyl-terephtalate (HTPA) is formed. Fluorescence spectra of HTPA in the absence and presence of H_2O_2 are shown in Figure VI.1 and Figure VI.2, respectively. A gradual increase in the intensity is observed with time, i.e., 0, 1, 3, 5 and 25 h under phosphate buffer. No significant changes seem to occur under MOPS buffer. The intensity of the spectra increased considerably upon addition of H_2O_2 under both buffers at the time of mixing, and did not change with time.

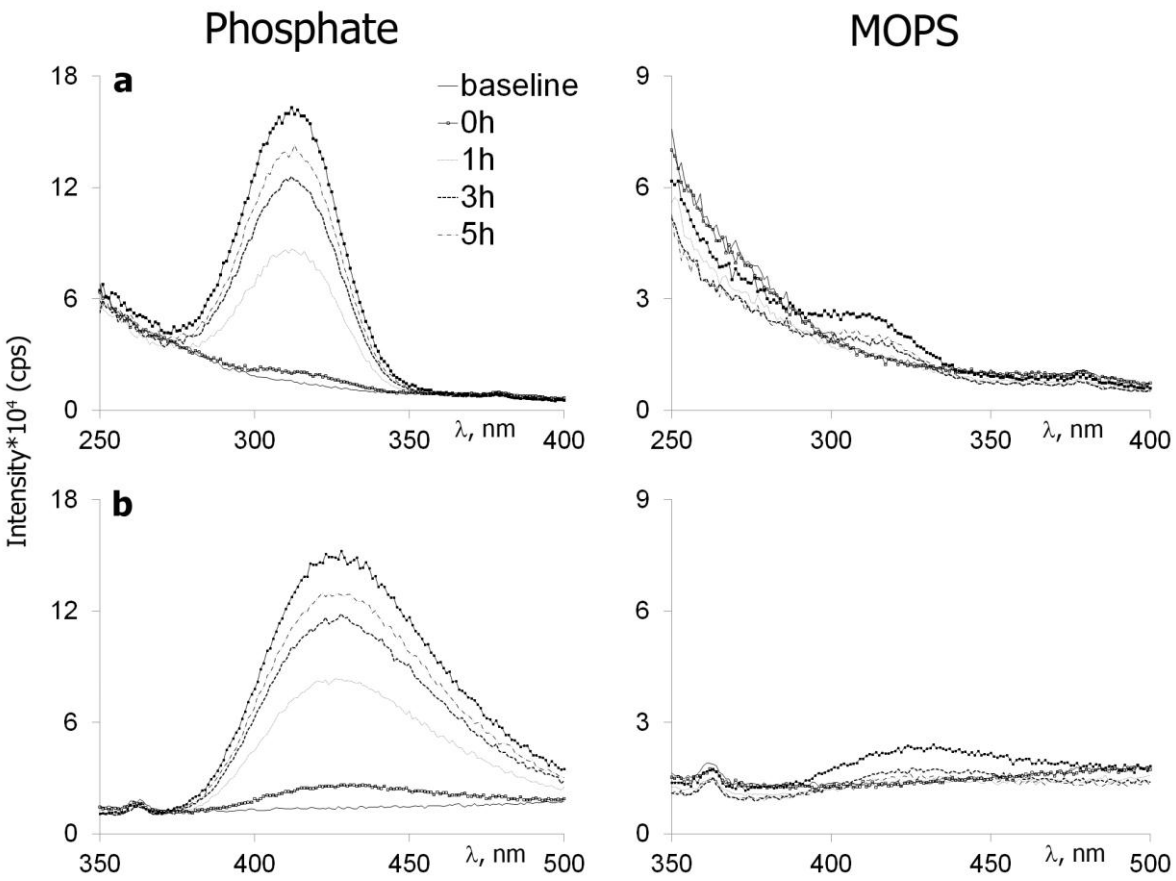

Figure VI.1. Fluorescence spectra of HTPA resulted from the reaction mixture of TPA (200 μM) and **1** (50 μM) under phosphate and MOPS buffers (5 mM) at the time of mixing, after 1, 3, 5 and 25 h. Excitation spectra (a) were scanned at emission of 435 nm, and emission spectra (b) - at 323 nm of excitation.

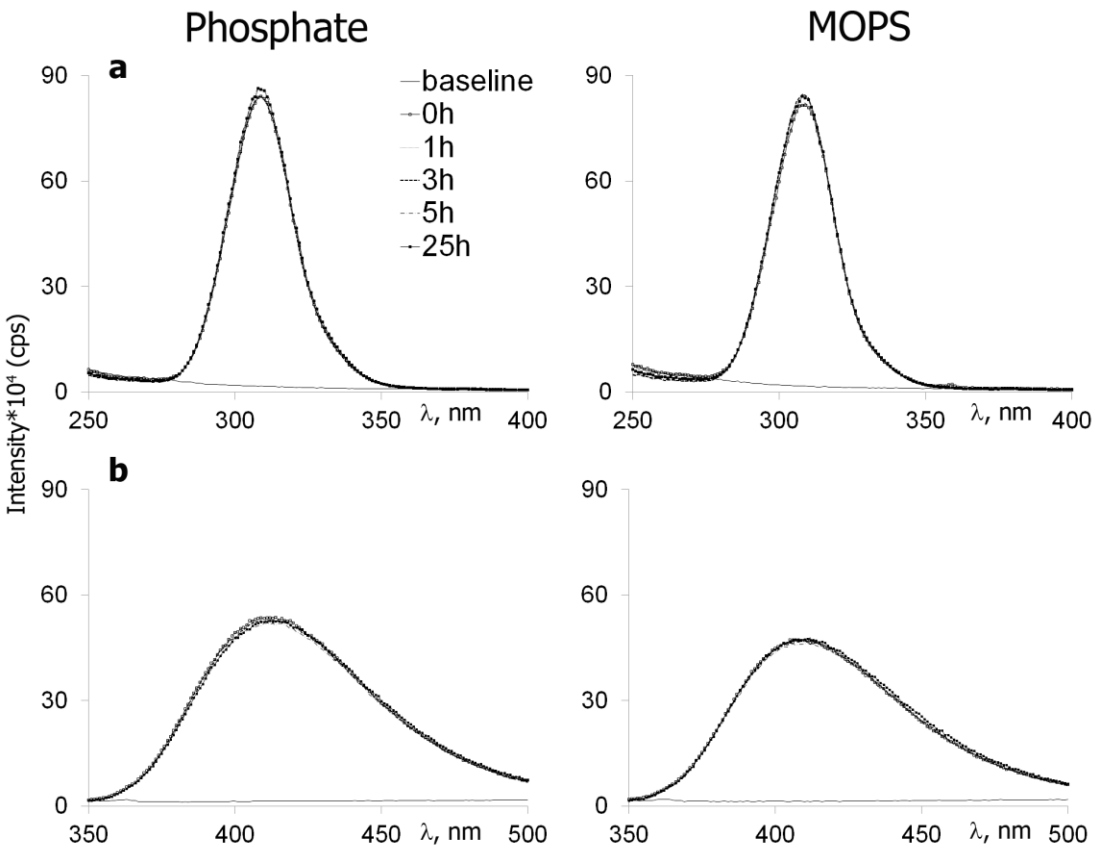

Figure VI.2. Fluorescence spectra of the reaction mixture of TPA (200 μM), **1** (50 μM) and excess of H_2O_2 under phosphate and MOPS buffers (5 mM) at the time of mixing, after 1, 3, 5 and 25 h.

Generation of hydroxyl radicals was also tested in the presence of **4** and **9** (Figure VI.3). Under phosphate buffer the formation of HTPA in the reaction with **9** seems to be rapid in the first hour, however, the intensity decreased considerably between 5 and 25 h. In the presence of **4** the hydroxylation of TPA is also observed, though to a small extent. The intensity does not change with time. Under MOPS buffer none of three complexes seem to induce the reaction of hydroxylation.

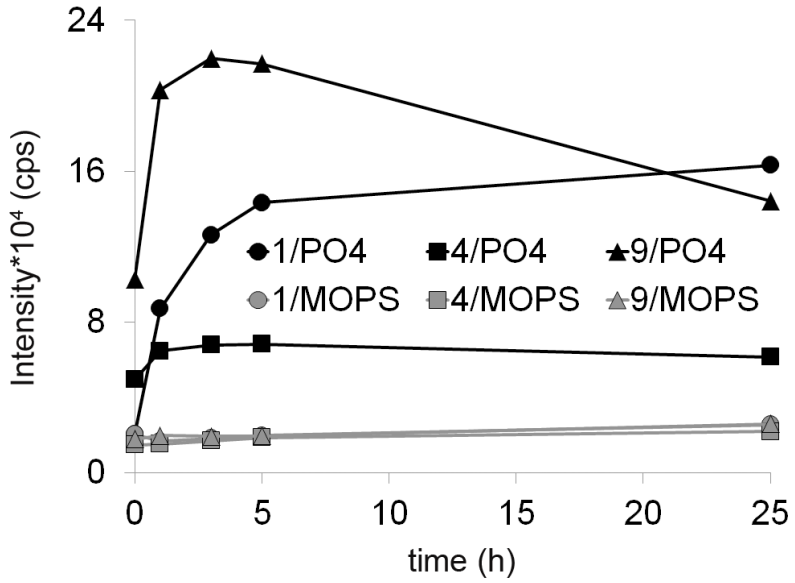

Figure VI.3. Fluorescence intensity *vs.* time. Reaction mixtures containing 200 µM TPA prepared in phosphate (black lines) or MOPS (grey) buffers with **1**, **4** and **9** (50 µM). Measurements were taken at the time of mixing, after 1, 3, 5 and 25 h.

To compare the efficiency of **1** in the formation of HTPA, the experiment in was carried out buffering the reaction medium with mixtures of phosphate and MOPS media. The reaction is always inhibited in the presence of MOPS even when phosphate is in a two-fold excess (MOPS/phosphate 5/10 mM) but proceeds with an intense hydroxylation of TPA when MOPS is absent (0/5 mM).

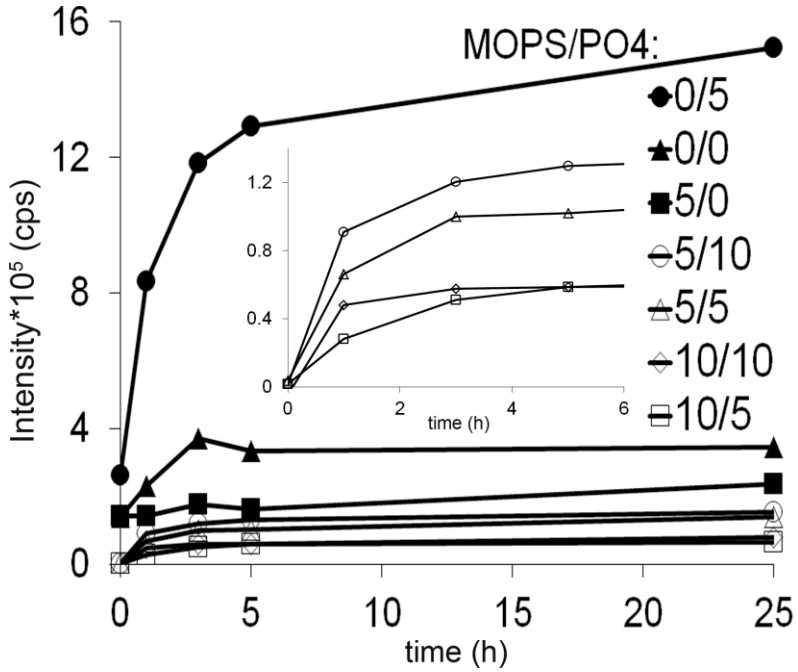

Figure VI.4. Change in the fluorescence intensity of the reaction mixtures with time (0, 1, 3, 5 and 25 h). TPA (200 µM) dissolved in MOPS (0, 5 and 10 mM) with addition of **1** (50 µM) prepared in 0, 5 and 10 mM of phosphate buffer. MOPS/phosphate buffer concentrations (in order of intensity decrease): 0/5, 0/0 (unbuffered), 5/0, 5/10, 5/5, 10/10, 10/5. The inset is the same graph with increased X and Y scales.

VI.1.2 Hydrolytic cleavage

Hydrolytic cleavage of two DNA model substrates, 4-nitrophenyl phosphate (NPP) and bis-4-nitrophenyl phosphate (BNPP), was examined by ^{1}H NMR in PBS and MOPS buffers. After mixing solution of **1** with NPP or BNPP, a ^{1}H NMR spectrum was recorded at different time increments, i.e., 0, 24, 47, 72, 168 and 240 h. An example of the whole spectra is shown in Figure VI.5. The remaining figures focus on the chemical shifts from 6.5 to 8.5 ppm, where peaks of NPP, BNPP and NP can be found, or from 1 to 4 ppm, where the peaks due to acac and MOPS are observed.

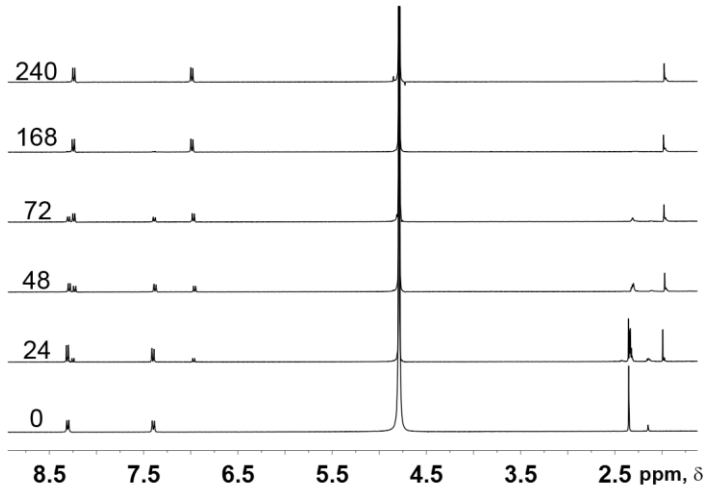

Figure VI.5. ^{1}H NMR spectrum of NPP hydrolysis in the presence of **1** under PBS buffer. Peak at 4.79 ppm is the reference peak of DSS.

^{1}H NMR spectra of **1** in D_2O is shown in Figure VI.6. There are four peaks observed: 1) a quartet at 3.65 ppm; 2) singlet at 2.07 ppm; 3) singlet at 1.44 ppm after 48 h that can be seen only when greatly zoomed; 4) triplet with peaks at 1.20, 1.18 and 1.17 ppm.

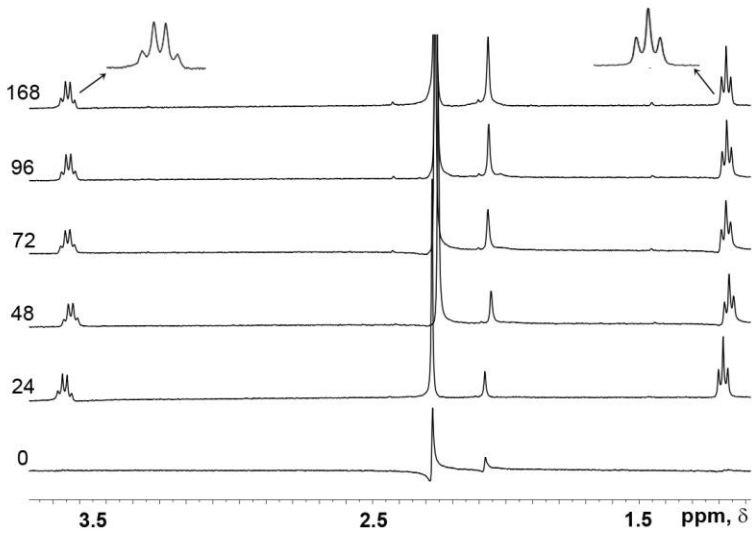

Figure VI.6. ^{1}H NMR spectra of **1** in D_2O along time. Numbers indicate hours after dissolution.

The spectra of control blank samples, i.e., NPP and BNPP under PBS and MOPS buffers with no added **1**, are shown in Figure VI.7. Initially only the two doublets characteristic of NPP and BNPP are observed close to 8.5 and 7.5 ppb. After 7 days two additional doublet peaks are observed in the spectrum of NPP under both PBS (8.21 and 8.19; 6.82 and 6.80 ppm.) and MOPS (8.11 and 8.09; 6.56 and 6.54) buffers. In the case of BNPP no changes are observed under PBS buffer, whereas in the presence of MOPS two new doublets appeared after 72 h.

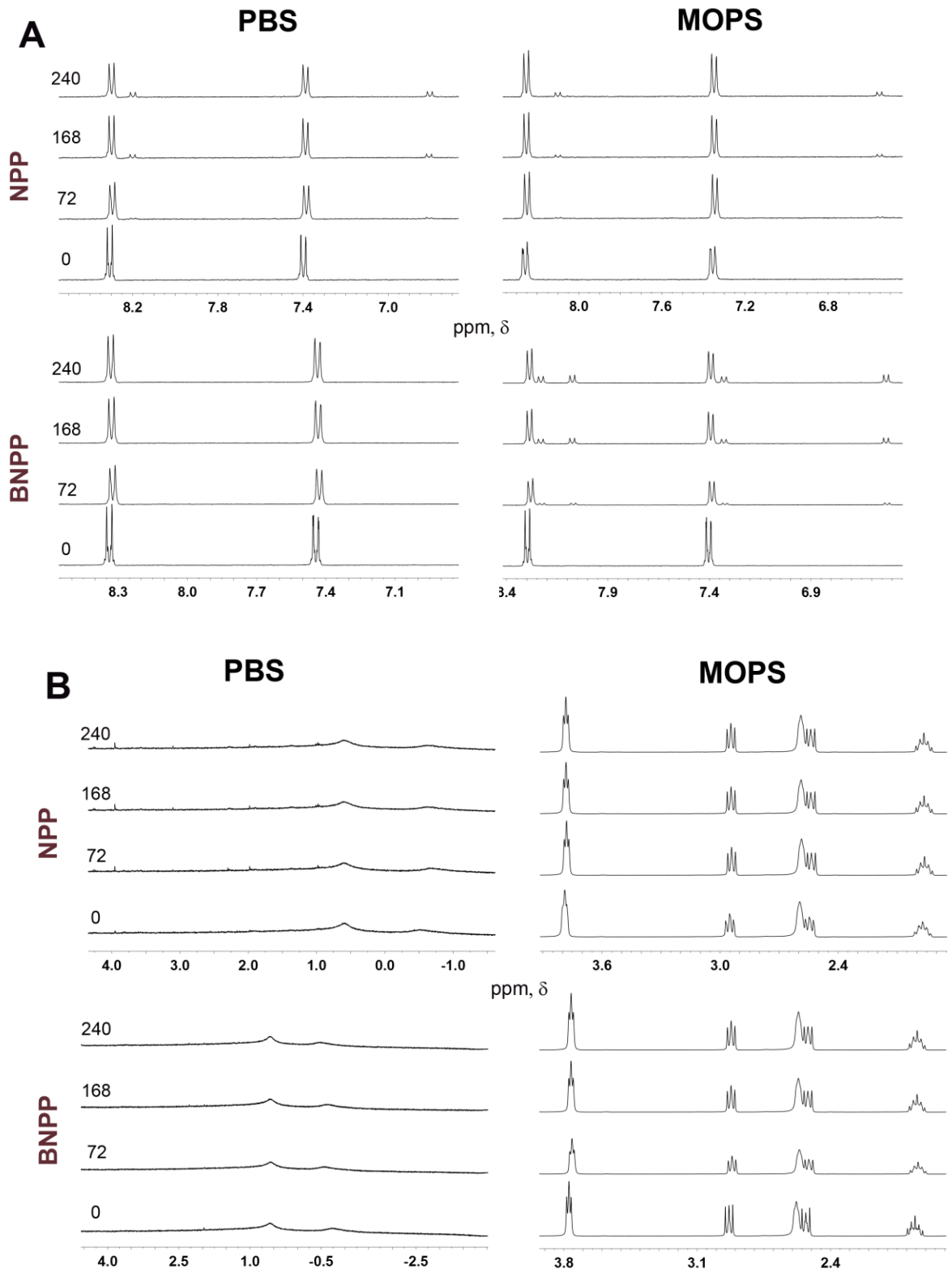

Figure VI.7. ^{1}H NMR spectra of NPP and BNPP under PBS and MOPS buffers (control samples) measured at different times (numbers indicate hours).

The results of ^{1}H NMR spectra of NPP and BNPP in the presence of **1** are summarized in Figure VI.8. Two doublets of NP, the product of hydrolysis, under PBS occur after 24 h in the case of NPP (8.26 and 8.24; 6.98 and 6.96 ppm). After 48 h a gradual decrease of NPP and increase of NP peaks is observed, until NPP peaks completely disappeared after 10 days and only the doublets of NP were left. After 24 h a peak that most probably belongs to 'free' acac is observed indicating a decomposition of **1**. In the case of BNPP the peaks of NP seems to only appear after 168 h (8.22 and 8.20; 6.93 and 6.91 ppm), however when zooming the spectrum (Figure VI.9), four doublets can be distinguished at the time of 24 h: 1) 8.29 and 8.27; 2) 8.22 and 8.19; 3) 7.40 and 7.38; 4) 6.93 and 6.91.

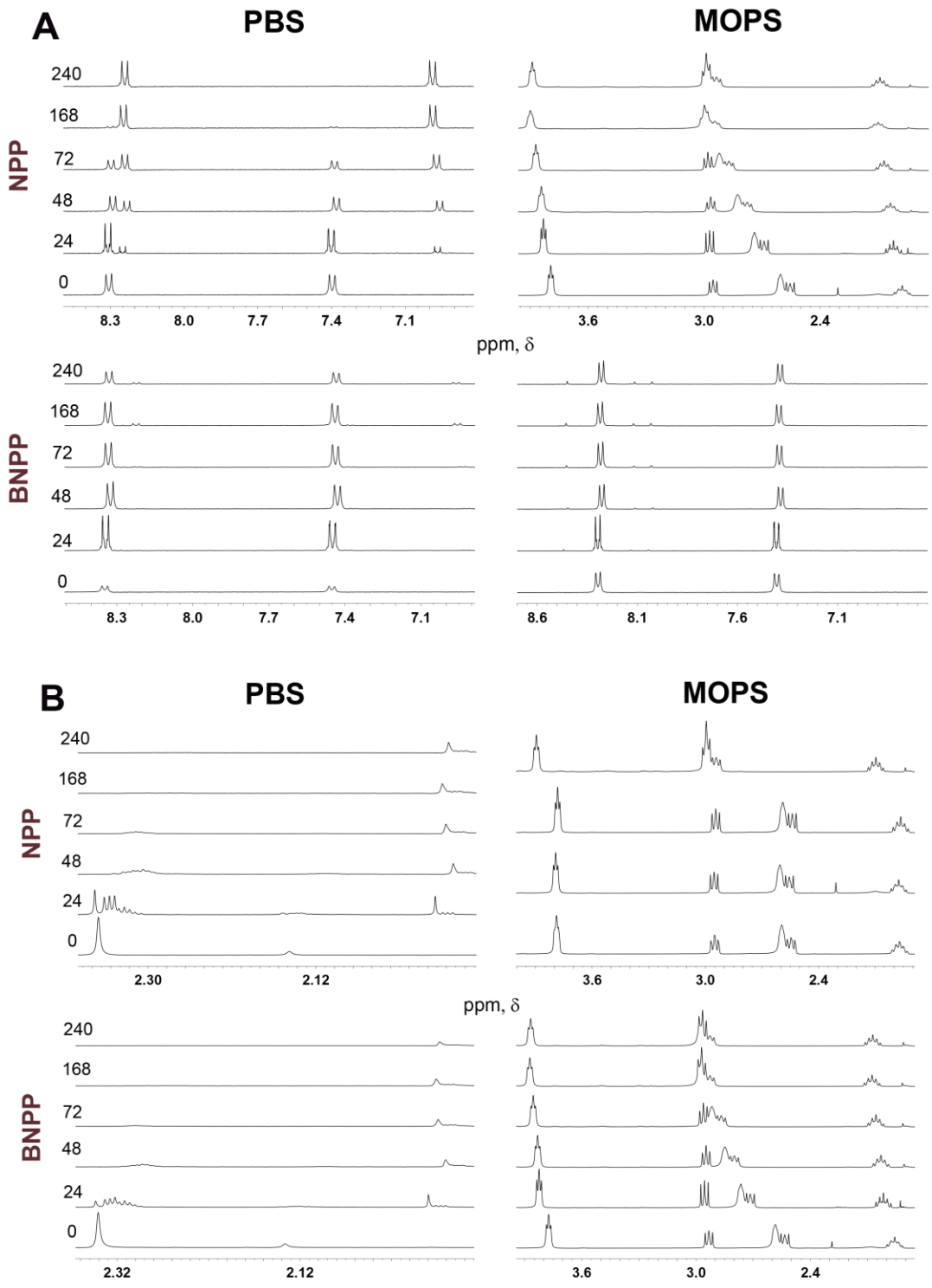

Figure VI.8. ^{1}H NMR spectra of the reaction of NPP (a) and BNPP (b) with **1** (d) measured at different times (numbers indicate hours) under PBS and MOPS buffers. NP (c) is the main product of the hydrolysis; 'e' is acac ligand.

Under MOPS, no hydrolysis of NPP or BNPP was observed, except after 7 days which can attributed to the natural degradation of NPP also observed in the blank control.

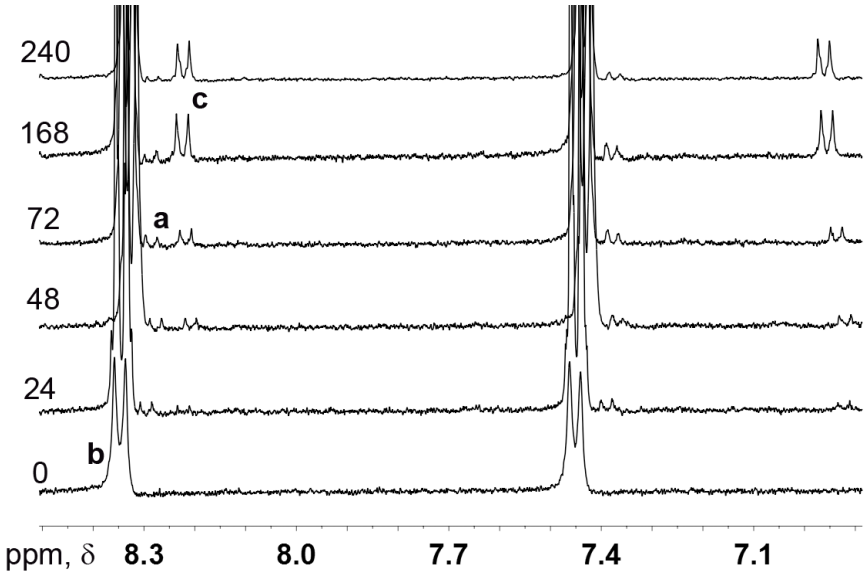

Figure VI.9. ^{1}H NMR spectra of the reaction of BNPP (b) with **1** measured at different times (numbers indicate hours) under PBS buffer. Zoomed version of the spectra shown in Figure VI.8.

Under MOPS buffer (Figure VI.10) peaks are detected after 24 h for both model substrates. In case of NPP, two doublets of NP at 8.17 and 8.15, 6.76 and 6.73 chemical shifts, respectively. In the spectra of BNPP, four doublets, two belong to NPP (8.25 and 8.22; 7.34 and 7.32) and two are of NP (8.13 and 8.11; 6.82 and 6.80). The resonances though look like doublets possess peaks of a different height: the left hand peak is much smaller than the right hand one. Also, there are two new peaks at 8.47 and 8.06 ppm which are not observed under PBS buffer.

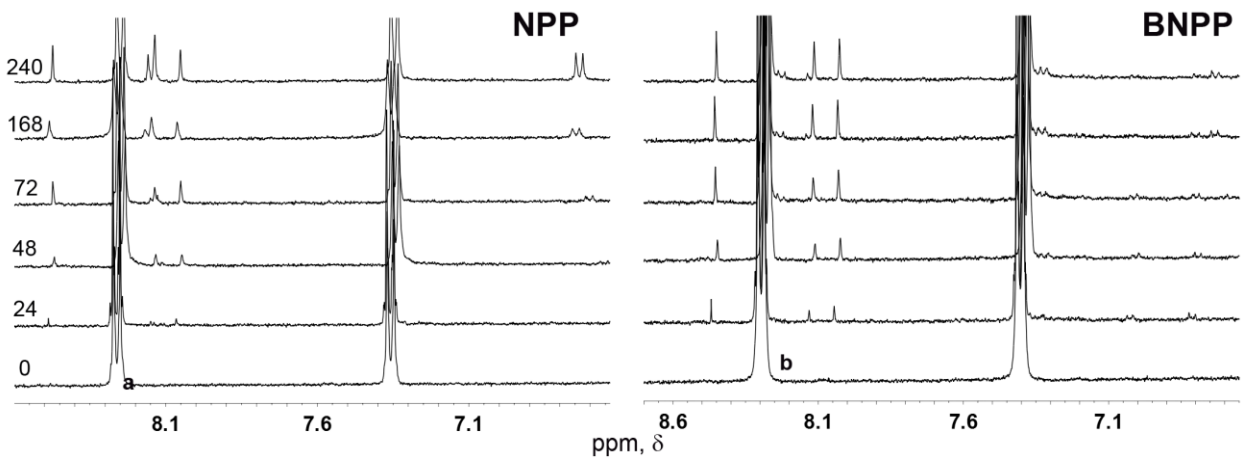

Figure VI.10. ^{1}H NMR spectra of the reaction of NPP (a) and BNPP (b) with **1** measured at different times (numbers indicate hours) under MOPS buffer. Zoomed version of the spectra shown in Figure VI.8.

The same four reaction mixtures, i.e., **1** with NPP/BNPP under PBS/MOPS, were used to measure ^{51}V NMR spectra to determine which vanadium species are responsible for the hydrolysis of phosphoesters (Figure VI.11). No peaks are observed immediately after mixing. Vanadate species are clearly formed after 24 h. Under PBS buffer two peaks at similar chemical shifts appeared in the spectra of both NPP (-570.42 and -578.26) and BNPP solutions (-572.0 and -580.0). Under MOPS buffer more V(V) peaks are observed, NPP/BNPP: 1) -548.6/-552.1; 2) -566.4/-567.7; 3) -572.4/-572.7; 4) -580.6/-581.3.

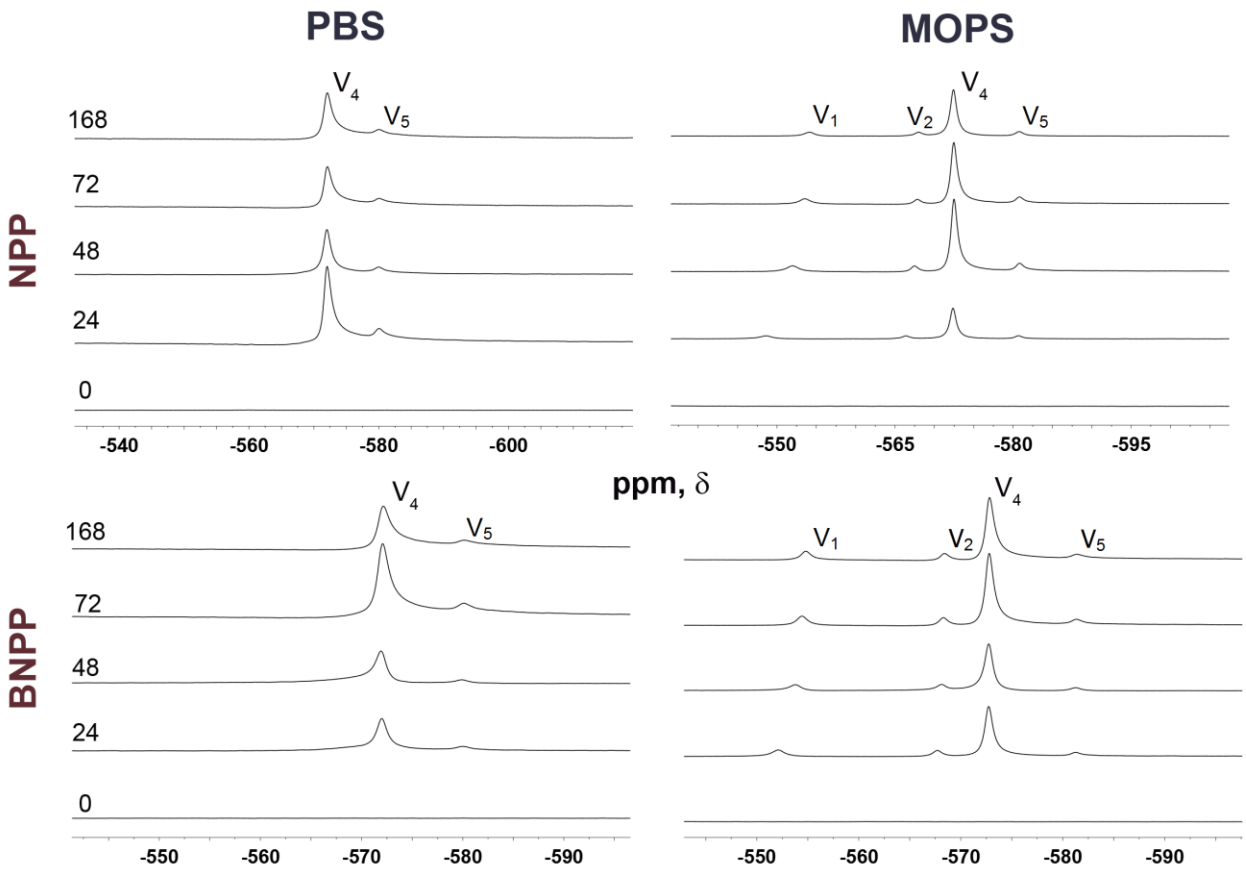

Figure VI.11. ^{51}V NMR spectra of the same solutions presented in Figure VI.7 and Figure VI.8 for the reaction of NPP and BNPP in solution of **1** under PBS and MOPS buffers.

VI.2 Discussion

The DNA cleavage by the metallonucleases typically proceeds via either a radical or a hydrolytic mechanism. Unlike the radical attack on the sugar or base moieties mediated by inorganic cleaving agents, the hydrolytic cleavage of the phosphodiester bond is reversible and is the path followed by natural nucleases.

Studies of the mechanism of DNA cleavage were to answer the following questions: Does ROS form in an aqueous solution of **1**? Does the buffer medium influence the generation of ROS? Is $VO(acac)_2$ capable of cleaving DNA hydrolytically? What is the

possibility of occurrence of mixed oxidative/hydrolytic mechanism during 1h complex-DNA digestion?

Based on the previous work of our group and according to the findings obtained by AGE in this work, a radical mechanism of DNA cleavage by **1** is considered and can be established.

VI.2.1 Oxidative Cleavage

The maximum fluorescence intensity at 323 nm (in excitation spectra) and 435 nm (in emission spectra) is interpreted as being proportional to the total number of ROS/hydroxyl radicals formed in solution during the experiment time. The interpretation of obtained results might be complicated because while the hydroxylation reaction of TPA by 'free' hydroxyl radicals has been a subject of intensive studies, similar reactions of TPA with other agents such as metals are not well understood. Oxidovanadium may itself be considered a ROS, and it is possible that species such as a metal complex with the superoxide anion will promote the hydroxylation of TPA, without the formation of 'free' hydroxyl radicals. For the effects of this study, it is understood that a ROS capable of promoting the hydroxylation of TPA is damaging for DNA.

No hydroxylation of TPA is observed in the absence of metal complexes. The situation changes dramatically upon addition of **1** and differs with buffer media. Figure VI.12 compares the fluorescence spectra of HTPA formed upon the addition of **1** under phosphate and MOPS buffers. It is clear that **1** induces the hydroxylation to the greater extent in phosphate than in MOPS buffer, especially after 25 h. The formation of HTPA in these conditions suggests that aqueous solutions of the V(IV) complexes are able to generate hydroxyl radicals or ROS in general that are capable of hydroxylating TPA.

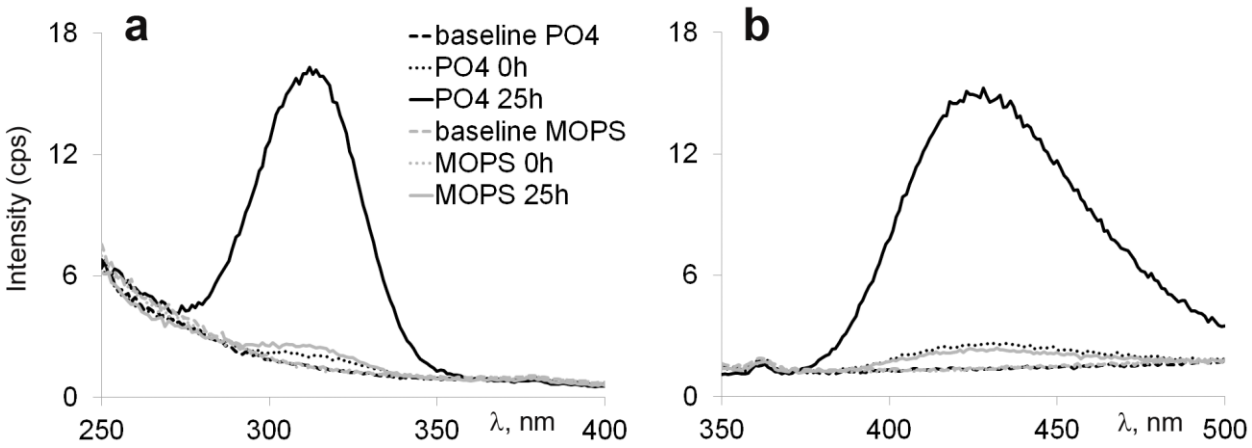

Figure VI.12. Fluorescence spectra for (a) excitation and (b) emission of HTPA formed in the reaction of TPA and **1** in freshly prepared reaction mixture and after 25 h, at neutral pH under phosphate or MOPS.

As expected, addition of hydrogen peroxide to solutions of **1** yields a strong formation of ROS (Figure VI.13) since in its presence, oxidovanadium(IV) complexes are known to produce large amounts of •OH in a Fenton-like reaction [431, 524]. Under both buffers the intensity after 25 h is as high as at the time of mixing, suggesting a fast completion of the reaction.

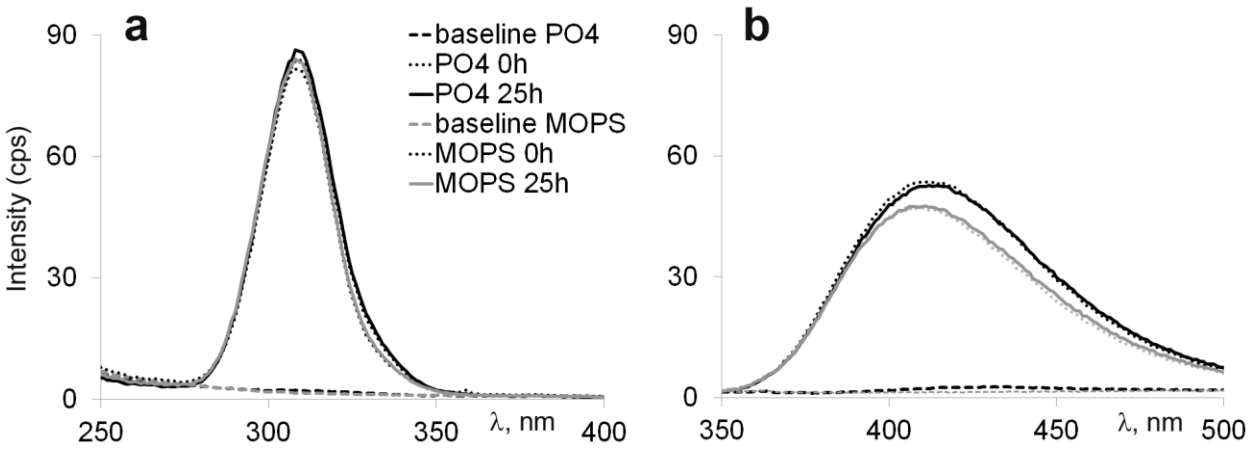

Figure VI.13. Fluorescence spectra of TPA (200 μM) in phosphate and MOPS buffers (5 mM) in the presence of **1** (50 μM) and excess of H_2O_2. Excitation spectra (a) were scanned at emission of 435 nm, and emission spectra (b) - at 323 nm of excitation.

Figure VI.3 compares the evolution of fluorescence intensities of complexes **1**, **4** and **9** with time. The strongest fluorescence is observed under phosphate buffer where the intensity of **1** increases along time and seems to stabilize after ca. 20 h, whereas in the case of **4** there is a modest increase which stabilizes after 4 h. This is in agreement with the nuclease activity results and corroborates the assumption that the DNA cleavage caused by these complexes follows a radical mechanism. Complex **4** is the least active, and also shows the lowest fluorescence intensity, thus it can be assumed that it generates less ROS capable of hydroxylating TPA and cleaving DNA. Complex **1** is the most active, and also generates more ROS.

Though in the presence of **9** the increase in the fluorescence is surprisingly high right from the time of mixing, the decrease observed after 3 h suggests low reproducibility observed in AGE results. Fluorescence intensities in this figure observed under MOPS are insignificant, also reflecting the low nuclease activity observed under organic buffers.

When dissolving TPA and **1** in solutions buffered by mixtures of MOPS and phosphate (Figure VI.4), increasing concentrations of phosphate increase the fluorescence intensity when MOPS is kept constant, suggesting that phosphate contributes to the generation of ROS, but the most striking results are obtained in the complete absence of MOPS, in which case fluorescence jumps to more than 10 fold higher than in its presence. This can be explained by the scavenging effect of MOPS on 'free' radicals [462].

AGE results of DNA cleavage induced by the same mixtures of buffers and **1** are in agreement with those obtained by fluorescence, i.e., the nuclease activity of **1** shows the same pattern, i.e. it is strikingly higher in the absence of MOPS (Figure IV.23). When MOPS buffer is absent linearization of DNA is observed. On the contrary, the DNA degradation is always inhibited when MOPS is added and the extent of the inhibition is higher for higher concentrations of MOPS.

According to the literature precedents, phosphate buffer is often used in the experiments involving the generation of 'free' radicals and is known to increase the rate of Fe(II) [447] and V(IV) [522, 523] autoxidation at neutral pH. The reaction products are Fe(III) and V(V) and superoxide (eq.VI.1 and VI.2).

When the reaction involves the addition of H_2O_2, vanadyl, in the same manner as ferrous in the Fenton reaction, appears to reduce it to OH^- generating •OH (eq.VI.3 and VI.4) in the vanadyl-initiated Fenton-like reaction [524]; formed radicals then rapidly react with TPA yielding a fluorescent HTPA. In the absence of H_2O_2, it is likely that, oxidovanadium coordinates to phosphate resulting in a metal-buffer complex, which in turn, induces the formation of 'non-free' ('crypto') radicals [384, 446, 449], causing the hydroxylation.

$$Fe(II) + O_2 \rightarrow Fe(III) + O_2^- \qquad \text{(eq.VI.1)}$$

$$V(IV) + O_2 \rightarrow V(V) + O_2^- \qquad \text{(eq.VI.2)}$$

$$Fe(II) + H_2O_2 \rightarrow Fe(III) + OH^- + \bullet OH \qquad \text{(eq.VI.3)}$$

$$V(IV) + H_2O_2 \rightarrow V(V) + OH^- + \bullet OH \qquad \text{(eq.VI.4)}$$

The effect of phosphate in the biological activity of V has been addressed indirectly by Saran, Reinke and Liochev [447,449,522,523]. V(IV) promotes the oxidative stress in cells, and *in vitro* studies show that phosphate buffer increases the activity of ROS caused by VC. As an example, an important role of phosphate buffer is described by Liochev in the oxidation of NAD(P)H by vanadate [522]. Vanadium(IV) would autoxidize rapidly in phosphate buffer at neutral pH with generation of the superoxide anion [the reaction in [1a], which would then be the ROS responsible for the oxidation of NAD(P)H. On the other hand, in the absence of phosphate the oxidation of V(IV) would normally be outrun by the formation of mixed V(V)-V(IV) stable polyacids, which would possibility decrease or prevent the production of O_2^- completely.

Altogether, the nature of the formed species in phosphate buffer is not clear. Liochev [522] explored that phosphate prevents the formation of a stable “green complex” of V(V)/V(IV). In this case superoxide formed during oxidation of V(IV) possibly together with the metal is likely to play the role of active radical. This is in agreement with Saran’s [447] findings in which the active species in iron Fenton chemistry is not the hydroxyl radical, but a metal species with the superoxide ion. Reinke [449] in turn, emphasizes the likelihood of ‘non-free’ radicals which he describes as an oxidizing intermediate formed from a direct reduction of molecular oxygen which is apparently different from the hydroxyl radicals.

The formation of divanadates is usually observed only for vanadium concentrations above 100 μM [527]. At the level of concentration of DNA cleavage experiments (ca. 2-100 μM) the proportion of any eventual vanadium polyacids should be negligible, thus Liochev’s proposal about the formation of oxo-bridged V(V)/V(IV) complexes may not be suitable for explaining the observed DNA cleavage activity under either of buffers. It is nevertheless reasonable to assume that phosphate-oxidovanadium species could form

under of ca. 10 mM phosphate, when phosphate:metal ratios vary from 100 to 5000. The results on the electrochemistry of these complexes show that these species are formed, and they have a reversible electrochemical behaviour that may facilitate the oxidation of V(IV) with generation of ROS in neutral aqueous solutions.

In summary, the obtained results show that VC can generate ROS in neutral aqueous solutions, even in the absence of hydrogen peroxide. Such ROS, possibly a mixed radical of superoxide with V or V-PO_4 'crypto' radical, are capable of hydroxylating TPA and are likely to be responsible for the nuclease activity observed in **1** and derivatives. The best conditions for hydroxylation reaction are the same as for DNA cleavage, i.e., under phosphate buffer. The present work started with $VO(acac)_2$ but in fact can be applied to more VC. We observed a similar behaviour for $VOSO_4$, although with low reproducibility due to precipitation. V oxidative stress has been clearly described in the presence of H_2O_2, but the results of this work show that it is also important in its absence. The oxidation of V(IV) at neutral pH, whether promoted by dissolved oxygen or by water itself, will, in the presence of phosphate, generate ROS that can hydroxylate TPA and cleave DNA. The oxidative (radical) mechanism can be established.

VI.2.2 Hydrolytic cleavage

Nitrophenyl phosphate (NPP) and bis-4-nitrophenyl phosphate (BNPP) are two known DNA substrates which are typically used as the models for studying interactions with DNA as they have the structure similar to that of phosphoester bonds. The presence of an activating nitro group in the structure of NPP and BNPP implies an extreme resistance towards P–O bond hydrolysis. The cleavage of both models is expected to result into formation of free phosphate, accompanied by the release of p-nitrophenol (NP), which is easily detected by ^{1}H NMR due to its characteristic aromatic resonance [290]. In the case of hydrolytic cleavage of BNPP, NPP is an intermediate product and is supposed to be detected together with NP. Peak assignment is shown in Figure VI.14.

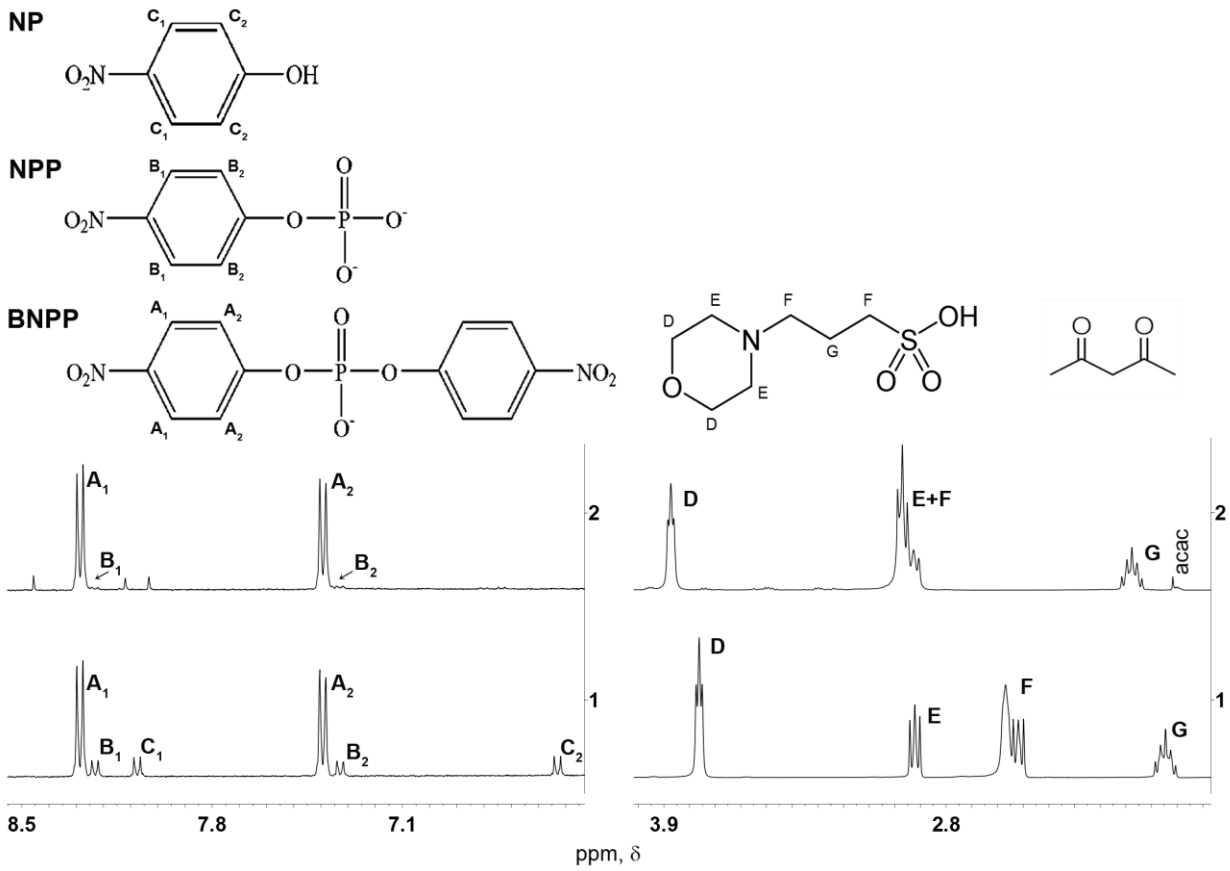

Figure VI.14. ^{1}H NMR spectra of BNPP in MOPS in the absence (1) and presence (2) of **1**, incubated at 50 ºC for 168 h. On the left side are the aromatic resonance peaks of BNPP, NPP and NP, while the right side are the chemical shifts of MOPS buffer.

The peaks at 1.93 and 5.16 ppm are the resonances due to CH_3 and CH protons that have been reported in free acetylacetone at 1.99 and 5.54 ppm, respectively [528, 529].

In the course of hydrolysis of both model substrates by **1**, the reaction mixture of NPP in PBS is the most favourable for the cleavage to occur: the ^{1}H NMR resonances attributed to the product of hydrolysis, NP, are easily observed after ca. 24 h increasing gradually with time. At ca. 200 h the reaction seems to be completed as at this point the ^{1}H NMR resonances of the aromatic protons in NPP disappear (Figure VI.3). In

agreement with the previously reported studies of this reaction [289], the hydrolysis of BNPP into NP is significantly slower than that of NPP. Under PBS, although the first signs of hydrolysis are also detected after 24 h, the peaks are too small to be visible in the spectrum (Figure VI.4). Also, as the hydrolysis of BNPP is expected to be a two-stage reaction in which NPP is an intermediate product, this might affect the rates of the cleavage. This reason, however, does not seem to be the main one because in the studies of this reaction [289], hydrolyses of BNPP is reported to be observed after ca. 7 h). Thus, the main reason for a very slow hydrolysis of BNPP obtained in our results is probably due to the occurred precipitation.

New peaks, singlets rather than doublets, that appear with time in experiments carried out with both substrates under MOPS (Figure VI.3), at chemical shifts 8.47 and 8.06 ppm are probably due to the degradation of MOPS induced by a reaction with ROS. This is the most likely explanation, since no peaks of possible MOPS degradation are observed in the control samples (Figure VI.12). The peaks assigned to MOPS in the range 2–4 ppm change position in time. This shows that the pH was not completely buffered. The concentration of MOPS was 40 mM while the concentration of vanadium was ~3 mM. The reason why the MOPS concentration was insufficient to buffer changes is the hydrolysis of vanadium. This difference is evidently observed when comparing the spectra of the samples with and without **1** in the proton resonances of MOPS buffer (Figure VI.14, right plot).

The phosphoester and phosphodiester hydrolysis is evidently much slower under MOPS than in the presence of PBS.

Except BNPP in PBS where no changes are observed within the timeframe of the experiment (i.e., 240 h), in the rest of the control samples some hydrolytic cleavage occurred. After ca. 72 h the presence of NP was detected in solutions of NPP both under PBS and MOPS; the presence of NPP as well as NP was also detected in solutions of BNPP under MOPS. This indicates that **1** is not responsible for the hydrolysis in the case of BNPP under MOPS. Nevertheless, under PBS the presence of **1** is determinant in increasing the rate of the reaction.

Regardless of a DNA model substrate and buffer medium, it is apparent that the longer the reactions mixtures are kept incubating at 50 ºC the greater the extent of hydrolytic cleavage. In fact, temperature is probably playing an important role in the hydrolysis of phosphoester structure. However, considering that the half-life of spontaneous cleavage for NPP and BNPP at 50 ºC is estimated to be respectively 135 and 27000 days, the possibility that the temperature is responsible for the hydrolytic cleavage in the absence of **1** is unlikely.

Monitoring the same reaction mixtures by ^{51}V NMR showed that after 24 h **1** has hydrolysed completely into inorganic vanadates (Figure VI.11).

The results show that **1** can promote the hydrolytic cleavage of DNA, but such a reaction is too slow to compete with the oxidative cleavage, which is the predominant mechanism and most likely the only one occurring during 1 h digestion of DNA.

It has been previously proven by Steens et al. [289,290] that vanadates can actually promote hydrolytic cleavage of the phosphodiester bond [530] – in particular di- and/or tetravanadates. It is possible that these species are the ones responsible for the observed hydrolytic activity in our experiments.

Hence, $VO(acac)_2$ induces the hydrolytic cleavage of the phosphoester bond under PBS buffer. This occurs more readily with NPP than BNPP. Under MOPS some hydrolysis was observed in the presence of $VO(acac)_2$ but it was indistinguishable from what occurs in the absence of the complex, suggesting that $VO(acac)_2$ does not play a role in this process. The reaction is extremely slow (>24 h at 50°C) comparing to the oxidative cleavage of plasmid DNA (<1 h at 37°C) with a completion of approximately 200h for NPP. The species responsible for the breakage of the phosphoester bond are probably tetravanadates.

It can be concluded that the hydrolytic mechanism does not play an important role in the DNA cleavage activity of $VO(acac)_2$.

Chapter VII

Conclusions

VII. Conclusions

The original motivation for this work has been to identify a vanadium complex species which would be responsible for the nuclease activity reported for many V(IV) complexes. While the search for one “culprit” species has been elusive, the information collected and conclusions derived are extremely important when considering the use of vanadium complexes in therapeutics.

The following main conclusions can be drawn from the previous chapters:

1. **All derivatives of $V^{IV}O(acac)_2$ studied, with the exception of V(V) derivatives, showed some degree of nuclease activity**. Some of these complexes (such as $VOSO_4$ and $VO(acac)_2$) have been reported in the literature as not showing nuclease activity. We believe the reason is that most research groups use commercial plasmid DNA, such as pBR322, which contains EDTA in concentrations ranging from 1 to 11 mM. EDTA is a very strong complexing agent which will change the metal speciation. All experiments in this work were conducted with pA1, a plasmid DNA which was amplified and purified in the laboratory, and dissolved in water only.

2. **The nuclease activity observed for the complexes under study is mainly caused by a radical mechanism.** Even though hydrolytic cleavage can occur, it is too slow to compete with the radical cleavage. The nuclease activity of these VC is indirect, i.e., it is a consequence of the generation of ROS caused by the VC. The active ROS are probably hydroxyl radicals, generated in a Fenton-like reaction of V(IV) complexes with water. Hence, all discussion on the nuclease activity of the complexes under study reflect their capacity of causing oxidative stress and is important in other aspects of metals in biological systems besides DNA cleavage

   .

3. **The activity of V(IV) complexes is closely dependent on the nature of the ligand**. Within the family of $VO(acac)_2$ derivatives, it was found that Cl-acac induced the highest activity, followed by acac and hd. Such evolution suggests that an electron-attracting group can increase the activity. Other acac derivatives substituted in C_3 with CH_3 and C_2H_5, as well as amine derivatives, show a much lower nuclease activity. These are also much less stable in aqueous solution.

4. **The activity of $VO(acac)_2$ derivatives is potentiated by phosphate.** As phosphate is ubiquitous in biological systems, it is extremely important to understand its role in this process. We have found that under phosphate buffer the most active and "stable" complexes **1**-**3** in fact react with phosphate to give a species with an electrochemical behaviour which is almost reversible. This is probably a mixed complex involving the ligand and phosphate. The less active complexes do not form this species, but instead they decompose into hydrolysis products. $VOSO_4$ forms a species with a similar reversible electrochemical behaviour but showing different reduction potentials. Assuming the electrochemical flexibility of these species is important for the oxidative stress, it would be expected that $VOSO_4$ would show a significant nuclease activity under phosphate buffer. In fact, we have observed that the nuclease activity of $VOSO_4$ is not very reproducible, but sometimes it is as high as for $VO(acac)_2$. The lack of reproducibility can be explained by its prompt precipitation as hydroxide at pH7. Cases where no activity of $VOSO_4$ is observed, as often reported in the literature, are probably due to a complete precipitation, or to complexation with EDTA when using commercial plasmid DNA.

5. **Other VC complexes studied do not show a buffer effect and are not potentiated by phosphate.** Unlike $VO(acac)_2$ derivatives, in the case of VO(oda) VO(oda)bipy and VO(oda)phen no significant difference is observed in nuclease activities under different pH buffers. The cleavage mechanism involves radicals. This is proved by the decreased activity following the addition of radical

scavengers. The extent of the decrease indicates that the cause for the buffer effect on the nuclease activity of $VO(acac)_2$ derivatives is not the scavenging effect of organic buffers, but the involvement of phosphate in the mechanism.

Further considerations

The reason for the high ROS activity of the mixed ligand – phosphate complexes is not clear. Previous studies have reached a similar conclusion and provided a few hypothesis.

The effect of phosphate in the biological activity of V has been addressed in the 1990s by Liochev [552,553], who observed a potentiation of the oxidation of NAD(P)H by vanadate under phosphate buffer when compared with other buffers. Liochev proposed that vanadium(IV) would autoxidize rapidly in phosphate buffer at neutral pH with generation of the superoxide anion, which would then be the ROS responsible for the oxidation of NAD(P)H. On the other hand, in the absence of phosphate the oxidation of V(IV) would normally be outrun by the formation of mixed V(V)-V(IV) stable polyacids, which would possibility decrease or prevent the production of superoxide completely.

Later, other groups [447,449] have described effects of the phosphate buffer on the Fenton generation of radicals by iron complexes. It was suggested that the active species in iron Fenton chemistry is not the hydroxyl radical, but a metal species containing the superoxide ion.

The formation of divanadates is usually observed only for vanadium concentrations above 100 μM [527]. At the level of concentration of DNA cleavage experiments (ca. 2-100 μM) the proportion of any eventual vanadium polyacids should be negligible, thus Liochev's proposal about the formation of oxo-bridged V(V)/V(IV) complexes may not be suitable for explaining the observed DNA cleavage activity under either of buffers. It is nevertheless reasonable to assume that phosphate-oxidovanadium species could form under ca. 10 mM phosphate, when phosphate:metal ratios vary from 100 to 5000.

Our results on the electrochemistry of these complexes show that these species are formed, and they have a reversible electrochemical behaviour that may facilitate the oxidation of V(IV) with generation of ROS in neutral aqueous solutions.

Based on the proposals by Liochev, Saran and Reinke [447,449,552,553], and on the results of this work, a tentative mechanism can be proposed:

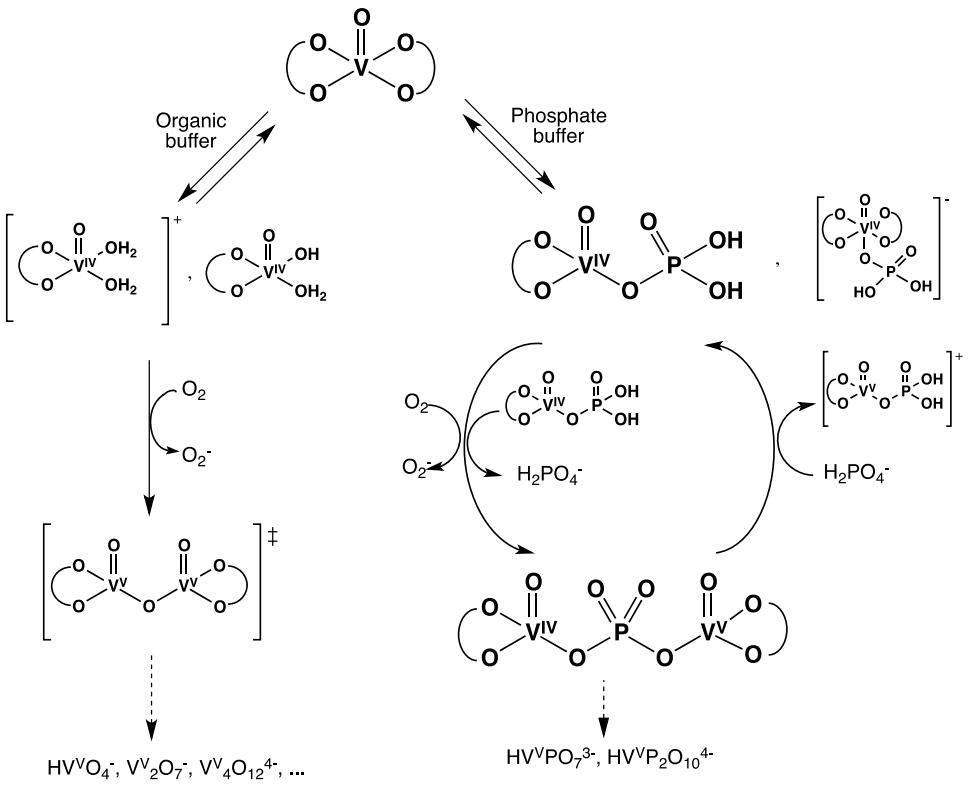

During this work we have tried to detect mixed ligand species containing acac and phosphate using Mass Spectrometry (MS-ESI) to analyse solutions of $VO(acac)_2$ under phosphate buffer, MOPS buffer and unbuffered solutions (results not shown in this thesis). Besides $V^{IV}O(acac)(H_2O)^+$ and $V^{IV}O(acac)_2.H^+$, a species formulated as $(VO)_2(acac)_3$ (M/z=431) was detected in all solutions.

One peak, M/z=449.4, was detected only in phosphate buffered solutions, and may be due to the species [$V^{IV}O(acac)V^{V}O(acac)PO_4$] proposed above, ionized with one Na^+. Nevertheless, MS-ESI spectra obtained for phosphate buffered solutions was subject to high noise due to the interference of refractive phosphate salts, therefore, these results must be confirmed.

Annexes

VIII. Annex A

Images of AGE Gels

$VO(acac)_2$ and derivatives

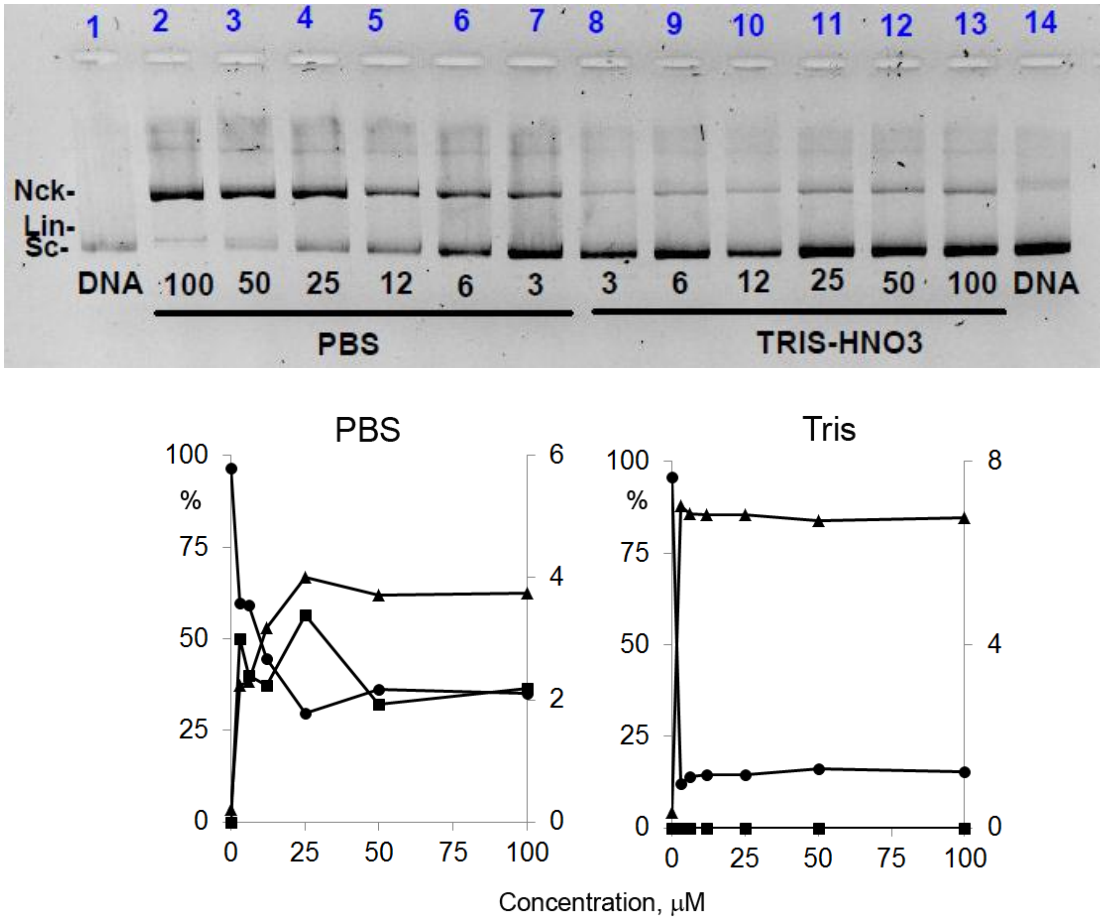

Figure A1. DNA cleavage activity of **1** at 3, 6, 12, 25, 50 and 100 μM (ri 0.2, 0.4, 0.8, 1.7, 3.3 and 6.7) under PBS and TRIS buffers. DNA" is the control for native DNA incubated in the absence of metal. 'Nck, Lin and Sc' indicate the position of the nicked, linear and supercoiled form of DNA, respectively. *Top*: Image of agarose gel. *Bottom*: graphic of the percentage of each DNA form *vs*. complex concentration

.

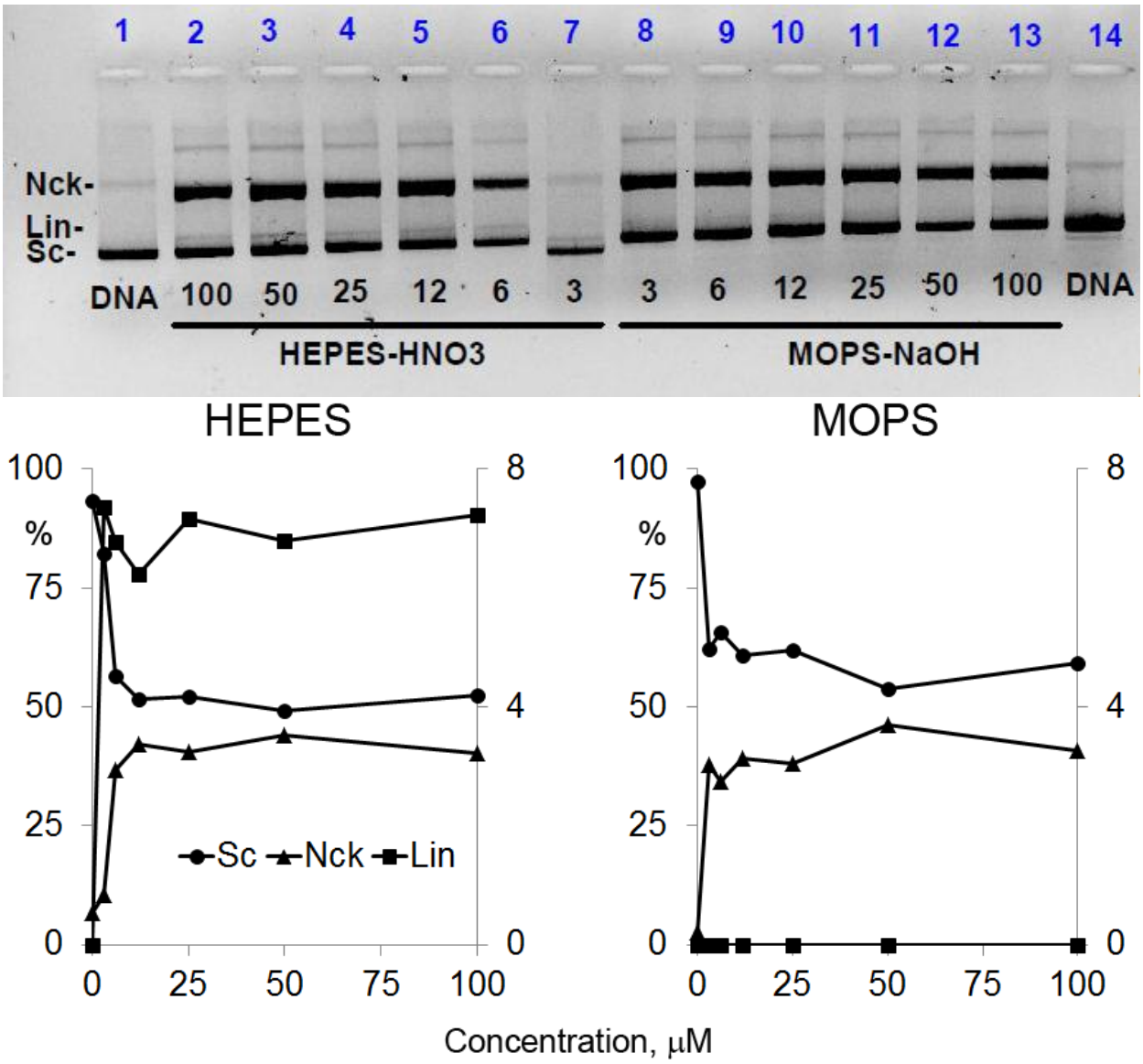

Figure A2. DNA cleavage activity of **1** at 3, 6, 12, 25, 50 and 100 μM (ri 0.2, 0.4, 0.8, 1.7, 3.3 and 6.7) under HEPES and MOPS buffers. *Top*: Image of agarose gel. *Bottom*: graphic of the percentage of each DNA form *vs*. complex concentration.

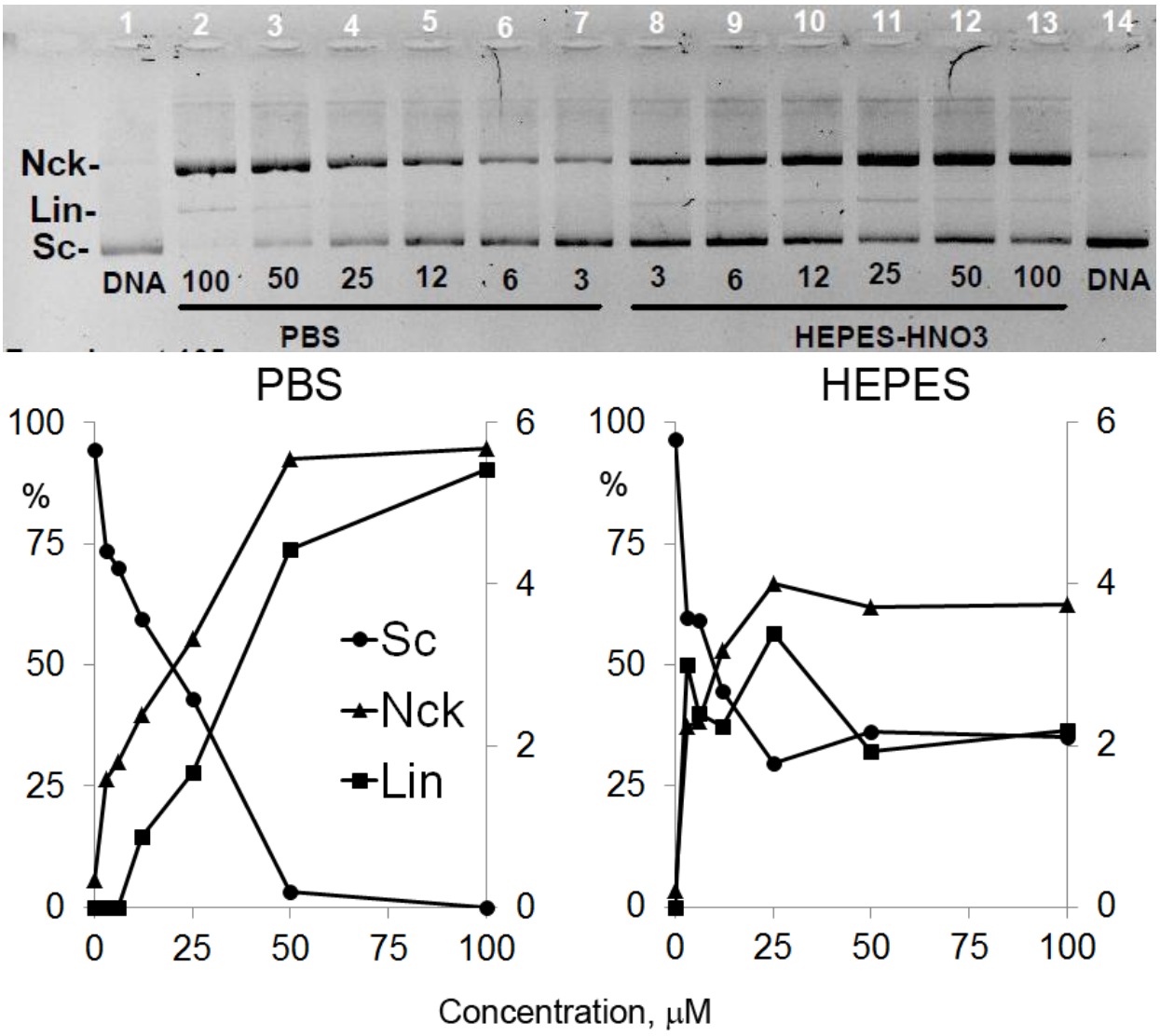

Figure A3. DNA cleavage activity of **1** at 3, 6, 12, 25, 50 and 100 μM (ri 0.2, 0.4, 0.8, 1.7, 3.3 and 6.7) under PBS and HEPES buffers. *Top*: Image of agarose gel. *Bottom*: graphic of the percentage of each DNA form *vs*. complex concentration.

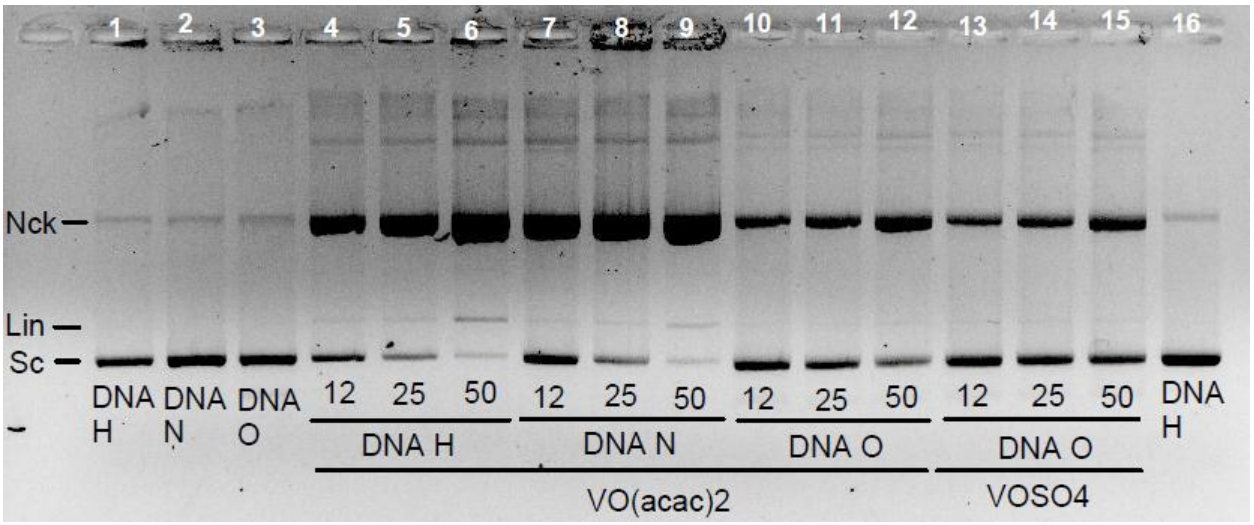

Figure A4. Comparison of the nuclease activity of **1** and **9** at 12, 25 and 50 µM (ri 0.8, 1.7 and 3.3) under phosphate buffer (pH 7.4) using three plasmids DNA obtained from different batches (i.e., DNA H, DNA N and DNA A).

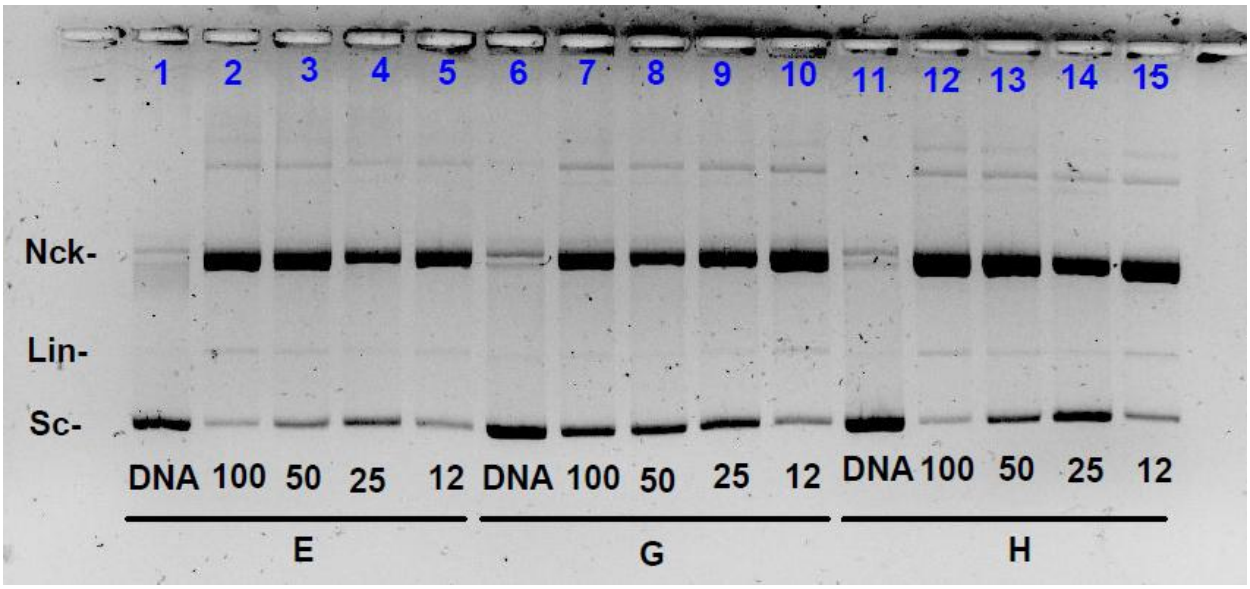

Figure A5. Comparison of the nuclease activity of **1** at 12, 25, 50 and100 µM (ri 0.8, 1.7, 3.3 and 6.7) under phosphate buffer (pH 7.4) using three plasmids DNA obtained from different batches (i.e., DNA E, DNA G and DNA H).

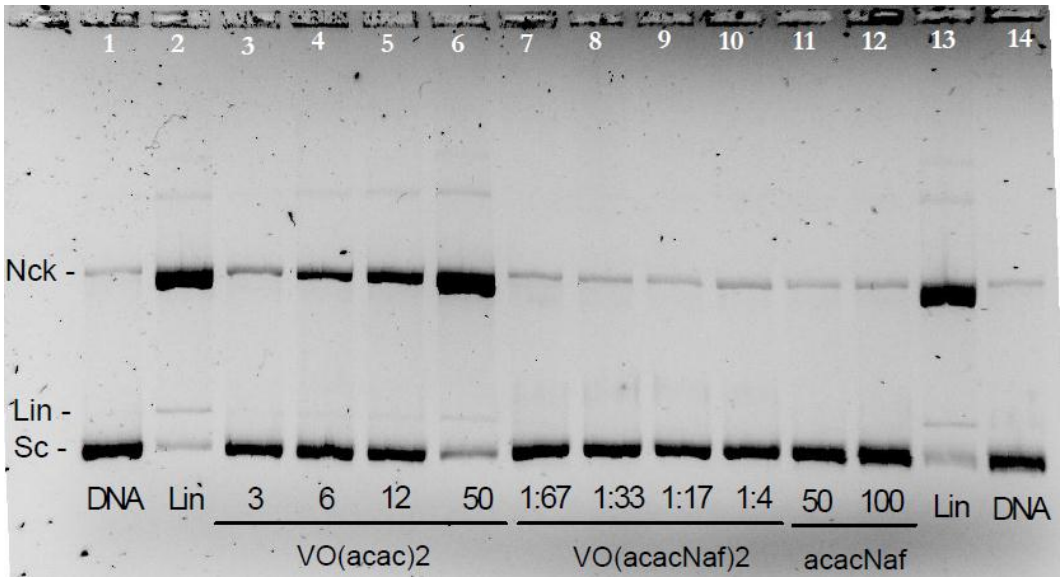

Figure A6. DNA cleavage activity of **1** and **10** under phosphate buffer. Concentration of **1** was 3, 6, 12 and 50 µM (ri 0.2, 0.4, 0.8 and 1.7). As complex **10** is poorly soluble in H_2O, dilutions (~1:4, 1:17, 1:33 and 1.67) were made from the stock solution prepared to be 200 µM. 'Lin DNA' is the control for linearized DNA (pA1 plasmid DNA digested with 50 µM of **1** under phosphate buffer). Ligand acac-Naf (Naf = naphthalene) was added for comparison.

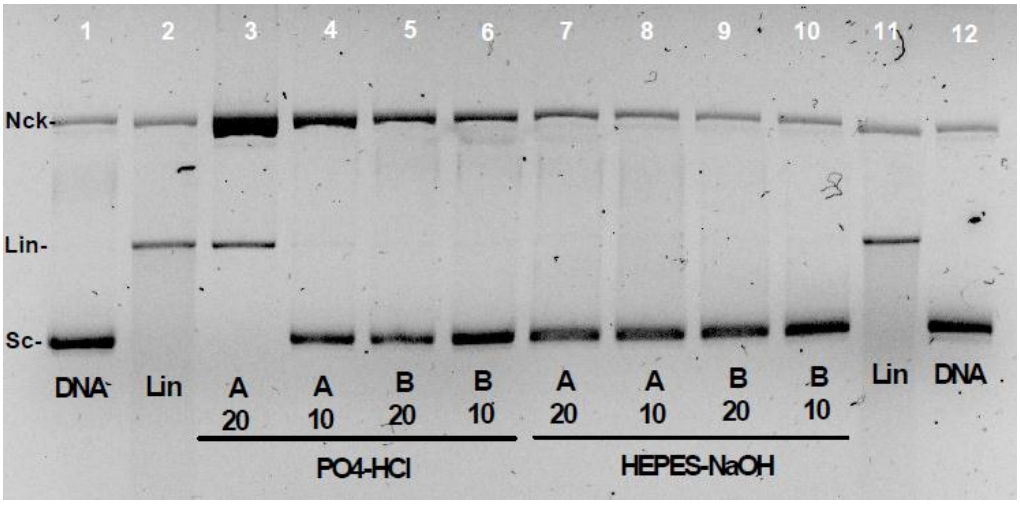

Figure A7. DNA cleavage activity of **1** (A) and **2** (B) 10 and 20 µM (ri 0.7 and 1.33) under phosphate and HEPES buffers.

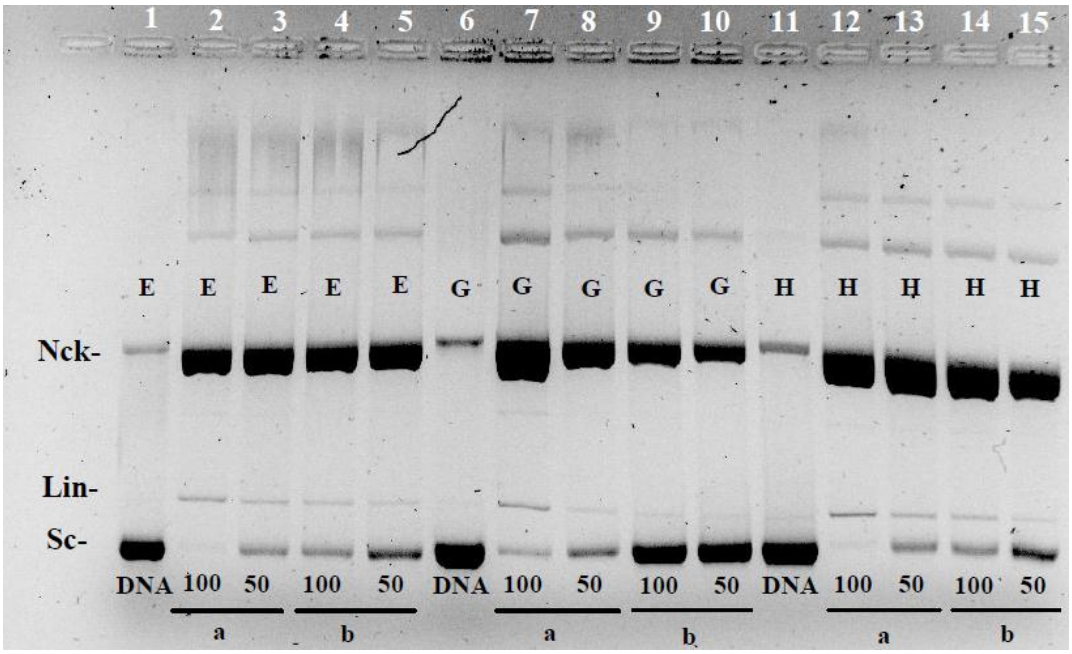

Figure A8. DNA cleavage activity of **1** (a) and **9** (b) at 50 and 100 µM (ri 3.3 and 6.7) under phosphate buffer using three plasmids DNA obtained from different batches (DNA E, DNA G and DNA H).

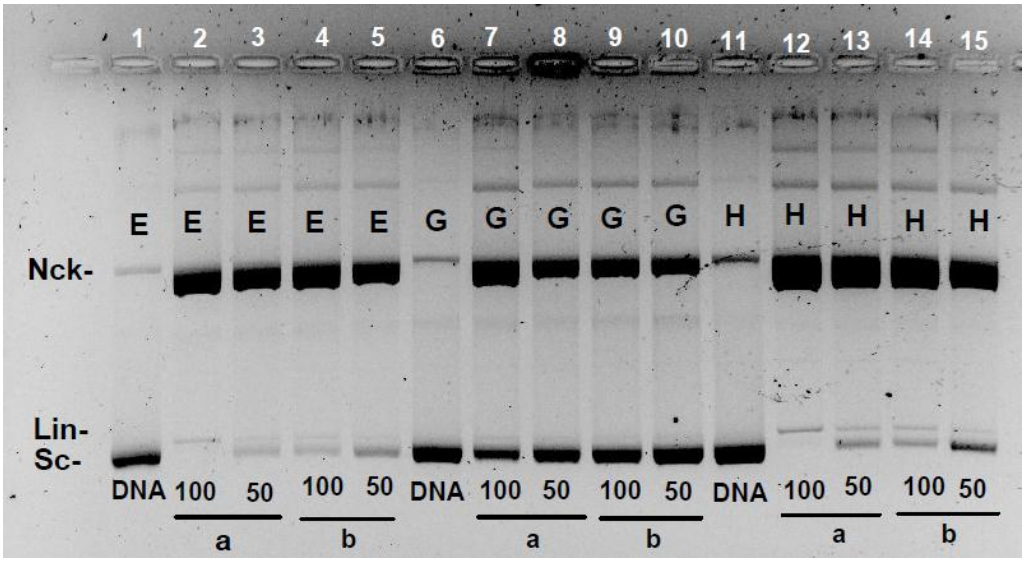

Figure A9. Replicate of the gel in Figure A8.

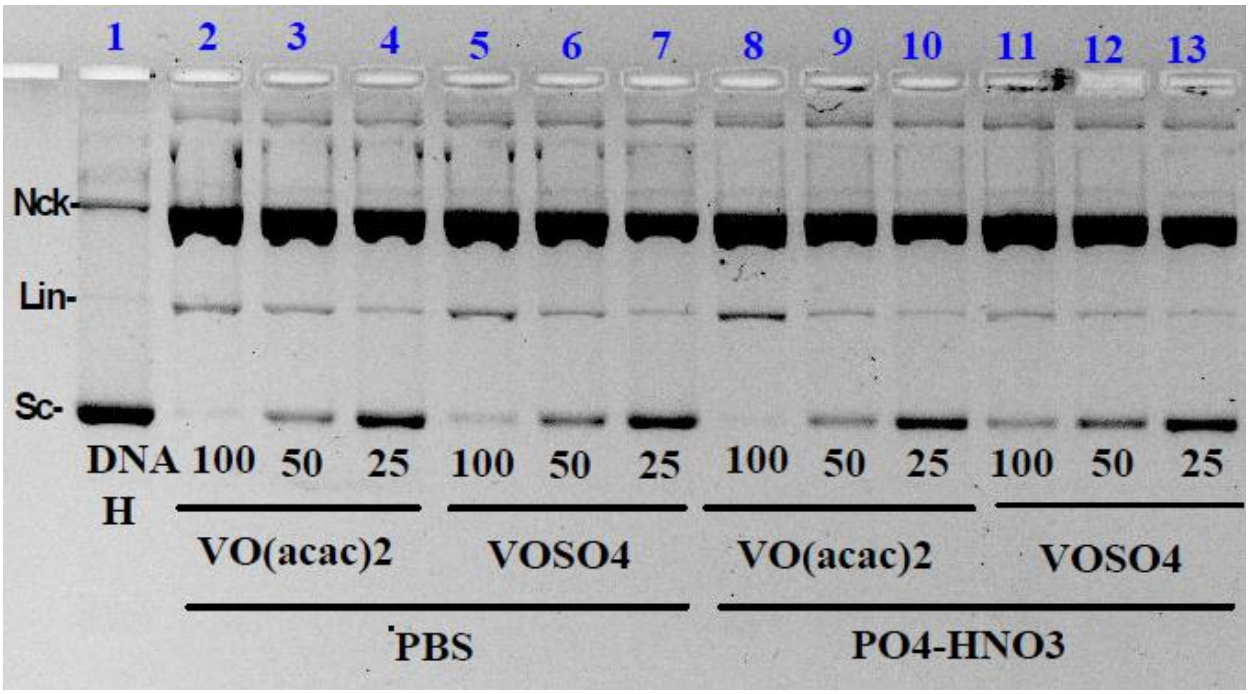

Figure A10. Comparison of DNA cleavage activity of **1** (a) and **9** (b) at 25, 50 and 100 μM (ri 1.7, 3.3 and 6.7) under PBS and phosphate buffer.

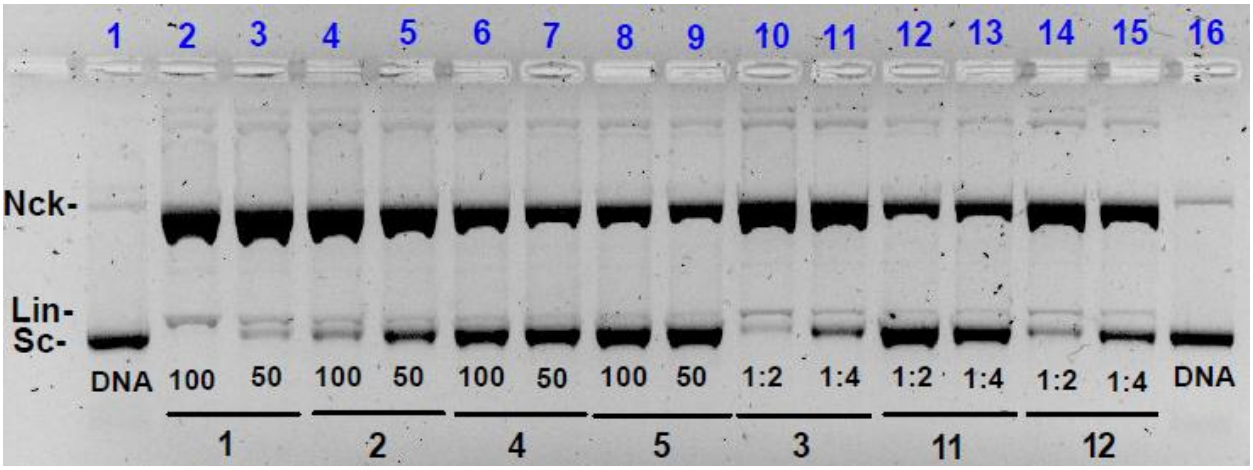

Figure A11. Comparison of DNA cleavage activity of **1**-**5**, **11** and **12** at 50 and 100 μM (ri 3.3 and 6.7) under PBS buffer. As complexes **3**, **11** and **12** are poorly soluble in water, a necessary amount of the solid was weighed to obtain 200 μM solution and corresponding dilutions 1:2 and 1:4 were made.

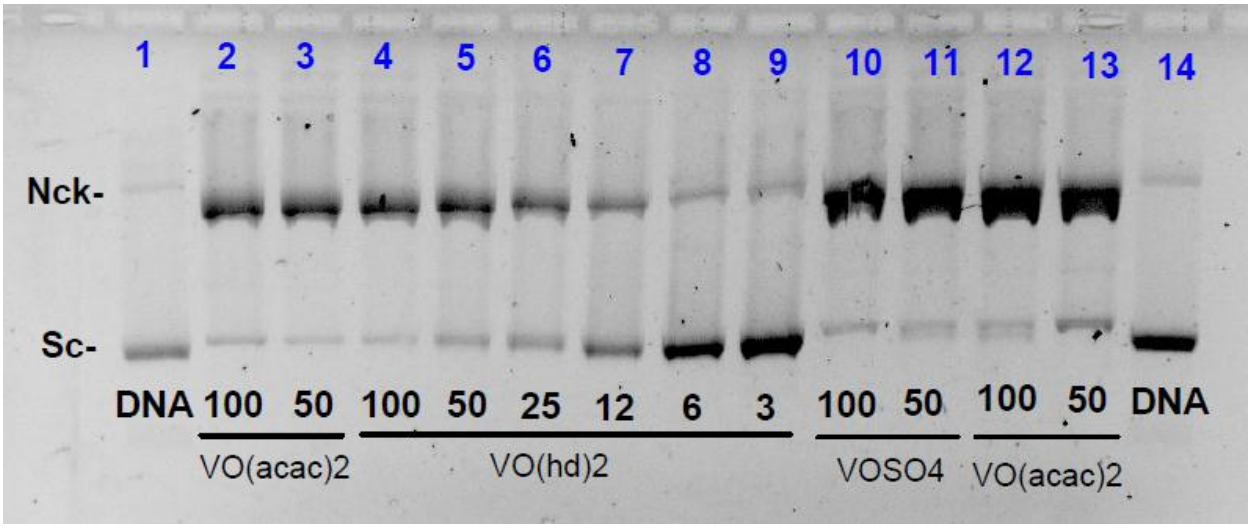

Figure A12. DNA cleavage activity of **2** at 3, 6, 12, 25, 50 and 100 µM (ri 0.2, 0.4, 0.8, 1.7, 3.3 and 6.7) under PBS buffer. Complex **1** and **9** were added for comparison.

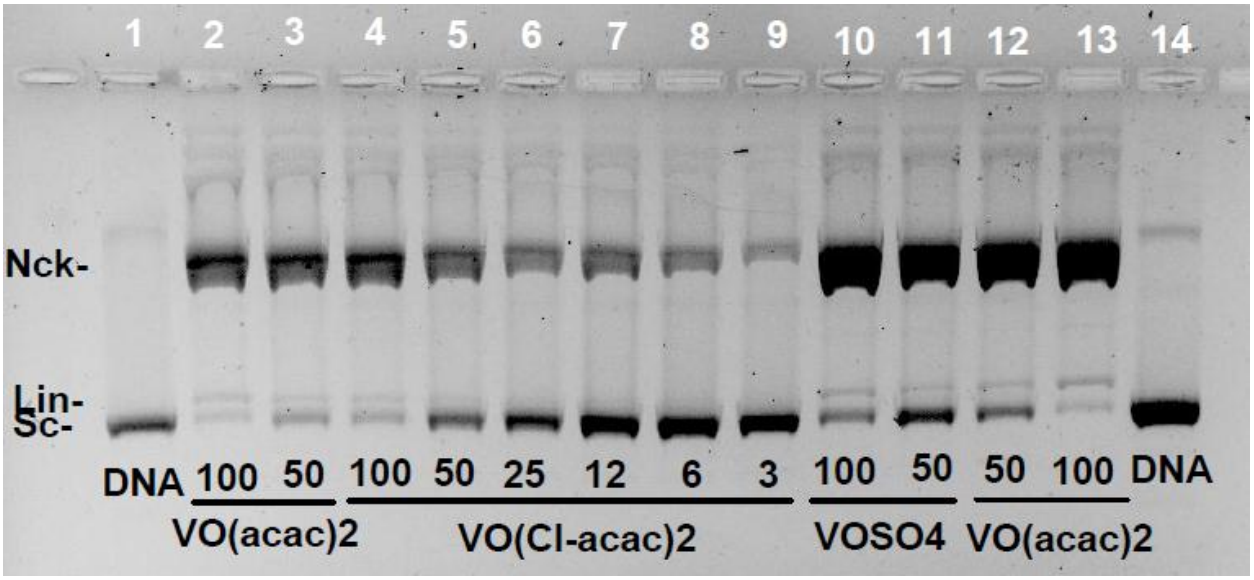

Figure A13. DNA cleavage activity of **3** at 3, 6, 12, 25, 50 and 100 µM (ri 0.2, 0.4, 0.8, 1.7, 3.3 and 6.7) under PBS buffer. Complex **1** and **9** were added for comparison.

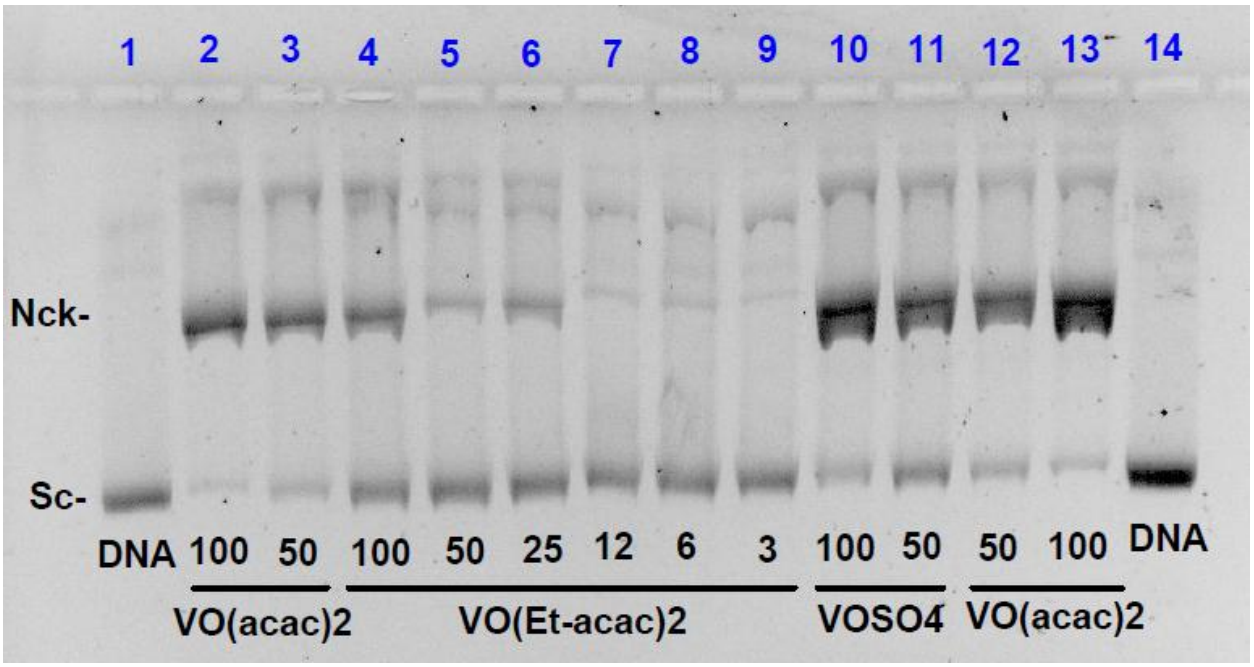

Figure A14. DNA cleavage activity of **4** at 3, 6, 12, 25, 50 and 100 μM (ri 0.2, 0.4, 0.8, 1.7, 3.3 and 6.7) under PBS buffer. Complex **1** and **9** were added for comparison.

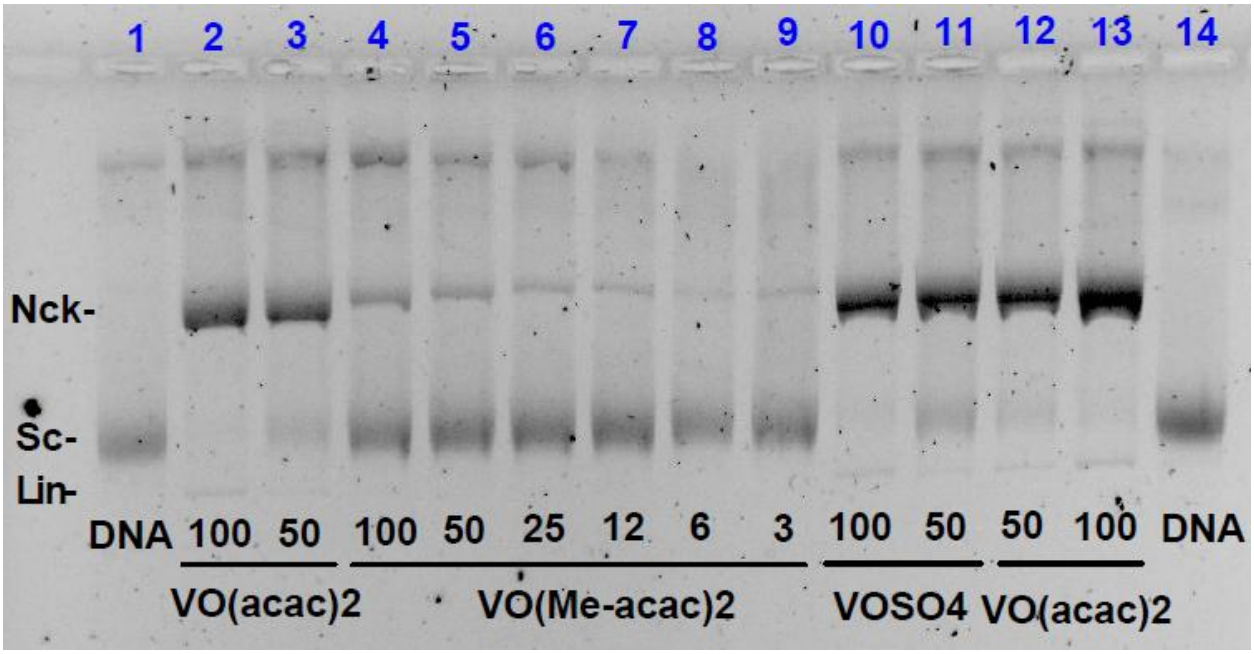

Figure A15. DNA cleavage activity of **5** at 3, 6, 12, 25, 50 and 100 μM (ri 0.2, 0.4, 0.8, 1.7, 3.3 and 6.7) under PBS buffer. Complex **1** and **9** were added for comparison.

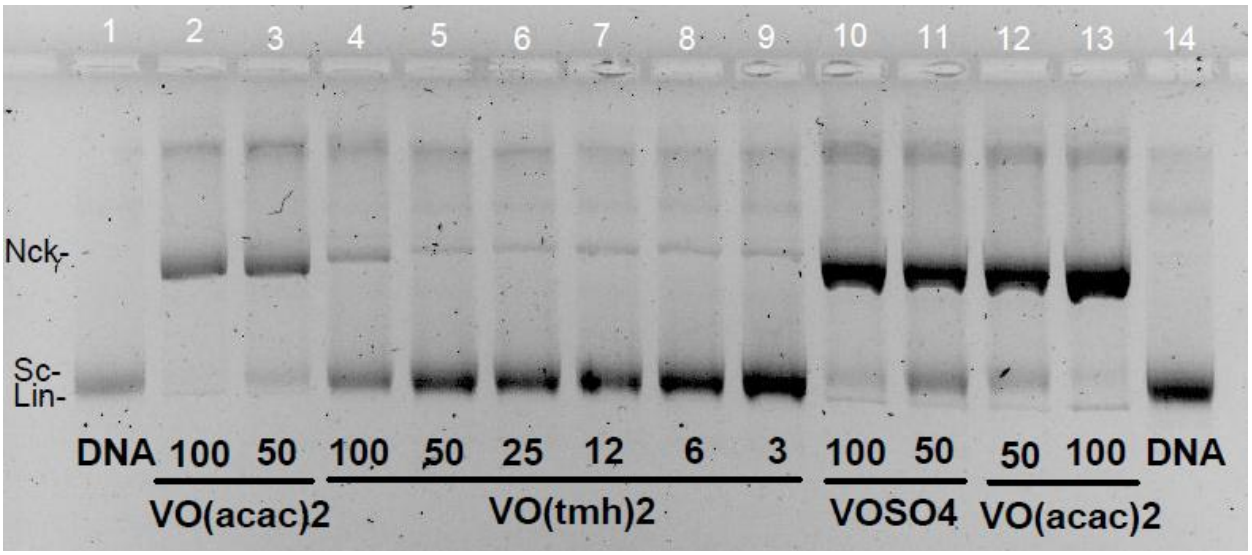

Figure A16. DNA cleavage activity of **11** at 3, 6, 12, 25, 50 and 100 μM (ri 0.2, 0.4, 0.8, 1.7, 3.3 and 6.7) under PBS buffer. Complex **1** and **9** were added for comparison.

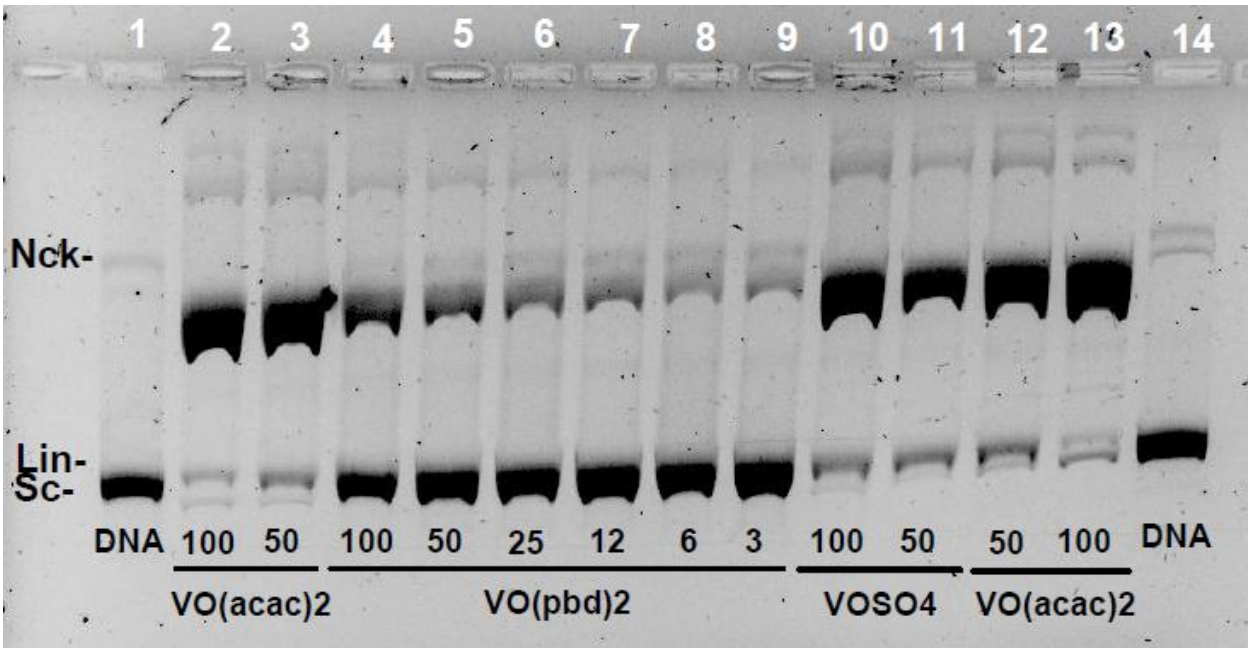

Figure A17. DNA cleavage activity of **12** at 3, 6, 12, 25, 50 and 100 μM (ri 0.2, 0.4, 0.8, 1.7, 3.3 and 6.7) under PBS buffer. Complex **1** and **9** were added for comparison.

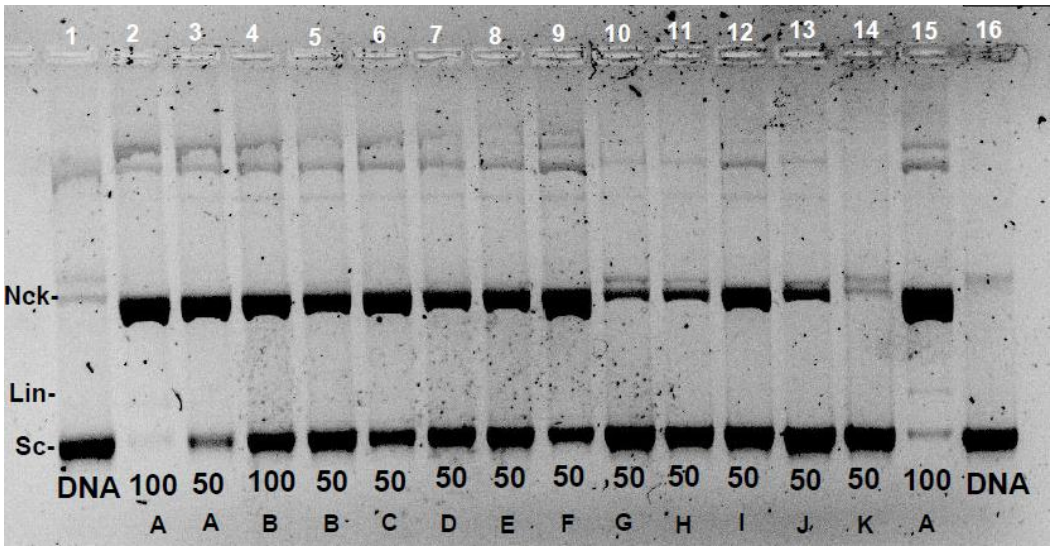

Figure A18. Comparison of the nuclease activity of **1** (A) at 50 and 100 µM (ri 3.3 and 6.7), **2** (B), **3** (C), **4** (D), **5** (E), **9** (F), **10** (K), **11** (J), **12** (I), **13** (H), **14** (G) at 50 µM under **PBS** buffer.

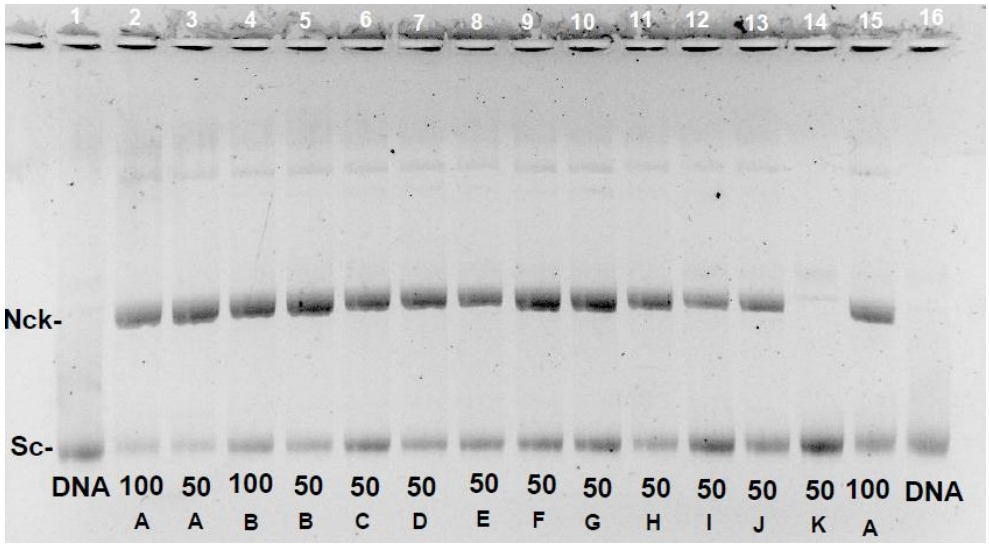

Figure A19. Comparison of the nuclease activity of **1** (A) at 50 and 100 µM (ri 3.3 and 6.7) **2** (B), **3** (C), **4** (D), **5** (E), **9** (F), **10** (K), **11** (J), **12** (I), **13** (H), **14** (G) at 50 µM under **MOPS** buffer.

Effect of incubation time

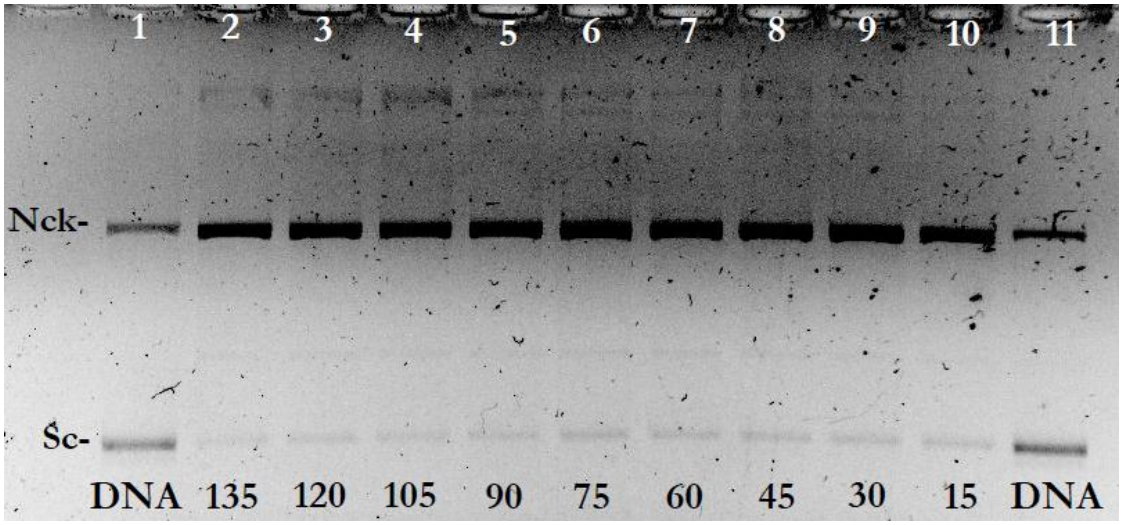

Figure A20. Effect of incubation time on the nuclease activity of **1** at 3 μM (ri 0.2) under phosphate buffer. The first sample containing **1** (lane 2) was incubated at 37 ºC for 135 min, the last one (lane 10) for 15 min. Interval between introducing samples into incubator was 15 min.

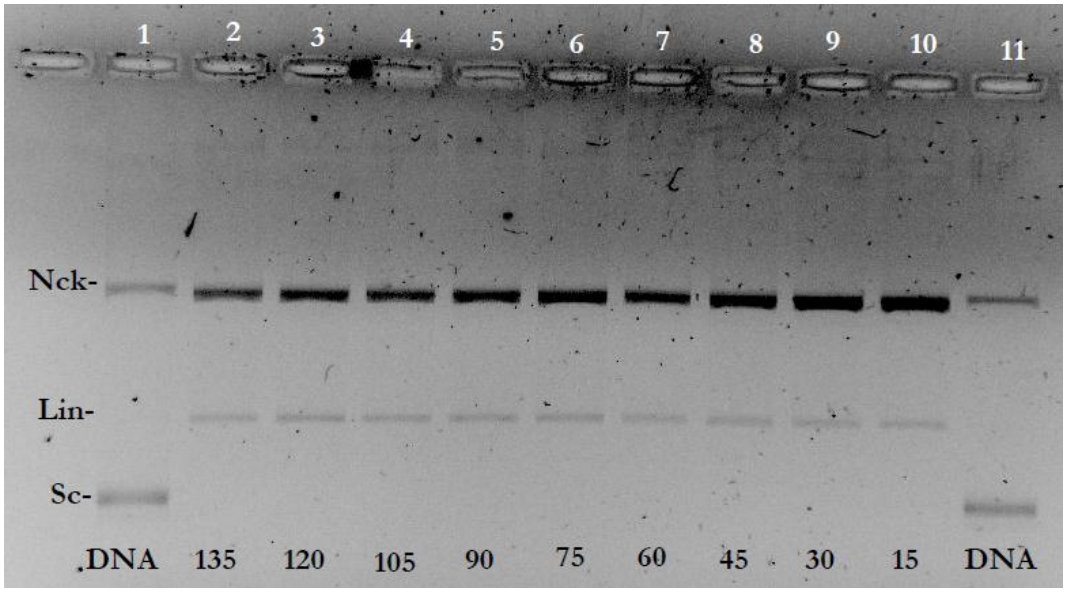

Figure A21. Effect of incubation time on the nuclease activity of **1** at 25 μM (ri 1.7) under phosphate buffer. The first sample containing **1** (lane 2) was incubated at 37 ºC for 135 min and the last one (lane 10) for 15 min with the interval of 15 min.

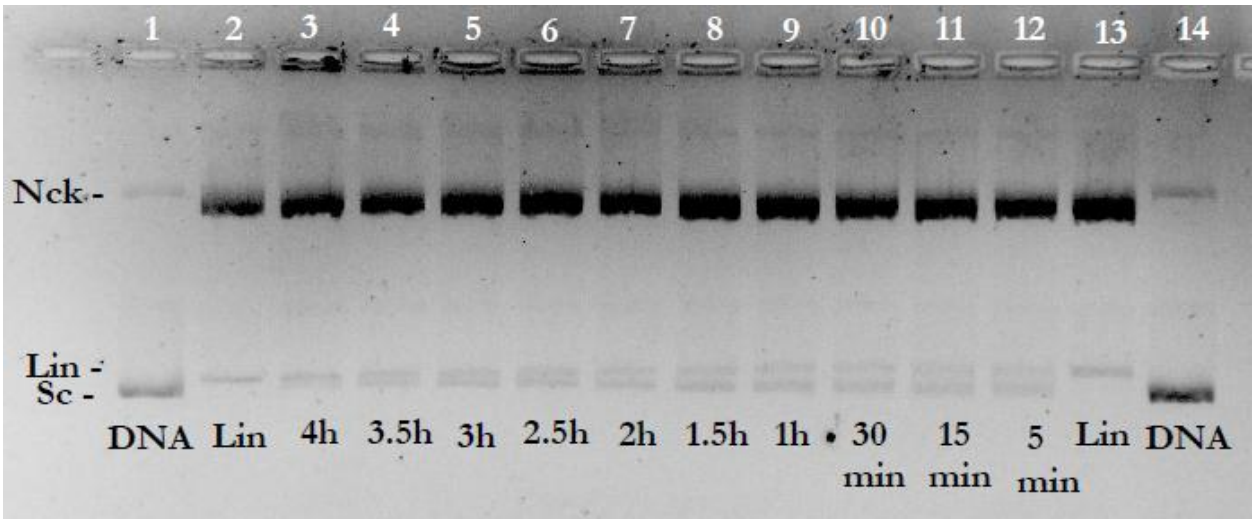

Figure A22. Effect of incubation time on the nuclease activity of **1** at 25 μM (ri 1.7) under phosphate buffer. Incubation time is indicated. Interval is 30 min. The first sample (lane 3) was incubated at 37 ºC for 4 h and the last one (lane 12) for 5 min.

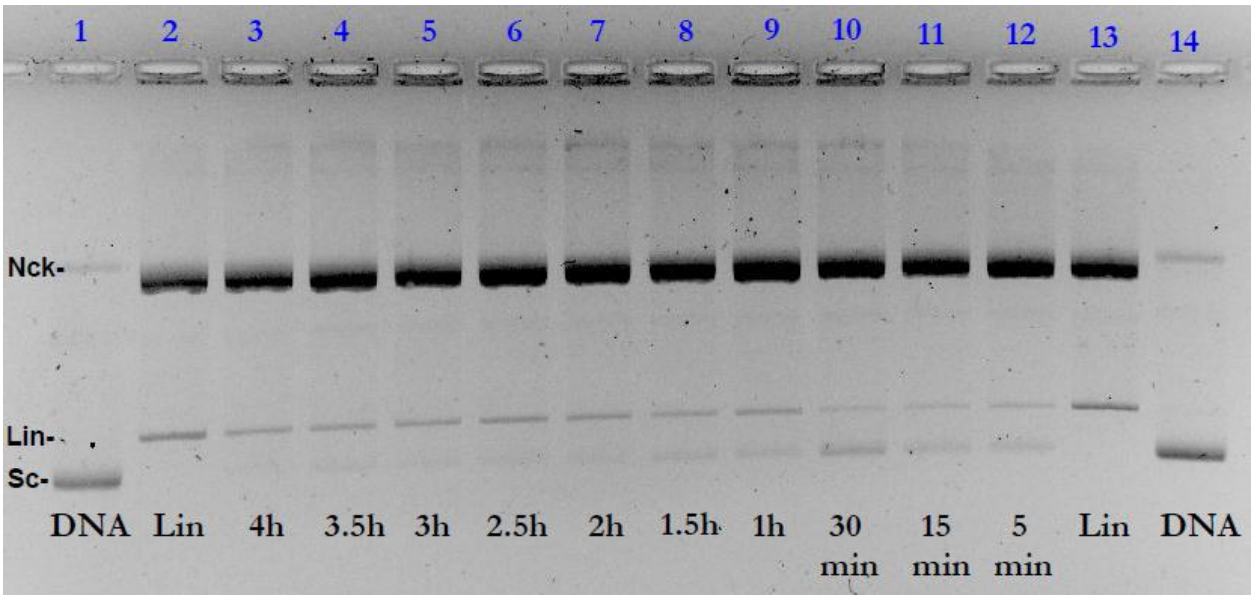

Figure A23. Replicate of the gel in Figure A22.

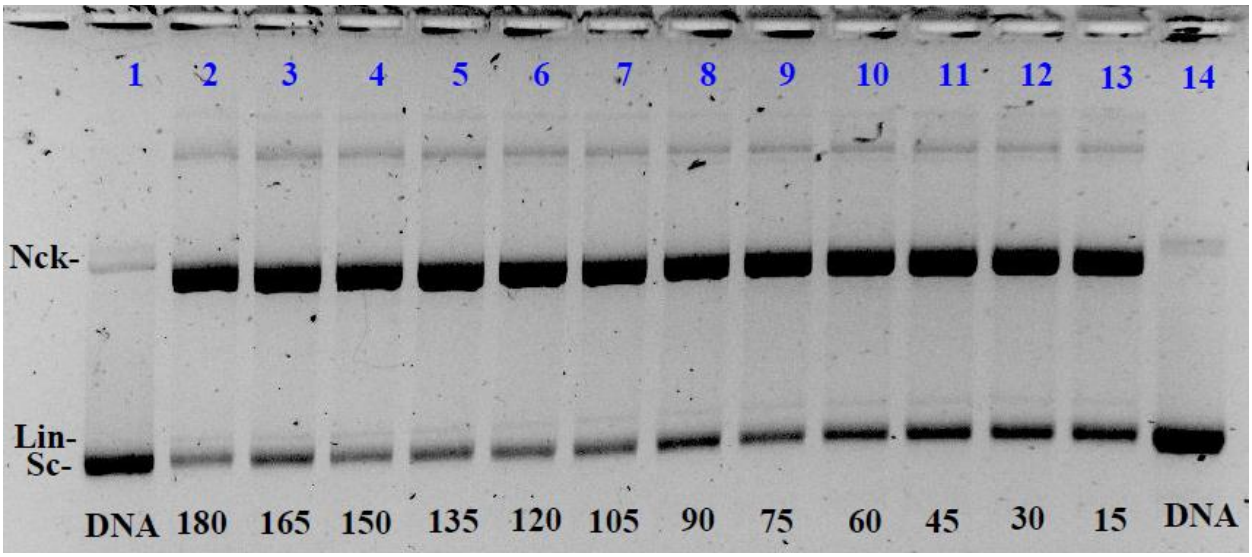

Figure A24. Effect of incubation time on the nuclease activity of **1** at 25 μM (ri 1.7) under phosphate buffer. Incubation interval was 15 min at 37 ºC. The first sample (lane 2) was incubated for 180 min and the last one (lane 10) for 15 min.

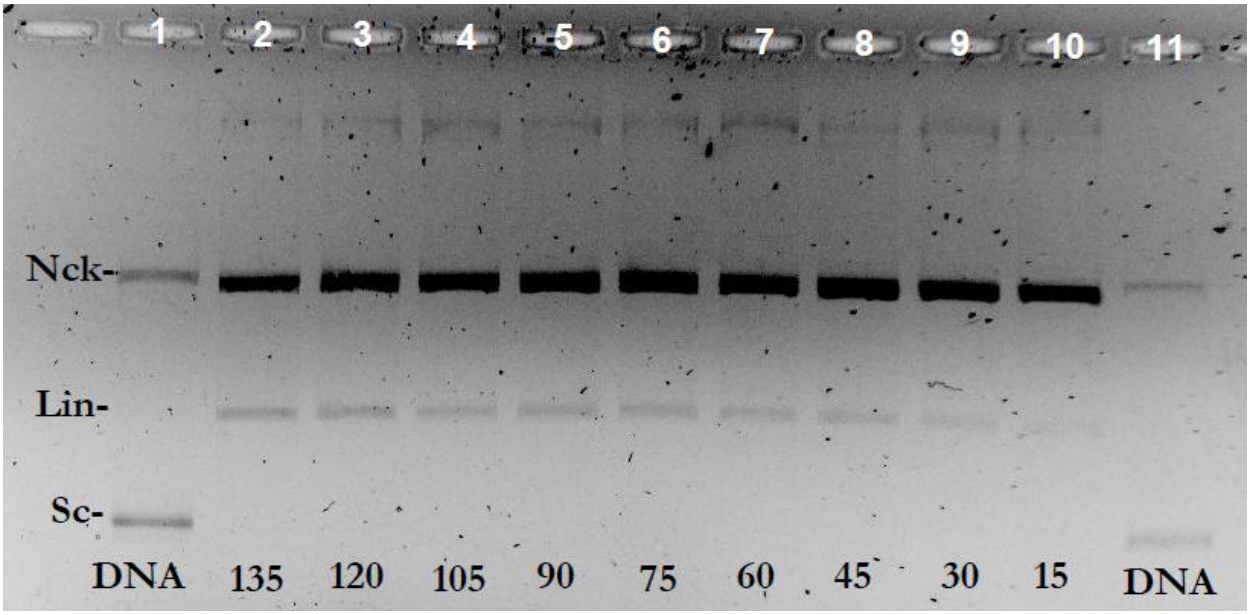

Figure A25. Effect of incubation time on the nuclease activity of **2** at 50 μM (ri 3.3) under phosphate buffer. Incubation interval was 15 min at 37 ºC. The first sample (lane 2) was incubated for 135 min and the last one (lane 10) for 15 min.

Effect of excess ligand

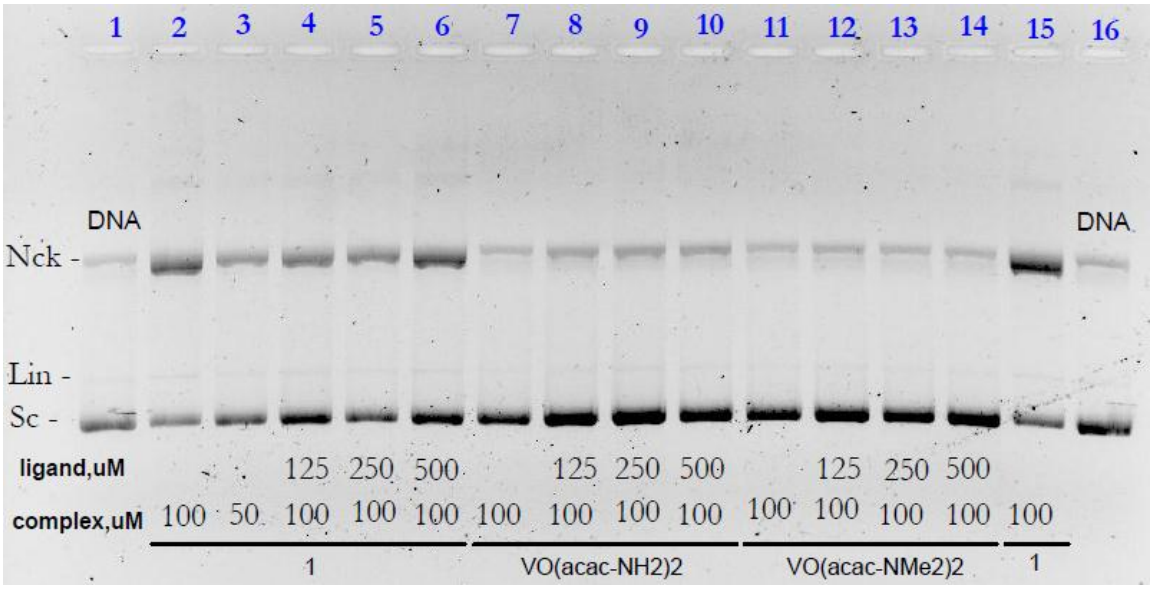

Figure A26. Nuclease activity of **1**, **13** and **14** affected by addition of excess ligands under phosphate buffer. Complex and ligand concentrations are 100 μM (ri 6.7) and 125, 250 and 500 μM (ri 8.3, 16.7, 33.3), respectively. Ligands were added prior to the addition of the complex. Ligand-to-metal (L/M) ratios for the $V^{IV}OL_2$ complex are 1.25 (lanes 4, 8 and 12), 2.5 (lanes 5, 9 and 13) and 5 (lanes 6, 10 and 14).

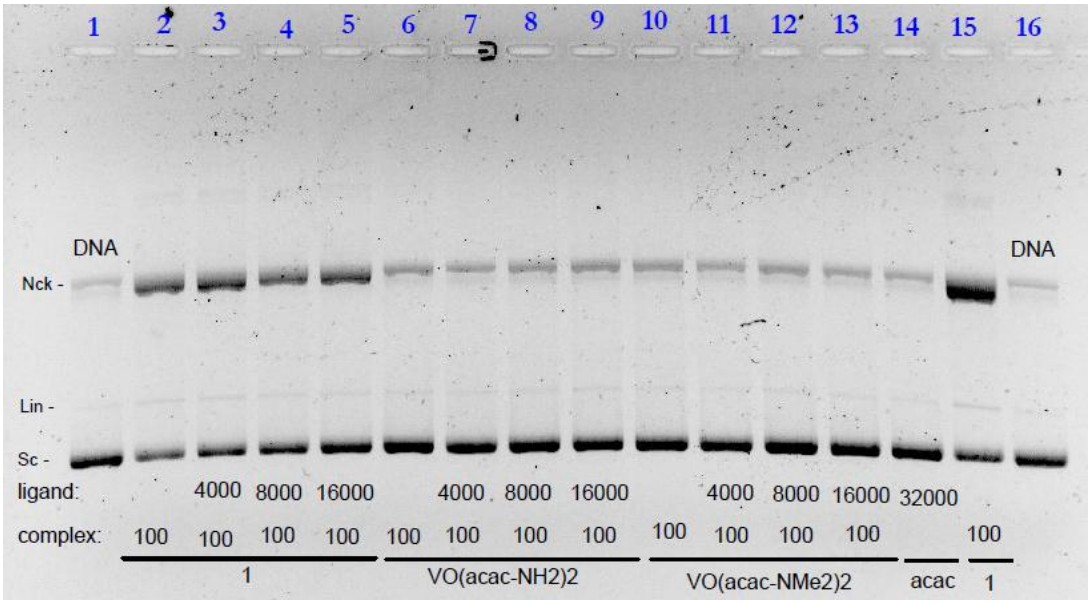

Figure A27. Effect of excess ligand on the nuclease activity of **1**, **13** and **14** at 100 μM (ri 6.7) under phosphate buffer. Ligand concentrations are 100 and 4000, 8000 and 16000 μM. Lane 14 is the control for acetylacetonate. Ligand-to-metal (L/M) ratios for the $V^{IV}OL^2$ complex are 40 (lanes 3, 7 and 11), 80 (lanes 4, 8 and 12) and 160 (lanes 5, 9 and 13).

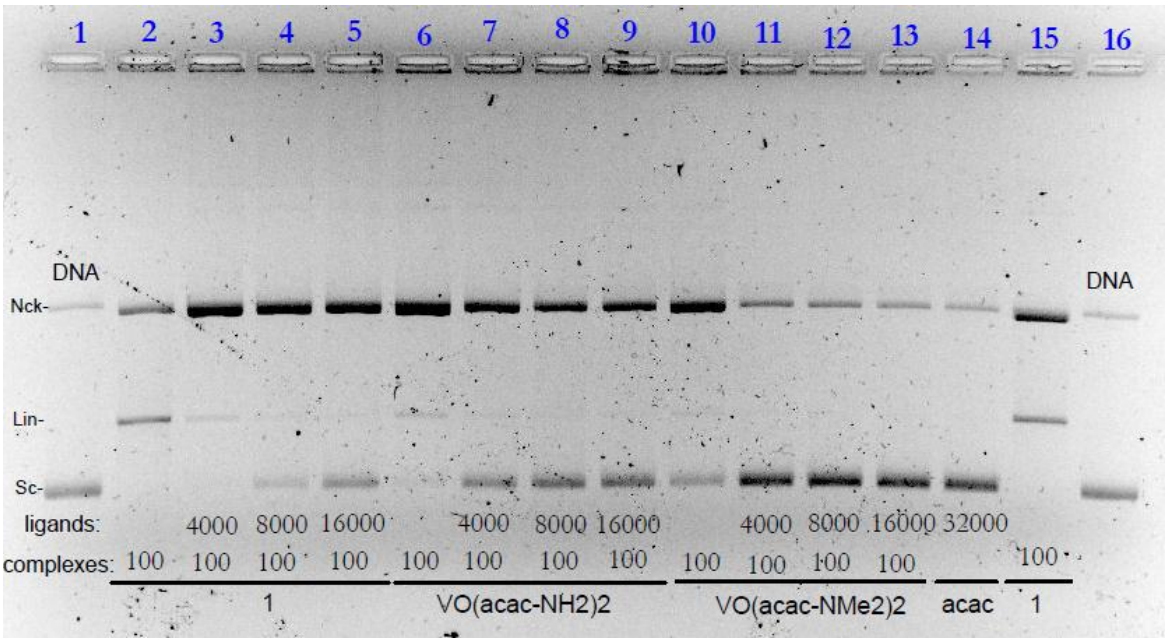

Figure A28. Replicate of the gel in Figure A27.

Effect of buffer media

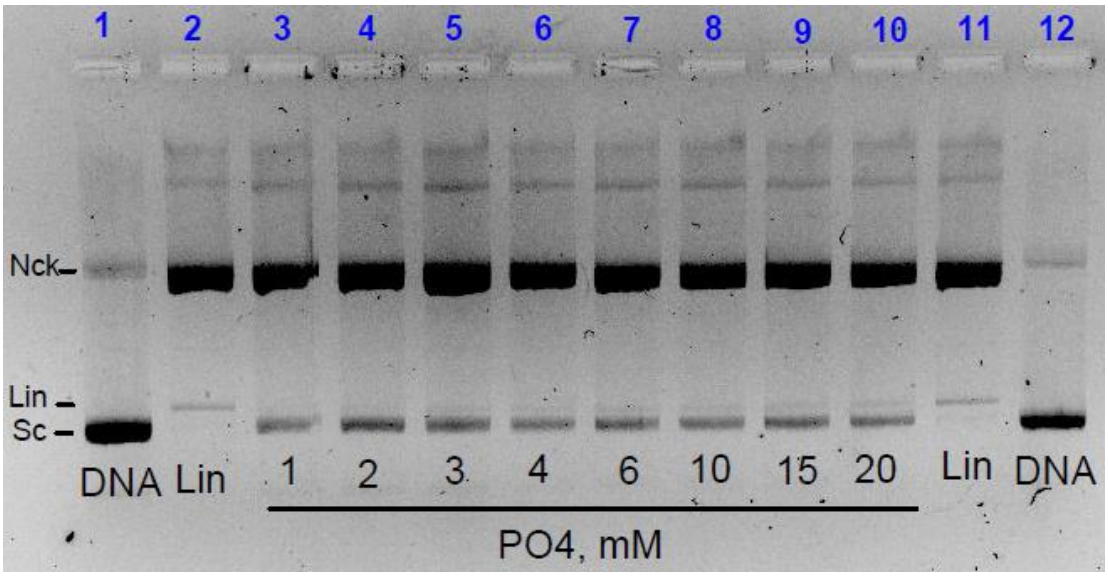

Figure A29. Effect of the concentration of phosphate buffer (1, 2, 3, 4, 6, 10, 15 and 20 mM) on the nuclease activity of **1** at 20 μM (ri 1.33).

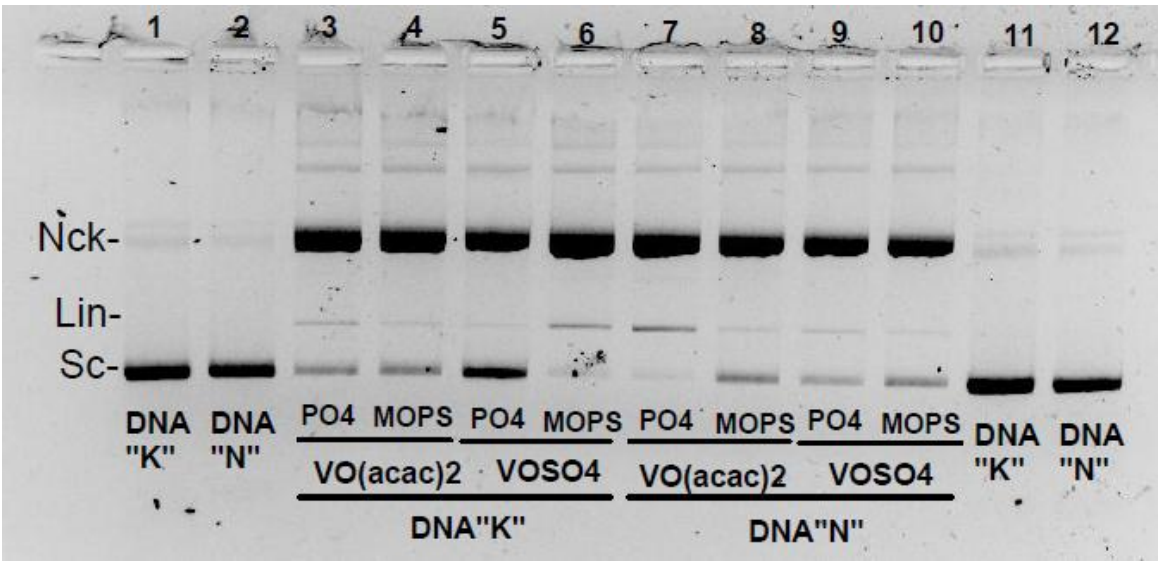

Figure A30. Effect of phosphate and MOPS buffers on the DNA cleavage activity of **1** and **9** at 50 μM (ri 3.3) using two plasmids DNA obtained from different batches.

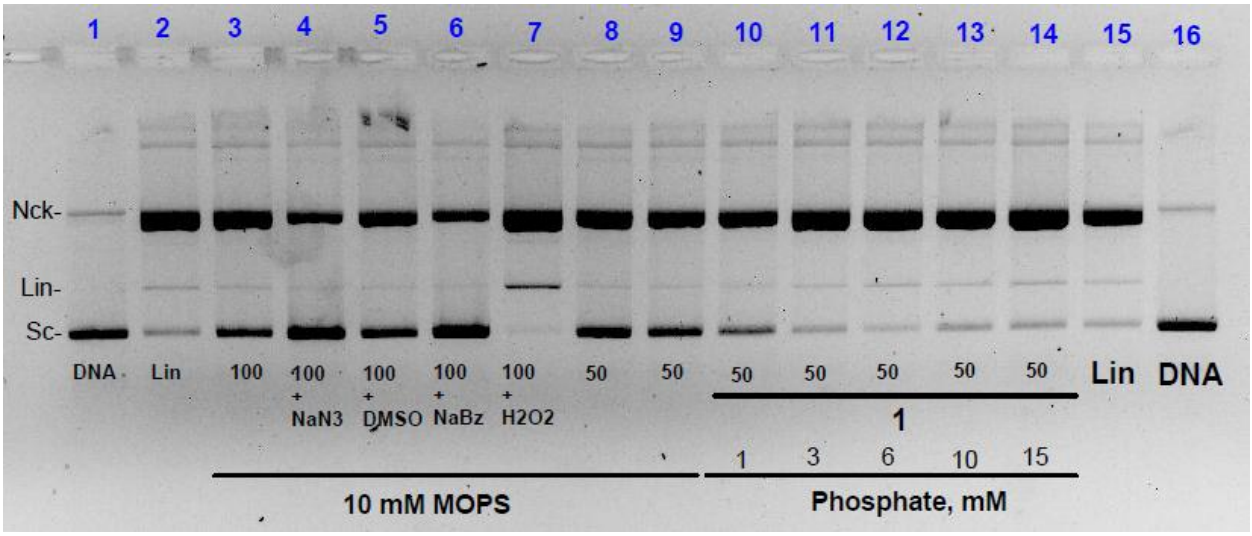

Figure A31. Effect of the concentration of phosphate buffer (1, 3, 6, 10 and 15 mM) on the nuclease activity of **1** at 50 μM (ri 3.3; lanes 10-14). Effect of scavengers on the DNA cleavage activity of VO(oda) at 100 μM (ri 6.7; lanes 3-7) under MOPS buffer. Complex **9** and $V^{IV}O(ClO_4)_2$ (ri 3.3; lane 8 and 9, respectively) are added for comparison.

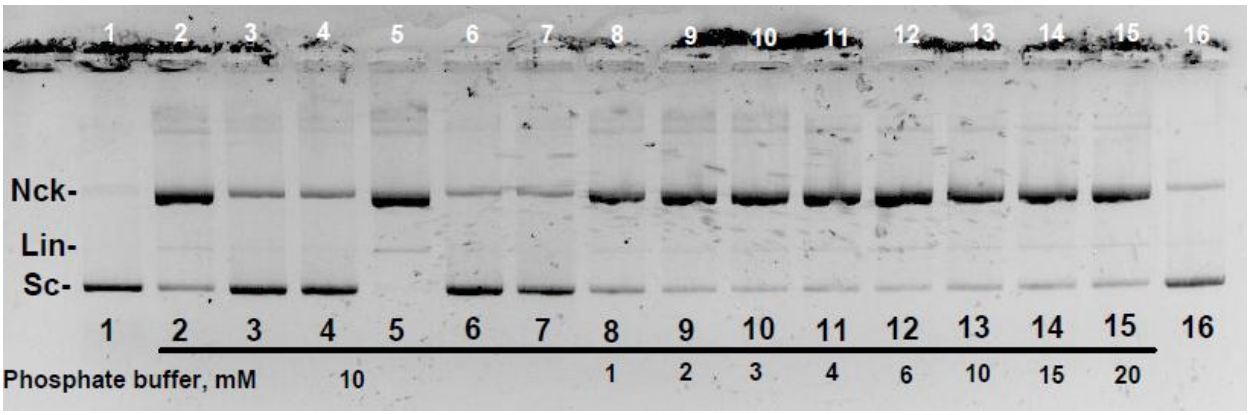

Figure A32. Effect of the concentration of phosphate buffer (1, 2, 3, 4, 6, 10, 15 and 20 mM) on the nuclease activity of **1** at 50 µM (ri 3.3, lanes 8-15). Effect of activating agents (MPA and oxone) on the DNA cleavage activity of **6** (ri 3.3, lanes 2-7) under 10 mM phosphate buffer Lanes 1, 16 - controls for native DNA; 2 - control for linearized DNA; 3 – **6**; 4 - **6** + MPA; 5 – **6** + oxone; 6 - control for MPA; 7 - control for oxone.

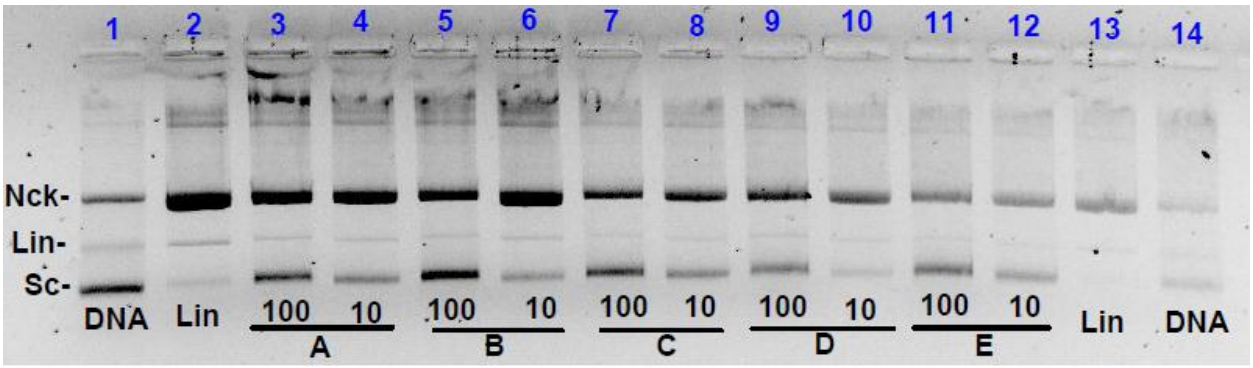

Figure A33. Comparison of the DNA cleavage activity of **1** (A), **9** (B), **13** (C), **4** (D) and **6** (E) at 12 µM (ri 0.8) under 10 and 100 mM phosphate buffer.

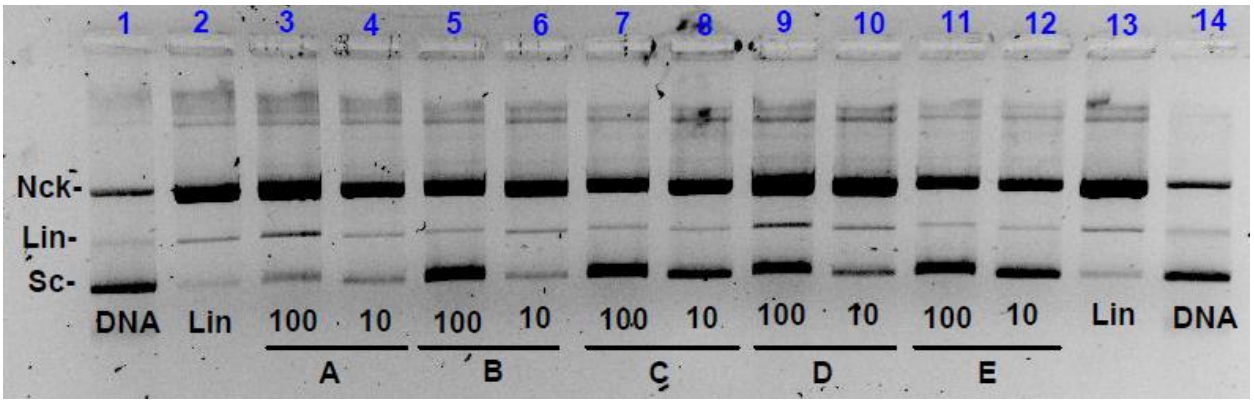

Figure A34. Replicate of the gel in Figure A33 at complex concentration of 25 µM instead of 12.

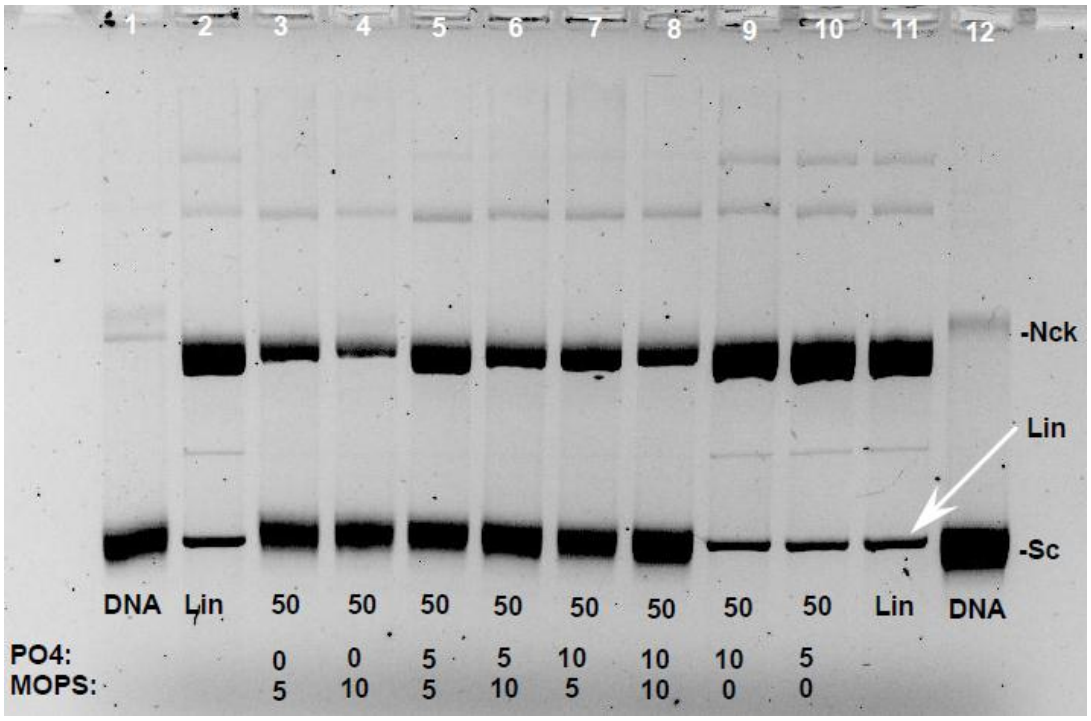

Figure A35. Nuclease activity of **1** at 50 µM (ri 3.3) in the presence of both phosphate and MOPS buffers (pH 7.4). Phosphate/MOPS: 0/5, 0/10, 5/5, 5/10, 10/5, 10/10, 10/0, 5/0 mM.

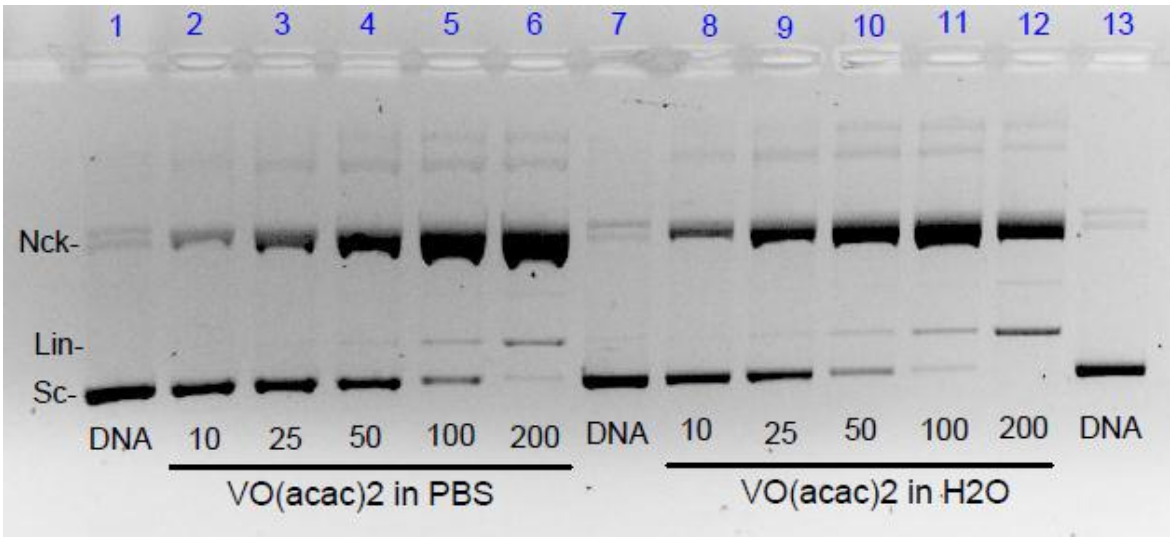

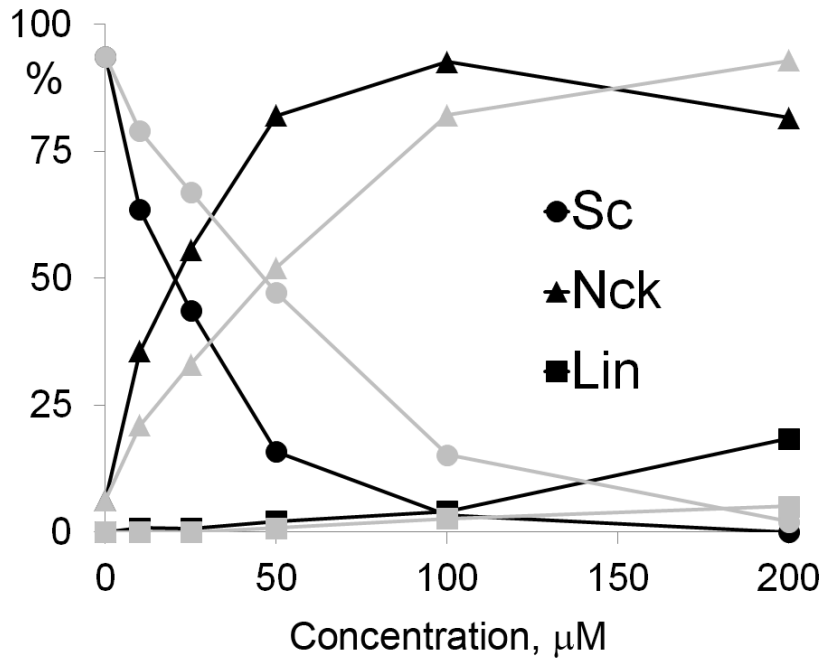

Figure A36. Comparison of the activity of **1** at 10, 25, 50, 100 and 200 μM (ri 0.7, 1.7, 3.3, 6.7 and 13.3) stock solution of which was prepared in PBS buffer (lanes 2-6) and, as typically, in water (lanes 8-12). In the latter case PBS was added into each sample before addition of plasmid and complex.

Effect of light

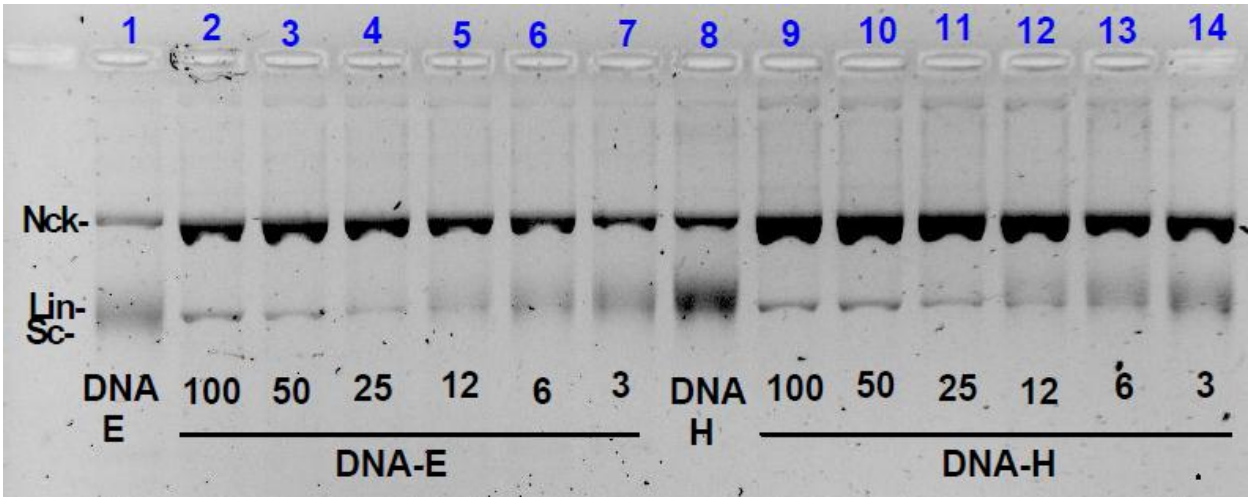

Figure A37. Effect of light on the DNA cleavage activity of **1** at 3, 6, 12, 25, 50 and 100 µM (ri 0.2, 0.4, 0.8, 1.7, 3.3 and 6.7) under PBS buffer using plasmids DNA obtained from different batches. Closed tubes with the samples were incubated under a 370-nm UV lamp for 1 h at 37 ºC.

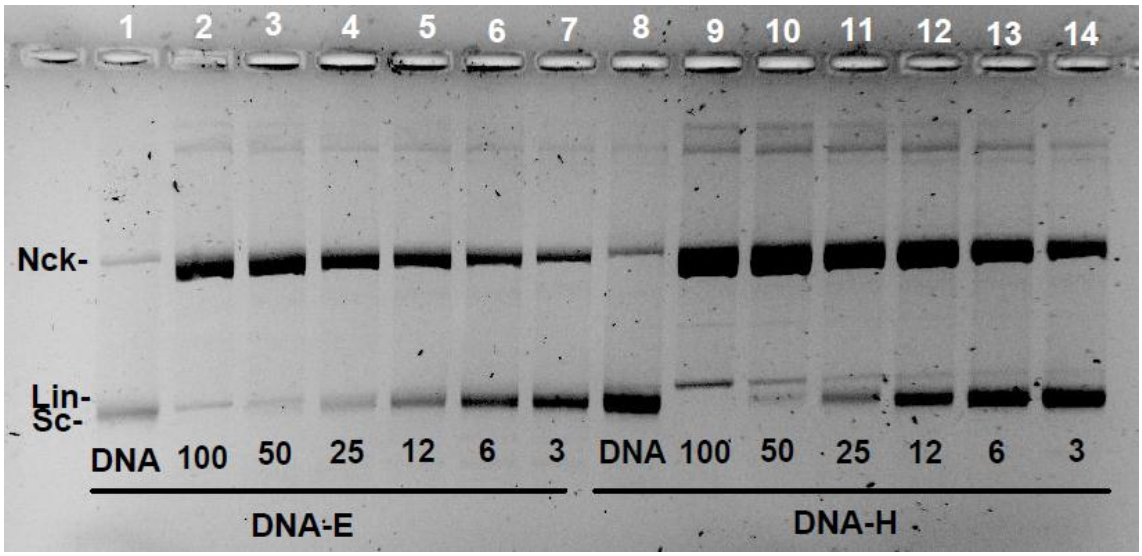

Figure A38. Effect of light on the DNA cleavage activity of **1** at 3, 6, 12, 25, 50 and 100 µM (ri 0.2, 0.4, 0.8, 1.7, 3.3 and 6.7) under phosphate buffer using plasmids DNA obtained from different batches. Eppendorfs containing sample mixtures were incubated wrapped in aluminium foil.

Effect of hydrogen peroxide

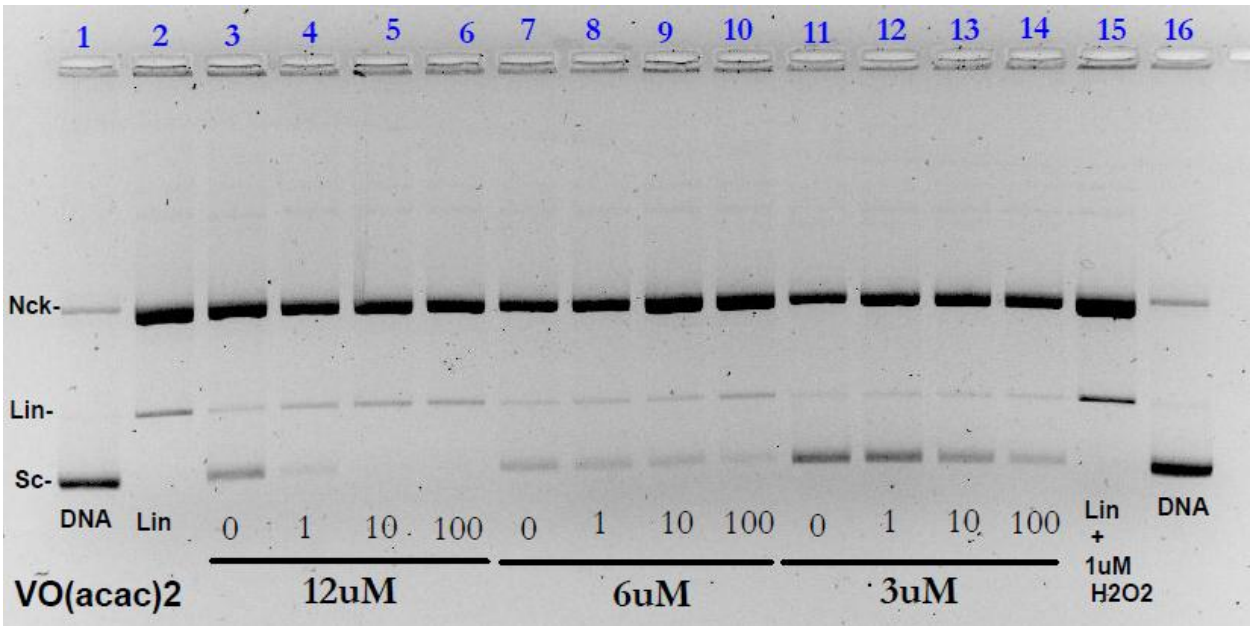

Figure A39. Effect of hydrogen peroxide on the nuclease activity of **1** at 3, 6 and 12 μM (ri 0.2, 0.4 and 0.8) under phosphate buffer. Concentrations of hydrogen peroxide are 1, 10 and 100 μM.

Effect of atmosphere (air and nitrogen)

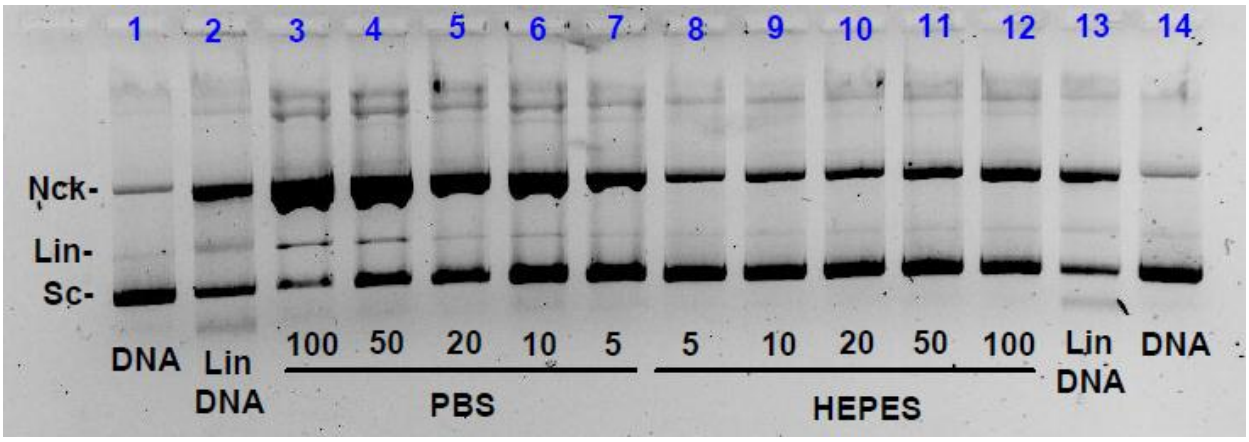

Figure A40. Cleavage of pA1 pDNA by **9** at 5, 10, 20, 50 and 100 μM (ri 0.3, 0.7, 1.7, 3.3 and 6.7.) under **inert atmosphere**. Samples were digested under phosphate and HEPES buffers.

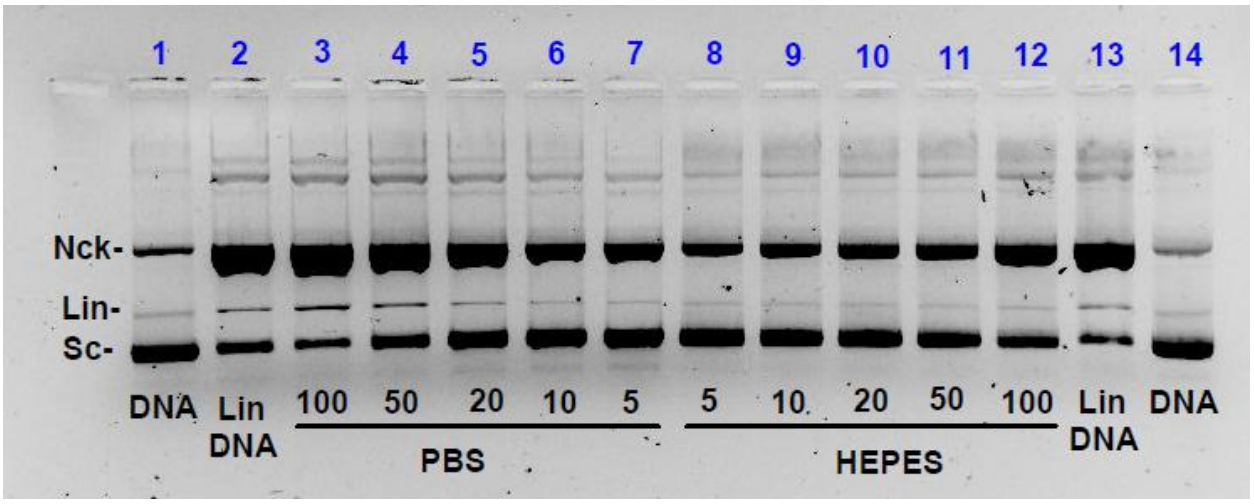

Figure A41. The cleavage of pA1 DNA by **9** at 5, 10, 20, 50 and 100 μM (ri 0.3, 0.7, 1.7, 3.3 and 6.7) under **air**. Samples were digested under phosphate and HEPES buffers.

$V^{IV}OSO_4$ (9)

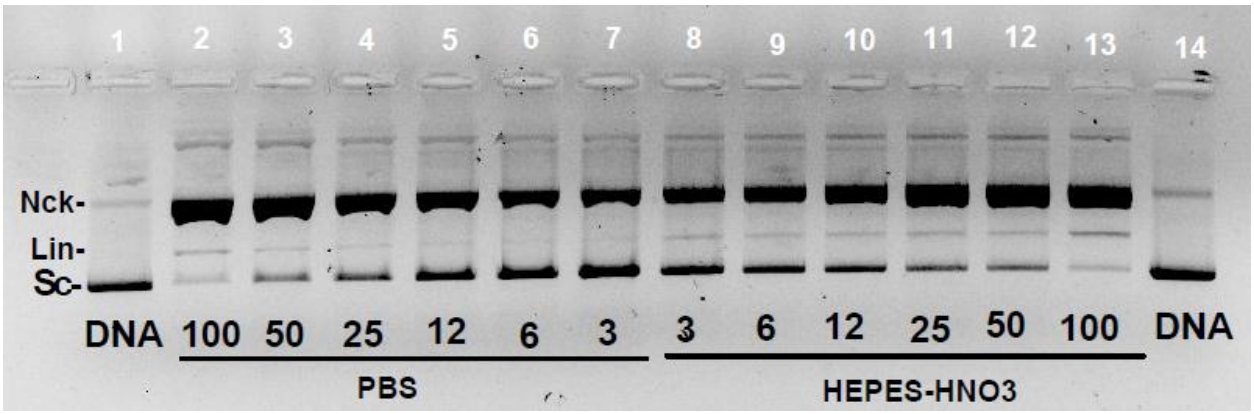

Figure A42. DNA cleavage activity of **9** at 3, 6, 12, 25, 50 and 100 μM (ri 0.2, 0.4, 0.8, 1.7, 3.3 and 6.7) under PBS and HEPES buffers.

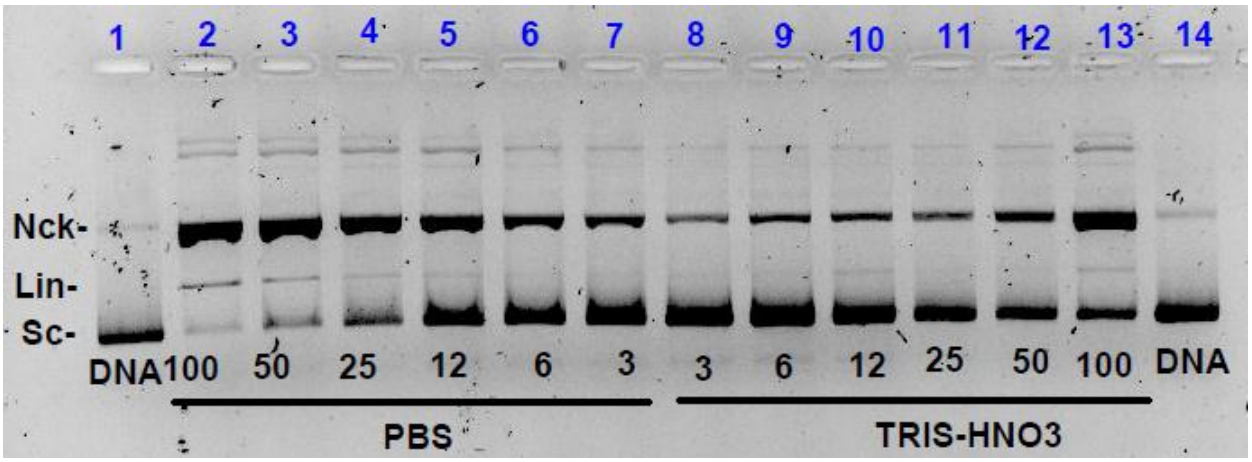

Figure A43. DNA cleavage activity of **9** at 3, 6, 12, 25, 50 and 100 μM (ri 0.2, 0.4, 0.8, 1.7, 3.3 and 6.7) under PBS and TRIS buffers.

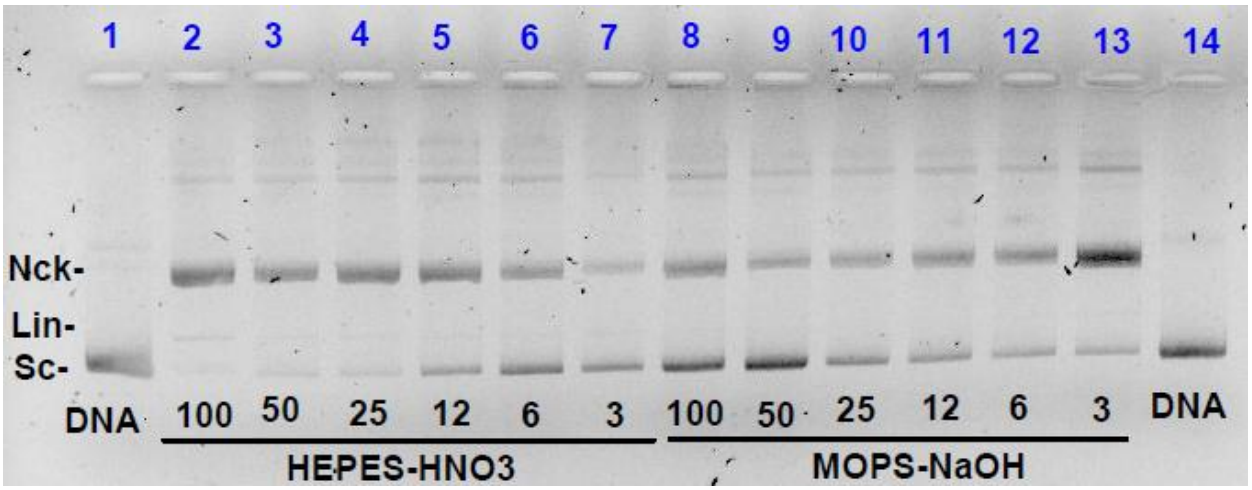

Figure A44. DNA cleavage activity of **9** at 3, 6, 12, 25, 50 and 100 μM (ri 0.2, 0.4, 0.8, 1.7, 3.3 and 6.7) under HEPES and MOPS buffers.

V(V) derivatives

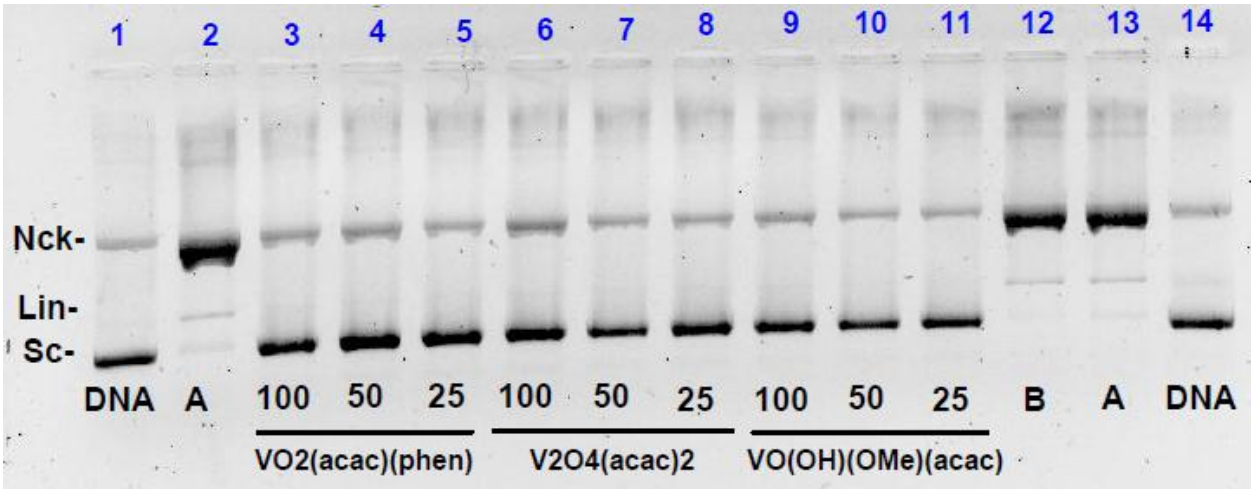

Figure A45. Nuclease activity of **6**-**8** at 25, 50 and 100 μM (ri 1.7, 3.3, 6.7) under phosphate buffer. Complexes **1** (A) and **9** (B) (50 μM, ri 3.3) were added for comparison.

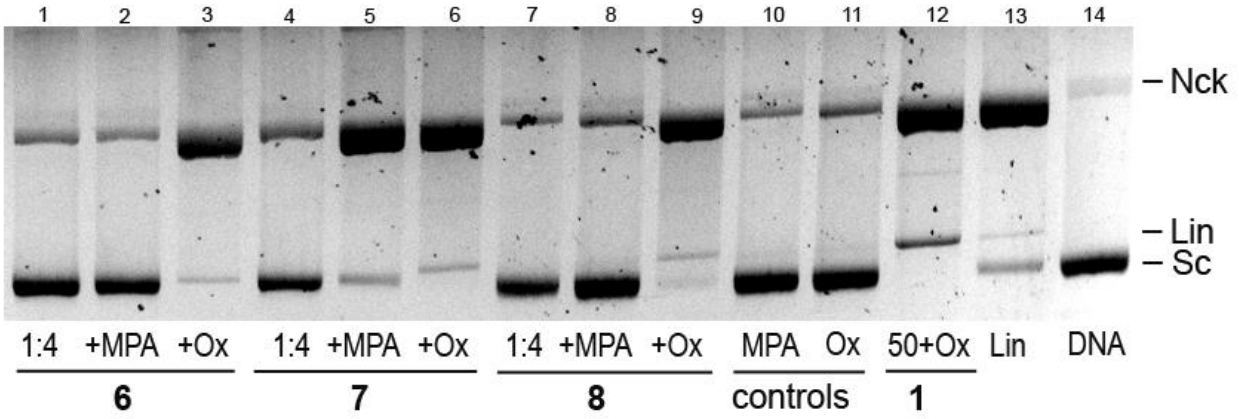

Figure A46. DNA cleavage activity of **6**-**8** under phosphate buffer in the presence of activating agents (MPA and oxone). Complexes did not dissolve completely and were diluted 1:4 from saturated stock solutions prepared to be 200 μM. Lanes 1, 4 and 7 are the complexes alone, 2, 5 and 8 are with added MPA; 3, 6 and 9 – with oxone; 10 and 11 – controls for MPA and oxone; 12 – 50 μM of **1** + oxone; 13 and 14 – controls for linearized DNA and native DNA.

Monovanadate

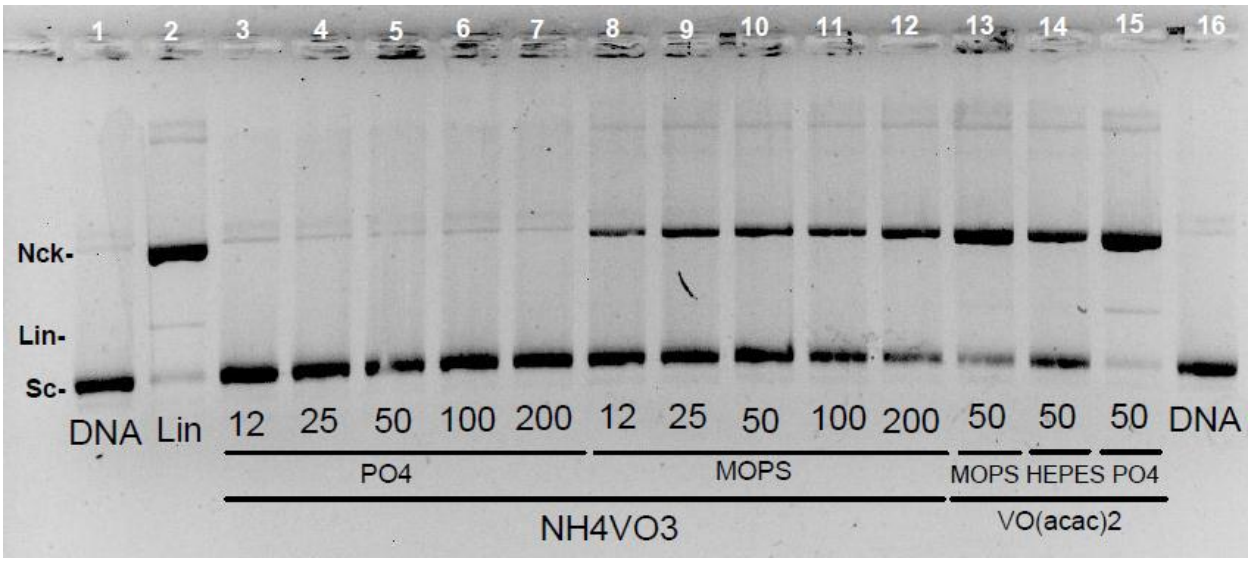

Figure A47. Nuclease activity of NH_4VO_3 (monovanadate, V_1) at 12, 25, 50, 100 and 200 μM (ri 0.8, 1.7, 3.3, 6.7 and 13.3.) under phosphate and MOPS buffers. Complex **1** (50, ri 3.3) under MOPS, HEPES and phosphate buffer was added for comparison.

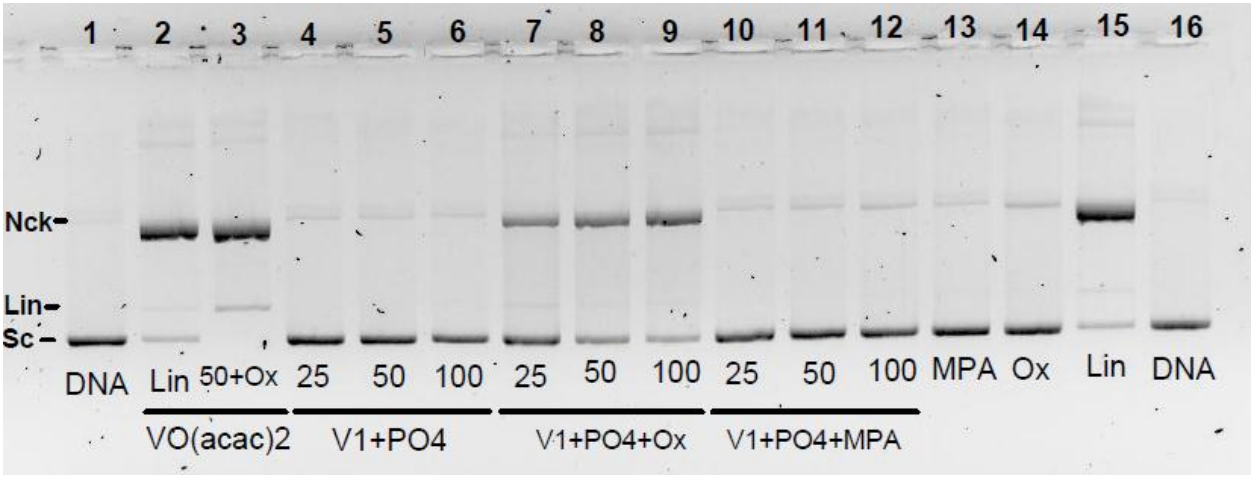

Figure A48. Effect of V_1 on pA1 DNA cleavage under **phosphate** buffer after addition of oxone and MPA. Lanes 1, 16 – controls for native DNA; 2, 15 – controls for linearized DNA; 3 – 50 μM (ri 3.3) of **1** + oxone; 4-6 – 25, 50 and 100 μM (ri 1.7, 3.3 and 6.7, respectively) of V_1; 7-9 – 25, 50 and 100 μM of V_1 + oxone; 10-12 – 25, 50 and 100 μM of V_1 + MPA; 13 and 14 – control for MPA and oxone.

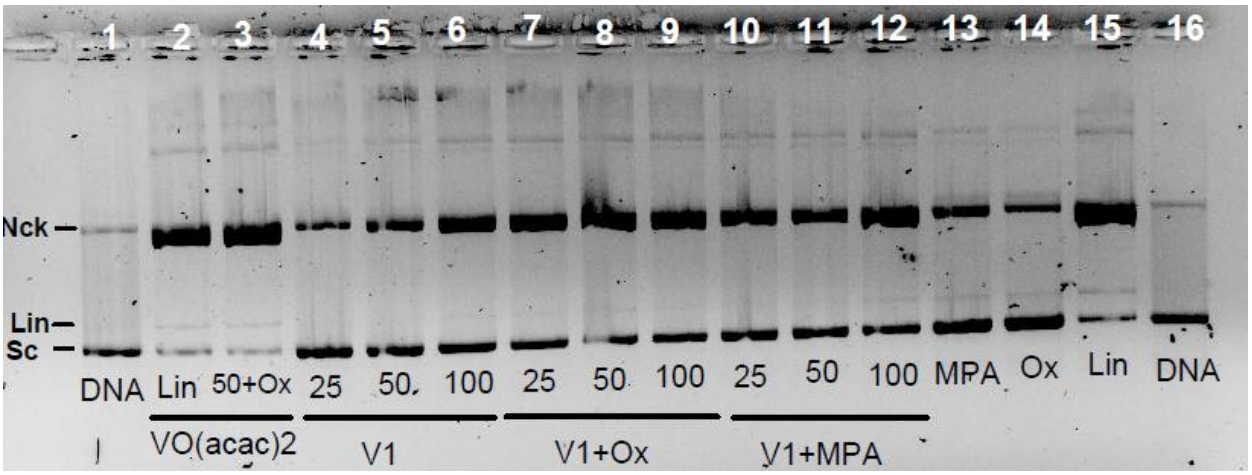

Figure A49. Effect of V1 on pA1 DNA cleavage under **MOPS** buffer after addition of oxone and MPA. Lanes 1, 16 – controls for native DNA; 2, 15 – controls for linearized DNA; 3 – 50 µM (ri 3.3) of 1 + oxone; 4-6 – 25, 50 and 100 µM (ri 1.7, 3.3 and 6.7, respectively) of V1; 7-9 – 25, 50 and 100 µM of V1 + oxone; 10-12 – 25, 50 and 100 µM of V1 + MPA; 13 and 14 – control for MPA and oxone.

$Cu(acac)_2$ (**15**) and $Ni(acac)_2$ (**16**)

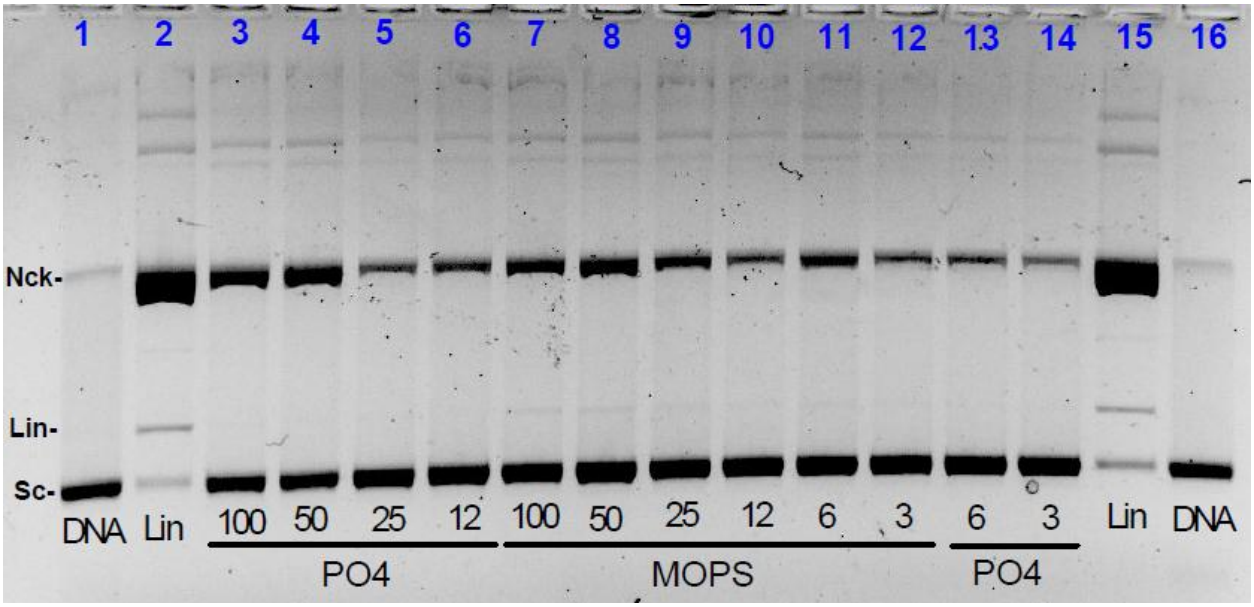

Figure A50. Nuclease activity of **15** at 3, 6, 12, 25, 50 and 100 µM (ri 0.2, 0.4, 0.8, 1.7, 3.3 and 6.7) under phosphate and MOPS buffers.

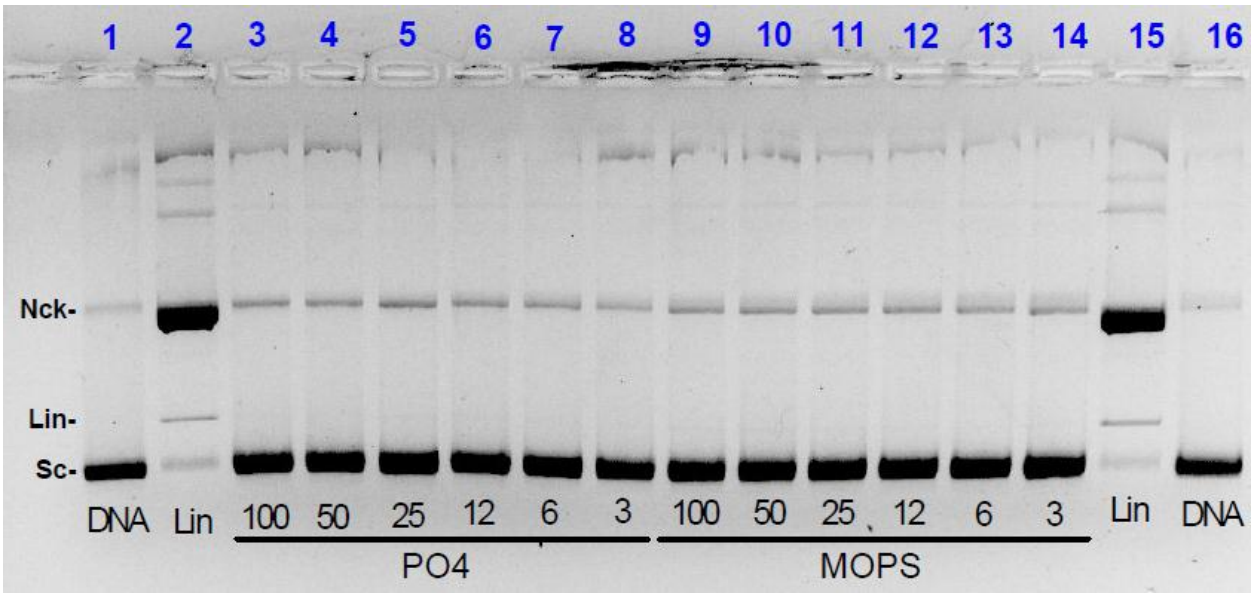

Figure A51. Nuclease activity of **16** at 3, 6, 12, 25, 50 and 100 µM (ri 0.2, 0.4, 0.8, 1.7, 3.3 and 6.7) under phosphate and MOPS buffers.

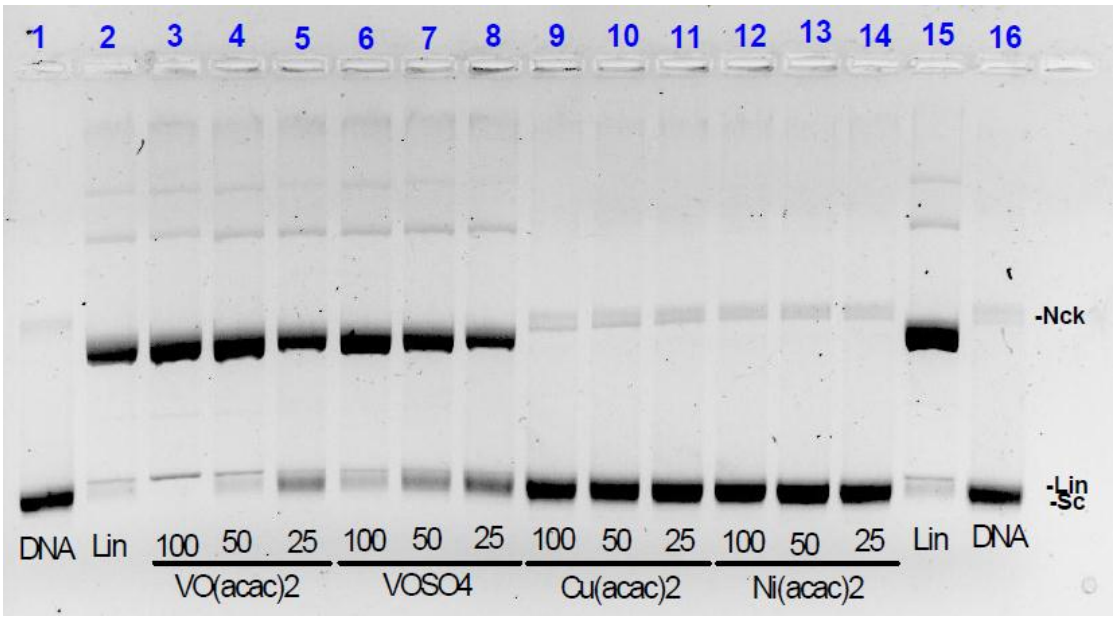

Figure A52. Comparison of the DNA cleavage activity of **1**, **9**, **15** and **16** at 25, 50 and 100 µM (ri 1.7, 3.3 and 6.7) under phosphate buffer.

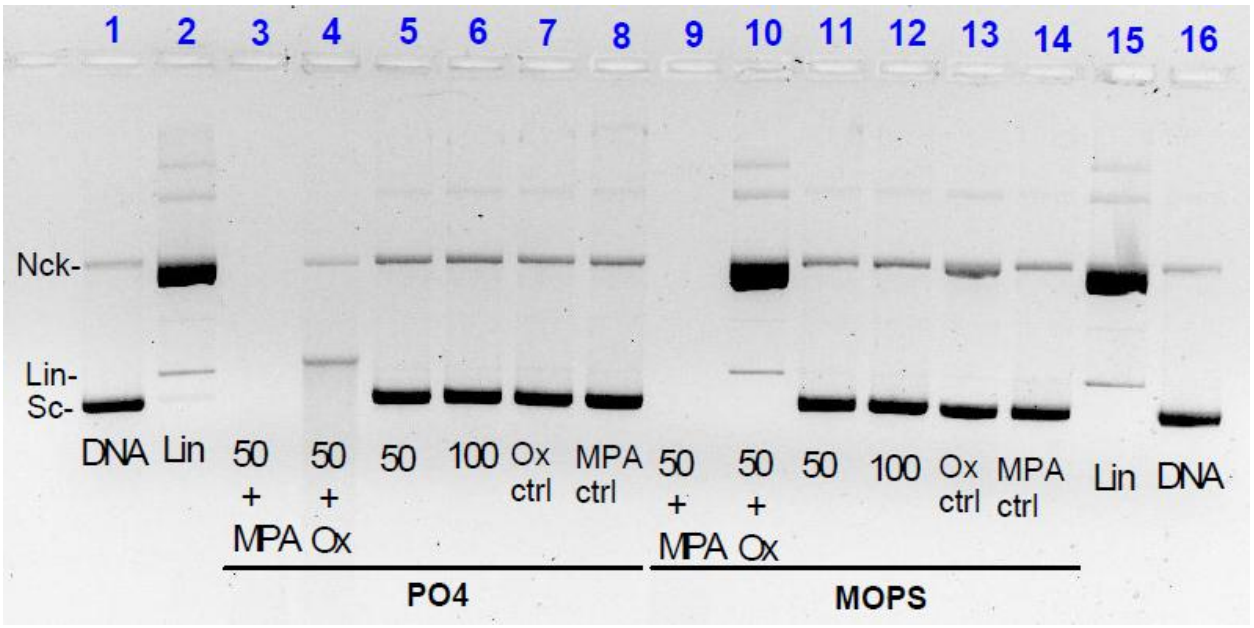

Figure A53. Nuclease activity of **15** at 50 and 100 µM (ri 3.3 and 6.7) under phosphate and MOPS buffers in the presence of MPA and oxone. Samples 7, 8 and 13, 14 are the controls for MPA and oxone under phosphate and MOPS buffers, respectively.

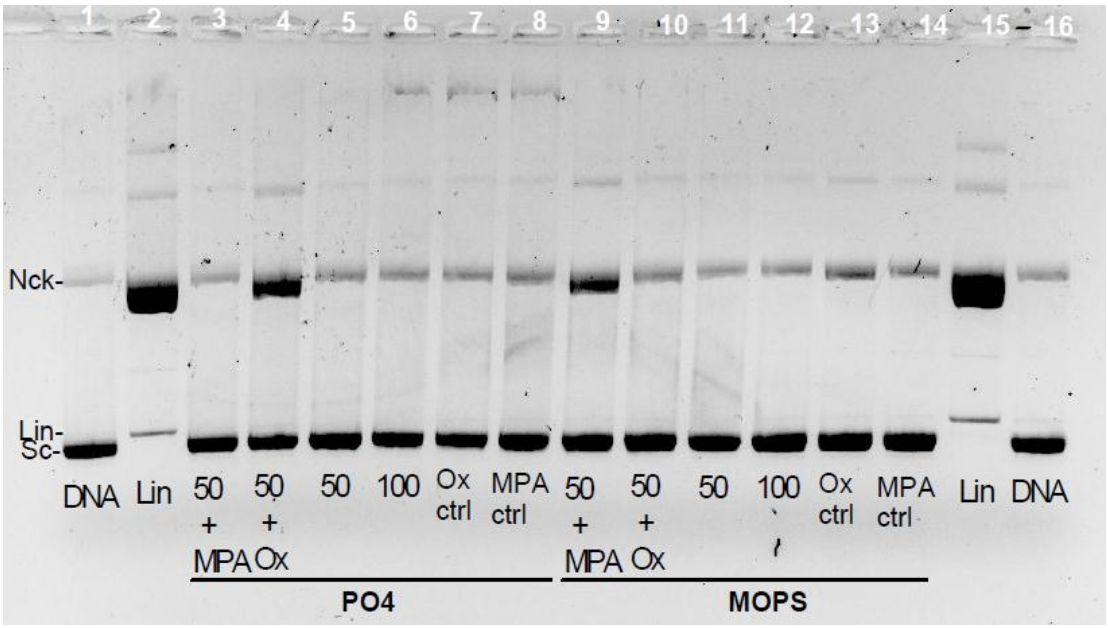

Figure A54. Nuclease activity of **16** at 50 and 100 µM (ri 3.3 and 6.7) under phosphate and MOPS buffers in the presence of MPA and oxone. Samples 7, 8 and 13, 14 are the controls for MPA and Ox under phosphate and MOPS buffers, respectively.

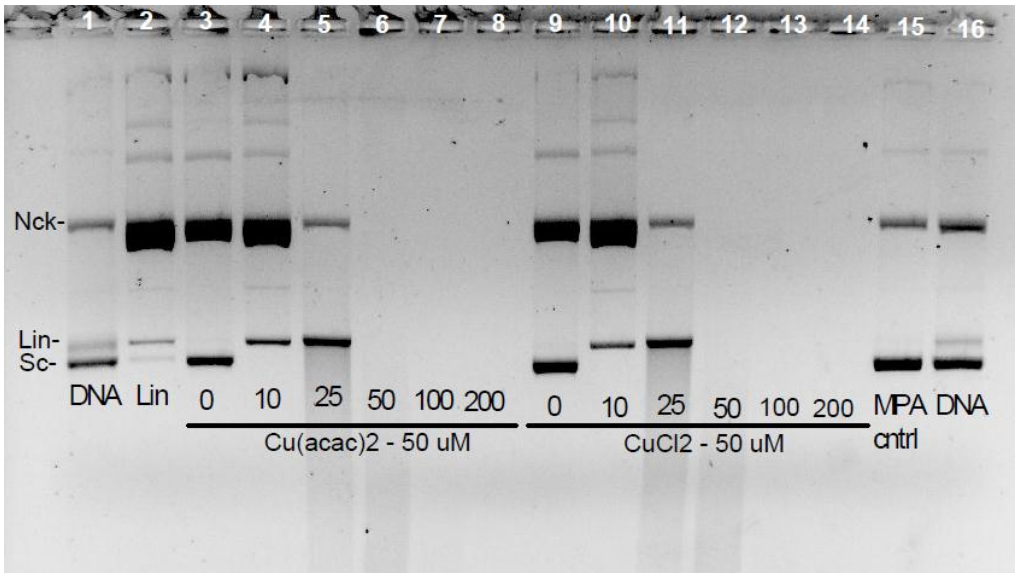

Figure A55. DNA cleavage activity of **15** and $CuCl_2$, at 50 μM (ri 3.3) under phosphate buffer changing the concentration of MPA (10, 25, 50, 100 and 200 μM).

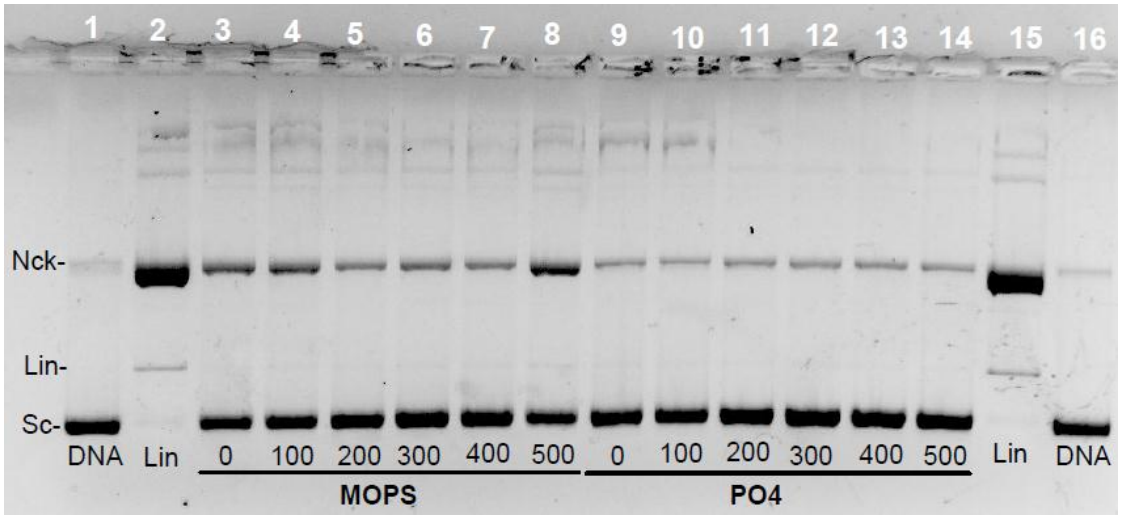

Figure A56. DNA cleavage activity of **16** at 50 μM (ri 3.3) under phosphate and MOPS buffers changing concentration of MPA (0, 100, 200, 300, 400 and 500 μM).

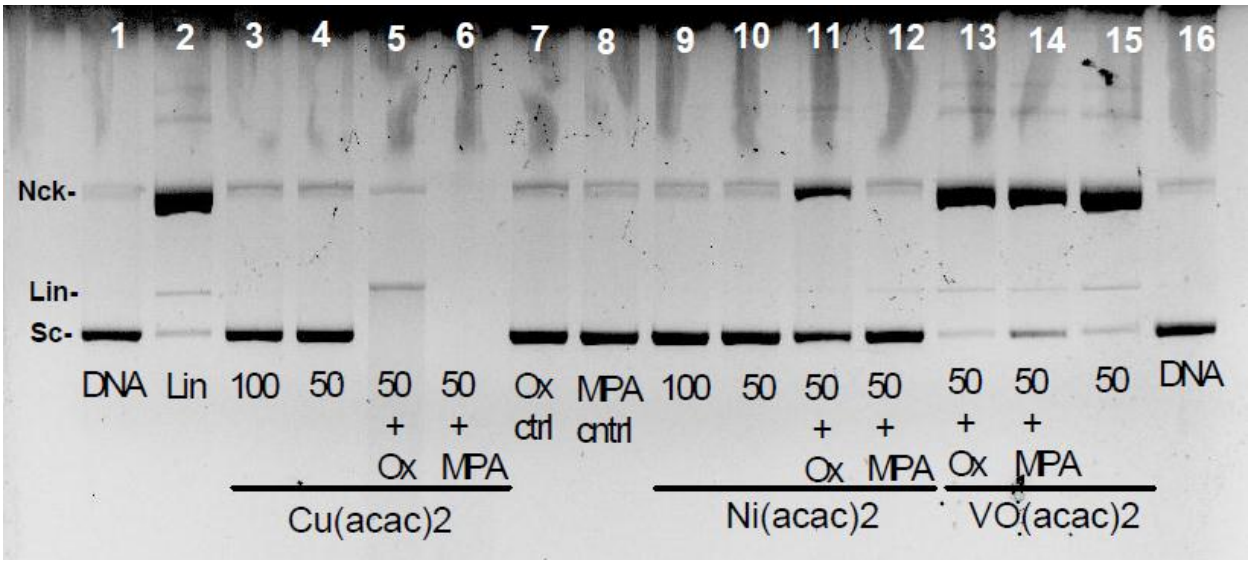

Figure A57. Comparison of the nuclease activity of **15** and **16** at 50 and 100 μM (ri 3.3 and 6.7) under phosphate buffer in the presence of oxone and MPA. Complex **1** (ri 3.3) is added for comparison.

Other oxovanadium complexes

*$VO(MPA)_2$ (**17**), $VO(dmpp)_2$ (**18**), $VO(PA)_2$ (**19**)*

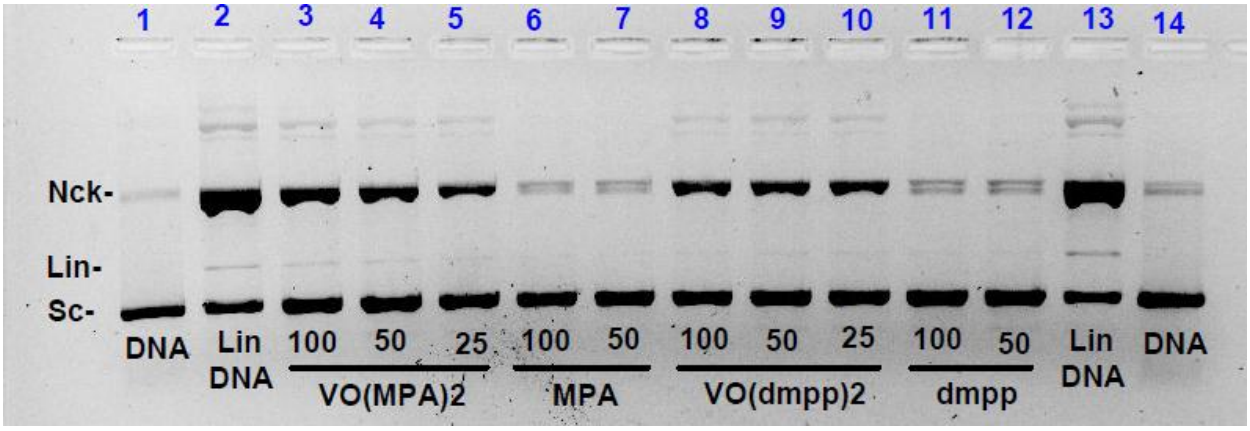

Figure A58. Nuclease activity of **17**, **18** and corresponding ligands at 25, 50 and 100 μM (ri 1.7, 3.3 and 6.7) under phosphate buffer (pH 7.4).

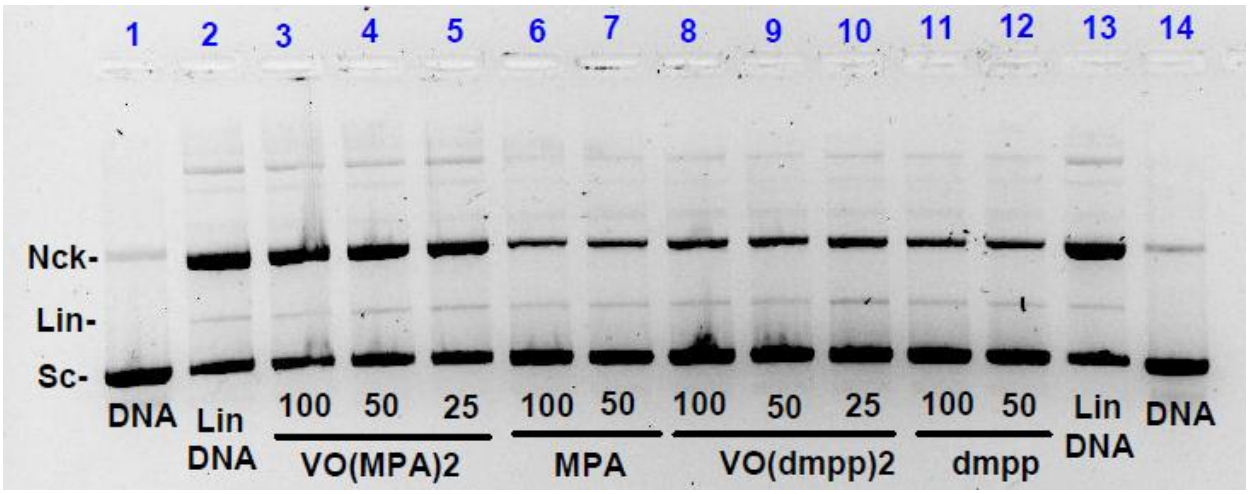

Figure A59. Nuclease activity of **17**, **18** and corresponding ligands at 25, 50 and 100 μM (ri 1.7, 3.3 and 6.7) under HEPES buffer (pH 6.97).

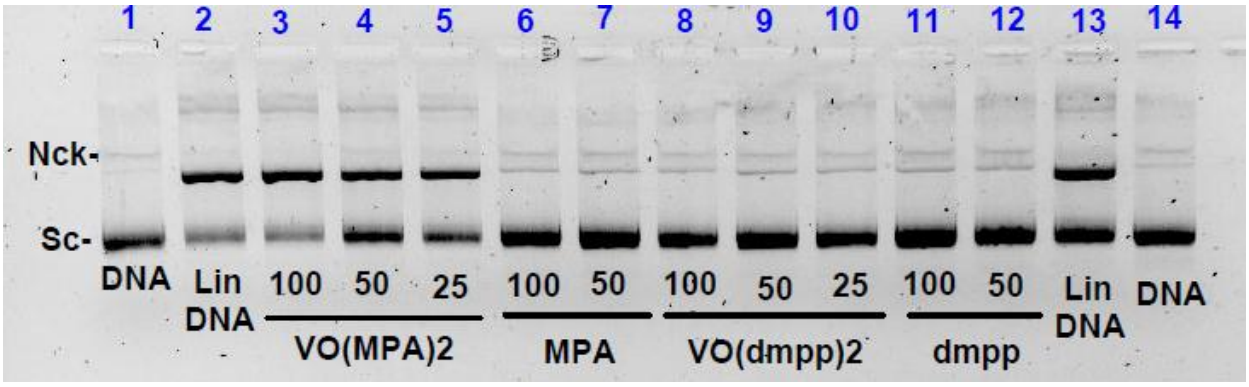

Figure A60. Replicate of the gel in Figure A59.

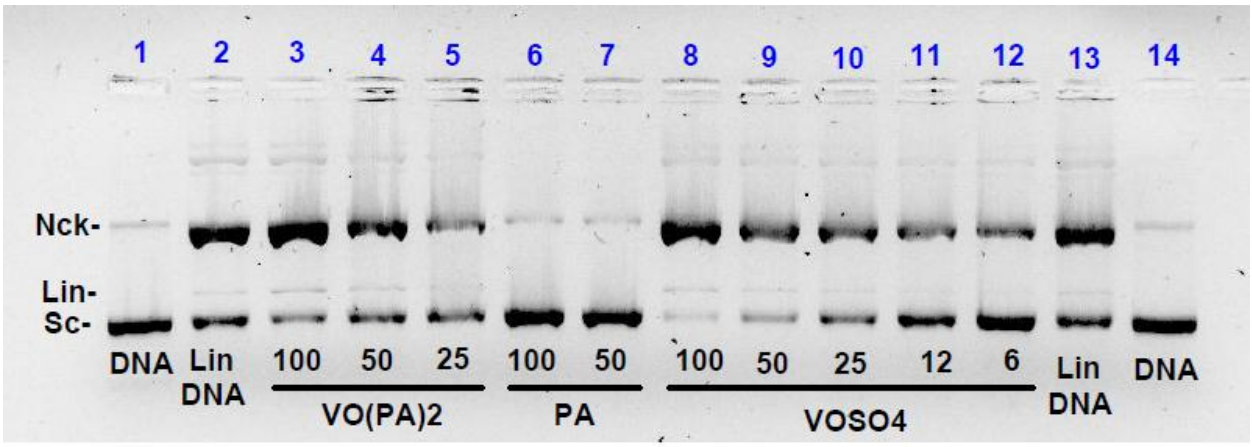

Figure A61. Nuclease activity of **19** and corresponding ligand at 25, 50 and 100 μM (ri 1.7, 3.3 and 6.7) under phosphate buffer (pH 7.4). Complex **9** at 6, 12, 25, 50 and 100 μM (ri 0.4, 0.8, 1.7, 3.3 and 6.7) was added for comparison.

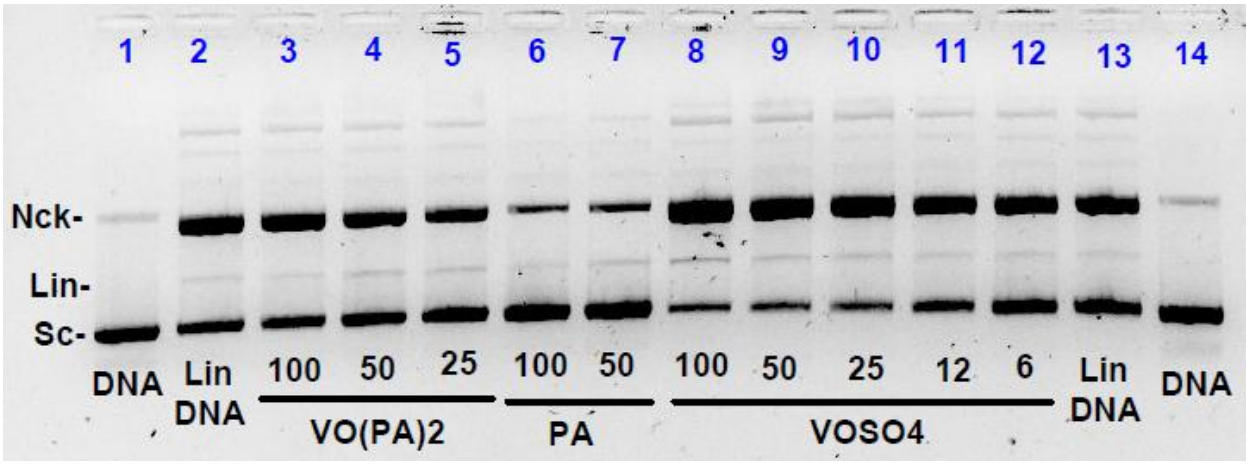

Figure A62. Nuclease activity of **19** and corresponding ligand at 25, 50 and 100 μM (ri 1.7, 3.3 and 6.7) under HEPES buffer (pH 6.97). Complex **9** at 6, 12, 25, 50 and 100 μM (ri 0.4, 0.8, 1.7, 3.3 and 6.7) was added for comparison.

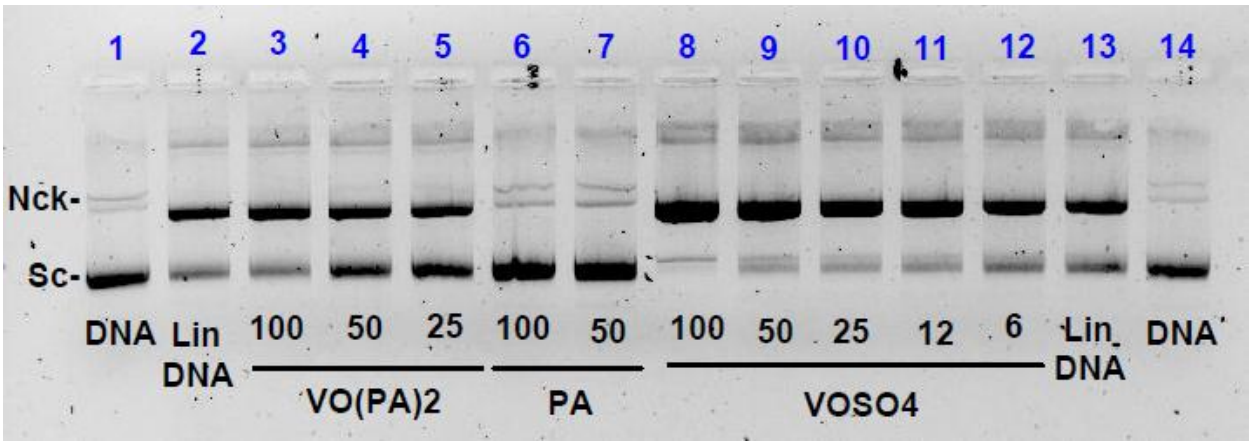

Figure A63. Replicate of the gel in Figure A62.

*VO(oda) (**20**), VO(oda)phen (**21**), VO(phen)$_2$ (**22**) VO(oda)bipy (**23**)*

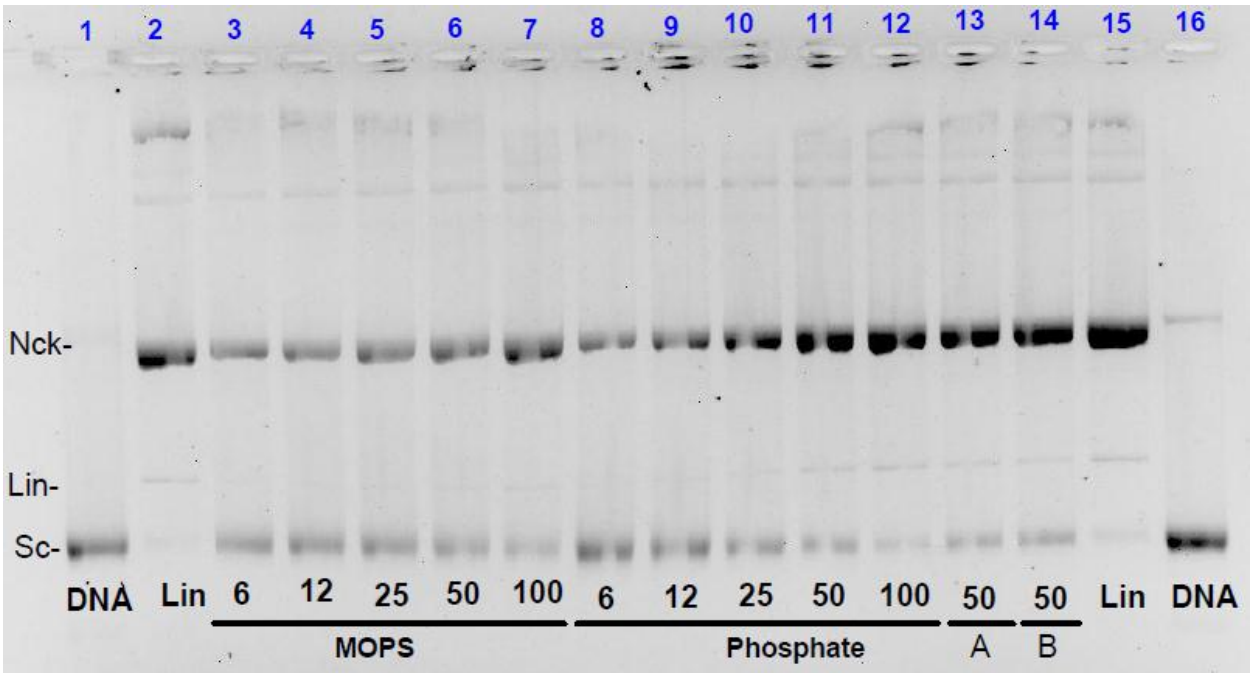

Figure A64. DNA cleavage activity of **20** at 6, 12, 25, 50 and 100 µM (ri 0.4, 0.8. 1.7, 3.3 and 6.7) under phosphate and MOPS buffers. Complex **9** (A) and $V^{IV}O(ClO_4)_2$ (B) at 50 µM under phosphate buffer were added for comparison.

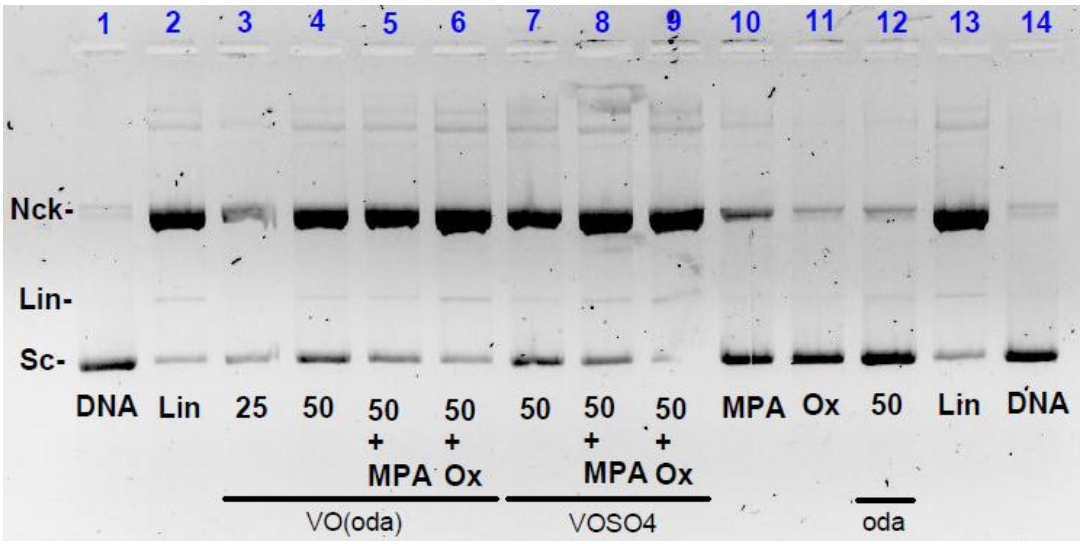

Figure A65. DNA cleavage activity of **20** and corresponding ligand at 25 and 50 μM (ri 1.7 and 3.3) under MOPS buffer in the presence of MPA and oxone. Complex **9** at 50 μM was added for comparison. “MPA” and “Ox” are the controls for the activating agents with no added complex.

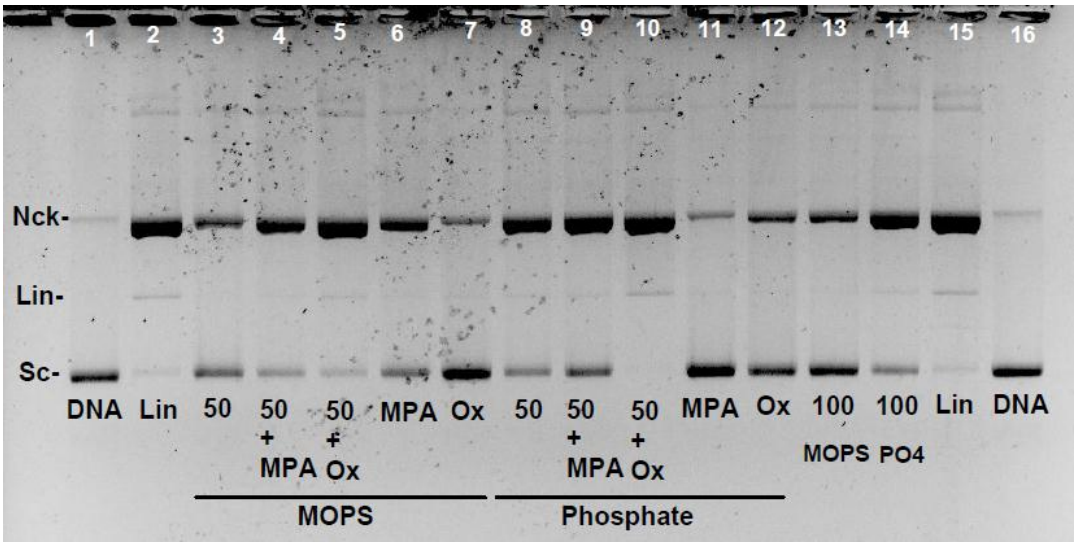

Figure A66. DNA cleavage activity of **20** at 50 and 100 μM (ri 3.3 and 6.7) under phosphate and MOPS buffers in the presence of MPA and oxone.

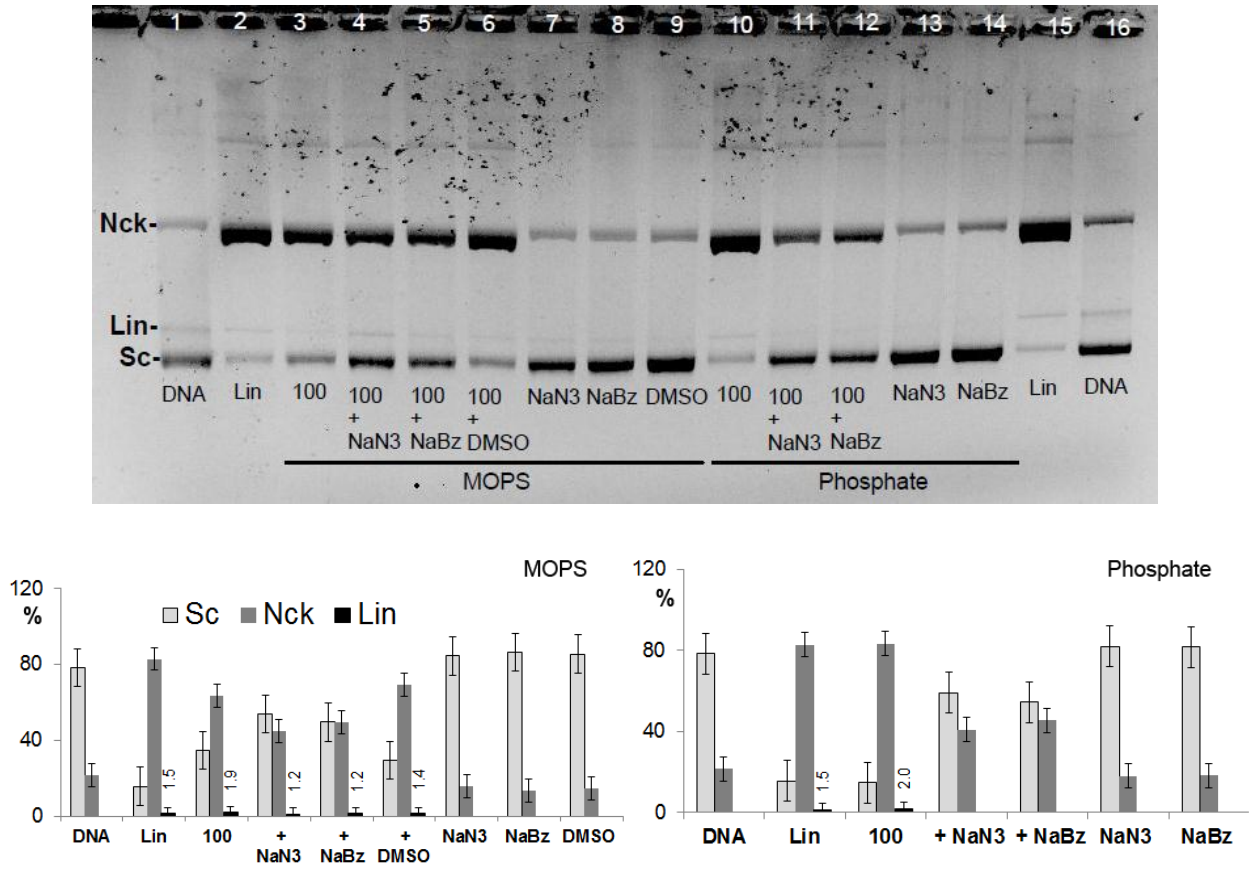

Figure A67. DNA cleavage activity of **20** at 100 μM (ri 6.7) under phosphate and MOPS buffers in the presence of scavengers (NaN_3, NaBz and DMSO). Lanes 7-9 present the controls of NaN_3, NaBz and DMSO in MOPS buffer; lanes 13 and 14 are the controls of NaN_3 and NaBz in phosphate buffer.

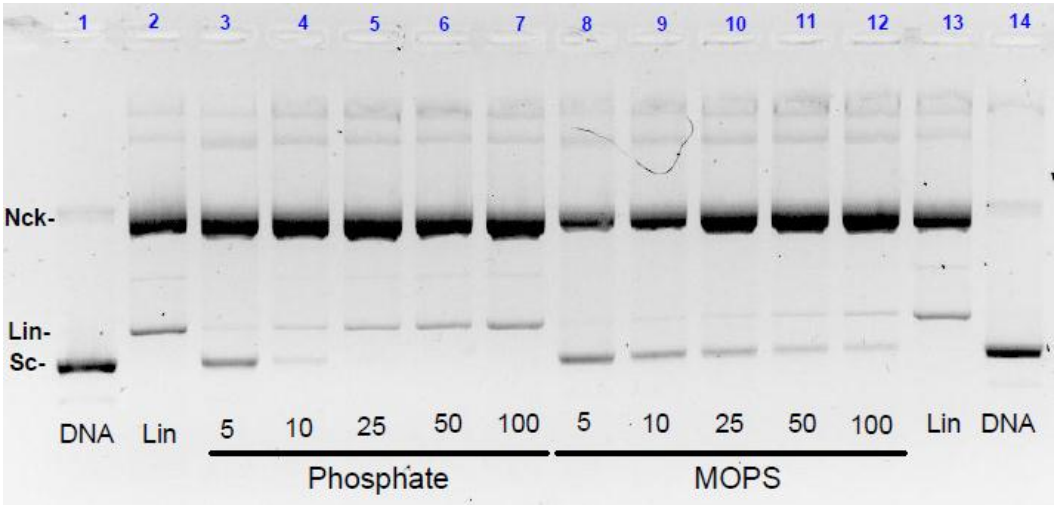

Figure A68. Nuclease activity of **21** at 5, 10, 25, 50 and 100 μM (ri 0.3, 0.7, 1.7, 3.3 and 6.7) under phosphate and MOPS buffers.

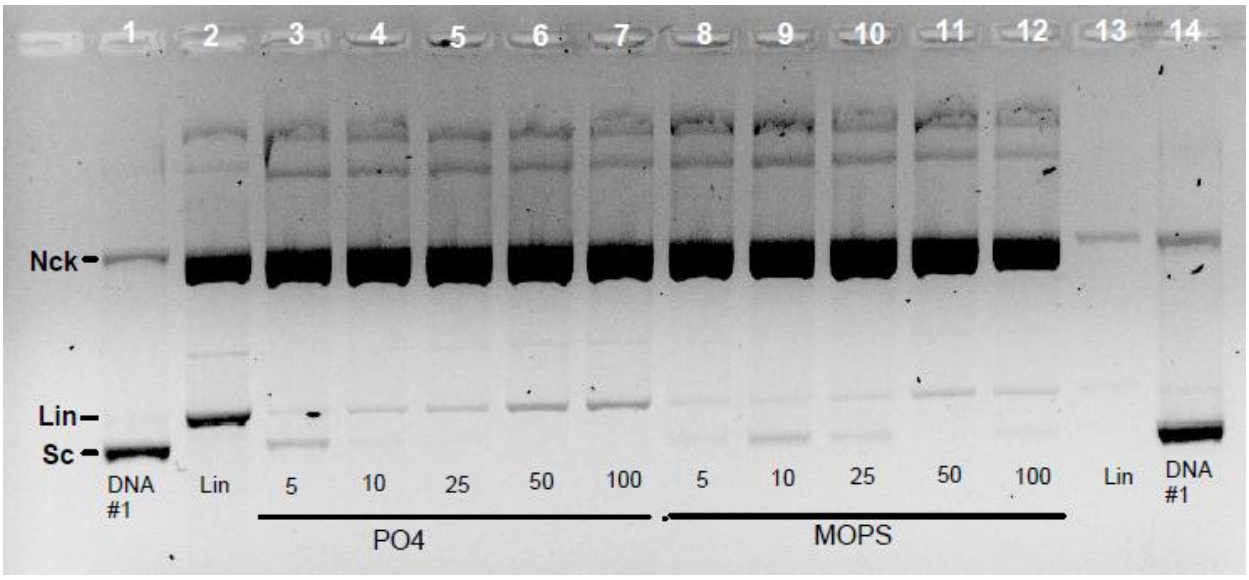

Figure A69. Replicate of the gel in Figure A68.

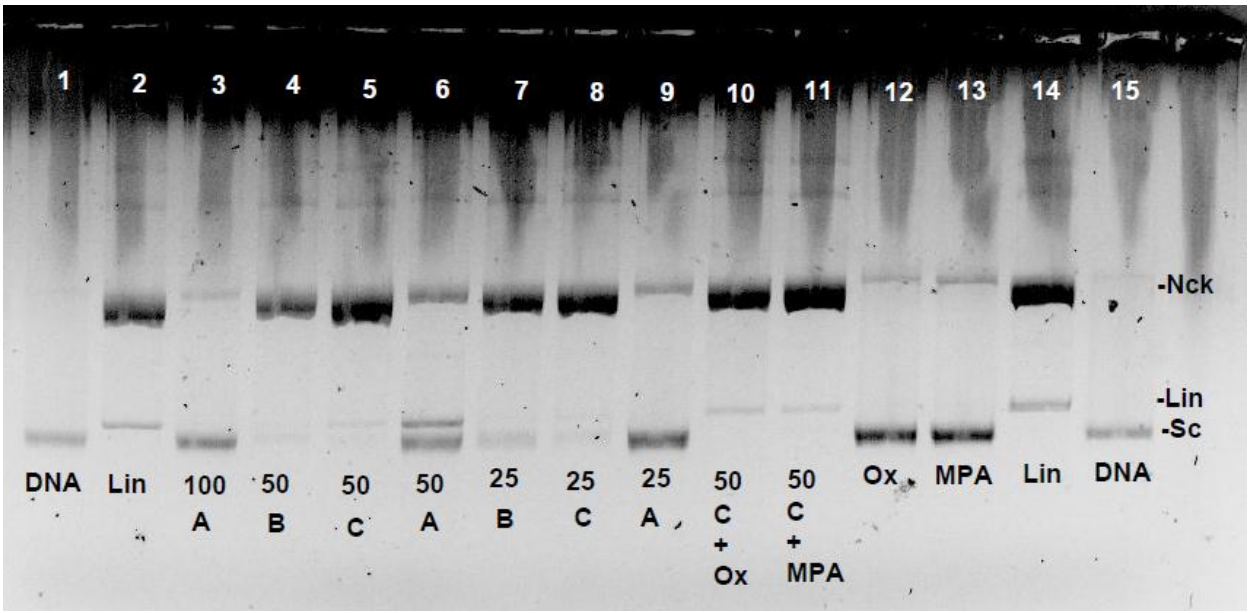

Figure A70. Nuclease activity of 1,10-phen (A), **22** (B) and **21** (C) at 25 and 50 μM (ri 1.7 and 3.3) under **phosphate** buffer (pH 7.4). Complex **21** is also tested in the presence of oxone and MPA. Lanes 13 and 14 are controls for respectively oxone and MPA.

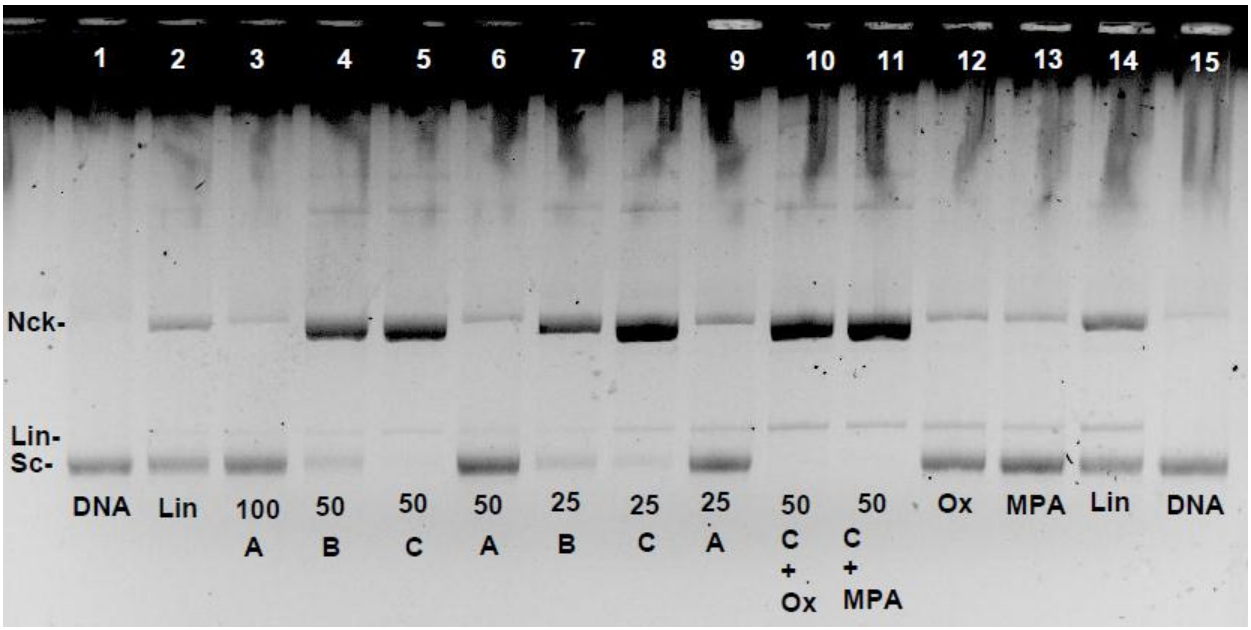

Figure A71. Nuclease activity of 1,10-phen (A), **22** (B) and **21** (C), at 25 and 50 μM (ri 1.7 and 3.3) under **MOPS** buffer (pH 7.4). Complex **21** is also tested in the presence of oxone and MPA. Lanes 13 and 14 are controls for respectively oxone and MPA.

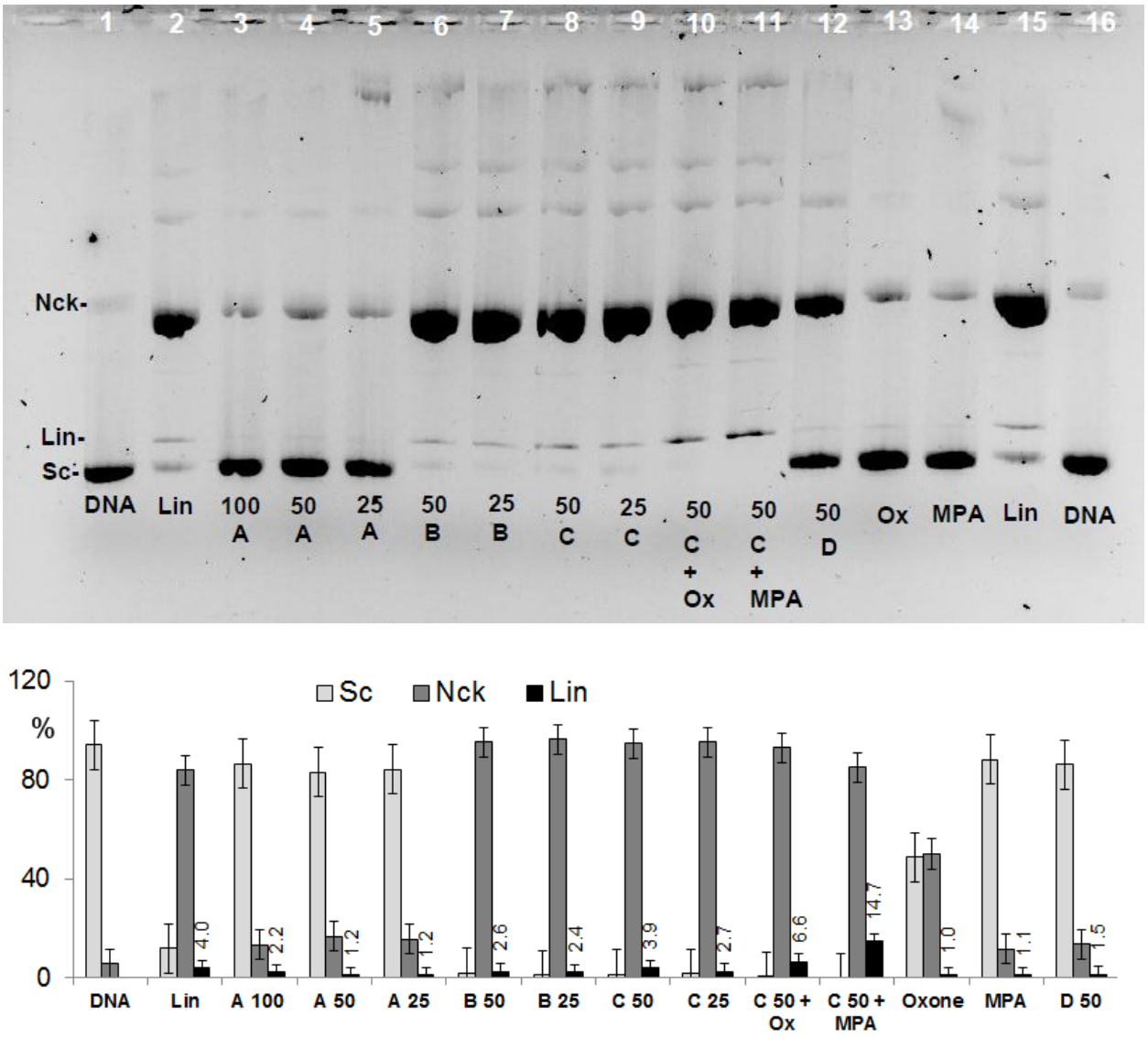

Figure A72. Nuclease activity of 1,10-phen (A), **22** (B) and **21** (C), at 25 and 50 µM (ri 1.7 and 3.3) under HEPES buffer (pH 7.4). Complex **21** is also tested in the presence of MPA and oxone. Lanes 13 and 14 are controls for respectively oxone and MPA. Complex **20** (D) at 50 µM (ri 3.3) was added for comparison.

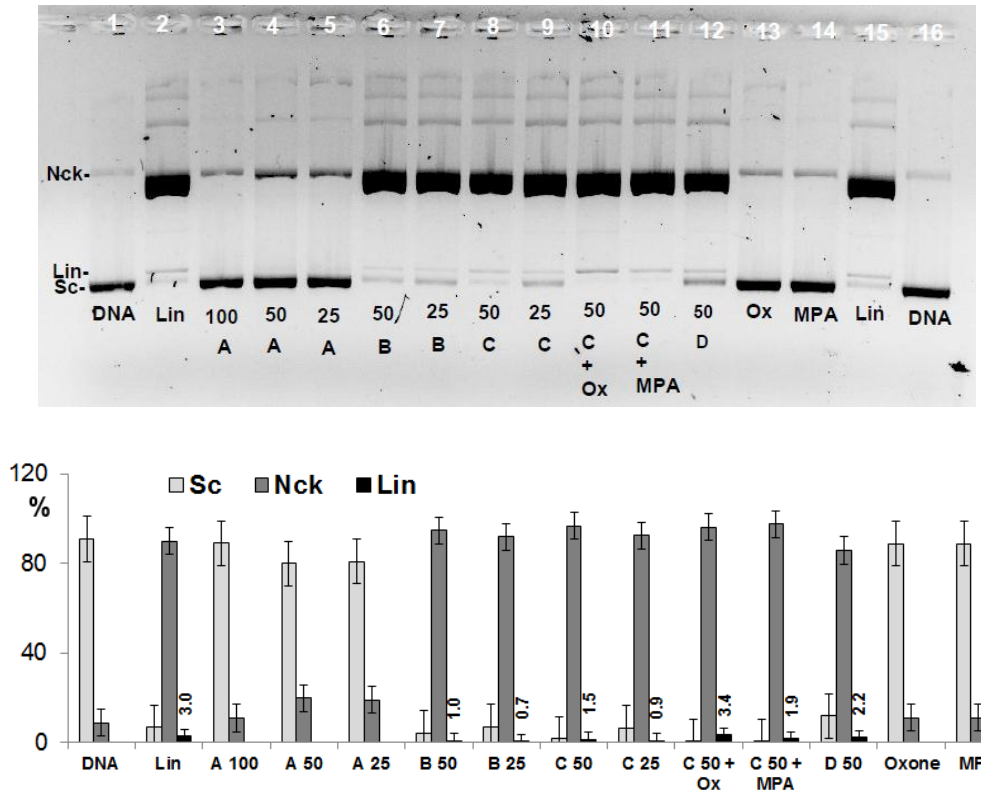

Figure A73. Replicate of the gel in Figure A70.

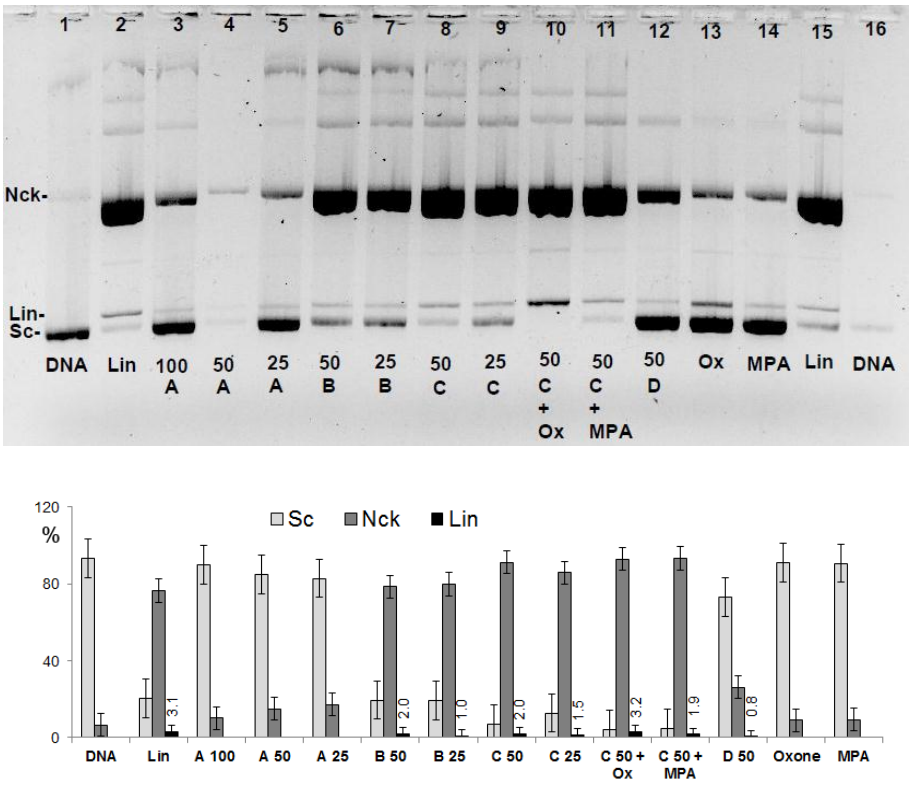

Figure A74. Replicate of the gel in Figure A71.

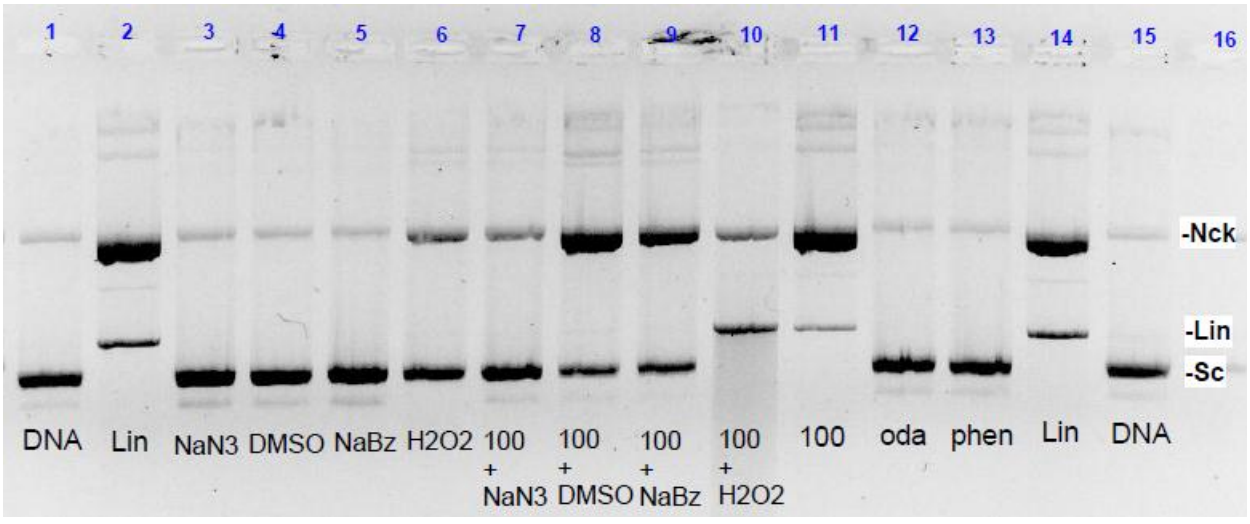

Figure A75. Nuclease activity of **21** at 100 µM (ri 6.7) under **phosphate** buffer in the presence of scavengers and H_2O_2. Ligands oda and phen were added for comparison. DNA 'N' and 'K' are plasmids DNA prepared in different batches.

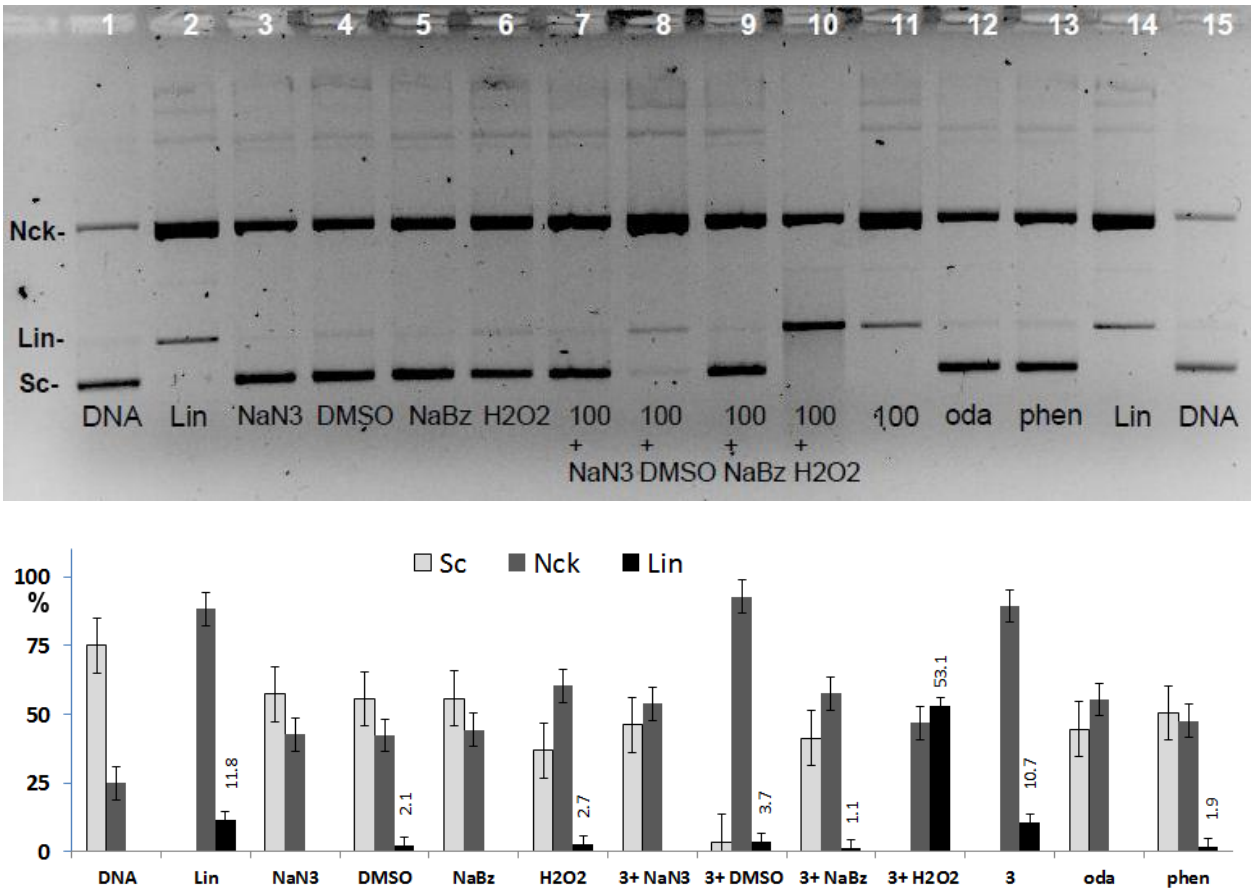

Figure A76. Replicate of the gel in Figure A75.

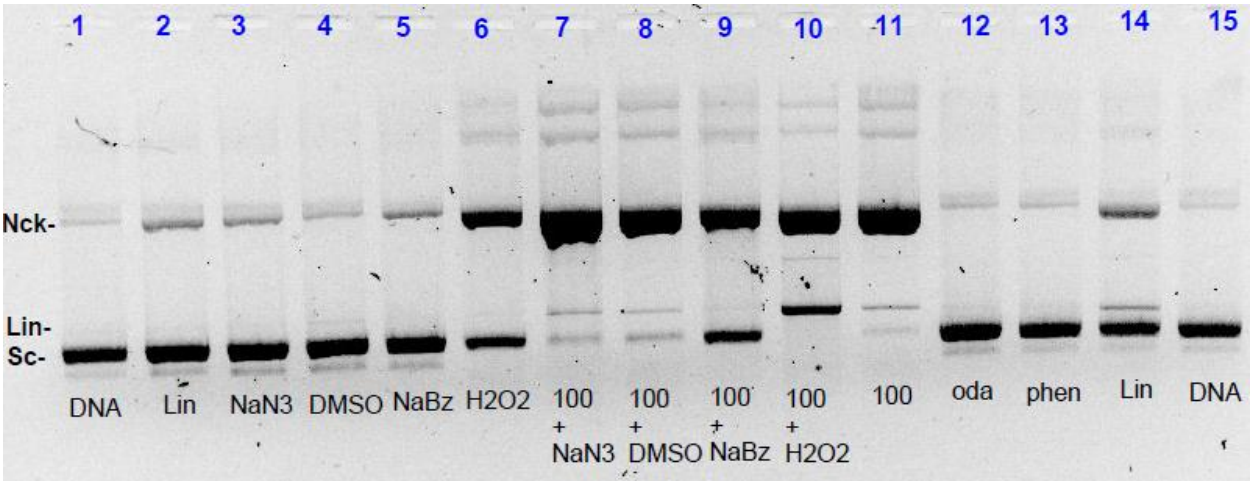

Figure A77. Nuclease activity of **21** at 100 μM (ri 6.7) under **MOPS** buffer in the presence of scavengers and H_2O_2. Ligands oda and phen were added for comparison. Lanes 3-6 are the controls for NaN_3, NaBz, DMSO and H_2O_2 with no added complex.

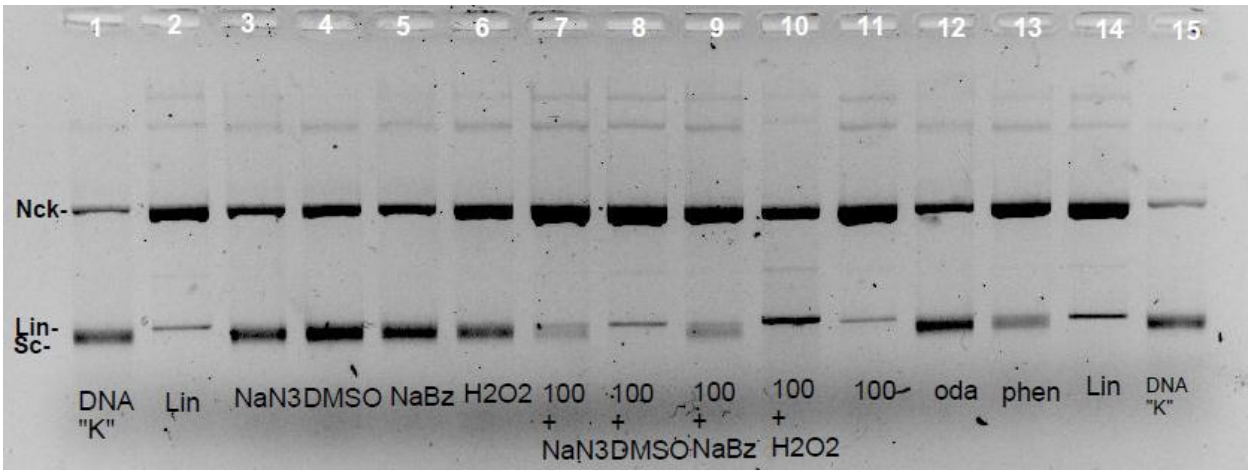

Figure A78. Replicate of the gel in Figure A77.

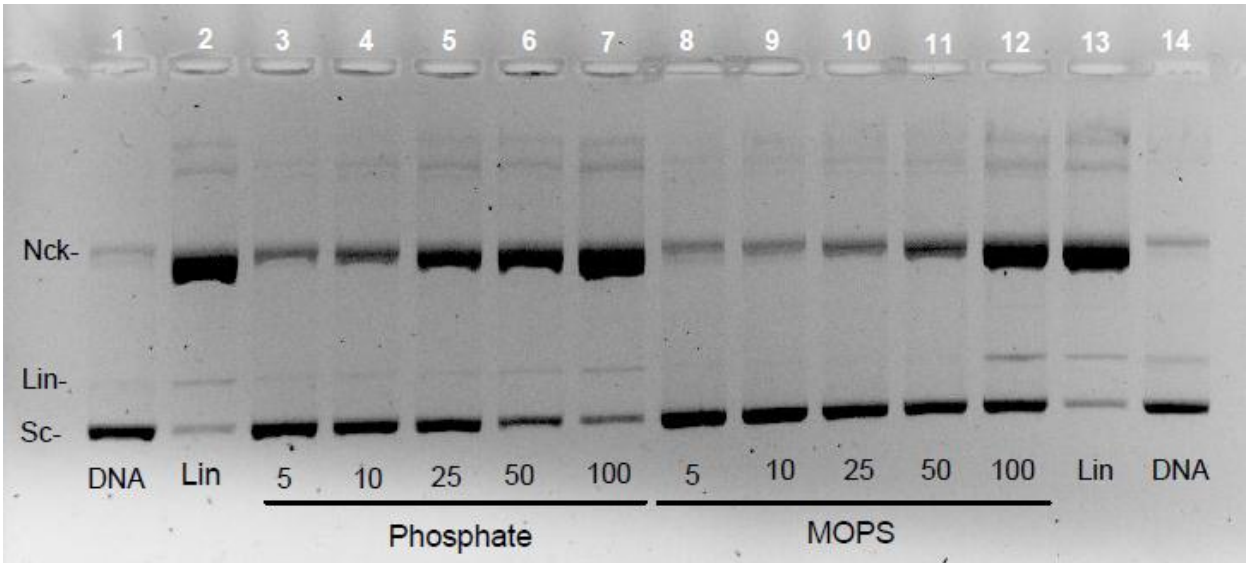

Figure A79. Nuclease activity of **23** at 5, 10, 25, 50 and 100 μM (ri 0.3, 0.7, 1.7, 3.3 and 6.7) under phosphate and MOPS buffers.

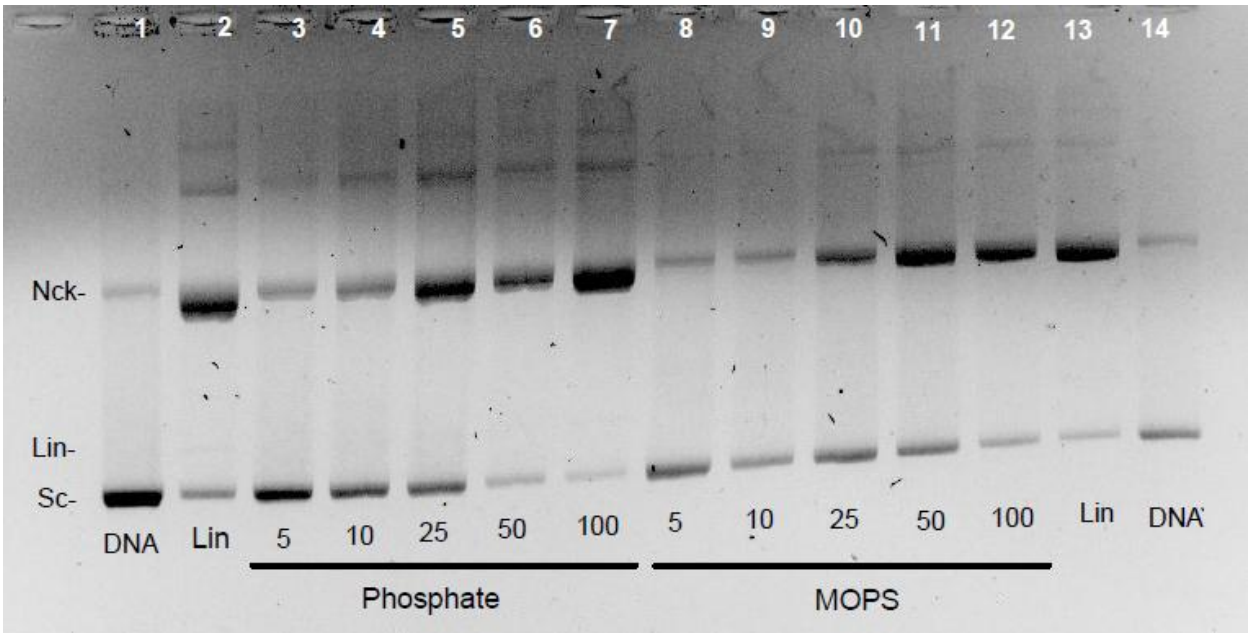

Figure A80. Replicate of the gel in Figure A79.

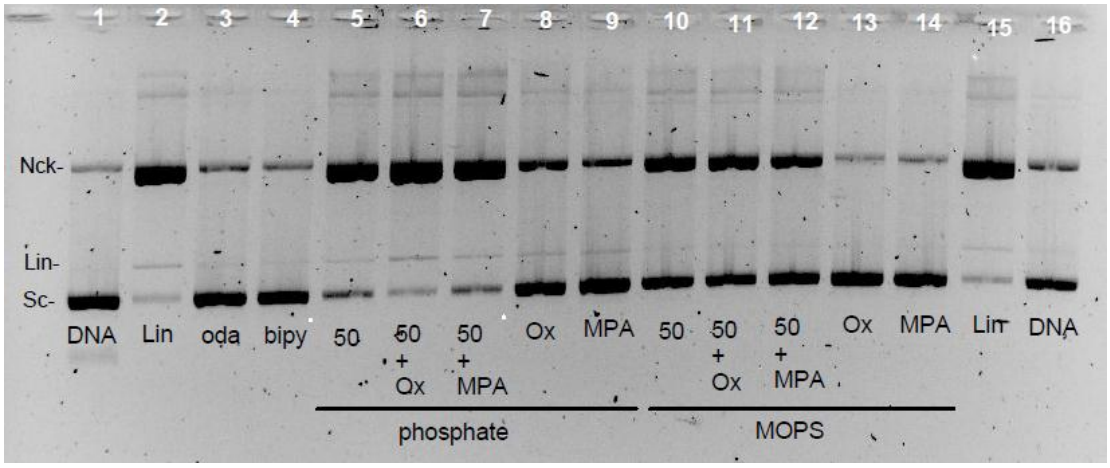

Figure A81. Nuclease activity of **23** at 50 μM (ri 3.3) under phosphate and MOPS buffers in the presence of oxone and MPA. Corresponding ligands, oda and bipy, were added for comparison.

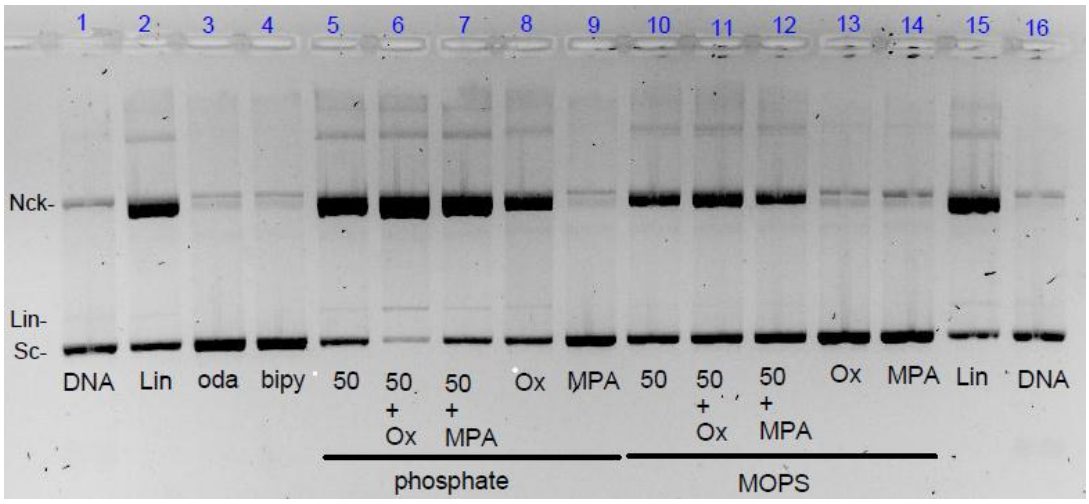

Figure A82. Replicate of the gel in Figure A81.

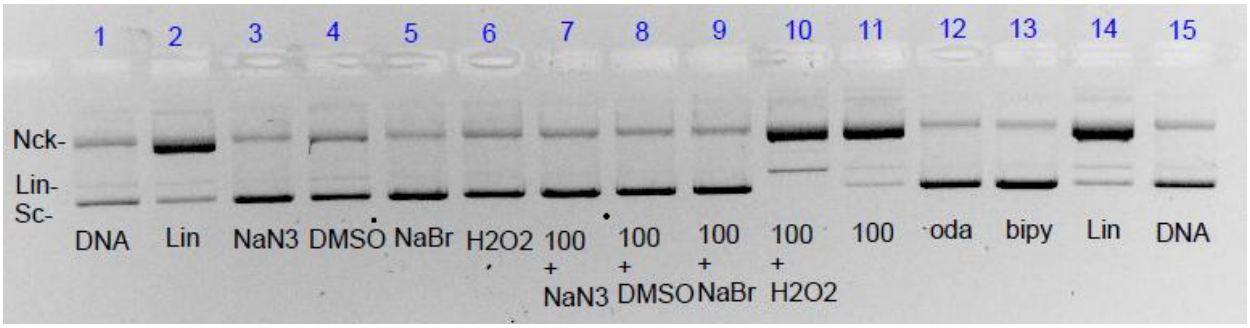

Figure A83. Nuclease activity of **23** at 100 μM (ri 6.7) under phosphate buffer in the presence of scavengers and H_2O_2. Corresponding ligands, oda and bipy, were added for comparison.

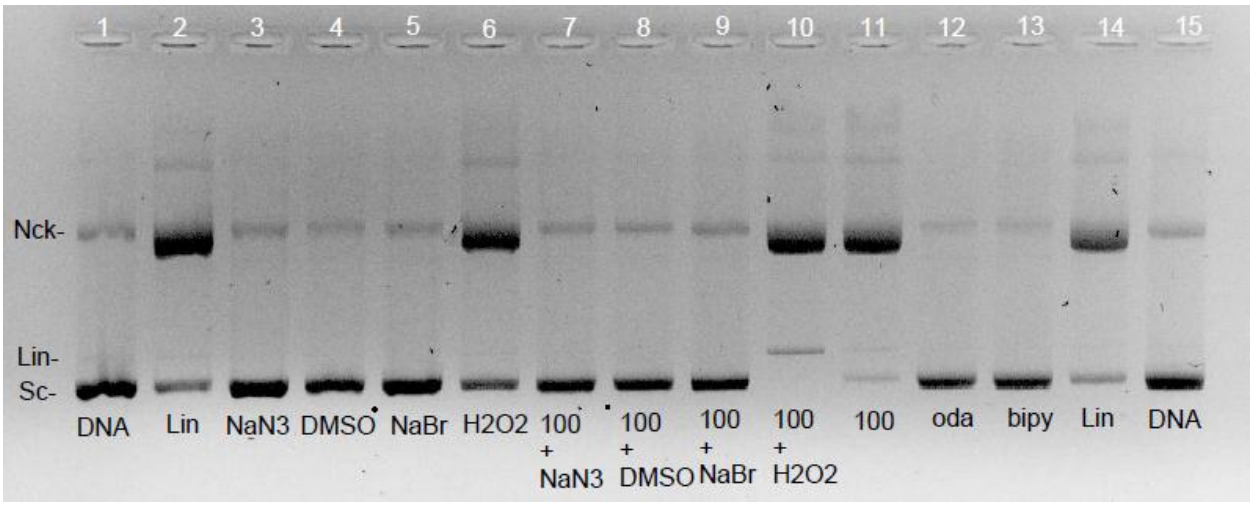

Figure A84. Replicate of the gel in Figure A83.

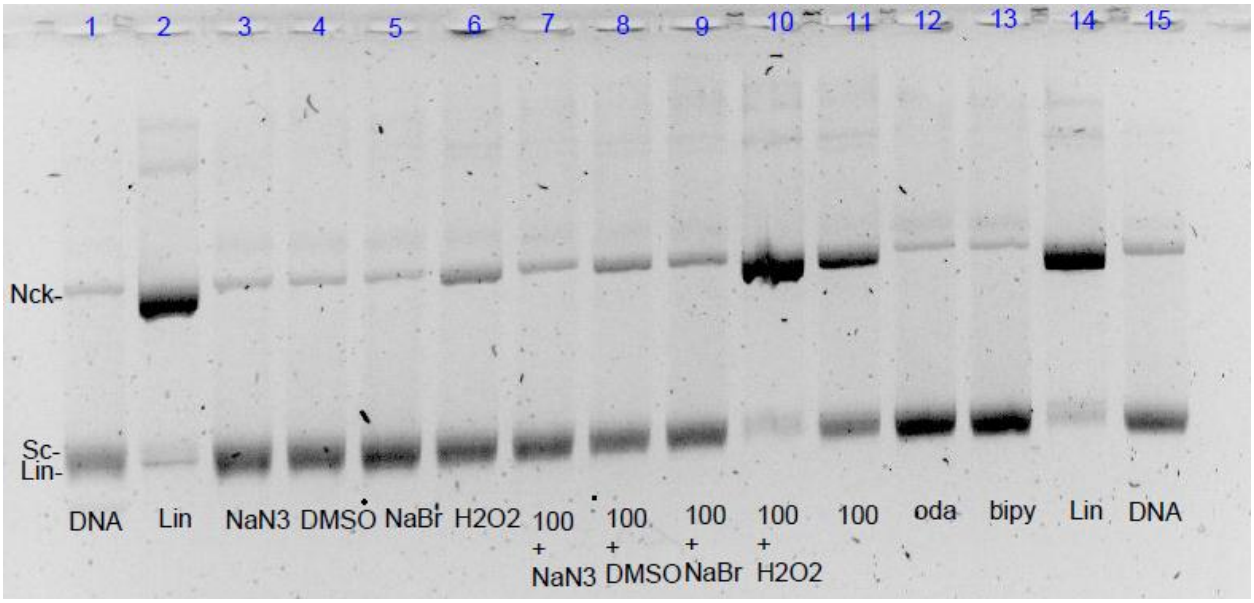

Figure A85. Nuclease activity of **23** at 100 μM (ri 6.7) under MOPS buffer in the presence of scavengers and H_2O_2. Corresponding ligands, oda and bipy, were added for comparison.

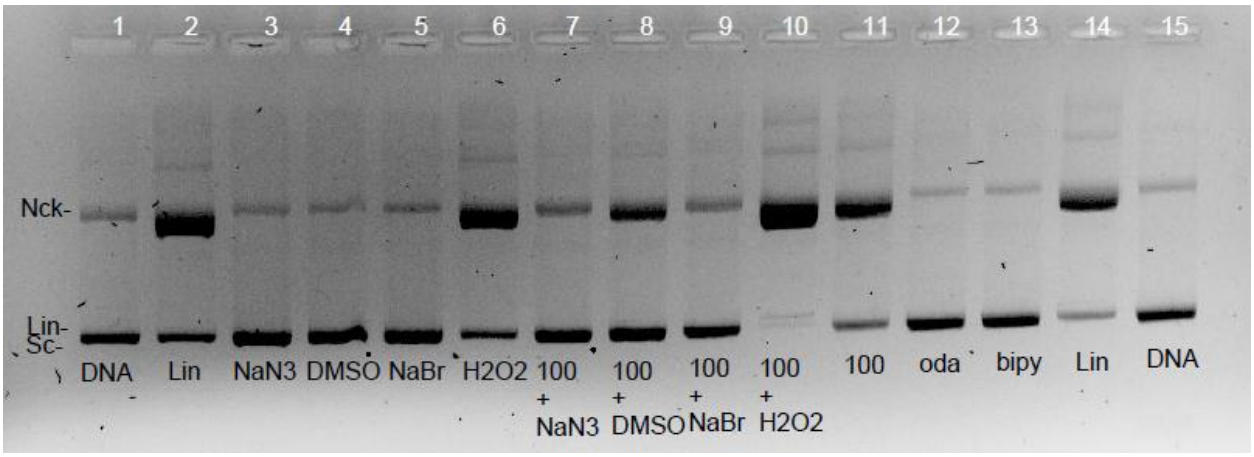

Figure A86. Replicate of the gel in Figure A85.

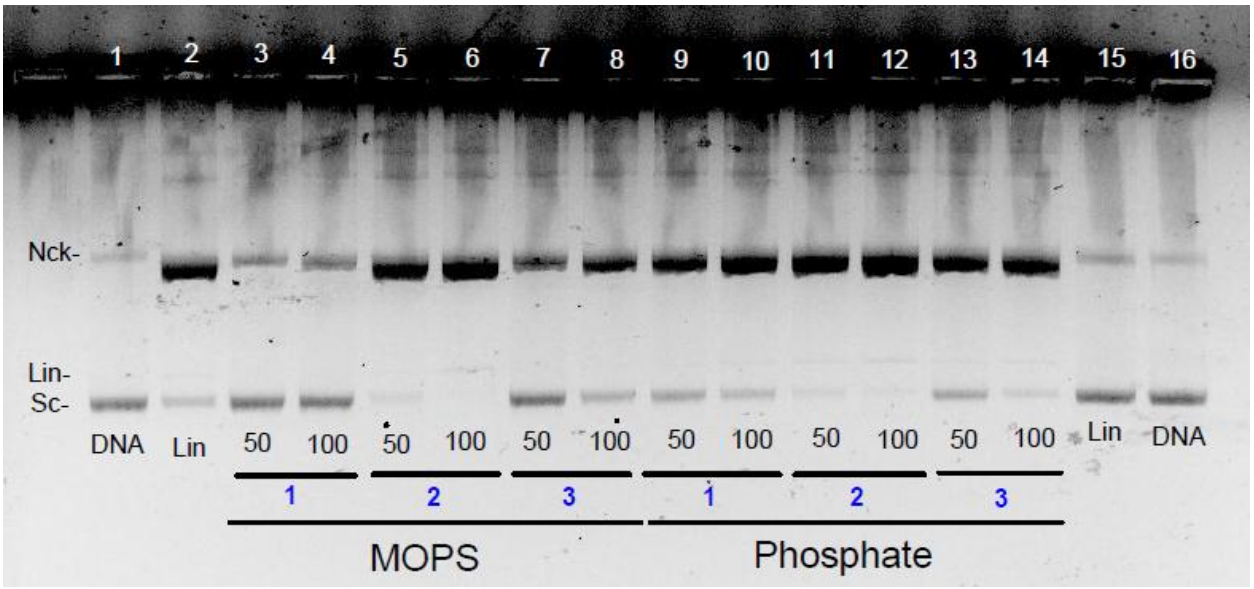

Figure A87. Comparison of DNA cleavage activity of **20** (1), **21** (2) and **23** (3) at 50 and 100 μM (ri 3.3 and 6.7) under MOPS and phosphate buffers.

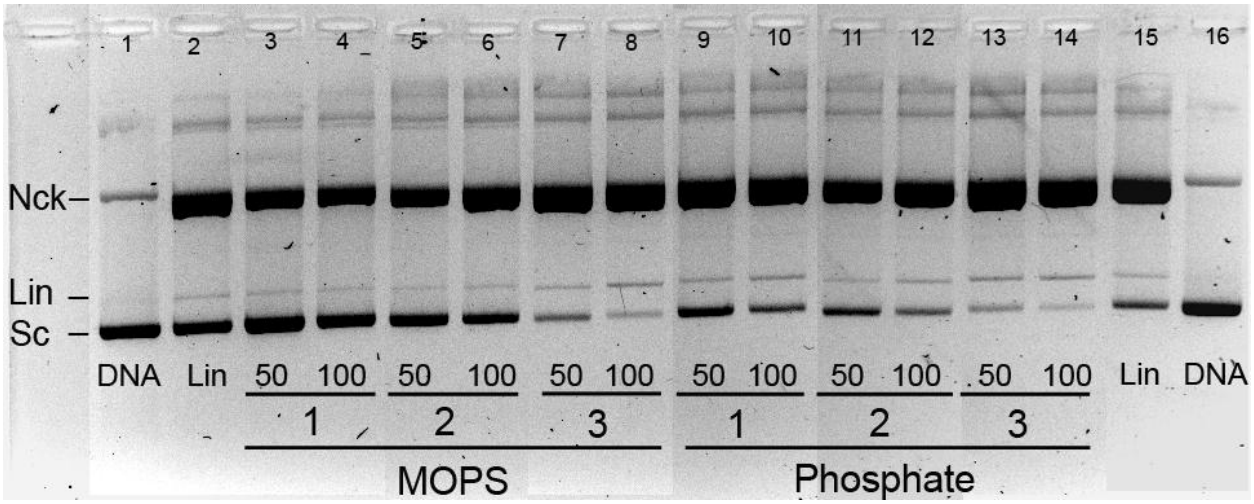

Figure A88. Replicate of the gel in Figure A87.

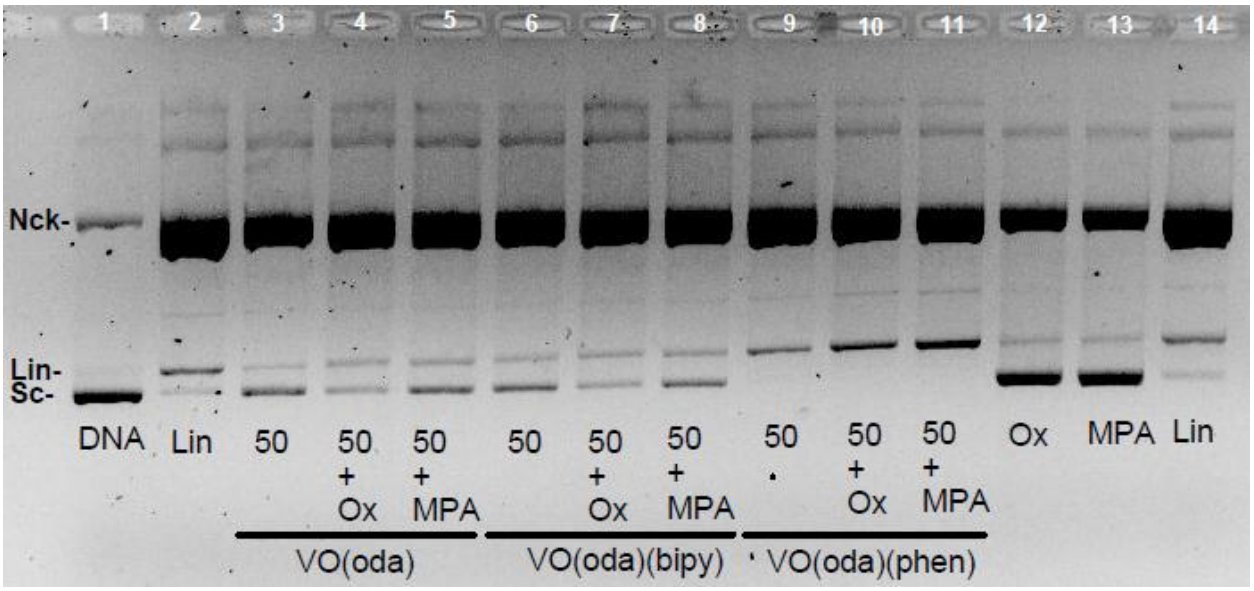

Figure A89. Comparison of the nuclease activity of **20** (lanes 3-5), **21** (lanes 9-11) and **23** (lanes 6-7) at 50 µM (ri 3.3) under **phosphate** buffer in the presence of oxone and MPA.

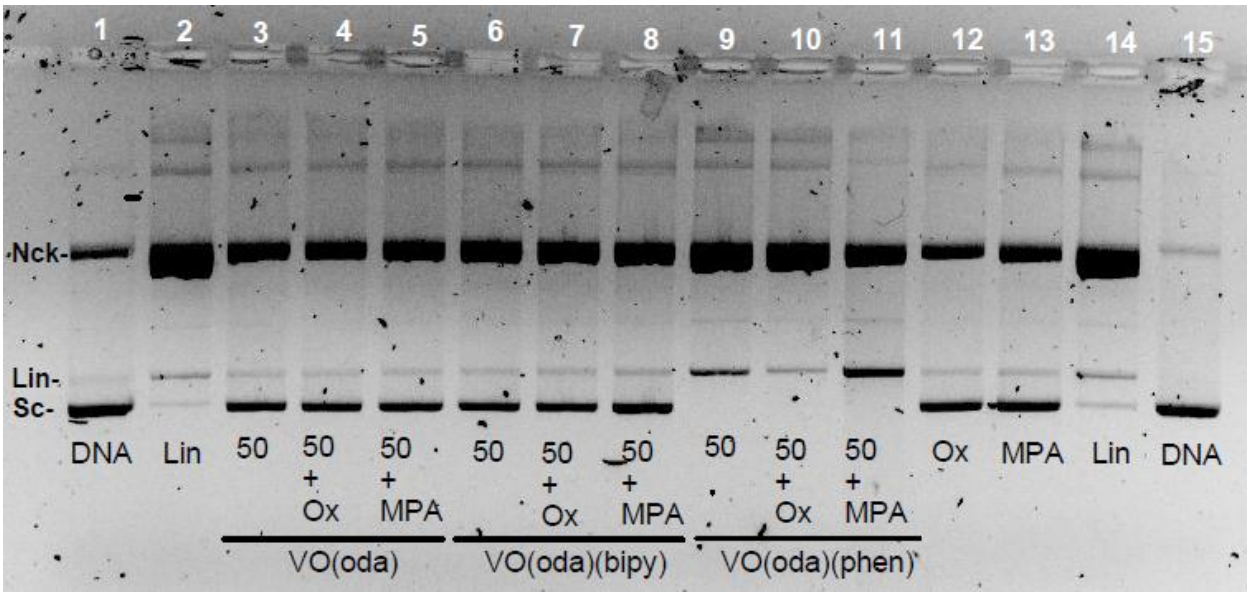

Figure A90. Comparison of the nuclease activity of **20**, **21** and **23** at 50 μM (ri 3.3) under **MOPS** buffer in the presence of oxone and MPA.

*$VO(crysin)_2$ (**24**), $VO(morin)_2$ (**25**), VO(clor) (**26**) and VO(silibinin) (**27**)*

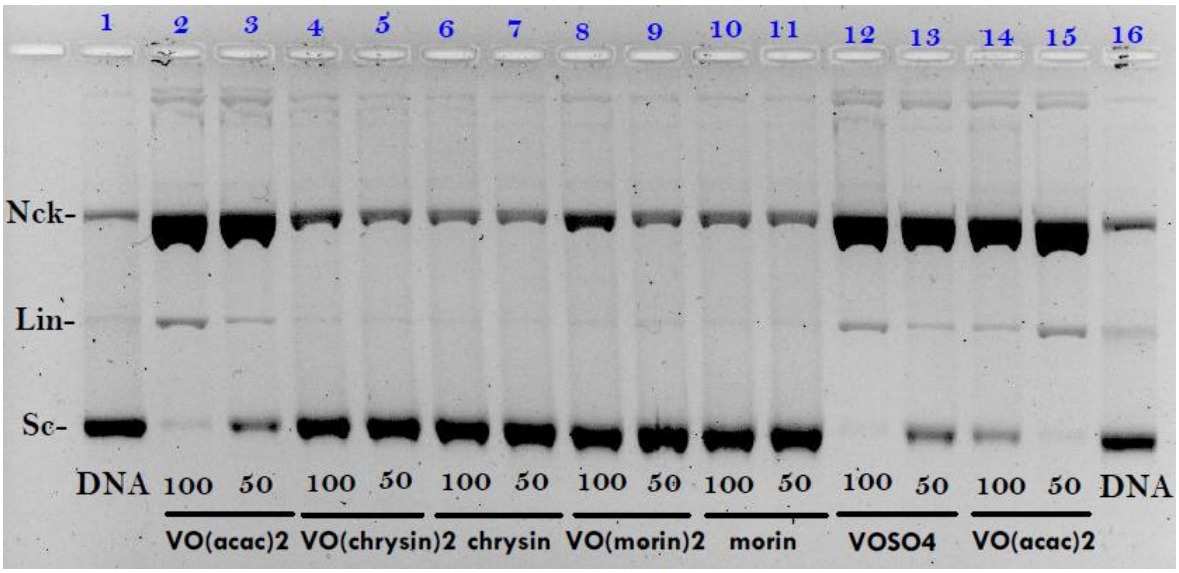

Figure A91. DNA cleavage activity of **24**, **25** and corresponding ligands at 50 and 100 μM (ri 3.3 and 6.7) under phosphate buffer. Complexes **1** and **9** were added for comparison.

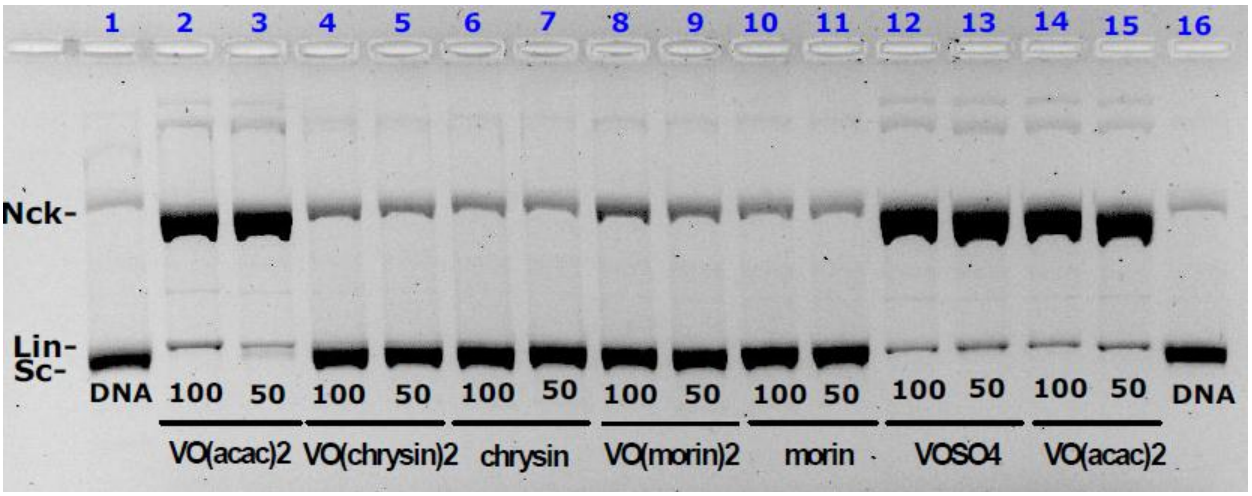

Figure A92. Replicate of the gel in Figure A91.

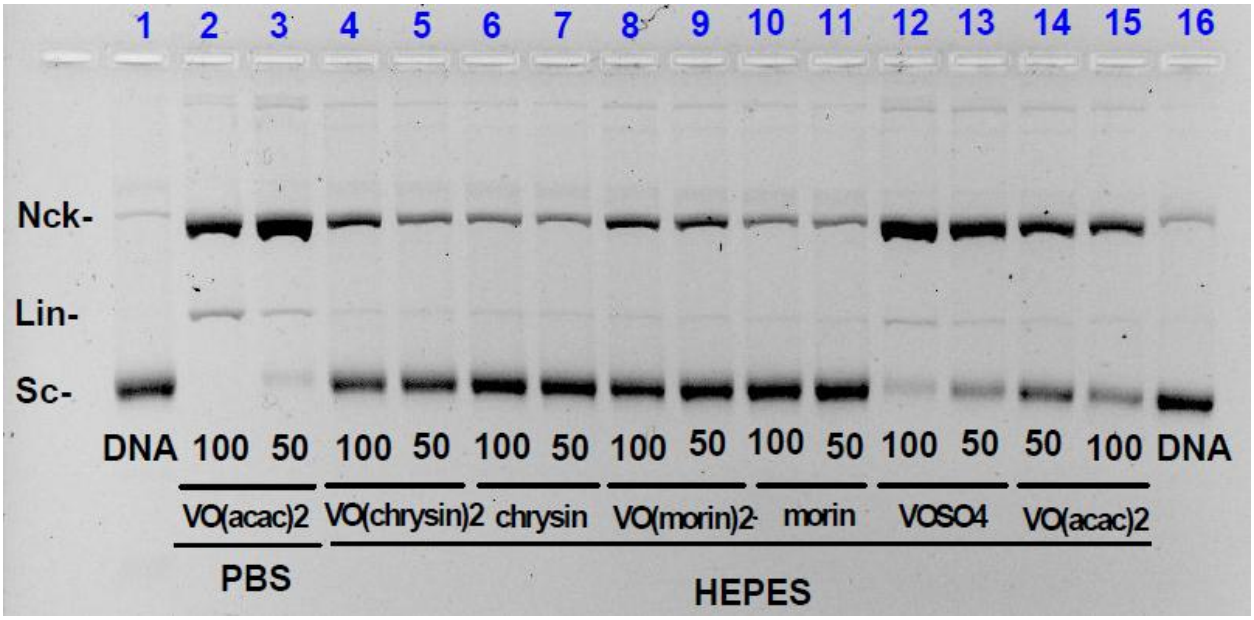

Figure A93. DNA cleavage activity of **24**, **25** at 50 and corresponding ligands at 50 and 100 μM (ri 3.3 and 6.7) under HEPES buffer. Complexes **1** and **9** were added for comparison.

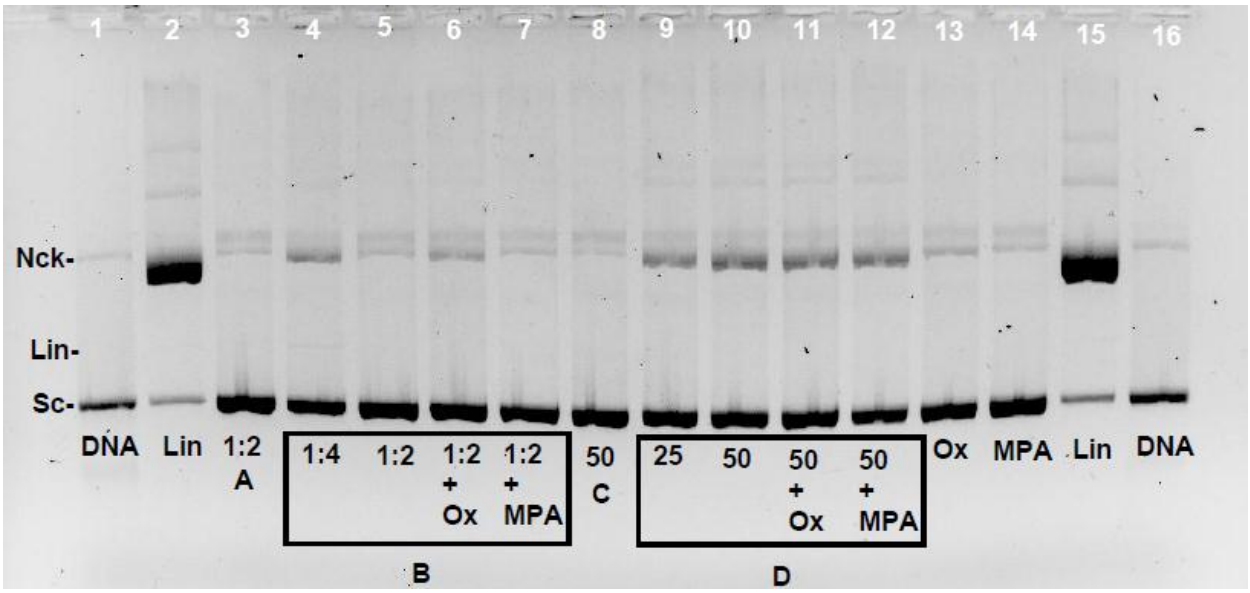

Figure A94. DNA cleavage activity of **25** (B) and **26** (D) and corresponding ligands (morin (A) and clor (C)) under **phosphate** buffer. A and B did not dissolve completely; the stock solution was prepared to be 200 μM and the corresponding dilutions 1:2 and 1:4 were made.

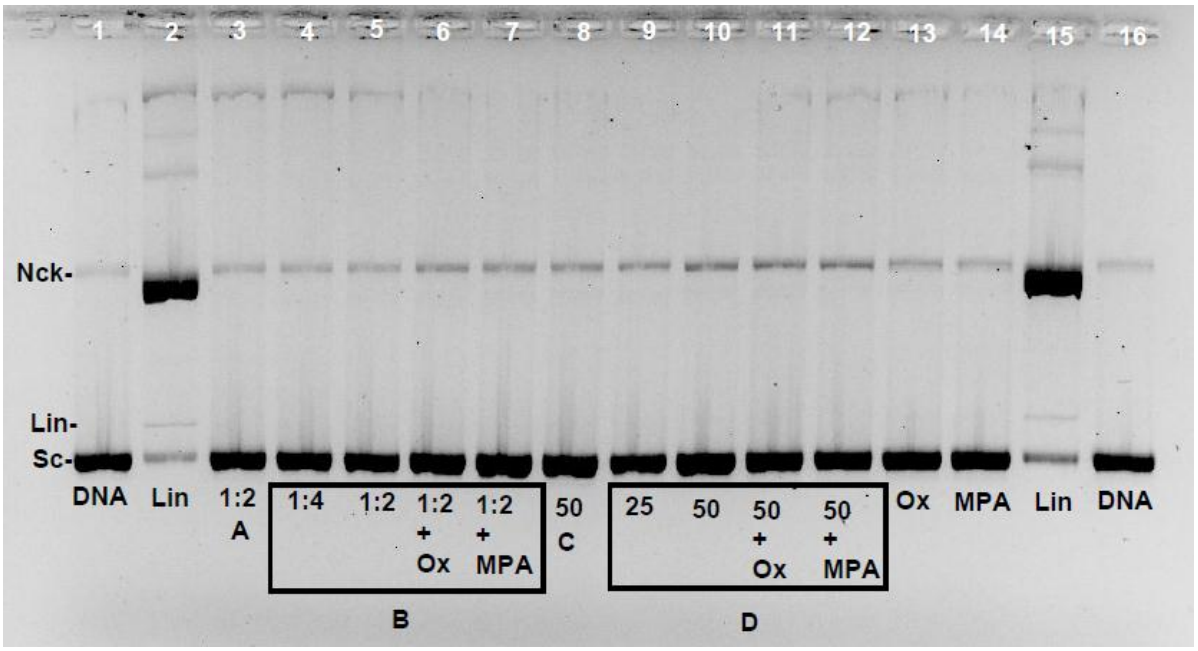

Figure A95. DNA cleavage activity of **25** (B) and **26** (D) and corresponding ligands (morin (A) and clor (C)) under **MOPS** buffer in the absence and presence of activating agents (oxone and MPA). A and B did not dissolve completely; the stock solution was prepared to be 200 μM and the corresponding dilutions 1:2 and 1:4 were made.

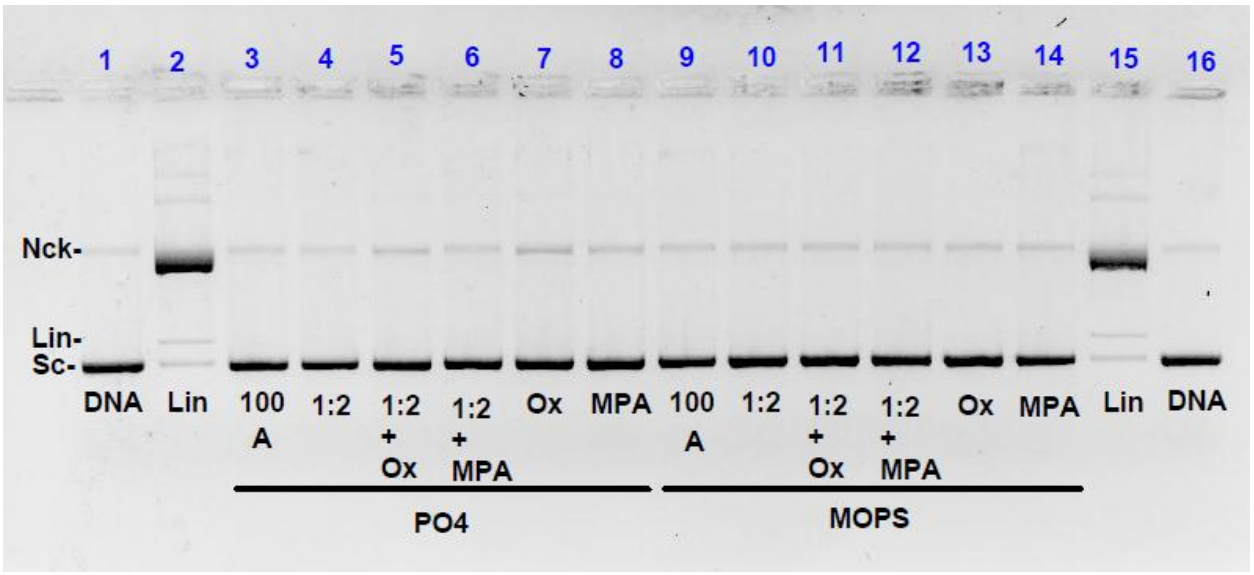

Figure A96. DNA cleavage activity of **25** and the corresponding ligand (morin (A)) under phosphate and MOPS buffers (pH 7.4). The complex and ligand were dissolved in 5% DMSO and in 1% ethanol, respectively. The final concentration for the ligand was 100 μM (ri 6.7). As the complex did not dissolve completely, the stock solution was prepared to be 100 μM and diluted 1:2 in order to ensure the concentration close to 50 μM (ri 3.3).

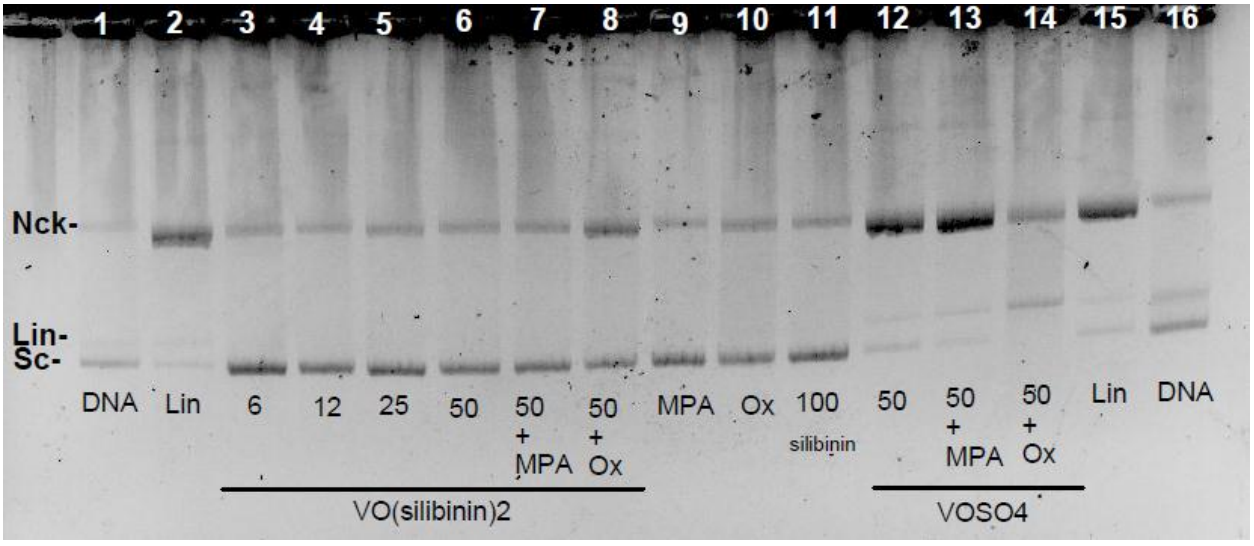

Figure A97. Effect of concentration and activating agents on the DNA cleavage activity of **27** ($Na_2[VO(silibinin)_2]•6H_2O$) at 6, 12, 25 and 50 μM (ri 0.4, 0.8, 1.7 and 3.3) under **phosphate** buffer. Complex **9** at 50 μM was added for comparison.

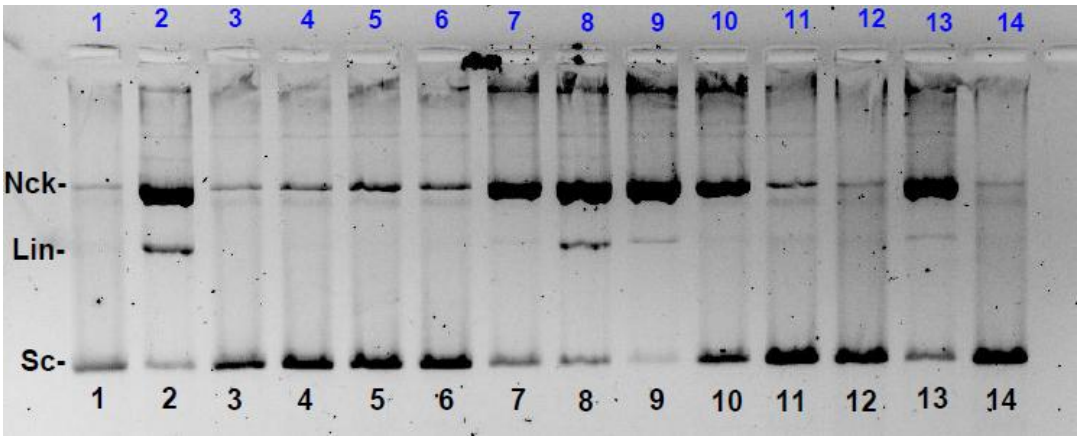

Figure A98. Effect of activating agents on the DNA cleavage activity of **27** under **MOPS** buffer. Lanes 1 and 14, 2 and 13 – controls for native and linearized DNA, respectively; 3 – 25 µM of **27** (ri 1.7); 4 – 50 µM of **27** (ri 3.3); 5 – 50 µM of **27** + MPA; 6 – 50 µM of **27** + oxone; 7 – 50 µM of **9**; 8 – 50 µM of **9** + MPA; 9 – 50 µM of **9** + oxone; 10 and 11 – controls for MPA; and oxone, respectively; 12 – 100 µM ligand silibinin.

Other vanadium and copper complexes: *Cu(Sal-Gly)(bipy)* (***28***), *Cu(Sal-Gly)(phen)* (***29***), *Cu(Sal-L-Phe)(phen)* (***30***), *VO(Sal-L-Phe)(bipy)* (***31***), *VO(Sal-L-Phe)(phen)* (***32***), *VO(Sal-Gly)(bipy)* (***33***), *VO(Sal-Gly)(phen)* (***34***), *VO(Sal-Gly)(H_2O)* (***35***), *VO(Sal-L-Phe)(H_2O)* (***36***)

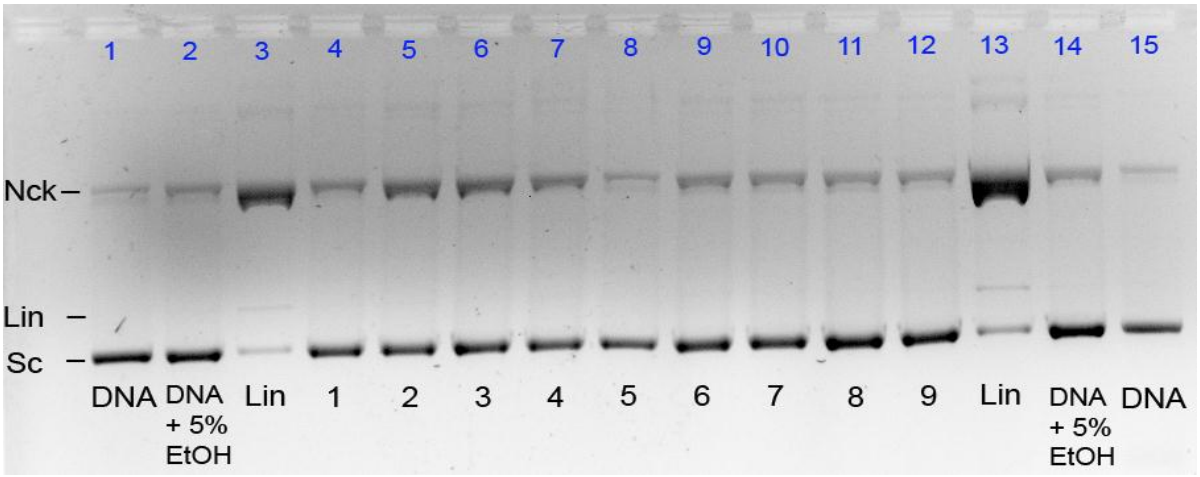

Figure A99. DNA cleavage activity of **28**-**36** (assigned as 1-9, respectively) at 50 µM (ri 3.3) under PBS buffer. The complexes were dissolved in 5% solution of EtOH. "DNA + 5% EtOH" is the control for the Sc DNA with 5% solution of EtOH. Reaction mixtures were incubated as typically, i.e., 1 h at 37 ºC.

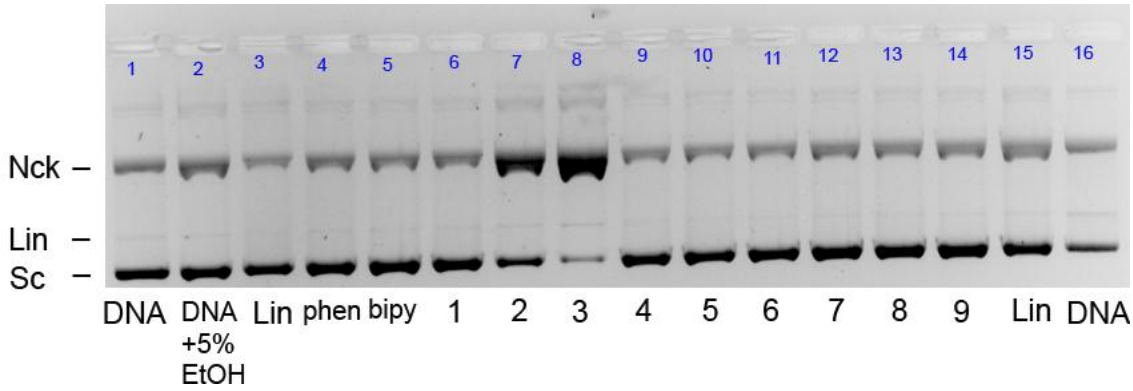

Figure A100. DNA cleavage activity of **28**-**36** (assigned as 1-9, respectively) at 100 µM (ri 6.7) under PBS buffer. The complexes were dissolved in 5% solution of EtOH. “Phen” and “bipy” are controls for 1,10-phenanthroline and 2,2´-bipyridyne. Reaction mixtures were incubated at for 5 h 37 ºC.

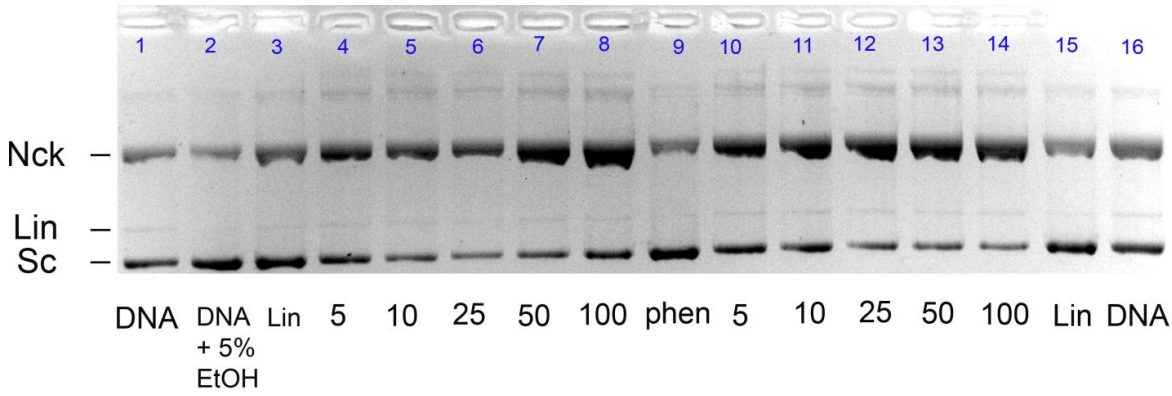

Figure A101. DNA cleavage activity of **29** and **30** at 5, 10, 25, 50 and 100 µM (ri 0.3, 0.7, 1.7, 3.3 and 6.7) under PBS buffer. The complexes were dissolved in 5% solution of EtOH. Reaction mixtures were incubated at 37 ºC for 5 h.

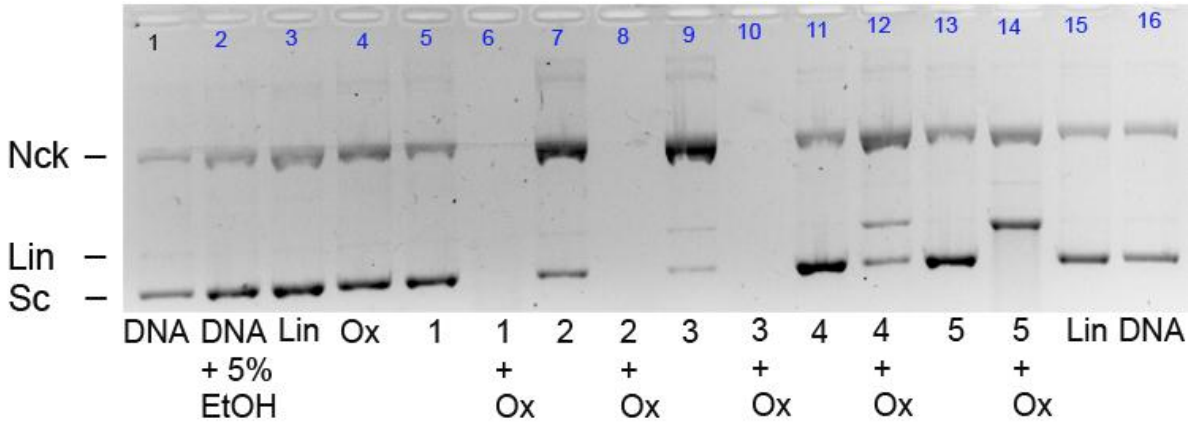

Figure A102. Cleavage of pA1 pDNA by **28**-**32** (assigned as 1-5, respectively) at 50 μM (ri 3.3) in the presence of oxone. The complexes were dissolved in 5% EtOH and 20 mM PBS. Final PBS concentration in a sample was 10 mM. "Ox" is the control for oxone without a complex. Samples were incubated at 37 ºC for 5 h (1-14), and 2 h (15 and 16).

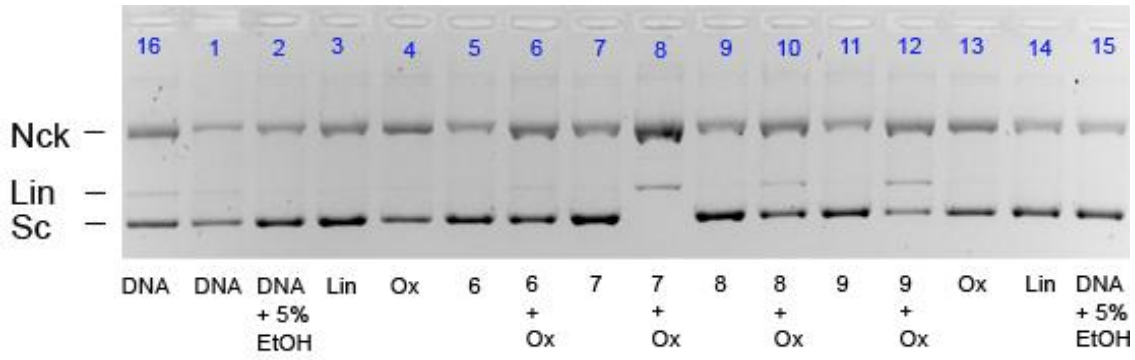

Figure A103. Cleavage of pA1 pDNA by **33**-**36** (assigned as 6-9, respectively) at 50 μM (ri 3.3) in the presence of oxone. The complexes were dissolved in 5% EtOH and 20 mM PBS. Final PBS concentration in a sample was 10 mM. Samples were incubated at 37 ºC for 5 h (1-12), 2 h (13-15) and at room temperature for 5 h (16).

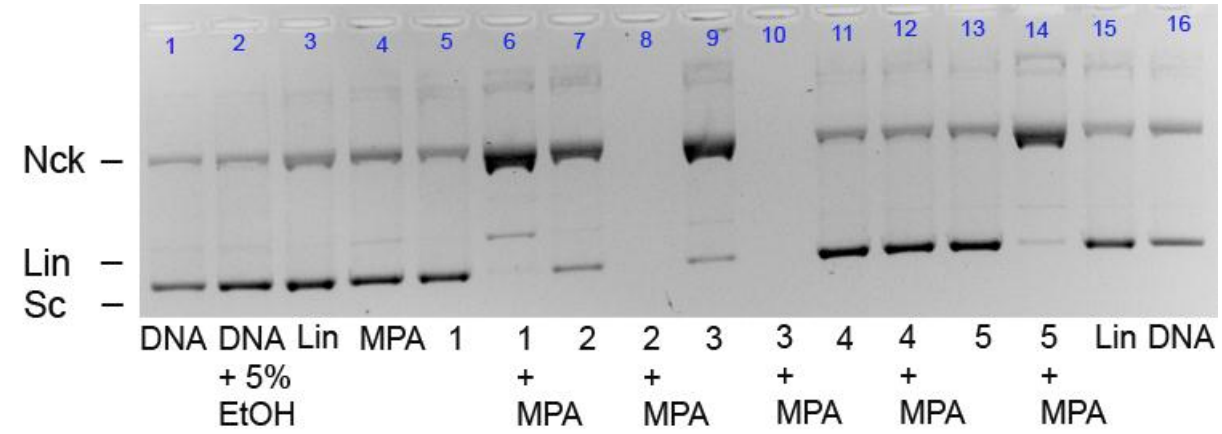

Figure A104. Cleavage of pA1 pDNA by **28**-**32** (assigned as 1-5, respectively) at 50 μM (ri 3.3) in the presence of MPA. The complexes were dissolved in 5% EtOH and 20 mM PBS. Final PBS concentration in a sample was 10 mM. "MPA" is the control for MPA without a complex. Samples were incubated at 37 ºC for 5 h (1-14), and 2 h (15 and 16).

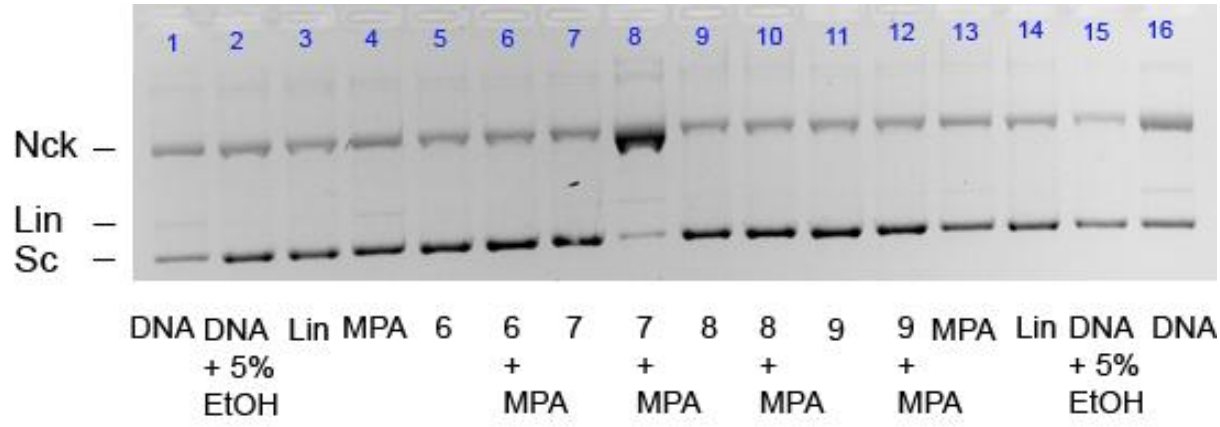

Figure A105. Cleavage of pA1 pDNA by **33**-**36** (assigned as 6-9, respectively) at 50 μM (ri 3.3) in the presence of MPA. The complexes were dissolved in 5% EtOH and 20 mM PBS. Final PBS concentration in a sample was 10 mM. Samples were incubated at 37 ºC for 5 h (1-12), 2 h (13-15) and at room temperature for 5 h (16).

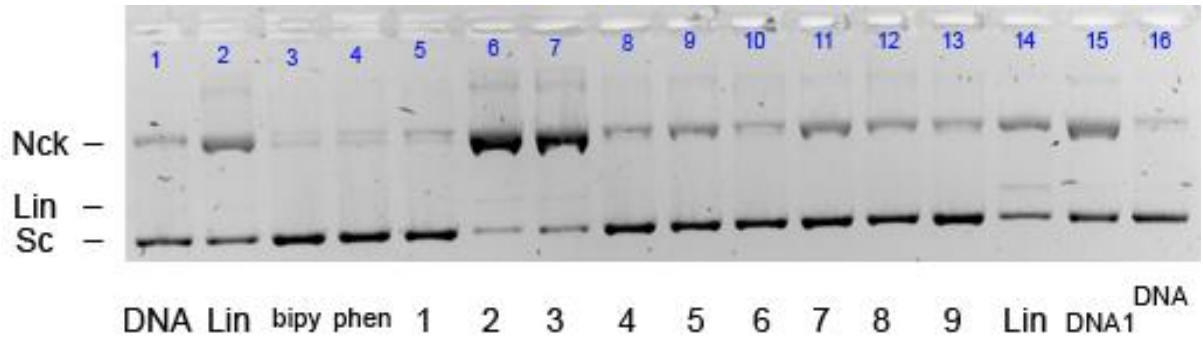

Figure A106. Cleavage of pA1 pDNA by **28**-**36** (assigned as 1-9, respectively) at 50 μM (ri 3.3) prepared in 20 mM PBS, no EtOH. Final concentration of PBS was 10 mM. "DNA1" is also the control for the Sc DNA but is from a different batch. "Phen" and "bipy" are controls for 1,10-phenanthroline and 2,2'-bipyridyne. Incubation 5 h at 37 ºC.

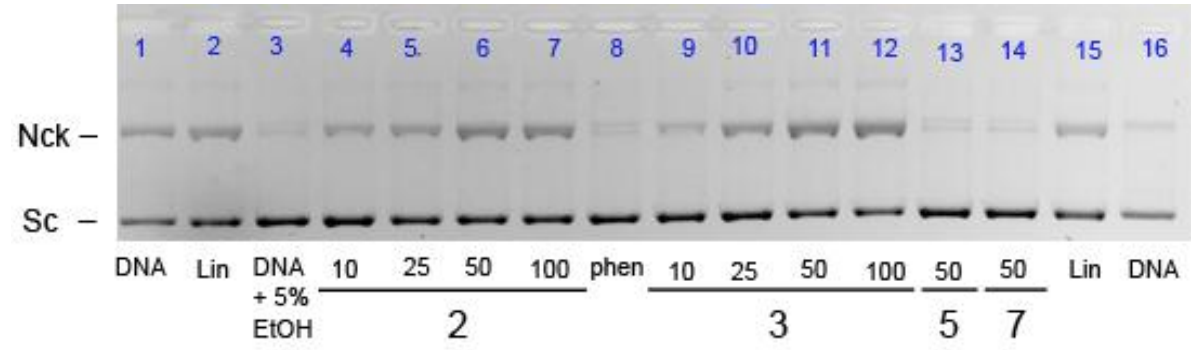

Figure A107. Nuclease activity of **29** and **30** (assigned as 2 and 3) at 10, 25, 50 and 100 μM (ri 0.7, 1.7, 3.3 and 6.7) prepared in 5% EtOH and 20 mM PBS. Complexes **32** and **34** (assigned 5 and 7, respectively) were added for comparison (ri 3.3). Final concentration of PBS was 10 mM. "DNA + 5% EtOH" is the control for the Sc DNA with 5% solution of EtOH. Samples were incubated at 37 ºC for 5 h (1-12) and 1 h (13-16).

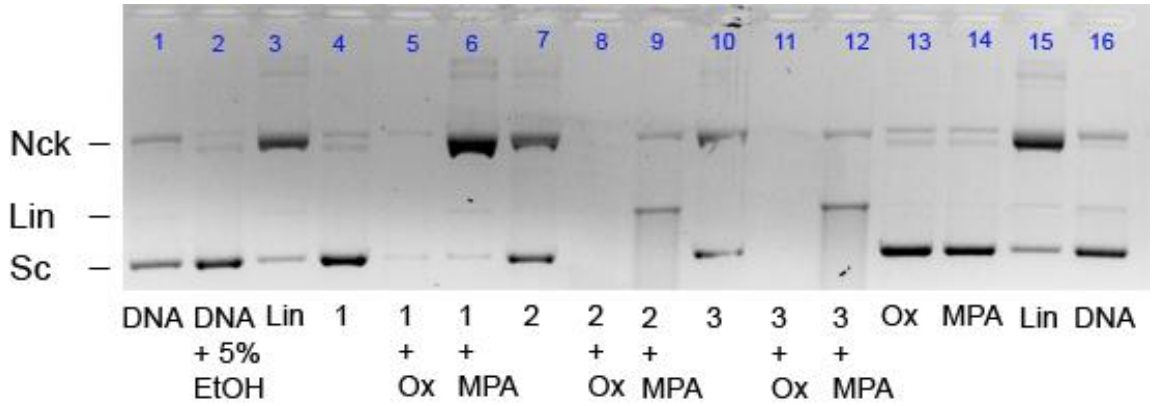

Figure A108. Effect of oxone and MPA on the nuclease activity of **28**-**30** (assigned as 1-3) at 50 µM (ri 3.3). The complexes were dissolved in 5% EtOH and 20 mM PBS. Final PBS concentration was 10 mM.

Phantom bands

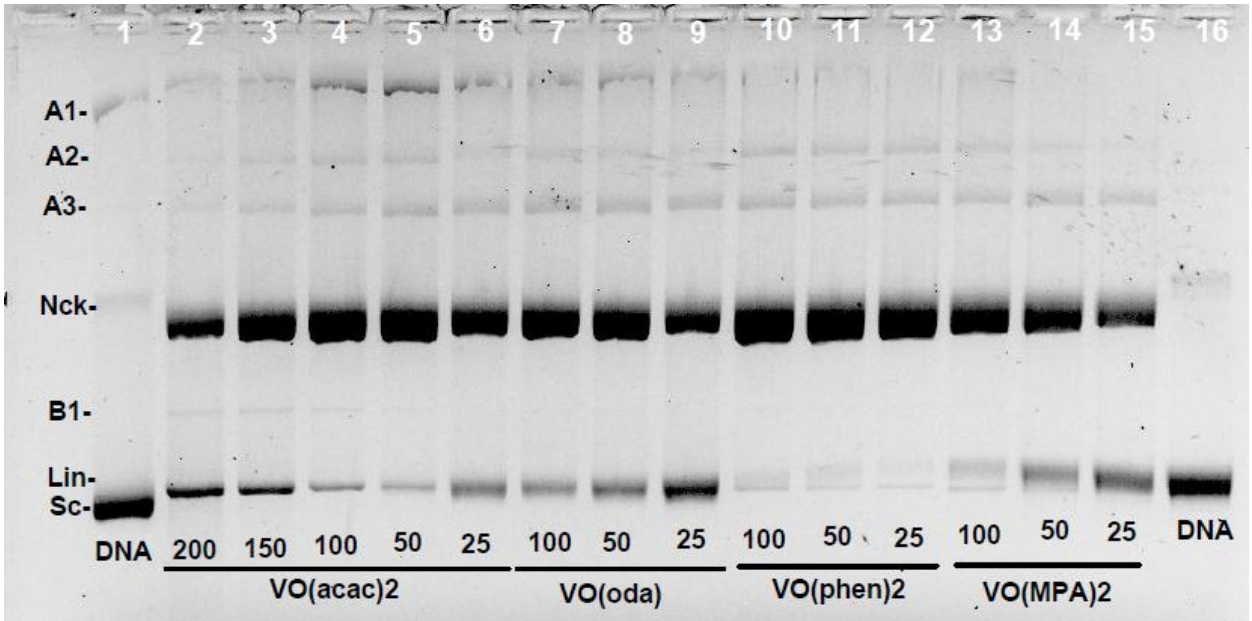

Figure A109. Understanding 'phantom bands'. Cleavage of pA1 DNA by **1**, **17, 20** and **22** under phosphate buffer. Tested concentrations are 25, 50, 100 and 200 µM (ri 1.7, 3.3, 6.7, 10 and 13.3). A1-A3 and B1 are so-called phantom bands detected when a complex promotes the scission of both single and double strands.

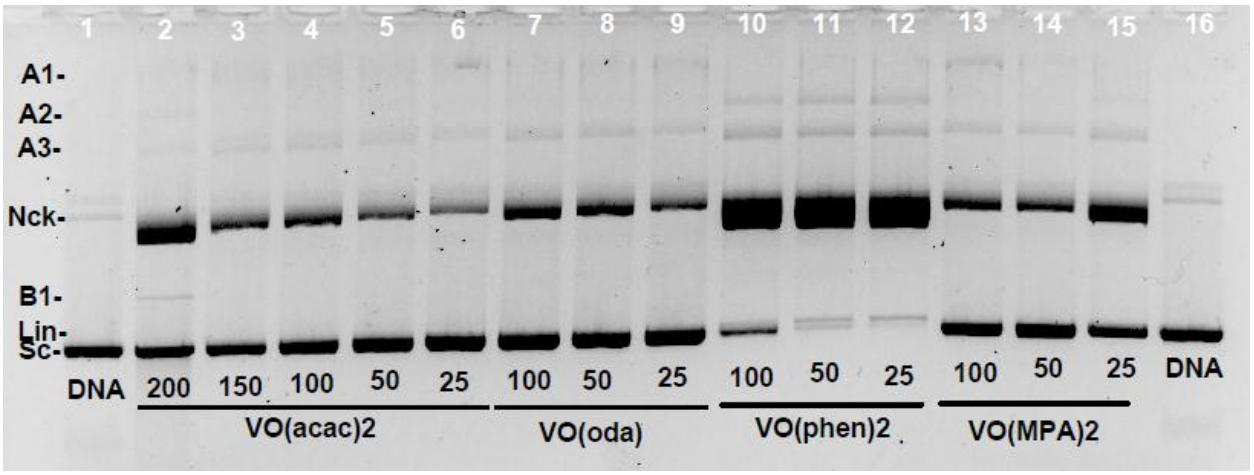

Figure A110. Understanding 'phantom bands'. Cleavage of pA1 DNA by **1**, **17, 20** and **22** under MOPS buffer. Tested concentrations are 25, 50, 100 and 200 µM (ri 1.7, 3.3, 6.7, 10 and 13.3). A1-A3 and B1 are so-called phantom bands detected when a complex promotes the scission of both single and double strands.

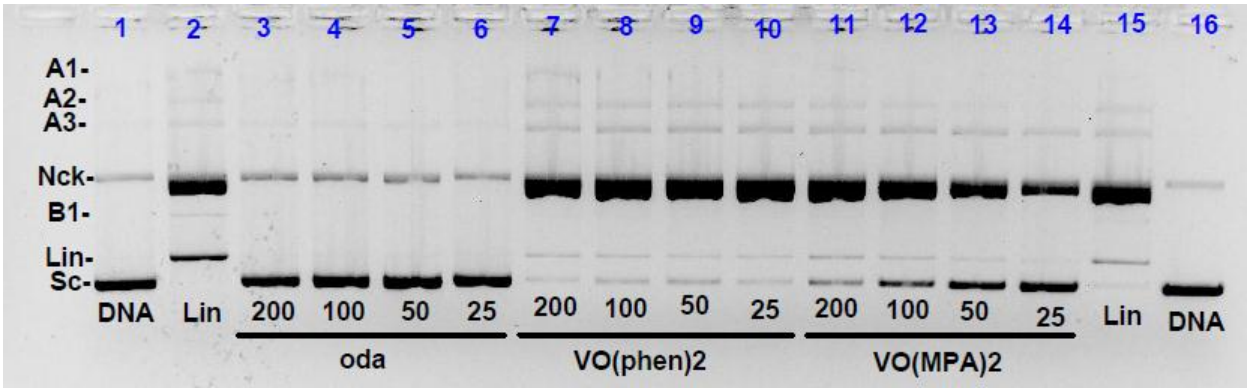

Figure A111. Understanding 'phantom bands'. Cleavage of pA1 DNA **17** and **22**at 25, 50, 100 and 200 µM (ri 1.7, 3.3, 6.7 and 13.3) under phosphate buffer (pH 7.4). Oda ligand was added for comparison as non-active agent towards pDNA activity. A1-A3 and B1 are observed phantom bands.

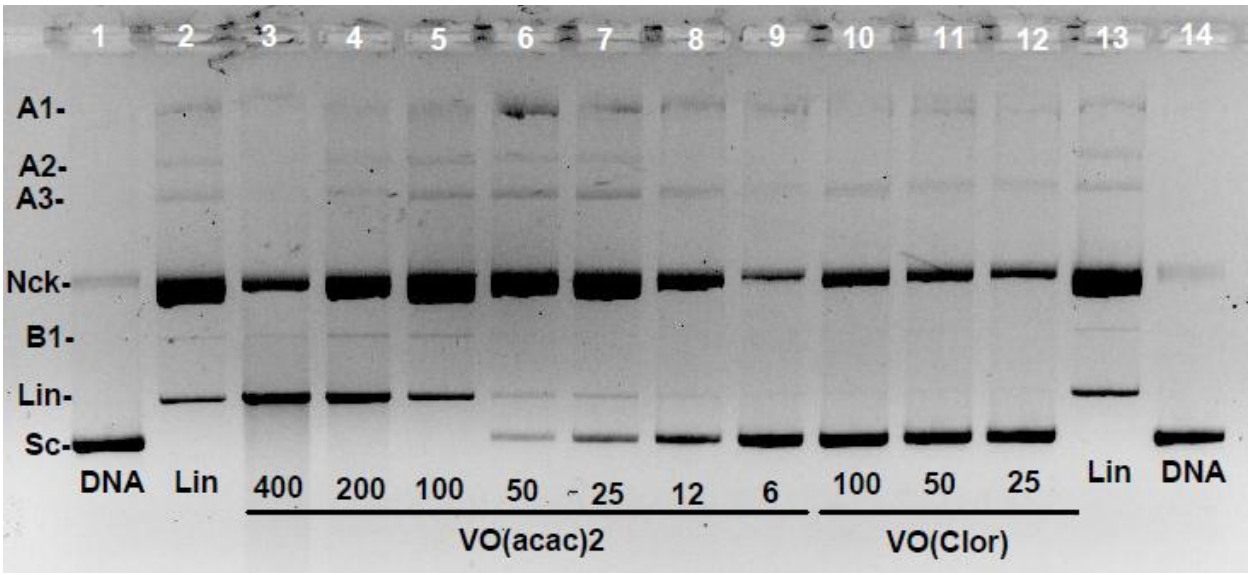

Figure A112. Understanding 'phantom bands'. Cleavage of pA1 DNA by **1** at 6, 12, 25, 50, 100, 200 and 400 (ri 0.4, 0.8, 1.7, 3.3, 6.7, 13.3 and 26.7) under phosphate buffer (pH 7.4). Complex **26** (ri 1.7, 3.3 and 6.7), as the one that does not induce significant cleavage, was added for comparison. A1-A3 and B1 are the observed phantom bands.

IX. Annex B

Cyclic and Square wave voltammograms of examined complexes

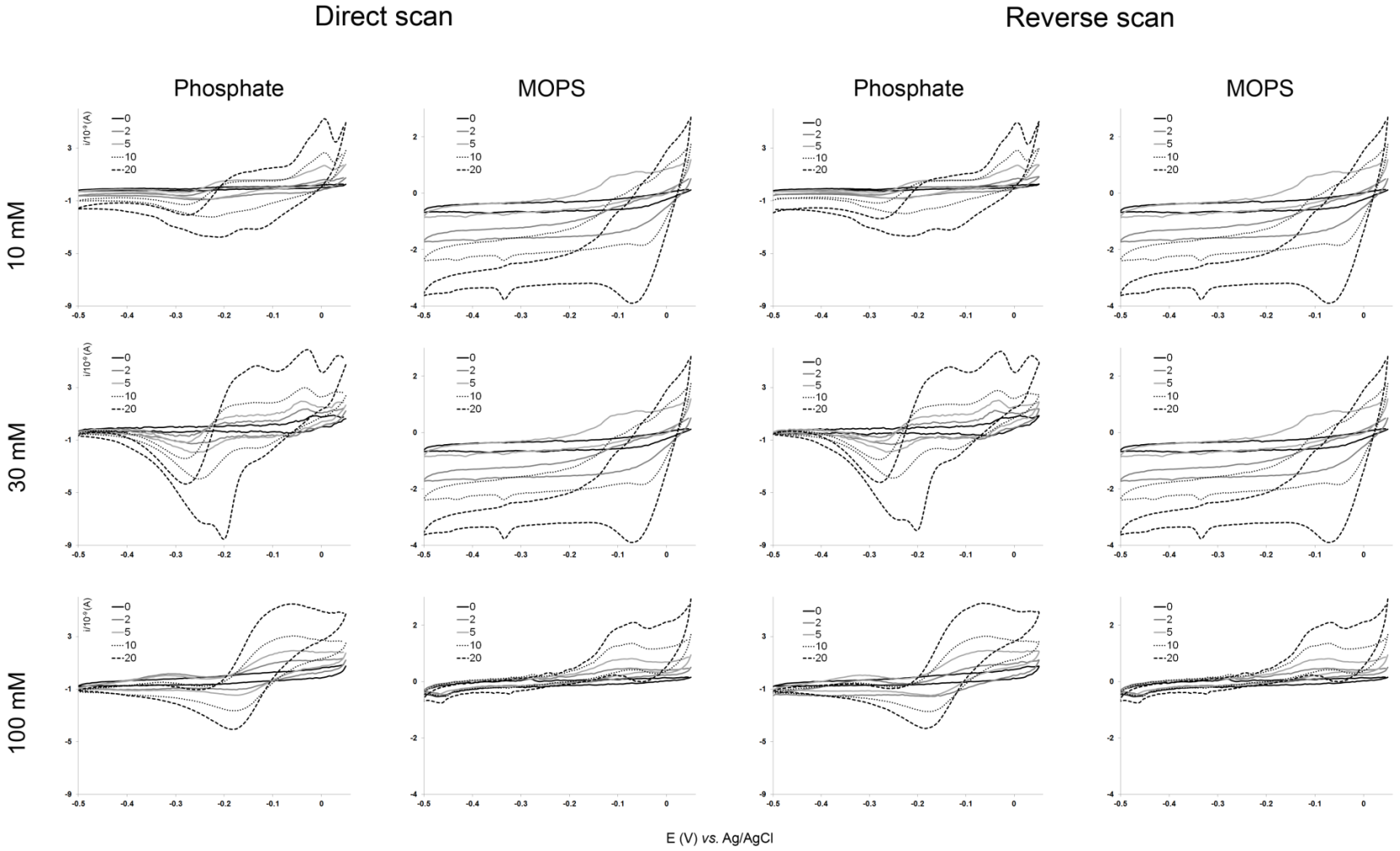

Figure B1. Cyclic voltammograms of 1 in 10, 30 and 100 mM phosphate and MOPS buffers.

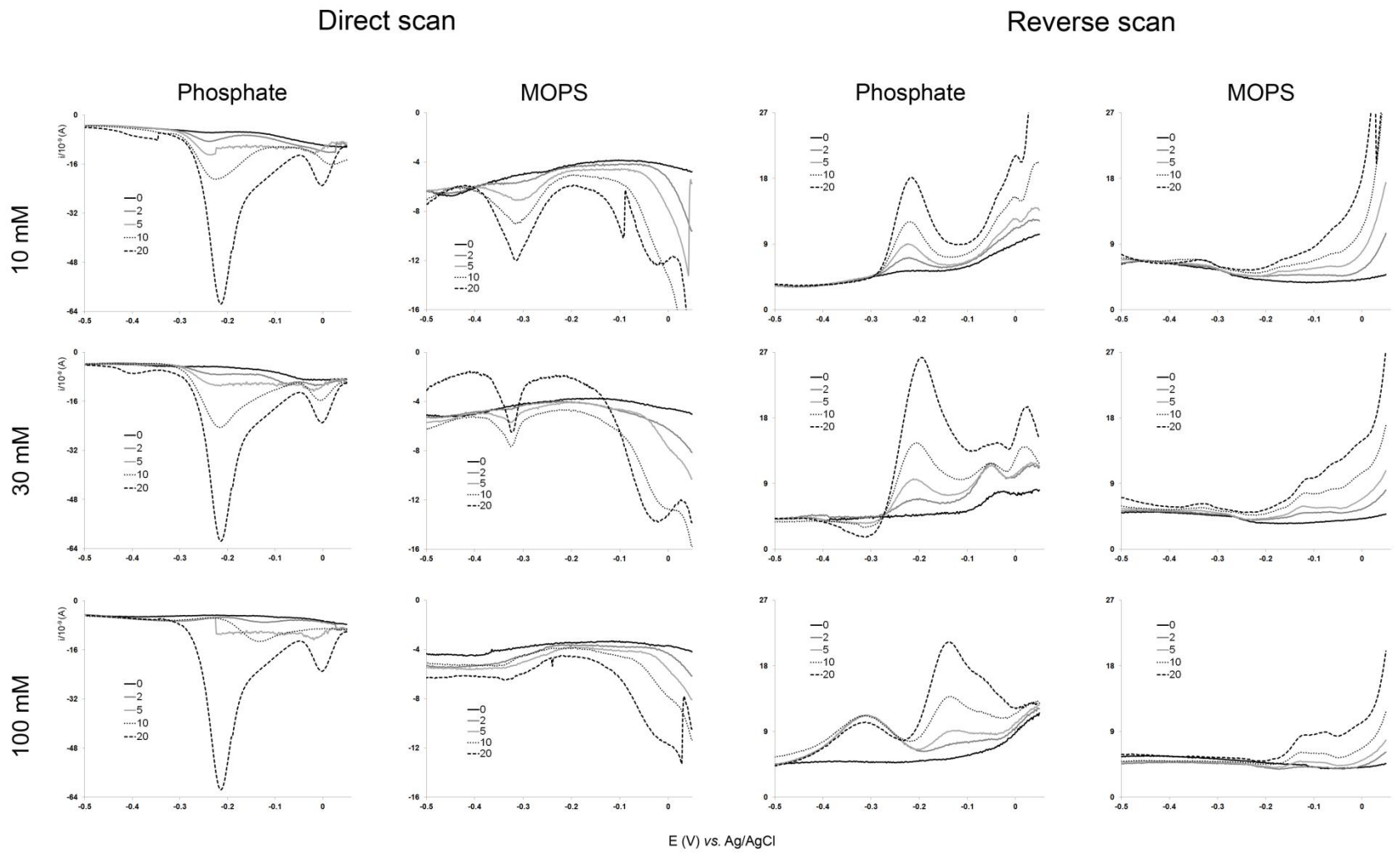

Figure B2. Square wave voltammograms of **1** in 10, 30 and 100 mM phosphate and MOPS buffers.

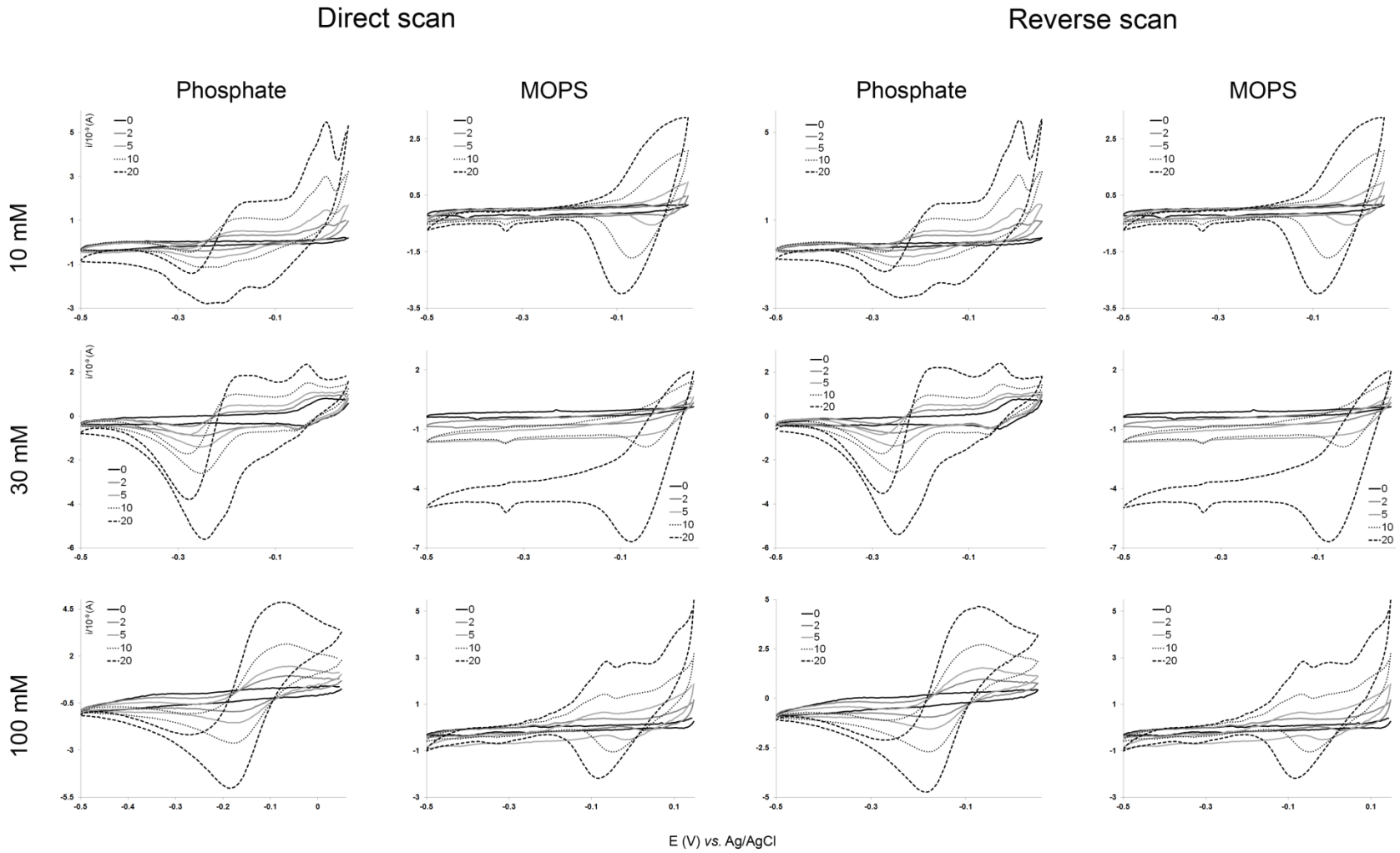

Figure B3. Cyclic voltammograms of **2** in 10, 30 and 100 mM phosphate and MOPS buffers.

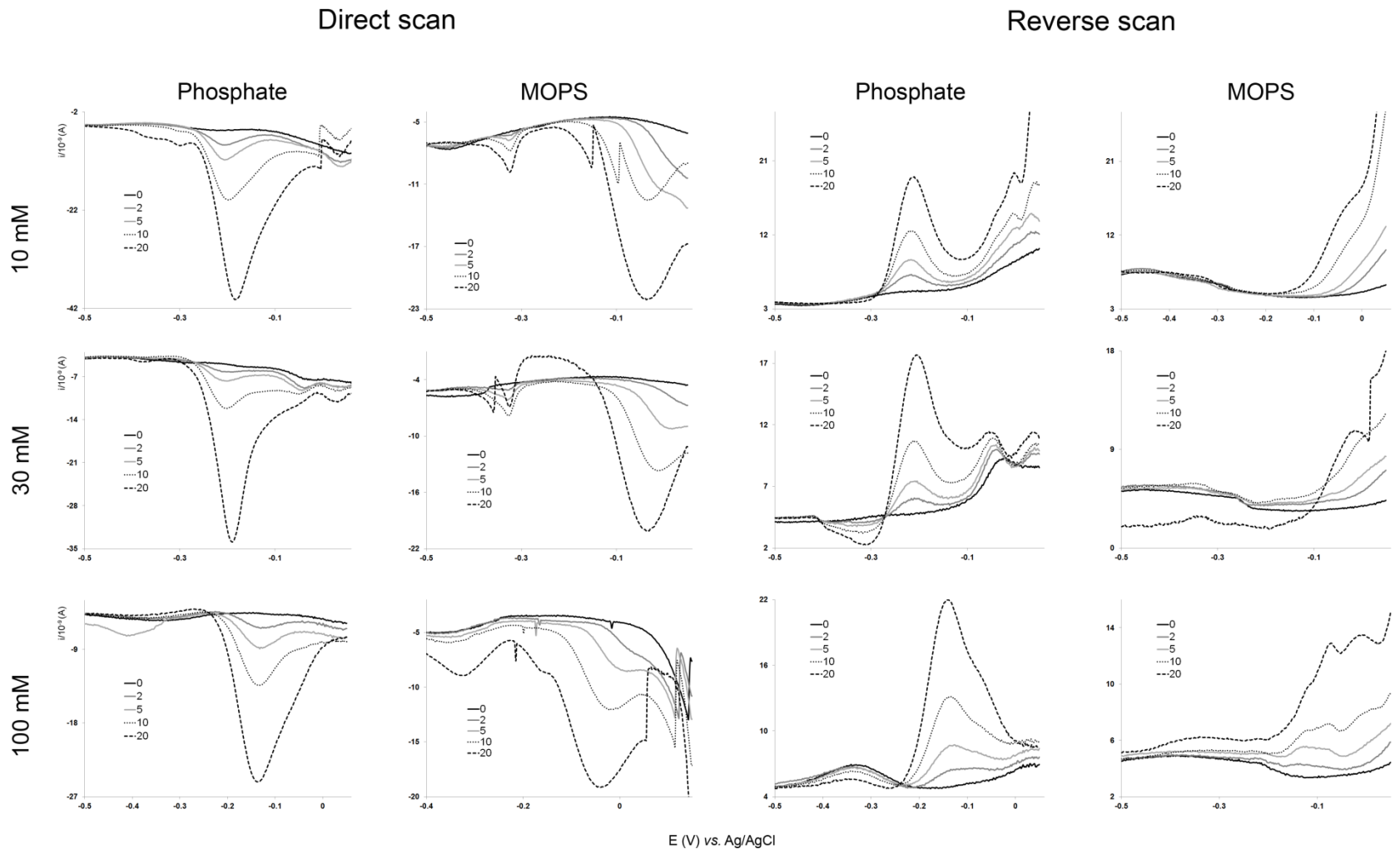

Figure B4. Square wave voltammograms of **2** in 10, 30 and 100 mM phosphate and MOPS buffers.

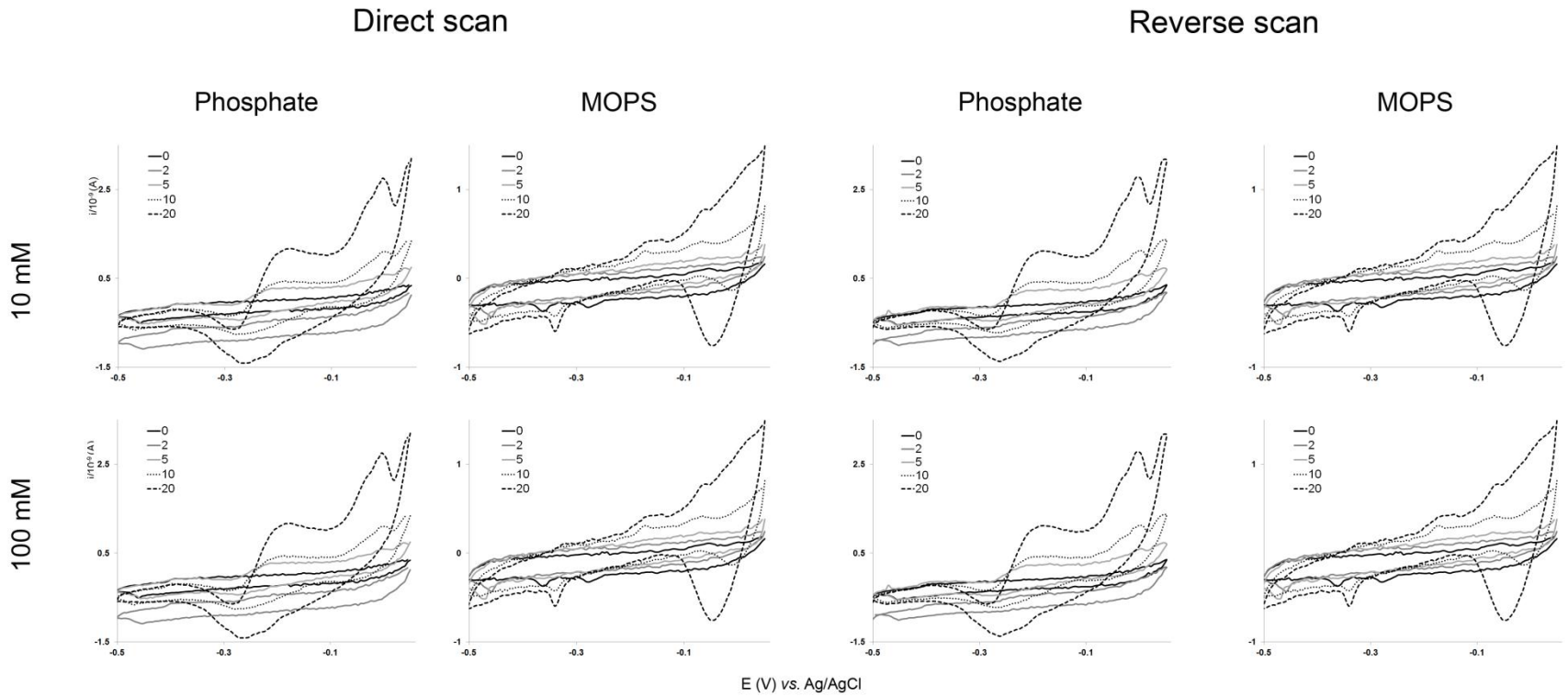

Figure B5. Cyclic voltammograms of **3** in 10 and 100 mM phosphate and MOPS buffers.

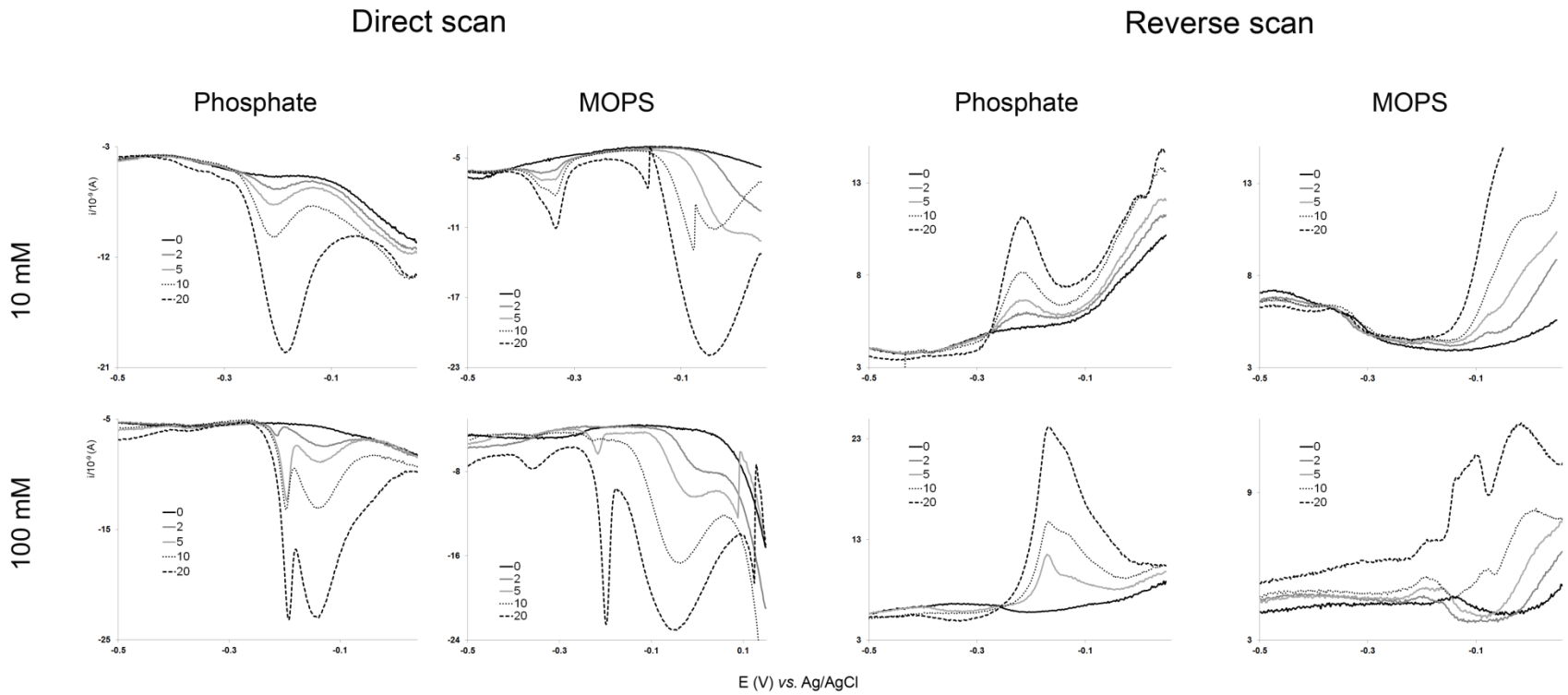

Figure B6. Square wave voltammograms of **3** in 10 and 100 mM phosphate and MOPS buffers.

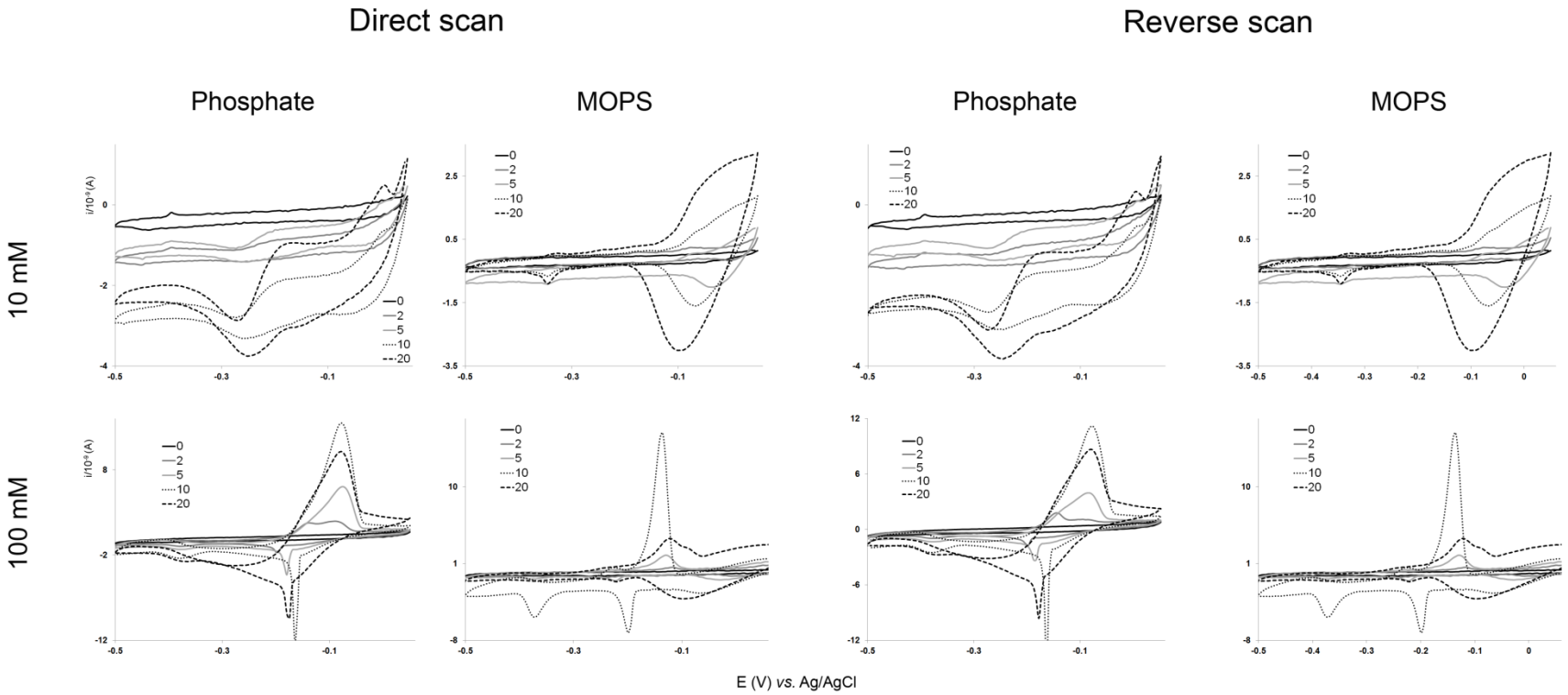

Figure B7. Cyclic voltammograms of **4** in 10 and 100 mM phosphate and MOPS buffers.

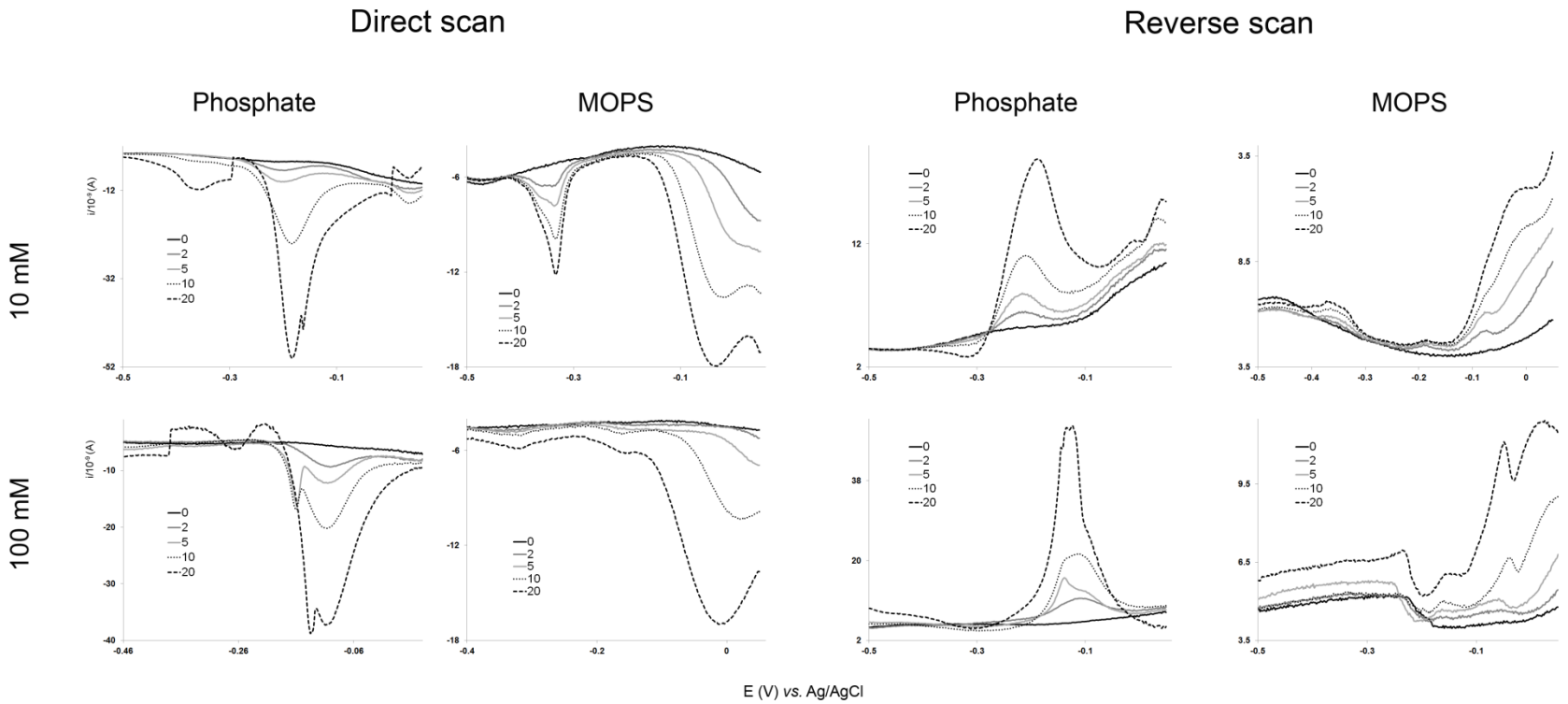

Figure B8. Square wave voltammograms of **4** in 10 and 100 mM phosphate and MOPS buffers.

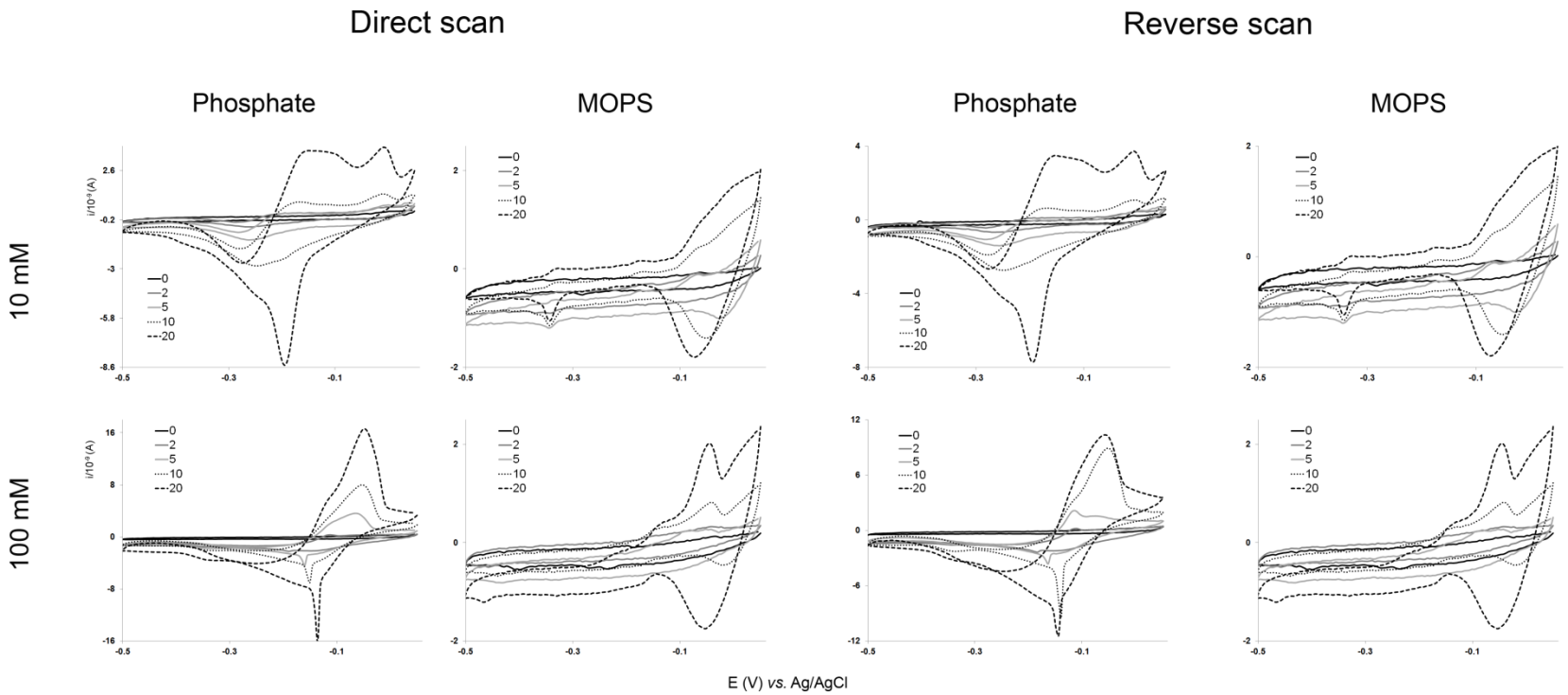

Figure B9. Cyclic voltammograms of **5** in 10 and 100 mM phosphate and MOPS buffers.

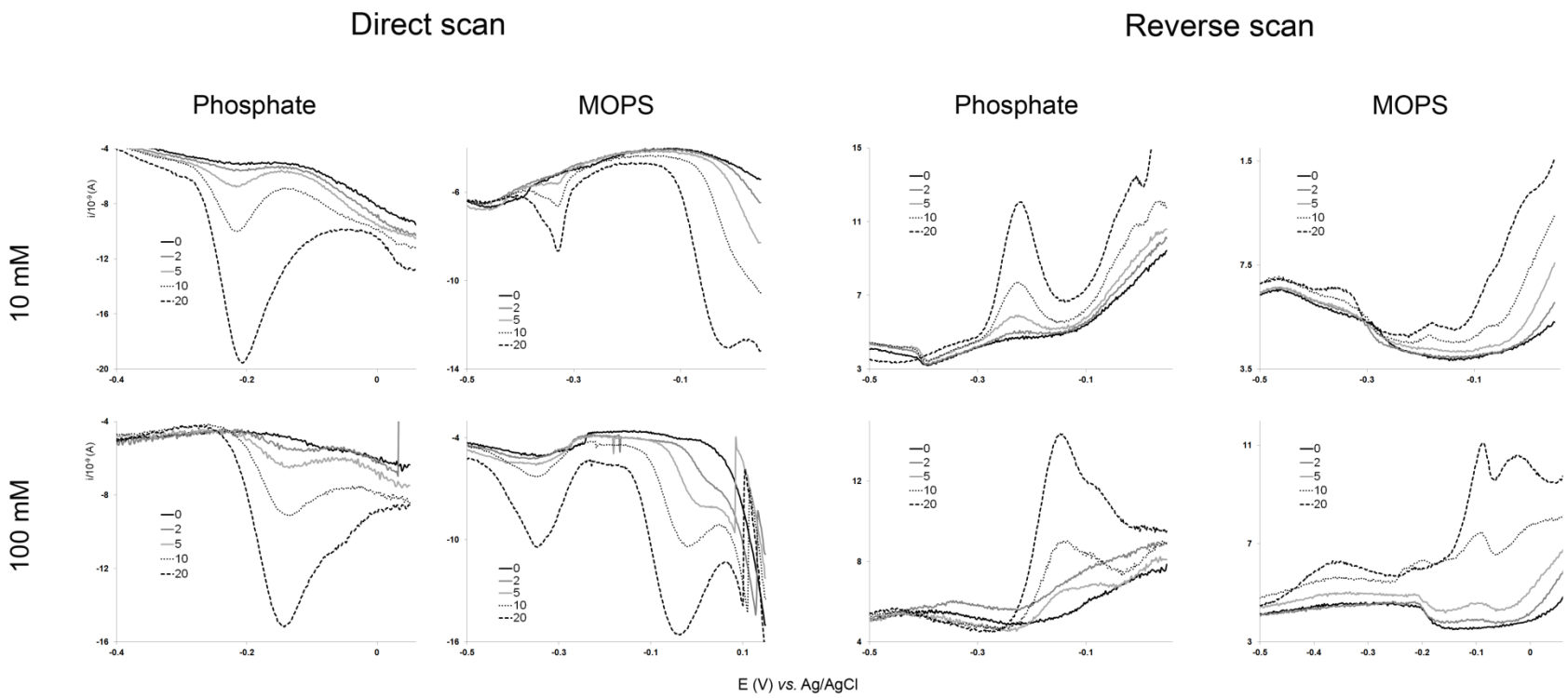

Figure B10. Square wave voltammograms of **5** in 10 and 100 mM phosphate and MOPS buffers.

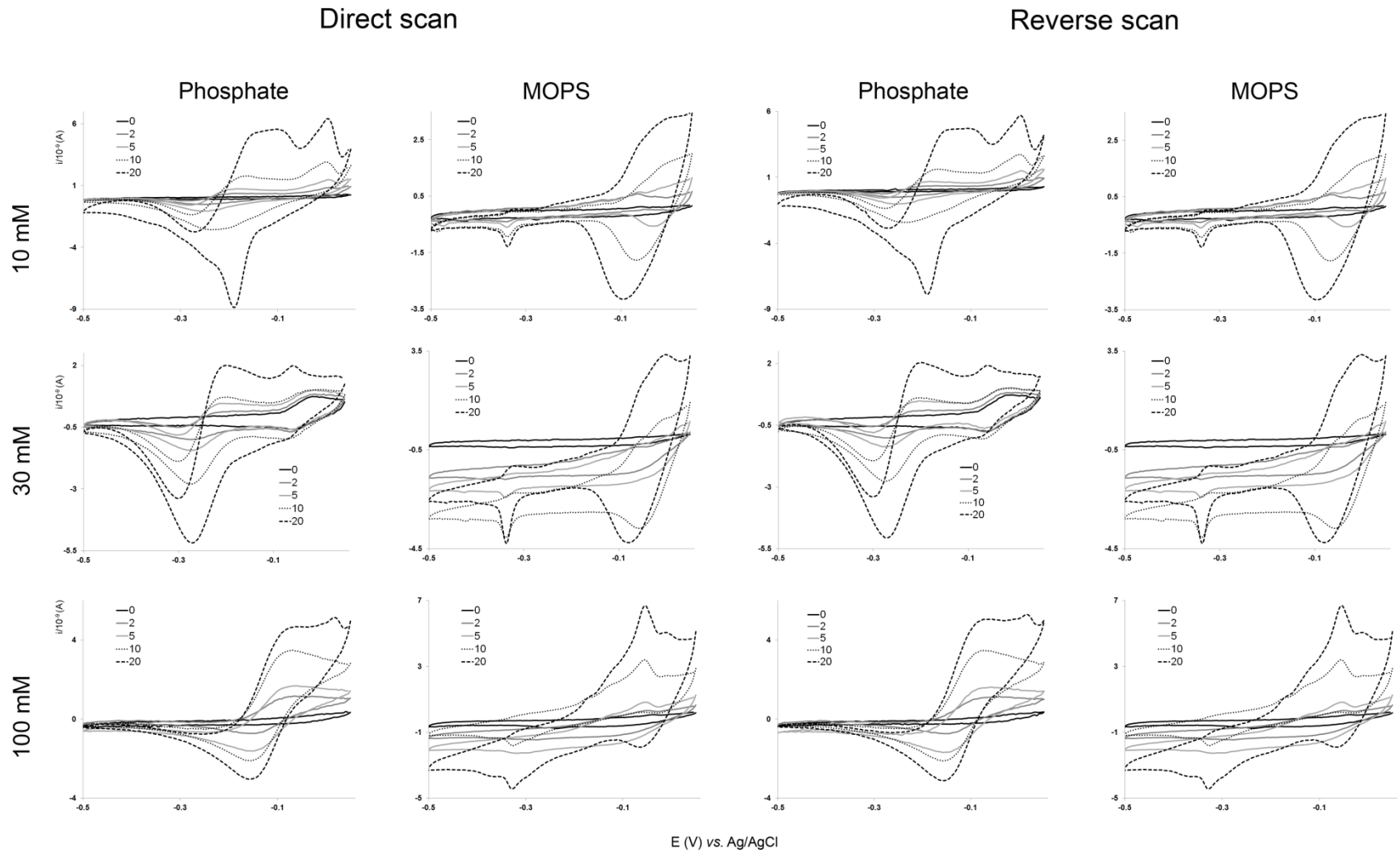

Figure B11. Cyclic voltammograms of **9** in 10, 30 and 100 mM phosphate and MOPS buffers.

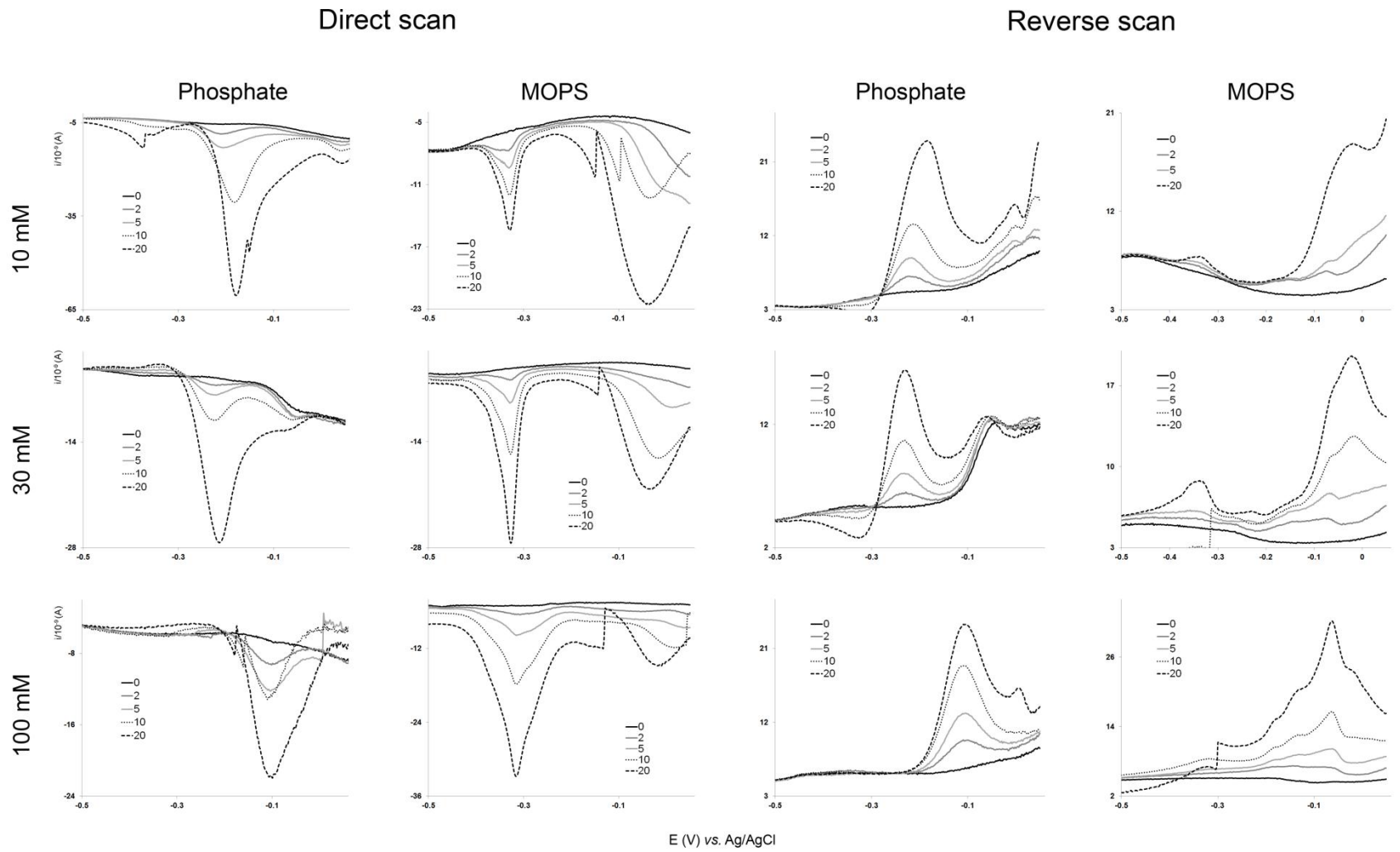

Figure B12. Square wave voltammograms of **9** in 10, 30 and 100 mM phosphate and MOPS buffers.

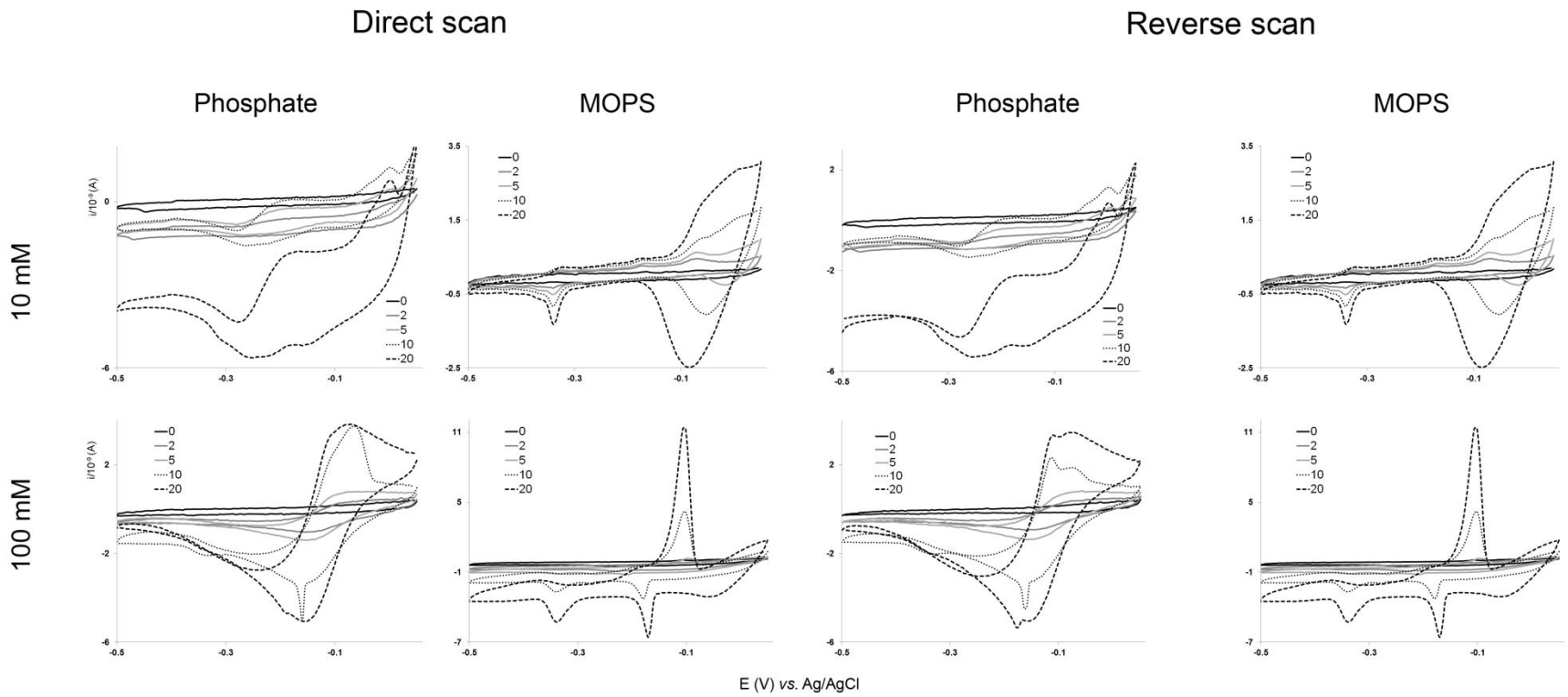

Figure B13. Cyclic voltammograms of VO(acac-NH_2)$_2$ in 10 and 100 mM phosphate and MOPS buffers.

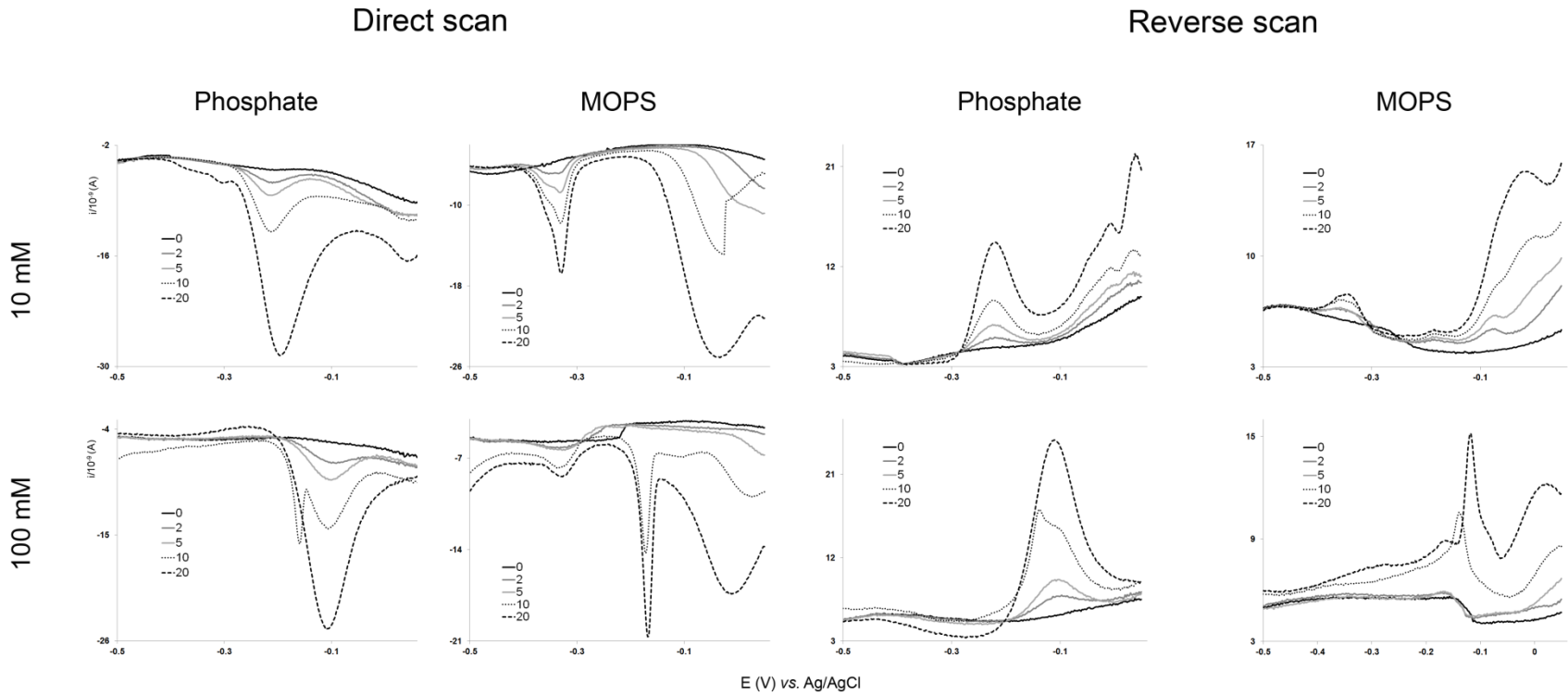

Figure B14. Square wave voltammograms of VO(acac-NH_2)$_2$ in 10 and 100 mM phosphate and MOPS buffers.

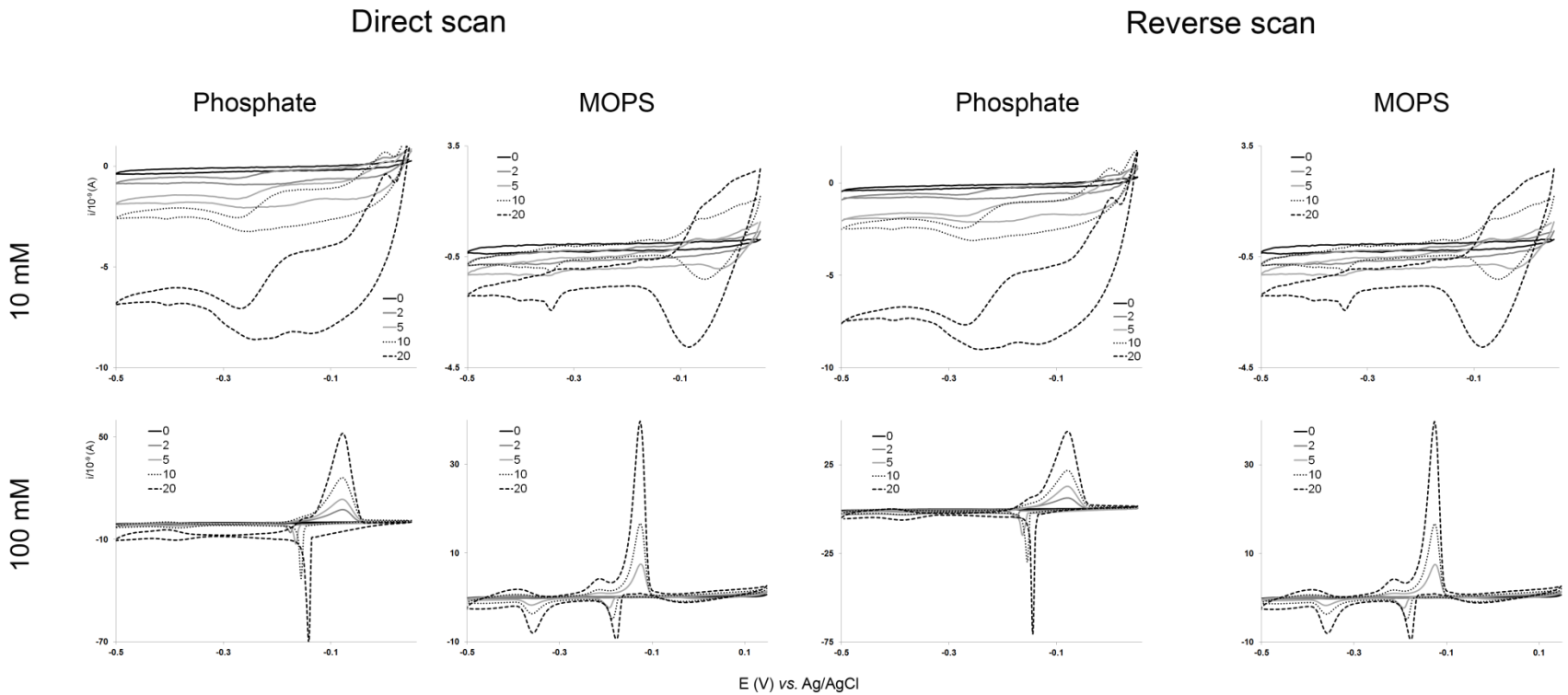

Figure B15. Cyclic voltammograms of VO(acac-NMe_2)$_2$ in 10 and 100 mM phosphate and MOPS buffers.

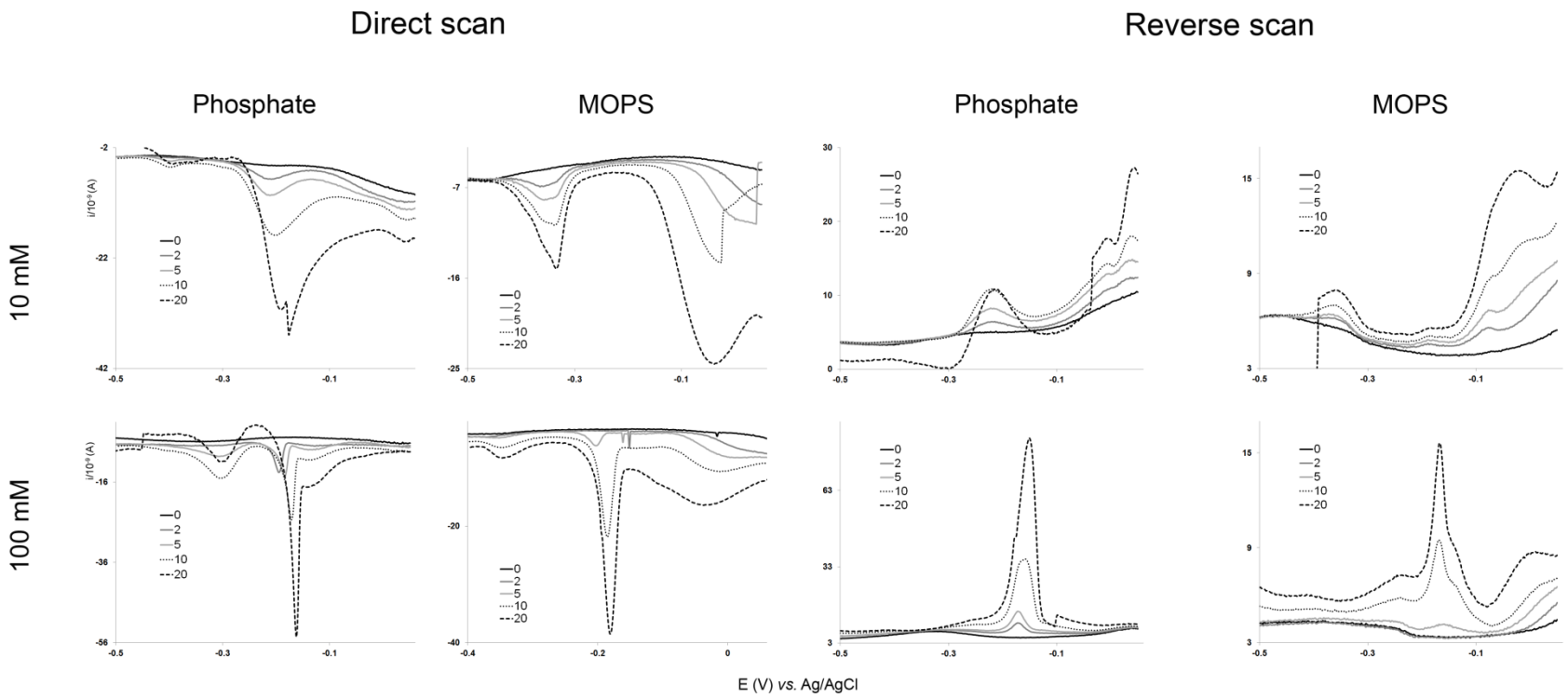

Figure B16. Square wave voltammograms of $VO(acac\text{-}NMe_2)_2$ in 10 and 100 mM phosphate and MOPS buffers.

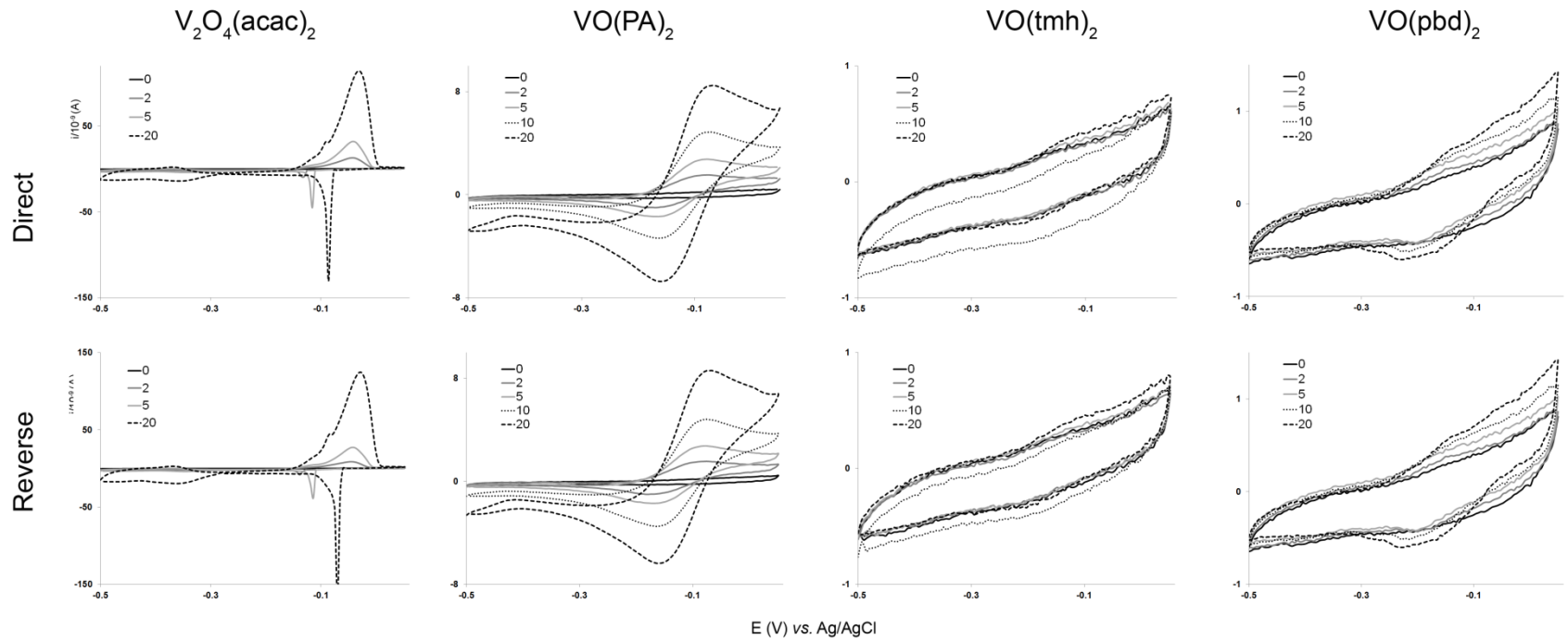

Figure B17. Cyclic voltammograms of **6**, $VO(PA)_2$, $VO(tmh)_2$ and $VO(pbd)_2$ under 100 mM phosphate buffer.

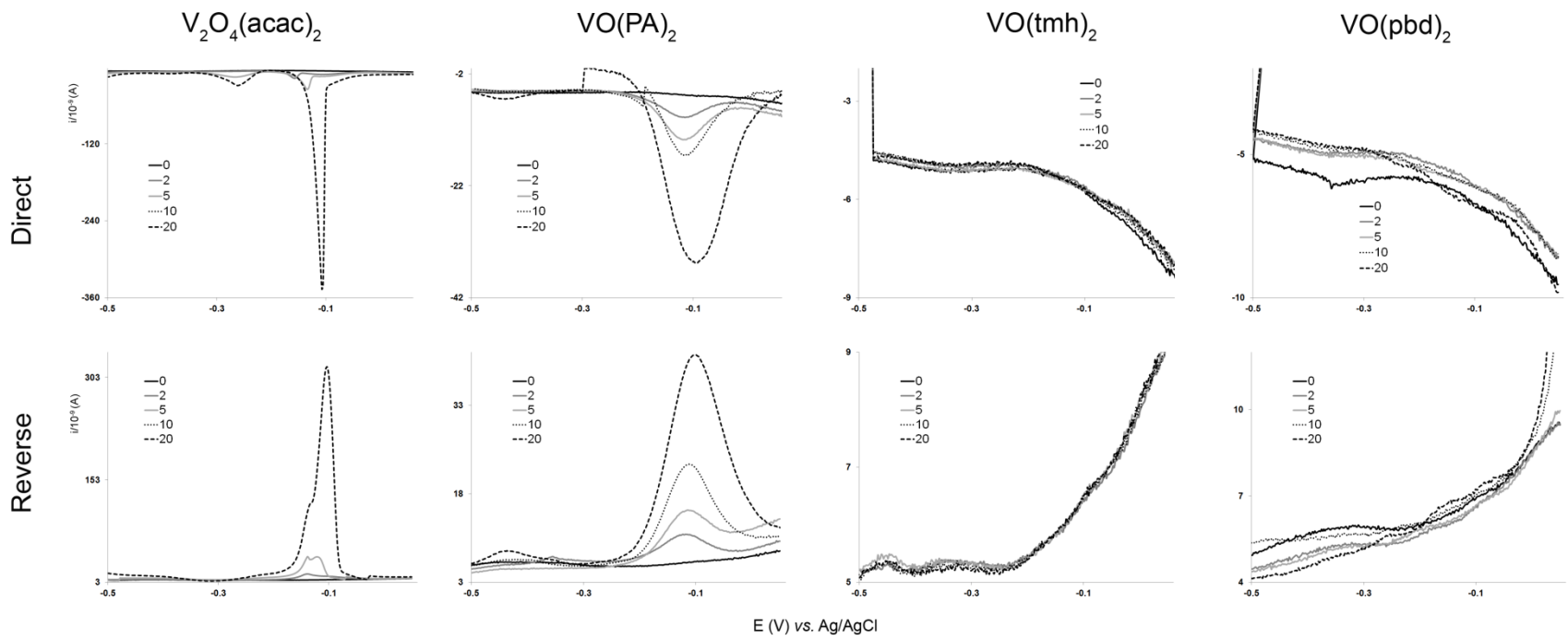

Figure B18. Square wave voltammograms of **6**, $VO(PA)_2$, $VO(tmh)_2$ and $VO(pbd)_2$ under 100 mM phosphate buffer.

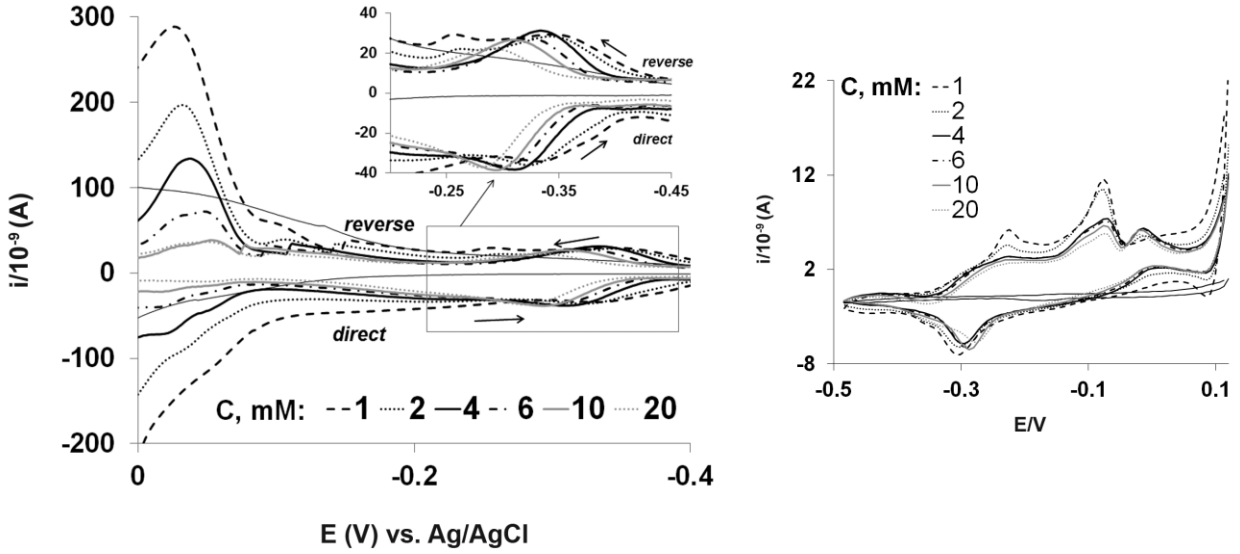

Figure B19. Square wave and cyclic (direct) voltammograms of **2** (50 µM) increasing concentration of phosphate buffer (1, 2, 4, 6, 10 and 20 mM).

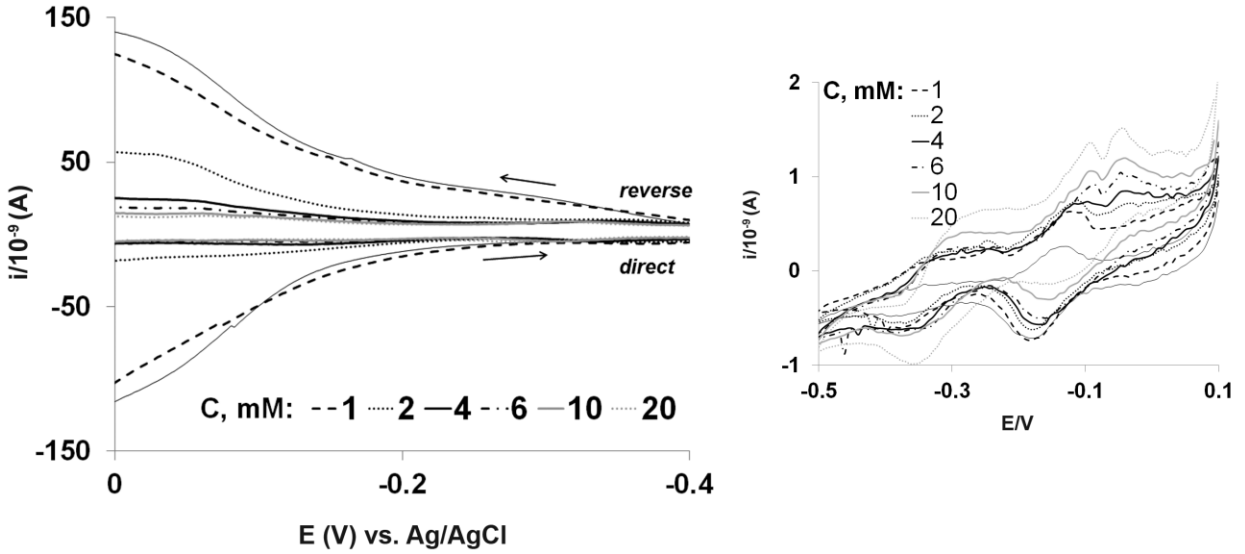

Figure B20. Square wave and cyclic (direct) voltammograms of **3** (50 µM) increasing concentration of phosphate buffer (1, 2, 4, 6, 10 and 20 mM).

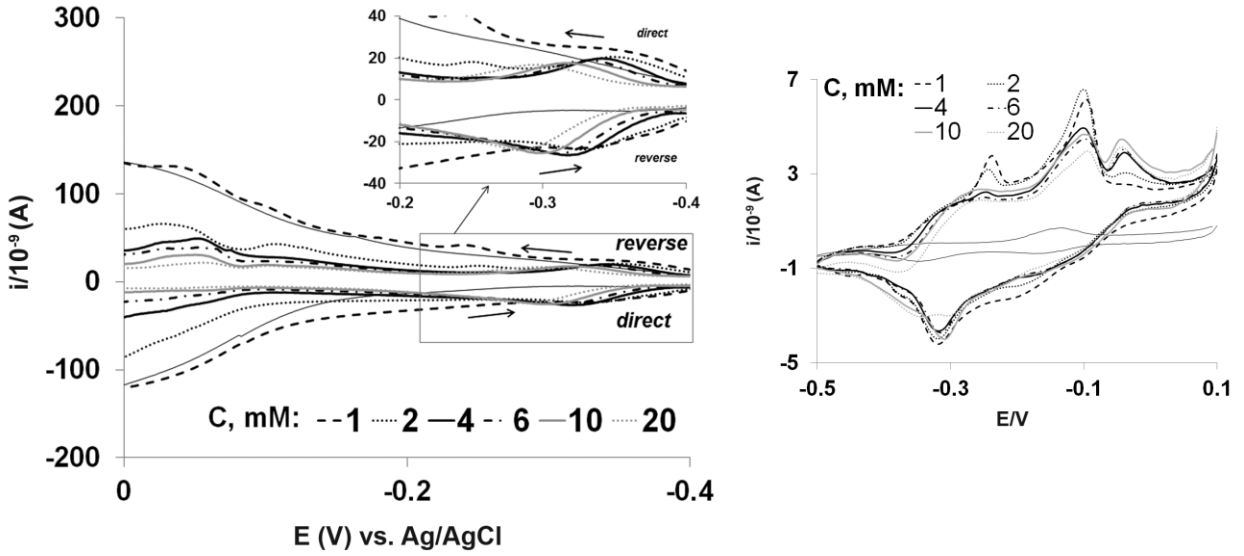

Figure B21. Square wave and cyclic (direct) voltammograms of **4** (50 µM) increasing concentration of phosphate buffer (1, 2, 4, 6, 10 and 20 mM).

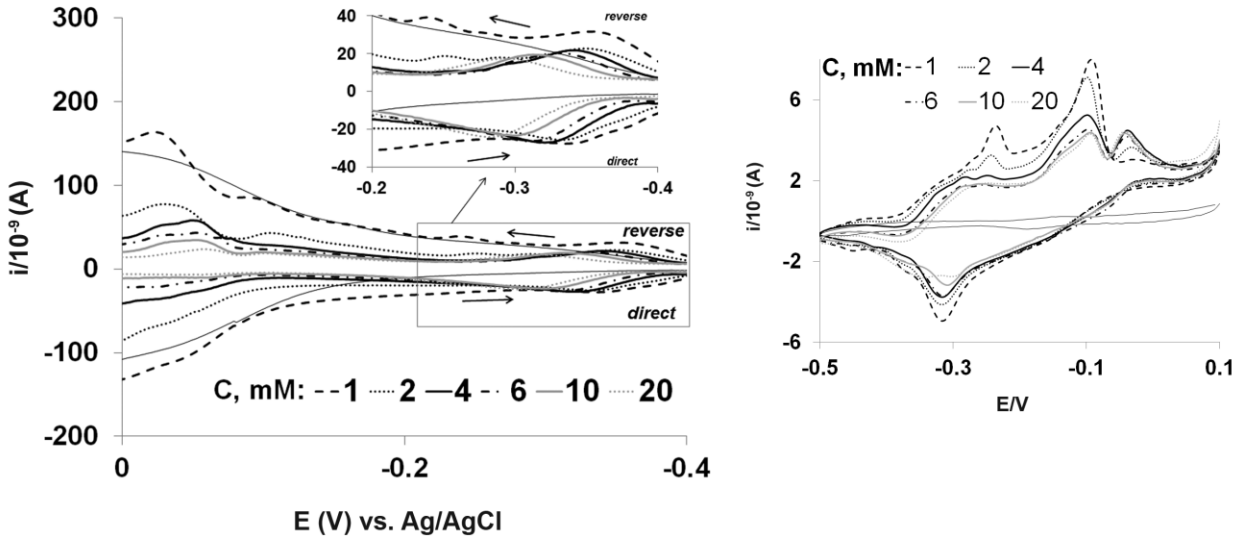

Figure B22. Square wave and cyclic (direct) voltammograms of **5** (50 µM) increasing concentration of phosphate buffer (1, 2, 4, 6, 10 and 20 mM).

References

X. References

1. Shechter, Y.; Shisheva, A. *Endeavour* **1993,** *17*, 27-31.
2. Orvig, C.; Caravan, P.; Gelmini, L.; Glover, N.; Herring, F.G.; Li, H.; McNeill, J.H.; Rettig, S.J.; Setyawati, I.A. *J. Am. Chem. Soc.* **1995**, *117*, 12759–12770.
3. Goldwaser, I.; Gefel, D.; Gershonov, E.; Fridkin, M.; Shechter, Y. *Biol. Inorg. Chem.* **2000**, *80,* 21-25.
4. Rehder, D.; Costa Pessoa, J.; Geraldes, C.F.G.C.; Castro, M.M.C.A.; Kabanos, T.; Kiss, T.; Meier, B.; Micera, G.; Pettersson, L.; Rangel, M.; Salifoglou, A.; Turel, I.; Wang, D. *Biol. Inorg. Chem.* **2002**, *7,* 384–396.
5. Evangelou, A.M. *Crit. Rev. Oncol. Hematol.* **2002**, *42,* 249–265.
6. Kostova, I. *Anti-Cancer Agents in Med. Chem.* **2009**, *9*, 827-842.
7. Weckhuysen, B.M.; Keller, D.E. *Catal. Today*, **2003**, *78*, 25-46.
8. Greenwood, N.N. *Catal. Today*, **2003**, *78*, 5-11.
9. Rehder, D. *Bioinorganic Chemistry of Vanadium*; John Wiley & Sons, Ltd: The Atrium, Southern Gate, Chichester, West Sussex, England, 2008; pp 31-34.
10. Rychcik M.; Skyllas-Kazacos, M. *J. Power Sources*, **1988**, *22*, 59-67.
11. Ligtenbarg, A.G.J; Hage, R.; Feringa, B.L. *Coord. Chem. Rev.* **2003***, 237*, 89-101.
12. Tracey, A.S.; Crans, D.C. In *Vanadium Compounds: Chemistry, Biochemistry, and Therapeutic Applications*; Tracey, A.S., Crans, D.C., Eds.; ACS Symposium Series 711; American Chemical Society: Washington, DC, 1998; pp 2-29.
13. Rehder, D. *Future Med. Chem.* **2012**, *4*, 1823-1837.
14. Burns, R.G. In *Mineralogical Applications of Crystal Field Theory*, 2nd ed.; Putris, A., Liebermann R.C. Eds.; Cambridge University Press: Cambridge, 1993.
15. Corathers, L.A., Gambogi, J.; Kuck, P.H.; Papp, J.F.; Polyak, D.E.; Shedd, K.B. In *Geological Survey Minerals Yearbook*: *Ferroalloys*; U.S. Geological Survey, 2010; pp 25.1-25.16.
16. Chasteen, N.D. In *Copper, Molybdenum and Vanadium in Biological Systems: Structure and Bonding;* Averill, B.A., Briggs, LeB.R., Chasteen, N.D., Gilbert, T.R., Kustin, K., McLeod, G.C., Penfield, K.W., Solomon, E.I., Wilcox D.E., Eds.; Springer: Berlin Heidelberg; 1983; Vol. 53, pp 105-138.
17. Boas, L.F.V.; Costa Pessoa, J. In *Comprehensive Coordination Chemistry: Vanadium*; Wilkinson, G., Gillard, R.D., McCleverty J.A. Eds.; Pergamon: Oxford, 1987; Vol. 3, pp 453–583.
18. Reul, B.A.; Amin, S.S.; Buchet, J.P.; Ongemba, L.N.; Crans, D.C.; Brichard, S.M. *British J. Pharmocol.* **1999**, *126*, 467-477.
19. Crans, D.C.; Bunch, R.L.; Theisen, L.A. *J. Am. Chem. Soc.* **1989**, *111,* 7597-7607.
20. Selling, A.; Andersson, I.; Pettersson, L.; Schramm, C.M.; Downey, S.L.; Grate, J.H. *Inorg. Chem.* **1994**, *33*, 3141-3150.
21. Pettersson, L.; Andersson, I.; Gorzsás, A. *Coord. Chem Rev.* **2003**, *237,* 77-87.
22. Gorzsás A.; Andersson, I.; Pettersson, L. *J. Inorg. Biochem.* **2009**, *103*, 517-526.
23. Gorzsás, A.; Getty, K.; Andersson, I.; Pettersson, L. *Dalton Trans*. **2004**, 2873-2882.
24. Andersson, I.; Gorzsás A.; Pettersson, L. *Dalton Trans*. **2003**, 2503-2511.
25. Andersson, I.; Gorzsás A.; Kerezsi, C.; Toth, I.; Pettersson, L. *Dalton Trans.* **2005**, 3658–3666.
26. Kiss, T.; Kiss, E.; Garribba, E.; Sakurai, H. *J. Inorg. Biochem.* **2000**, *80*, 65-73.
27. Crans, D.C.; Jiang, F.; Boukhobza, I.; Bodi, I.; Kiss, T. *Inorg. Chem.* **1999**, *38,* 3275-3282.
28. Kiss, T.; Kiss, E.; Micera, G.; Sanna, D. *Inorg. Chim. Acta* **1998**, *283*, 202-210.
29. Crans, D.C.; Yang, L.; Jakush, T.; Kiss, T. *Inorg. Chem.* **2000**, *39*, 4409-4416.
30. Jakush, T.; Jin, W.; Yang, L.; Kiss, T.; Crans, D.C. *J. Inorg. Biochem.* **2003**, *95*, 1-13.
31. Crans, D.C.; Smee, J.J.; Gaidamauskas, E.; Yang L. *Chem. Rev*. **2004**, *104*, 849-902.
32. Jakush, T.; Costa Pessoa, J.; Kiss, T. *Coord. Chem. Rev.* **2011**, *255*, 2218-2226.
33. Correia, I.; Jakush, T.; Cobbinna, E.; Mehtab, S.; Tomaz, I.; Nagy, N.V.; Rockenbauer, A.; Costa Pessoa, J.; Kiss, T. *Dalton Trans*. **2012**, *41*, 6477–6487.
34. Alberico, E.; Micera, G. *Inorg. Chim. Acta* **1994**, *215*, 225-227.
35. Butler, A.; Clague, M.J.; Meister, J.E. *Chem. Rev*. **1994**, *94*, 625-638.
36. Dikanov, S.A.; Liboiron, B.D.; Orvig, C. *J. Am. Chem. Soc.* **2002**, *124*, 2969-2978.
37. Ishii, T.; Nakai, I.; Numako, C.; Okoshi, K.; Otake, T. *Naturwissenschaften* **1993**, *80*, 268-270.

38. Kanda, T.; Nose, Y.; Wuchiyama, J.; Uyama, T.; Moriyama, Y.; Michibata, H. *Zool. Sci*. **1997**, 14, 37-42.
39. Orvig, C.; Thompson, K.H.; Liboiron, B.D.; McNeill, J.H.; Yuen, V.G. *J. Inorg. Biochem*. **2003**, *96*, 14 (abstr. presented by C. Orvig at ICBIC 11, Cairns, QLD, Australia, 2003).
40. Antipov, A.N.; Lyalikova, N.N.; Khijniak, T.V.; L'vov, N. P. *FEBS Lett.* **1998**, *441*, 257-260.
41. Antipov, A. N.; Sorokin, D. Y.; L'Vov, N. P.; Kuenen, J. G.*Biochem. J.* **2003**, *369*, 185-189.
42. French, R. J.; Jones, P.J.H. *Life Science* **1993**, *52*, 339-346.
43. Costa Pessoa, J.; Tomaz, I. *Curr. Med. Chem*. **2010**, *17*, 3701-3738.
44. Rehder, D. *Angew. Chem. Int. Ed. Engl*. **1991**, *30,* 148-167.
45. Crans, D.C. *Pure Appl. Chem.* **2005**, *77*, 1497–1527.
46. Oltz, E.M.; Bruening, R.C.; Smith, M.J.; Kustin, K.; Nakanishi, K. *J. Am. Chem. Soc.*, **1988**, *110*, 6162–6172.
47. Michibata, H.; Uyama, T.; Kanamori, K. In *Vanadium Compounds: Chemistry, Biochemistry and Therapeutic Applications*; Tracey, A.S., Crans, D.C., Eds.; ACS Symposium Series 711; American Chemical Society: Washington, DC, 1998; pp 248-258.
48. Michibata, H.; Yamaguchi, N.; Uyama T.; Ueki, T. *Coord. Chem. Rev*. **2003**, *237*, 41–51.
49. Treberg, J.R.; Stacey, J.E.; Driedzic, W.R. *Comp. Biochem. Physiol. B* **2012**, *161*, 323–330.
50. Garner, C.D.; Armstrong, E.M.; Berry, R.E.; Beddoes, R.L.; Collison, D.; Cooney, J.J.A.; Ertok, S.N.; Helliwell, M. *J. Inorg. Biochem.* **2000**, 80, 17–20.
51. Matoso, C.M.M.; Pombeiro, A.J.L.; Fraústo da Silva, J.J.R.; Silva, M.F.C.G.; Silva, J.A.L.; Baptista-Ferreira, J.L.; Pinho-Almeida, F. *In Vanadium Compounds: Chemistry, Biochemistry and Therapeutic Applications; Tracey, A.S., Crans, D.C., Eds.; ACS Symposium Series 711; American Chemical Society: Washington, DC, 1998;* Chapter 18, pp 241-247.
52. Silva, J.A.L.; Frausto da Silva, J.J.R.; Pombeiro, A.J.L. *Chem. Commun.* **2013**, 2388-2400.
53. Guedes da Silva, M.F.C.; Silva, J.A.L; Fraústo da Silva, J.J.R.; Pombeiro, A.J.L.; Amatore, C.; Verpeaux, J.N. *J. Am. Chem. Soc*.**1996**, *118*, 7568-7573.
54. Reis, P.M.; Silva, J.A.L.; Palavra, A.F.; Frausto da Silva, J.J.R.; Kitamura, T.; Fujiwara, Y.; Pombeiro, A.J.L. *Angew. Chem., Int. Ed*. **2003**, 42, 821-823.
55. Hubregtse, T.; Neeleman, E.; Maschmeyer, T.; Sheldon, R.A.; Hanefeld, U.; Arends, I.W.C.EJ. Inorg. Biochem. **2005**, *99*, 1264–1267.
56. Wever, R., Tromp, M.C.M.; Krenn, B.E.; Marjani A.; Van Tol, M. *Environ. Sci. Technol.* **1991**, *25*, 446–449.
57. Eady, R. R. *Coord. Chem. Rev.* **2003**, *237*, 23-30.
58. Robson, R.L.; Eady, R.R.; Richardson, T.H.; Miller, R.W.; Hawkins M. Postgate, J.R. *Nature* **1986**, *322*, 388–390.
59. Dilworth, M.J.; Eady, R.R. *Biochem. J*. **1991**, *277*, 465–468.
60. Fay, A.W.; Blank, M.A.; Lee, C.C. *J. Am. Chem. Soc.* **2010**, *132*, 12612–12618.
61. Hu, Y.; Lee, C.C.; Ribbe, M.W. *Science* **2011**, *333*, 753–755.
62. Rehder, D. *Inorg. Chem. Comm*. **2003**, *6*, 604–617.
63. Thompson, K.H., Orvig C. *J. Inorg. Biochem.* **2006**, *100,* 1925–1935.
64. Elvingson, K.; Crans, D. C.; Pettersson, L. *J. Am. Chem. Soc.* **1997**, *119*, 7005-7012.
65. Crans, D.C.; Simone, C.M.; Blanchard, J.S. *J. Am. Chem. Soc.* **1992**, *114*, 4926-4928.
66. Crans, D.C.; Marshman, R.W.; Nielsen, R.; Felty, I. *J. Org.Chem.* **1993**, *58*, 2244-2252.
67. Lindquist, R.N.; Lynn, J.L. Jr.; Lienhard, G.E. *J. Am. Chem.Soc.* **1973**, *95*, 8762-8768.
68. Berger, S.L.; Birkenmeier, C.S. *Biochem.* **1979**, *18*, 5143-5149.
69. Brichard, S.M.; Henquin J.C. *Trends Pharm. Sci.* **1995**, *16*, 265-270.
70. Thompson, K.H.; McNeill, J.H.; Orvig C. *Chem. Rev*. **1999**, *99*, 2561-2562.
71. Sakurai, H. *Chem. Records* **2002**, *2*, 237-248.
72. Sakurai, H.; Tamura, A.; Fugono, J.; Yasui, H.; Kiss, T. *Coord. Chem. Rev.* **2003**, *245*, 31–37.
73. Srivastava, A.K. Mehdi, M.Z. *Diabetic Medicine*, **2004**, *22*, 2–13.
74. Thompson, K.H.; Orvig, C. *Met. Ions Biol. Syst.* **2004**, *41*, 221–252.
75. Sakurai, H.; Katoh, A.; Yoshikawa, Y. *Bull. Chem. Soc. Jpn*. **2006**, *79*, 1645–1664.
76. Goc, A. *Centr. Europ. J. Biol*. **2006**, *1,* 314–332.

77. Thompson, K.H.; Lichter, J.; LeBel, C.; Scaife, M.C.; McNeill, J.H.; Orvig, C. *J. Inorg. Biochem*. **2009**, *103*, 554–558.
78. Desoize, B. *Crit. Rev. Oncol. Hematol.* **2002**, *42*, 1-3.
79. Somerville, J.; Davies, B. *Am. Heart J.* **1962**, *64*, 54–56.
80. Kivelson, D.; Lee, S.L.; *J. Chem. Phys*. **1964**, *41*, 1896–1903.
81. Tolman, E.L.; Barris, E.; Burns, M.; Pansini A.; Partridge, R. *Life Sci.* **1979**, *25*, 1159–1164.
82. Shechter, Y.; Karlish, S.J.D. *Nature* **1980**, *284*, 556–558.
83. Heyliger, C.E.; Tahiliani, A.G.; McNeill, J.H. *Science* **1985**, *227*, 1474–1477.
84. Kadota, S.; Fantus, I.G.; Deragon, G.; Guyda, H.J.; Hersh B.; Posner, B.I. *Biochem. Biophys. Res. Commun*. **1987**, *147*, 259–266.
85. Fantus, I.G.; Kadota, S.; Deragon, G.; Foster, B.; Posner, B.I. *Biochem*. **1989**, *28*, 8864–8871.
86. Brichard, S.M.; Pottier, A.M.; Henquin, J.C. *Endocrin*. **1989**, *125*, 2510–2516.
87. Pederson, R.A.; Ramanadham, S.; Buchan, A.M.J.; McNeill, J.H. *Diabetes* **1989**, *38* 1390–1395.
88. Brichard, S.M.; Bailey, C.J.; Henquin, J.-C. *Diabetes* **1990**, *39*, 1326–1332.
89. Thompson, K.H.; Leichter, J.; McNeill, J.H. *Biochem. Biophys. Res.Commun*. **1993**, *197*, 1549–1555.
90. Ramanadham, S.; Mongold, J.J.; Brownsey, R.W.; Cros G.H.; McNeill, J.H. *Am. J. Physiol*. **1989**, *257*, 904–911.
91. Villani, P.; Cordelli, E.; Leopardi, P.; Siniscalchi, E.; Veschetti, E.;Fresegna, A.M.; Crebelli, R. *Toxicol. Lett.* **2007**, *170*, 11–18.
92. Sakurai, H.; Tsuchiya, K.; Nukatsuka, M.; Kawada, J.; Ishikawa, S.; Yoshida, H.; Komatsu, M. *J. Clin. Biochem. Nutr.* **1990**, *8*, 193–200.
93. McNeill, J.H.; Yuen, V.G.; Hoveyda, H.R.; Orvig, C. *J. Med. Chem.* **1992**, *35*, 1489–1491.
94. Orvig, C.; Thompson, K.H.; Battell, M.; McNeill, J.H. *Met. Ions Biol. Syst.* **1995**, *31*, 575–594.
95. Caravan, P.; Gelmini, L.; Glover, N.; Herring, F.G.; Li, H.; McNeill, J.H.; Rettig, S.J.; Setyawati, I.A.; Shuter, E.; Sun, Y.; Tracey, A.S.; Yuen, V.G.; Orvig, C. *J. Am. Chem. Soc.* **1995**, *117*, 12759–12770.
96. Thompson, K.H.; Yuen, V.G.; McNeill, J.H.; Orvig, C. In *Vanadium Compounds: Chemistry, Biochemistry and Therapeutic Applications*; Tracey, A.S., Crans, D.C., Eds.; ACS Symposium Series 711; American Chemical Society: Washington, DC, 1998; pp 329–343.
97. Sakurai, H.; Fujii, K.; Watanabe, H.; Tamura, H. *Biochem. Biophys. Res. Commun*. **1995**, *214*, 1095-1101.
98. Fujimoto, S.; Fujii, K.; Yasui, H.; Matsushita, R.; Takada, J.; Sakurai, H. *J. Clin. Biochem. Nutr.* **1997**, *23*, 113-129.
99. Melchior, M.; Thompson, K.H.; Jong, J.M.; Retting, S.J.; Shuter, E.; Yuen, V.; Zhou, Y.; McNeill, J.H.; Orvig, C. *Inorg. Chem.* **1999**, *38*, 2288–2293.
100. Takino, T.; Yasui, H.; Yoshitake, A.; Hamajima, Y.; Matsushita, R.; Takada, J.; Sakurai, H. *J. Biol. Inorg. Chem.* **2005**, *6*, 133-142.
101. Esbak, H.; Enyedy, E.A.; Kiss, T.; Yoshikawa, Y.; Sakurai, H.; Garribba. E.; Rehder, D. *J. Inorg. Biochem.* **2009**, *103*, 590–600.
102. Willsky, G.R; Chi, L-H.; Godzala, M.; Kostyniak, P.J.; Smee, J.J.; Trujillo, A.M., Alfano, J.A.; Ding, W.; Hu, Z.; Crans, D.C. *Coord. Chem. Rev.* **2011**, *225*, 2258–2269.
103. Goldfine, A.B.; Simonson, D.C.; Folli, F.;Patti, M-E.; Kahn, R. *J. Clin. Endocrinol. Metab*. **1995**, *80*, 3311–3320.
104. Goldfine, A.B.; Willsky, G.R.; Kahn, C.R. In *Vanadium Compounds: Chemistry, Biochemistry and Therapeutic Applications*; Tracey, A.S., Crans, D.C., Eds.; ACS Symposium Series 711; American Chemical Society: Washington, DC, 1998; pp 353–368.
105. Buglyó, P.; Kiss, E.; Fábián, I.; Kiss, T.; Sanna, D.; Garribba, E.; Micera, G. *Inorg. Chim. Acta* **2000**, *306*, 174–183.
106. Kiss, E.; Garribba, E.; Micera, G.; Kiss, T.; Sakurai, H. *J. Inorg.Biochem.* **2000**, *78*, 97–108.
107. Buglyó, P.; Kiss, T.; Kiss, E.; Sanna, D.; Garribba, E.; Micera, G. *J. Chem. Soc., Dalton Trans.* **2002**, *11*, 2275–2282.
108. Dörnyei, A.; Marcão, S.; Costa Pessoa,J.; Jakusch, T.; Kiss, T. *Eur. J. Inorg. Chem.* **2006**, 3614–3621.
109. Jakusch, T.; Hollender, D.; Enyedy, E.A.; González, C.S.; Montes-Bayón, M.; Sanz-Medel, A.; Costa Pessoa, J.; Tomaz, I.; Kiss, T. *Dalton Trans*. **2009**, *13*, 2428–2437.

110. Sanna, D.; Bíró, L.; Buglyó, P.; Micera, G.; Garribba, E. *J. Inorg. Biochem*. **2012**, *115*, 87–99.
111. Vincent, J.B.; Love, S. *Biochim. Biophys. Acta* **2012**, *1820 (3)*, 362–378.
112. Sakurai, H.; Yoshikawa, Y.; Yasui, H. *Chem. Soc. Rev*. **2008**, *37*, 2383–2392.
113. Delgado, T.C., Tomaz, I.; Correia, I.; Costa Pessoa, J.; Jones, J.G.; Geraldes, C.F.G.C.; Castro, M.M.C.A. *J. Inorg. Biochem.* **2005**, *99*, 2328-2339.
114. Li, J.; Elberg, G.; Crans, D.C.; Shechter, Y. *Biochem*. **1996**, *35*, 8314-8318.
115. Crans, D.C. *J. Inorg Biochem.* **2000**, *80*, 123–131.
116. Amin, S.S.; Cryer, K.; Zhang, B.; Dutta, S.K.; Eaton, S.S.; Anderson, O.P.; Miller, S.M.; Reul, B.A.; Brichard, S.M.; Crans, D.C. *Inorg Chem*. **2000**, *39*, 406-416.
117. Ou, H.; Yan, L.; Mustafi, D.; Makine, M.W.; Brady, M.J. *J. Biol. Inorg. Chem.* **2005**, *10*, 874–886.
118. Durai, N.; Saminathan, G. *J. Clin. Biochem. Nutr*. **1997**, *22*, 31-39.
119. Costa Pessoa, J.; Cavaco, I.; Correia, I.; Tomaz, I.; Adão, P.; Vale, I.; Ribeiro, V. Castro, M.M.C.A.; Geraldes, C.C.F.G. In *Vanadium: The Versatile Metal*; Kustin, K., Costa Pessoa, J., Crans, D.C., Eds.; ACS Symposium Series 974; American Chemical Society: Washington, DC, 2007; Chapter 24, pp 340–351.
120. Sakurai, H.; Sano, H.; Takino, T.; Yasui, H. *Chem. Lett.* **1999**, 913-914.
121. Takeshita, S.; Kawamura, I.; Yasuno, T.; Kimura, C.; Yamamoto, T.; Seki, J.; Tamura, A.; Sakurai, H.; Goto, T. *J. Inorg. Biochem.* **2001**, *85*, 179-186.
122. Melchior, M.; Rettig, S.J.; Liboiron, B.D.; Thompson, K.H.; Yuen, V.G.; McNeill, J.H.; Orvig, C. *Inorg. Chem*. **2001**, *40*, 4686–4690.
123. Li, M.; Smee J.J.; Ding, W.; Crans, D.C. *J. Inorg. Biochem.* **2009**, *103*, 585–589.
124. Saatchi, K.; Thompson, K.H.; Patrick, B.O.; Pink, M.; Yuen, V.G.; McNeill, J.H.; Orvig, C. *Inorg. Chem.* **2005**, *44*, 2689-2697.
125. Adachi,Y.; Yoshida, J.; Kodera, Y.; Kahto, A.; Takada, J.; Sakurai, H. *J. Med. Chem.* **2006**, *49*, 3251–3256.
126. Hiromura, M.; Adachi, Y.; Machida, M.; Hattori, M.; Sakurai, H. *Metallomics* **2009**, *1*, 92–100.
127. Yoshikawa, Y.; Ueda, E.; Kojima, Y.; Sakurai, H. *Life Sci*. **2004**, *75*, 741-751.
128. Mehdi, M. Z. ; Srivastava, A. K., Arch. Biochem. Biophys **2005**, *440*, 158–164
129. Monga, V.; Thompson, K.H.; Yuen, V.G.; Sharma, V.; Patrick, B.O.; McNeill, J.H.; Orvig, C. *Inorg. Chem*. **2004**, *44*, 2678–2688.
130. Yasui, H.; Tamura, A.; Takino, T.; Sakurai, H. *J. Inorg. Biochem*. **2002**, *91*, 327–338.
131. Thompson, K.H.; Chiles, J.; Yuen, V.G.; Tse, J.; McNeill, J.H.; Orvig, C. *J. Inorg. Biochem*. **2004**, *98,* 683–690.
132. Straganz, G.D.; Glieder, A.; Brecker, L.; Ribbons, D.W.; Steiner, W. *Biochem*. *J.* **2003**, *369*, 573–581.
133. Beskid, M.; Jachimowicz, J.; Taraszewska, A.; Kukulska, D. *Exp. Toxicol. Pathol*. **1995**, *47*, 25–30.
134. Domingo, J.L. *J. Toxicol. Environ. Health* **1994**, *42*, 123–141.
135. Ding, M.;Li, J-J.; Leonard, S.S.; Ye, J-P.; Shi, X.; Colburn, N.H.; Castranova, V. Vallyathan, V. *Carcinogenesis* **1999***, 20*, 663–668.
136. Rojas, E.; Herrera, L.A.; Poirier, L.A.; Ostrosky-Wegman, P. *Mutation Res.* **1999**, *443*, 157–181.
137. Bode, A.M.; Dong, Z. *Crit. Rev. Oncol. Hematol.* **2002**, *42,* 5-24.
138. Chen, F.; Vallyathan, V.; Castranova, V.; Shi, X. *Molec. Cellular Biochem*. **2001**, *222* 183–188.
139. Waris, G.; Ahsan, H. *J. Carcinogenesis* **2006**, *5*, 1-8.
140. Hallenbeck, P.L.; Stevenson, S.C. In *Cancer Gene Therapy: Past Achievements and Future Challenges.* Habib, N.A., Ed.; New York: Kluwer Academic/ Plenum 2000; pp 37-46.
141. Clemmons, D.R. In *Insulin-like Growth Factors and Cancer: From Basic Biology to Therapeutics, Cancer Drug Discovery and Development.* LeRoith D., Ed.; Springer New York: Humana Press, 2012; Chapter 10, pp193-213.
142. Cancer, fact sheet #297, reviewed January 2013: http://www.who.int/mediacentre/factsheets/fs297/en/index.html (last access 24/10/13), part of the World Health Organization website. http://www.who.int/en/
143. Fricker, S.P. *Dalton Trans*. **2007**, 4903–4917.
144. Lovejoy, K.S.; Lippard, S. J. *Dalton Trans.* **2009**, 10651–10659.
145. Lippert, B. *BioMet.* **1992**, 195–208

146. Choy, H.; Park, C.; Yao, M. *Clin. Cancer Res.* **2008**, ***14***, 1633-1638.
147. Clarke, M.J.; Zhu, F.; Frasca, D.R. *Chem. Rev*. **1999**, *99*, 2511-2533.
148. Pizarro, A.M.; Habtemariam, A.; Sadler, P.J. *Top Organomet. Chem.* **2010**, *32*, 21-56.
149. Hartinger, C.G.; Jakupec, M.A.: Zorbas-Seifried, S.; Groessl, M.; Egger, A.; Berger, W.; Zaboras, H.; Dyson, P.; Keppler, B.K. *Chem. Biodiver.* **2008**, *5*, 2140-2155.
150. Alessio, E.; Mestroni, G.; Bergamo, A.; Sava, G. *Curr. Topics in Med. Chem*. **2004**, *4*, 1525-1535.
151. Bratsos, I.; Jedner, S.; Gianferrara, T.; Alessio, E. *Chimia* **2007***, 61*, 692–697.
152. Antonarakis, E.S.; Emadi, A. *Cancer Chemother. Pharmacol.* **2010***, 66,* 1-9.
153. Dyson, P.J.; Sava, G. *Dalton Trans.* **2006**, 1929-1933.
154. Boerner, L.J.K.; Zaleski, J.M. *Curr. Opin. in Chem. Biol*. **2005**, *9,* 135–144.
155. Cortizo, A.M.; Molinuevo, M.S.; Barrio, D.A.; Bruzzone, L. *Intern. J. Biochem. Cell Biol.* **2006**, *38*, 1171–1180.
156. Naso, L.; Ferrer, E.G.; Lesama, L; Rojo, T.; Etcheverry, S.B.; Williams, P. *J. Biol. Inorg. Chem.* **2010**, *15*, 889-902.
157. Naso, L.G.; Lezama L.; Rojo, T.; Etcheverry, S.B.; Valcarcel, M.; Roura, M.; Salado, C.; Ferrer, E.G.; Williams, P.A.M. *Chem.-Biol. Interact.* **2013**, *206*, 289-301.
158. Köpf-Maier, P.; Köpf, H. *Drugs Future* **1986**, *11*, 297–319.
159. Liu, T-T.; Liu, Y-J.; Wang, Q.; Yang, X-G.; Wang, K. *J. Biol. Inorg. Chem*. **2012**, *17*, 311-320.
160. Aubrecht, J.; Narla, R.K.; Ghosh, P.; Stanek, J.; Uckun, F.M.. Toxicol. Appl. Pharm. **1999**, *154*, 228–235.
161. Narla, R.K.; Dong, Y.; D'Cruz, O.J.; Navara, C.; Uckun, F.U. Clinic. Cancer Res. **2000**, *6*, 1546–1556.
162. D'Cruz, Osmond J.; Uckun, F.M. *Toxic. Appl. Pharmac.* **2000**, *166*, 186–195.
163. D'Cruz, O.J.; Uckun, F.M. Expert Opin. Investig. Drugs, **2002**, *11*, 1829-1836.
164. Bishayee, A.; Waghray, A.; Patel, M.A., Chatterjee, M. *Cancer Lett.* **2010**, *294*, 1–12.
165. Fichtner, I.; Claffey, J.; Deally, A.; Gleeson, B.; Hogan, M.; Rivera Markelova, M.; Mueller-Bunz, H.; Weber, H.; Tacke, M. *J. Organomet. Chem*. **2010**, *695*, 1175–1181.
166. Gleeson, B.; Deally, A.; Müller-Bunz, H.; Patil, S.; Tacke, M. *Aust. J. Chem*. **2010**, *63*, 1514–1520.
167. Leon, I.E.; Porro, V.; Di Virgilio, A.L.; Naso, L.G.; William, P.A.M.; Bollati-Fogolin, M.; Etcheverry, S.B. J Biol. Inorg. Chem. **2013**, Manuscript accepted (ID: JBIC-13-06-00093.R2).
168. Papaioannou, A.; Manos, M.; Karkabounas, S.; Liasko, R.; Evangelou, A.M.; Correia, I.; Kalfakakou, V.; Costa Pessoa, J.; Kabanos, T. *J. Inorg. Biochem*. **2004**, *98*, 959-968.
169. Noblía, P.; Vieites, M.; Parajón-Costa, B.S.; Baran, E.J.; Cerecetto, H.; Draper, P.; Gonzalez, M.; Piro, O.E.; Castellano, E.E.; Azqueta, A.; Ceráin, A.L.; Monge-Vega, A.; Gambino, D. *J. Inorg. Biochem.* **2005**, *99*, 443-451.
170. Fu, Y.; Wang, Q.; Yang, X-G.; Yand, X-D.; Wang, K. *J. Biol. Inorg. Chem*. **2008**, *13*, 1001-1009.
171. Mustafi, D.; Foxley, S.; Zamora, M.; Makinen, M.W.; Karczmar, G.S. *Proc. Intl. Soc. Mag. Reson. Med.* **2006**, *14*, 684.
172. Barrio, D.A.; Williams, P.A.M.; Cortizo, A.M.; Etcheverry, S.B. *J. Biol. Inorg. Chem.* **2003**, *8*, 459–468.
173. Bishayee, A.; Roy, S.; Chatterjee, M. Oncol. Res. **1999**, *11*, 41–53.
174. Molinuevo, M.S.; Barrio, D.A.; Cortizo, A.M.; Etcheverry, S.B. *Cancer Chemother. Pharmacol.* **2004**, *53*, 163–172.
175. Liasko, R.; Kabanos, T.A.; Karkabounas, S.; Malamas, M.; Tasiopoulos, A.J; Stefanou, D.; Collery, P., Evangelou, A. *Anticancer Res*. **1998**, *18*, 3609-3613.
176. Maier, R.H.; Purser, S.M.; Nicholson, D.L.; Pories, W.J. *In Vitro Cell Dev. Biol. Anim.* **1997**, *33*, 218-221.
177. Choi, Y-J.; Lim, S-Y.; Woo, J-H.; Kim, Y-H., Kyu Kwon, Y.; Suh, S.; Lee, S-H.; Choi, W-Y.; Kim, J-G.; Lee, I-S.; Park, J-W.; Kyu Kwon, T. *Biochem. Biophys. Res. Comm.* **2003**, *305*, 176-185.
178. D'Cruz, O.J.; Uckun, F.M.; *Expert Opin. Investig. Drugs*. **2002**, *11*, 1829-1836.
179. Wozniak, K.; Blasiak, *J. Arch Toxicol*. **2004**, *78*, 7-15.
180. Cruz, T.F.; Morgan, A.; Min, W. *Mol. Biochem.* **1995**, *53*, 161-166.
181. Murthy, M.S.; Rao LN, Kuo LY, Toney JH, Marks TJ. Inorg Chim Acta **1988**;152:117-124.
182. Gambino, D. *Coord. Chem. Rev.* **2011**, *255*, 2193–2203.

183. Turner, T.L.; Nguyen, V.H.; McLaughlan, C.C.; Dymon, Z.; Dorsey, B.M.; Hooker, J.D.; Jones, M.A. *J. Inorg. Biochem.* **2012**, *108*, 96–104.
184. Benítez, J.; Guggeri, L.; Tomaz, I.; Costa Pessoa, J.; Moreno; Lorenzo, J.; Aviles, F.X.; Garat, B.; Gambino, D. *J. Inorg. Biochem.* **2009**, *103*, 1386-1394.
185. Benítez. J.; Guggeri, L.; Tomaz, I. Arrambide, G.; Navarro, M.; Costa Pessoa, J.; Garat, B.; Gambino, D.*J. Inorg. Biochem.* **2009**, *103*, 609–616.
186. Maurya, M.R.; Khan, A.A.; Azam, A.; Ranjan, S.; Mondal, N.; Kumar, A.; Avecilla, F.; Costa Pessoa, J. *Dalton Trans.* **2010**, *39*, 1345-1360.
187. Maurya, M.R.; Kumar, A.; Bhat, A.R.; Azam, A.; Bader, C.; Rehder, D. *Inorg. Chem.* **2006**, *45*, 1260-1269.
188. Maurya, M.R.; Khan, A.A.; Irfan, I.; Azam, A.; Kumar, A.; Costa Pessoa, *J. Eur. J. Inorg. Chem.* **2009**, 5377-5390.
189. Ghosh, P.; D'Cruz, O.J.; DuMez, D.D.; Peitersen, J.; Uckun, F.M. *J. Inorg. Biochem*. **1999**, *75*, 135-143.
190. D'Cruz, O.J.; Waurzyniak, B.; Uckun, F.M.. *Toxicol.* **2002**, *170*, 31-43.
191. Shigeta, S.; Mori, S.; Yamase, T.; Yamamoto, N.; Yamamoto, N. *Biomed. Pharmacother*. **2006**, *60*, 211-219.
192. D'Cruz, O.J.; Dong, Y.H.; Uckun, F.M. *Biochem. Biophys. Res. Commun*. **2003**, *302*, 253-264.
193. Wong, S.Y.; Sun, R.W.Y.; Chung, N.P.Y.; Lin, C.L.; Che, C.M. *Chem. Commun*. **2005**, 3544-3546.
194. Wai-Yin Sun, R.; Ma, D-L.; Lai-Ming Wong, E.; Che, C-M. *Dalton Trans.* **2007**, 4884–4892.
195. Ross, A.; Soares, D.C.; Covelli, D.; Pannecouque, C.; Budd, L.; Collins, A.; Robertson, N.; Parsons, S.; De Clercq, E.; Kennepohl, P.; Sadler,P.J. *Inorg. Chem.* **2010**, *49*, 1122–1132.
196. Maiti, A.; Ghosh, S. *J. Inorg. Biochem*. **1989**, *36*, 131-139.
197. David, S.; Barros, V.; Cruz, C.; Delgado, R. *FEMS Microbiol. Lett*. **2005**, *251*, 119-124.
198. da S. Maia, P.I.; Pavan, F.R.; Leite, C.Q.F.; Lemos, S.S.; de Sousa, G.F.; Batista, A.A.; Nascimento, O.R.; Ellena, J.; Castellano, E.E.; Niquet, E.; Deflon, V.M. *Polyhedron*, **2009**, 28, 398–406.
199. Morgan, G.T.; Moss, H.W. *J. Chem Soc.* **1914**, *103*, 78-90.
200. Dodge, R.P.; Templeton, D.H.; Zalkin, A. *J. Chem Phys.* **1961**, *35,* 55-67.
201. Guyard A. *Bull. Soc. Chim.* ***1876****, 25,* 350.
202. Taguchi, H.; Isobe, K.; Nakamura, Y.; Kawaguchi, *S. Chem. Lett*. **1975**, 757-760.
203. Selbin, J.; Manning, H.R.; Cessac, G.J. *Inorg. Nucl. Chem.* **1963**, *25*, 1253-1258.
204. Atherton, N.M.; Gibbon, P.J.; Shohoji, M.C.B. *J. Chem. Soc., Dalton Trans*. **1982**, 2289-2290.
205. Nakamoto, K.; Morimoto, Y.; Martell, A.E. *J Amer. Chem. Soc.* **1961**, *83*, 4533-4536.
206. Vlčková, B.; Strauch, B.; Horák, M. *Collect. Czech. Chem. Comm*, **1987**, *52*, 686-695.
207. Selbin, J. *Coord. Chem. Rev.* **1966**, *1*, 293-314.
208. Baran, E.J. *J. Coord. Chem.* **2001**, *54*, 215-238
209. Santos Claro, P.C.; González-Baró, A.C.; Parajón-Costa, B.S.; Baran, E.J. *Z. Anorg. Allg. Chem*. **2005**, *631*, 1903–1908.
210. Kaneda, K.; Jitsukawa, K.; Itoh, T.; Teranishi, S. *J. Org. Chem*. **1980**, *45*, 3004-3009.
211. Conte, V.; Di Furia, F.; Moro. S. *J. Phys. Org. Chem*. **1996**, *9*, 329-336.
212. Hirao, T. *Chem. Rev*. **1997**, *97*, 2707-2724.
213. Wender, P. A.; Rice, K. D.; Schnute, M. E. *J. Am. Chem. Soc*. **1997**, *119*, 7897-7898.
214. Jiang, F.; Anderson, O. P.; Miller, S. M.; Chen, J. Mahroof-Tahir, M.; Crans, D.C. *Inorg. Chem.* **1998**, *37*, 5439-5451.
215. Rio, D.; Galindo, A.; Tejedo, J.; Bedoy, F.J.; Ienco, A.; Mealli, C. *Inorg.Chem. Comm*. **2000**, *3*, 32–34.
216. Maurya, M.R. *Coord. Chem. Rev.* **2003**, *237*, 163-181.
217. Jang, Y.J.; Lee, U.; Bon Kweon Koo, B.K. *Bull. Korean Chem. Soc*. **2005**, *26*, 72-76.
218. Sarkar, A.; Pal, S. *Inorg. Chim. Acta* **2008**, *361*, 2296–2304.
219. Itoh, T.; Jitsukawa, K.; Kaneda, K.; Terashini, S. *J. Am. Chem. Soc*. **1979**, *101*, 159–169.
220. Csanyi, L.J.; Jaky, K.; Galbacs, G. *J. Mol. Catal.* **2002**, *179*, 65–72.
221. Nawi, M.A.; Riechel, T.L. *Inorg. Chem.* **1981**, *20*, 1974-1978.
222. Mustafi, D.; Makinen. M.W. *Inorg. Chem.* **2005***, 44*, 5580-5590.
223. Garribba, E.; Micera, G.; Sanna, D. *Inorg. Chim. Acta* **2006**, *359*, 4470-4476.

224. Wisley, J.; Michael, K.M.; Philip, J.S. *Endocrin.* **2006**, *147*, 493-501.
225. Makinen, M.W.; Brady, M.J. *J. Biol. Chem.*, **2002**, *277*, 12215–12220.
226. Nawi, M.A.; Riechel, T.L. *Inorg. Chem.* **1982**, *21*, 2268-2271.
227. Taguchi, H.; Isobe, K.; Nakamura, Y.; Kawaguchi, S. *Bull. Chem. Soc. Jpn.* **1978**, *51*, 2030-2035.
228. Doadrio, A.; Carro, A.G. *An. R. Soc. Esp. Fis. Quim.* **1964**, *60*, 495-504.
229. Grybos, R.; Samotus, A.; Popova, N.; Bogolitsyn, K. *Transit. Met. Chem.* **1997**, *22*, 61-64.
230. Mahroof-Tahir, M.; Brezina, D.; Fatima, N.; Choudhary, M.; Atta-ur-Rahman *J. Inorg. Biochem*. **2005**, *99*, 589-599.
231. Crans, D.C.; Khan, A.R.; Mahroof-Tahir, M.; Mondal, S.; Miller, S.M.; Cour, A.; Anderson, O.P.; Jakusch, T.; Kiss T. *J. Chem. Soc*. *Dalton Trans*. **2001**, 3337–3345.
232. Correia, I.; Mota, A.; Hallett, J.P.; Kuznetsov, M.L. *Physical Chemistry Chemical Physics* **2011**, *13*, 15094–15102.
233. Ziegler, A.J.; Florian, J.; Ballicora, M.A; Herlinger, A.W. *J. Enz. Inhib. Med. Chem*. **2009**, *24*, 22–28.
234. Holloway, C.E.; Melnik, M. *Rev. Inorg. Chem*. **1985**, *7*, 75-159.
235. Linert, W.; Herlinger, E.; Margl, P.; Boca, R. *J.Coord.Chem*. **1993** *28* 1-16.
236. Carlin, R.L.; Walker, F.A. *J. Am. Chem. Soc.* **1965**, *87*, 2128-2133.
237. Isobe, K.; Nakamura, Y.; Kawaguchi, S. *J. Inorg. Nucl. Chem.* **1978**, *40*,607-–611.
238. Cornman, C.R.; Kampf, J.; Lah, M.S.; Pecoraro, V.L. *Inorg. Chem.* **1992**, *31*, 2035-2043.
239. Schmidt, H.; Bashirpoor, M.; Rehder, D. *J. Chem. Soc., Dalton Trans*. **1996**, 3865-3870.
240. Crans, D.C.; Keramidas, A.D.; Amin, S.S.; Anderson, O.P.; Miller, S.M. *J. Chem. Soc., Dalton Trans*. **1997**, 2799-2812.
241. Kuriakose M.; Kurup P. M.R.; Suresh, E. *Polyhedron* **2007**, *26*, 2713–2718.
242. Barnum, D.W. *J. Inorg. Nucl. Chem*. **1961**, *21*, 221-237.
243. Selbin, J.; Ortolano, T.R. *J. Inorg. Nucl.Chem.* **1964**, *26*, 37-40.
244. Ballhausen, C.J; Gray, J.B. *Inorg. Chem.* **1962**, *1*, 111-122.
245. Barton J.K. In *Bioinorganic Chemistry.* Bertini, I., Eds.; Sausalito, California: University Science Books, 1994; pp. 455-503.
246. Jiang, Q.; Xiao, N.; Shi, P.; Zhu, Y.; Guo, Z. *Coord. Chem. Rev.* **2007**, *251*, 1951–1972.
247. Hegg, E.L.; Burstyn, J.N. *Coord. Chem. Rev.* **1998**, *173,* 133–165.
248. Mancin, F.; Scrimin P.; Tecilla P.; Tonellato U. *Chem. Commun.* **2005**, 2540-2548.
249. Burrows, C.J.; Muller, J.G. *Chem. Rev*. **1998**, *98*, 1109-1151.
250. Armitage, B. *Chem. Rev.* **1998**, *98,* 1171-1200.
251. Sigman, D.S.; Bruice, T.W.; Mazumder, A.; Sutton, C. *Acc. Chem. Res.* **1993**, *26*, 98-104.
252. Erkkila, K.E., Odom, D.T. Barton J.K. *Chem. Rev.* **1999**, *99,* 2777-2795.
253. Cowan, J. A. *Curr. Opin. in Chem. Biol.* **2001**, *5*, 634–642.
254. Sigman, D.S.; Mazumder, A.; Perrin, D.M. *Chem. Rev.* **1993**, *93*, 2295-2316.
255. Liu, C.; Wang, M.; Zhang, T.; Sun, H. *Coord. Chem. Rev.* **2004**, *248*, 147–168.
256. Morrow, J.R.; Iranzo, O. *Curr. Opin. Chem. Biol.* **2004**, *8*, 192–200.
257. Sigman, D.S. *Biochem.* **1990**, *29*, 9097-9105.
258. Dupureur, C.M. *Curr. Opin. Chem. Biol*. **2008**, *12*, 250–255.
259. Livieri, M.; Mancin, F.; Saielli, G.; Chin, J.; Tonellato, U. *Chem. Eur. J.* **2007**, *13*, 2246-2256.
260. Liu, C.; Wang, L. *Dalton Trans.* **2009**, 227-239.
261. Zhang, J.J; Shao, Y.; Wei, L.; Li, Y.; Sheng, X.; Liu, F.; Lu, G.Y. *Sci. China Ser. B-Chem.* **2009**, *52*, 402-414
262. Crespy, D.; Landfester, K.; Schubert, U.S.; Schiller, A. *Chem. Commun.* **2010**, *46*, 6651-6662.
263. Gyurcsik, B.; Czene, A. *Future Med. Chem.* **2011**, *3*, 1935-1966.
264. Mancin, F.; Scrimina, P.; Tecilla, P. *Chem. Commun.* **2012**, *48*, 5545–5559.
265. Kuwahara, J.; Suzuki, T.; Sugiura, Y. *Biochem. Biophys. Res.Commun*. **1985**, *129*, 368-374.
266. Sakurai, H.; Nakai, M.; Miki, T.; Tsuchiya, K.; Takada, J.; Matsushita, R. *Biochem. Biophys. Res. Commun.* **1992**, *189*, 1090-1095.
267. Sakurai, H.; Tamura, H.; Okatani, K. *Biochem. Biophys. Res.Commun.* **1995**, *206*, 133-137.
268. Shi, X.; Jiang, H.; Mao, Y.; Ye, J.; Saffiotti, U. *Toxicol*. **1996**, *106*, 27-38.
269. Hiort, C.; Goodisman, J.; Dabrowiak, J.C. *Mol. Cell. Biol.* **1995**,*153*, 31-36.
270. Sam, M.; Hwang, J.H.; Chanfreau, G.; Abu-Omar, M.M. *Inorg.Chem*. **2004**, *43*, 8447-8455.

271. Kwong, D.W.J.; Chan, O.Y.; Shek, L.K.; Wong, R.N.S. *J. Inorg. Biochem.* **2005**, *99*, 2062-2073.
272. Kwong, D.W.J.; Chan, O.Y.; Wong, R.N.S.; Musser, S.M.; Vaca, L.; Chan, S. I. *Inorg. Chem.* **1997**, *36*, 1276-1277.
273. Hiort, C.; Goodisman, J.; Dabrowiak, J.C. *Biochem.* **1996**, *35*, 12354-12362.
274. Chen, C.-T.; Lin, J.-S.; Kuo, J.-H.; Weng, S.-S.; Cuo, T.-S.; Lin, Y.-W.; Cheng, C.-C.; Huang, Y.-C.; Yu, J.-K.; Chou, P.-T. *Org. Lett.* **2004**, *6*, 4471-4474.
275. Heater, S.J.; Carrano, M.W.; Rains, D.; Walter, R.B.; Ji, D.; Yan, Q.; Czernuszewicz, R.S.;. Carrano, C.J. *Inorg. Chem*. **2000**, *39,* 3881-3889.
276. Stemmler, A.J.; Burrows, C.J. *J. Biol. Inorg. Chem.* **2001**, *6*, 100-106.
277. Verquin, G.; Fontaine, G.; Bria, M.; Zhilinskaya, E.; Abi-Aad, E.; Aboukais, A.; Baldeyrou, B.; Bailly, C.; Bernier, J.-L. *J. Biol. Inorg. Chem*. **2004**, *9,* 345-353.
278. Sasmal, P.K; Saha, S.; Majumdar, R.; Dighe, R.R.; Chakravarty, A.R. *Chem. Comm.* **2009**, 1703-1705.
279. Sasmal, P.K; Saha, S.; Majumdar, De, S.; Dighe, R.R.; Chakravarty, A.R. *Dalton Trans*. **2010**, *39*, 2147–2158.
280. Sasmal, P.K; Saha, S.; Majumdar, R.; Dighe, R.R.; Chakravarty, A.R. *Inorg. Chem*. **2010**, *49*, 849-859.
281. Prasad, P.; Sasmal, P.K; Majumdar, R.; Dighe, R.R.; Chakravarty, A.R. *Inorg. Chim. Acta* **2010**, *363,* 2743–2751.
282. Prasad, P.; Sasmal, P.K.; Khan, I.; Kondaiah, P.; Chakravarty, A.R. *Inorg. Chim. Acta* **2011**, *372*, 79-87.
283. Leelavathy, L.; Anbu, S.; Kandaswamy, M.; Karthikeyan, N.; Mohan, N., *Polyhedron* **2009**, *28*, 903-910.
284. Du, Y.F.; Lu, J.Z.; Guo, H.W.; Ping, J.J.; Chen, C.F.; Pan, J.M. *Trans. Met. Chem.* **2010**, *35*, 859–864.
285. Prasad, K.S.; Kumar, L.S.; Shekar, S.C.; Prasad, M.; Revanasiddappa, H.D. *Chem. Scien. J.* **2011**, *12*, 1-10.
286. Raman, N.; Jeyamurugan, R.; Subbulakshmi, M.; Boominathan, R.; Yuvarajan C.R. *Chem. Papers* **2010**, *64*, 318-328.
287. Patel, M.N.; Patel, S.H.; Chhasatia, M.R.; Desai, C.R. Nucleos. Nucleot. Nucl. Acids **2010**, *29*, 200-215.
288. Islam, M.N.; Kumbhar, A.A.; Kumbhar, A.S.; Zeller, M.; Butcher, R.J.; Dusane, M.B.; Joshi, B.N. *Inorg. Chem.* **2010**, *49*, 8237-8246.
289. Steens, N.; Ramadan, A.M.; Parac-Vogt, T.N. *Chem. Commun*. **2009**, 965-967.
290. Steens, N.; Ramadan, A.M.; Absillis, G.; Parac-Vogt, T.N. *Dalton Trans.* **2010**, *39*, 585-592.
291. Ho, P.H., Breynaert, E.; Kirschhock, C.E.A.; Parac-Vogt, T.N**.** *Dalton Trans*. **2011**, *40*, 295-300.
292. Ho, P.H.; Mihaylov, T.; Pierloot, K.; Parac-Vogt, T.N. *Inorg. Chem*. **2012**, *51*, 8848-8859.
293. Mihaylov, T.; Parac-Vogt, T.N.; Pierloot, K. *Inorg. Chem*. **2012**, *51*, 9619-9628.
294. Ren, Y.-G.; Kirsebom, L.A.; Virtanen, A. J. Biol. Chem. **2004**, *279*, 48702-48706.
295. Robertazzi, A.; Platts, J. A. *J Biol. Inorg. Chem.* **2005**, *10*, 854–866.
296. Casellato, U.; Tamburini, S.; Tomasin P.; Vigato, P.A. *Inorg. Chim. Acta* **2004**, *357,* 4191-4207.
297. Takenaka, S.; Ihara, T.; Takegi, M. *J. Mol. Recognit.* **1990**, *3*,156–162.
298. Williams, N.H.; Takasaki, B.; Wall M.; Chin, J. *Acc. Chem. Res.* **1999**, *32*, 485–493.
299. Komiyama, M.; Takeda, N.; Shigekawa, H. *Chem. Commun.* **1999**, 1443–1451.
300. Niittymaki, T.; Lonnberg, H. *Org. Biomol. Chem.* **2006**, *4*, 15–25.
301. Mancin, F.; Tecilla, P. *New J. Chem.* **2007**, *31*, 800–817.
302. Roigk, A.; Hettich, R.; Schneider, H. *Inorg. Chem.* **1998**, *37*, 751-756.
303. Takasaki, B.K.; Chin, J. *J. Am. Chem. Soc*., **1994**, *116*, 1121–1122.
304. Morrow, J. R.; Buttrey, L.A.; Shelton, V. M.; Berback, K.A. *J. Am. Chem. Soc.* **1992**, 114, 1903-1905.
305. Matsumoto, Y.; Komiyama, M. *Nucleic Acids Symp. Ser.* **1992**, *27*, 33-34.
306. Komiyama, M. *J. Biochem.* **1995**, *118*, 665-670.
307. Jurek, P.E.; Jurek, A.M.; Martell, A.E. *Inorg. Chem*. **2000**, *39*, 1016–1020.
308. Komiyama, M.; Shiiba, T.; Kodama, T.; Takeda, N.; Sumaoka J.; Yashiro, M. *Chem. Lett*. **1994**, *23*, 1025–1028.

309. Sumaoka, J.; Igawa, T.; Furuki, K.; Komiyama, M. *Chem. Lett*. **2000**, *29*, 56–57.
310. Sigman, D.S. Graham, D.R.; D'Aurora, V.; Stern, A.M. *J. Biolog. Chem*. **1979**, *254*, 12269-12272.
311. Pope, L.M.; Reich, K.A.; Graham, D.R. Sigman, D.S. *J. Biolog. Chem*. **1982**, *257*, 12121-12128.
312. Sigman, D.S. *Acc. Chem. Res.* **1986**, *19*, 180-186.
313. Chen. C.B. Sigman, D.S. *J. Am. Chem. Soc*. **1988**, *110*, 6570-6572.
314. Oyoshi, T.; Sugiyama, H. *J. Am. Chem. Soc.* **2000**, *122,* 6313-6314.
315. Lu, L-P.; Zhu, M-L.; Yang, P. *J. Inorg. Biochem.* **2003**, *95*, 31–36.
316. Zhang, S.; Zhu, Y.; Tu, C.; Wei, H, Yang, Z.; Lin, L.; Ding, J.; Zhang, J.; Guo, Z. *J. Inorg. Biochem*. **2004**, *98,* 2099–2106.
317. Pitie, M.; Croisy, A.; Carrez, D.; Boldron, C.; Meunier, B. *ChemBioChem.* **2005**, *6*, 686–691.
318. Thomas, A.M.; Nethaji, M.; Chakravarty, A.R. *J. Inorg. Biochem*. **2004**, *98*, 1087–1094.
319. Hirohama, T.; Kuranuki, Y.; Ebina, E.; Sugizaki, T.; Arii, H.; Chikira, M.; Selvi, P.T.; Palaniandavar, M. *J. Inorg. Biochem*. **2005**, *99*, 1205–1219.
320. Reddy, P.R.; Shilpa, A. *Polyhedron* **2011**, *30*, 565–572.
321. Chen, C-H.B.; Milne, L.; Landgraf, R.; Perrin, D.M.; Sigman, D.S. ChemBioChem **2001**, *2*, 735-740.
322. Ramakrishnan, S.; Palaniandavar, M. *J. Chem. Sci.* **2005**, *117*, 179–186.
323. Patra, A.K.; Bhowmick, T.; Ramakumar, S.; Nethajia, M.; Chakravarty, A.R. *Dalton Trans.* **2008**, 6966-6976.
324. Zuber, G.; Quada, J.C.; Hecht, S.M. *J. Am. Chem. Soc.* **1998**, *120,* 9368-9369.
325. Dhar, S.; Nethaji M.; Chakravarty, A.R. *Dalton Trans.* **2004**, 4180-4184.
326. Ward, B.; Skorobogaty, A.; Dabrowiak, J.C. *Biochem.* **1986**, *25*, 6875-6883.
327. Le Doan, T.; Perrouault, L.; Helene, C.; Chassignol, M.; Thuong, N.T. *Biochem.* **1986**, *25*, 6136-6739.
328. Groves, J.T.; Farrell, T P. *J. Am. Chem. Soc.* **1989**, *111*, 4998-5000.
329. Yoshino, M.; Haneda, M.; Naruse, M.; Murakami, K. *Molec. Genet. Metab*. **1999**, *68*, 468-472.
330. Macías, B.; Villa, M.V.; Sanz, F.; Borras, J.; Gonzalez-Alvarez, M.; Alzuet, G. *J. Inorg. Biochem.* **2005**, *99*, 1441-1448.
331. Ueda, J.; Takai, M.; Shimazu, Y.; Ozawa, T. *Arch. Biochem. Biophys.* **1998**, *357,* 231-239.
332. Reddy, P.A.N.; Santra, B.K.; Nethaji, M.; Chakravarty, A.R. *J. Inorg. Biochem.* **2004**, *98*, 377-386.
333. Zan, J.; Yan, H.; Guo, Z.-f.; Lu, Z.-L. *Inorg. Chem. Comm.* **2010**, 1054-1056.
334. McMillin, D.R.; McNett, K.M. **1998**, *98*, 1201-1219.
335. Patra, A.K.; Dhar, S.; Nethaji, M.; Chakravarty, A.R. *Dalton Trans.* **2005**, 896-902
336. He, J.; Hu, P.; Wang, Y.-J.; Tong, M.-L.; Sun, H.; Mao, Z.-W.; Jia, L-N. *Dalton Trans.* **2008**, 3207-3214.
337. Kirin, S.I.; Happel, K.M.; Hrubanova, S.; Weyhermüller, T.; Klein, C.; Metzler-Nolte, N. *Dalton Trans.* **2004**, 1201–1207.
338. Das, S.; Madhavaiah, C.; Verma, S.; Bharadwaj, P.K. *Inorg. Chim. Acta* **2005**, *358*, 3236-3240.
339. Li, L.; Karlin, K.D.; Rokita, S.E. *J. Amer. Chem. Soc.* **2005**, *127*, 520-521.
340. Kong, D.; Reibenspies, J.; Mao, J.; Clearfield, A.; Martell, A. E. *Inorg. Chim. Acta* **2003**, *342*, 158-170.
341. Macías, A.; Villa, M.V.; Salgado, M.; Borras, J.; Gonzalez-Alvarez, M.; Sanz, F. *Inorg. Chim. Acta* **2006**, *359*, 1465-1472.
342. Jimenez-Garrido, N.; Perello, L.; Ortiz, R.; Alzuet, G.; Gonzalez-Alvarez, M.; Canton, E.; Liu-Gonzalez, M.; Garcıa-Granda, L.; Perez-Priede, M. *J. Inorg. Biochem*. **2005**, *99,* 677–689.
343. Chetana, P.R; Rao, R.; Roy, M.; Patra, A.K. *Inorg. Chim. Acta* **2009**, *362*, 4692-4698.
344. Krishnamoorthy, P.; Sathyadevi, P.; Cowley, A.H.; Butorac, R.R.; Dharmaraj, N. *Europ. J. of Med. Chem*. **2011**, *46*, 3376-3387.
345. Li, D.-D.; Tian, J.-L.; Gu, W.; Liu, X.; Yan, S-P.; *Eur. J. Inorg. Chem.* **2009**, 5036-5045.
346. Raman, N.; Selvan, A. *J. Coord. Chem.* **2011**, *64*, 534-553.
347. Modak, A.S.; Gard, J.K.; Merriman, M.C.; Winkeler, K.A.; Bashkin, J.K.; Stern, M.K. *J. Am. Chem. Soc*. **1991**, *113*, 283-291.
348. Burstyn, J.N.; Kim A.D. *Inorg. Chem.* **1993**, *32*, 3585-3586.
349. Deal, K.A.; Burstyn, J.N. *Inorg. Chem.* **1996**, *35*, 2792–2798.
350. Hegg E.L.; Burstyn, J.N. *Inorg. Chem*. **1996**, *35*, 7474-7481.

351. Deck, K.M.; Tseng, T.A.; Burstyn, J.N. *Inorg. Chem*. **2002**, *41*, 669–677.
352. Reddy, P.R.; Shilpa, A. *Indian J. Chem.* **2010**, *49A*, 1003-1015.
353. Sissi, C.; Mancin, F.; Gatos, M.; Palumbo, M.; Tecilla, P.; Tonellato, U. *Inorg, Chem.* **2005**, *44*, 2310-2317.
354. Anbu, S.; Kandaswamy, M.; Kamalraj, S.; Muthumarry, J.; Varghesec, B. *Dalton Trans.* **2011**, *40*, 7310–7318.
355. Subat, M.; Woinaroschy, K.; Gerstl, C.; Sarkar,B.; Kaim, W.; Konig, B. *Inorg. Chem.* **2008**, *47*, 4661-4668.
356. Desbouis, D.; Troitsky, I.P.; Belousoff, M.J; Spiccia, L., Graham, B. *Coord. Chem. Rev*. **2012**, *256*, 897–937.
357. Roy, M.; Dhar, S.; Maity, B.; Chakravarty, A.R. *Inorg. Chim. Acta* **2011**, *375*, 173–180.
358. Zhang, C.X.; Lippard, S.J. *Curr. Opin. Chem. Biol.* **2003**, *7*, 481-489.
359. Malinge, J-M.; Giraud-Panis, M-J.; Leng, M. *J. Inorg. Biochem*. **1999**, *77*, 23-29.
360. Jamieson, E.R.; Lippard, S.J. *Chem. Rev*. **1999**, *99*, 2467-2498.
361. Mounir, M.; Lorenzo, J.; Ferrer, M.; Prieto, M.J.;Rossell, O.; Aviles, F.; Moreno, V. *J. Inorg. Biochem*. **2007**, *101*, 660–666.
362. Lippard, S.J. In *Bioinorganic Chemistry.* Bertini, I., Gray, H.B., Lippard, S.J., Valentine, J.S., Eds.; Mill Valley: University Science Books, 1994; Chapter 9; pp 505-583.
363. Vashisht Gopal, Y.N.; Jayaraju, D.; Kondapi, A.K. *Biochem.* **1999**, *38*, 4382-4388.
364. Neyhart, G.A.; Grover, N.; Smith, S.R.; Kalsbeck, W.K.; Fairley, T.A.; Cory, M.; Thorp, H.H. *J. Amer. Chem. Soc*. **1993**, *115*, 4423-4428.
365. Janaratne, T.K.; Yadav, A.; Ongeri, F.; MacDonnell, F.M. *Inorg. Chem.* **2007**, *46*, 3420-3422.
366. Ghosh, A.; Mandoli, A.; Kumar, K.; Singh Yadav, N.; Ghosh, T. Jha, B.; Thomas, J.A.; Das, A. *Dalton Trans*. **2009**, 9312–9321.
367. Bicek, A.; Turel, I.; Kanduser, M.; Miklavcic, D. *Bioelectrochem*. **2007**, *71*, 113–117.
368. Arounaguiri, S.; Easwaramoorthy, D.; Ashokkumar, A.; Dattagupta, A.; Maiya, B.G. *Proc. Indian Acad. Sci. (Chem. Sci.)* **2000**, *112*, 1–17.
369. Tan, C.; Liu, J.; Chen L.; Shi, S.; Ji, L. *J. Inorg. Biochem.* **2008**, 1644-1653.
370 Otero, L.; Smircich, P.; Vieites, M.; Ciganda, M.; Severino, P.C.; Terenzi, H.; Cerecetto, H.; Gambino, D.; Garat, B. *J. Inorg. Chem.* **2007**, *101*, 74-79.
371. Deshpande, M.S.; Kumbhar, A.A.; Khumbar, A.S. *Inorg. Chem.* **2007**, *46*, 5450-5452.
372. Yan, Y.K.; Melchart, M.; Habtemariam, A.; Salder, P.J. *Chem. Commun*. **2005**, 2764-4776.
373. Vock, C.A.; Ang, W.H.; Scolaro, C.; Phillips, A.D.; Lagopoulos, L.; Juillerat-Jeanneret, L.; Sava, G.; Scopelliti, R.; Dyson, P.J. *J. Med.Chem.* **2007**, *50*, 2166-2175.
374. Burger, R.M. *Chem. Rev.* **1998**, *98*, 1153-1169.
375. Claussen, C.A.; Long, E.C. *Chem. Rev*. **1999**, *99*, 2797-2816.
376. Hecht, S.M. *J. Nat. Prod.* **2000**, *63,* 158-168.
377. Pogozelski, W.J.; McNeese, T.J.; Tullius, T.D. *J. Am. Chem. Soc.* **1995**, *117*, 6428-6433.
378. Hertzberg, R.P.; Dervan, P.B. *Biochem*. **1984**, *23*, 3934-3945.
379. Chen, X.; Wang, J; Sun, S.; Fan, J; Wu, S.; Liu, J.; Ma, S.; Zhang, L.; Peng, X.; *Bioorg. Medic. Chem. Lett*. **2008**, *18*, 109–113.
380. Roy, M.; Santhanagopal, R.; Chakravarty, A.R. *Dalton Trans*. **2009**, 1024–1033.
381. Roy, M.; Bhowmick, T.; Santhanagopal, R.; Ramakumarb, S.; Chakravarty, A.R. *Dalton Trans*. **2009**, 4671–4682.
382. Kowalski, K.; Suwaki, N.; Zakrzewski, J.; White, A.J.P.; Long, N.J.; Mann, D.J. *Dalton Trans*. **2007**, 743–748.
383. Proteggente, A.R.; England, T.G.; Rice-Evans, C.A.; Halliwell, B. *Biochem. Biophys. Res. Comm.* **2001**, *288*, 245-251.
384. Flemming, J.; Arnhold, J. *Eur Biophys J*. **2007**, *36*, 377–384.
385. Liu, C.; Yu, S.; Li, D.; Liao, Z.; Sun, X.; Xu, H. *Inorg. Chem.* **2002**, *41*, 913-922.
386. Neves, A.; Terenzi, H.; Horner, R.; Horn Jr., A.; Szpoganicz, B.; Sugai, J. *Inorg. Chem. Comm.* **2001**, *4*, 388-391.
387. Livieri, M.; Mancin, F.; Tonellato, U; Chin, J. *Chem*. *Commun*. **2004**, 2862–2863.

388. Boseggia, E.; Gatos, M.; Lucatello, L.; Mancin, F.; Moro, S.; Palumbo, M.; Sissi, C.; Tecilla, P.; Tonellato, U.; Zagotto, G. *J. Am. Chem. Soc.* **2004**, *126*, 4543-4549.
389. Penkova, L.V.; Macia, A.; Rybak-Akimova, E.V.; Haukka, M.; Pavlenko, V.A.; Iskenderov, T.S.; Kozlowski, H.; Meyer, F.; Fritsky, I.O. *Inorg. Chem.* **2009**, *48*, 6960–6971.
390. Qian, J; Wang, L; Gu, W; Liu, X; Tian, J.; Yan, S. *Dalton Trans.,* **2011**, *40*, 5617-5624.
391. Jun, T.; Bochua, W.; Liancai, Z.; *Bioorgan. Medic. Chem. Lett.* **2007**, *17,* 1197–1199.
392. Qian, J.; Ma X.-F.; Xu, H.-Z.; Tian, J.-L.; Shang, J.; Zhang, Y.; Yan, S.-P. *Eur. J. Inorg. Chem.* **2010**, 3109–3116.
393. Bernadou, J.; Pratviel G.E; Bennis, F.; Girardet, M.; Meunier, B. *Biochem.* **1989**, *28*, 7268-7275.
394. Mandal, S.S.; Kumar, K.V.; Varshney, U.; Bhattacharya, S. *J. Inorg. Biochem.* **2006***, 63*, 265-272.
395. Oikawa, S.; Hiraku, Y.; Fujiwara, T.; Saito, I.; Kawanishi, S. *Chem. Res. Toxicol*. **2002**, *15*, 1017-1022.
396. Anbu, S.; Shanmugaraju, S.; Kandaswamy, M. *RSC Adv*. **2012**, *2*, 5349–5357.
397. Qian, J.; Ma, X.; Tian, J.; Gu, W.; Shang, J.; Liu, X.; Yan, S. *J. Inorg. Biochem*. **2010**, *104*, 993–999.
398. Levina, A.; Lay, P.A.; Dixon, N.E. *Inorg. Chem.* **2000**, *39*, 385-395.
399. Vijayalakshmi, R.; Kanthimathi, M.; Subramanian, V.; Unni Nair, B. *Biochem. Biophys. Comm*. **2000**, *271*, 731-734.
400. Kawanishi, S.; Inoue, S.; Sano, S. *J. Biol. Chem.* **1986**, *261*, 5952-5958.
401. Absillis, G.; Van Deun, R; Parac-Vogt, T.N. *Inorg. Chem.* **2011**, *50*, 11552-11560.
402. Ho, P.H.; Stroobants, K.; Parac-Vogt, T.N. *Inorg. Chem.* **2011**, *50*, 12025-12033.
403. Uchida, K.; Pyle, A.M.; Morii, T.; Barton, J.K., *Nucleic Acids Res*. **1989**, *17*, 10259-10279.
404. Gómez-Tagle, P. Yatsimirsky, A.K. *J. Chem. Soc. Dalton Trans.* **2001**, 2663–2670.
405. Camargo, M.A.; Neves, A.; Szpoganicz, B.; Bortoluzzi, A.J.; Fischer, F.L.; Terenzi, H.; Castellano, E.E. *Inorg. Chem.* **2010**, *49*, 3057–3063.
406. Gravert, D.J.; Griffin, J.H. *Inorg. Chem.* **1996**, *35*, 4837-4847.
407. Burrows, C.J.; Rokita, S.E. *Acc. Chem. Res.* **1994**, *27*, 295-301.
408. Routier, S.; Bernier, J.-L.; Waring, M.J. Colson, P.; Houssier, C.; Baily, C. *J. Org. Chem.***1996**, *61*, 2326-2331.
409. Lamour, E.; Routier, S.; Bernier, J.-L.; Catteau, J.-P.;Baily, C.; Vezin, H. *J. Amer. Chem. Soc.* **1999**, *121*, 1862-1869.
410. Mandal, S.S.; Varshney, U.; Bhattacharya, S. *Bioconjugate Chem.* **1997**, *8*, 798-812.
411. Cheng, C-C.; Lu, Y.-L. *J. Chinese Chem. Soc.***1998**, *45*, 611-617.
412. Routier, S.; Vezin, H.; Bernier, J.-L.; Catteau, J.-P.;Baily, C. *Nucleic Acids Res.***1999**, *27*, 4160-4166
413. Clever, G.H.; Sçltl, Y.; Burks, H.; Spahl, W.; Carell, T. *Chem*. *Europ. J.* **2006**, *12*, 8708-8718
414. Rodger. A.; Norden, B. In *Circular Dichroism and Linear Dichroism.* Oxford University Press: Oxford; 1997.
415. Pingoud, A.; Alves J.; Geiger, R. In *Enzymes in Molecular Biology.* Method in Molecular Biology. Burrell, M.M., Ed.; Totowa, NJ: Humana Press Inc.; 1993; Vol, 16, Chapter 8, pp 107-200.
416. Mancin, F.; Teclilla, P. In *Metal Complex-DNA Interactions*, Hadjiliadis, N.; Sletten E., Eds.; UK: Willey, Blackwell Publishing Ltd.; 2009; pp 369-394.
417. Radzicka, A.; Wolfenden, R.; *Science* **1995**, *267*, 90-93.
418. Hendry, P.; Sargeson, A.M. *Prog. Inorg. Chem.* **1990**, 38, 201-258.
419. Cowan, J.A. *Chem. Rev.* **1998**, *98*, 1067-1087.
420. Blasko, A.; Bruice, T.C. *Acc. Chem. Res.* **1999**, *32*, 475-484.
421. Hirt, H.; Apel, K. *Annu. Rev. Plant. Biol.* **2004**, *55*, 373-399.
422. Halliwell, B.; Gutteridge, J.M.C. *Molec. Aspects. Med.* **1985**, 8, 89-193.
423. Halliwell, B. *Mutation Res.* **1999**, *443*, 37–52.
424. Valko, M.; Leibfritz, D.; Moncola, J.; Cronin, M.T.D.; Mazur, M.; Telser, J. *The Intern.J. Biochem. Cell Biol.* **2007**, *39*, 44–84.
425. Wiseman, H.; Halliwell, B. *Biochem. J.* **1996**, *313*, 17-29.
426. Halliwell, B. *Plant Physiol*. **2006**, *141*, 312-322.
427. Valko, M.; Rhodes, C.J.; Moncola, J.; Izakovic, M.; Mazur. M. *Chemico-Biolog. Interac.* **2006**, *160*, 1-40.
428. Halliwell, B. *Drugs Aging* **2001**, *18*, 685-716.

429. Kuznetsova, A.A.; Knorre, D.G.; Fedorova, O.S. *Russian Chem. Rev*. **2009**, *78,* 659-678.
430. West, J.D.; Marnett, L.J. *Chem. Res. Toxicol.* **2006**, *19*, 173-194.
431. Valko, M.; Morris, H.; Cronin, M.T.D. *Curr. Medic. Chem.* **2005**, *12*, 1161-1208.
432. Halliwell, B.; Gutteridge, J. M. C. *Meth.Enzymol*. **1990**, *186*, 1-85.
433. Freinbichler, W.; Colivicchi, M.A.; Stefanini, C.; Bianchi, L.; Ballini, C.; Misini, B.; Weinberger, P.; Linert, W.; Vareslija, D.; Tipton, K.F.; Corte, L.D. *Cell. Mol. Life Sci*. **2011**, *68*, 2067–2079.
434. Rehmana, A.; Nourooz-Zadehb, J.; Moëllerc, W.; Tritschlerc, H.; Pereirad, P.; Halliwell, B. *FEBS Lett.* **1999**, *448*, 120-122.
435. Floyd, R.A. Carcinogenesis **1990**, *11*, 447–1450.
436. Whiteman, M.; Hong, H.S.; Jenner, A.; Halliwell, B. *Biochem. Biophys. Res. Commun.* **2002**, *296*, 883-889.
437. Haber, F.; Weiss, J. *Proc. R. Soc. Lond. A* **1934**, *147*, 332-351.
438. Fenton, H.J.H. *J. Chem. Soc. Trans.* **1894**, *65*, 899-910.
439. Sawyer, D.T.; Valentine, J.S. *Acc. Chem .Res.* **1981**, *14*, 393-400.
440. Bielsky, B.H.J.; Cabelli, D.E.; Ravindra, L.A. *J. Phys. Chem. Ref. Data* **1985**, *14*, 1041-1100.
441. Fridovich, I. *Arch. Biochem.Biophys.* **1986**, *247*, 1-11.
442. Hassan, H.M.; Fridovich, I. *J. Biol. Chem.* **1978**, *253*, 8143-8148.
443. Kearns, D.R. *Chem. Rev.* **1971**, *71*, 395-427.
444. Basu-Modak, S.; Tyrrell, R. M. *Cancer Res.* **1993**, *53*, 4505-4510.
445. Schweitzer, C.; Schmidt, R. *Chem. Rev.* **2003***, 103,* 1685-1757.
446. Youngman, R.J.; Elstner, E.F. *FEBS Lett.* **1981**, *129*, 265-268.
447. Saran, M.; Michel, C.; Stettmaier, K.; Bors, W. *Free Rad. Res.* **2000**, *33*, 567-579.
448. Gutteridge, J.M.C. *Biochem. J.* **1984**, *224*, 761-767.
449. Reinke, L.A.; Rau, J.M.; MacCay, P.B. *Free Rad. Biol. Med.* **1994**, *16*, 485-492.
450. Tadolini, B. *Free. Rad. Biol. Med.* **1987**, *4*, 149-160.
451. Burkitt, M.J.; Gilbert, B.C. *Free Rad. Res. Commun*. **1991**, *14*, 107-123.
452. Tero-Kubota, S.; Ikegami, Y.; Kurokawa, T.; Sasaki, R.; Sugioka, K.; Nakano, M. *Biochem. Biophys. Res. Commun.* **1982**, *108*, 1025-1031.
453. Koppenol, W.H.; Butler, J. Adv. Free Rad. Biol. Med. **1985**, *1*, 91-131.
454. Makrigiorgos, G.M.; Bump, E.; Huang, C.; Baranowska-Kortylewicz, J.; Kassis, A.I. *Free Radic. Biol. Medicin.* **1995**, *18*, 669-678.
455. Gutteridge, J.M.C. *Biochem. J.* **1987**, *243*, 709-714.
456. Inoue, S.; Kawanishi, S. *Canc. Res.* **1987**, *47*, 6522-6527.
457. Evans, P.J.; Halliwell, B. *Methods in Enzym.* **1994**, *233*, 82-92.
458. Fisher, A.E.O.; Maxwell, S.C.; Naughton, D.P. *Biochem. Biophys. Res. Commun.* **2004**, *316*, 48-51.
459. Anipsitakis, G.; Dionysiou, D.D. *Environ. Sci. Technol*. **2004**, *38*, 3705-3712.
460. Moriwaki, H.; Osborne, M.R.; Phillips, D.H. *Toxicol. in Vitro* **2008**, *22*, 36–44.
461. Halliwell, B.; Gutteridge, J.M.C. *FEBS* **1992**, *307,* 108-112.
462. Halliwell, B.; Gutteridge, J.M.C. *Free Radicals in Biology and Medicine*. Oxford University Press: Oxford; 2007.
463. Sawyer, D.T.; Sobkowiak, A.; Matsushita, T. *Acc. Chem. Res*. **1996**, *29*, 409-416.
464. Kremer, M.L. *J. Inorg. Biochem.* **2000**, *78*, 255–257.
465. Halliwell, B.; Gutteridge, J.M.C. *Arch. Biochem. Biophys*. **1986**, *246*, 501-514.
466. Halliwell, B.; Guttcridge, J.M.C. *Arch. Biochem. Biophys*. **1990**, *280*, 1-8.
467. Pogozelski, W.K; Tullius, T.D. *Chem.l Rev.* **1998**, *98*, 1089-1107.
468. Sinha, R.P.; Häder, D.-P. *Photochem. Photobiol. Sci*. **2002**, *1*, 225-236.
469. Sambrook, J.; Russel, D.W. *Molecular Cloning, A laboratory Manual;* 3rd Ed. Cold Spring Harbor Laboratory Press, Cold Spring Harbor, New York, **2001**; Vol. 1, pp 1.1-1.170.
470. Villareal, V.; Zhang, Y.; Zurita, C.; Moran, J.;Silva, I.; Gomez, F.A. *Anal.Lett.* **2003**, *36*, 451–463.
471. Stellwagen, N.C. *Electrophoresis* **2009**, *30*, S188-S195.
472. Silverstein, R.M.; Webster, F.X. *Spectrometric Identification of Organic Compounds,* 6th Ed. John Wiley & Sons, Inc: USA; 1997; pp 144-216.
473. *Handbook of Spectroscopy*. Gauglitz, G., Vo-Dinh, T., Eds.; WILEY-VCH Verlag GmbH & Co. KGaA: Weinheim; 2003; Vol. 1.

474. Pavia, D.L.; Lampman, G.M.; Kriz, G.S.; Vyvyan, J.A. *Introduction to Spectroscopy,* 4th Ed.; Brooks/Cole, Cengage Learning Publishers: Belmont, CA, USA; 2009; pp 381-417.
475. Sutherland, J.C. In *Modern Techniques for Circular Dichroism and Synchrotron Radiation Circular Dichrosim Spectroscopy*. Wallace, B.A., Janes, R.W., Eds.; IOS Press: Amsterdam; 2009; Vol. 1, pp 19-72.
476. Kelly, S.M.; Price, N.C. *Biochim. Biophys Acta* **1997**, *1338*, 161-185.
477. Kelly, S.M.; Jess, T.J; Price, N.C. *Biochim. Biophys Acta* **2005**, *1751*, 119-139.
478. Bard, A.J.; Faukner, L.R. *Electrochemical methods*: *Fundamentals and applications,* 2nd Ed.; John Wiley & Sons, Inc: Republic of Singapore; 2001.
479. Brett, C.M.A.; Brett, A.M.O. *Electrochemistry: Principles, Methods, and Applications*, Oxford University Press: Oxford; 1993.
480. Wang, J. *Analytical electrochemistry,* 2nd Ed.; John Wiley & Sons, Inc: New York; 2001; pp 28-39.
481. Christensen, P.A.; Hamnett, A. *Techniques and Mechanisms in Electrochemistry*. Blackie Academic & Professional, an imprint by Chapman & Hall: Glasgow; 1994; pp 55-66.
482. O'Dea, J.J.; Wojciechowski, M.; Osteryoung, J.G. *Anal. Chem*. **1985**, *57,* 954-955.
483. Helfrick Jr, J.C.; Bottomley, L.A. *Anal. Chem*. **2009**, *81*, 9041–9047.
484. Saran, M.; Summer, K.H. *Free Rad. Res*. **1999**, *31*, 429-436.
485. Linxiang, L.; Abe, Y.; Nagasawa, Y.; Kudo, R.; Usui, N.; Imai, K.; Mashino, T.; Mochizuki, M.; Miyata, N.; *Biomed. Chromatogr*. **2004**, *18*, 470-474.
486. Freinbichler, W.; Bianchi, L.; Colivicchi, M.A.; Ballini, C.; Tipton, K.F.; Linert, W.; Corte, L.D. *J. Inorg. Biochem.* **2008**, *102*, 1329-1333.
487. Mason, T.J.; Lorimer, J.P.; Bates D.M.; Zhao Y. *Ultrason. Sonochem.* **1994**, *1*, S91-S95.
488. Barreto, J.C.; Smith, G.S.; Strobel, N.H.; McQuillin, P.A.; Miller, T.A. *Life Sci.* **1995**, *56*, PL-89–PL-96.
489. Yan, E.B.; Unthank, J.K.; Castillo-Melendez, M.; Miller, S.L.; Langford, S.J.; Walker D.W. *J. Appl. Physiol.* **2005**, *98*, 2304–2310.
490. Mishin, V.M.; Thomas, P.E. *Biochem. Pharmacol.* **2004**, *68*, 747–752.
491. Dai, G.D.; Cui, L.B.; Song, L.; Zhao, R.Z.; Chen, J.F.; Wang, Y.B.; Chang, H.C.; Wang, X.R. *Biomed. Environ. Sci.* **2006**, *19*, 8–14.
492. Montgomery, J.; Ste-Marie, L.; Boismenu, D.; Vachon, L. *Free Rad. Biol. Med.* **1995**, *19*, 927-933.
493. Teismann, P.; Ferger, B.; *Brain Res. Protoc*. **2000**, *5*, 204-2010.
494. Luo, H.; Lehotay, D. *Clinic. Biochem.* **1997**, *30*, 41-46.
495. Lakowicz, J.R. *Principles of Fluorescence Spectroscopy*; 3rd Ed.; Springer, 2006; pp 1-60.
496. Hore, P.J. *Nuclear Magnetic Resonance* Oxford University Press: Oxford; 1995.
497. Roat-Malone, R.M. *Bioinorganic chemistry. A Short Course*, 2nd Ed.; John Wiley & Sons, Inc., Hoboken: New Jersey; 2007, 98-122.
498. Lambert, J.B.; Mazzola, E. Nuclear Magnetic Resonance Spectroscopy: *An Introduction to Principles, Applications, and Experimental Methods* Pearson Education Ins.: New Jersey; 2004.
499. Fisher, M.B.; Thompson, S.J.; Ribeiro, V.; Lechner, M.C.; Rettie, A. *Arch. Biochem. Biophys*. **1998**, *356,* 63-70.
500. Plasmid DNA Purification User Manual NucleoSpin® Plasmid 2009 Macherey-Nagel.
501. Birnboim, H.C.; Doly, J. *Nucl. Acids Res.* **1979**, *7*, 1513-1523.
502. Nigam, S. Validation of methods for measuring efficiency of inorganic nucleases, MSc Thesis (European Master in Quality in Analytical Laboratories), University of Algarve, Faro, **2011**.
503. Aureliano, M.; Gândara, R.M.C. *J. Inorg. Biochem*. **2005**, *99, 979-985*.
504. Aureliano, M.; Crans, D.C. *J. Inorg. Biochem*. **2009**, 103*, 536-546*.
505. Mueller, S.; Riedel, H.-D.; Stremmel, W. *Anal. Biochem*. **1997**, *245*, 55–60.
506. Slebodnick, C.; Pecorraro, V.; *Inorg. Chi. Acta* **1998** *283,* 37-43
507. Sreedhara, A.; Freed, J.D.; Cowan, J.A. *J. Am. Chem. Soc*. **2000**, *122*, 8814–8824.
508. Loganathan, R.; Ramakrishnan, S.; Suresh, E.; Riyasdeen, A.; Akbarsha, M.A.; Palaniandavar, M. *Inorg Chem.* **2012**, *51*, 5512-5532.
509. Good, N.E; Winget, G.D.; Winter, W.; Connolly, T.N.; Izawa, S.; Sing, R.M.M. *Biochem* **1966**, *5*, 467-477.
510. Good, N.E.; Izawa, S. *Meth. Enzymol.* **1972***, 24*, 53-68.

511. Ferguson, W.J.; Braumschweiger, K.L.; Braumscheiger, W.R.; Smith, J.R.; McCormick, J.J.; Wasman, C.C.; Jarivis, N.P.; Bell, D.H.; Good, N.E. *Anal. Biochem.* **1980**, *104, 300-310.*
512. Haveles, K.S.; Georgakilas, A.G.; Sideris, E.G.; Sophianopoulou, V. *Int. J. Radiat. Biol.* **2000**, *76*, 51–59.
513. Harris, W.R. *Clinic. Chem*. **1992**, *38*, 1809-1818.
514. Buglyó, P.; Kiss, T.; Alberico, E.; Micera, G.; Dewaele, D. *J. Coord. Chem*. **1995**, *36*, 105–116.
515. Kiss, T.; Kiss, E.; Garribba, E.; Sakurai, H. *J. Inorg. Biochem*. **2000**, 80, 65–73.
516. Veal, J.M.; Merchant, K.; Rill, R.L. *Nucleic Acids Res***. 1991**, *19*, 3383-3388.
517. Fridovich, I. *Meth. Enzymol.* **1984**, *105*, 59-61.
518. Ohno, Y.; Gallin, J.I. *J. Biol. Chem.* **1985**, *260*, 8438-8446.
519. Szczepanik, W.; Kaczmarek, P.; Jezowska-Bojczuk, M. *J. Inorg. Biochem*. **2004**, *98*, 2141–2148.
520. Liochev, S.I.; Fridovich, I. *Arch. Biochem. Biophys*. **1986**, *250*, 139-145.
521. Liochev, S.I.; Fridovich, I. *Arch. Biochem. Biophys*. **1989**, *275,* 40-43.
522. Liochev, S.I.; Fridovich, I. *Arch. Biochem. Biophys*. **1990**, *279*, 1-7.
523. Liochev, S.I.; Fridovich, I. *Arch. Biochem. Biophys*. **1987**, *255,* 274-278.
524. Carmichael, A.J. *FEBS* **1990**, *261*, 165-170.
525. Rajendiran, V.; Karthik, R.; Palaniandavar, M.; Stoeckli-Evans, H.; Periasamy, V.S.; Akbarsha, M.A.; Srinag, B.S.; Krishnamurthy, H. *Inorg. Chem.* **2007**, *46*, 8208–8221.
526. Bortolini, O; Conte, V. *Mass Spectrom. Rev*. **2006**, *25*, 724–740.
527. Larson, J.W. *J. Chem. Eng. Data* **1995**, *40*, 1276-1280.
528. Smith, J.A.S. Wilkins, E.J. *J. Chem. Soc*. **1966**, 1749.
529. Straganza, G.; Breckerb, L.; Weberb, H-J.; Steinera, W.; Ribbons D.W. *Biochem. Biophys. Res. Comm.* **2002**, *297*, 232-236.
530. Crans, D.C.; Trujillo, A.M.; Pharazyn, P.S.; Cohen, M.D. *Coord. Chem. Rev.* **2011**, *255*, 2178-2192.